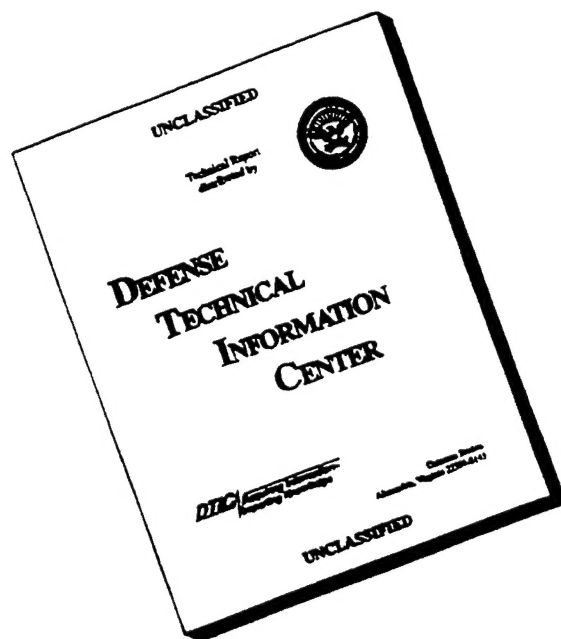


REPORT DOCUMENTATION PAGE			Form Approved OMB No. 0704-0188	
Public reporting burden for this collection of information is estimated to average 1 hour per response, including the time for reviewing instructions, searching existing data sources, gathering and maintaining the data needed, and completing and reviewing the collection of information. Send comments regarding this burden estimate or any other aspect of this collection of information, including suggestions for reducing this burden to Washington Headquarters Services, Directorate for Information Operations and Reports, 1215 Jefferson Davis Highway, Suite 1204, Arlington, VA 22202-4302, and to the Office of Management and Budget, Paperwork Reduction Project (0704-0188), Washington, DC 20503.				
1. AGENCY USE ONLY (Leave blank)	2. REPORT DATE September 1996	3. REPORT TYPE AND DATES COVERED Final		
4. TITLE AND SUBTITLE Three Component Micro and Small Aperture Arrays and Local Networks in Noisy Environment. Development of Statistical Data Processing Techniques: Coherent Noise Suppression, Signal Azimuth and Apparent Velocity Estimation, Generic Automated Event Source Location, Seismic Source Identification		5. FUNDING NUMBERS SPC-95-4045		
6. AUTHOR(S) Alexander Fedorovich Kushnir, Andrey Nikolaevich Gashin, Leonid Matveevich Haikin, Victor Mikhailovich Lapshin, Andrey Dmitrievich Rasskazov, Mikhail Vladimirovich Rozhkov, Boris Mikhailovich Shoubik, Vladimir Vladimirovich Starostin, Evgeny Valerievich Troitsky				
7. PERFORMING ORGANIZATION NAME(S) AND ADDRESS(ES) Synapse Science Center 119034 Ostojenka 13/12 bld 1-AB Moscow Russia		8. PERFORMING ORGANIZATION REPORT NUMBER SPC-95-4045		
9. SPONSORING/MONITORING AGENCY NAME(S) AND ADDRESS(ES) EOARD PSC 802 BOX 14 FPO AE 09499-0200		10. SPONSORING/MONITORING AGENCY REPORT NUMBER SPC-95-4045		
11. SUPPLEMENTARY NOTES				
12a. DISTRIBUTION/AVAILABILITY STATEMENT Unlimited			12b. DISTRIBUTION CODE	
13. ABSTRACT (Maximum 200 words) Automatic discrimination of weak explosions and earthquakes at local distances is an important problem for CTBT monitoring in regions where commercial mining operations and quarry blasting generate a large number of seismic recordings on a daily basis. Development of reliable discrimination techniques to solve this problem involve selection of regionally dependent parameters (which have to be automatically extracted from seismograms) and estimation of misclassification probabilities intrinsic for a given region. Discrimination between weak regional or local earthquakes and explosions remains a serious challenge for state-of-the-art CTBT monitoring. In particular, the known fact that discrimination features proved to be efficient in one seismic region are often useless in another region is a serious obstacle for refinement and standardization of source discrimination techniques. Another important unsolved task in seismic discrimination is to estimate the probability of event misclassifications inherent to the seismic region under investigation.				
14. SUBJECT TERMS			15. NUMBER OF PAGES 272	
			16. PRICE CODE	
17. SECURITY CLASSIFICATION OF REPORT UNCLASSIFIED	18. SECURITY CLASSIFICATION OF THIS PAGE UNCLASSIFIED	19. SECURITY CLASSIFICATION OF ABSTRACT UNCLASSIFIED	20. LIMITATION OF ABSTRACT U/L	

DISCLAIMER NOTICE

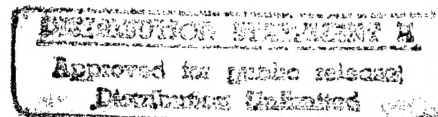


**THIS DOCUMENT IS BEST
QUALITY AVAILABLE. THE
COPY FURNISHED TO DTIC
CONTAINED A SIGNIFICANT
NUMBER OF PAGES WHICH DO
NOT REPRODUCE LEGIBLY.**

SYNAPSE Science Center

**THREE COMPONENT MICRO AND SMALL
APERTURE ARRAYS AND LOCAL NETWORKS
IN NOISY ENVIRONMENT**

**Development of statistical data processing techniques:
coherent noise suppression, signal azimuth and apparent
velocity estimation, generic automated event source
location, seismic source identification**



**Report on
SPECIAL PROJECT SPC-95-4045**

ERIC QUALITY INSPECTED 2

Moscow, September 1996

19961113 144

List of participants of the Project

Gashin Andrey Nikolaevich, researcher, program developer,
Researcher of SYNAPSE Science Center

- *Chapter 4: sections 4.1-4.6; Chapter 6: sections 6.1-6.6.*

Haikin Leonid Matveevich, System SNDA developer,
Ph.D., Senior Researcher of SYNAPSE Science Center

- *Chapter 5, Appendix for Report .*

Kushnir Alexander Fedorovich, **Principal investigator**,
Dr.Sc.,Prof., Senior Researcher of SYNAPSE Science Center

- *Chapters 1, 3, Chapter 4: section 4.7, Report editing.*

Lapshin Victor Mikhailovich, researcher, program developer,
Ph.D., Senior researcher of Institute of Physics of the Earth, RAS

- *Chapter 6: sections 6.7, 6.8.*

Rasskazov Andrey Dmitrievich, researcher, program developer,
System engineer of SYNAPSE Science Center - *Chapter 1: section 1.9.2.*

Rozhkov Mikhail Vladimirovich, researcher, program developer,
Scientific Director of SYNAPSE Science Center - *Chapter 1: section 1.9.2.*

Shoubik Boris Mikhailovich, researcher, program developer,
Ph.D., Senior researcher of Institute of Physics of the Earth, RAS

- *Chapter 2: sections 2.1 - 2.7.*

Starostin Vladimir Vladimirovich, researcher, program developer,
Ph.D., Senior Researcher of SYNAPSE Science Center

- *Chapter 2: section 2.8*

Troitsky Evgeny Valerievich, researcher, program developer,
Ph.D., Assistant professor of Moscow University of Communications and Informatics

- *Chapter 1.*

Acknowledgments:

Participants of the project are grateful to:

- SYNAPSE administration: SYNAPSE Director T.T. Taguizade, SYNAPSE Scientific Director M.V. Rozhkov;
- SYNAPSE system manager V.A.Gurevich; system programmers V.E Kamensky, I.E. Starovoitov, D. Mishin; system engineer A.D.Rasskazov for the help and advises while using SYNAPSE local computer network in the process of project developing;
- SYNAPSE engineer E.V. Kapichnikov for the help in report preparing;
- Dr. A. Dainty, Prof. E.Husebye, Dr. F.Ringdal, Dr.T.Kvaerna and Dr. E.Kremenetskaya for the valuable discussions on the Project subjects.

SYNAPSE address: 119034 Ostojenka 13/12, bld 1-AB, Moscow, Russia

Telephones (095) 201 2516; (095) 202-6934

FAX (095) 956-3033

E-mail kushnir@synapse.ru

CONTENTS

1. EARTHQUAKE-EXPLOSION SEISMOGRAM DISCRIMINATION

1.1. Introduction	1
1.2. Overview of theoretical methods for statistical classification, feature selection and error probability estimation	4
1.2.1. Statistical approach to the classification problem	4
1.2.2 Feature selection	9
1.2.3. Estimation of misclassification probability	12
1.3. Seismogram processing for event source identification: feature extraction, feature selection and misclassification probability estimation..	15
1.4. Results of experimental data processing and discussion;	18
Tables	20
1.5. Conclusions and recommendations;	32
Figures	
1.6. Description of program package for statistical identification of seismic source type	35
1.6.1 Program "LD"	35
1.6.2 Program "LDSTST"	37
1.6.3. Program "FSEL"	41
1.6.4. Program "RECLLD"	43
1.6.5. Program "EXAMLD"	45
1.6.6. Program "EXAMQD"	47
1.7. References	50
1.8. Appendix I.....	52
1.8.1. Script for selection of explosions for classification	52
1.8.2. Script for measuring of earthquake P and S power features	53
1.8.3. Labels of features obtained with the help of "filtration" method for "pure" variant	62

1.8.4. Script for statistical classification, feature selection and error probability estimation	62
1.9 Appendix II	
1.9.1. Application of statistical source identification package for teleseismic event discrimination	64
1.9.2. Neural network approach to discrimination of regional events based on seismic trace sonograms	65
2. SCANLOC: AUTOMATIC SEISMIC EVENT LOCATION IN SPACE AND TIME BASED ON THE PRINCIPLES OF EMISSION TOMOGRAPHY	
2.1. Introduction	1
2.2. Analytical formulation	2
2.3. SCANLOC program package and results of data processing	5
2.4. Conclusions and recommendations	9
2.5. Tables and figures	10
2.6. References	11
2.7. Appendix: Descriptions of SNDA JCL scripts and SCANLOC input file	12
2.8. Study of Israel regional velocity model on the basis of Israel Seismic Network catalogue of local events.....	17
Figures	24
3. ADAPTIVE PROCESSING OF 3-COMPONENT SMALL APERTURE AND MICRO-ARRAY DATA (THEORY AND ALGORITHMS)	
3.1. Mathematical models of 3-component small aperture seismic array records	1
3.2. Coherent noise suppression and seismic waveform extraction using data from 3-component arrays	7
3.2.1. Introduction	7
3.2.2. Statistically optimal group filter (Wiener filter)	8
3.2.3. Adaptation of optimal group filter to variations of noise spectrum	10

3.2.4. Spatial Rejecting Group Filter	12
3.2.5. Optimal group filter with additional constraints	14
3.3. Adaptive statistical algorithms for estimation of azimuth and apparent velocity of seismic phases using data from 3-component arrays	16
3.3.1. Introduction	16
3.3.2. Mathematical models of observations as a random time series with informative and nuisance parameters	17
3.3.3. Asymptotically efficient estimates of apparent slowness vector for random signal waveforms	19
3.3.4. Asymptotically efficient estimates of apparent slowness vector for small signal-to-noise ratio	22
3.3.5. Apparent slowness estimates for completely unknown signal waveforms	24
3.4. References	27
4. EXPERIMENTAL STUDY OF ADAPTIVE ALGORITHM APPLICATIONS TO 3-COMPONENT VERY BROAD BAND SMALL APERTURE ARRAY DATA PROCESSING	
4.1 Introduction.....	1
4.2. Geyocha array noise feature study.....	2
4.3. Simulating experiments with real Geyocha 3C noise recordings.....	5
4.4. Analysis of Geyocha 3C seismograms from Lop Nor explosion on 07.10.1994.....	6
4.4.1. P-phase arrival direction estimation.....	6
4.4.2. Extracting of phase waveforms from background noise.....	7
4.5. Analysis of Geyocha 3C seismograms from Lop Nor explosion on 10.06.1994.....	9
4.5.1. P-phase arrival direction estimation.....	9
4.5.2. Extracting of phase waveforms from background of noise and coda of previous phases.....	11
4.6. Analysis of Geyocha 3C seismograms from Oman gulf earthquake on 18.10.1993.....	14
4.6.1. Onset time estimation of the event wave phases.....	14

4.6.2. Extraction of body wave phase waveforms using adaptive array seismogram processing	17
4.6.3. Study of event surface wave characteristics	19
Figures.....	
4.7. Detection and parameter estimation of explosion signal obscured by coda of strong interfering earthquake using data from small aperture array.....	21
Figures	
4.8. References.....	24
5. FURTHER DEVELOPMENT OF THE SNDA SYSTEM	2
5.1. New high level language	2
5.2. Surfer	6
5.3. Map	7
5.4. Cluster	8
5.5. Other developments	10
6. DESCRIPTION OF PROGRAMS FOR 3-COMPONENT ARRAY DATA PROCESSING	
6.1. Program "MODELS" Modeling of 3-component array seismograms...	1
6.2. Program "POL" Polarization filtering of data from single 3-component station by Flinn method	7
6.3. Program "POLCFLTS" Vector polarization filtering of multichannel data	11
6.4. Program "ARMAFS" Estimating of inverse matrix power spectral density of multichannel data by ARMA modeling	14
6.5. Program "GRFILTF5" Optimal Wiener group filtering of 3-component array data for different types of wave polarization	18
6.6. Program "GRFLTFCS" Extraction of waveforms of differently polarized seismic phases using 3-component array data with the help of optimal Wiener group filtering	25
6.7. Program "GRFLTFK" Adaptive 3-component F-K analysis	32
6.8. Program SP3C Adaptive multimode F-K analysis of 3-component array data	37

1. EARTHQUAKE-EXPLOSION SEISMOGRAM DISCRIMINATION

CONTENTS

1.1. Introduction	1
1.2. Overview of theoretical methods for statistical classification, feature selection and error probability estimation	4
1.2.1. Statistical approach to the classification problem	4
1.2.2 Feature selection	9
1.2.3. Estimation of misclassification probability	12
1.3. Seismogram processing for event source identification: feature extraction, feature selection and misclassification probability estimation	15
1.4. Results of experimental data processing and discussion;	18
Tables	20
1.5. Conclusions and recommendations;	32
Figures	
1.6. Description of program package for statistical identification of seismic source type	35
1.6.1 Program "LD"	35
1.6.2 Program "LDSTST"	37
1.6.3. Program "FSEL"	41
1.6.4. Program "RECLLD"	43
1.6.5. Program "EXAMLD"	45
1.6.6. Program "EXAMQD"	47
1.7. References	50
1.8. Appendix I.....	52
1.8.1. Script for selection of explosions for classification	52
1.8.2. Script for measuring of earthquake P and S power features	53
1.8.3. Labels of features obtained with the help of "filtration" method for "pure" variant	62
1.8.4. Script for statistical classification, feature selection and error probability estimation	62
1.9 Appendix II	
1.9.1. Application of statistical source identification package for teleseismic event discrimination	64
1.9.2. Neural network approach to discrimination of regional events based on seismic trace sonograms	65

1. EARTHQUAKE-EXPLOSION SEISMOGRAM DISCRIMINATION

1.1. Introduction

Automatic discrimination of weak explosions and earthquakes at local distances is an important problem for CTBT monitoring in regions where commercial mining operations and quarry blasting generate a large number of seismic recordings on a daily basis. Development of reliable discrimination techniques to solve this problem involve selection of regionally dependent parameters (which have to be automatically extracted from seismograms) and estimation of misclassification probabilities intrinsic for a given region.

Discrimination between weak regional or local earthquakes and explosions remains a serious challenge for state-of-the-art CTBT monitoring. In particular, the known fact that discrimination features proved to be efficient in one seismic region are often useless in another region is a serious obstacle for refinement and standardization of source discrimination techniques. Another important unsolved task in seismic discrimination is to estimate the probability of event misclassifications inherent to the seismic region under investigation.

In recent years the success has been achieved in techniques for discriminating between earthquake and explosion sources by artificial neural networks. Nevertheless, the potential of the conventional statistical discrimination approach is not exhausted yet. Two general statistical approaches may be distinguished in the seismic discrimination problem [1,2]:

1. Waveform discrimination approach: employment of the statistically optimal technique for testing hypothesis for discrimination between explosion and earthquake seismograms. The latter is modeled in this approach as realizations of zero mean stochastic processes with unknown but different power spectral densities (PSD). The discrimination is based on the well known fact that typical normalized PSD of P and S phases are different for explosions and earthquakes. This difference is due to distinction of physical nature of the sources. The various divergence measures between stationary stochastic processes (used for modeling explosion and earthquake seismograms) were proposed in [1,2] to construct the hypotheses testing statistics. There are the following measures: quadratic informant, minimum discriminative information, ϵ -entropy Renyi, Kullback-Leibler J divergence, Chernoff quasi-distance and so on. The summary of this approach is presented in [20].

Practical application of the above approach to seismic source discrimination demands estimating PSD of P and S phases belonging to different classes using learning sets of explosions and earthquakes. These estimates have to be substituted into classification algorithms instead of unknown PSD of stochastic processes which are modeling the different classes. Our experiments showed that seismograms of weak local earthquakes and explosions demonstrate considerable diversity of spectral estimates. Therefore, simple averaging of spectral estimates calculated for learning seismograms belonging to the same classes inevitably should result in great smoothing which leads to poor classification capability. This did not encourage us to use the approach recommended in [1,2] for discrimination of weak local events.

2. Feature extraction - feature discrimination approach: statistical discrimination of relevant numerical features extracted from seismograms according to some heuristic considerations. Some power or spectral numerical characteristics of seismograms which are typically different for earthquakes and explosions are used as the discrimination features. The discrimination problem is solved by application of classical statistical pattern recognition technique to processing of the feature sets. Numerous investigations in discriminate analysis [3-6] demonstrated that selection of a small number of most informative features is extremely useful in this approach. It was proved that few carefully selected features may provide a smaller error classification probability as compared with the all set of the features. This is so-called "pick-effect" or "multivariate effect". Of course, the optimal feature subset selected for given region data is able not be the same as one for another region. But automatic feature selection procedure allows to select the individual optimal subsets of features for different regions of interest.

Note, that there exists a vast amount of statistical nonparametric pattern recognition methods (Parzen's "kernels", "potential functions" methods and other [10]). Various unstatistical methods of classification such as "nearest neighbor" and "k-nearest neighbor" rules, are also frequently used in different applications [10] The logical classification algorithm "KORA" and his numerous modifications are widely employed for predictions of future earthquake epicenter locations [21]. Nevertheless at our opinion, parametric statistical approach is the most appropriate in our problem, because the criterion of classification quality can be most generally formulated in

terms of the probability theory and error classification probabilities can be rather easily calculated. Besides:

a). The parametric statistical classification theory is well developed. In particular, it allows to obtain under quite realistic assumptions the theoretical estimates of error classification probabilities and to perform the theoretically optimal feature selection;

b). Often the optimal parametric statistical algorithms are coincide with ones resulting from some heuristic consideration;

c). The parametric statistical algorithms are rather simple for realization as automated computer tool for different monitoring purposes.

The theoretical assumption concerning to multidimensional Gaussian (normal) distribution of the feature vectors used for theoretical substantiation of many parametric statistical algorithms is not so severe due to possibility to implement a feature nonlinear transformation of the vectors (as known Box-Kox's transformation used in this research) which leads to normalization of their distributions. The statistical methods mentioned above are not widely used until present time in seismic monitoring practice for selection of appropriate earthquake and explosion discrimination parameters and for ensuring of reliability of earthquake-explosion discrimination in a given region.

In this study we made an attempt to implement the parametric statistical classification methods for discrimination between weak earthquakes and chemical explosions recorded by Israel local seismic network. A learning set of 28 earthquakes and 25 explosions with magnitudes 1.1-2.6 recorded at distances of 30-200 km. was used in the study. The events were recorded by the Israel Seismic Network (ISN) which is operated by the Seismological Division of the Institute for Petroleum Research and Geophysics (IPRG), Israel. The data base supplied with ground truth information was collected by Dr. Y.Gitterman (IPRG) and used in [19]. The wave forms and ISN bulletin information were prepared and transferred by Dr. V. Pinsky (IPRG).

A variety of discrimination parameters based on the relative power spectral distributions of P and S phases was extracted from the event wavetrains and processed by special statistical procedures with purpose to select the most informative features and attain the minimum of probability of discrimination errors. Estimates of the

power spectrum of seismic noise at intervals preceding the event wavetrains were used to improve the quality of discrimination feature measurement in conditions of poor signal-to-noise ratio which are typical for weak event recordings.

The feature selection procedures allowed us to extract by an automatic procedure the 5 most informative features from more the 20 seemed to be relevant for discrimination from heuristic considerations. Implementation of noise refinement and feature selection procedures, feature nonlinear transformation and quadratic discrimination allowed to achieve the average misclassification probability (estimated with the help of a statistically consistent cross-validation method) equal to 3.8%: only 2 events (explosions) were incorrectly classified from 53 events under study.

An automated seismogram discrimination technique was developed to provide implementation of the proposed algorithms in seismic monitoring practice. It was designed with the help of Seismic Network Data Analysis (SNDA) System, a problem-oriented programming shell developed at the Moscow IRIS Data Analysis Center/SYNAPSE Science Center [7] in which the program package for statistical identification was incorporated

1.2. Overview of theoretical methods for statistical classification, feature selection, and error probability estimation

1.2.1. Statistical approach to the classification problem.

There exists an extensive bibliography on the statistical methods of discriminant analysis. The reviews on this problem may be found in [5,8-12]. Below we give the very brief sketch of statistical approach to the discriminant analysis.

Let us consider the following parametric model of a set of p -dimensional distributions in p -dimensional feature space R_p ; let the set can be parametrized by k -dimensional parameter θ : $\{P_\theta; \theta \in \Theta \subset R_k\}$. Denote the corresponding set of probability density functions (p.d.f) as $\{f(x; \theta); \theta \in \Theta \subset R_k\}$. The p.d.f. $f(x; \theta)$ can be regarded as known function of argument x and parameter θ . The two distributions P_1 and P_2 with corresponding p.d.f. $f(x; \theta_1)$ and $f(x; \theta_2)$ is the probabilistic model of some two classes of feature vector variations.. The learning vector samples $X_{n1} = \{x_{11}(1), x_{21}(1), \dots, x_{n1}(1)\}$ and $X_{n2} = \{x_{12}(2), x_{22}(2), \dots, x_{n2}(2)\}$ are regarded as the mutually independent random vectors with p.d.f. $f(x; \theta_1)$ and $f(x; \theta_2)$ respectively. The vector x to be classified is regarded as random vector independent from the learning samples X_{n1} and X_{n2} and

having p.d.f $f(x; \theta_0)$ where parameter θ_0 is unknown but can be equal only to θ_1, θ_2 . The discrimination problem is then be interpreted in the terminology of theoretical statistic as the testing of composite statistical hypothesis on the basis of the observations $X = \{x, X_{n1}, X_{n2}\}$. The hypothesis are: $H_1: \theta_0 = \theta_1$; $H_2: \theta_0 = \theta_2$. This most general so-called three-samples statistical interpretation of the classification problem was suggested by C.R.Rao in 1954 [13]. There are few strategies and approaches for this problem solution [11], such as Bayesian, maximum likelihood ratio, minimax, adaptive and so on. We briefly discuss below some of this approaches.

In the Bayesian classification approach θ_1 and θ_2 are regarded as independent random variables with a priori probability density functions $p(\theta_1)$ and $p(\theta_2)$ correspondingly. The learning sample sets X_{n1}, X_{n2} are treated as sequences of independent observations of vector variables from R_p with conditional p.d.f. $f(x|\theta_1)$ and $f(x|\theta_2)$, where fixed θ_1, θ_2 are sample values of random variables from R_k with p.d.f. $p(\theta_1)$ and $p(\theta_2)$. The vector x to be classified is regarded as a sample value of vector variable with conditional p.d.f. $f(x|\theta_0)$ where θ_0 is a sample value of random variable from R_k with unknown a priori distribution: $p(\theta_1)$ or $p(\theta_2)$, every can exist with a priori probabilities P_1 and $P_2 = 1 - P_1$. It is known that the statistic of Bayesian discrimination rule (which minimizes the average Bayesian risk) has the form of averaged likelihood ratio ([11] eq.(32)). In the important particular case where $f(x|\theta_l)$, $l=1,2$ are the multivariate Gaussian distributions $\mathcal{N}(\mu_l, S)$, with random mean vectors μ_1 and μ_2 having different Gaussian distributions and random matrix $T = S^{-1}$ having the Wishart distribution, the Bayesian discrimination rule can be calculated analytically ([12] formula (57)). For practical applications of this rule the a priori information concerning parameters of a priori distributions of μ_l and T is required. If this information is absent, the asymptotic form of the Bayesian rule may be used for natural asymptotic where this a priori information "disappears", i.e. dispersions of all a priori distributions tend to infinity and P_1, P_2 tend to $1/2$. This asymptotic Bayesian statistic has the form ([12], eq.62):

$$B_{as} = \frac{\Gamma(\frac{n_2}{2})}{\Gamma(\frac{n_2-p}{2})} \frac{\Gamma(\frac{n_1-p}{2})}{\Gamma(\frac{n_1}{2})} \left(\frac{n_1+1}{n_2+1}\right)^{\frac{p}{2}} \left(\frac{|\Sigma_1|}{|\Sigma_2|}\right)^{\frac{1}{2}} \times$$

$$\frac{\left[1 + \frac{1}{n_1+1} (x - \bar{x}^{(1)})^T \Sigma_1^{-1} (x - \bar{x}^{(1)})\right]^{\frac{n_1}{2}}}{\left[1 + \frac{1}{n_2+1} (x - \bar{x}^{(2)})^T \Sigma_2^{-1} (x - \bar{x}^{(2)})\right]^{\frac{n_2}{2}}} \quad (1)$$

where: $\bar{x}^{(1)}$ $\bar{x}^{(2)}$ and Σ_1 Σ_2 are sample means and sample covariance matrices of the learning sector sets X_{n1} , X_{n2} , $|\Sigma_l|$, $l=1,2$, are the discriminants of the sample matrices. If $B_{as} > 1$, the decision is made that hypothesis H_2 is true; if $B_{as} < 1$, the decision is made that the opposite hypothesis H_1 is true. Note, that only learning vector data X_{n1} , X_{n2} and being classified vector x are used in equation (1)

The maximum likelihood discrimination rule has the form ([11], p.24):

if $r > 1$, the hypothesis H_2 is adopted

if $r < 1$, the hypothesis H_1 is adopted,

where

$$r = \frac{\sup_{(\theta_1, \theta_2) \in \Theta \otimes \Theta} f(x|\theta_2) f(X_{n1}|\theta_1) f(X_{n2}|\theta_2)}{\sup_{(\theta_1, \theta_2) \in \Theta \otimes \Theta} f(x|\theta_1) f(X_{n1}|\theta_1) f(X_{n2}|\theta_2)} \quad (2)$$

In the case where $f(x; \theta_1)$ and $f(x; \theta_2)$ are the multivariate Gaussian distributions $\mathfrak{N}\{\mu_l, S\}$, $l=1,2$, with a common covariance matrix S the statistic r in eq.(2) coincides with the well known Anderson's maximum likelihood statistic M ([12] p.46, eq.(29)):

$$M = \frac{n_1}{n_1+1} (x - \bar{x}^{(1)})^T S_{n1+n2}^{-1} (x - \bar{x}^{(1)}) - \frac{n_2}{n_2+1} (x - \bar{x}^{(2)})^T S_{n1+n2}^{-1} (x - \bar{x}^{(2)}),$$

where S_{n1+n2}^{-1} is unbiased estimate of the common covariance matrix of observations S using total learning vector set.

In the case where $f(x; \theta_1)$ and $f(x; \theta_2)$ are the multivariate Gaussian distributions $\mathfrak{N}\{\mu_l, S_l\}$, $l=1,2$, with different covariance matrices S_1 and S_2 statistic r in eq.(2) is defined by formula ([12] eq.(30)):

$$r = \left(\frac{n_1}{n_1 + 1} \right)^{\frac{p(n_1+1)}{2}} \left(\frac{n_2 + 1}{n_2} \right)^{\frac{p(n_2+1)}{2}} \frac{|\Sigma_1|^{\frac{1}{2}} \left[1 + \frac{n_1}{(n_1 + 1)^2} (x - \bar{x}^{(1)})^T \Sigma_1^{-1} (x - \bar{x}^{(1)}) \right]^{\frac{n_1+1}{2}}}{|\Sigma_2|^{\frac{1}{2}} \left[1 + \frac{n_2}{(n_2 + 1)^2} (x - \bar{x}^{(2)})^T \Sigma_2^{-1} (x - \bar{x}^{(2)}) \right]^{\frac{n_2+1}{2}}} \quad (3)$$

In accordance with the minimax strategy one has to find the discrimination rule that provides a minimum (in comparison with any other rule) of a risk function $\rho(\theta_1, \theta_2)$ maximum value attained for all possible $\theta_1, \theta_2 \in \Theta$. This strategy is very difficult for realization. In the case of multivariate Gaussian distributions $\mathcal{N}(\mu_l, S)$, $l=1,2$ with a common and known covariance matrix S the minimax discrimination rule was derived in 1973 by Das S. Gupta [8]. He found that in this case the minimax statistic coincides with the Anderson's maximum likelihood statistic (3) where Σ_l^{-1} , $l=1,2$, have to be substituted by the known covariance matrix S .

Adaptive ("plug-in") discrimination rules get historically the most development. In particular, the adaptive rules based on likelihood ratio calculated for known parameters of observation $X = \{x, X_{n1}, X_{n2}\}$ distributions under hypothesis H_1 and H_2 , are most commonly used. Adaptive rule of this type has the form:

if $\ln(\hat{L}(x)) > 0$, the hypothesis H_2 is adopted;

if $\ln(\hat{L}(x)) \leq 0$, the hypothesis H_1 is adopted,

where $\hat{L}(x) = f(x; \hat{\theta}_1) / f(x; \hat{\theta}_2)$, $\hat{\theta}_1, \hat{\theta}_2$ are consistent estimators of θ_1, θ_2 .

Adaptive rules of this type usually provide rather simple and relevant in practical applications discrimination algorithms. From the theoretical point of view they are asymptotically optimal (under weak restrictions) if estimators $\hat{\theta}_1, \hat{\theta}_2$ are consistency ones. It means that minimum of misclassification probability is guaranteed when amounts n_1, n_2 of learning vectors tend to infinity and assumed conditional p.d.f. $f(x; \theta)$ corresponds to real distribution of observations belonging to different classes if parameter θ get some values θ_1, θ_2 .

In the case of multivariate Gaussian distributions $\mathcal{N}(\mu_l, S)$, $l=1,2$ with a common covariance matrix S we get the well known discrimination rule based on the linear discriminant function (LDF)

If $LDF > 0$, the hypothesis H_2 is adopted;

If $LDF < 0$, the hypothesis H_1 is adopted,

where

$$LDF = [x - \frac{1}{2}(\bar{x}^{(2)} + \bar{x}^{(1)})^T S_{n_1+n_2}^{-1}(\bar{x}^{(2)} - \bar{x}^{(1)})^T]. \quad (4)$$

In the case of multivariate Gaussian distributions $\mathbf{x} \sim \{\mu_l, \mathbf{S}_l\}$, $l=1,2$ with different covariance matrices \mathbf{S}_1 and \mathbf{S}_2 we get well known discrimination rule based on the quadratic discriminant function (QDF)

If $QDF > 0$, the hypothesis H_2 is adopted;

If $QDF < 0$, the hypothesis H_1 is adopted,

where

$$QDF = (x - \bar{x}^{(1)})^T S_{n_1}^{-1}(x - \bar{x}^{(1)}) - (x - \bar{x}^{(2)})^T S_{n_2}^{-1}(x - \bar{x}^{(2)}) + \ln \frac{|S_{n_1}|}{|S_{n_2}|} \quad (5)$$

It was proved in [12], that in the case of multivariate Gaussian distributions $\mathbf{x} \sim \{\mu_l, \mathbf{S}_l\}$, $l=1,2$, with different covariance matrices \mathbf{S}_1 and \mathbf{S}_2 the asymptotic Bayesian discrimination rule (1), maximum likelihood rule (3) and rule founded on QDF (5) are asymptotically equivalent if amounts of learning vectors n_1, n_2 tend to infinity. The same is valid for the rules (2) and (4) based on the Anderson M-statistic and the LDF (for the Gaussian case with common covariance matrix).

In our experimental studies we used the discrimination rules based on the LDF and QDF because these rules are asymptotically optimal in the case of multivariate Gaussian distributions and are easy for realization. Besides, these rules are optimal in the following heuristic sense: the LDF and QDF compare p -dimension distances from the vector \mathbf{x} being classified to the centers of classes determined by the sample means $\bar{x}^{(1)}$ and $\bar{x}^{(2)}$, and assign the vector \mathbf{x} to the class corresponding to the minimal distance. The distances are calculated for generalized Euclidean metrics defined by the matrices $S_{n_1}^{-1}$ and $S_{n_2}^{-1}$ (which are equal in the LDF case). The restriction for practical application of LDF and QDL, connected with the necessity of multidimensional Gaussian (normal) distribution of observations can be relaxed by the nonlinear transformation of the features: there exist some transformations (for example, the simplest ones: $y=\log(x)$ and Box-Kox's $y=\alpha(x^\alpha-1)$) which being applied to the discrimination feature make their distribution close to Gaussian one.

In practical application of the LDF and QDF some computational difficulties may occur while inverting of sample matrices $S_{n_1+n_2}$, S_{n_1} , S_{n_2} : the latter can be bad-posed if the some features are strongly correlated. These difficulties can be overcome

by the regularization of the sample covariance matrices, for example, by substituting their diagonal elements s_{ii} by the values $s_{ii}(1+\rho)$ where ρ is the coefficient of regularization chosen from some heuristic considerations.

1.2.2. Feature selection.

The feature selection problem in the statistical discriminant analysis is a part of more general problem of the multivariate statistical analysis connected with decreasing of dimension of random variables being processed. The different dimension decreasing methods are used in the discriminant analysis such as regression and correlation analysis, method of canonical variables, principal component method, method of two discriminant directions and so on [10]. The main idea of these approaches is to pass to some space of linear combinations of input variables which has a smaller dimension. The lack of these methods is difficulties connected with a "physical" interpretation of used linear combinations. The simplest alternative method for dimension decreasing used in the discriminant analysis is selection of a subset of the "most informative features" from the total feature set. At the early stage of discriminant analysis development it seemed that increasing of amount of features improves the classification quality or do not make it at least worse. Then it was realized that this assertion is correct only for situation where all parameters of feature distributions are a priori known for every class, but as a rule, it is incorrect for situation where the unknown parameters have to be estimated using learning feature vector sets with bounded sample size. Numerous investigations in discriminant analysis [3-6] demonstrated that few carefully selected features may provide a smaller error classification probability as compared with the all feature set. This is so-called "pick-effect" or "multivariate effect". The effect may be explained in the following manner: the number of parameters to be estimated using bounded learning sets rapidly (often in quadratic manner) increases together with rising of the amount of features used; random variations of the estimated parameters are strongly correlated and as a rule, are summated during the procedure of discrimination statistic calculation that gains the random variations of the statistic; this results in growth of the classification error probability. From the other hand, increasing of the feature amount k leads to growth of the Kullback-Leibler's distance between the feature multidimensional distributions corresponding the two classes. This results in decreasing of the

classification error probability. These two tendencies operating in the opposite directions allow to expect an appearance of minimum in a course of the error probability curve $P(k)$ while increasing of k . The more thorough investigations revealed that this minimum is realized when the Kullback-Leibler's distance growth with rising of k is exhausted for large values of k .

The quantitative analysis of the "pick effect" is the very difficult mathematical task so derivation of an analytical expressions for the error probability curve $P(k)$ was accomplished only for few simplest cases, in particular, for the case of two multivariate Gaussian (normal) feature distributions with equal covariance matrices. For these distributions the Kullback-Leibler's distance coincides with the Mahalanobis distance $D(k)$. An asymptotic expansion for the average error probability $P_L(k)$ provided in this case by the linear discrimination function (LDF) was studied by A.D. Deev [3]. He derived the rather simple asymptotic formula (Kholmogorov-Deev formula) for $P(k)$ in the asymptotic where sizes of learning vector sets n_1 and n_2 and amount of features k tend to infinity while k/n_1 , k/n_2 and Mahalanobis distance tend to constants. This asymptotic is very relevant for describing of typical practice situation where amount of features gathered for discriminant analysis is commensurable with amounts of learning feature vectors available. The idea to apply this asymptotic for investigation of discriminant analysis quality was put forward by A.N. Kholmogorov and it appeared to be the very productive idea used in numerous further investigations.

The Kholmogorov-Deev formula was used in our study for design of step-wise feature selection procedure. This procedure generates an optimal feature subset consisting of k_0 features providing the error probability equal (or close) to minimum of $P_L(k)$ probability curve. The procedure is recurrent one and allows to avoid a exhaustive search through the all feature subsets. The few types of step-wise (recurrent) feature selection procedures can be constructed using the following selection strategies: one by one addition of features, one by one elimination of features, step-wise addition of one with elimination of another feature and so on. In this study we used the step-wise procedure with one by one feature addition. This procedure is comparable with the exhaustive search procedure in reliability of attaining of the $P_L(k)$ minimum but significantly less time consuming.

Feature selection is based on processing of learning vectors $\{x_l(j); j \in (1, n_l), l \in (1, 2)\}$ where l is the number of class; n_l is the number of vectors in the learning set. Initially each vector consists of p features gathered as relevant for a given discrimination problem. The feature selection procedure consists of p steps. At any intermediate step k only some $k < p$ features are involved, so the $x_l(j)$ are the k -dimensional feature vectors at this step. We use as a base for the feature selection the informational distance between two k -dimensional probability distributions of learning vectors which is called the Makhalonobious distance

$$R(k) = (m(k, 1) - m(k, 2))^T S^{-1}(k) (m(k, 1) - m(k, 2)), \quad (6)$$

where: $m(k, 1)$, $m(k, 2)$ are the sample mean k feature vectors for the 1-st and 2-nd classes; $S^{-1}(k)$ is the $(k \times k)$ inverse sample covariance matrix calculated for these features using learning data for the both classes.

At the first step of selection procedure p values of the $R(1)$ distance are calculated for every feature. The maximum from these p values is attained for some $j(1)$ feature which is thus selected as optimal one. At the second step $p-1$ values of the $R(2)$ distance are calculated for the feature pairs. The first member of every pair is always the previously selected feature with number $j(1)$, the second member is any rest feature. The second optimal feature is selected as providing a maximum among these $R(2)$ values. At the k -th step of selecting procedure $p-k+1$ values of the $R(k)$ distance are calculated for the vectors composed by the k features. The first $k-1$ components of these vectors are the optimal features which have been selected at the previous steps, the k -th component is any feature from the remaining $p-k+1$ ones.

The procedure described rearranges the initial order of features in the learning vectors to provide the most rapid increasing of the Makhalonobious distance. To select the most informative subset of the features the estimate of misclassification probability $P_L(k)$ is calculated for every step k ($k = 2, \dots, p$) of the procedure using the Kholmogorov-Deev formula [3]:

$$P_L(k) = (1/2)[1 - T_k(R(k)/\sigma(k)) + T_k(-R(k)/\sigma(k))], \quad (7)$$

where

$$\sigma^2(k) = [(t+1)/t][r_1 + r_2 + R(k)]; \quad t = [(r_1 + r_2)/r_1 r_2] - 1; \quad r_1 = k/n_1; \quad r_2 = k/n_2$$

$$T_k(z) = F(z) + (1/(k-1)) (a_1 - a_2 H_1(z) + a_3 H_2(z) - a_4 H_3(z)) f(z),$$

$F(z)$ - is the cumulative function of standard Gaussian probability distribution ; $f(z)$ is the density of this distribution; $H_i(z)$ is the Hermitian polynomial with order i , $i=1,2,3$; a_j , $j=1,\dots,4$ are some coefficients depending on k , n_1 , n_2 and $R(k)$ [3].

The selection method is based on the theoretical interpretation of the fact that in practice the Mahalanobious distance $R(k)$ is a monotonically increasing function of k with growth tending to be exhausted while $k \rightarrow p$. For this condition the function $P_L(k)$ has a minimum at a some step k_0 between 1 and p . Thus in result of a procedure execution one gets the set of optimal (most informative) features with initial numbers $j(1), j(2), \dots, j(k_0)$, i.e. the set of features selected at the steps $1, \dots, k_0$.

Note that such selected optimal features provide the absolute minimum of average misclassification probability only in the case where the multivariate feature distributions are the Gaussian ones with equal covariance matrices and discrimination itself is performed with the help of linear discrimination function. If these assumptions are not valid there are no theoretical guarantee that this set is the best solution. Nevertheless numerous tests, practical applications of the procedure described and some heuristic consideration ensure us that the optimality of the such selected feature set is preserved outside of mentioned confining assumptions. However the estimated value of the $P_L(k)$ minimum seems to be, as a rule, excessively pessimistic. So the real misclassification probability provided by the employed (not necessary linear) discrimination function operating with the optimal feature set has to be independently estimated with the help of statistically consistent procedures. Such procedures are discussed below.

The feature selection algorithm explained above is realized in the computer program "fsel".

1.2.3. Estimation of misclassification probability.

At least four types of misclassification probability are used in the discriminant analysis. They are the following ones:

P_B - this is the Bayesian misclassification probability: absolute minimum of misclassification probability value provided by Bayesian decision rule under assumptions that the feature multivariate distributions a priori completely known but a priori probabilities of classes P_{C1} , $l=1,2$ are known (equal 1/2, for example);

$P = P_{C1} P_{21} + P_{C2} P_{12}$ ($P_{C1} = P_{C2} = 1/2$, for example) - this is the conditional misclassification probability provided by some fixed discrimination function (decision

rule) under condition of fixed learning data. Here P_{21} , P_{12} are the conditional misclassification probabilities for classes 1 and 2 accordingly. Note, that P is really a random variable;

P_{as} - this is the asymptotic (limit) P value for infinitely increasing sizes of the learning sets: $n_1, n_2 \rightarrow \infty$;

$P_{av} = P_{C1} P_{av21} + P_{C2} P_{av12} = E\{P\}$ - this is the average P value: the mathematical expectation of random P value using distributions of the learning vectors. Note that it is calculated for some fixed decision rule. In the asymptotic $n_1, n_2 \rightarrow \infty$ P_{av} tends to P_{as} for the any reasonable discriminant function. However, for not so large n_1, n_2 values of P and P_{av} can significantly differ.

The average misclassification probability P_{av} seems to be the most relevant and convenient one for characterizing the discrimination procedure quality: though it is related to the discriminant function used for decision making, it is independent with respect to the set of learning observations. However, the calculation of P_{av} for a given discriminant function is much more difficult mathematical task as compare with the P calculation. The Kholmogorov -Deev formula gives the asymptotic approximation for the average misclassification probability P_{av} provided by linear discriminant function under assumption that feature distributions are Gaussian ones with equal covariance matrices. It serves as a basis for design of the fast and effective procedure for feature selection [4,5]. However, due to the asymptotic method of its derivation it often gives higher probabilities of misclassifications than those really achievable in simulation experiments with mediate amounts (several ten) of learning vectors.

The more or less realistic estimates of misclassification probability are provided by different modifications of the frequency ratio method. The essence of the method is very simple: some part of learning set is used for adjusting (learning) of discriminant function, the another part (possibly crossing with the first) is subjected to classification by the learned discriminant function; the fraction of misclassified vectors with respect to the total number of tested vectors is used as an estimate of misclassification probability. Let us denote: as $m(j)$ - the number of vectors from class j , subjected to classification by the discriminant function; as $m(i|j)$ - the number of vectors from class j classified as belonging to class i ; $i, j=1, 2$. Then $v(i|j) = m(i|j)/m(j)$ is the frequency ratio of misclassifications for class j ; $v = (1/2)(v(1|2) + v(2|1))$ is the total frequency ratio of misclassifications for the both classes

The next modifications of frequency ratio method are most often used.

a) Reclassification method (R-method). By this method the adaptation (learning) of discriminant function is made using all learning vectors being available. Then the same vectors are classified with the help of this discriminant function. The disadvantage of the R-method is that the frequency ratio v is in this case the biased estimator of the P , and P_{av} values: it gives as a rule the too optimistic values for misclassification probability (even asymptotically - for infinitely increasing sizes of the learning vectors). The bias of this estimator may be decreased by the boot-strap method.

b) Sample-Check method (C-method). By this method the every class learning vector set is divided in two parts. The first part is used for adaptation (learning) of discriminant function and the second part - for classification by this discriminant function. The frequency ratio for C-method provides a consistent estimator for P , P_{as} and P_{av} values: $v \rightarrow P_{as}$, when $n_1, n_2 \rightarrow \infty$. The disadvantage of C-method is that the learning data is used not so economically: being divided in two parts their size in practice became rather small to guarantee as the good adaptation (learning) of the discriminant function as the good misclassification probability estimation by the frequency ratio method. As result, the latter is subjected by serious statistical variations if the numbers n_1 and n_2 of learning vector sets are not sufficiently large.

c) The cross-validation (Jack-knife) method (CV-method). The most realistic estimate of P_{av} is provided by examination of the learning vector sets with the cross-validation procedure [18]. In our experiments, we used the described above linear discrimination function (LDF) and quadratic discrimination function (QDF). for making the classification decisions. It is, of course, possible to implement more sophisticated statistical discrimination rules or artificial neural network algorithms. In all cases the cross-validation algorithm became the same as described below.

At the every step of cross-validation procedure one of the learning vectors $x_l(j)$, $j=1, n_l$, $l=1, 2$ is eliminated from the learning vector set. The remaining vectors are used as the data for LDF or QDF adaptation (learning). The eliminated vector is then classified by thus learned LDF or QDF. If this vector is classified incorrectly, i.e. attributed to a class 2 instead 1 or vice versa, the appropriate count $m(1|2)$ or $m(2|1)$ is increased by one. The eliminated feature vector is then returned to the learning data set and the next vector $x_l(j)$ is extracted. This procedure is repeated with the all (n_l

$+n_2$) learning vectors. The values $v(1|2)=m(1|2)/n_2$, $v(2|1)=m(2|1)/n_1$, $v=(v(1|2)+v(2|1))/2$ are asymptotically unbiased and consistence estimates for P_{av12} , P_{av21} and P_{av} for a wide class of feature multidimensional distributions satisfying to some weak restrictions [18].

The LDF and/or QDF values for both classes produced by the cross-validation procedure can be ranked in magnitude. The two ranked LDF and/or QDF sequences allow to investigate the physical reasons for misclassifications due to outliers of the feature values.

1.3. Seismogram processing for event source identification: feature extraction, feature selection and misclassification probability estimation. (scheme of experimental study).

One of the goals of this study was a development of flexible automated interactive technique for processing of weak seismic event recordings provided by a local or regional seismic network with the purpose of source type identification. The prototype of such technique was tested using the SNDA System data handling and interactive graphic facilities and consisted of the next stages:

1) Mapping of relative location of event epicenter and network stations, visualization of event seismograms recorded by the stations; interactive measurement of distances from epicenter to stations and ordering the seismograms at the screen according to epicenter distances.

2) Selection of the best quality seismograms for the further identification processing. Two seismograms were selected from the total seismogram set for every event: one recorded by a "nearby" station and another by a "far" station. Thus, four sets seismograms were formed: "near earthquakes", "far earthquakes", "near explosions", "far explosions". The purpose of this selection was to investigate the influence of epicenter distance on identification of weak local events: from one hand the small epicenter distance guarantees the high signal to noise ratio, but from another hand at the small distances the wave field characteristics of different wave phases are not ascertained due to overlapping of phase waveforms.

3) Interactive setting at every selected seismogram time intervals for which the P and S phase waveforms have to be processed with the purpose of discrimination feature extracting.

4) Automatic measurement of discrimination spectral feature set from all earthquake and explosion seismograms.

5) Improving the quality of feature estimation in condition of poor signal-to-noise ratio by evaluation of the seismic noise power spectral density at interval preceding the event wavetrain.

6) 3-dimensional visualization of feature vector data with the purpose to study the scattering of the features for earthquake and explosions and their separating in distinct clusters. The visualization is performed for various triplets of the total feature set and allows to select those features which provides the best visual separation between sets of seismogram and explosion points in 3-dimensional subspaces of feature space and make a decision to apply some nonlinear transformations of the features with the purpose to decrease their scattering degree.

7) Feature transforming by some nonlinear function with the purpose to make their distribution more close to the Gaussian one.

8) Manual and automatic selecting of a feature subset from the initial feature set to provide the minimum of misclassification probability attainable in the given region (while using the statistical identification algorithms)

9) Estimation of error classification probabilities provided by different classifiers with the help of reclassification and cross-validation methods using learning earthquake and explosion observations.

10) Identification of "unknown" events from this region which have not been used for learning of classification algorithms (if they are available) with the purpose of revision of error classification probability estimate made by the cross validation method.

The stages 1-7 are really the preliminary seismogram processing providing the feature vector sets as proper input data for statistical (or other) classification algorithm. The stages 7 - 10 are the classification procedure itself with accompanying data manipulations. The preliminary processing steps (stages 1-7) are illustrated by Fig.1. The stages 1, 2 were performed with the help of special scripts (with names: "*selearthq.scr*" and "*selexpl.scr*") - the programs written in internal language of the SNDA System. The scripts are similar and differ only by the tables of event names; the code of the "*selexp.scr*" program is given in the Appendix 1 to this section.

The stages 3-6 were performed with the help of the SNDA scripts "*earthspmeas.scr*", "*explspmeas.scr*", "*fftearthmeas.scr*", "*fftexplmeas.scr*". The code of the 1-st script is given in the Appendix 2, the other scripts have the same structure and differ from 1-st only by the tables of event names and some processing routines. The measurements of spectral features of seismogram P and S phase waveforms were performed in this study by two competitive computational methods:

a) by filtering of P and S phases in the frequency bands: $D0=(1-15)Hz$, $D1=(1-3)Hz$, $D2=(3-6)Hz$, $D3=(6-10)Hz$, $D4=(10-15)Hz$ with the subsequent calculating of the following spectral ratios:

$$\begin{aligned} & avp(P, Di)/avp(P, D0); \quad avp(S, Di)/avp(S, D0); \quad i=1, \dots, 4; \\ & avp(S, Di)/avp(P, Di); \quad maxp(S, Di)/maxp(P, Di); \quad i=0, \dots, 4, \end{aligned}$$

where $av(\bullet, Di)$ and $max(\bullet, Di)$ denote the average power and peak power of the corresponding phase waveforms in the corresponding frequency bands. The 18 features are calculated by this method with the help of the scripts "*earthspmeas.scr*" and "*explspmeas.scr*"

b).by discrete Fast Fourier Transforming (FFT) of P and S phase waveform with the subsequent calculating of the following spectral ratios:

$$\begin{aligned} & avp(P, Di)/avp(P, D0); \quad avp(S, Di)/avp(S, D0); \quad i=1, \dots, 4; \\ & avp(S, Di)/avp(P, Di); \quad Maxsd(S, Di)/Maxsd(P, Di); \quad f_{max}(P, Di); \quad f_{max}(S, Di); \quad i=0, \dots, 4 \end{aligned}$$

where: $Maxsd(S, Di)/Maxsd(P, Di)$ denotes the ratios of power spectral density peak values for S and P phases in different frequency bands; $f_{max}(P, Di)$, $f_{max}(S, Di)$ denote frequencies inside the frequency bands Di for which the peak values of P and S phases power spectral densities are attained. The 23 spectral ratio features are calculated by this method with the help of scripts "*fftearthmeas.scr*" or "*fftexplmeas.scr*".

Note that the features calculated with the help of both methods are relative ones i.e. do not depend on event magnitudes or recording scale factors.

To make the feature measurement procedure more robust to the affecting of seismic noise, the values of average noise power were measured in the same frequency bands Di in a noise window preceding the P-wave onset. The noise power values are subtracted from the corresponding signal phase power values. This ensures more precise feature measurement of an event wavetrain even if the signal-to-noise ratio in the event recording is poor. Thus, two variants of feature sets are created: with

subtracting of noise power values ("pure" variant) and without this subtracting ("noise" variant).

As the result of accomplishing of the processing stages 1 - 5 the eight feature data sets are prepared for earthquakes and explosion seismograms according to variants: 1) "pure" ("p") or "noise" ("n") variants; 2) "Far" ("F") or "Near" ("N") events; 3) Type of feature extraction: filtration in the frequency bands ("p" or "b") or the fast Fourier transformation ("s") (see Fig.1 and Fig.2). As an example, the list of 18 feature labels obtained with the help of "filtration" method for "pure" variant and the list of 16 feature labels obtained with the help of "FFT" method for "pure" variant with are given in the Appendix 3 to this section.

To utilize the advantages of the both methods for feature extraction, two combined feature sets were prepared (for the "Pure" variant): 1) "b+s" set: three features ("Ipsmfp", "6ssmfp", "11rmspp") from "FFT" method were combined with 18 features of "filtration" method; 2) "s+b" set: five features ("9msprp0", "10msprp1", "11msprp2", "12msprp3", "13msprp4") from "filtration" method were combined with 16 features of "FFT" method.

The processing stages 6 - 10 corresponding to feature selecting, error probability estimating and event classification procedures with accompanying data manipulations are performed in the framework of special SNDA script "*selfeat.scr*" composed with the programs "*ld*", "*ldstst*", "*fsel*", "*reclld*", "*examld*", "*examqd*" (described in Section 6) and some SNDA stack commands. The last provides feature nonlinear transformation: $y = \log(x)$ and Box-Kox' normalizing transformation: $z = \alpha(y^\alpha - 1)$ with the exponent power $\alpha=1/7$, visualization of three dimensional scattering diagrams of feature vectors with the help of SNDA Stack command "cluster" and the two dimensional scattering diagrams with the help of the standard UNIX routine "*plotxy*". The script code is given in the Appendix 4 to this section.

1.4. Results of experimental data processing and discussion

The statistical classification approach described in Section 2 was applied to discrimination of weak earthquakes and explosions in the region of Israel. The set of seismograms of weak events recorded by stations of the local Israel seismic network was used as learning data for classification. The set consisted of recordings of 28

earthquakes with magnitudes 1.1-2.6 and 25 chemical explosions with magnitudes 1.3-2.6; each event was recorded by several stations of the network. For every event two vertical seismograms were selected: one recorded by a nearby station (with distance less than 100 km) and another - by a rather far station (with distance mostly from 100 km to 200 km). The location of earthquake and explosion epicenters and disposition of stations which have recorded the selected seismograms are shown in Fig. 3. One can see from this figure, that all events analyzed: as earthquake, as explosions, occurred in the same rather small region with size 80×80 Km. The identical geological conditions in the both type source areas, of course, facilitate the source type identification because the differences in source excitation mechanisms are not masking in seismograms by the impact of different hypocentral zone geological conditions (as it is often happened in identification practice).

In Fig. 4. the sets of earthquake and explosion seismograms recorded at near and far distances are presented: onsets of P-waves are aligned, seismograms are ordered according to epicenter distances and scaled to the waveform maximum. Comparison of the event waveforms indicates that earthquake and explosion seismograms reveal some visual differences which are more explicitly manifested at far distance set. In Fig. 4c and 4d we see that the earthquakes S-waves are more powerful relatively to the P-waves in comparison with the explosions. This is evident for the majority of event wavetrains in spite of rather poor signal-to-noise ratio for some seismograms. Note that for the "near" distances (Fig.4a,b) this divergence of earthquake and explosion seismograms is not so explicit. The example depicted is encouraging one for employment of the conventional P-S spectral ratio discriminants in the problem of local earthquake and explosion discrimination.

The interactive automated procedure for discrimination feature extraction from seismogram was described in Section 3. It is illustrated by the flow-chart in Fig.1. The two different methods used for measuring of P and S phase spectral characteristics are illustrated by Fig.5. Fig.5a shows the seismograms of local earthquake with magnitude 1.5 and depth $10. \pm 1.1$ km registered at distances 48 and 143 km. Note that the recordings are made with the rather good signal to noise ratio and the explicit P and S+Lg phases are seen at the seismograms. (The second phase of local earthquake which really is a superposition of different S-type phases and Lg phase we will shortly name as S-phase).

Fig.5b illustrates the method of power feature extraction from the different frequency bands of P and S phase waveforms with the help of Fast Fourier Transform. The figure shows the FFT power spectra of preceding seismic noise, P and S waveforms. The spectra are calculated for the "far" earthquake seismogram in the time intervals (2-44), (47.5-56) and (65.3-73-.7) sec., correspondingly (these intervals are marked at Fig.5c by the vertical lines). The vertical lines at Fig.5b mark the margins of frequency bands used for evaluation of discriminant features, such as average and maximal values of P and S spectra estimated in every frequency band.

Fig.5c and Fig.5d illustrates the feature extracting with the help of band filtering. The traces 2-5 at Fig.5c are the output wavetrains of band-pass 5-th order Butterworth filters with frequency bands indicated at start of the traces. Fig.5d shows the S-phase current powers traces for frequency bands under consideration. The figure illustrates the procedure for evaluation of averaged and maximum values of the S-phase current power in different bands.

The eight sets of learning feature vectors were prepared for every class with the help of described automated feature extraction procedure (the earthquakes we denoted as 1 class, the explosions - as 2 class). The sets differ in the 3 parameters used in their notations (Fig. 2): parameter *p-n* means: noise compensation is implemented or not; parameter *N-F* means: "near" or "far" seismograms are used; parameter *b-s* means: the band filtering or the FFT method was employed for feature extraction. Comparison of classification results achieved by using of every set allows to refine the statistical source identification technique being developed. The essence of these results is reflected in the Tables 1- 4 (see end of this section). General conclusions implying from analysis of the experimental study results are discussed in the Section 5.

Let us consider in details the processing of "pFb" feature vector set by following the sequence of procedures composing the script "*selfeatrs.scr*" (described in Section 3). The notation "pFb" means that the "far" seismograms were used, noise compensation was implemented and band filtering was applied for feature extraction.

The "value traces" of "pFb" features after their nonlinear transformations by functions $y=\log(x)$ and $z=\alpha(y^\alpha - 1)$, $\alpha=1/7$, are shown in Fig.6. Along the horizontal X-axis the event numbers are indicated: the first 28 points correspond to earthquakes and the remaining 25 points - to explosions. Along the vertical axis of every trace the corresponding feature values are set in the integer X-points and linear interpolations

are made between integer points. The number and label of every trace is the same as for corresponding feature, the feature labels (which meanings are explained in the Appendix 2 of Section 3) are disposed at the left side of the plot. This graphical representation of feature vector sets allows to catch an impression about tendencies in feature behavior for different classes. For this example one can say, that features with numbers 9-18 differ appreciably in their means and dispersions corresponding to earthquake and explosion classes. This fact is encouraging for success of application to these features the statistical discrimination techniques.

Analysis of feature pair correlation coefficients made in the program *"ldstst"* (see description of this program in Section 5) shows that feature pairs: (*"9msprp0"*, *"12msprp3"*) and (*"11msprp2"*, *"13msprp4"*) are strongly correlated (their correlation coefficient exceeds 0.75). The program *"ldstst"* recommended to eliminate features *"9msprp0"* and *"11msprp2"* because their one dimensional distributions have less Mahalanobious distances between the classes in comparison with their counterparts in the above pairs.

The remaining 16 features were processed by the program *"fsel"* which accomplished automated selection of the most informative features providing the minimum of error classification probability (see Section 2 for theoretical explanations, Section 5 for description of the program). Fig.7 illustrates results of the program execution for the "pFb" feature vector set. It shows Mahalanobious distance $\rho^2(p)$ and classification error probability $Pr(p)$ in depend on the amount p of informative features selected at the first p steps. Minimum of $Pr(p)$ is reached on step 5. The sense of first 5 features selected by the program *"fsel"* from the total set of features composing the "pFb" learning vectors are given below (in the order of their discrimination rank):

- 1) *"18asprp4"* = $avp(S,D4)/avp(P,D4)$ - the ratio of S-phase and P-phase average powers in the highest frequency band (10-15) Hz;
- 2) *"7srbp3"* = $avp(S,D3)/avp(S,D0)$ - the fraction of S-phase averaged power belonging to the high frequency band (6-10)Hz;
- 3) *"10msprp1"* = $maxp(S,D1)/maxp(P,D1)$ - the ratio of S-phase and P-phase peak powers in the lowest frequency band (1-3)Hz;
- 4) *"17asprp3"* = $avp(S,D3)/avp(P,D3)$ - the ratio of S-phase and P-phase average powers in the high frequency band (6-10)Hz

5) "*5srbp1*" = $avp(S,D1)/avp(S,D0)$ - the fraction of S-phase averaged power belonging to the lowest frequency band (1-3)Hz;

The features with rank numbers 1 and 4 characterizes the excess of share wave high frequency energy for earthquakes in comparison with explosions. This is well explained by the shift mechanism of earthquake sources typical for shallow events [14-17, 6]. The selection of feature with rank number 3 can be explained in the same way - by excess of P-phase low frequency energy for explosions in comparison with earthquakes that is typical for explosion mechanism. The appearance of features with rank numbers 2 and 5 is also connected with more high frequency content of S-waves for explosions in comparison with earthquakes.

The SNDA graphic program "Cluster" allows to inspect the three dimensional scattering diagrams of selected features. Four such diagrams for different feature triplets composed from the selected features are shown in Fig.8. The triplets of features with rank numbers (1,3,4) and (1,2,3) (see the list above) provide the best visual separation of the earthquake and explosion clusters. The diagram for (1,3,4) triplet seems to be the most impressive and it is shown in Fig.9 in a large scale with indication of the earthquake and explosion numbers. The numbers are given in according of the event lists used in the study (see Appendix 2 to Section 3). Explosions with numbers 9 and 23 produced the features close to the earthquake cluster and earthquakes with numbers 24 and 26 - to the explosion cluster. Thus scattering diagrams are an effective tool for revealing of features providing the best cluster separation and for detecting of outlying events: the earthquakes with characteristics similar those for explosions and vice versa.

It becomes obvious from analysis of Fig.8 scattering diagrams that only 4 misclassifications from total 53 observations may occur if to cut the 3-dimensional space of features with rank numbers (1,2,3) or (1,3,4) by an appropriate plane. It is shown below that the linear discriminant function constructed on the basis of 5 optimal features gives the exactly 4 wrongly classified events with mentioned numbers. The Fig. scattering diagrams indicate also that earthquake feature points demonstrates more tight clustering then explosions ones. This well corresponds to the fact that the optimal features have a greater dispersion for the explosions than for earthquakes (it is seen, for example from Fig.).

The estimation of error probability was made in this study by the three methods theoretically grounded in Section 2:

- 1) Reclassification by the linear discriminator (program *"recalled"*);
- 2) Examination (cross-validation) by the linear discriminator (program *"exhaled"*);
- 3) Examination (cross-validation) by the quadratic discriminator (program *"examqd"*).

We will discuss the results for all these cases.

1) The linear discrimination function (LDF) values calculated by the program *"reclld"* for the earthquake and explosion learning vector sets using the 5 optimal features are depicted in Fig.10. To make the decisions an LDF value is to be compared with zero threshold:

if $LDF > 0$, then the vector examined belongs to an explosion;

If $LDF < 0$, then the vector examined belongs to an earthquake.

One can see in Fig.10 that one earthquake and two explosions were wrongly classified by the reclassification procedure, however one of correctly classified earthquakes produces the LDF value which is very close to the zero threshold (one may say that it lies in the "uncertainty" zone).

2) The LDF values calculated by the program *"examld"* for the same as in the previous case 5 optimal features and earthquake and explosion learning sets are depicted in Fig.11. Two earthquakes and two explosions were wrongly classified by this procedure. Emerging of four mistakes in the result of cross-validation procedure instead of three mistakes for reclassification procedure is natural: it is theoretically known that the reclassification method provides as a rule more optimistic error probability estimates as compared with cross-validation method.

3) The values of quadratic discrimination function (QDF) calculated by the program *"examqd"* for the same as in the previous cases 5 features and earthquake and explosion learning sets are depicted in Fig.12. Only two explosions from total 53 events were wrongly classified by quadratic discriminator in the result of cross-validation procedure instead of four mistakes made by the LDF. Thus the total error probability estimate is equal in this case to 3.8%. Note, that the QDF provides also the rather wide "robust classification zone" which size is approximately equal to 20% of the amplitude between minimum and maximum QDF cross-validation values. Any shift of classification threshold inside this zone keeps the error probability constant

(equal to 3.8%). This allows to hope that moderate changes in computational procedures for extracting of features from seismograms should not lead to increasing of the discrimination error probability. It is interesting also, that the explosion QDF values compose the three explicit clusters, though for the earthquake QDF values exists only single cluster. This can be interpreted as testimony that different types of explosion sources have existed and in contrast, that the earthquake sources in the region have rather similar characteristics.

The numbers of wrongly classified explosions are 9 and 23 (in accordance with the event list used). These are the same numbers as for the outlier explosion points in Fig.9 scattering diagram. The same numbers also have the explosions wrongly classified by the LDF (see Fig.10 and Fig.11 plots). The original and band filtered seismograms of these explosions are shown in Fig.13 and Fig.14. The misclassification of explosion with number 9 can be apparently explained by the insufficient duration of time interval at which the explosion wavetrain was registered: the S-phase waveform was cut off before the phase power begins to decrease. This could result in overestimating the average S-phase power in all frequency bands. As result, the event feature vector have got into the earthquake cluster.

The misclassification of explosion with number 23 is almost evidently connected with its poor signal to noise ratio. The incorrect attempt to "improve" the seismogram was made at the stage of preliminary data processing: the clipping of noise amplitude spikes was accomplished with the help of SNDA interactive tool (it is seen in Fig.14 first seismogram). This could lead to incorrect noise compensation (this procedure was implemented while creating "pFb" feature vectors).

The reclassification and cross-validation procedures for Linear Discriminator and cross-validation procedure for Quadratic Discriminator were accomplished also using the best three features ("*18asprp4*", "*10msprp1*", "*17asprp3*") manually selected with the help of scattering diagrams. The classification quality for these best three features turned out to be the same as for the five optimal features automatically selected by the program "*fsel*": the same misclassification probabilities and the same numbers of wrongly classified events were achieved. Even the relative widths of "robust zones" between the clusters of points belonging to different classes are roughly the same for the both cases. This is convincing argument in favor of automated feature selection facility provided by the program "*fsel*".

It is quite interesting to compare the results discussed above with ones produced by the same processing applied to the seismograms recorded by the "near" station (with epicenter distances less than 100 Km). The preprocessing of these seismograms generated the feature vector sets which we denoted as "pNb" data. The processing of this data by the feature selection - error probability estimation procedures gave the following. Five features ("4prbp4", "10msprp1", "11msprp2", "14asprp0", "15asprp1") were eliminated due to strong pair correlation (exceeding 0.75). The feature vectors composed by remaining 13 features were used as the input data for the program "fsel". The course of automated feature selecting is illustrated by the plots in Fig.15. The six optimal features were chosen:

- 1) $18asprp4 = avp(S,D4)/avp(P,D4)$ - the ratio of *S*-phase and *P*-phase average powers in the highest frequency band (10-15) Hz;
- 2) $5srbp1 = avp(S,D1)/avp(S,D0)$ - the fraction of *S*-phase averaged power belonging to the lowest frequency band (1-3)Hz;
- 3) $13msprp4 = maxp(S,D4)/maxp(P,D4)$ - the ratio of *S*-phase and *P*-phase peak powers in the highest frequency band (10-15)Hz;
- 4) $1prbp1 = avp(P,D1)/avp(P,D0)$ - the fraction of *P*-phase averaged power belonging to the lowest frequency band (1-3)Hz;
- 5) $8srbp4 = avp(S,D4)/avp(S,D0)$ - the fraction of *S*-phase averaged power belonging to the highest frequency band (10-15)Hz;
- 6) $9msprp0 = maxp(S,D0)/maxp(P,D0)$ - the ratio of *S*-phase and *P*-phase phase peak powers in the highest frequency band (10-15)Hz

Note, that this feature set is different from the optimal feature set for the case of "far" station seismograms. However the two features: "18asprp4" and "5srbp1" are selected by the "fsel" program in the both cases, moreover the feature "18asprp4" has the highest rank in the both cases and being used alone for discrimination provides the (theoretically estimated) error probability equal about 20%. Although (judging to our experiments) the station epicenter distances impact on the contents of optimal feature sets, the physical sense of all selected features remains the same: they reflect the relative *S* and *P* phase powers in the highest and lowest parts of frequency range being analyzed.

Three dimensional scattering diagrams for different feature triplets taken from the optimal feature set are shown in Fig.16. The clustering of the earthquake and

explosion points in the "Near" station case is slightly worse than for the "Far" case. The feature triplet with the rank numbers (1, 2, 3) and labels ("*18asprp4*", "*5srbp1*", "*13msprp4*") seems to be the most instructive one. Note that again the triplet recommended by the program "*fsel*" as providing the steepest slope of error probability curve, is proved to be the most attractive from the point of view of clustering capability. The different projections of these three dimensional feature clusters are shown in Fig.17 (plot pairs (a)-(b) and (c)-(d) are the projections from the opposite directions but have the same rotation angles). This figure was depicted to convince a critical reader that the rather good separation of earthquake and explosion clusters is not illusion due to specially chosen displaying projection. Analysis of Fig.17 ensures us that no more than five classification mistakes from total 53 events can be get if to cut this triplet three-dimensional space by a proper separating plane.

The error probability estimation accomplished on the basis "pNb" data with the help of programs "*reclld*", "*examld*", "*examqd*" gave the results presented in Fig.18-20. Comparison of these results with analogous ones for "pFb" data (Fig.10-12) shows that the discrimination capability of Quadratic Discriminator in the case of "pNb" data is slightly worse: four mistakes are got for cross-validation (7.6%) instead two ones (3.8%). However, for Linear Discriminator the results are quantitatively the same: four mistakes are got for cross-validation and three mistakes for reclassification in the both cases. Nevertheless, the "robust classification zones" between earthquake and explosion clusters for "pNb" data are narrower as compared with "pFb" data. These facts may be predicted from scrutinizing the seismograms registered by the "Far" and "Near" stations (Fig.4).

The interesting result here is that the all earthquakes are classified correctly and the list of numbers of four wrongly classified explosions (2, 3, 25, 8 - for QDF and 2,8,25,14 - for LDF) does not include the numbers (9, 23) of misclassified explosions for the "Far" case. This confirms the conclusion made above that the wrong classifications of (9, 23) explosions are related with the shortages in event wavetrain registering. The "Near" station seismograms of wrongly classified explosions (2, 8, 25) are plotted in Fig.21. One can see from this figures that explosions 8 and 25 are registered at the very small distances: 24 and 28 km correspondingly, and for this reason the P and S phases are overlapping in the seismograms. This can result in S/P spectral ratios which are not typical for the

explosions. The explosion (2) was registered at the distance 89 Km and has the distinct P and S-phase waveforms. However one can see in the seismogram that the S-phase waveform contains an intensive high frequency pulse (having, probably, a technogeneous origin). This pulse undoubtedly brought additional high frequency energy in the average S-wave spectrum, that leads to wrong discrimination feature values for this event.

The next part of the Section is devoted to analysis of robustness of the feature selection and error probability estimation techniques proposed. Deviations of classification results are studied in response of changes of structure or parameters of the processing algorithms.

The change a value of the parameter α in the Box-Kox normalizing transformation: $z = \alpha(y^\alpha - 1)$, from $1/7$ to $1/5$ leads (for the case of "pFb" feature vectors) to deterioration of the classification quality. Execution of the program "*recld*", "*examld*" and "*examqd*" with "pFb" data subjected to transformation $z = (1/5)(y^{1/5} - 1)$ gives the results shown in Fig.22-24. Comparison these figures with Fig.10-12 reveals, that the program "*examqd*" gave three mistakes instead two mistakes (the event with number 11 was additionally wrongly classified), the programs "*examld*" and "*recld*" gave the same mistakes but the robustness of classification was significantly deteriorated: the "empty zones" between the LDF clusters corresponding to earthquakes and explosions, became nearer. Nevertheless, the numbers of wrongly classified events and events whose discrimination statistic values lie close to the threshold (in the "uncertainty zone") did not change.

The elimination of the Box-Kox transformation leads to increasing of the error classification probability up to 7.5% (see Table 1 and Table 3) and significantly worsen the classification robustness. Our experiments allow to assert that the theoretically well grounded Box-Kox normalizing transformation proved to be helpful for the refinement of statistical discrimination technique.

Effectiveness of noise compensation procedure being a part of automated feature measurement algorithm was tested by analysis of discrimination capability of the "nFb" feature vectors produced while the noise compensation was omitted. The best three optimal features selected by the program "*fsel*" using "nFb" data appeared to be same as for "pFb" data: "*18asprp4*", "*10msprp1*", "*17asprp3*". The QDF values for "nN3" vectors composed with these 3 features are depicted in Fig.25. Comparison

of this figure with analogous one for "pFb" data (Fig.12) shows that the classification capability of "nFb" data is slightly worse than in the "pFb" case (the program *"examqd"* gave three mistakes (5.7%) instead two ones (3.8%) in the "pFb" case). Nevertheless, the three "worst" explosions corresponding to three smallest QDF values had numbers 9,23,11 and are the same in both cases and. The remarkable fact is that the explosion with number 23 wrongly classified with "pFb" data, for "nFb" data gave the QDF value below the threshold, so was classified correctly. This confirms our hypothesis that it's previous misclassification was due to improper noise compensation caused by the incorrect "far" seismogram preprocessing.

The four "worst" earthquakes corresponding to the four largest QDF values had in "nFb" case numbers 13, 24, 26, 2, while in "pFb" case the three "worst" ones had numbers 24, 26, 2. We get here the good coincidence and may suspect that earthquake with number 13 was eliminated from the list of the "worst" earthquakes because the application of noise compensation procedure. The evident advantage of the noise compensation is enlarging of the "robust classification zone" which is manifested in the "pFb" case in comparison with "pNb" case.

As it mentioned above, the combined data types ("*b+s*" and "*s+b*") were also prepared. The results of experiments with "pF(*b+s*)" data are presented in Fig.26-28. The four features "*9msprp0*", "*11msprp2*", "*13msprp4*", "*14asprp0*" were eliminated because strong pair correlation, exceeding 0.75. The remaining 17 features were processed by the program *"fsel"* which selected the next nine optimal features:

- 1) *18asprp4* = $av(S,D4)/av(P,D4)$ - the ratio of average *S*-power to average *P*-power in the highest frequency band (10-15)Hz;
- 2) *7srbp3* = $av(S,D3)/av(S,D0)$ - the fraction of average *S*-power belonging to the high frequency band (6-10)Hz;
- 3) *10msprp1* = $max(S,D1)/max(P,D1)$ - the ratio of maximum *S*-power to maximum *P*-power in the lowest frequency band (1-3)Hz;
- 4) *17asprp3* = $av(S,D3)/av(P,D3)$ - the ratio of average *S*-power to average *P*-power in the high frequency band (6-10)Hz;
- 5) *19psmfp* = $fmax(P)$ - the frequency where maximum of *P*-spectrum is attained;
- 6) *5srbp1* = $av(S,D1)/av(S,D0)$ - the fraction of average *S*-power belonging to the lowest frequency band (1-3)Hz;
- 7) *21rmspp* = $Max(S)/Max(P)$ - the ratio of maximums of *P* and *S* spectra;

8) $1prbp1 = av(P,D1)/av(P,D0)$ - the fraction of average P -power belonging to the lowest frequency band (1-3)Hz;

9) $6ssmfp = fmax(S)$ - the frequency where maximum of P -spectrum is attained

Let us emphasize the the following:

1. The first four optimal features: "18asprp4", "7srbp3", "10msprp1", "17asprp3" selected from "pF(b+s)" feature set coincide with the "best" four features for "pFb" data;

2. The feature "5srbp1" was chosen on sixth step for "pF(b+s)" data and on fifth step for "pFb" data;

3. The features "19psmfp", "6ssmfp" specific and quite essential for the "s" selection method were included in the optimal feature subset of the "pF(b+s)" data.

The comparison of results of cross validation procedure applied to 9 optimal features of "pF(b+s)" data (Fig.28) with analogous results for 5 optimal features of "pFb" data (Fig.12) shows that classification quality is same for the both data types: two mistakes (3.8%) was got with the same numbers (9,23) of wrongly classified events

The total information about classification quality achieved using different variants of learning data set with application of the feature logarithmic transformation: $y=\ln(x)$, and additional Box-Kox's transformation $z=(1/7)(y^{1/7} - 1)$, is accumulated in Tables 1-4. The analysis these tables allows to make the next conclusions:

1. Data from "far" stations provide as a rule a smaller error probability as compared with data from "near" stations.

2. Employment of the Box-Kox normalizing transformation tangibly decreases the identification error probability if decision is made using statistical identification rules.

2. "Pure" data got after the noise compensation procedure demonstrate usually smaller error probability as compared with "noise" data do not subjected to this procedure.

3. Band filtering method for measurement of phase averaged and maximal powers in different frequency bands turn out to be more effective in sense of error probability than Fast Fourier Transform method. This is experimental fact and we fail

to explain it at the moment. Possibly there is needed some refinement of the FFT method.

4. The "b+s" learning vectors composed from the features measured by the band filtering method with addition of several specific features provided by the FFT method (see Section 3) gave in our experiments the same discrimination mistakes as the "b"-type learning vectors. Nevertheless we hope that this augmented assortment of the discrimination features will be the most effective in further experiments.

Table 1

**Error probabilities cross-validations estimates (%)
for Linear Discriminator with feature transformation
by function $y = \log(x)$**

Features	Unselected	Selected	Unselected	Selected
Type of data	pFb16	pFb8	pFs15	pFs6
Error probab. %	11.5	7.5	7.5	7.5
Type of data	nFb12	nFb8	nFs14	nFs5
Error probab. %	11.0	11.0	9.4	9.4
Type of data	pNb11	pNb3	pNs13	pNs4
Error probab. %	13.5	11.0	11.3	9.4
Type of data	nNb12	nNb6	nNs12	nNs5
Error probab. %	9.4	9.4	9.4	7.5

Table2

**Numbers of events incorrectly classified
by Linear Discriminator with transformation
of features by function $y = \log(x)$**

Features	Unselected	Selected	Unselected	Selected
Type of data	pFb16	pFb8	pFs15	pFs6
Earthquakes	4, 14, 15	4, 15	5, 24	15, 21, 24
Explosions	9, 11, 15	9, 11	9, 15	9
Type of data	nFb12	nFb8	nFs14	nFs5
Earthquakes	4, 14, 15, 21, 24	4, 14, 15, 24	14, 15, 21, 24	14, 15, 21, 24
Explosions	9	6, 9	9	9
Type of data	pNb11	pNb3	pNs13	pNs4
Earthquakes	20, 25	20, 25	20, 22, 25	20, 22, 25
Explosions	2, 3, 6, 8, 14, 20	2, 3, 14, 20	2, 20, 25	2, 20
Type of data	nNb12	nNb6	nNs12	nNs5
Earthquakes	20, 25	20, 25	20, 25	20, 22, 25
Explosions	2, 14, 20	2, 14, 20	2, 20	2, 14

Table 3

Error probability cross validation estimates (%) for Linear and Quadratic discriminators with features transformation by functions
 $y = \log(x)$, $z = 7(y^{1/7}-1)$

Features	Unselected		Selected		Unselected		Selected	
Type of data	pFb16		pFb5		pFs15		pFs7	
Discriminator	LD	QD	LD	QD	LD	QD	LD	QD
Error probab. %	13.8	9.6	7.5	3.8	20.7	5.8	11.3	5.8
Type of data	nFb14		nFb3		nFs		nFs	
Discriminator	LD	QD	LD	QD	LD	QD	LD	QD
Error probab. %	9.4	7.5	7.5	5.5				
Type of data	pNb13		pNb6		pNs15		pNs8	
Discriminator	LD	QD	LD	QD	LD	QD	LD	QD
Error probab. %	9.4	7.5	7.5	7.5	11.3	9.4	7.5	9.4
Type of data	nNb		nNb		nNs		nNs	
Discriminator	LD	QD	LD	QD	LD	QD	LD	QD
Error probab. %								
Type of data	pF(b+s)18		pF(b+s)9		pF(s+b)18		pF(s+b)9	
Discriminator	LD	QD	LD	QD	LD	QD	LD	QD
Error probab. %	13.2	5.7	9.4	3.8	17.0	7.5	5.7	9.4

Table 4

Numbers of events incorrectly classified by Linear and Quadratic Discriminators with transformation of features by functions $y = \log(x)$; $z = 7(y^{1/7}-1)$

Features	Unselected		Selected		Unselected		Selected	
Type of data	pFb16		pFb5		pFs15		pFs7	
Discriminator	LD	QD	LD	QD	LD	QD	LD	QD
Earthquakes	24	2,9	24,26	----	24,13	13		
Explosions	15,14,6 23,25,9	9,23, 11	9,23	9,23	15,14,9, 25,23,28 13,20	9,11		
Type of data	nFb14		nFb11		nFs		nFs	
Discriminator	LD	QD	LD	QD	LD	QD	LD	QD
Earthquakes	24,13	2,13	24,13	13,24				
Explosions	3,9,23	23,9	3,9	9				
Type of data	pNb13		pNb6		pNs15		pNs8	
Discriminator	LD	QD	LD	QD	LD	QD	LD	QD
Earthquakes	-----	6,8	-----	-----	14	20,25,22	----	22,20,25,3
Explosions	2,8,25 20,14	25,2	2,8,25 14	2,3,25 8	20,2,8 14,25	2,25	14,8 2,25	2
Type of data	nNb		nNb		nNs		nNs	
Discriminator	LD	QD	LD	QD	LD	QD	LD	QD
Earthquakes								
Explosions								
Type of data	pF(b+s)18		pF(b+s)9		pF(s+b)18		pF(s+b)9	
Discriminator	LD	QD	LD	QD	LD	QD	LD	QD
Earthquakes	-----	2,9	24	-----	24	2,13	24	13,2,24
Explosions	15,14, 2325,9,	9	9,14, 23,20	9,23	14,15,25 9,23,18	9,11	9,23	18,9

1.5. Conclusions and recommendations

1. The flexible automated technique for seismograms processing aimed to discriminating small earthquakes and explosions was developed. The technique was designed in the framework of the Seismic Network Data Analysis System (SNDA) - a problem-oriented programming shell developed at SYNAPSE Science Center /Moscow IRIS Data Analysis Center. The program package for statistical discrimination with selection of the most informative features and estimation of the error probability was built in the SNDA. This technique is intended to be a component of automated data analysis system for CTBT monitoring.

The preliminary testing of the technique was made using teleseismic P-wave + P-coda recordings of 32 nuclear explosions at Semipalatinsk test site and 35 earthquakes occurred in Eastern Kazakhstan were analyzed. The data were the same as used in [6]. The results of this testing experiment were described in [20]. A thorough investigation of discrimination capabilities of the statistical technique was undertaken on the basis of local event seismograms from 28 small earthquakes and 25 industrial chemical explosions registered by Israel's local seismic network. Spectral characteristics of the data are described in [19].

2. Proposed technique for seismogram discrimination is founded on the statistical approach and provides measurement of various spectral features of seismogram wave phases, selection of a set of those features which are optimal for earthquake-explosion discrimination in given region and making the decision about the tested event seismogram to attribute it to an explosion or earthquake. Our experiments showed that the conventional P-S spectral ratio discriminants were in every case included in the optimal feature set by the automated feature selection procedure along with other (regionally dependent) features.

3. The powerful graphic tool was designed in the SNDA System for 3-dimensional visualization of clustering of feature vectors corresponding to earthquakes and explosions. Interactive manual selection with the help of this tool of the optimal feature triplets demonstrating the most distinct clustering confirmed the results of automated feature selection. We hope that the serious problem of "transportation" of discriminants efficient in one region to be used in another region can be facilitated by the automated and interactive feature selection procedures proposed.

4. The important component of proposed technique is the precise estimation of discrimination error probabilities. By comparison of different estimation methods it was proved that the cross-validation procedures have to be used as the consistent estimator of misclassification probability intrinsic to a given region. It is especially helpful if numbers of learning earthquake and explosion observations are not so large.

5. Transformations of feature by the nonlinear functions such as $\log(x)$ and Box-Kox's normalizing function: $z = \alpha(y^\alpha - 1)$, considerably decrease the discrimination error probability while the conventional statistic linear and quadratic discriminators (optimal for Gaussian feature distributions) are used for decision making.

6. Implementation of the noise suppression procedure provides as a rule an increasing of discrimination quality and allow to involve into discrimination processing seismograms with small signal to noise ratio.

7. The proposed technique for seismogram discrimination was thoroughly tested by applying to discrimination between earthquakes and chemical explosions recorded by Israel local seismic network. The pre-selection of event seismograms registered by the network, implementation of noise refinement and feature selection procedures, feature nonlinear transformation and employment of statistic quadratic discriminator allowed to get for this data the average misclassification probability (estimated with the help of cross-validation procedure) equal 3.8% (only 2 events (explosions) were misclassified from 53 events). The classification mistakes can apparently be explained by the insufficient quality of seismogram recording and small signal-to-noise ratio.

8. Capability of local event source discrimination tends to be improved with increasing of a distance of a recording station from an event source. In our experiments the misclassification probability of events recorded at distances of about 60 km is equal to 7.8% while for the same events recorded at distances of about 140 km, - to 3.8%. Besides, the robust classification zone for seismograms recorded at "far" distances" is wider as compared with "near" station seismograms.

9. Possible improvements of the discrimination technique can be made in the following directions:

Extension of the set of relevant features automatically measured from seismograms (by including, for example, the features characterizing various functional distances between estimates of power spectra for different phases.

Development of an advanced feature selection procedure. This can be made by following ways:

a) by using some error probability theoretic formulae for nonlinear classification rules; such formulae are derived, for example, for quadratic discriminator [22,23] and it is natural to employ them at the stage of feature selection if the final decision making is to be done by the quadratic discriminator.

b) by employment of more sophisticated (but more computer resource consuming) recurrent procedures for selection of a feature set providing a global minimum of discrimination probability. For example, the exhaustive search could be employed at the initial steps of recurrent procedure when the number of features being selected is not so great.

c) by adoption of cross-validation error probability estimate for using at every step of recurrent feature selecting procedure instead of any theoretical formula. Such complex procedure is the most robust and flexible to changes of classification rules and can be used for optimization of the total discrimination scheme.

Implementation of more sophisticated classification rules (providing separation of feature space by more complex functions than hypo-plane and hypo-sphere as it was used in our experiments). Such a rule can be designed on the basis of learned neural network, but application of this technique for estimating of misclassification probably by cross validation method or for feature selection is extremely time consuming.

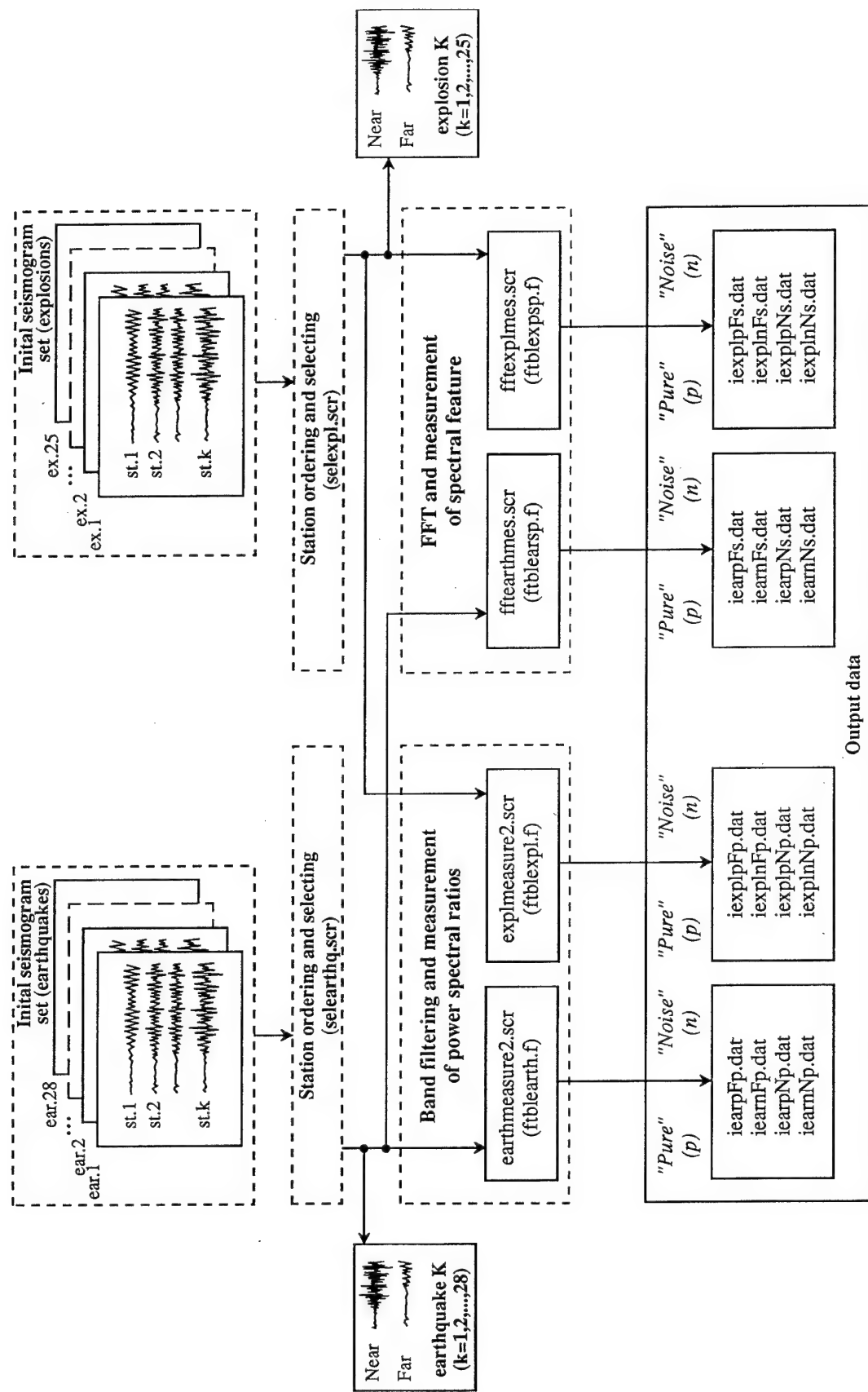


Fig. 1. Data preparing for classification.

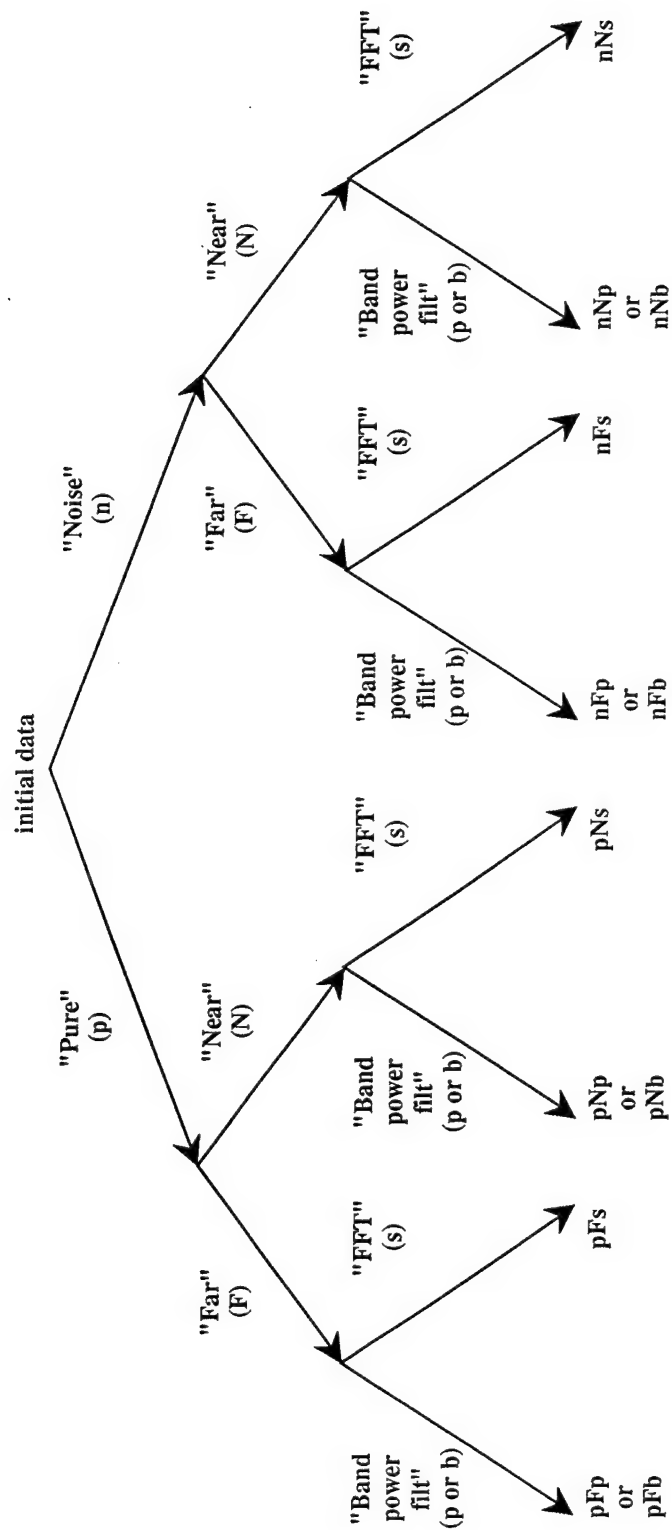
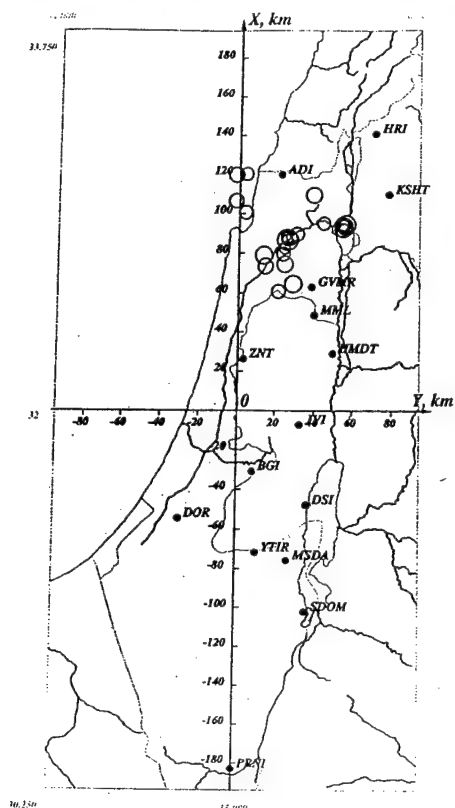


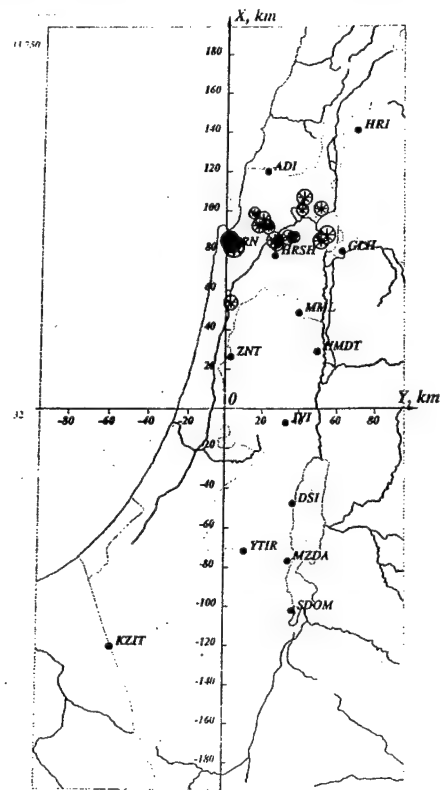
Fig. 2. Graph of data types.

Israel seismic local network
Map of earthquakes and stations registered them



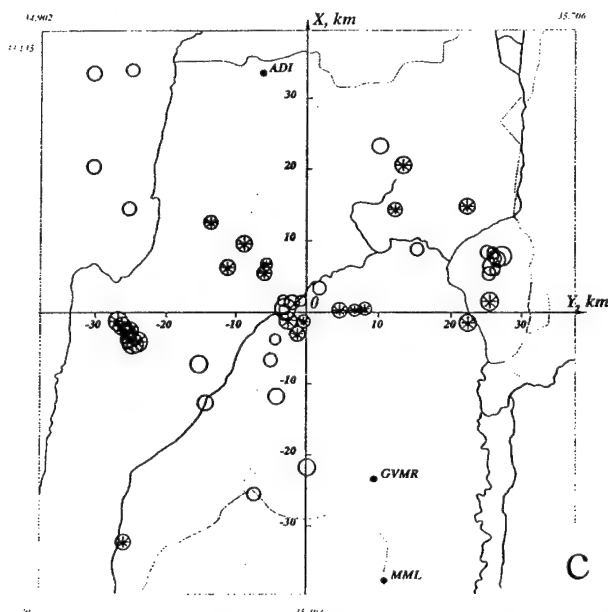
a

Israel seismic local network
Map of explosions and stations registered them



b

Map of earthquakes and explosions locations



c

EARTHQUAKES

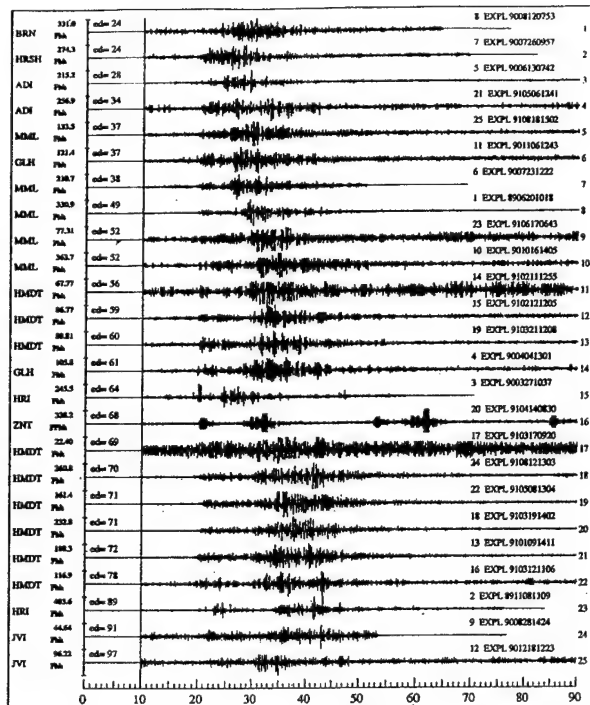
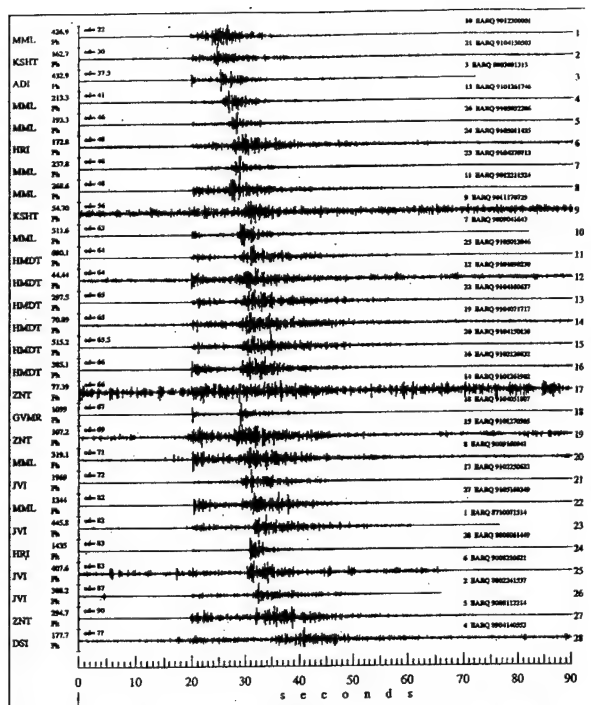
N	MAGN	HIPO. DEPTH km
1	1.9 ± 0.2	12.0 ± 1.1
2	1.5 ± 0.1	10.0 ± 1.2
3	1.1 ± 0.2	12.0 ± 1.5
4	2.1 ± 0.2	12.0 ± 0.9
5	1.7 ± 0.2	21.0 ± 1.4
6	1.8 ± 0.2	11.0 ± 1.0
7	1.8 ± 0.1	16.0 ± 2.3
8	1.5 ± 0.1	12.0 ± 2.0
9	1.6 ± 0.1	12.0 ± 0.9
10	1.2 ± 0.0	17.0 ± 2.9
11	1.5 ± 0.0	10.0 ± 1.1
12	1.5 ± 0.2	23.0 ± 3.0
13	1.1 ± 0.0	20.0 ± 1.6
14	2.6 ± 0.0	1.0 ± 3.1
15	1.1 ± 0.0	3.0 ± 5.9
16	1.5 ± 0.2	4.0 ± 5.4
17	1.4 ± 0.1	8.0 ± 1.5
18	2.0 ± 0.1	21.0 ± 1.2
19	1.4 ± 0.1	17.0 ± 3.6
20	1.3 ± 0.0	0.0 ± 1.5
21	2.4 ± 0.1	14.0 ± 4.2
22	1.5 ± 0.2	0.0 ± 2.3
23	1.9 ± 0.2	6.0 ± 1.4
24	1.3 ± 0.0	0.0 ± 3.9
25	1.2 ± 0.2	0.0 ± 1.7
26	2.2 ± 0.2	6.0 ± 1.3
27	1.0 ± 0.2	6.0 ± 5.6
28	1.7 ± 0.2	10.0 ± 1.3

EXPLOSIONS

MAGN	HIPO DEPTH km
2.6 ± 0.1	3.0 ± 10.5
2.6 ± 0.1	3.0 ± 10.5
1.3 ± 0.0	0.0 ± 3.2
2.4 ± 0.2	0.0 ± 1.4
1.7 ± 0.1	7.0 ± 3.5
1.4 ± 0.1	0.0 ± 1.6
1.5 ± 0.0	0.0 ± 4.9
1.9 ± 0.0	0.0 ± 5.1
1.7 ± 0.1	0.0 ± 1.3
2.2 ± 0.1	0.0 ± 2.6
2.1 ± 0.1	0.0 ± 0.9
2.2 ± 0.1	3.0 ± 30.0
2.2 ± 0.2	0.0 ± 3.2
2.0 ± 0.0	0.0 ± 1.5
2.0 ± 0.0	0.0 ± 3.0
2.0 ± 0.0	0.0 ± 3.0
1.3 ± 0.0	0.0 ± 4.5
1.3 ± 0.0	0.0 ± 2.2
1.8 ± 0.0	0.0 ± 1.3
1.8 ± 0.0	2.0 ± 5.3
1.8 ± 0.0	0.0 ± 3.0
1.8 ± 0.0	4.0 ± 1.4
1.6 ± 0.2	0.0 ± 2.6
2.6 ± 0.1	0.0 ± 3.9
1.8 ± 0.0	0.0 ± 5.9

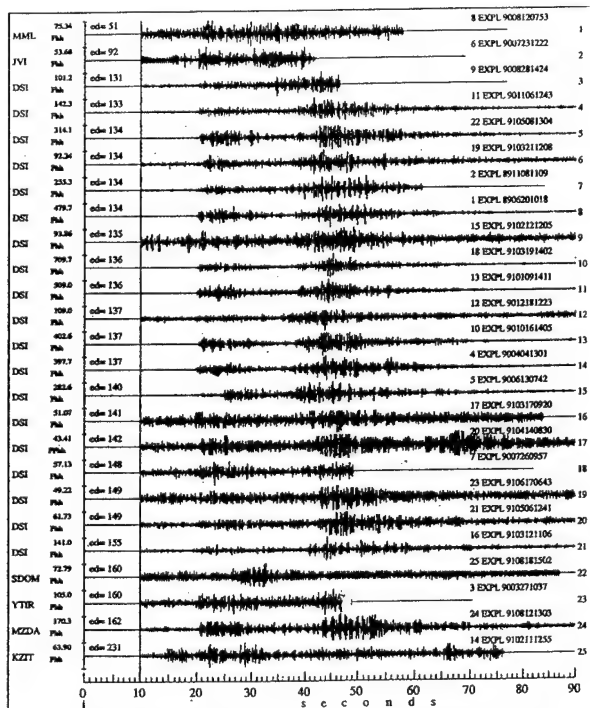
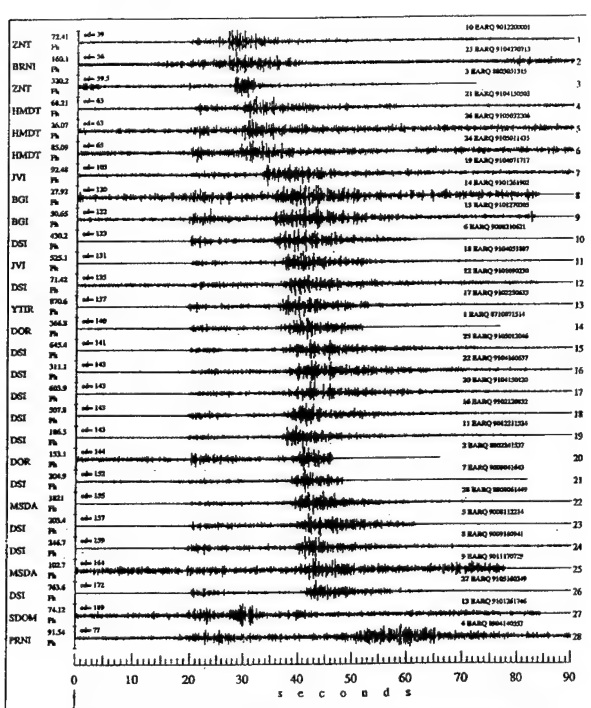
d

Fig. 3. Location of Israel local network stations and seismic events used in source discrimination study.
a,b. Location of stations recorded earthquakes and explosions. c. Location of earthquake and explosion sources. d. Magnitudes and focal depths of events.



Base time: 20.12.90 00.01.55.874
Seconds from start: 0.000
ISRAEL LOCAL NETWORK EARTHQUAKES
USED FOR SOURCE DISCRIMINATION
NEAR STATIONS: DIST = 20 - 100 km.

Base time: 18.08.91 15.02.00.990
Seconds from start: 0.000
ISRAEL LOCAL NETWORK EXPLOSIONS
USED FOR SOURCE DISCRIMINATION
NEAR STATIONS: DIST 24 - 100 KM.



Base time: 20.12.90 00.01.55.874
Seconds from start: 0.000
ISRAEL LOCAL NETWORK EARTHQUAKES
USED FOR SOURCE DISCRIMINATION
FAR STATIONS: DIST = 40 - 200 km.

Base time: 18.08.91 15.02.00.990
Seconds from start: 0.000
ISRAEL LOCAL NETWORK EXPLOSIONS
USED FOR SOURCE DISCRIMINATION
FAR STATIONS: DIST 50 - 230 KM.

Fig. 4. Set of event seismograms used in discrimination study.
a,b Earthquake and explosion seismograms at near distances: 20-100km.
c,d Earthquake and explosion seismograms at far distances: 70-200km.
Two seismograms from stations at different distances were used for every event.

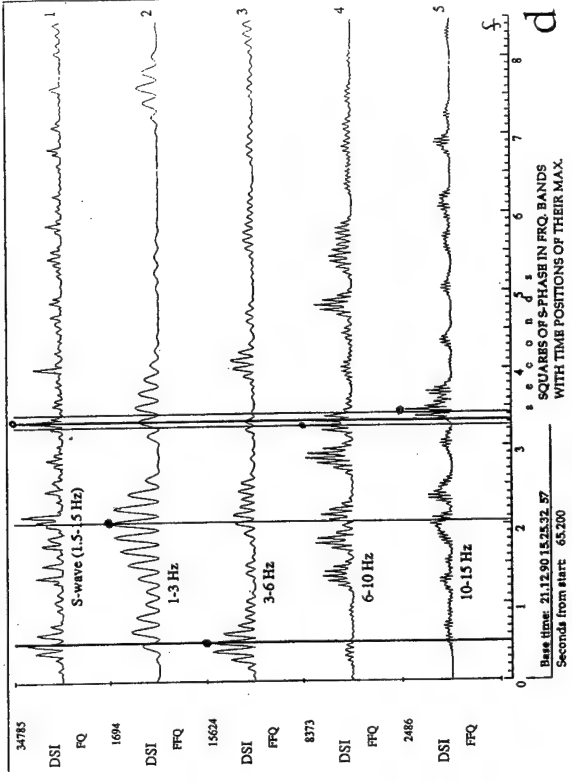
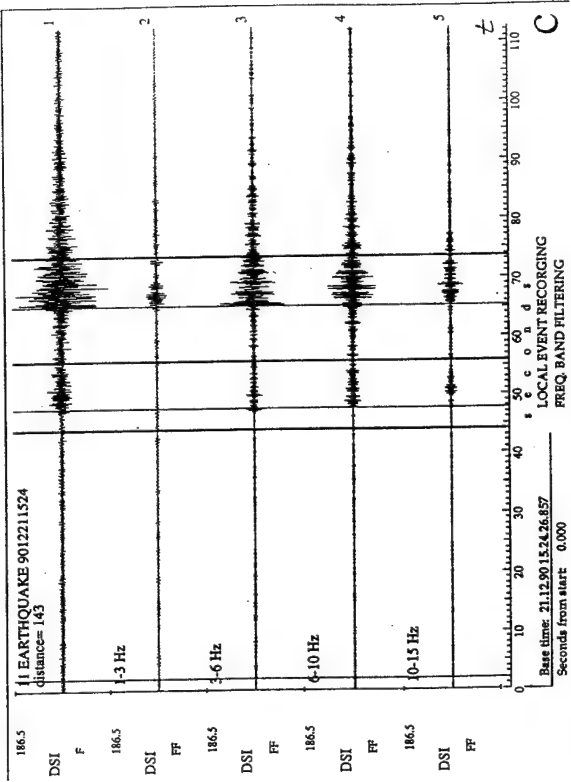
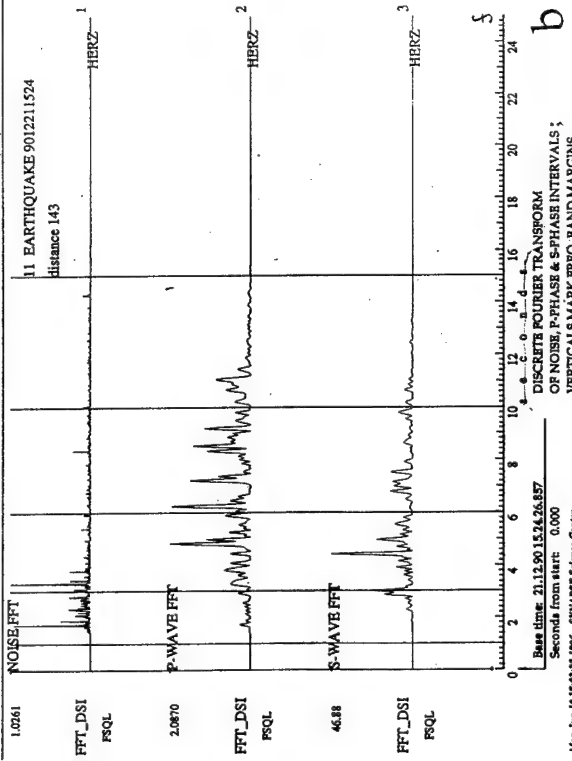
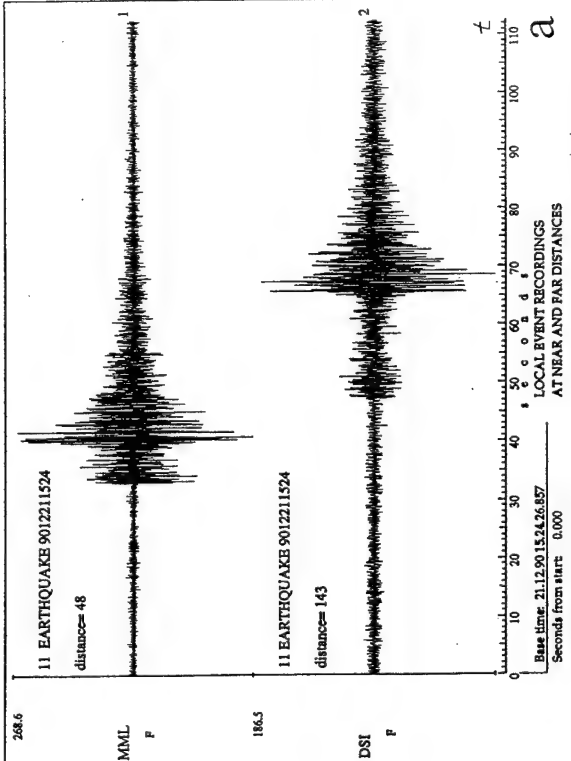


Fig. 5. Automated extraction of features for source discrimination from an event seismogram.

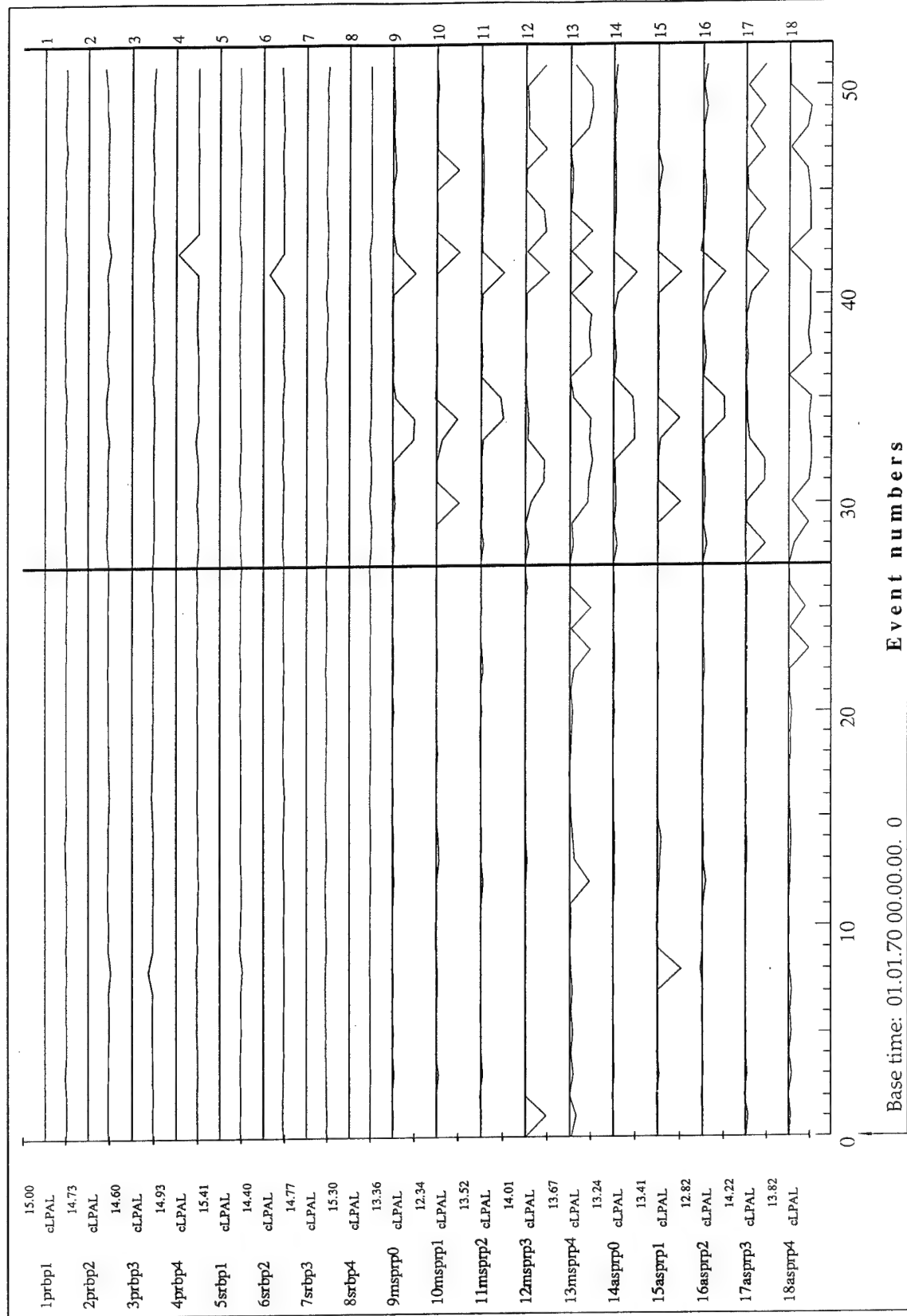
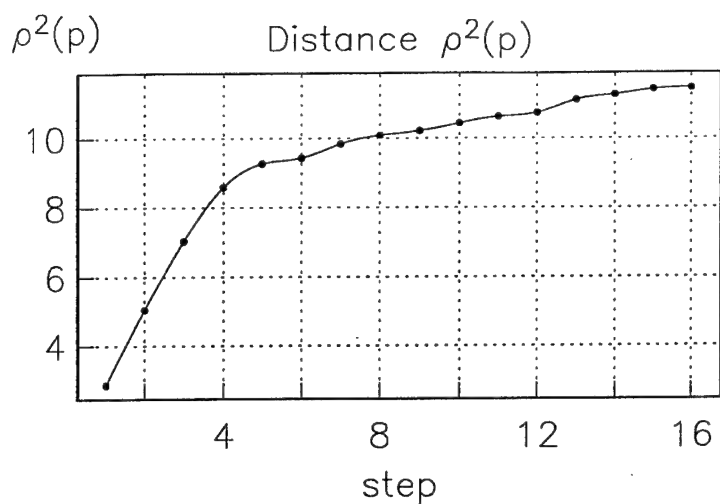
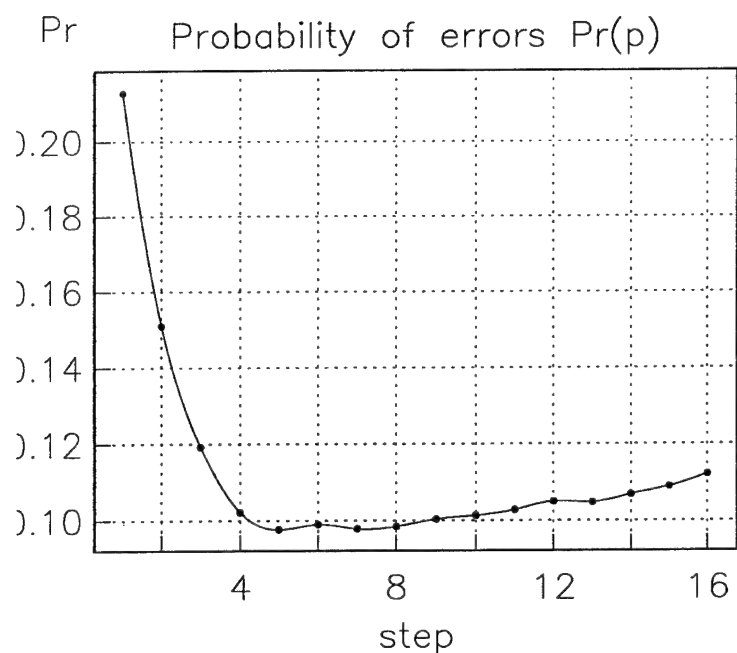


Fig. 6. "Value traces" of pFb features



Selected features:

St.: 1	18asprp4
St.: 2	7srbp3
St.: 3	10msprp1
St.: 4	17asprp3
St.: 5	5srbp1
St.: 6	14asprp0
St.: 7	6srbp2
St.: 8	8srbp4
St.: 9	16asprp2
St.:10	2prbp2
St.:11	3prbp3
St.:12	15asprp1
St.:13	4prbp4
St.:14	13msprp4
St.:15	1prbp1
St.:16	12msprp3



Min of Pr is riched on step 5

Fig. 7. Results of execution of the program "fsl" for the "pFb" feature vector set.

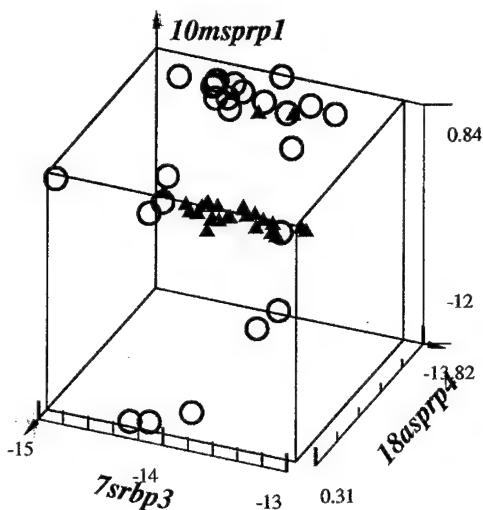


Fig. 8a Scatplt for: 18, 7, 10.

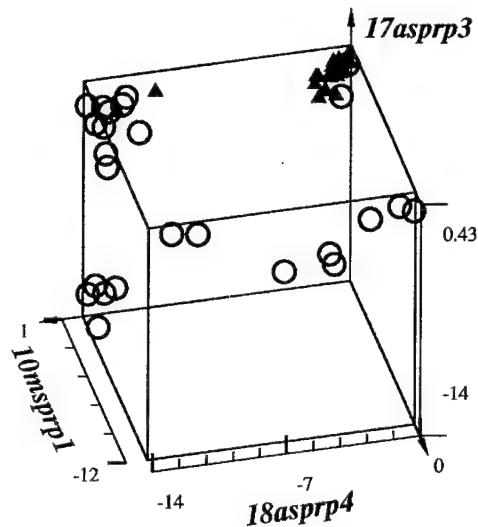


Fig. 8b. Scatplt for: 18, 10, 17

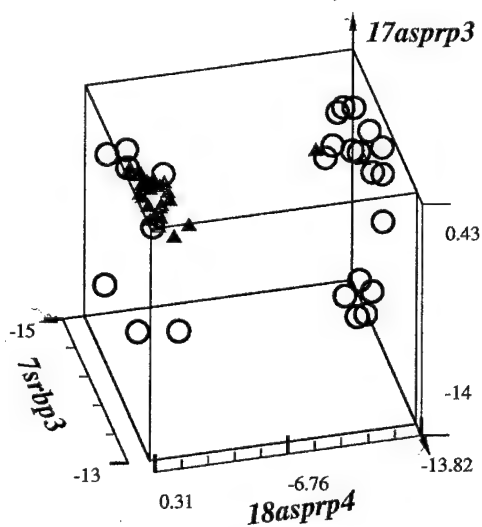


Fig. 8c. Scatplt for: 18, 7, 17

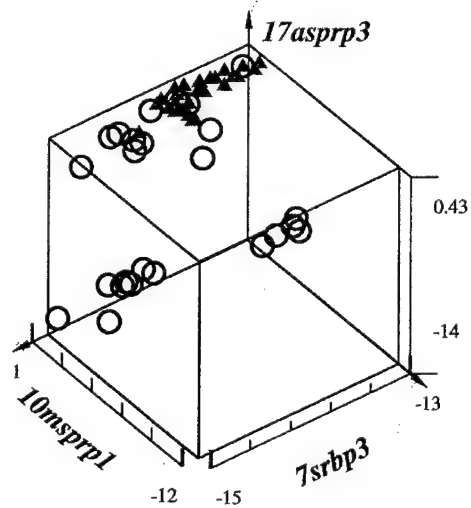


Fig. 8d. Scatplt for: 7, 10, 17

- ▲ Class 1 Red triangles: Israel local earthquakes
- Class 2 Blue circles: Israel local explosions

Fig. 8. Four diagrams for different feature triplets composed from the selected optimal features

- ▲ Class 1 Red triangles: Israel local earthquakes
- Class 2 Blue circles: Israel local explosions

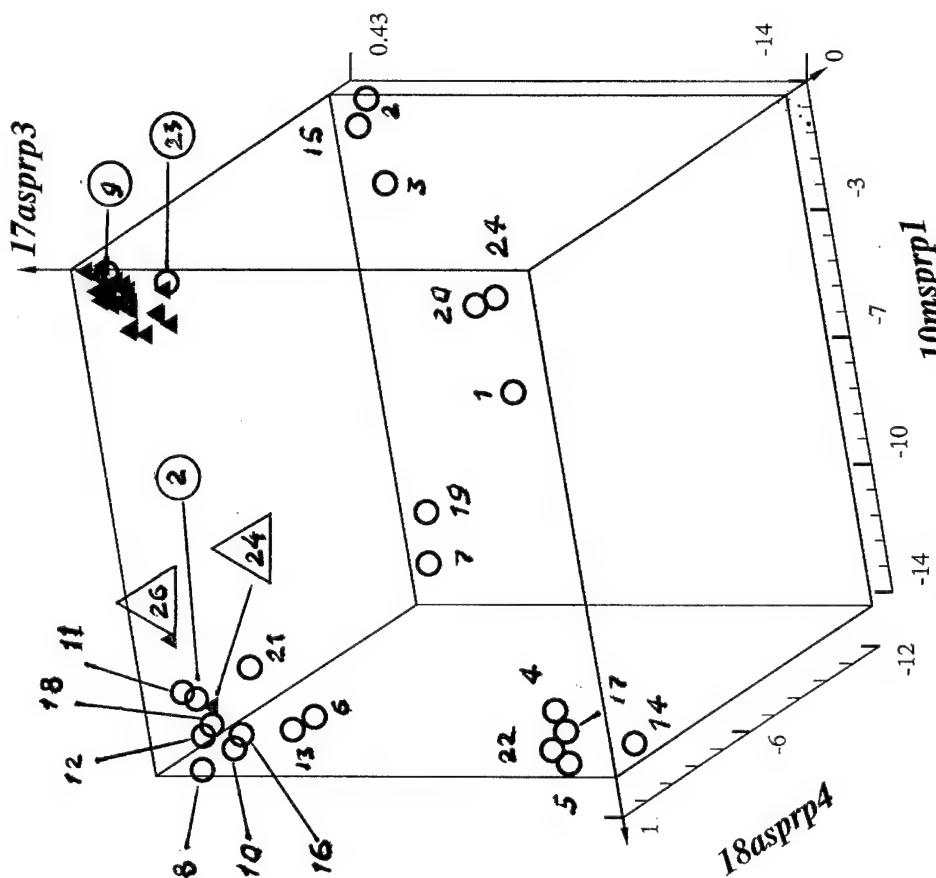


Fig. 9. Three dimensional scatterplot for feature numbers 18,10,17

Number of observations
rearranged by LD (class 1)

Number of observations
rearranged by LD (class 2)

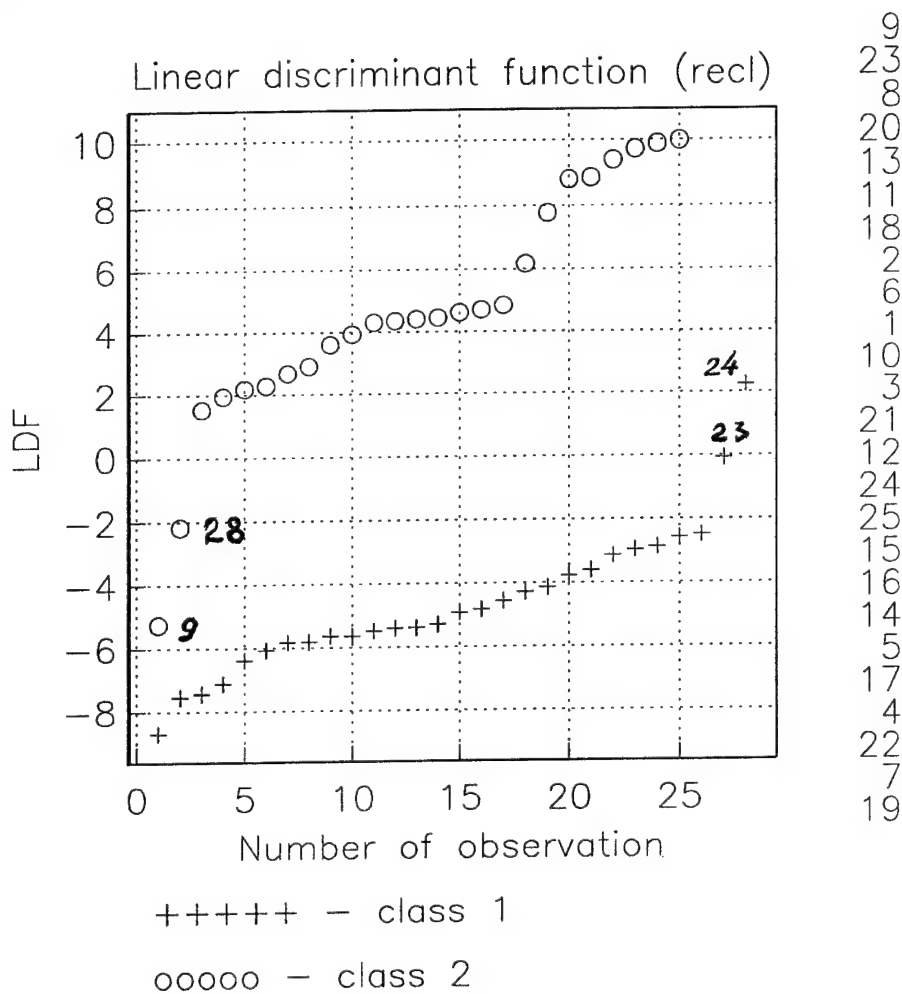


Fig. 10. Linear discrimination function calculated by the program "reclld" for the earthquake and explosion learning vector sets using the 5 optimal features.

Number of observations
rearranged by LD (class 1)

Number of observations
rearranged by LD (class 2)

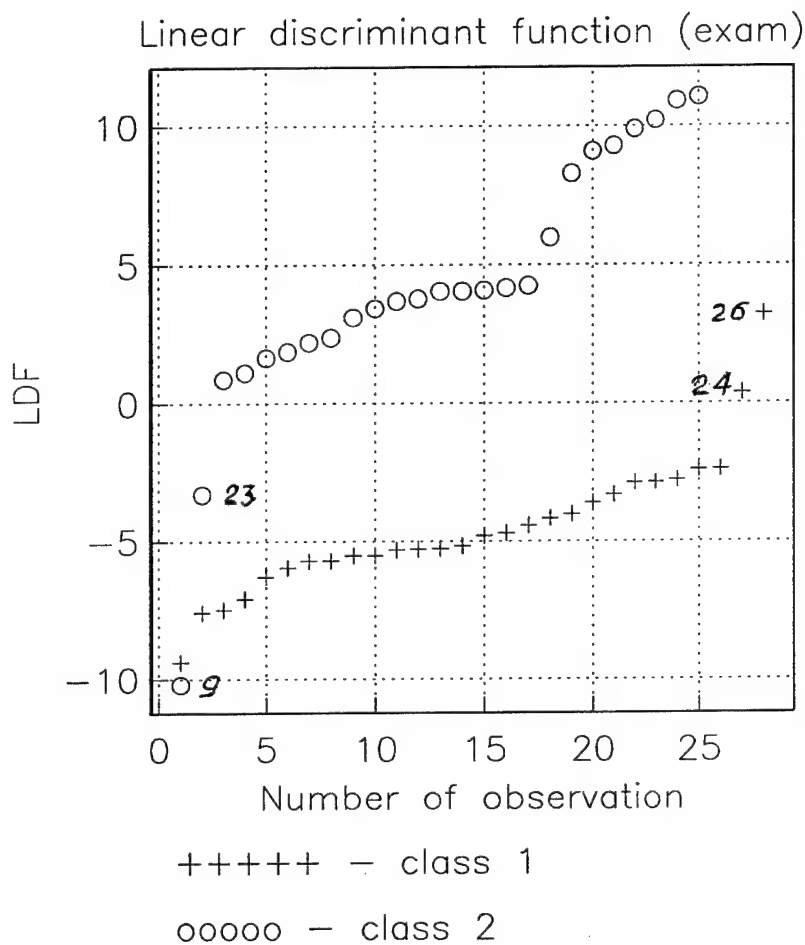


Fig. 11. Linear discrimination function calculated by the program "examld" for the earthquake and explosion learning vector sets using the 5 optimal features.

Number of observations
rearranged by QD (class 1)

Number of observations
rearranged by QD (class 2)

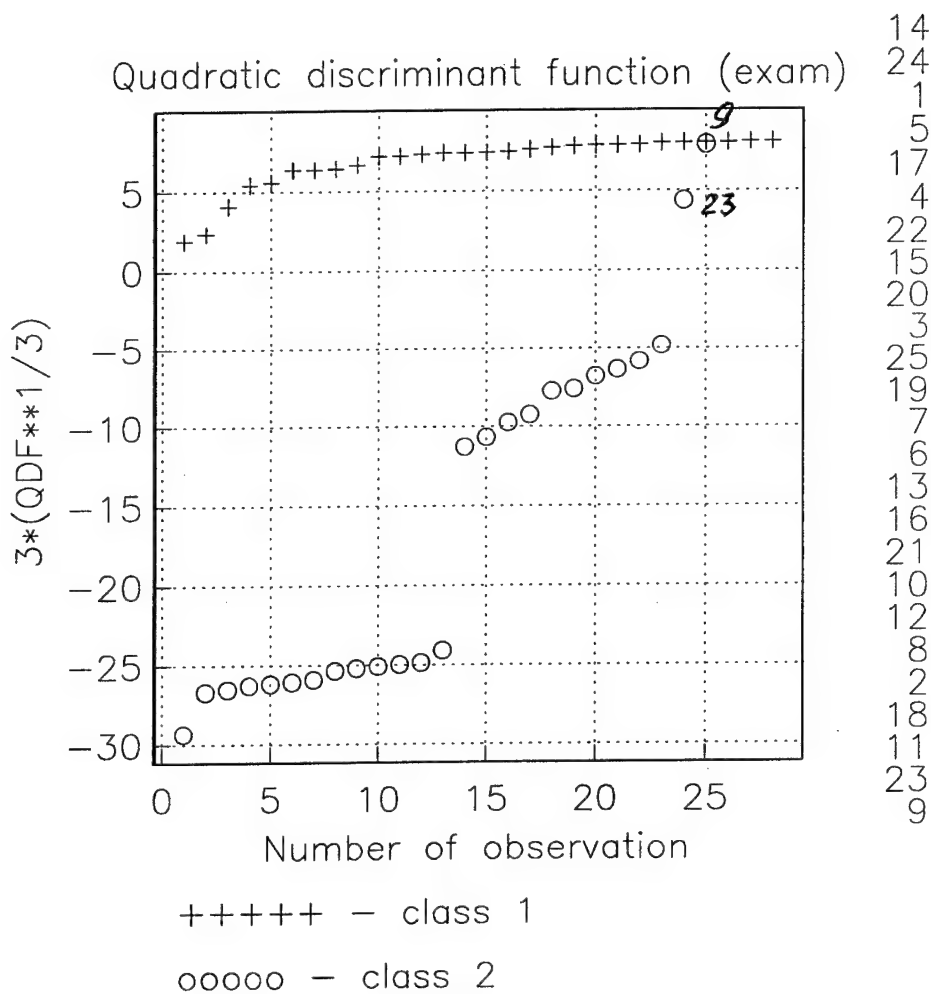


Fig. 12. Quadratic discrimination function
calculated by the program "examqd" for the earthquake
and explosion learning vector sets using the 5 optimal features

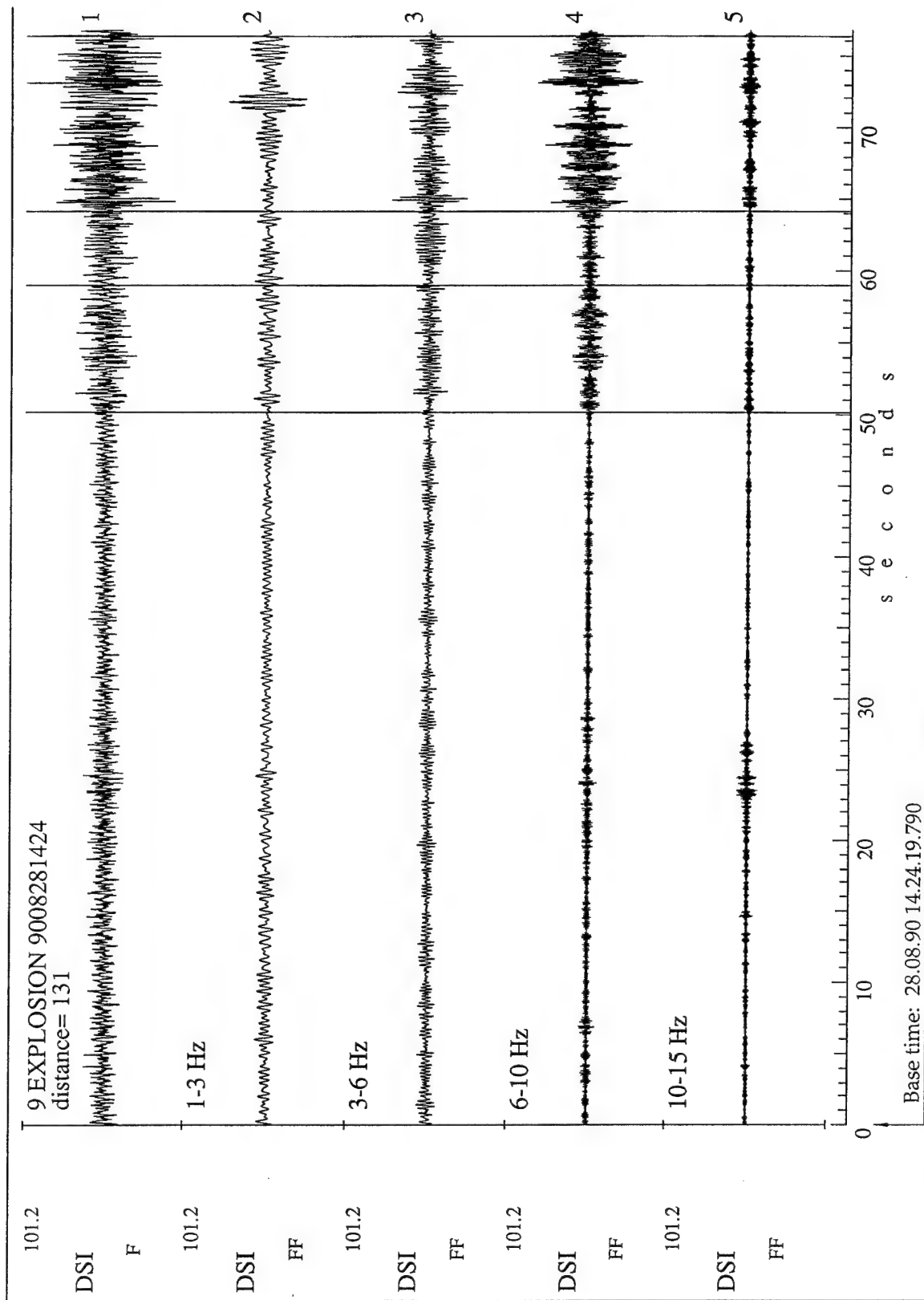


Fig. 13. The original and band filtered seismograms of the explosion N9.

Seconds from start: 0.000

Tue Jul 30 20:05:57 1996 SYNAPSE Science Center

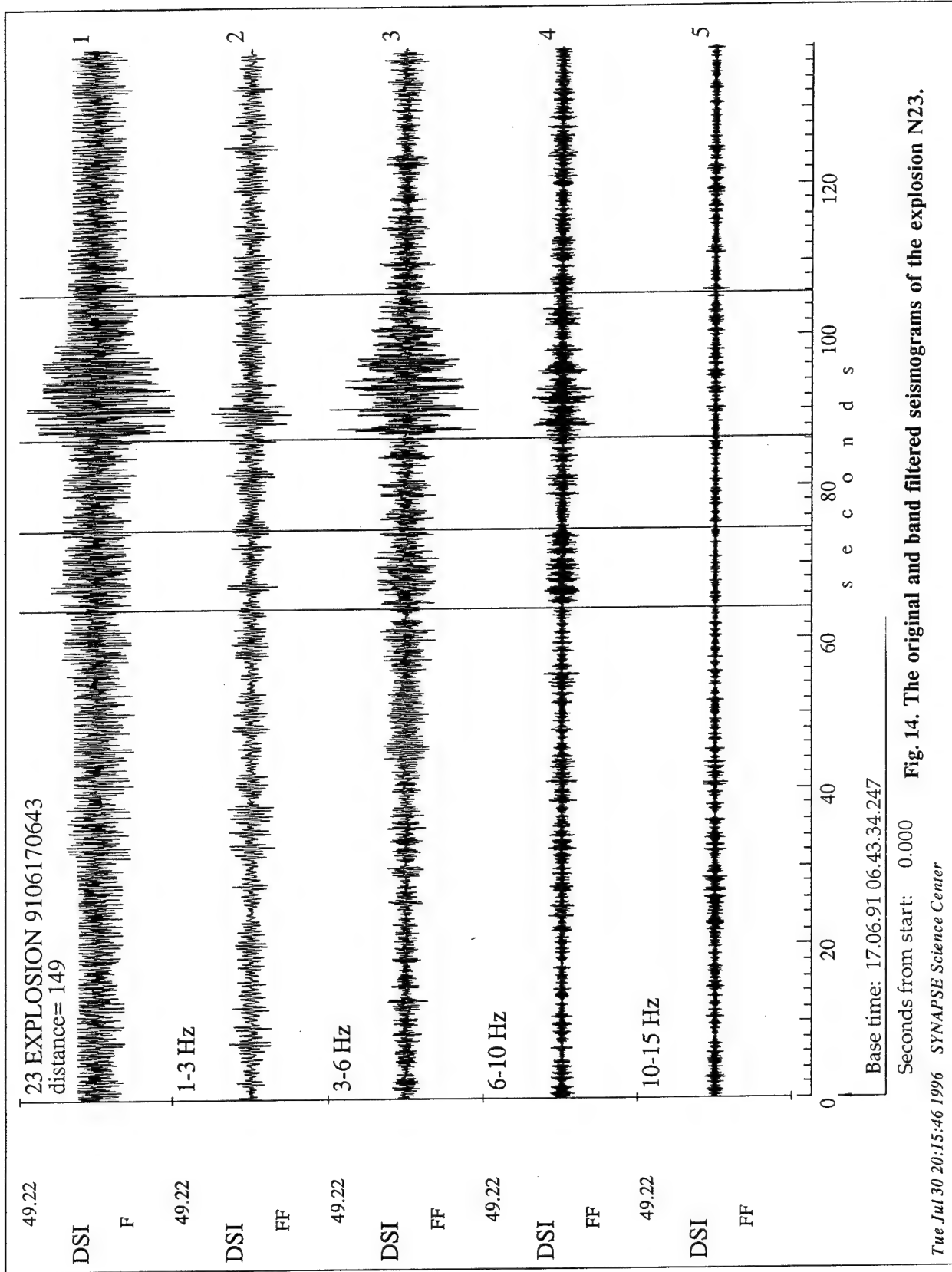
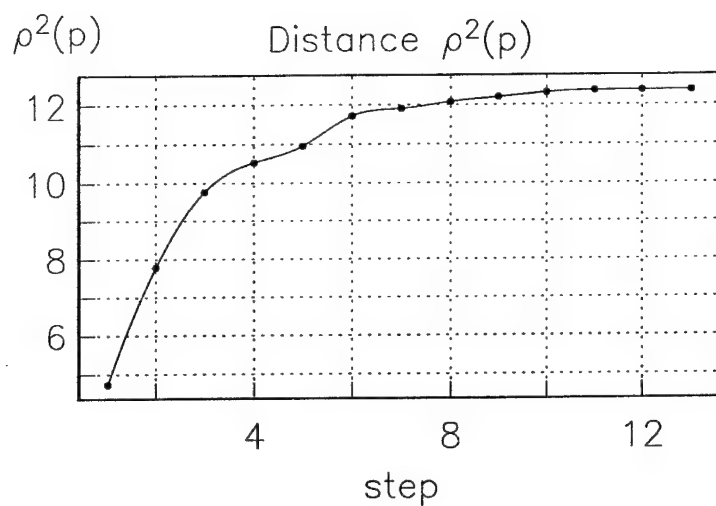
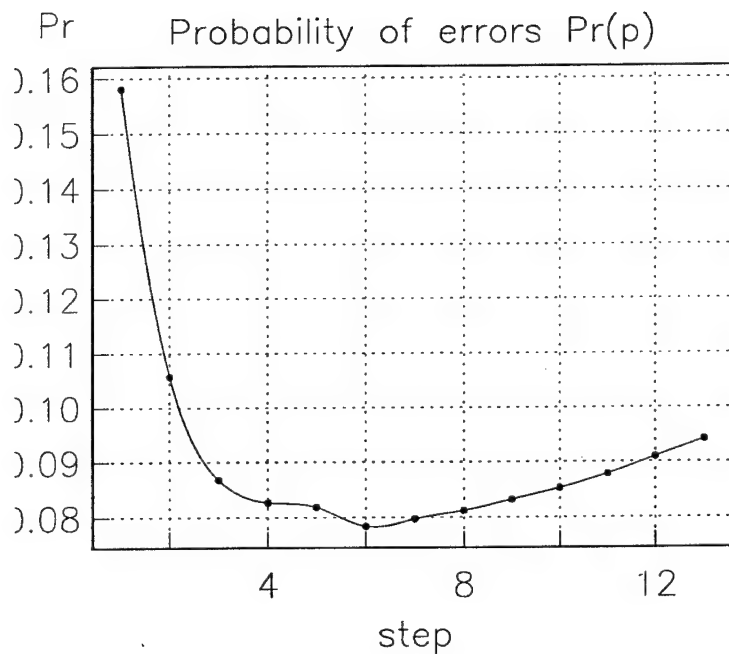


Fig. 14. The original and band filtered seismograms of the explosion N23.



Selected features:

St.: 1	18asprp4
St.: 2	5srbp1
St.: 3	13msprp4
St.: 4	1prbp1
St.: 5	8srbp4
St.: 6	9msprp0
St.: 7	12msprp3
St.: 8	16asprp2
St.: 9	7srbp3
St.:10	17asprp3
St.:11	2prbp2
St.:12	3prbp3
St.:13	6srbp2



Min of Pr is riched on step 6

Fig. 15. Automated feature selecting for the "pNb" data by the "fsel" program.

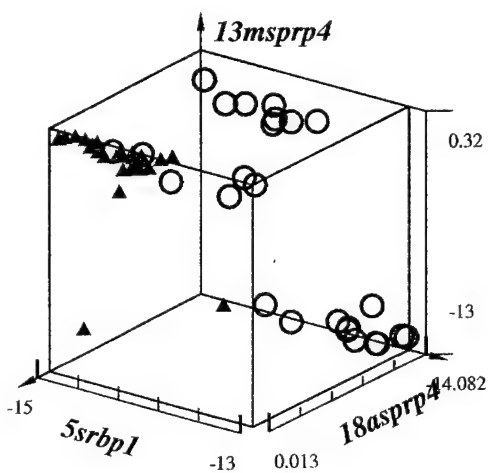


Fig. a Scplt for 18, 5, 13

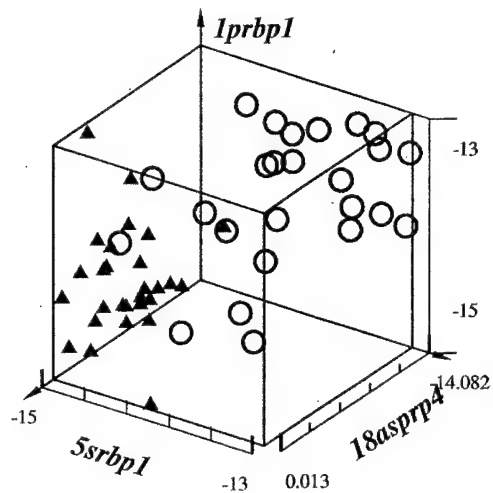


Fig. b Scplt for 18, 5, 1

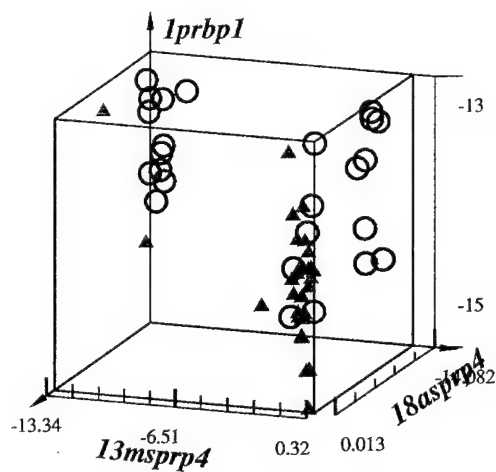


Fig. c Scplt for 18, 13, 1

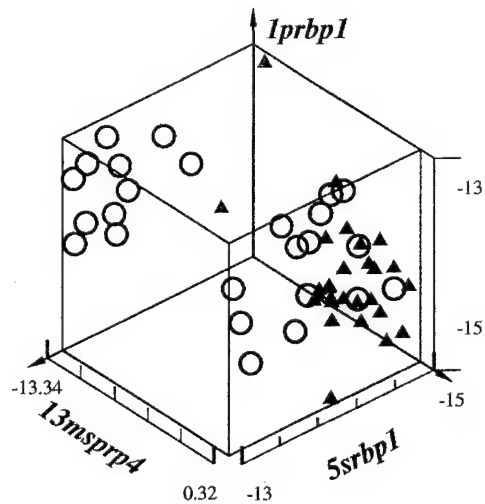


Fig. d Scplt for 5, 13, 1

- ▲ Class 1 Red triangles: Israel local earthquakes
- Class 2 Blue circles: Israel local explosions

Fig. 16. Three dimensional scattering diagrams for different feature triplets chosen from the optimal features

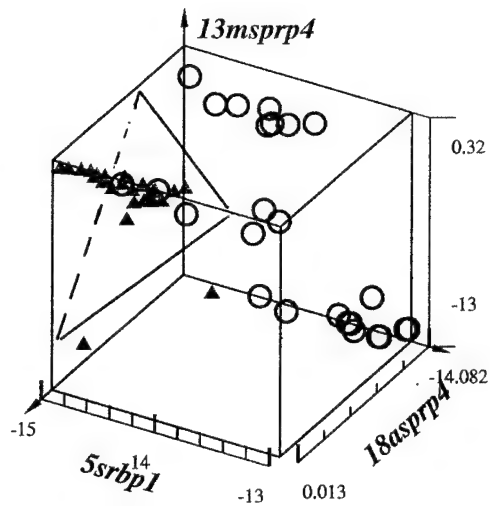


Fig. a

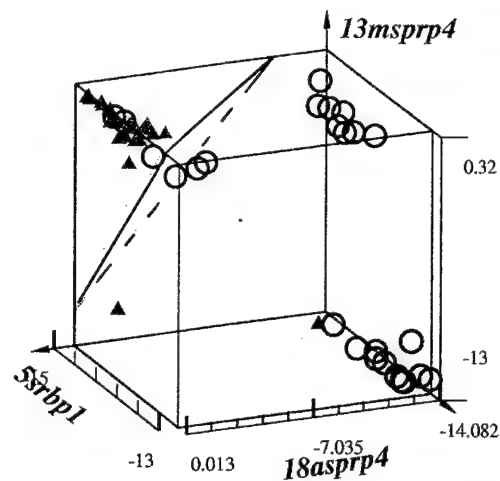


Fig. b

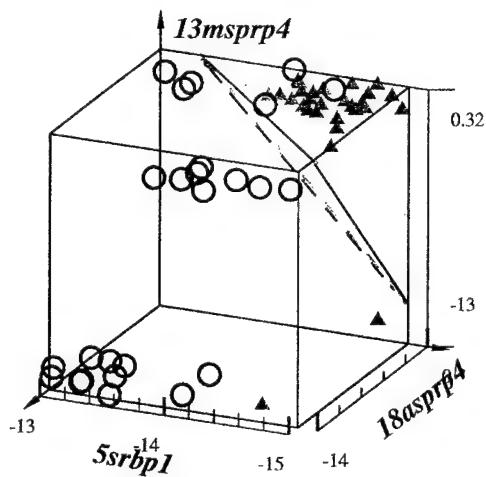


Fig. c

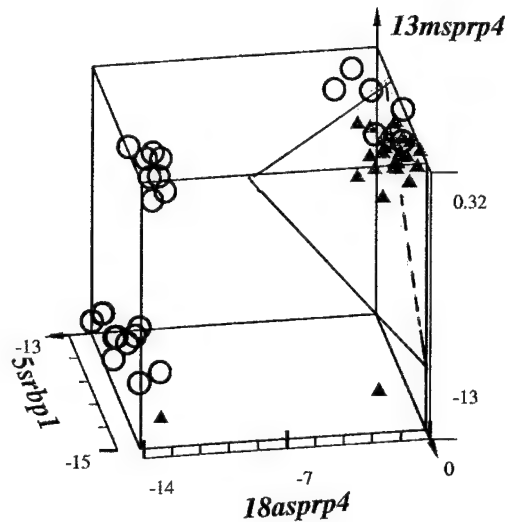


Fig. d

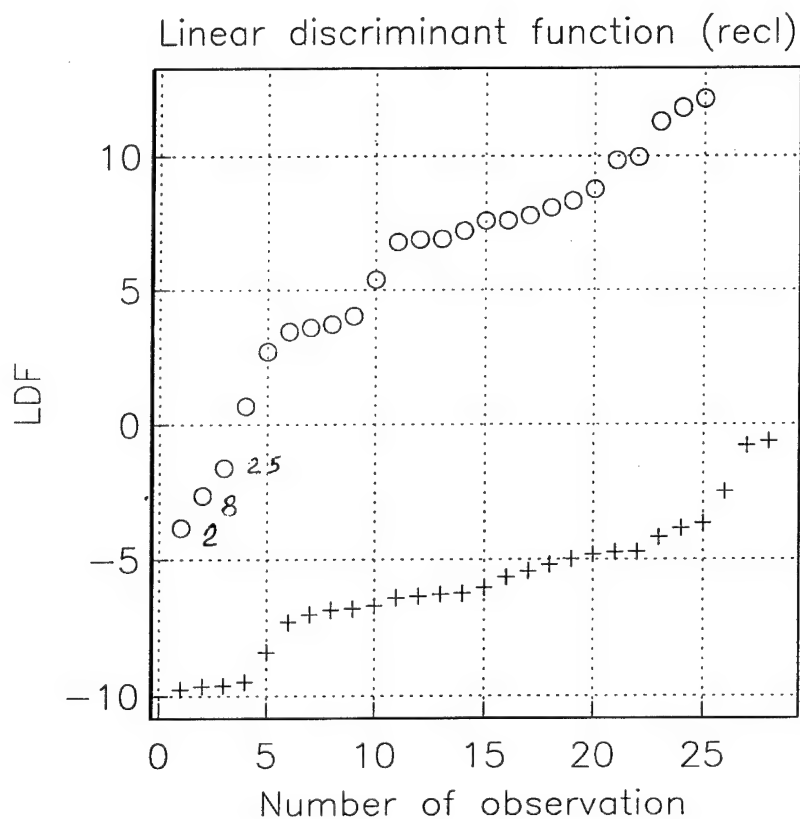
- ▲ Class 1 Red triangles: Israel local earthquakes
- Class 2 Blue circles: Israel local explosions

Fig. 17. Different projections of three dimensional space of the optimal features.

Number of observations
rearranged by LD (class 1)

Number of observations
rearranged by LD (class 2)

11
7
10
13
14
15
12
28
9
6
18
17
27
2
5
4
8
26
1
24
23
21
19
16
3
22
20
25



2
8
25
14
23
20
12
9
6
18
13
24
1
10
4
7
19
3
22
5
15
11
21
16
17

+++++ - class 1

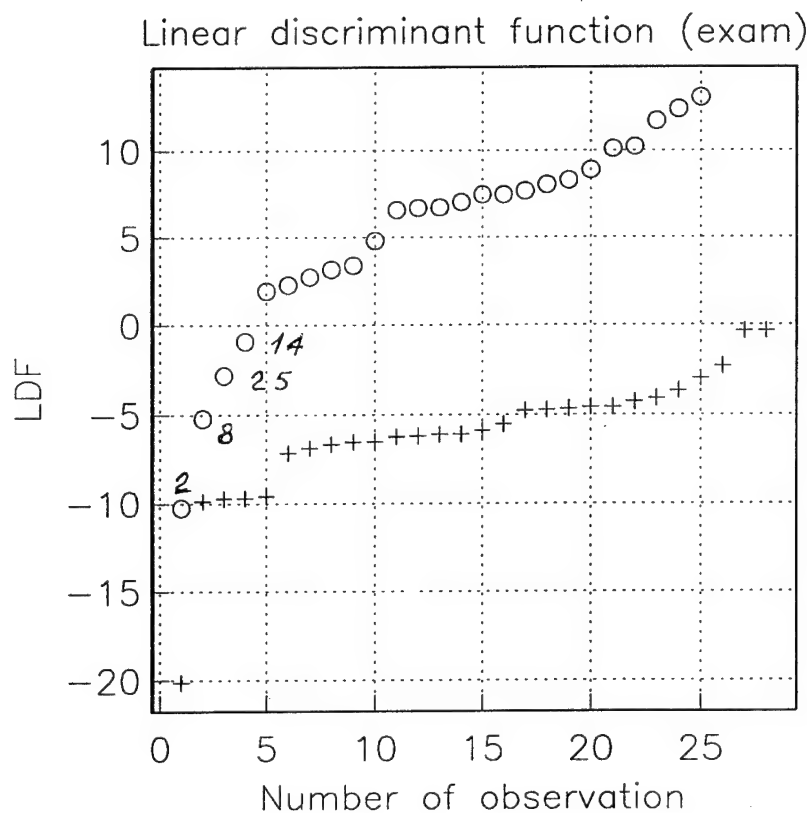
ooooo - class 2

**Fig. 18. Results of the error probability estimation
accomplished on the basis "pNb" data
with the help of program "reclld".**

Number of observations
rearranged by LD (class 1)

Number of observations
rearranged by LD (class 2)

14
11
7
10
13
15
12
28
6
9
18
17
27
2
5
4
1
26
24
21
23
8
19
16
3
22
20
25



2
8
25
14
23
20
12
9
6
18
13
1
24
10
4
7
19
3
22
5
15
11
21
16
17

+++++ - class 1

ooooo - class 2

**Fig. 19. Results of the error probability estimation
accomplished on the basis "pNb" data
with the help of program: "examld".**

Number of observations
rearranged by QD (class 1)

Number of observations
rearranged by QD (class 2)

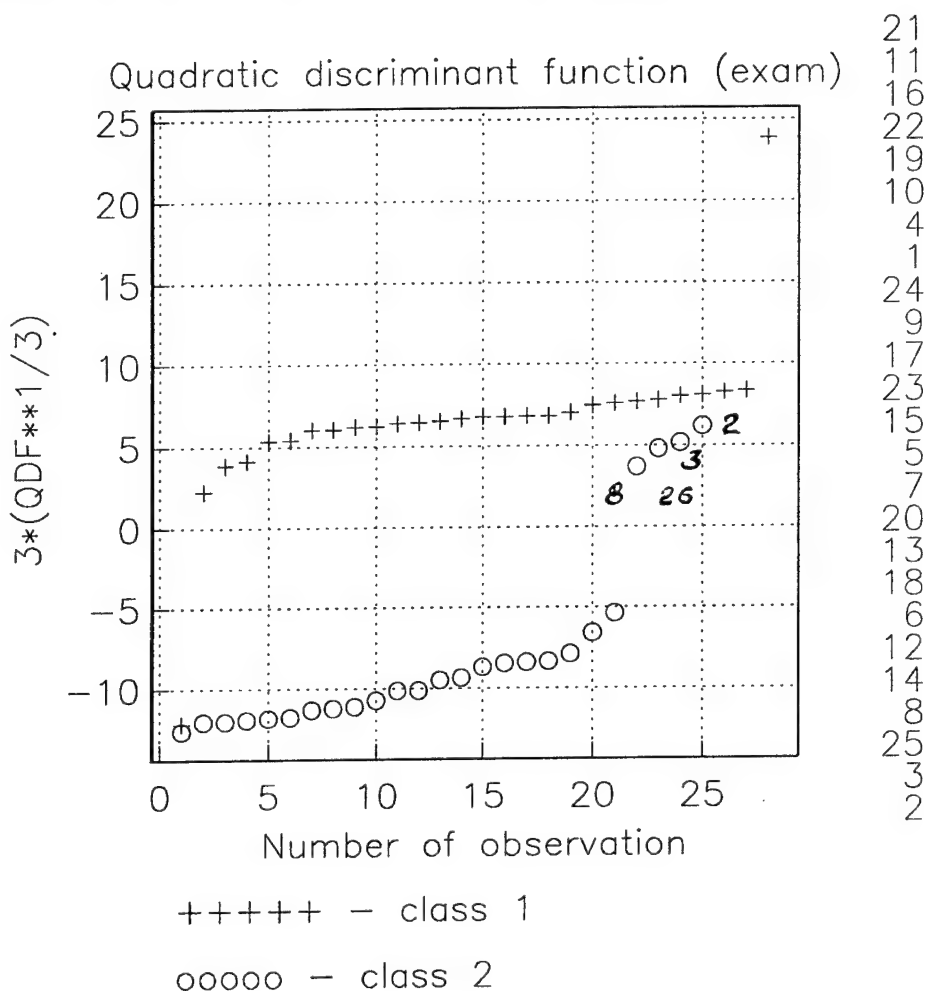


Fig. 20. Results of the error probability estimation
accomplished on the basis "pNb" data
with the help of program. "examqd".

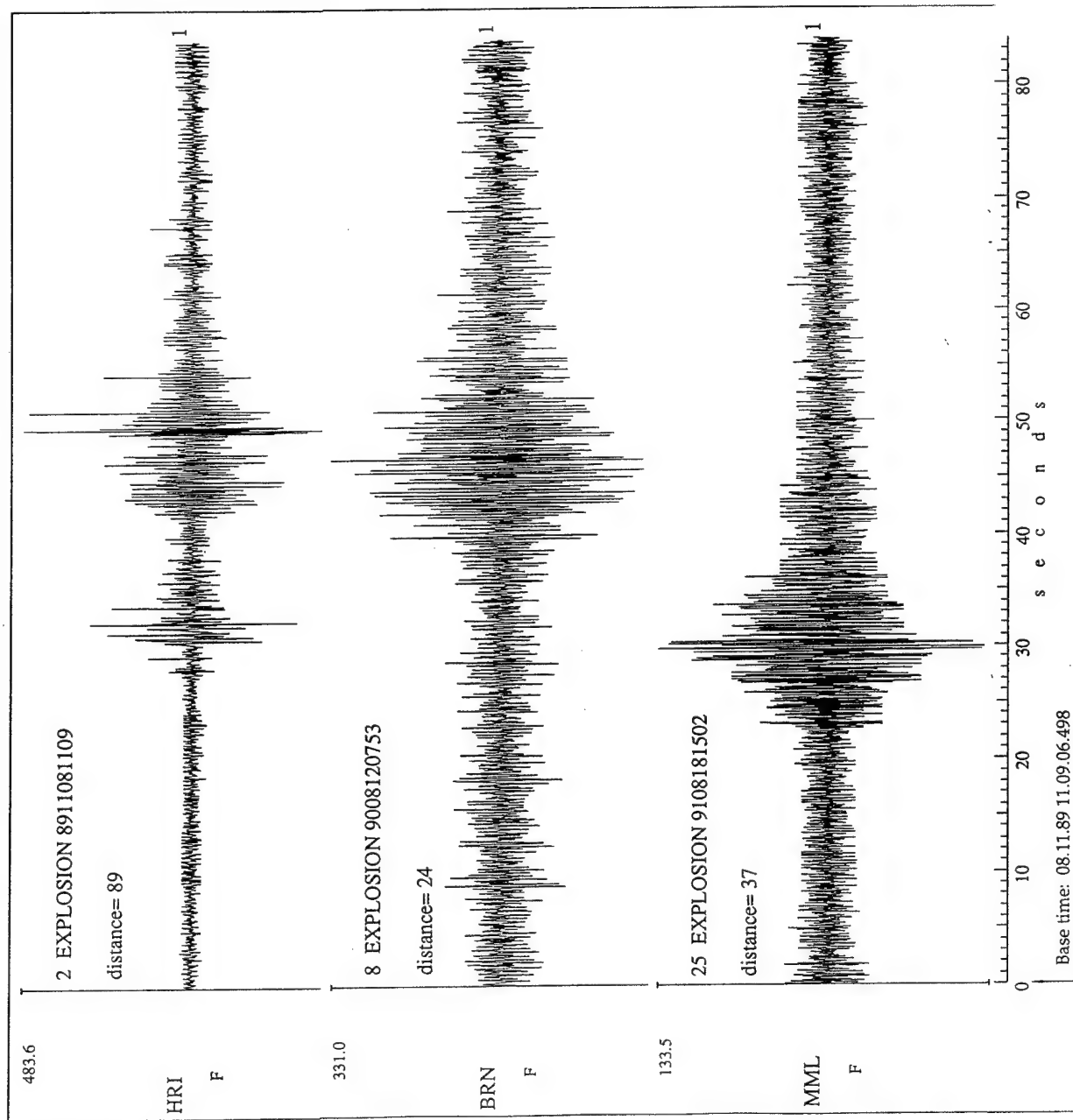


Fig. 21. "Near" station seismograms of wrongly classified explosions

Number of observations
rearranged by LD (class 1)

Number of observations
rearranged by LD (class 2)

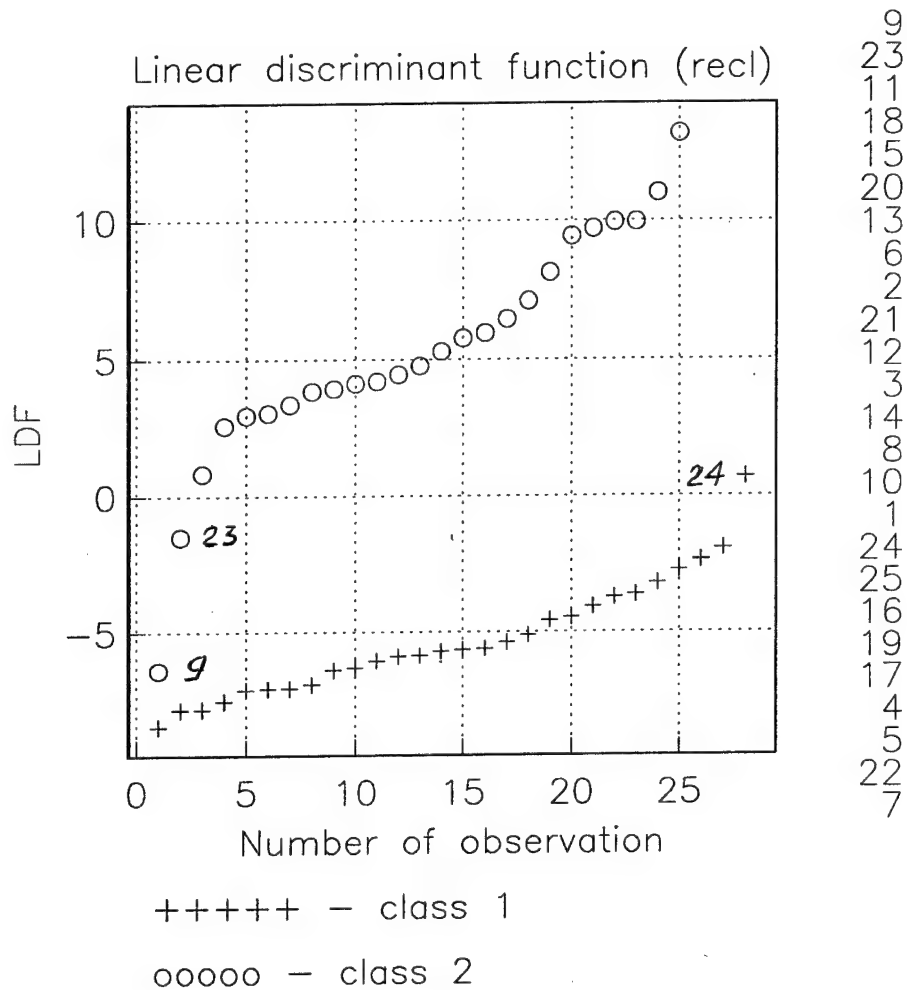


Fig. 22. Results of execution of the program "reclld"
with "pFb" data transformed by function $z = (1/5)(y^{1/5} - 1)$.

Number of observations
rearranged by LD (class 1)

Number of observations
rearranged by LD (class 2)

28
12
9
17
3
7
11
5
16
18
27
6
8
23
22
13
10
1
20
25
19
21
2
14
15
4
26
24

14
9
23
11
15
18
20
6
13
2
3
12
21
8
10
1
24
25
16
17
4
5
19
22
7

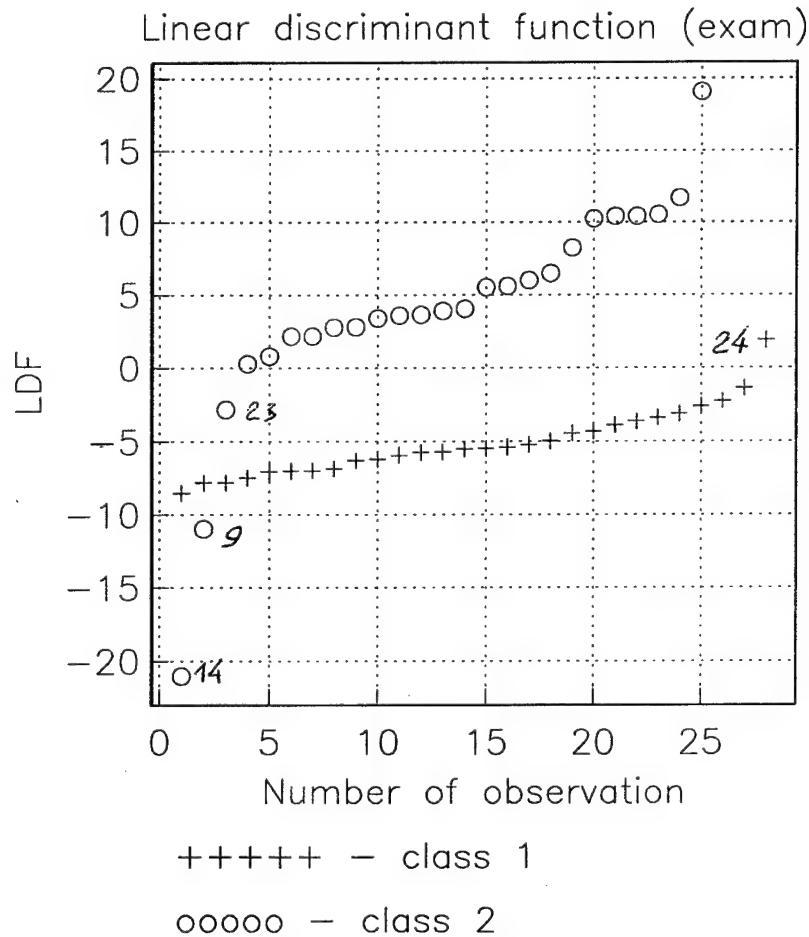


Fig. 23. Results of execution of the program "examld" with "pFb" data transformed by function $z = (1/5)(y^{1/5} - 1)$.

Number of observations
rearranged by QD (class 1)

Number of observations
rearranged by QD (class 2)

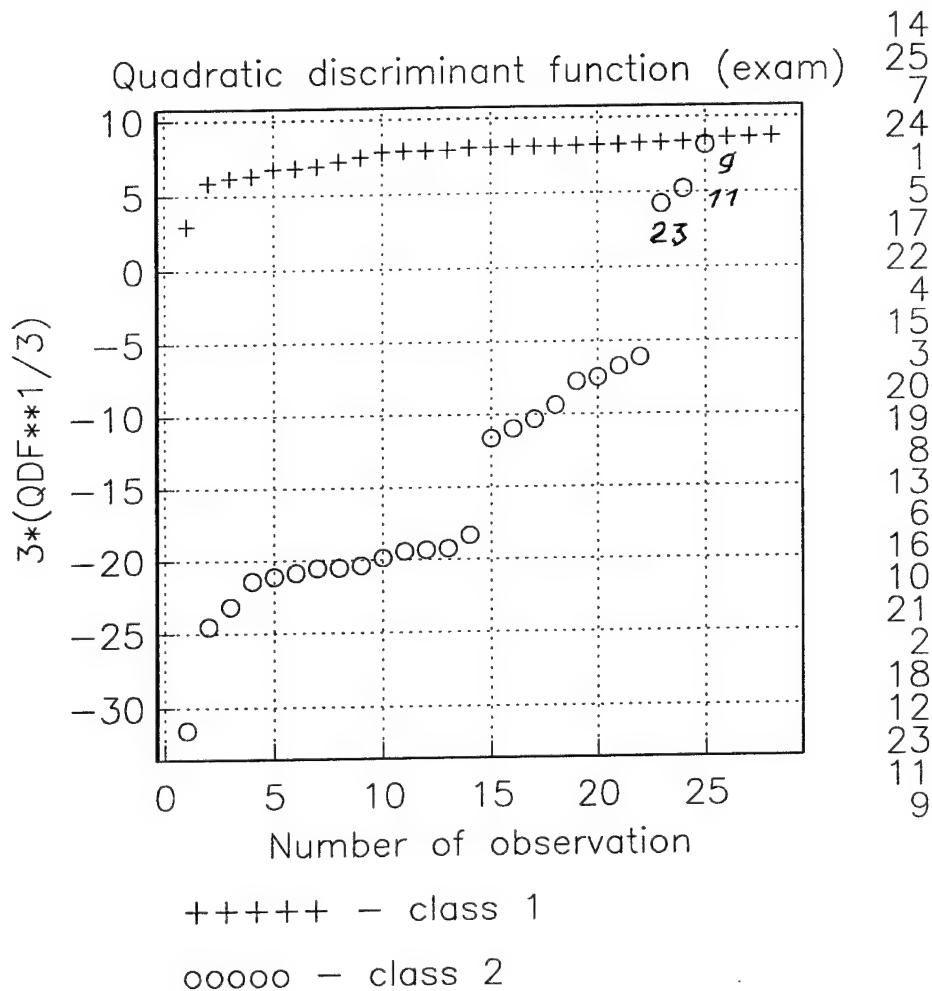
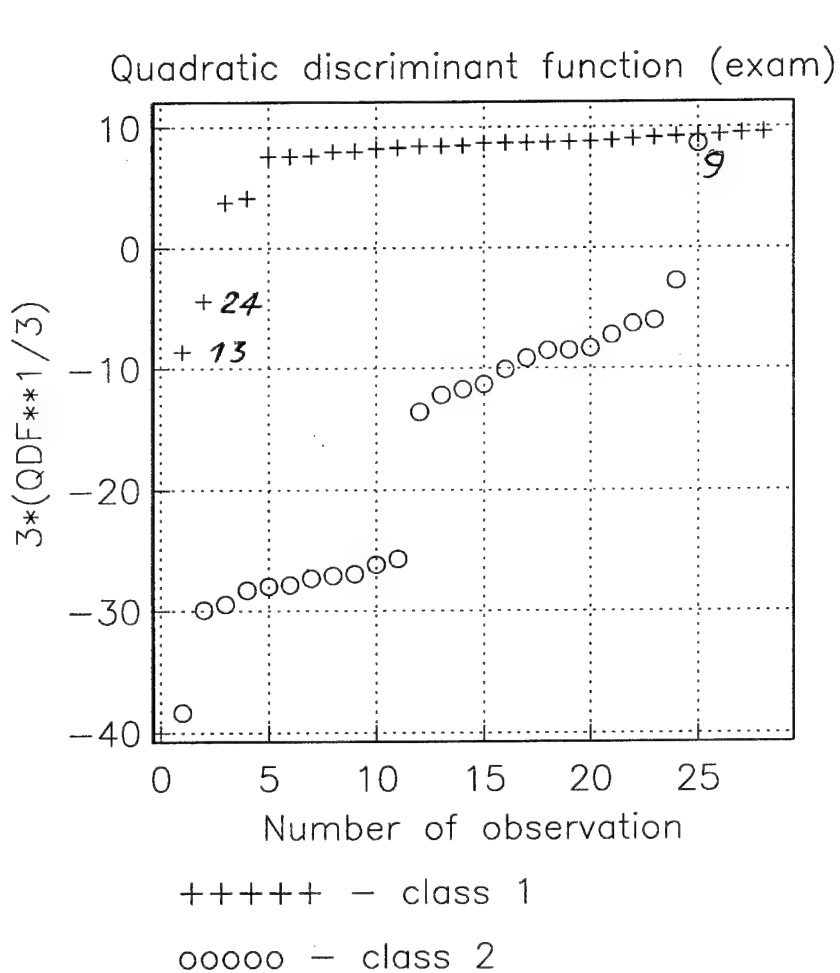


Fig. 24. Results of execution of the program "examqd" with "pFb" data transformed by function $z = (1/5)(y^{1/5} - 1)$.

Number of observations
rearranged by QD (class 1)

Number of observations
rearranged by QD (class 2)

13
24
26
2
15
14
21
4
10
1
23
19
3
25
12
11
22
17
20
28
7
27
9
8
5
16
6
18



14
6
7
24
8
1
5
22
4
17
20
25
13
10
16
21
2
3
19
12
15
18
11
23
9

Fig. 25. Results of QDF cross-validation
for "nFb" data with 3 optimal features.

Number of observations
rearranged by LD (class 1)

Number of observations
rearranged by LD (class 2)

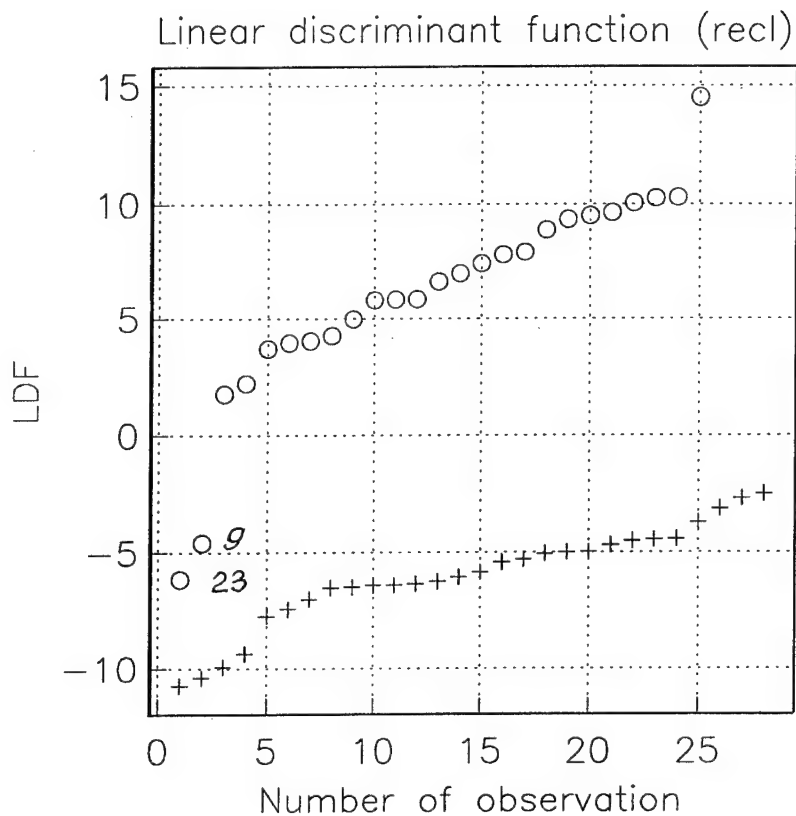
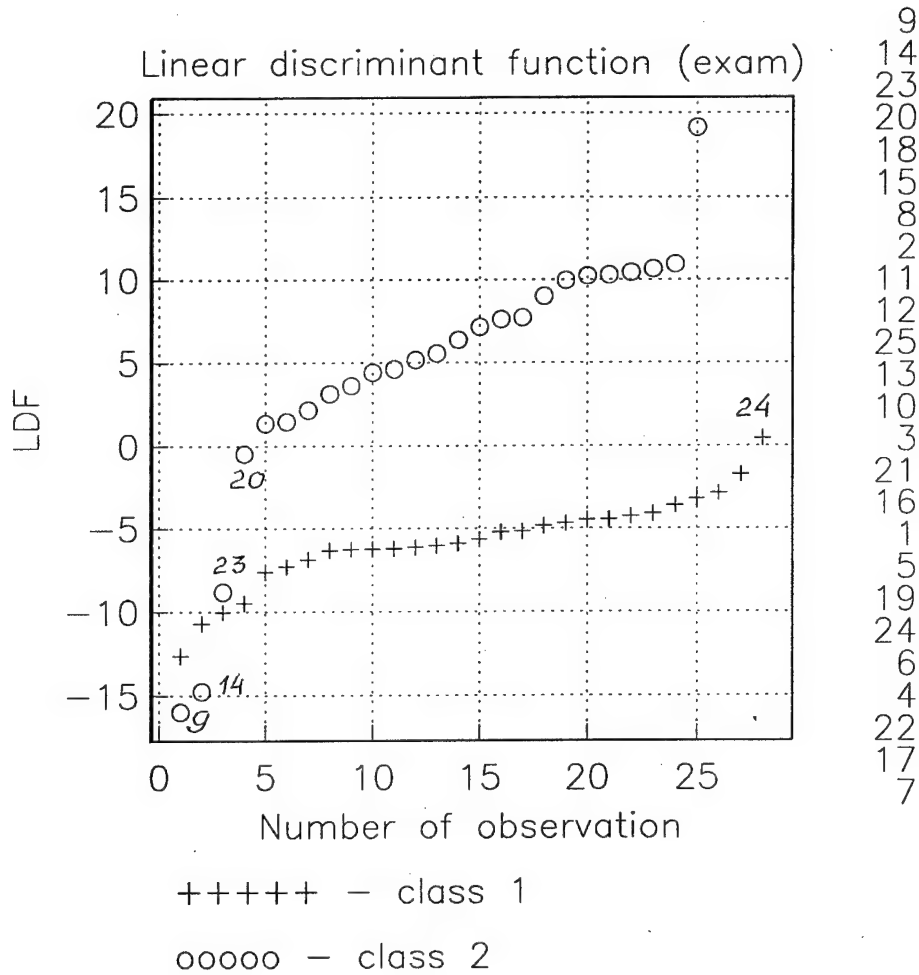


Fig. 26. Results of LDF reclassification
for combined "pF(b+s)" data with 9 optimal features.

Number of observations
rearranged by LD (class 1)

Number of observations
rearranged by LD (class 2)

9
13
12
28
19
11
6
3
8
16
17
7
5
23
18
27
25
22
2
1
4
20
10
15
14
21
26
24



9
14
23
20
18
15
8
2
11
12
25
13
10
3
21
16
1
5
19
24
6
4
22
17
7

Fig. 27. Results of LDF cross-validation
for combined "pF(b+s)" data with 9 optimal features.

Number of observations
rearranged by QD (class 1)

Number of observations
rearranged by QD (class 2)

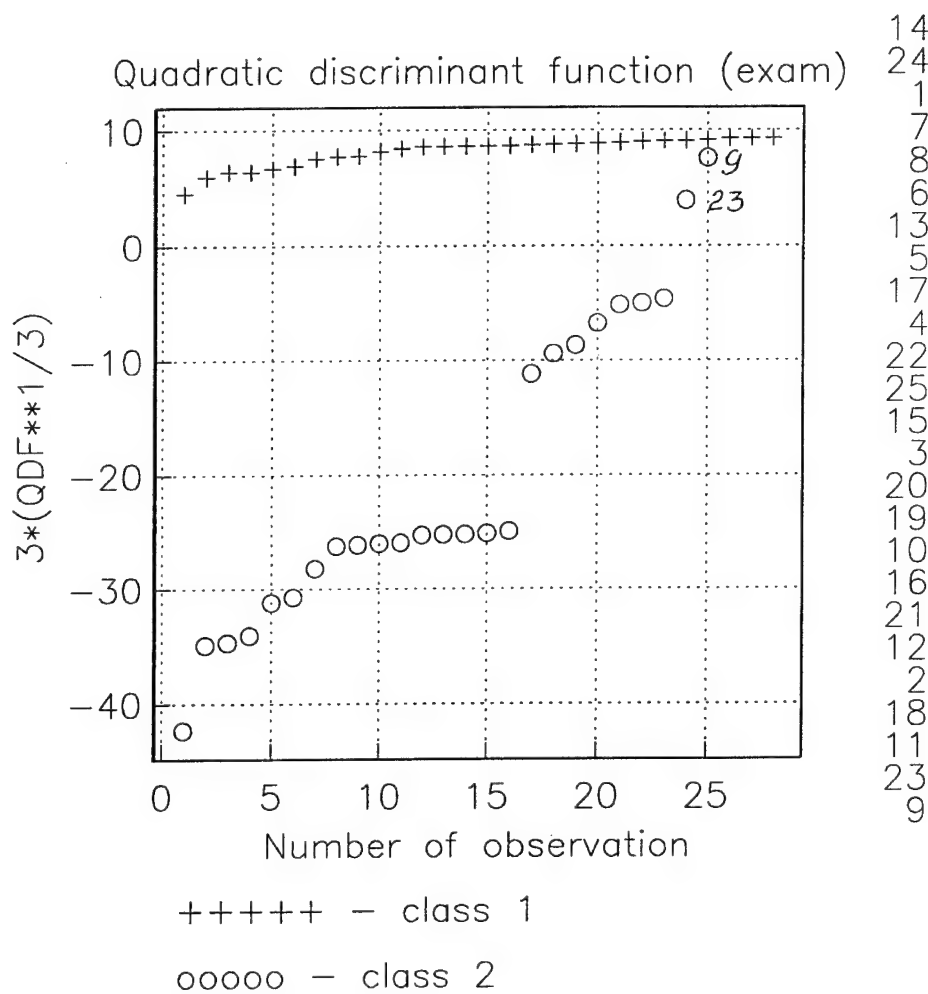


Fig. 28. Results of QDF cross-validation
for combined "pF(b+s)" data with 9 optimal features.

1.6. Description of program package for statistical identification of seismic source type

1.6.1 Program "LD"

Input data for learning and classification in the SNDA stack

The program "LD" is designed to provide some auxiliary transformations of feature vectors intended for facilitate treating of learning vectors and vectors with unknown class attributes by the subsequent procedures of statistical classification package. It reads the vector data from input files and writes them to the System SNDA Stack and some auxiliary files with the purpose to deliver them to the next procedures. In result every channel of the System SNDA Stack contains data of someone feature. So, if the number of features is equal p , the p channels are produced in the Stack. The feature values corresponding to 1 and 2 class learning vectors and vectors to be classified are arranged in the channels sequentially. So, if the number of learning vectors from class 1 is equal to n_1 , from class 2 - n_2 and number of inattributed vectors (from unknown classes) is equal to n_0 , then the number of every channel points is $(n_1+n_2+n_0)$. In the reclassification mode the learning vectors serves also as the vectors to be classified, so they are written to the Stack twice. In this mode $n_0=n_1+n_2$ and the total number of stack channel points is equal to $2(n_1+n_2)$. To provide the reclassification mode the program "ld" reads the vectors for classification from two distinct input files.

The allocation of the data in the SNDA stack allows a user to display them at the screen with the help of the SNDA graphic facilities in the form of "channel traces". This facilitates the manual selection of the most informative features and detecting of data outliers. The parameters of the learning data and the data for classification are saved to the file "gl.dat" and are used by the all other programs of statistical classification package (participating in given identification session).

Program input parameters

All input parameters of the program are to be contained in the file "ld.inp".
Example of this input file is given below

```
****INPUT FILE FOR PROGRAM "LD"(2 CL. VERSION): standard****
NUMBER OF CLASSES (maximum 2 in this version)
2
NUMBER OF FEATURES (maximum 25)
18
```

```

NUMBERS OF LEARNING VECTORS (maximum 100)
28 25
NAME OF FILE FOR 1 CLASS LEARNING VECTORS
data/troitsky/iearpFp.dat
NAME OF FILE FOR 2 CLASS LEARNING VECTORS
data/troitsky/iexplpFp.dat
NAME OF FILE FOR FEATURE LABELS
data/troitsky/lblpb.18
NAME OF FILE 1 FOR VECTORS FOR CLASSIFICATION
data/troitsky/iearpFp.dat
NAME OF FILE 2 FOR VECTORS FOR CLASSIFICATION
data/troitsky/iexplpFp.dat

```

Explanation of input file parameters

NUMBER OF CLASSES (2 in this version)

The parameter defines the number of classes assumed in the given classification session. In this simple version of the package the number of classes is restricted by two classes and this adjusting is not necessary

NUMBER OF FEATURES (maximum 25)

The parameter defines the number of features in learning and in attributed vectors. This value is delivered to the other package programs participating in the given classification session

NUMBERS OF LEARNING VECTORS (maximum 100 in this version)

These two parameters define the numbers of learning vectors from class 1 and class 2

NAME OF FILE FOR LEARNING VECTORS OF CLASS 1 (input file)

This is a name of file containing learning vectors of class 1. The file must have the form of ASCII matrix; the every column of the matrix is composed by someone feature observations. The number of columns is equal to the number of features p . The number of rows is equal to the number of observations n_1 for class 1.

NAME OF FILE FOR LEARNING VECTORS OF CLASS 2 (input file)

This is a name of file containing learning vectors of class 2. The file must have the form of ASCII matrix; the every column of the matrix is composed by someone feature observations. The number of columns is equal to the number of features p . The number of rows is equal to the number of observations n_2 for class 2.

NAME OF FILE FOR FEATURE LABELS (input file)

This is a name of file containing feature labels. The labels must consist of no more 8 ASCII symbols and be written as the column.

NAME OF FILE 1 FOR VECTORS FOR CLASSIFICATION (input file)

This is a name of file containing vectors for classification. In the plain classification mode this file contains inattributed vectors belonging to unknown classes. In the reclassification mode this file contains learning vectors from class 1. The file must have the form of ASCII matrix; the every column of the matrix is composed by observations of someone feature. The number of columns is equal number of features p . The number of rows is equal number of observations n_0 of inattributed vectors to be classified.

NAME OF FILE 2 FOR VECTORS FOR CLASSIFICATION (input file)

This parameter is valid only for reclassification mode. In this case the directory and name of file contains learning vectors from class 2 must be assigned here. The format of this file is the sam as one described above. For the mode of classification of new unattributed vectors the name of file has to contain the no less then 5 blanks.

1.6.2. Program "LDSTST" Evaluation of standard learning data statistics

The program "ldstst" provides a user by means for manual selecting of the identification features and calculates the general statistics of the learning data used in the subsequent programs of the statistical classification package. It accomplishes the following actions:

1) Reading of learning vectors and vectors for classification from the System SNDA Stack. The vectors read contain only subset of the features selected for further processing and specified by the program input parameter. The selecting of features can be, in particular, made with the help of imaging by the SNDA graphic tool the "feature traces" (i.e. graphical representation of feature value sequences for the observations of 1 and 2 class and observations to be classified) or feature 3-dimension scattering diagrams

2) Forming of output files with class 1 and class 2 vectors composed by the specified features. The files are used by the SNDA program CLUSTER providing the 3 dimensional scattering diagrams of the features.

3) Calculating of the following statistics of learning data:

a) the mean vectors $m(k)$ for every class $k = 1, 2$;

- c) the sample covariance ($p \times p$) matrix C (where p is the number of features selected);
- b) the ($p \times p$) matrix R which elements $r(jl)$ are the estimates of correlation coefficients between the features with numbers j and l ; the maximum absolute value of correlation coefficients $r(jl)$ for all $j, l = 1, \dots, p$ and numbers j_{max} , l_{max} of the features, for which this value is attained;
- e) Mahalanobis distances $d(k)$, $k=1, \dots, p$ of the one-dimensional feature distributions corresponding to 1 and 2 classes, the minimum value of $d(k)$ and number k_{min} of feature for which its value is attained.

The information obtained in items d) and e) is displayed on the screen and allows to choose the proper feature set for the further processing by excluding one of the feature from highly correlated pairs and/or the features with small Mahalanobis distances.

4) Plotting of the 2 dimensional scattering diagrams of the features with the help of standard UNIX routine "plotxy".

5) Forming of auxiliary output data files for the subsequent package programs.

The mean vectors $m(k)$ are calculated by the equation: $m(k) = (1/n_k)(X_k(1) + \dots + X_k(n_k))$, $k = 1, 2$, where $X_k(i)$ is the i -th feature vector from class k ;

The elements $r(jl)$ of matrix R are defined by the formula: $r(jl) = c(jl) / (c(jj)c(ll))^{1/2}$, $j, l = 1, 2, \dots, p$, where $c(jl)$ are the elements of unnormalized covariance matrix C :

$$C = \sum_{k=1}^2 \left\{ \sum_{i=1}^{n_k} (X_k(i) - m(k))(X_k(i) - m(k))^T \right\}$$

T - is the sign of vector transposition.

In the geometrical sense $m(k)$ are the "centers" of classes in the p -dimensional feature space. The large distance between the "centers" of classes implies the low error probabilities of discrimination. The analysis of matrix R allows one to reveal groups of uncorrelated features and/or pairs of strong correlated features. It is recommended to eliminate one feature of the pair if $|r(jl)| > 0.75$ for this pair. It is also recommended to eliminate the features with small one dimensional Mahalanobis distances between distributions of 1 and 2 class. The selecting of features is accomplished by assigning the proper Stack channel numbers in the program input file.

Scatterplots for different feature pairs of can be exposed on the screen with the help of standard UNIX routine "plotxy". This plotting is managed in the following manner: one of the features is being chosen as the "basic", and p-1 plots with scattering diagrams of this feature with the remaining ones are displayed on the screen. At every plot the points with X-Y coordinates equal to given features pair values for the 1 & 2 class observations are drawn on the screen. The points corresponding to different classes are plotted by different symbols. As a result, some clusters of points attributed to different classes can be seen on the diagrams. By analyzing the scatterplots a user may select the most separated pairs of features. Besides that, it is possible to estimate the proximity of feature two-dimensional distributions to the Gaussian one .

Program input parameters

All input parameters of the program are to be contained in the file "ldstst.inp".

Example of this input file is given below

```

****INPUT FILE FOR PROGRAM "LDSTST": standard****
STACK CHANNELS (FEATURES) TO BE USED: 8; (1-8 10 12-18); all
(18 7 10 17 5)
NAME OF OUTPUT FILE FOR VECTORS FOR CLASSIFICATION
data/troitsky/newvect.dat
NAME OF OUTPUT FILE FOR MEAN VECTORS AND COVARIANCE MATRIX OF LEARNING
VECTORS
data/troitsky/resku.dat
NAME OF GRAPHIC CONTROL FILE
plot/troitsky/gr.gr
NUMBER OF REFERENCE FEATURE FOR SCATTERING DIAGRAMS
1
NAME OF OUTPUT FILE WITH CLASS 1 VECTORS (FOR CLUSTER IMAGING)
data/troitsky/clast1.dat
NAME OF OUTPUT FILE WITH CLASS 2 VECTORS (FOR CLUSTER IMAGING)
data/troitsky/clast2.dat

```

Explanation of program input parameters

STACK CHANNELS (FEATURES) BEING USED (input information)

This string defines the numbers of features selected for the subsequent analysis. If the all features are kept, "all" must be written here. In other case numbers of features (channels) to be kept are given according to notation CHANNELS used for the SNDA Stack commands.

NAME OF OUTPUT FILE FOR VECTORS FOR CLASSIFICATION

This is a name of file with unattributed vectors (to be classified) composed with the selected features.

NAME OF OUTPUT FILE FOR MEAN VECTORS AND COVARIANCE MATRIX OF LEARNING VECTORS

This is a name of file containing the mean vectors $m(k)$, $k=1,2$ for every class; the normalized correlation matrix R ; the unnormalized covariance matrix C for selected set of features and some service information needed for execution of the following programs.

NAME OF GRAPHIC CONTROL FILE

This is a name of control file for the "plotxy" UNIX routine containing commands for displaying feature scattering diagrams.

NUMBER OF THE REFERENCE FEATURE FOR SCATTERING DIAGRAM

This feature is used for design of $p-1$ scattering diagrams. On every diagram this feature values corresponding different observations are set along the X axis, and along the Y-axis - the values of one from remaining features.

NAME OF OUTPUT FILE WITH CLASS 1 VECTORS (FOR CLUSTER IMAGING)

This is a name of file containing selected feature vectors of class 1. The file is used by the other programs of the package, in particular, the SNDA program "CLUSTER" providing the three dimensional plotting of feature scattering diagrams.

NAME OF OUTPUT FILE WITH CLASS 2 VECTORS (FOR CLUSTER IMAGING)

This is a name of file containing selected feature vectors of class 2. The file is used by the other programs of the package, in particular, the SNDA program "CLUSTER" providing the three dimensional plotting of feature scattering diagrams.

1.6.3. Program "FSEL"

Automatic selection of informative features providing minimum of classification probability error estimate

The program "fsel" accomplishes the following operations:

- 1) the automatic stepwise selecting of most informative features providing the least error probabilities for the classification based on the given set of learning data;
- 2) calculating of a function $R(k)$, $k = 1, \dots, p$, which is a Makhalanobious distance in depend on an amount k of features used for classification;
- 3) calculating of a function $P(k)$, $k=1, \dots, p$ which is a theoretic total probability of classification errors in depend on an amount k of features used for classification;
- 4) calculating of the value k_0 for which the function $P(k)$ attains its minimum ($k_0 = \operatorname{argmin} P(k)$);
- 5) plotting of the calculated functions $R(k)$ and $P(k)$ on the screen using the standard UNIX routine "plotxy" with displaying on this plot the numbers and labels of features chosen at every selection step.

The Makhalanobious distance between two k -dimensional distributions of k feature vectors (corresponding to 1 and 2 classes) is defined by the quadratic form:

$$R(k) = (\mathbf{m}(k,2) - \mathbf{m}(k,1))^T \mathbf{S}^{-1}(k) (\mathbf{m}(k,2) - \mathbf{m}(k,1)),$$

where: $\mathbf{m}(k,1)$, $\mathbf{m}(k,2)$ - are the sample mean vectors of learning data for 1 and 2 classes calculated for a k feature vectors; $\mathbf{S}(k) = \mathbf{C}(k)/(n_1+n_2)$ is the sample covariance matrix calculated for a k feature vectors using total learning data for the both classes; T is the sign of vector transposition.

At the first step of the selecting procedure p values of the $R(1)$ functional are calculated for every feature. The maximum of these p values is attained at some $j(1)$ feature which is thus selected. At the second step $p-1$ values of the $R(2)$ functional are calculated for the pairs of features: the first member of this pairs is always the previously selected feature $j(1)$, the second member - is an arbitrary feature from the remaining ones. Then the second feature is selected which ensure the maximum of these $R(2)$ values. At the k -th step of this selecting procedure $p-k+1$ values of the $R(k)$ functional are calculated for k feature vectors. The first $k-1$ components in these vectors are the features which were selected at the previous steps, the k -th component is an arbitrary feature from the remaining ones. On the each step $k = 1, 2, \dots, p$ of the

selecting procedure the number $j(k)$ and label of the feature selected are stored and the theoretical value of total error probability $P(k)$ is calculated. The value $P(k)$ (for $k > 1$) is calculated by the formula:

$$P(k) = (1/2)[1 - T_k(R(k)/\sigma(k)) + T_k(-R(k)/\sigma(k))],$$

where

$$\sigma^2(k) = [(t+1)/t][r_1+r_2+R(k)]; \quad t = [(r_1+r_2)/r_1r_2]-1; \quad r_1=k/n_1; \quad r_2=k/n_2$$

$$T_k(z) = F(z) + (1/(k-1)) (a_1 - a_2 H_1(z) + a_3 H_2(z) - a_4 H_3(z)) f(z),$$

$F(z)$ - is the cumulative function of standard Gaussian probability distribution; $f(z)$ is the density of this distribution; $H_i(z)$ is the Hermitian polynomial with order i , $i=1,2,3$; $a_j, j=1,\dots,4$ are some coefficients depending on k, n_1, n_2 and $R(k)$ [1].

This formula was derived via an asymptotic expansion of the distribution function for conventional linear discriminator under the assumption that the number of features p and numbers of learning vectors n_1, n_2 for both the classes are simultaneously increasing with the same rate.

The program "fsel" then defines a number k_0 of that selecting step for which a minimum of function $P(k)$, $k=1,\dots,p$, is attained: $k_0 = \operatorname{argmin} P(k)$. Thus the optimal set of features with the numbers $j(1), j(2), \dots, j(k_0)$ become determined. These features provide the minimal total error probability.

Program input parameters

All input parameters of the program are to be contained in the file "fsel.inp". Example of this input file is given below

```
****INPUT FILE FOR PROGRAM "FSEL": stanard****
NAME OF FILE FOR MEAN VECTORS AND COVARIANCE MATRIX OF LEARNING DATA
data/troitsky/resku.dat
NAME OF FILE FOR GRAPHIC RESULTS:
plot/troitsky/mygr.gr
```

Explanation of input file parameters

NAME OF FILE FOR MEAN VECTORS AND COVARIANCE MATRIX OF LEARNING DATA

This is name of file containing the covariance matrix and mean values of the features, calculated by the program "ldstst".

NAME OF FILE FOR GRAPHIC RESULTS (output file):

This is name of control file for the UNIX routine "plotxy", containing the commands providing displaying of Makhalanobius distance curve $R(k)$ and probability error curve $P(k)$, along with the numbers and labels of selected features.

Program output files with standard names

- 1) File "perr.dat": the file contains values of classification error probabilities, corresponding to selected features in the order of their selection in the program.
- 2) File "jnum.dat": the file contains the selected feature numbers in the order of their selection in the program.
- 3) File "sumr.dat": the file contains values of Makhalanobius distances corresponding to selected features in the order of their selection in the program.

1.6.4. Program "RECLLD"

Reclassification of learning vectors by the linear discriminator

The program "reclld" accomplishes the following operations:

1. Classifying of given unattributed feature vectors X_1, \dots, X_r as belonging to one of two classes. The classification is performed by the linear discrimination function (LDF) which is "learned" using the estimates of class mean vectors and covariance matrix provided by the "ldstst" program on the basis of learning data. There exists the two modes: classification of "new" vectors X_i , and the reclassification mode when the learning vectors from classes 1 and 2 are regarded as unattributed and are newly classified by the LDF (previously learned with their help).
2. Plotting of the ranked LDF values corresponding to vectors attributed by the program to classes 1 and 2. The plot is produced with the help of standard UNIX routine "plotxy".

A classification in the program "reclld" is performed using the LDF. The input data for the program are the statistics of the learning feature vectors: sample mean vectors $m(k)$ for every class $k=1,2$, and sample covariance matrix S (the same for both classes) and feature vectors X_1, \dots, X_r to be classified. For every class $k=1,2$ the program calculates the "informants":

$$I(k) = X^T S^{-1} (m(k) - (1/2) m(k)^T S^{-1} m(k)), \quad k = 1, 2.$$

Then the program calculates number k_0 providing a maximum for the values $I(k)$, $k=1,2$ and thus classifies the vector X as belonging to the class with number k_0 . This decision making procedure is equivalent to comparison of a value of the Linear Discrimination Function:

$$L=I(2) - I(1)$$

with the threshold equal 0.

Program input parameters

All input parameters of the program are to be contained in the file "reclld.inp". Example of this input file is given below

```
*****INPUT FILE FOR PROGRAM "RECLLD": standard*****
NAME OF INPUT FILE FOR MEAN VECTORS AND COVARIANCE MATRIX OF LEARNING
DATA
data/troitsky/resku.dat
NAME OF FILE FOR VECTORS FOR CLASSIFICATION
data/troitsky/newvect.dat
CLASSIFICATION MODE: RECLASSIFICATION OF LEARN. VECTORS = 0;
CLASSIFICATION OF NEW VECTORS = 1
0
FEATURES TO BE USED OF UNSELECTED = 0; SELECTED = 1
0
NAME OF OUTPUT FILE FOR CLASSIFICATION RESULTS
data/troitsky/ldres.dat
NAME OF GRAPHIC CONTROL FILE FOR PLOTTING OF CLASSIFICATION RESULTS
plot/troitsky/reclplt.cnt
```

Explanations of program input file parameters

NAME OF INPUT FILE FOR MEAN VECTORS AND COVARIANCE MATRIX OF LEARNING DATA

This is a name of file for reading of the Linear Discrimination Function parameters. File is produced by the program "ldstst".

NAME OF INPUT FILE FOR VECTORS FOR CLASSIFICATION

This is a name of file containing the unattributed vectors which have to be classified by the program. File is produced by the program "ldstst".

CLASSIFICATION MODE: RECLASSIFICATION OF LEARN. VECTORS = 0;
CLASSIFICATION OF NEW VECTORS = 1

The parameter switches the program to one of two modes connected with origin of vectors to be classified.

FEATURES TO BE USED OF UNSELECTED = 0; SELECTED = 1

The parameter defines the feature set to be used for the classification of unattributed vectors. If 0 is assigned, the program uses for classification the initial feature set, if 1 is assigned, only the features selected by the program "fsel" are used in the classification procedure.

NAME OF OUTPUT FILE FOR CLASSIFICATION RESULTS

This is a name of file contains the table with numbers of unattributed vectors and numbers of classes to which this vectors is related in the result of classification.

NAME OF GRAPHIC CONTROL FILE FOR PLOTTING OF CLASSIFICATION RESULTS

This a name of control file for the UNIX routine "plotxy" containing the commands for displaying of the program classification results.

1.6.5. Program "EXAMLD Estimation of error probability by cross-validation method using linear discriminator.

The program "examld" calculates by the statistically consistent cross-validation method (synonyms: Jack-knife, "plug-in" method) the estimates of classification error probabilities which linear discrimination function (LDF) provides for given set of learning observations. The LDF values obtained for every class learning vectors are ranked in their magnitudes. The points corresponding this two ranked sets are displayed on the screen by using the standard UNIX routine "plotxy". This provides the descriptive graphical representation of the linear discriminator classification capability in regard of the given set of learning observations.

The equations for calculation of linear discrimination function are given in the description of program "reclld". The estimates $v(1|2)$, $v(2|1)$, of first and second types of classification error probabilities $p(1|2)$, $p(2|1)$ are calculated in the program by the equations:

$$v(1|2) = n(1|2)/n_2, \quad v(2|1) = n(2|1)/n_1,$$

where: $n(j|k)$ - is an amount of vectors from class k attributed by the LDF to

class j in the result of cross validation procedure, $j, k=1, 2$, n_k - is a total amount of vectors from class $k=1, 2$. The estimate of the averaged classification error probability p_{av} is defined as following: $v_{av} = (1/2)(v(1|2)+v(2|1))$ and the estimate of the total classification error probability p_{tot} is defined by the formula:

$v_{tot} = (n_2/n_{tot})v(1|2) + (n_1/n_{tot})v(2|1)$, where $n_{tot} = n_1 + n_2$.

The well known cross-validation procedure consists of $n_{tot} = n_1 + n_2$ steps. On every step one of the learning vectors belonging to the class j ($j=1,2$) is eliminated from the learning set. The remaining vectors are used as the learning data for calculating the LDF adjusting parameters. The eliminated vector is then classified by this LDF. If this vector is classified incorrectly, the value $n(k|j)$, $k=3-j$ is increased by the unit. The eliminated vector is then returned into the learning set and then the next vector is extracted. This procedure is repeated with the all learning vectors. Values $v(1|2)$, $v(2|1)$, v_{av} and v_{tot} , evaluated by the cross-validation method is asymptotically unbiased estimate of the classification error probabilities $p(1|2)$, $p(2|1)$, p_{av} and p_{tot} , when n_1 , n_2 tend to infinity with the same rate. The program displays the values $v(1|2)$, $v(2|1)$, v_{av} and v_{tot} (in percents) on the screen.

The program calculates also the sequences $L_I(i)$, $i=1, \dots, n_1$ and $L_{\mathcal{I}}(j)$ $j=1, \dots, n_2$ of LDF values obtained during cross validation procedure for the observations from the class 1 and 2 respectively. These sequences are ranked in the order of their magnitudes and are plotted on the screen by using the standard UNIX routine "plotxy". Values $L_I(i)$ are marked by the symbol "+", values $L_{\mathcal{I}}(j)$ - by the symbol "o". The plots of $L_I(i)$ and $L_{\mathcal{I}}(j)$ functions enable a user with following possibilities: to detect incorrectly classified observations; to select the observations corresponding to the "uncertain" classification area defined by the condition $-c < L(i) < c$, where c equal to some fraction of $A = (max L_{\mathcal{I}}(j) - min L_I(i))$; and at last, to estimate distributions of L_1 , L_2 for correction of the classification threshold in accordance with these distributions.

Program input parameters

All input parameters of the program are to be contained in the file "examld.inp". Example of this input file is given below

```
****INPUT FILE FOR PROGRAM EXAMLD: standard****
NAME OF FILE FOR MEAN VECTORS AND COVARIANCE MATRIX OF LEARNING DATA
data/troitsky/resku.dat
FEATURES TO BE USED OF UNSELECTED = 0; SELECTED = 1
0
NAME OF FILE FOR GRAPHIC RESULTS
plot/troitsky/examld.gr
```

Explanation of the program input parameters

NAME OF FILE FOR MEAN VECTORS AND COVARIANCE MATRIX OF LEARNING DATA

This is a name of file for reading of the Linear Discrimination Function parameters. File is produced by the program "ldstst".

FEATURES BEING USED: UNSELECTED = 0, SELECTED = 1

The parameter defines the feature set to be used for the cross validation procedure. If 0 is assigned, the program uses in this procedure the initial feature set, if 1 is , only the features selected by the program "fsel" are used in the procedure.

NAME OF GRAPHIC CONTROL FILE FOR PLOTTING OF CLASSIFICATION RESULTS

This a name of control file for the UNIX routine "plotxy" containing the commands for displaying of the program classification results.

1.6.6. Program "EXAMQD"

**Estimation of error probability by cross-validation method
using quadratic discriminator.**

The program "examqd" calculates by the statistically consistent cross-validation method (synonyms: Jack-knife, "plug-in" method) the estimates of classification error probabilities which quadratic discrimination function (QDF) provides for given set of learning observations. The QDF values obtained for every class learning vectors are ranked in their magnitudes. The points corresponding to this two ranked sets are displayed on the screen by using the standard UNIX routine "plotxy". This provides the descriptive graphical representation of the linear discriminator classification capability in regard of the given set of learning observations.

Quadratic discrimination function from feature vector X to be classified is defined by the equation:

$$Q(X) = \sum_{j=1}^p (x_j - m_j(2))^2 / \sigma_j^2(1) - \sum_{j=1}^p (x_j - m_j(1))^2 / \sigma_j^2(2) + \sum_{j=1}^p \ln(\sigma_j^2(1) / \sigma_j^2(2)),$$

where: x_j is j -th component of vector X being classified; $m_j(k)$ is j -th component of sample mean values vector $m(k)$ for learning vectors from class $k=1,2$; $\sigma_j^2(k)$ is the sample dispersion of j -th component for learning vectors vector from class $k=1,2$.
If $Q(X) > 0$, the quadratic classification algorithm relates the vector X to the class 2, else - to the class 1.

The equation above is derived under assumption that features are statistically independent. This assumption leads to simplified version of well known Quadratic Discrimination Function but allows to avoid difficulties accompanying to inversion of often near to singular sample covariance matrices for classes 1 and 2

The well known cross validation procedure for the case of QDF is completely the same as one for LDF (explained in the description of program "examld"). The program "examqd" generates the same output data as the program "examld".

Comparison of the probability error estimates provided by the programs "examld" and "examqd" allow to chose the most appropriate statistical classification algorithm: LDF or QDF, that guarantees the least misclassification probability for those statistical characteristic of the features which have been revealed from analysis of the learning vectors.

Program input parameters

All input parameters of the program are to be contained in the file "examqd.inp". Example of this input file is given below

```
****INPUT FILE FOR PROGRAM EXAMLD: standard****
NAME OF FILE FOR MEAN VECTORS AND COVARIANCE MATRIX OF LEARNING DATA
data/troitsky/resku.dat
FEATURES TO BE USED OF UNSELECTED = 0; SELECTED = 1
0
NAME OF FILE FOR GRAPHIC RESULTS
plot/troitsky/examqd.gr
```

Explanation of the program input parameters

NAME OF FILE FOR MEAN VECTORS AND COVARIANCE MATRIX OF LEARNING DATA

This is a name of file for reading of the Quadratic Discrimination Function parameters. File is produced by the program "ldstst".

FEATURES BEING USED: UNSELECTED=0, SELECTED=1

The parameter defines the feature set to be used for the cross validation procedure. If 0 is assigned, the program uses in this procedure the initial feature set, if 1 is assigned, only the features selected by the program "fsel" are used in the procedure.

NAME OF GRAPHIC CONTROL FILE FOR PLOTTING OF CLASSIFICATION RESULTS

This a name of control file for the UNIX routine "plotxy" containing the commands for displaying of the program classification results.

1.7. References

1. R.H. Shumway (1995) Statistical approach to seismic discrimination. *E. Husebye, A. Dainty (eds.) Monitoring of Comprehensive Test Ban Treaty*, pp. 791-805, NATO ASI Series, Kluwer Academic Publishers.
2. Y.Kakizawa, R.H. Shumway , M.Taniguchi (1996). Discrimination and clustering for multivariate time series. *Preprint of the paper submitted to Bull. Seism. Soc. Am*
3. A.D. Deev (1970) Representation of statistics of discrimination analysis and their asymptotic expansion for space dimension comparable with sample size. *Docl. Acad Nauk USSR*, v.195, pp. 759-762 (in Russian)
4. B.R. Levin, E.V. Troitsky (1970) Total probability error in classification of Gaussian populations differing in vectors of means. *Automatica and Telemekhanika*, n.1, pp. 54-56. (in Russian)
5. Sh. Yu. Raudis (1976) Limitations of sample size in classification problem. *Statistical Problems of Control*, issue N18, Publ. of Institute Physics and Mathematics AN Lit. SSR, Vilnius, (in Russian)
6. S.L. Tsvang, V.I. Pinsky, E.S. Husebye (1993) Enhanced seismic discrimination using NORESS recordings from European events. *Geophys. J. Intern*, v.112, pp. 1-14.
7. L.M.Haikin A.F.Kushnir, "Seismic network data analysis (SNDA)". Seismological problem oriented computer system. *Appendix to the Final report on EOARD Special Project SPC-95-4045*.
8. Das Gupta S. (1973). Theories and methods in classification. *Discriminant analysis and applications*. Ed. T.Cacoullos, Athens, Greece Academic Press, N-Y, L., pp. 77-137.
9. Sh. Yu. Raudis (1984). The influence of sample volume on classification quality. *Statistical Problems of Control*, issue N66, Publ. of Institute of Physics and Mathematics AN Lit. SSR, Vilnius, (in Russian).
10. S.A.Ivazian, V.M. Bukhshtaber, I.S.Eniukov, L.D.Meshalkin (1989). Applied Statistics.: Classification and decreasing of dimension. *Moscow. Finance and Statistics*.
11. E.V.Troitsky (1986). The classification of random observations 1. (The statistical methods of construction of the classification decision rules). *The mathematical methods of the geophysical information processing*. Publ. of Inst. Physics of Earth AN USSR, pp. 3-27 (in Russian).
12. E.V.Troitsky (1986). The classification of random observations 2. (The classification of the Gaussian distributed populations). *The mathematical methods of the geophysical information processing*. Publ. of Inst. Physics of Earth AN USSR, pp. 28-66 (in Russian).
13. C.R.Rao (1954). A general theory of discrimination when information about alternative populations is based on samples. *Ann. Math. Stat.*, V25, Num.4.

14. P.S. Dissart, J.J. Pulli (1990) Regional seismic event discrimination at the NORESS array: seismological measurements and the use of trained neural networks. *Bull. Seism. Soc. Am.*, V.80, N6, pp. 1910-1993.
15. D.N. Anderson, K.K. Anderson, D.N. Hagedorn, S.R. Sain, C.J. Young (1995). Statistical frameworks for seismic discrimination. *Proceedings of the 17th annual seismic research symposium on monitoring a comprehensive test ban treaty. AFOSR, USA*, pp. 18-26.
16. Indra N. Gupta (1995). Study of broadband Lg/P and its application to source discrimination *Proceedings of the 17th annual seismic research symposium on monitoring a comprehensive test ban treaty. AFOSR, USA*, pp. 38-46.
17. W.-Y. Kim, V. Aharonian, G. Abbers, A. Lerner-Lam and P. Richards (1995). Discrimination of earthquakes and explosions in Southern Russia using regional high frequency data from IRIS/JSP Caucasus network. *Proceedings of the 17th annual seismic research symposium on monitoring a comprehensive test ban treaty. AFOSR, USA*, pp. 68-77.
18. K. Fukunaga, D.L. Kessel (1971) Estimation of classification errors. *IEEE Trans. on Comp.* v.C-20, N12, pp. 136-143.
19. Gitterman, Y. and T. van Eck, (1993). Spectra of quarry blasts and microearthquakes recorded at local distances in Israel, *Bull. Seism. Soc. Am.*, 83, pp. 1799-1812.
20. A.F.Kushnir (Ed.) Three component micro and small aperture arrays in noisy environment: development of statistical data processing techniques. *Feasibility study report on Special project SPC-95-4045. Moscow IRIS Data Analysis Center/SYNAPSE Science Center, EOARD, September 1995.*
21. V.I.Keilis-Borok, E.N.Lukina, I.M.Rotvine, E.Harn (1982) Long-term seismological predictors of strong earthquakes. Bursts of aftershocks in South America. *Mathematical models of the Earth structure and the earthquake prediction.*(Computational seismology, issue N14) M. "Nauka" (in Russian)
- 22.Sh.Y.Raudis (1975) Classification errors for quadratic discriminant function. *Statistical problems of control, issue N14. Publ of Institute of Physics and Mathematics Vilnius, AN Lit. SSR*, pp.33-49. (in Russian).
23. E.V.Troitsky (1981) Comparison of linear and quadratic discriminators in condition of limited size of learning samples. *Statistical problems of control, issue N50. Publ of Institute of Physics and Mathematics ,Vilnius, AN Lit. SSR*, pp.31-47. (in Russian).

1.8. Appendix

Appendix 1

```

#   SCRIPT FOR SELECTION OF EXPLOSIONS FOR CLASSIFICATION
#
#       script troitsky/isrdtp/selexpl1.scr
. char path[]="/detseis/seis/alex/data/israel/explos/"
. int i
. char dt[26][10],      k[26][6],      f[26][10],      r[26][10],      d[26][10]
#       identifier      initial keep      flush poor      final keep      dist: near far
.&& t[1]="8906201018"; k[1]="42"; f[1]="35 40"; r[1]="12 23"; d[1]="49 134"
.&& t[2]="8911081109"; k[2]="42"; f[2]="35 40"; r[2]="17 22"; d[2]="87 144"
.&& t[3]="9003271037"; k[3]="42"; f[3]="35 40"; r[3]="14 25"; d[3]="77 160"
.&& t[4]="9004041301"; k[4]="42"; f[4]="35 40"; r[4]="16 22"; d[4]="61 137"
.&& t[5]="9006130742"; k[5]="42"; f[5]="35 40"; r[5]="7 22"; d[5]="28 140"
.&& t[6]="9007231222"; k[6]="42"; f[6]="35 40"; r[6]="12 19"; d[6]="39 92"
.&& t[7]="9007260957"; k[7]="42"; f[7]="28 29"; r[7]="7 23"; d[7]="24 192"
.&& t[8]="9008120753"; k[8]="42"; f[8]="28 29"; r[8]="7 13"; d[8]="46 145"
.&& t[9]="9008281424"; k[9]="36"; f[9]="28 29"; r[9]="10 15"; d[9]="37 91"
.&& t[10]="9010161405"; k[10]="42"; f[10]="36 39"; r[10]="11 23"; d[10]="52 137"
.&& t[11]="9011061243"; k[11]="42"; f[11]="36 39"; r[11]="11 23"; d[11]="37 133"
.&& t[12]="9012181223"; k[12]="42"; f[12]="36 39"; r[12]="21 23"; d[12]="97 137"
.&& t[13]="9101091411"; k[13]="42"; f[13]="36 39"; r[13]="18 24"; d[13]="72 136"
.&& t[14]="9102111255"; k[14]="42"; f[14]="36 39"; r[14]="12 35"; d[14]="56 231"
.&& t[15]="9102121205"; k[15]="42"; f[15]="36 46"; r[15]="12 23"; d[15]="59 135"
.&& t[16]="9103121106"; k[16]="46"; f[16]="36 46"; r[16]="17 27"; d[16]="78 155"
.&& t[17]="9103170920"; k[17]="46"; f[17]="36 46"; r[17]="17 27"; d[17]="69 185"
.&& t[18]="9103191402"; k[18]="48"; f[18]="36 46"; r[18]="21 28"; d[18]="71 136"
.&& t[19]="9103211208"; k[19]="50"; f[19]="36 46"; r[19]="17 28"; d[19]="60 134"
.&& t[20]="9104140830"; k[20]="50"; f[20]="36 46"; r[20]="22 28"; d[20]="68 142"
.&& t[21]="9105061241"; k[21]="50"; f[21]="36 46"; r[21]="10 28"; d[21]="34 150"
.&& t[22]="9105081304"; k[22]="50"; f[22]="36 46"; r[22]="22 29"; d[22]="71 134"
.&& t[23]="9106170643"; k[23]="44"; f[23]="36 44"; r[23]="16 17"; d[23]="52 72"
.&& t[24]="9108121303"; k[24]="50"; f[24]="36 44"; r[24]="22 31"; d[24]="70 164"
.&& t[25]="9108181502"; k[25]="50"; f[25]="36 44"; r[25]="12 33"; d[25]="37 160"

. for (i=1; i<26; i=i+1)
    clearstack
    && unix uncompress &path.&t[i]..a.Z ; readmem &path.&t[i]..a
    filterB all -L2.0 -H15.0 -THP -P2
    && keep &k[i]; plot all -y; flush (&f[i]); episort1; plot all -y
    savepack &path.&t[i]..pk
    && flist all plot/troitsky/mask1; map plot/troitsky/israel.par
    && keep (&r[i]); plot all -y ; savepack &path.&t[i].sel.pk;
    && unix compress &path.&t[i]..a ; pause
. endfor

```

Appendix 2

```

.
#      SCRIPT FOR MEASURING OF EARTQUAKE P AND S POWER FEATURES
#      script troi/isrdtp/earthmeas.scr

. char nr[28], far[28], text[80], evnm[28], evtp[80]
. char dist[10], path[80], qualn[10], qualf[10], text1[80]
. int count, cyc, mod, nc, ncl

# ASSINING TIME INTERVALS OF P AND S PHASES:  mod = 0 ;
# PARAMETER MEASURING:  mod = 1
. mod = 0;  evtp ="EARTHQUAKE";  path ="data/israel/earthq/"

. char identif[29][12]
. && identif[1] = "8802241537" ;  identif[15] = "8802241537"
. && identif[2] = "8802241537" ;  identif[16] = "8802241537"
. && identif[3] = "8802241537" ;  identif[17] = "8802241537"
. && identif[4] = "8802241537" ;  identif[18] = "8802241537"
. && identif[5] = "8802241537" ;  identif[19] = "8802241537"
. && identif[6] = "8802241537" ;  identif[20] = "8802241537"
. && identif[7] = "8802241537" ;  identif[21] = "8802241537"
. && identif[8] = "8802241537" ;  identif[22] = "8802241537"
. && identif[9] = "8802241537" ;  identif[23] = "8802241537"
. && identif[10] = "8802241537" ;  identif[24] = "8802241537"
. && identif[11] = "8802241537" ;  identif[25] = "8802241537"
. && identif[12] = "8802241537" ;  identif[26] = "8802241537"
. && identif[13] = "8802241537" ;  identif[27] = "8802241537"
. && identif[14] = "8802241537" ;  identif[28] = "8802241537"

. for (cyc=1; cyc<29; cyc= cyc+1)
.   evnm = identif[cyc]
.   sndf11=0; sndf12=0; sndf21=0; sndf22=0; sndf31=0; sndf32=0
.   sndf41=0; sndf42=0; sndf51=0; sndf52=0; sndf61=0; sndf62=0
.   perform switcher # SET NEXT EARTHQUAKE PARAMETERS
.   clearstack
.   dist = "distance="
.   perform readwave # READING WAVETRAIN
.   for (count =0; count <2; count = count+1)
.     perform multfilt # WAVETRAIN MULTIBAND FILTERING
.     when (mod =1)
.       perform calcspec # CALCULATING SPECTRA
.       perform measuring # MEASURING PHASE BAND POWER FEATURES
.       perform savepar # SAVING SPECTRAL FEATURES FOR SIGN+NOISE
.       echo GO TO FAR EVENT
.     endwhen
.     flush 5
.   endfor
.   echo END OF EVENT FEATURE MEASURING
.   echo GO TO ANOTHER EVENT
. endfor
. return

##### EVENT SWITCER #####

# LIST OF EVENT INFORMATION
# NEAR EVENTS:
# sndf11 = Start point of noise (sec)
# sndf12 = Length of noise (sec)
# sndf21 = Start point of P-wave (sec)
# sndf22 = Length of P-wave (sec)
# sndf31 = Start point of S-wave (sec)

```



```

# sndf32 = Length of S-wave (sec)

# FAR EVENTS:
# sndf41 = Start point of noise (sec)
# sndf42 = Length of noise (sec)
# sndf51 = Start point of P-wave (sec)
# sndf52 = Length of P-wave (sec)
# sndf61 = Start point of S-wave (sec)
# sndf62 = Length of S-wave (sec)

. switcher block
.   when (cyc=1) # St JVI, St DOR
.     && qualn = "h"; nr = "82"; sndf11 = 0.1; sndf12 = 34
.     && sndf21 = 35.5; sndf22 = 5; sndf31 = 47; sndf32 = 10
.     && qualf = "h"; far = "140"; sndf41 = 0.1; sndf42 = 43
.     && sndf51 = 44.5; sndf52 = 5; sndf61 = 62.5; sndf62 = 9
.   elseif (cyc=2) # St JVI, St DOR
.     && qualn = "h"; nr = "82"; sndf11 = 21.862; sndf12 = 6.45
.     && sndf21 = 31.2; sndf22 = 5; sndf31 = 42.8; sndf32 = 8.4
.     && qualf = "m"; far = "144"; sndf41 = 1.1; sndf42 = 34.9
.     && sndf51 = 39.5; sndf52 = 6.2; sndf61 = 59.2; sndf62 = 4.7
.   elseif (cyc=3) # St ADI, St PRNI
.     && qualn = "h"; nr = "37.5"; sndf11 = 1.; sndf12 = 25.5
.     && sndf21 = 29.; sndf22 = 3.9; sndf31 = 34.; sndf32 = 2.6
.     && qualf = "m"; far = "59.5"; sndf41 = 19.36; sndf42 = 11.6
.     && sndf51 = 33.4; sndf52 = 4.9; sndf61 = 41.; sndf62 = 4.3
.   elseif (cyc=4) # St DSI, St ZNT
.     && qualn = "m"; nr = "??"; sndf11 = 1.9; sndf12 = 35.8
.     && sndf21 = 42.8; sndf22 = 4.7; sndf31 = 58.6; sndf32 = 12.2
.     && qualf = "m"; far = "??"; sndf41 = 3.; sndf42 = 53.
.     && sndf51 = 61.4; sndf52 = 9.2; sndf61 = 94.; sndf62 = 13.6
.   elseif (cyc=5) # St ZNT, St DSI
.     && qualn = "h"; nr = "90"; sndf11 = 0.9; sndf12 = 41.6
.     && sndf21 = 44.9; sndf22 = 4.5; sndf31 = 56.8; sndf32 = 8.4
.     && qualf = "h"; far = "157"; sndf41 = 0.9; sndf42 = 51.6
.     && sndf51 = 55.5; sndf52 = 8; sndf61 = 76; sndf62 = 9
.   elseif (cyc=6) # St JVI, St DSI
.     && qualn = "l"; nr = "83"; sndf11 = 19.3; sndf12 = 10.9
.     && sndf21 = 50.; sndf22 = 4.7; sndf31 = 61.1; sndf32 = 9.5
.     && qualf = "l"; far = "123"; sndf41 = 0.7; sndf42 = 52.9
.     && sndf51 = 55.8; sndf52 = 4.6; sndf61 = 71.9; sndf62 = 9.7
.   elseif (cyc=7) # St MML, St DSI
.     && qualn = "h"; nr = "63"; sndf11 = 2.; sndf12 = 35.5
.     && sndf21 = 39.6; sndf22 = 2.8; sndf31 = 48.1; sndf32 = 4.6
.     && qualf = "m"; far = "152"; sndf41 = 1.2; sndf42 = 45.7
.     && sndf51 = 53.6; sndf52 = 5.7; sndf61 = 72.4; sndf62 = 5.9
.   elseif (cyc=8) # St MML, St DSI
.     && qualn = "m"; nr = "71"; sndf11 = 1.9; sndf12 = 25.9
.     && sndf21 = 34.6; sndf22 = 5.3; sndf31 = 44.; sndf32 = 13.8
.     && qualf = "h"; far = "159"; sndf41 = 1.5; sndf42 = 43.8
.     && sndf51 = 47.9; sndf52 = 6.; sndf61 = 68.2; sndf62 = 6.8
.   elseif (cyc=9) # St KSHT, St MSDA
.     && qualn = "l"; nr = "56"; sndf11 = 2.1; sndf12 = 30.4
.     && sndf21 = 35.9; sndf22 = 5.; sndf31 = 45.9; sndf32 = 5.5
.     && qualf = "l"; far = "164"; sndf41 = 3.; sndf42 = 48.8
.     && sndf51 = 54.7; sndf52 = 7.2; sndf61 = 75.4; sndf62 = 10.1
.   elseif (cyc=10) # St MML, St ZNT
.     && qualn = "h"; nr = "22"; sndf11 = 2.1; sndf12 = 22.9
.     && sndf21 = 28.1; sndf22 = 3.0; sndf31 = 32.0; sndf32 = 6.3
.     && qualf = "m"; far = "39"; sndf41 = 1.8; sndf42 = 27.4
.     && sndf51 = 30.6; sndf52 = 4.1; sndf61 = 37.5; sndf62 = 4.3
.   elseif (cyc=11) # St MML, St ZNT

```

```

.      && qualn = "h";      nr = "48";      sndf11 = 2.2;      sndf12 = 28.6
.      && sndf21 = 33.;      sndf22 = 4.4;      sndf31 = 39.1;      sndf32 = 5.7
.      && qualf = "h";      far = "143";      sndf41 = 2.0 ;      sndf42 = 42.
.      && sndf51 = 47.7;      sndf52 = 8.1;      sndf61 = 65.2;      sndf62 = 8.5
.  elseif (cyc=12) # St HMDT, St DSI
.      && qualn = "m";      nr = "64";      sndf11 = 2.1;      sndf12 = 36.6
.      && sndf21 = 43.2;      sndf22 = 5.9;      sndf31 = 52.1;      sndf32 = 7.8
.      && qualf = "m";      far = "135";      sndf41 = 1.8 ;      sndf42 = 48.5
.      && sndf51 = 53.7;      sndf52 = 6.4;      sndf61 = 70.9;      sndf62 = 7.8
.  elseif (cyc=13) # St MML, St SDOM
.      && qualn = "h";      nr = "41";      sndf11 = 2.;      sndf12 = 31.9
.      && sndf21 = 35.9;      sndf22 = 4.8;      sndf31 = 41.5;      sndf32 = 5.
.      && qualf = "m";      far = "189";      sndf41 = 3.5 ;      sndf42 = 39.8
.      && sndf51 = 48.1;      sndf52 = 4.8;      sndf61 = 56.;      sndf62 = 3.1
.  elseif (cyc=14) # St ZNT, St BGI
.      && qualn = "l";      nr = "66";      sndf11 = 2.5;      sndf12 = 33.5
.      && sndf21 = 40.7;      sndf22 = 7.2;      sndf31 = 51.8;      sndf32 = 5.3
.      && qualf = "l";      far = "120";      sndf41 = 3.5 ;      sndf42 = 39.8
.      && sndf51 = 48.8;      sndf52 = 4.6;      sndf61 = 64.9;      sndf62 = 9.8
.  elseif (cyc=15) # St ZNT, St BGI
.      && qualn = "m";      nr = "69";      sndf11 = 1.5;      sndf12 = 34.6
.      && sndf21 = 41.8;      sndf22 = 5.;      sndf31 = 49.6;      sndf32 = 11.1
.      && qualf = "m";      far = "122";      sndf41 = 1.7 ;      sndf42 = 42.9
.      && sndf51 = 49.6;      sndf52 = 6.1;      sndf61 = 65.2;      sndf62 = 17.9
.  elseif (cyc=16) # St HMDT, St DSI
.      && qualn = "h";      nr = "66";      sndf11 = 2.;      sndf12 = 41.8
.      && sndf21 = 48.1;      sndf22 = 6.6;      sndf31 = 57.1;      sndf32 = 10.4
.      && qualf = "h";      far = "143";      sndf41 = 2.;      sndf42 = 55.
.      && sndf51 = 60.5;      sndf52 = 8.6;      sndf61 = 79.;      sndf62 = 11.8
.  elseif (cyc=17) # St JVI, St YTIR
.      && qualn = "h";      nr = "72";      sndf11 = 8.9;      sndf12 = 28.6
.      && sndf21 = 40.4;      sndf22 = 5.7;      sndf31 = 49.6;      sndf32 = 12.1
.      && qualf = "h";      far = "137";      sndf41 = 2.2 ;      sndf42 = 43.3
.      && sndf51 = 50.6;      sndf52 = 7.;      sndf61 = 67.1;      sndf62 = 18.1
.  elseif (cyc=18) # St GVMR, St JVI
.      && qualn = "h";      nr = "67";      sndf11 = 1.1 ;      sndf12 = 36.2
.      && sndf21 = 39.7;      sndf22 = 5.1;      sndf31 = 48.9;      sndf32 = 7.3
.      && qualf = "h";      far = "131";      sndf41 = 1.6;      sndf42 = 45.4
.      && sndf51 = 49.1;      sndf52 = 8.1;      sndf61 = 65.9;      sndf62 = 17.5
.  elseif (cyc=19) # St HMDT, St JVI
.      && qualn = "m";      nr = "65";      sndf11 = 1.7;      sndf12 = 34.5
.      && sndf21 = 39.8;      sndf22 = 7.2;      sndf31 = 48.4;      sndf32 = 8.9
.      && qualf = "m";      far = "103";      sndf41 = 1.7;      sndf42 = 39.3
.      && sndf51 = 45.8;      sndf52 = 9.9;      sndf61 = 59.;      sndf62 = 11.8
.  elseif (cyc=20) # St HMDT, St DSI
.      && qualn = "h";      nr = "65.5";      sndf11 = 1.6 ;      sndf12 = 37.7
.      && sndf21 = 43.3;      sndf22 = 7.5;      sndf31 = 52.4;      sndf32 = 15.1
.      && qualf = "h";      far = "143";      sndf41 = 2.3 ;      sndf42 = 50.1
.      && sndf51 = 55.4;      sndf52 = 12.5;      sndf61 = 72.4;      sndf62 = 19.
.  elseif (cyc=21) # St KSHT, St HMDT
.      && qualn = "m";      nr = "30";      sndf11 = 2.5;      sndf12 = 2
.      && sndf21 = 31.4;      sndf22 = 2.5      sndf31 = 35.;      sndf32 = 8.5
.      && qualf = "m";      far = "63";      sndf41 = 5.9 ;      sndf42 = 23.3
.      && sndf51 = 36.5;      sndf52 = 5.9;      sndf61 = 44.5;      sndf62 = 15.7
.  elseif (cyc=22) # St HMDT, St DSI
.      && qualn = "h";      nr = "65";      sndf11 = 2.5;      sndf12 = 38.9
.      && sndf21 = 44.2;      sndf22 = 6.4;      sndf31 = 53.4;      sndf32 = 10.1
.      && qualf = "m";      far = "143";      sndf41 = 2.5 ;      sndf42 = 48.1
.      && sndf51 = 56.2;      sndf52 = 8.9;      sndf61 = 73.8;      sndf62 = 17.6
.  elseif (cyc=23) # St MML, St BRNI
.      && qualn = "m";      nr = "48";      sndf11 = 1.2 ;      sndf12 = 26.7
.      && sndf21 = 30.7;      sndf22 = 5.5;      sndf31 = 37.7;      sndf32 = 8.9

```

```

.      && qualf = "l";   far = "56";   sndf41 =1.4 ;   sndf42 =24.7
.      && sndf51 =34.6;   sndf52 =4.;   sndf61 =41.3;   sndf62 =13.2
.      elseif (cyc=24) # St HRI, St HMDT
.      && qualn = "m";   nr = "48";   sndf11 =2.;   sndf12 =28.4
.      && sndf21 =33.3;   sndf22 =5.8;   sndf31 =40.6;   sndf32 =13.7
.      && qualf = "l";   far = "65";   sndf41 =2.2 ;   sndf42 =28.2
.      && sndf51 =35.7;   sndf52 =6.4;   sndf61 =44.6;   sndf62 =12.2
.      elseif (cyc=25) # St HMDT, St DSI
.      && qualn = "h";   nr = "64";   sndf11 = 2.4;   sndf12 =38.6
.      && sndf21 =43.9;   sndf22 =5.1;   sndf31 =52.6;   sndf32 =17.3
.      && qualf = "h";   far = "141";
sndf41 =2.1 ; sndf42 =50.1
.      && sndf51 =55.9;   sndf52 =7.2;   sndf61 =73.2;   sndf62 =21.2
.      elseif (cyc=26) # St MML, St HMDT
.      && bqualn = "m";   nr = "46";   sndf11 = 1.7;   sndf12 =26.7
.      && sndf21 =30.8;   sndf22 =4.9;   sndf31 =37.5;   sndf32 =6.4
.      && qualf = "l";   far = "63";   sndf41 =1.1 ;   sndf42 =29.
.      && sndf51 =33.5;   sndf52 =6.2;   sndf61 =42.6;   sndf62 =8.3
.      elseif (cyc=27) # St MML, St DSI
.      && qualn = "h";   nr = "82";   sndf11 =1.7 ;   sndf12 =41.4
.      && sndf21=45.6;   sndf22 =7.3;   sndf31 =54.8;   sndf32 =18.7
.      && qualf = "h";   far = "172";   sndf41 =2.2;   sndf42 =53.4
.      && sndf51 =59.3;   sndf52 =9.8;   sndf61 =80.;   sndf62 =18.5
.      elseif (cyc=28) # St HRI, St MSDA
.      && qualn = "h";   nr = "83";   sndf11 =2. ;   sndf12 =30.8
.      && sndf21=35.2;   sndf22 =4.7;   sndf31 =45.8;   sndf32 =6.4
.      && qualf = "h";   far = "155";   sndf41 =2.4;   sndf42 =40.7
.      && sndf51 =47.5;   sndf52 =7.5;   sndf61 =66.8;   sndf62 =12.9

.endblock of switcher

```

``` ##### READING WAVETRAINS AND FILTERING ##### ```

```

. block readwave
.   text = "0 -3. 0.14"
.   text1 = "SPECTRA OF EARTHQUAKE PHASES AND PRECEEDING NOISE"
.   unix /usr/bin/rm data/troitsky/spctl.bb
.   savevar data/troitsky/spctl.bb text text1

.   echo READING WAVETRAIN
.   text = "sel.pk"
.   readpack &path.&evnm.&text
.   notes (1) 1 0.7 m &cyc &evtp &evnm
.   notes (1) 1 0.4 m &dist &nr
.   notes (2) 1 0.7 m &cyc &evtp &evnm
.   notes (2) 1 0.4 m &dist &far
.   plot all -y
.   #savepack &path.&evnm.&text
.endblock

```

``` ##### WAVETRAIN MULTIBAND FILTERING ##### ```

```

. block multfilt
. echo WAVETRAIN MULTIBAND FILTERING
filterB (1) -L1. -H3. -R5 -TBP -P2
notes (1) 1 0.7 m 1-3 Hz
&& move 1 2; filterB (1) -L3. -H6. -R5 -TBP -P2
notes (1) 1 0.7 m 3-6 Hz
&& move 1 3; filterB (1) -L6. -H10. -R5 -TBP -P2
notes (1) 1 0.7 m 6-10 Hz
&& move 1 4; filterB (1) -L10. -H15. -R5 -TBP -P2
notes (1) 1 0.7 m 10-15 Hz
move 1 5

. float vert

```

```

vertical
. when (count = 0)
    vertical b o &sndf11;
.    vert = sndf11 + sndf12
    && vertical b o &vert; vertical u o &sndf21
.    vert = sndf21 + sndf22
    && vertical u o &vert; && vertical r o &sndf31
.    vert = sndf31 + sndf32
    vertical r o &vert
. else
    vertical b o &sndf41
.    vert = sndf41 + sndf42
    && vertical b o &vert; vertical u o &sndf51
.    vert = sndf51 + sndf52
    && vertical u o &vert; vertical r o &sndf61
.    vert = sndf61 + sndf62
    vertical r o &vert
. endwhen
plot 5
.endblock
##### CALCULATING SPECTRA #####
. block calcspec
. echo CALCULATING SPECTRA
. char epidis[25]
. when (count = 0)
.    && epidis = nr; text = "nr"
    winon &sndf11 &sndf12
. else
.    epidis = far; text = "far"
    winon &sndf41 &sndf42
. endwhen
&& powspec (1) 50 5; rename (1) NOISE_&text
&& notes (1) 1 0.7 m &cyc &evtp &evnm &dist &epidis

    winoff
. when(count = 0)
    winon &sndf21 &sndf22
.    text = "nr"
. else
    winon &sndf51 &sndf52
.    text = "far"
. endwhen
&& powspec (2) 50 5; rename (1) P-WAVE_&text
&& notes (1) 1 0.7 m &cyc &evtp &evnm &dist &epidis

    winoff
. when (count = 0)
    winon &sndf31 &sndf32
.    text = "nr"
. else
    winon &sndf61 &sndf62
.    text = "far"
. endwhen
&& spec (3) 50 5; rename (1) S-WAVE_&text
&& notes (1) 1 0.7 m &cyc &evtp &evnm &dist &epidis; winoff
#-----#-----#-----#-----#-----#-----#-----#-----#-----#
. echo PLOTTING AND SAVING EVENT SPECTRA
#plotspec (1-3) -GO
#plotspec (1-3) -GO -Cdata/troitsky/spctl.bb
#plot all -y
#pause
#unix lpr -P1 plot/snda.ps

```

```

&& chanon 3;    savepack &path.&evnm.&text.sp.pk
&& chanoff;    flush 3
#pause
. endblock
#####
. block measuring
. echo MEASURING PHASE BAND POWER FEATURES
. echo SAVING EVENT NAME, STAION DISTANCES AND PHASE INTERVALS
. text = " "
. savevar data/troitsky/earthpf.bb cyc
. savevar data/troitsky/earthpf.bb evtp evnm
. text = "noise_start, noise_len, P_start, P_len, S_start, S_len"
. when (count = 0)
.   savevar data/troitsky/earthpf.bb dist nr
.   savevar data/troitsky/earthpf.bb text ;
.   savesnd data/troitsky/earthpf.bb
sndf11,sndf12,sndf21,sndf22,sndf31,sndf32
. else
.   savevar data/troitsky/earthpf.bb dist far
.   savevar data/troitsky/earthpf.bb text
.   savesnd data/troitsky/earthpf.bb
sndf41,sndf42,sndf51,sndf52,sndf61,sndf62
. endwhen
sqr (1-5) total
. echo NOISE MEASURING
.float strt, len
. when (count = 0)
.   && strt = sndf11; len = sndf22
. else
.   && strt = sndf41; len = sndf42
. endwhen
. float np[5]
mean (1-5) &strt &len np
. text = "Av N band powers"
. savevar data/troitsky/earthpf.bb text
. savevar data/troitsky/earthpf.bb np
#-----#-----#-----#-----#-----#-----#-----#-----#-----#
. echo P-WAVE MEASURING
. when (count = 0)
.   && strt = sndf21; len = sndf22
. else
.   && strt = sndf51; len = sndf52
. endwhen
# P+N MAX POWER IN FRQ BANDS
. float tmx[5], pamx[5]
tmax (1-5) &strt &len tmx pamx
#. text = "Max(P+N) band squar amplitudes"
#. savevar data/troitsky/earthpf.bb text
. savevar data/troitsky/earthpf.bb pamx

winon &strt &len
. float tmxw[5]
. for (nc = 0; nc < 5; nc = nc+1)
.   tmxw[nc] = tmx[nc] - strt
. endfor
&& vertical; vertical r o &tmxw[0]; vertical b o &tmxw[1]
&& vertical u o &tmxw[2]; vertical r o &tmxw[3];
vertical u o &tmxw[4]
. text = "P-wave"
&& notes (1) 1 -0.4 m &text; plot 5 -y; winoff

# 'Pure' P MAX POWER IN FRQ BANDS

```



```
&& notes (1) 1 -0.4 m &text; plot 5 -y

winoff
. for (nc=0; nc<5; nc = nc+1)
.   tmxw[nc] = tmx[nc] - 0.5
.endfor
. float spm[5], snpm[5]
. for (nc=0; nc<5; nc = nc+1)
.   && ncl=nc +1; spm[nc]=aux[0]; snpm[nc]=spm[nc]-np[nc]
.     mean (&ncl) &tmxw[nc] 1 aux
. endfor
. text = "Max(S+N) band powers"
. savevar data/troitsky/earthpf.bb text
. savevar data/troitsky/earthpf.bb spm
. text = "'Pure' MaxS band powers"
. savevar data/troitsky/earthpf.bb text
. savevar data/troitsky/earthpf.bb snpm

# S+N AVERAGED POWERS IN FRQ BANDS
. float sp[5]
. mean (1-5) &strt &len sp
. text = "Av(S+N) band powers"
. savevar data/troitsky/earthpf.bb text
. savevar data/troitsky/earthpf.bb sp

# "PURE" S AVERAGED POWERS IN FRQ. BANDS
. float snp[5]
. for (nc=0; nc<5; nc = nc+1)
.   snp[nc] = sp[nc] - np[nc]
. endfor
. text = "'Pure' AvS band powers"
. savevar data/troitsky/earthpf.bb text
. savevar data/troitsky/earthpf.bb snp

# S+N SPECTRAL SHAPE; 'PURE' S SPECTRAL SHAPE

. float srb[4], srbn[4]
. for (nc=0; nc<4; nc = nc+1)
.   srb[nc] = sp[nc+1] / sp[0]
.   srbn[nc] = snp[nc+1] / snp[0]
. endfor
. text = "Av(S+N) ratios of band powers to total power"
. savevar data/troitsky/earthpf.bb text ;
. savevar data/troitsky/earthpf.bb srb
. text = "'Pure'AvS ratios of band powers to total power"
. savevar data/troitsky/earthpf.bb text ;
. savevar data/troitsky/earthpf.bb srbn
#-----#-----#-----#-----#-----#-----#-----#-----#-----#-----#-----#-----#
. echo CALCULATION OF S-P FREQ.BAND POWER RATIOS

# RATIOS OF SQUARES OF MAX S+N AMPL TO MAX P+N AMPL
. float mspar[5], mspr[5], mnspr[5], spr[5], nspr[5]
. for (nc=0; nc<5; nc = nc+1)
.   mspar[nc] = samx[nc] / pamx[nc]
.   mspr [nc] = spm[nc] / ppm[nc]
.   mnspr[nc] = snpm[nc] / pnpm[nc]
.   spr [nc] = sp[nc] / pp[nc]
.   nspr[nc] = snp[nc] / pnp[nc]
. endfor
. text = "Max(S+N)/Max(P+N) square amplitude ratios in fr. bands"
. savevar data/troitsky/earthpf.bb text
. savevar data/troitsky/earthpf.bb mspar
```

```

. text = "Max(S+N)/Max(P+N) ratios for band powers "
. savevar data/troitsky/earthpf.bb text
. savevar data/troitsky/earthpf.bb mspr
. text = "'Pure' MaxS/MaxP ratios for band powers "
. savevar data/troitsky/earthpf.bb text
. savevar data/troitsky/earthpf.bb mnspr
. text = "Av(S+N)/Av(P+N) ratios for band powers "
. savevar data/troitsky/earthpf.bb text
. savevar data/troitsky/earthpf.bb spr
. text = " 'Pure' AvS/AvP ratios for band powers"
. savevar data/troitsky/earthpf.bb text
. savevar data/troitsky/earthpf.bb nspr
. endblock of measuring
##### SAVING SPECTRAL FEATURES FOR SIGN+NOISE #####

```

```

.block savepar
. echo SAVING SPECTRAL FEATURES FOR SIGN+NOISE

. text = "Av(P+N) band powers"
. savevar data/troitsky/earthpf.bb text
. savevar data/troitsky/earthpf.bb pp
. text = "Max(P+N) band powers"
. savevar data/troitsky/earthpf.bb text
. savevar data/troitsky/earthpf.bb ppm
. text = "Av(S+N) band powers"
. savevar data/troitsky/earthpf.bb text
. savevar data/troitsky/earthpf.bb sp
. text = "Max(S+N) band powers"
. savevar data/troitsky/earthpf.bb text
. savevar data/troitsky/earthpf.bb spm
. text = "Av(P+N) ratios of band powers to total power"
. savevar data/troitsky/earthpf.bb text
. savevar data/troitsky/earthpf.bb prb
. text = "Av(S+N) ratios of band powers to total power"
. savevar data/troitsky/earthpf.bb text
. savevar data/troitsky/earthpf.bb srb
. text = "Av(S+N)/Av(P+N) ratios for band powers "
. savevar data/troitsky/earthpf.bb text
. savevar data/troitsky/earthpf.bb spr
. text = "Max(S+N)/Max(P+N) amplitude ratio"
. savevar data/troitsky/earthpf.bb text
. savevar data/troitsky/earthpf.bb mspar
. text = "Max(S+N)/Max(P+N) ratios for band powers "
. savevar data/troitsky/earthpf.bb text
. savevar data/troitsky/earthpf.bb mspr
. echo SAVING SPECTRAL FEATURES FOR FOR 'PURE' SIGNAL
. text = "'Pure' AvP band powers"
. savevar data/troitsky/earthpf.bb text
. savevar data/troitsky/earthpf.bb pnp
. text = "'Pure' MaxP band powers"
. savevar data/troitsky/earthpf.bb text
. savevar data/troitsky/earthpf.bb pnpm
. text = "'Pure' AvS band powers"
. savevar data/troitsky/earthpf.bb text
. savevar data/troitsky/earthpf.bb snp
. text = "'Pure' MaxS band powers"
. savevar data/troitsky/earthpf.bb text
. savevar data/troitsky/earthpf.bb snpm
. text = "'Pure' AvP ratios of band power to total power"
. savevar data/troitsky/earthpf.bb text
. savevar data/troitsky/earthpf.bb prbn
. text = " 'Pure'AvS ratios of band powers to total power"

```



```

. savevar data/troitsky/earthpf.bb text
. savevar data/troitsky/earthpf.bb srbn
. text = " 'Pure' AvS/AvP ratios for band powers"
. savevar data/troitsky/earthpf.bb text
. savevar data/troitsky/earthpf.bb nspr
. text = " 'Pure' MaxS/MaxP ratios for band powers "
. savevar data/troitsky/earthpf.bb text
. savevar data/troitsky/earthpf.bb mnspr
.endblock
end of script
*****

```

Appendix 3.

Labels of features obtained with the help of
"filtration" method for "pure" variant

1prbp1 avp (P, D1) / avp (P, D0)	10msprp1-	maxp (S, D1) / maxp (P, D1)
2prbp2 avp (P, D2) / avp (P, D0)	11msprp2-	maxp (S, D2) / maxp (P, D2)
3prbp3 avp (P, D3) / avp (P, D0)	12msprp3-	maxp (S, D3) / maxp (P, D3)
4prbp4 avp (P, D4) / avp (P, D0)	13msprp4-	maxp (S, D4) / maxp (P, D4)
5srbp1 avp (S, D1) / avp (S, D0)	14asprp0-	avp (S, D0) / avp (P, D0)
6srbp2 avp (S, D2) / avp (S, D0)	15asprp1-	avp (S, D1) / avp (P, D1)
7srbp3 avp (S, D3) / avp (S, D0)	16asprp2-	avp (S, D2) / avp (P, D2)
8srbp4 avp (S, D4) / avp (S, D0)	17asprp3-	avp (S, D3) / avp (P, D3)
9msprp0	maxp (S, D0) / maxp (P, D0)	18asprp4-
		avp (S, D4) / avp (P, D4)

The labels of features obtained with the help of "FFT" method for "pure" variant

1psmfp fmax (P)	9sbrp3 avp (S, D3) / avp (S, D0)
2pbrp1 avp (P, D1) / avp (P, D0)	10sbrp4
3pbrp	avp (P, D2) / avp (P, D0)
4pbrp3 avp (P, D3) / avp (P, D0)	11rmspp
5pbrp4 avp (P, D4) / avp (P, D0)	Maxsd (S, D0) / Maxsd (P, D0)
6ssmfp fmax (S)	12spbrp0-
7sbrp1 avp (S, D1) / avp (S, D0)	avp (S, D0) / avp (P, D0)
8sbrp2 avp (S, D2) / avp (S, D0)	13spbrp1-
	avp (S, D1) / avp (P, D1)
	14spbrp2-
	avp (S, D2) / avp (P, D2)
	15spbrp3-
	avp (S, D3) / avp (P, D3)
	16spbrp4-
	avp (S, D4) / avp (P, D4)

Appendix 4

```

#          SCRIPT FOR STATISTICAL CLASSIFICATION FEATURE SELECTION
#          END ERROR PROBABILITY ESTIMATION
#          script troitsky/stcl/selfeatrs.scr
clearstack
# INPUT DATA TO THE STACK
# THE VARIANTS OF FEATUR SETS
#BY THE PROGRAM "LD"
. char[40] ldinp
ldinp = "troitsky/ldpFb.inp"
#ldinp = "troitsky/ldpFb+s.inp -c"
#ldinp = "troitsky/ldtest.inp -c"
#ldinp = "troitsky/ldnFb.inp -c"
#ldinp = "troitsky/ldpNb.inp -c"
#ldinp = "troitsky/ldnNb.inp -c"
#ldinp = "troitsky/ldpFs.inp -c"
#ldino = "troitsky/ldpFs+b.inp -c "
#ldinp = "troitsky/ldnFs.inp -c"
#ldinp = "troitsky/ldpNs.inp -c"
#ldinp = "troitsky/ldnNs.inp -c"

```

```

ld &ldinp
list
# DISPLAYING DATA TRACES &
# SCATTERING DIAGRAMS
vertical r b 27
vertical b b 52
plot all -y -x
cluster patr.par -c
##### FEATURE NONLINEAR TRANSFORM.
# BOX-COX NORMALIZING TRANSFORM.
log all
plot all -y -x
. float exp
. exp=1./7.
power all &exp
addc all -1.
scale all 7.
plot all -y -x
##### CALCULATION STATISTICS
# OF LERANING DATA FOR DIFFERENT
# DATA SETS BY THE PROGRAM "LDSTST"
. char[40] ldststinp
#ldststinp = "troitsky/ldststpFb.inp -c"
#ldststinp = "troitsky/ldststpFb+s.inp -c"
#ldststinp = "troitsky/ldststnNb.inp -c"
#ldststinp = "troitsky/ldststnFs.inp -c"
#ldststinp = "troitsky/ldststpNs.inp -c"
#ldststinp = "troitsky/ldststnNs.inp -c"
#ldststinp = "troitsky/ldststpNb.inp -c"
#ldststinp = "troitsky/ldststpFs.inp -c"
#ldststinp = "troitsky/ldststpFs+b.inp -c"
#ldstst inp = "troitsky/ldststnFb.inp -c"
ldstst &ldststinp
XYplot troitsky/gr.gr
unix lpr -P0 plot/snda.ps
# SELECTION OF THE MOST INFORMATIVE
# FEATURES BY THE PROGRAM "FSEL"
fsel troitsky/fsell.inp -c
XYplot troitsky/mygr.gr
unix lpr -P0 plot/snda.ps
sort data/troitsky/jnum.dat
plot all -y -x
unix lpr -P0 plot/snda.ps
pause
cluster patr.par -c

# RECLASSIFICATION OF LEARNING VECTORS
# BY THE PROGRAM "RECLLD"
reclld troitsky/reclld.inp -c
unix textedit data/troitsky/ldres.dat &
unix textedit data/troitsky/qdres.dat &
XYplot troitsky/reclplt.cnt

# CROSS VALIDATION EXAMINATION
# OF LEARNING VECTORS BY LINEAR &
# QUADRATIC DISCRIMINATORS:
# PROGRAMS "EXAMLD", "EXAMQD"
examld troitsky/examld.inp -c
XYplot troitsky/examld.gr
examqd troitsky/examqd.inp -c
XYplot troitsky/examqd.gr
# END OF SCRIPT

```

1.9 Appendix II

Appendix 1

Application of statistical source identification package for teleseismic event discrimination.

Performance of statistical source identification program package was also tested by its application to discriminating between teleseismic earthquakes and explosions. Seismograms of 28 underground nuclear explosions at Semipalatinsk test site and 33 earthquakes occurred in Eastern Kazakhstan were analyzed. Following the paper [6] we considered the normalized powers of P-phase and the P-coda waveforms in eight spectral bands, ordered in the 0.2-5.0 Hz range as the features characterizing shapes of P-phase and P-coda power spectra. The frequencies of spectral peaks for P-phase and P-coda and the ratio of maximums of P-wave and P-coda power spectra were also used as the additional features. The method for the most informative feature extraction implemented in this test was the same as described in Section.

Only eight the most informative features were selected from the initial 19 features. They provide the minimum of estimated probability of misclassifications. The dominant features were the ratio of maximums of P-phase and P-coda power spectra and the P-wave and P-coda normalized powers in the low frequency bands. The linear discriminant function was implemented for seismogram classification and error probability estimation based on the selected features.

Below we designate as X_1, X_2, \dots, X_8 the features, corresponding to the logarithms of normalized P-phase power fractions in the eighth frequency bands, as X_9-X_{16} - the similar P-coda power fractions, as X_{17}, X_{18} - the logarithms of frequencies of P-phase and P-coda spectral peaks and as X_{19} - the logarithm of ratio of spectral maximums for P-phase and P-coda.

The 18 scattering diagrams of the "basic" feature X_{19} with the rest 18 features were visually analyzed. The conclusion was made that the pairs of features (X_{10}, X_{19}) and (X_1, X_{19}) seem to be the most informative for the discrimination. The scattering diagram for the first pair is shown in Fig.1. The scattering diagram for the pair (X_1, X_{19}) is shown on Fig.2. One can see from these figures that properly drawn straight lines can divide the earthquake and explosion clusters without any mistakes.

The result of automatic stepwise selection of the most informative features (the output of program *"fsel"*) is displayed in Fig.3. Dependence of error probability $P(k)$ from the number k of selected features shows, that the 8 features corresponding to the first 8 selection steps may be chosen as the best for the discrimination. Note, that visually selected features 19,1 and 10 are enter to the set (19,1,17,10) of features with the highest ranks (19,1,17,10). The ranked values of linear discriminant function applied to selected features (the output of program 'exam') are displayed in Fig.4. The symbol '0' is used for earthquakes and symbol 'x' - for explosions. We see that the all learning observations for the given learning set of explosions and earthquakes are classified correctly, but the robust classification zone is rather narrow.

Appendix 2

Neural network approach to discrimination of regional events based on seismic trace sonograms

The sonogram representation of a seismogram is one of promising tools for seismic data analysis. The time-spectrum maps of seismic traces can reveal obscured signal features. These maps may be also processed by neural network tools. Standard feedforward neural models are widely used now for seismic events recognition [1,2]. The software and sonogram discrimination analysis methodology described below provides either interactive or batch modes of discrimination analysis built in the seismic array data processing system.

The neural computer networks for image processing are available now in several signal processing software packages (e.g. in MATLAB). There is also a neural network routine in the popular SAC package for seismic data analysis. Unfortunately these tools lack of capabilities of sonogram processing. The SNDA package for seismic array data analysis provides the capability of easy installation of user defined data processing programs. The following functions for sonogram discrimination analysis are implemented in SNDA :

- Seismic trace-sonogram conversion program,
- Sonogram visualization tool,
- Sonogram clusterisation tool by the ART2 neural network model,
- Supervised learning tool by the backpropagation neural network model,

Recognition tool for seismic event discrimination.

There is also an auxiliary tool for supervised learning network adjustment.

The sonograms of explosions and earthquakes may be discriminated by several features extracted from sonogram image. The experiments with explosion recognition showed stable discrimination within the same seismic region [2]. Unfortunately experiments with classification of seismograms from different regions using the same neural network discriminator demonstrates much less reliability.

There may be several hypothesis in seismic event discrimination: chemical explosion, nuclear blast, distant earthquake etc. So the straightforward feedforward model for learning and recognition may be extremely difficult to use. The more flexible technique with several stages of data processing including clustering and learning/recognition is preferable.

We propose the following data processing technique for seismic event discrimination using neural network programs. It consists of the next stages:

1. Trace to sonogram conversion;
2. Sonogram clustering;
3. Pattern learning;
4. Pattern recognition;
5. Neural network model adjustment and tuning.

A short description of each step is given below

1) The seismic traces in CSS or ASCII are converted to the time-frequency (sonogram)map image. The image size is set to 32x32 (1024) pixels. Then the patterns of 16x16 pixels located in a sonogram map area which is the most informative for discrimination are cut from every image. These patterns are used then for learning, clustering and recognition.

2) The learning set of sonogram patterns is applied to ART2 neural network with variable threshold [3,4]. This program performs clustering of the sonogram pattern set by assessing every sonogram as belonging to one of different clusters. So the number of different clusters is estimated and may be used to assign the number of output nodes of the supervised learning network used at the next processing stage .

3) At the stage of pattern learning the standard feedforward neural network with Backpropagation (or Quickpropagation) learning function [3,4] is implemented. The number of output attributes can be obtained from the previous stage. As a rule

the output attributes for learning are assumed to be binary values. So network designed for explosion-earthquake recognition have to have the two output nodes.

4) A sonogram of seismic trace with unknown source type is put to the trained network. The "True" value of the binary output is used as a pointer for attributing sonogram to a signal source class.

5) If some learning patterns are wrongly classified in the test (the output is not exact binary "TRUE" value) the pattern is included in the pattern set for the next learning cycle. The number of network outputs is incremented. The new output node represents the new signal class.

The technique described was tested using seismograms of Semipalatinsk nuclear tests and regional earthquakes from Southern Kazakhstan registered by Talgar seismic observatory. Vertical component trace data were used for neural network algorithm training. The learning set consisted of 10 nuclear explosion patterns, 6 earthquake patterns and 2 noise patterns.

The data clustering was performed by ART-2 model with variable threshold. The learning set of seismograms was correctly divided in three clusters.

Feedforward and Elman-Jordan neural network models were used for sonogram learning and recognition. The network was constructed with 256-nodes input layer, 2 hidden layers with 16 nodes in each, and 2-node output layer. The best learning performance was gained by the simple feedforward network with the Quickpropagation learning algorithm. The learning procedure required about 10000 cycles.

The following software tools were used as network prototypes [3,4]: SNNS v4.0, PlaNet 5.7, NBtest (X-based backpropagation-ART2 tool for sonogram processing). The NBtest program provides the automated network adjustment feature. The output layer adjustment procedure was tested in comparison with Cascade Correlation learning algorithm. This simplified adaptive procedure provides much advantage in learning cycle time.

The sonogram evaluation program operates with "wfdisk" files of the CSS-format recordings. This tool picks up the arrival point and sample rate in automated mode. The results of classification of the seismogram learning set described above by the neural network algorithm is depicted in the following table (the seismogram patterns are denoted by CSS trace labels)

Event	Class	Neural network output	
		explosion = 1	earthquake = 0
8051305	(nuclear explosion)	1.0;	0.
08081510	(nuclear explosion)	1.0;	0.
08081604	(nuclear explosion)	1.0;	0.
08081605	(nuclear explosion)	0.0;	1.
08081510	(nuclear explosion)	1.0;	0.
08081610	(nuclear explosion)	1.0;	0.
08081609	(nuclear explosion)	0.0;	1.
08081608	(nuclear explosion)	0.0;	1.
08081707	(nuclear explosion)	1.0;	0.
08050404	(nuclear explosion)	1.0;	0.
088258040108	(earthquake)	0.0;	1.
088292034130	(earthquake)	0.0;	1.
089043041625	(earthquake)	0.0;	1.
089048040240	(earthquake)	0.0;	1.
089245041825	(earthquake)	0.0;	1.
089292095115	(earthquake)	0.0;	1.

We see that the all earthquakes were classified correctly, but there were 3 mistakes in nuclear explosion classifications. This result prompts us to choose a more informative pattern set from event sonograms or to use additional seismogram features.

References

1. P.S. Dysart, J.J.Pulli (1990). Regional seismic event discrimination at the NORESS array: seismological measurements and the use of trained neural networks. *Bull. Seism. Soc. Am.* v.80, n.6, 1910-1933
2. F.U. Dowla (1995) Neural networks in seismic discrimination. *E.Husebye, A.Dainty (eds.) Monitoring of Comprehensive Test Ban Treaty, 777-790, NATO ASI Series, Kluwer Academic Publishers.*
3. SNNS, Stuttgart Neural Network Simulator, *User Manual, Version 4.0, Report No 6/95.*
4. Yoh-Han Pao (1990) Adaptive Pattern Recognition and Neural Networks, *Case Western Reserve University, Addison-Wesley Publishing Co. Inc.*

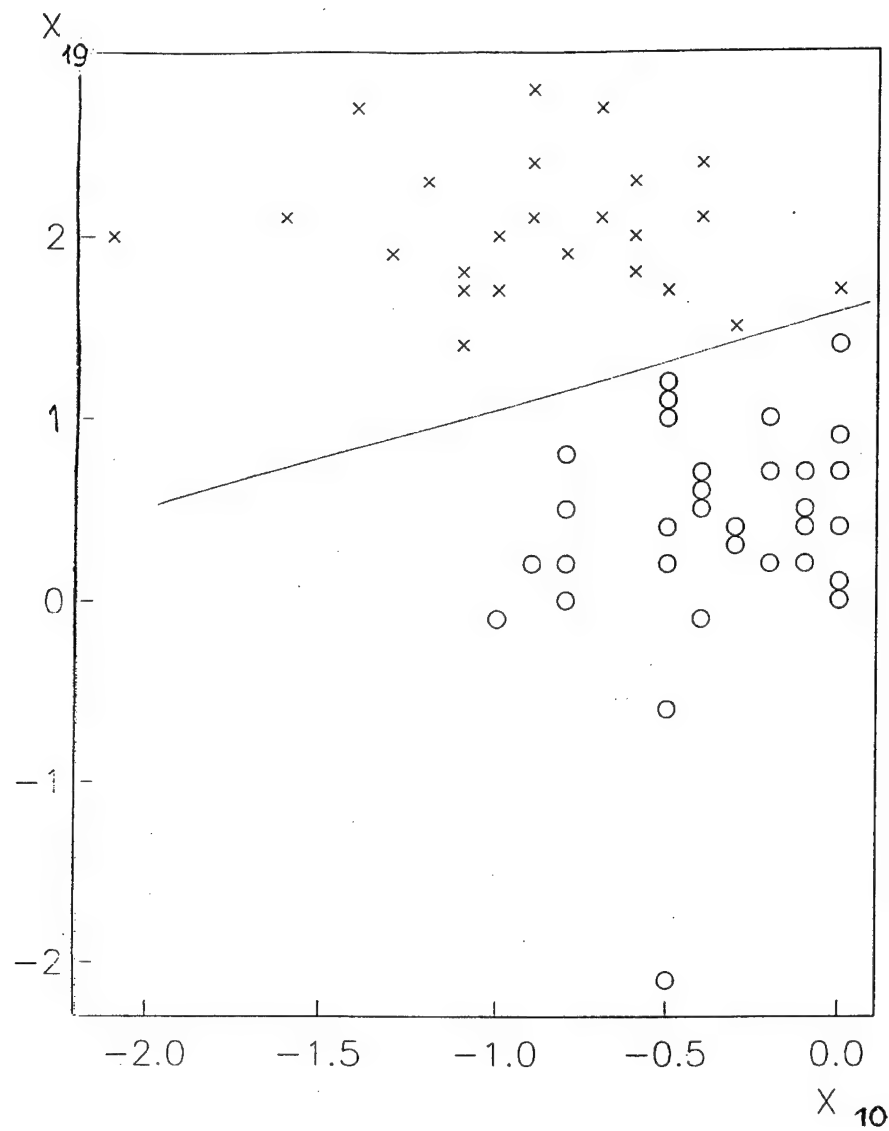


Fig. 1. Scattering diagram between features 10 and 19.
Feature 10 is the logarithm of normalized P-coda power
in the low frequency band, feature 19 is the logarithm of ratio
of spectrum maximums for P-wave P-coda.

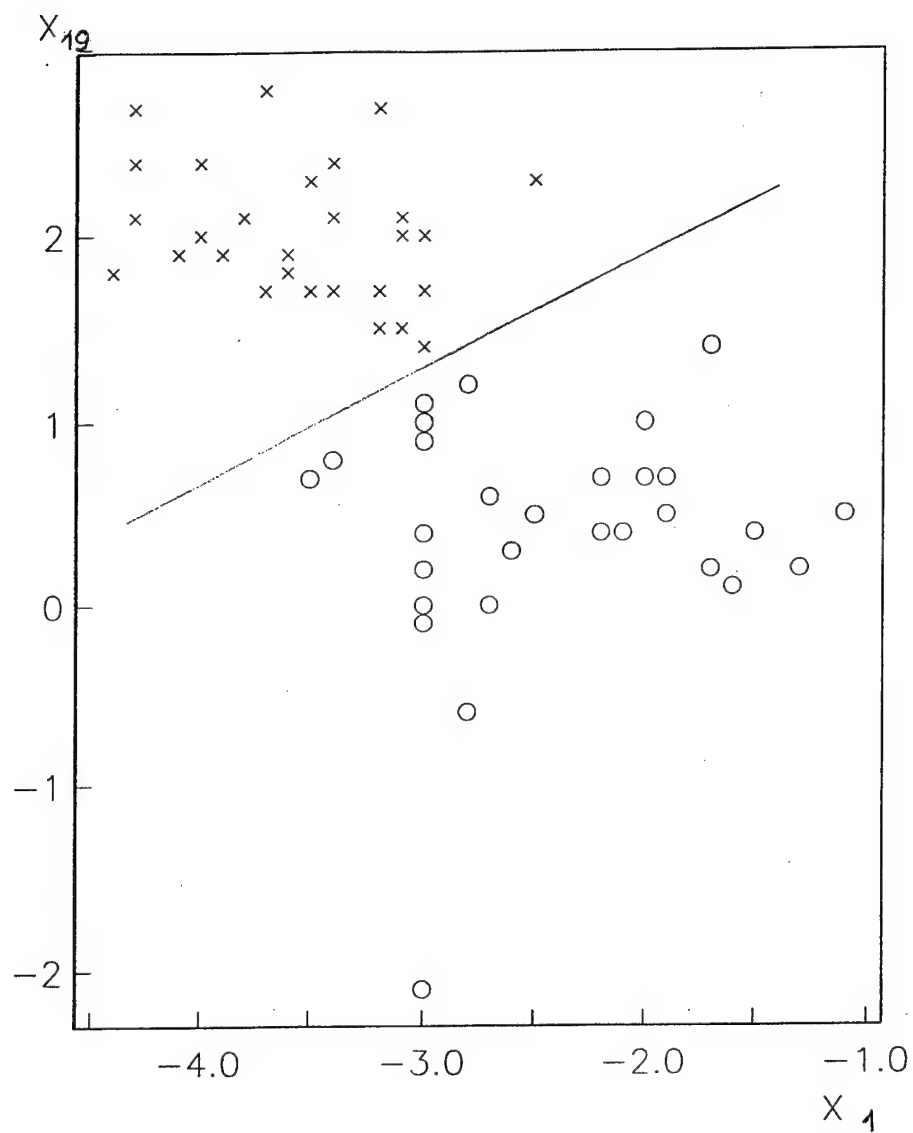
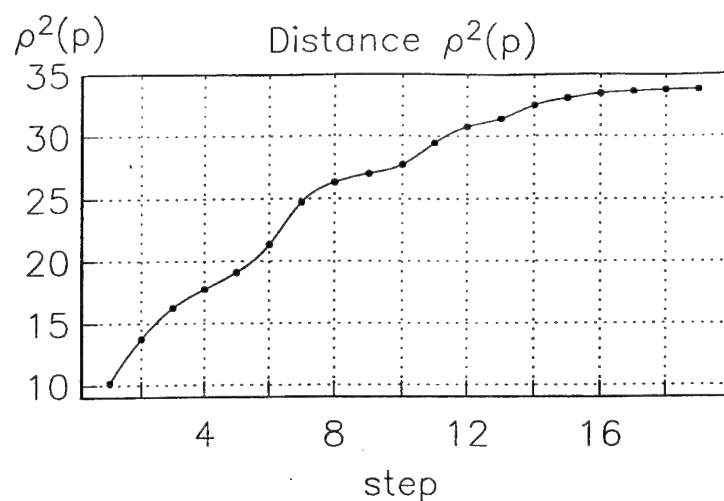


Fig. 2. Scattering diagram between features 1 and 19.
Feature 1 is the logarithm of normalized P-phase power in
the low frequency band.



Selected features:

Step: 1; number: 19
 Step: 2; number: 1
 Step: 3; number: 17
 Step: 4; number: 10
 Step: 5; number: 8
 Step: 6; number: 13
 Step: 7; number: 18
 Step: 8; number: 4
 Step: 9; number: 16
 Step: 10; number: 15
 Step: 11; number: 7
 Step: 12; number: 5
 Step: 13; number: 3
 Step: 14; number: 2
 Step: 15; number: 6
 Step: 16; number: 14
 Step: 17; number: 9

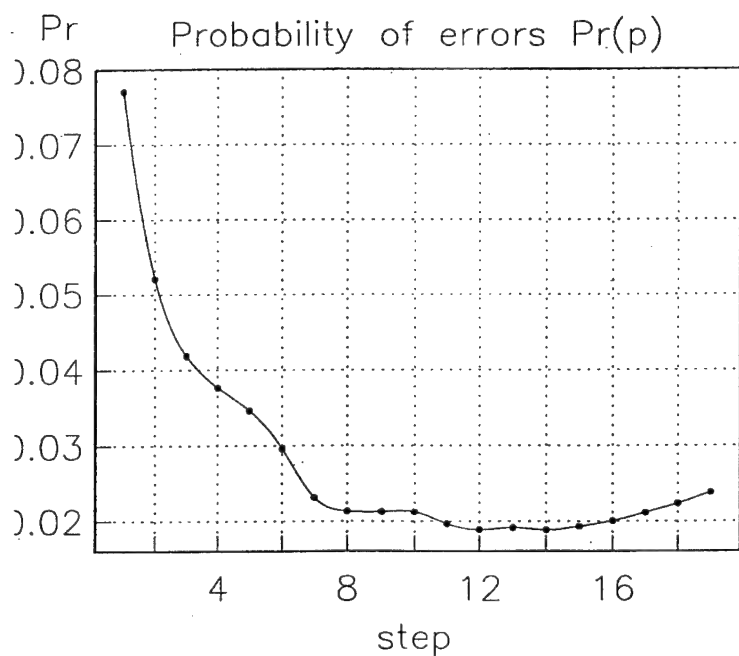
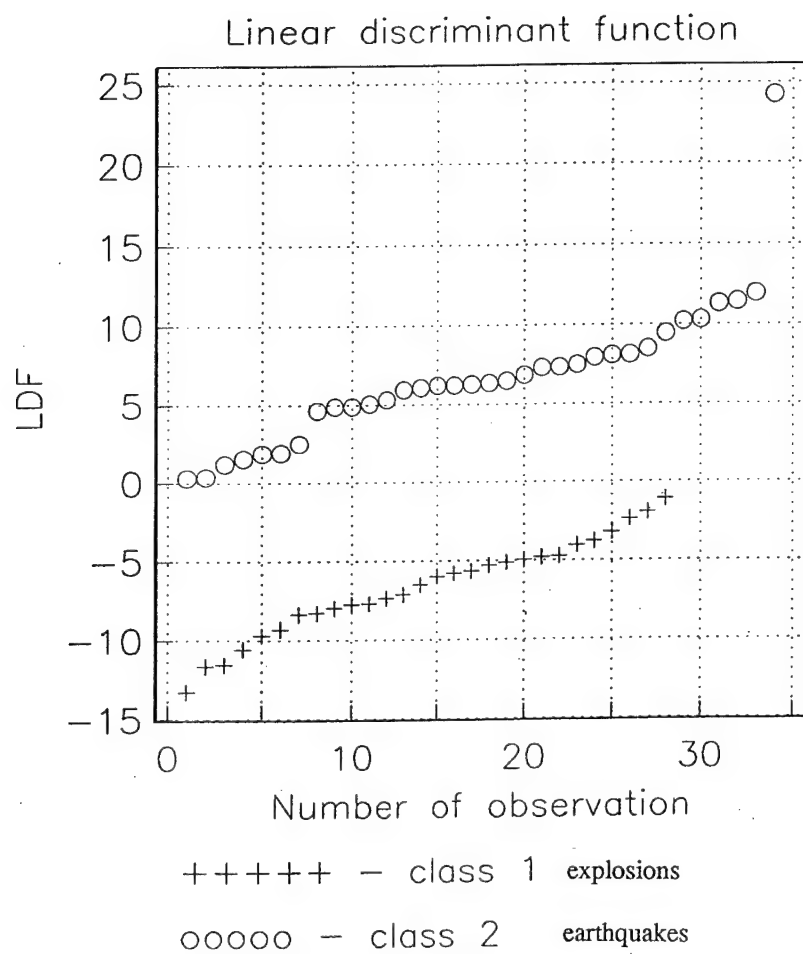


Fig. 3. Results of feature arranging in the order of increasing discrimination power.
 This allows one to select the most informative features.



**Fig. 4. Results of explosion and earthquake set discrimination with the help of learning data examination by the cross-validation method.
The learning observations are classified correctly.**

2. SCANLOC: AUTOMATIC SEISMIC EVENT LOCATION IN SPACE AND TIME BASED ON THE PRINCIPLES OF EMISSION TOMOGRAPHY

CONTENTS

2.1. Introduction	1
2.2. Analytical formulation	2
2.3. SCANLOC program package and results of data processing	5
2.4. Conclusions and recommendations	9
2.5. Tables and figures	10
2.6. References	11
2.7. Appendix: Descriptions of SNDA JCL scripts and SCANLOC input file	12
2.8. Study of Israel regional velocity model on the basis of Israel Seismic Network catalogue of local events.....	17
Figures	24

2. SCANLOC: AUTOMATIC SEISMIC EVENT LOCATION IN SPACE AND TIME BASED ON THE PRINCIPLES OF EMISSION TOMOGRAPHY

2.1. Introduction

Robust methods for automatic event location and origin time determination of numerous weak earthquakes and mining explosions at local and regional distances is an important part of modern CTBT monitoring technology. The goal of the current research is to design a reliable method for fast automatic event location based on local seismic network data. This is important for monitoring in industrialized or seismically active regions and for wide range of other seismic applications. The major effort was made to eliminate any need in the location procedure for the analyst verification of seismic wave phase detection and parameter estimation (that is routine practice in conventional monitoring systems).

The conventional methods for seismic event location (and evaluation of other event parameters) traditionally are based on detection, identification and precise measurement of seismic phase parameters by individual processing of recordings from every seismic network station (Kennett, 1996). Automatic methods designed using this paradigm have low computational efficiency because of difficulty to develop algorithms which adequately reproduce the operations of skillful geophysicist. Interestingly, the current methods of computer treatment of seismology data virtually do not use the advantages provided by multichannel data processing. From general point of view, registering of the event wavefield by a network consisting of identical sensors allows us to consider the set of recordings obtained from all receivers as a single multichannel seismogram. In many respects, this seismogram is similar to those conventionally used in seismic prospecting and deep seismic sounding. Powerful methods for optimal processing of multichannel data have been developed in these fields, and some of them can be used in solving the problems of seismic event location. Multichannel approaches to automatic analysis of seismic data for location purpose are under investigation by a number of research groups (Ryzhikov et al., 1995; Young et al., 1995; Ringdal and Kvarna, 1989). Promising results have been obtained, demonstrating that new techniques specifically oriented to automated computer data processing are useful for solving many traditional problems in seismology.

In the framework of this project we developed and tested a new automatic event location method based on processing of multichannel recordings from local and regional seismic networks. The approach is based on the principles of seismic emission tomography technique. The essence of our approach is to look for a "bright spot" in the medium by scanning the medium area under investigation with a sounding seismic beam in the units of given scanning grid. An advantage of the method is that it does not require a detection and parameter measurement of the event seismic phases.

The results of experimental processing of Israel regional network data obtained in our study showed that the method allows to determine the event epicenters and hypocenters with errors which do not exceed 1-3 steps of scanning grid (in our experiments the errors were less than 15 km). The computation time for scanning of a square area with 255 km x 255 km size while processing data from 10-20 sensors with sampling rate 50 Hz does not exceed 10-20 sec for a SPARC-2 Workstation. Thus, a near real-time automatic location technique could be designed on this basis.

2.2. Analytical formulation

Emission tomography proper is the method for reconstructing the object internal structure through the use of signals emitted by sources located within the medium. There are number of methods for solving this problem. In contrast to classic tomography based on solution of the inverse Radon's problem we obtain 3 dimensional (3D) image of emission's sources by scanning the medium volume under study by a sounding beam being formed from seismic array recording. This approach was proposed by A.V.Nikolaev and P.A.Troitsky, 1987. Lately this method was successfully implemented for mapping the zones of microseismic activity in hydrothermal area in NE Iceland (Shoubik et al., 1991; Shoubik and Kiselevich, 1993; Gurevich et al., 1994, Shoubik et al., 1996). The presence of microseismic sources or contrast inhomogeneties within the Earth results in the appearance of coherent time distributed components in a stochastic seismic wave field recorded on the surface by seismic array. By careful processing of seismic array data these coherent components can be used to develop a 3D model of microseismic activity in the medium under study or an image of noise radiating objects.

The essence of the processing algorithm consists of comparative assessment of coherent signal power irradiated from different points (or small volumes) of the area

under study. The area is portioned into an equidistant scanning grid and values of beam power are calculated for every unit of the grid. The beam power are assessed by observed value of Signal To Noise Ratio (*SNR*). If coordinates of some unit are equal or closest to the true emitter coordinates the *SNR* value calculated for this unit exceeds the *SNR* values calculated for the adjacent points. The set of calculated *SNR* values (2D or 3D *SNR*-map) reflects a spatial distribution of emitters in the area under study. The main idea of the current research consists in the use of above formulated approach to spatial and temporal location of natural and artificial seismic events sources rather than seismic noise sources.

Fig.1 illustrates the principle of the method. $P_1, P_2, \dots, P_m, \dots, P_M$ denote sensors of seismic array. The volume (V) below the array is scanned by beam formed from seismic array P_1, \dots, P_M in the units of scanning grid. X_i, Y_j, Z_k are coordinates of the grid unit and ϕ_{ijk} is the signal irradiated from this point.

The processing algorithm is based on a linear additive model of signals and noise at the network sensors:

$$f_m(t) = \alpha_{mijk} \phi_{ijk}(t - \tau_{mijk}) + \epsilon_m(t) \quad (1)$$

where:

$m = 1, 2, \dots, M$ is the number of sensors;

$f_m(t)$ is the seismic trace recorded by the m -th sensor; t is the receiver time;

$\phi_{ijk}(t)$ is a signal emitted from the source in the grid unit with coordinates X_i, Y_j, Z_k ;

α_{mijk} is the amplitude decay factor due to geometric spreading, angle of incidence and attenuation (absorption and scattering) of the signal $\phi_{ijk}(t)$ at the path from grid unit with coordinates X_i, Y_j, Z_k to m -th sensor;

τ_{mijk} is the time delay determined by the signal travel time;

$\epsilon_m(t)$ is the sum of stochastic noise and signals emitted from other sources not coinciding with X_i, Y_j, Z_k .

The location problem is reduced to a comparative assessment of the energy of signals (ϕ_{ijk}) radiated by different elements (i, j, k) of the medium volume under study (V). In order to assess the energy of the correlated components $\phi_{ijk}(t - \tau_{mijk})$ presenting in the multichannel recording ($f_m(t)$, $m=1, 2, \dots, M$) the two functional are most commonly used: Semblance (S) (Nadel and Taner, 1971) and Signal to Noise Ratio (*SNR*) (Katz and Shoubik, 1986). Let us designate:

$$A_{ijk}(t_n) = \left\{ \sum_{m=1}^M \beta_{mijk} f_m(t_n + \Delta_{mijk}) \right\}^2 \quad (2)$$

$$B_{ijk}(t_n) = \sum_{m=1}^M \{ \beta_{mijk} f_m(t_n + \Delta_{mijk}) \}^2 \quad (3),$$

then the Semblance functional is equal to:

$$S_{ijk} = \sum_{n=1}^N A_{ijk}(t_n) / M \sum_{n=1}^N B_{ijk}(t_n) \quad (4)$$

and the *SNR* functional is equal to:

$$SNR_{ijk} = \sum_{n=1}^N (A_{ijk}(t_n) - B_{ijk}(t_n)) / \sum_{n=1}^N (M B_{ijk}(t_n) - A_{ijk}(t_n)) \quad (5)$$

where:

β_{mijk} is the amplitude normalizing factor theoretically or experimentally chosen to approximate the reciprocal value of the amplitude decay factor α_{mijk} for the signal radiated from the medium element at X_i, Y_j, Z_k (i.e., $\beta_{mijk} \sim 1/\alpha_{mijk}$);

N is the number of samples in the time window for which the estimate of an average correlated signal power is calculated;

Δ_{mijk} is the estimation of time delay τ_{mijk} , of the signal due to propagation from the (i,j,k) volume element to the m -th receiver. This estimation computed for the *a priori* medium velocity model.

It can be shown that for a linear additive model (1) and uncorrelated random noise $\epsilon_m(t)$ in different sensors, the Semblance (S) converges to the ratio of coherent signal power to total average seismogram power, varying from 0 to 1; the Signal to Noise Ratio (*SNR*) converges to the ratio of coherent signal power to noise power, varying from 0 to infinity. If the (i,j,k) medium element contains the seismic source, the *SNR* value calculated for this element exceeds the *SNR* values calculated for neighboring grid points. The set of *SNR* values (5) calculated for every point X_i, Y_j, Z_k of the scanned medium surface area or the scanned medium volume produces 2D or 3D *SNR*-map. This map reflects the spatial distribution of seismic sources in the region under study.

We attempted to employ the above described emission tomography method, initially formulated and successively applied for seismic noise analysis in the rather small areas of microseismic activity, for the search of seismic event source as a radiator of seismic energy in the significantly larger Earth crust area. The method described above may be thought of as scanning the medium by a sounding beam formed by seismic network "antenna".

Actual implementation of these principles vary depending on the epicenter distance and the seismic network scale (regional network, local network, array with aperture of first dozen km). Array data from seismic events typically exhibit coherency (correlation) between signals recorded at different array sensors, at least a certain frequency range. In this situation it would probably be effective to use coherent stacking in (2) to scan the medium area. However, this is likely to be ineffective in local or regional seismic networks. In this case the incoherent analysis in course of the grid scanning should be preferable. In other words, one should use a suitable mask-filter (e.g., Shoubik, 1980) to transform the initial wave forms (1) into low frequency mask signals. As such low frequency signal models the functional of envelope function, STA/LTA function and of output signals of proper detector (polarization, amplitude, spectral, etc.). can be used.

2.3. SCANLOC program package and results of data processing

Following the above described approach the program package SCANLOC was developed and first results obtained in processing data recorded by the Israel Regional Seismic Network (ISN). ISN is operated by the Seismological Division of the Institute for Petroleum Research and Geophysics (IPRG) in Holon, Israel. The database supplied with ground truth information was collected by Dr. Y.Gitterman (IPRG) and used in the discrimination study (Y.Gitterman and T. van Eck, 1993). The waveforms and ISN bulletin information were kindly prepared and transferred by Dr. V.Pinsky (IPRG).

The SCANLOC package oriented to automatic event location includes the next main programs:

- Forward modeling using an *a priori* velocity model of a stratified laterally homogeneous medium. The procedure calculates the time delays, angles of incidence

and amplitude decay factor the specified number of seismic phases and for a given set of grid point and station coordinates.

- One-channel low frequency mask-filter. If the incoherent stacking is used the procedure transforms the original waveforms to a low frequency signal models.
- Grid scanning procedure. The procedure calculates the 2D or 3D *SNR*-maps, i.e., the set of *SNR* values (5) for all grid units. This *SNR*-map reflects the spatial distribution of seismic emitters in the area under study. The quality and accuracy of the event location can be assessed by relationship between the maximum map *SNR* value and the estimate of *SNR* dispersion through the total map.

An efficient methods for scanning through the grid points and for forward modeling were implemented in the package. In the current version of the SCANLOC package the computing time for processing data from 10-20 stations with sampling rate 50 Hz while scanning about 3000 grid points does not exceed 10-20 sec for a SPARC-2 Workstation. This means that it is possible to develop a near real-time automatic location procedure.

Note that the current version of the SCANLOC package developed in this project presents only the first stage of investigation of a new method for event location. This version was adapted to ISN data which were accessible to us in this project and it demonstrated a promising results on these data. These results encourage us to continue investigation in this direction. A wide testing, adjusting and improving of the package based on a range of medium models, network's data with different event types and signal/noise levels, etc. should be carried out in order to obtain a high efficiency program product.

This version of SCANLOC package is written in standard C language and interacts with the Seismic Processing Shell SNDA (Kushnir et al., 1995) by using of compatible formats of input and output files and by employing the various multichannel data handling and interactive graphic SNDA tools. This version is available now as the object module included in the latest version of the SNDA System. Descriptions of the input and output files of SCANLOC package and the SNDA JCL scripts used for the ISN data preparing and processing are presented in the **Appendix** to this chapter (**infloc.inp**, **ecsel.scr**, **locproc.scr**, **locview.scr**).

The package is working with standard input and output files. The input data file named "indat" contents the original event seismograms selected from ISN database

with the help of SNDA script "**recsel.scr**". These seismograms are presented in the internal SNDA data format and saved in files with the extension "***.pk**". Another standard input file named "**infloc.inp**" contents parameters in the ASCII format inquired by current version of the SCANLOC program for processing "**indat**" recordings. The description of these parameters, their recommended and margin values are given in the Appendix to this Section. Standard output file named "**outdat**" contents output data matrix in ASCII format (*SNR*-map) calculated by the SCANLOC program for seismogram from file "**indat**" and the parameter values from file "**infloc.inp**". The data in "**outdat**" file are presented in the ascending order of scanning area coordinates X_i (first index) and Y_j (second index). This format is compatible with SNDA "**surfer**" program.

The seismograms of 19 events recorded by ISN were processed during the course of this project. For this experiment only good quality station recordings were selected for every events from the available ISN database. The list of the events used with ground truth information is presented below in Table 1. This table contains the number, date, magnitude, geographical coordinates and hypocenter depth for 19 selected events. This information selected from IPRG event catalogue file. SNDA script "**recsel.scr**" was used for seismograms screening, selecting and obtaining the local coordinates of selected stations. The number of stations being selected for further data processing varied from 8 stations up to 24 stations. For solving the epicenters and hypocenters location tasks we have used the homogeneous *a priori* seismic velocity model with velocities of P and S waves equal to: $V_p = 6.196$ km/sec and $V_s = 3.367$ km/sec. The validity of simplest media model at local distances and the velocity were proved by the regression analysis of onset times of P and S phases measured at seismograms of numerous local earthquakes and explosions recorded by the Israel Seismic Network. The peculiarities of this analysis (performed by Dr. V.V.Starostin) are described in Section 2.8. The epicenters of the all 19 selected events are located within the 255km x 255km area. This area was covered by the scanning grid with the step equal to 5km (51 x 51=2601 grid units were used).

Some results of event epicenter and hypocenter location are presented in Table 2 and illustrated by Fig. 2(a,b,c,d,e), Fig 3(a,b,c,d). Table 2 contains list of processed events. Event date and time are given in the second column by a 10 digit event label containing the year, month, day, hour, minute (2 digits each). The third column shows

the number of stations which recorded specified event and were selected from ISN database for processing by **SCANLOC** method. The 4th and 5th columns contain the event coordinates (X_{cat} , Y_{cat}) from the catalogue file produced with the help of conventional location procedure implemented at IPRG, and 6th, 7th, 8th and 9th columns contain the coordinates (X_{m1} , Y_{m1}) corresponding the maxima of event *SNR*-maps, and the coordinates (X_{m2} , Y_{m2}) of the map points which values are the nearest to maximum. The latter serve as some measure of map dispersion (they characterize the width of map peaks). The coordinates are given in a local orthogonal system: the geographical coordinates of the system center (0.0, 0.0) coincide with coordinates of the epicenter of first processed event and equal to $LAT = 32.671N$, $LON = 35.260E$. The last column of Table2 shows the epicenter location error rounded off to integer km. One may see that 80% of the location errors do not exceed the scanning grid interval (5 km).

Fig. 2 (a,b,c,d,e) and Fig. 3 (a,b,c,d) illustrate the epicenter and hypocenter location procedure for 2 from 19 events in more detail. Fig. 2 illustrates some processing results for the first event from Table 1 (event 8710071514). The deployment of stations which recorded the event seismograms is shown in Fig. 2a. The circle on the map marks both the origin of coordinates and the event epicenter, as discussed above. The event seismograms are shown in Fig. 2b. The seismograms are ordered according to the station-epicenter distance. The **SCANLOC** output *SNR*-map is presented in Fig. 2c in the form of a mesh perspective diagram and in Fig. 2d in the form of a contour map. Some results of hypocenter location for this event are shown in Fig. 2e. Here are presented 9 *SNR*-maps for scanning squares located on the next depths: 0 km, 5 km, 10 km, 15 km, 20 km, 25 km, 30 km, 40 km and 50 km. The values of *SNR*-map maxima are shown below each *SNR*-map. One can see that the general pattern of *SNR* functional spatial distributions is rather stable up to 40 km depth and it is completely destroyed below 40 km depth. The value of *SNR*-map maxima (printed below every *SNR*-map) monotonically increase with the depth growing up to depth about 25 km and they decrease for depths lower this level. Also one can notice that the ratio of the maximum *SNR* value to the dispersion of *SNR*-map also increase with the depth growing up to 25 km and it sharply decreases below this depth. These observations demonstrate that the developed event location method could be very useful tool for near real time evaluation of event depth. The depth of event hypocenter is determined in the

catalogue as 12 ± 1.1 km. Most likely this deviation in hypocenter location is related with inaccuracy of the simplest seismic velocity model used. It is important to note that *a priori* medium velocity model can be refined in the framework of SCANLOC event location method: the peak value of calculated *SNR*-map can serve as a performance criterion of the velocity model used: a better velocity model provides a greater peak.

Fig. 3 illustrates some processing results for event No 13 from Table 2 (event 9104150120). The deployment of stations which recorded the event seismograms is shown in Fig. 3a. The circle in the map marks the event epicenter. The event seismograms are shown in Fig. 3b. The seismograms are ordered according to the station-epicenter distances. The SCANLOC output *SNR*-map is presented in Fig. 3c in the form of a mesh perspective diagram and in Fig. 3d in the form of a contour map.

2.4 Conclusions and recommendations

1). The new SCANLOC method for automated event location based on local seismic network data was developed and tested. The processing is founded on the principles of seismic emission tomography. The results of experiments with Israel Local Network data revealed the high reliability and precision of weak local event epicenter and hypocenter location by this technique. The software written can serve as the basis for developing a near real-time location tool for seismic monitoring at local and regional distances. A wide testing, adjusting and improving of the package based on a range of medium models, network's data with different event types and signal/noise levels, etc. should be carried out in order to obtain a high efficiency program product.

2). It is possible to refine the medium velocity model within the framework of the event location method. The peak value of calculated *SNR*-map can serve as a performance criterion of the velocity model used: a better velocity model provides a greater peak.

3). The processing approach can be implemented for coherent and incoherent multichannel seismogram analysis. The precision of weak event location can be increased by implementing one-channel seismic phase detectors which are more sensitive than the conventional STA/LTA detector used in our experiments.

2.5 Figures and tables

Table 1.

List of events, selected for processing by the SCANLOC program

No	Year	Month	Day	Origin time	M	Lat	Long	Depth km+/-err
1	1987	10	07	15:15:4.7	1.9	32.671N	35.260E	12+/-1.1
2	1988	02	24	15:37:26.6	1.5	32.717N	35.251E	10+/-1.2
3	1990	08	21	6:22:23.0	1.8	32.663N	35.152E	16+/-2.3
4	1990	09	16	9:41:44.4	1.6	32.961N	34.981E	12+/-0.9
5	1990	11	17	7:30:16.1	1.2	32.792N	35.270E	17+/-2.9
6	1990	12	21	15:24:50.4	1.5	32.853N	35.571E	23+/-3.0
7	1991	01	09	2:30:42.2	1.1	32.781N	35.272E	20+/-1.6
8	1991	01	26	17:46:55.7	2.6	32.782N	35.273E	1.0+/-3.1
9	1991	01	27	3:5:37.2	1.5	32.808N	35.324E	4.0+/-5.4
10	1991	02	12	8:32:56.9	1.4	32.857N	35.468E	8.0+/-1.5
11	1991	02	25	6:33:55.4	2.0	32.581N	35.306E	21+/-1.2
12	1991	04	07	17:18:19.7	1.3	32.845N	35.584E	0.0+/-1.5
13	1991	04	15	1:21:28.3	2.4	32.848N	35.594E	14+/-4.2
14	1991	04	15	5:3:49.8	1.5	32.826N	35.574E	0.0+/-2.3
15	1991	04	16	6:38:1.3	1.9	32.844N	35.587E	6.0+/-1.4
16	1991	04	27	7:13:22.3	1.3	32.852N	35.580E	0.0+/-3.9
17	1991	05	01	20:47:12.1	2.2	32.835N	35.578E	6.0+/-1.3
18	1991	05	03	22:7:19.2	1.0	32.830N	35.583E	6.0+/-5.6
19	1991	05	16	2:50:17.2	1.7	33.080N	34.981E	10+/-1.3

Table2.

Results of event location by the SCANLOC program

No	Event Date	Num. of stat	Xcat km	Ycat km	Xm1 km	Ym1 km	Xm2 km	Ym2 km	Error km
1	8710071514	8	0.0	0.0	0.0	0.0	0.0	5.0	0
2	8802241537	8	0.844	5.101	-5.0	5.0	0.0	0.0	4
3	9008210621	14	-10.13	-0.882	-5.0	-15.0	-10.0	-5.0	15
4	9009160941	12	-26.08	32.196	-30.0	35.0	-30.0	30.0	5
5	9011170729	10	0.937	13.419	0.0	10.0	5.0	10.0	3
6	9012211524	13	29.113	20.227	30.0	20.0	30.0	25.0	0
7	9101090230	12	1.124	12.199	5.0	10.0	-5.0	10.0	4
8	9101261746	9	1.218	12.310	0.0	15.0	-5.0	15.0	3
9	9101270305	9	5.994	15.195	-5.0	15.0	5.0	15.0	10
10	9102120832	21	19.470	20.647	25.0	20.0	20.0	20.0	5
11	9102250633	23	4.319	-9.980	5.0	-10.0	0.0	-15.0	1
12	9104071717	12	30.332	19.344	30.0	20.0	35.0	15.0	1
13	9104150120	24	31.268	19.679	35.0	15.0	35.0	20.0	5
14	9104150503	15	29.403	17.234	30.0	20.0	-35.0	5.0	3
15	9104160637	19	30.614	19.234	40.0	20.0	45.0	20.0	10
16	9104270713	9	29.956	20.119	30.0	20.0	30.0	15.0	1
17	9105012046	24	29.774	18.233	35.0	15.0	40.0	20.0	6
18	9105032206	11	30.244	17.680	35.0	15.0	30.0	20.0	5
19	9105160249	20	26.050	45.395	-35.0	45.0	-30.0	45.0	11

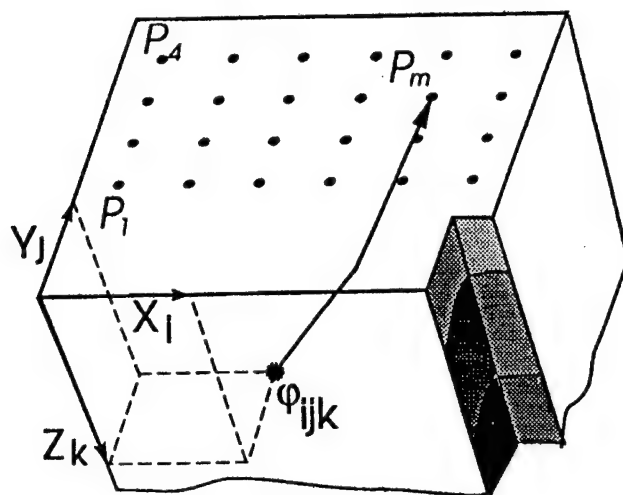


Fig. 1. Principle of emission tomography method.

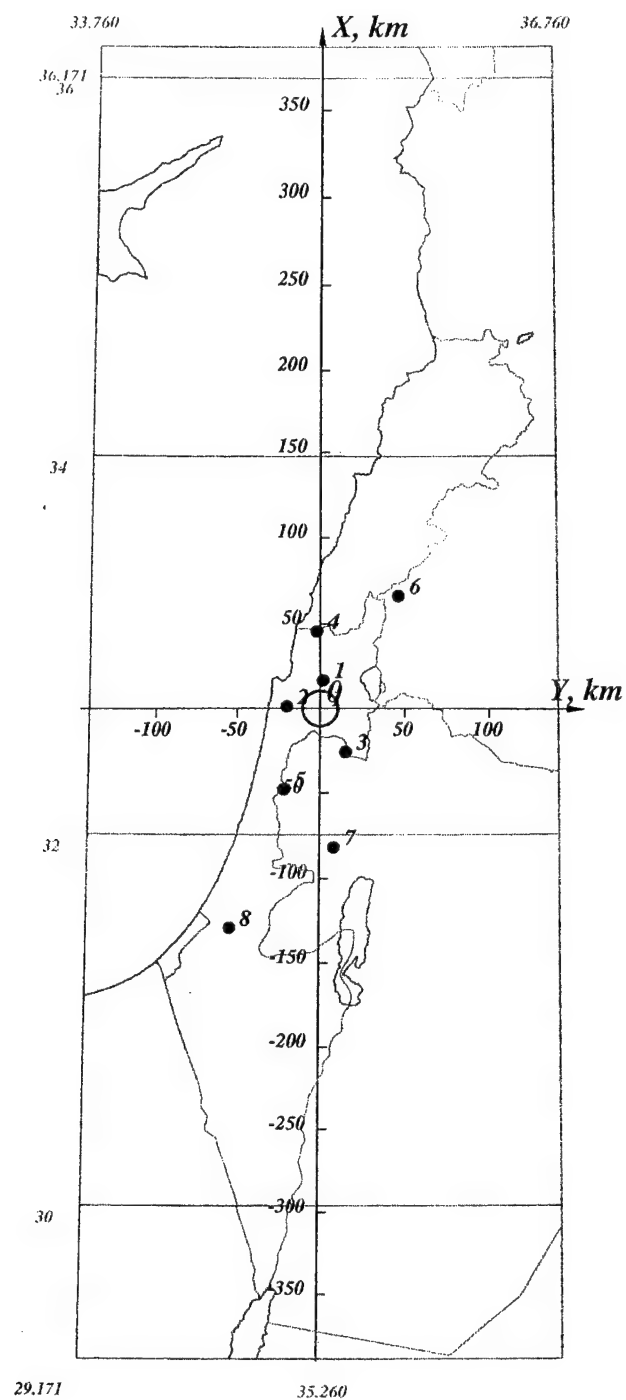


Fig. 2a. The deployment of Israel Seismic Network station which recorded the event 8710071514.

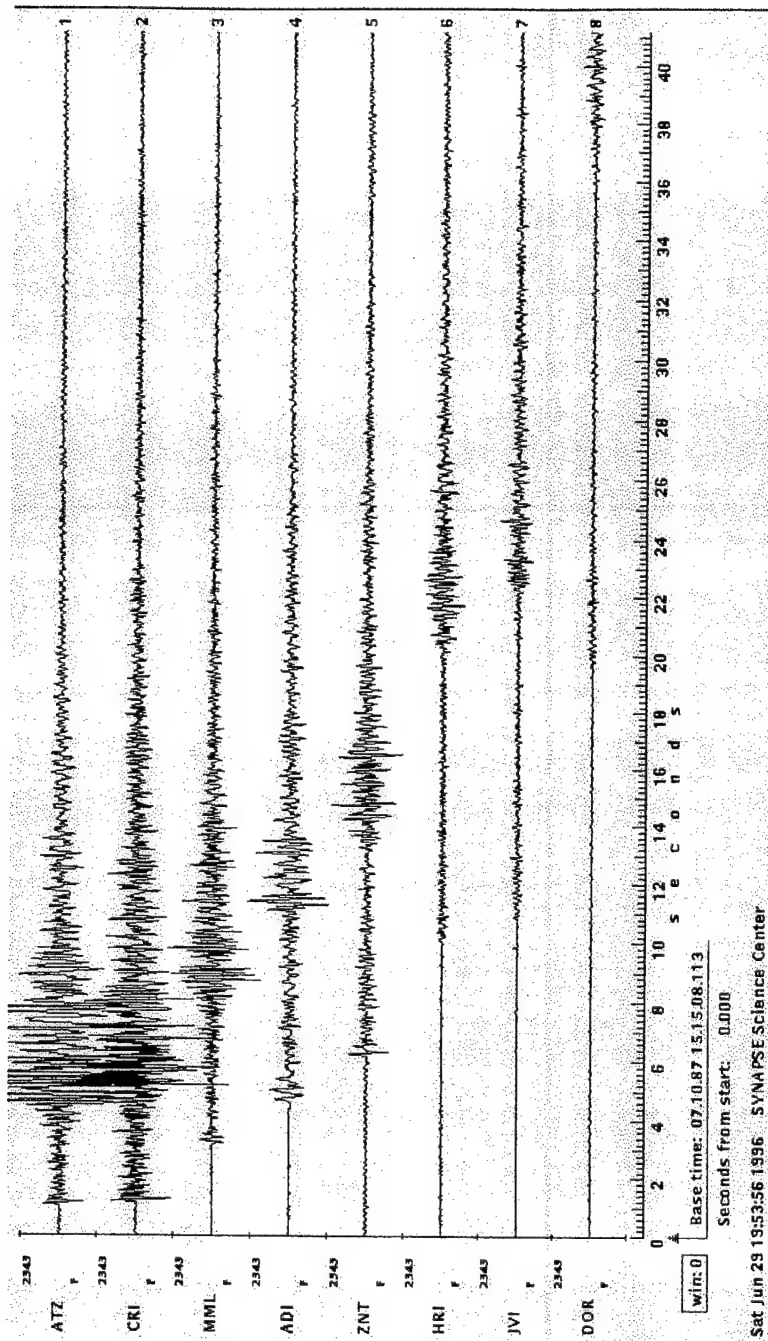


Fig. 2b. The seismogram of event 8710071514 recorded by 8 selected Israel Seismic Network stations.

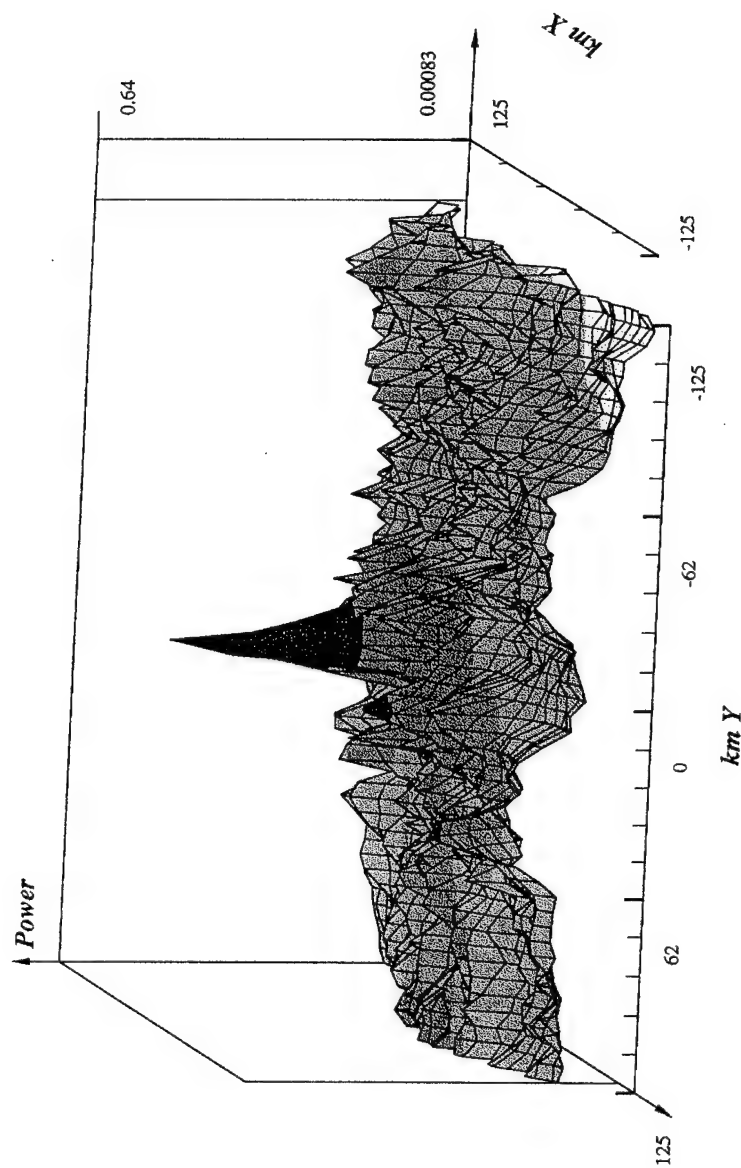
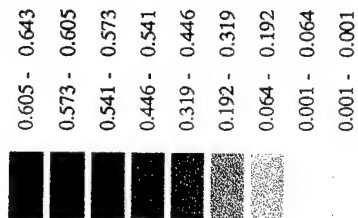


Fig. 2c. The output *SNR*-map, calculated by SCANLOC program.
 Scanning grid area is 255 km x 255 km,
 grid intervals are 5 km, depth is 0 km.

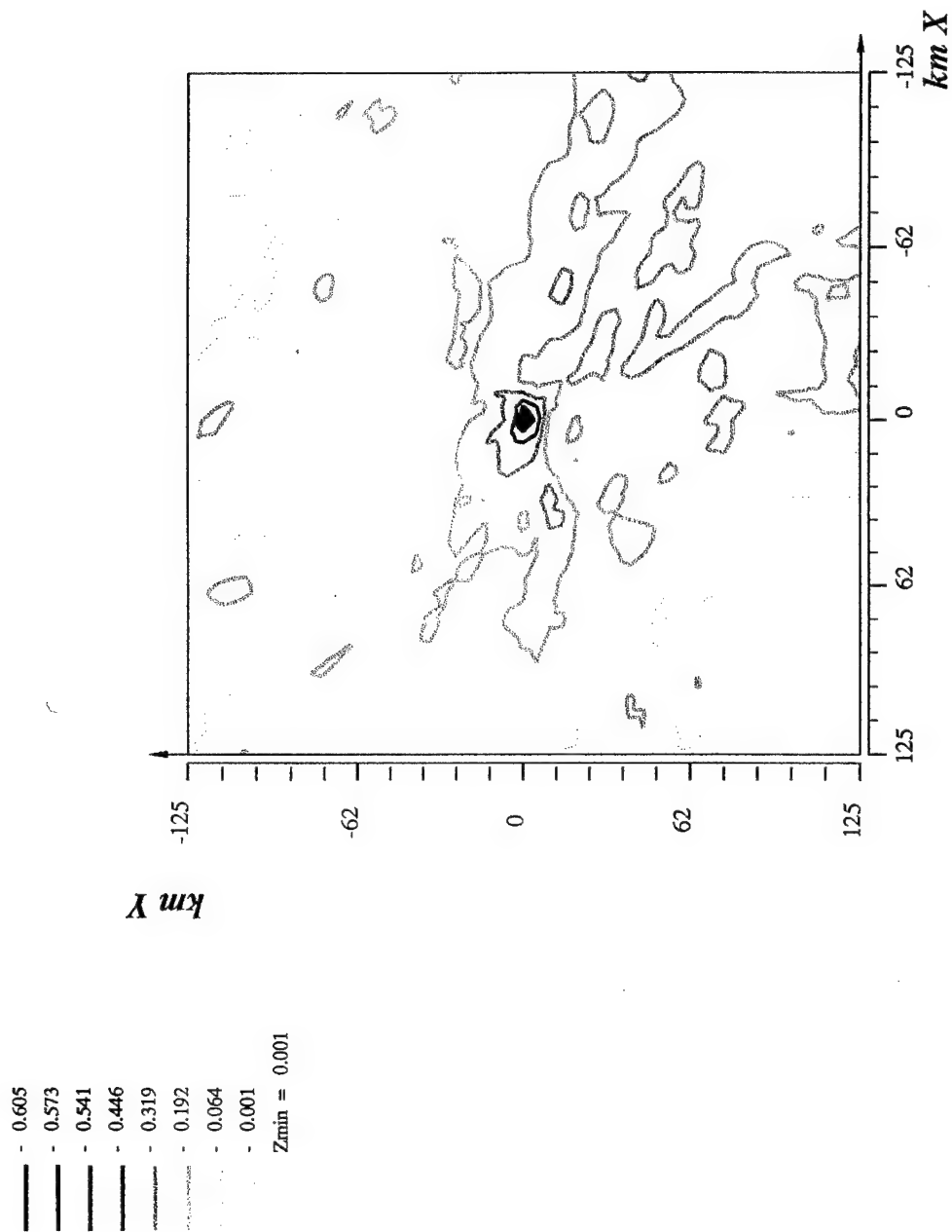


Fig. 2d. The output contour SNR-map, calculated by SCANLOC program.
 The scanning grid area is 255 km x 255 km,
 grid intervals are 5 km, depth is 0 km.

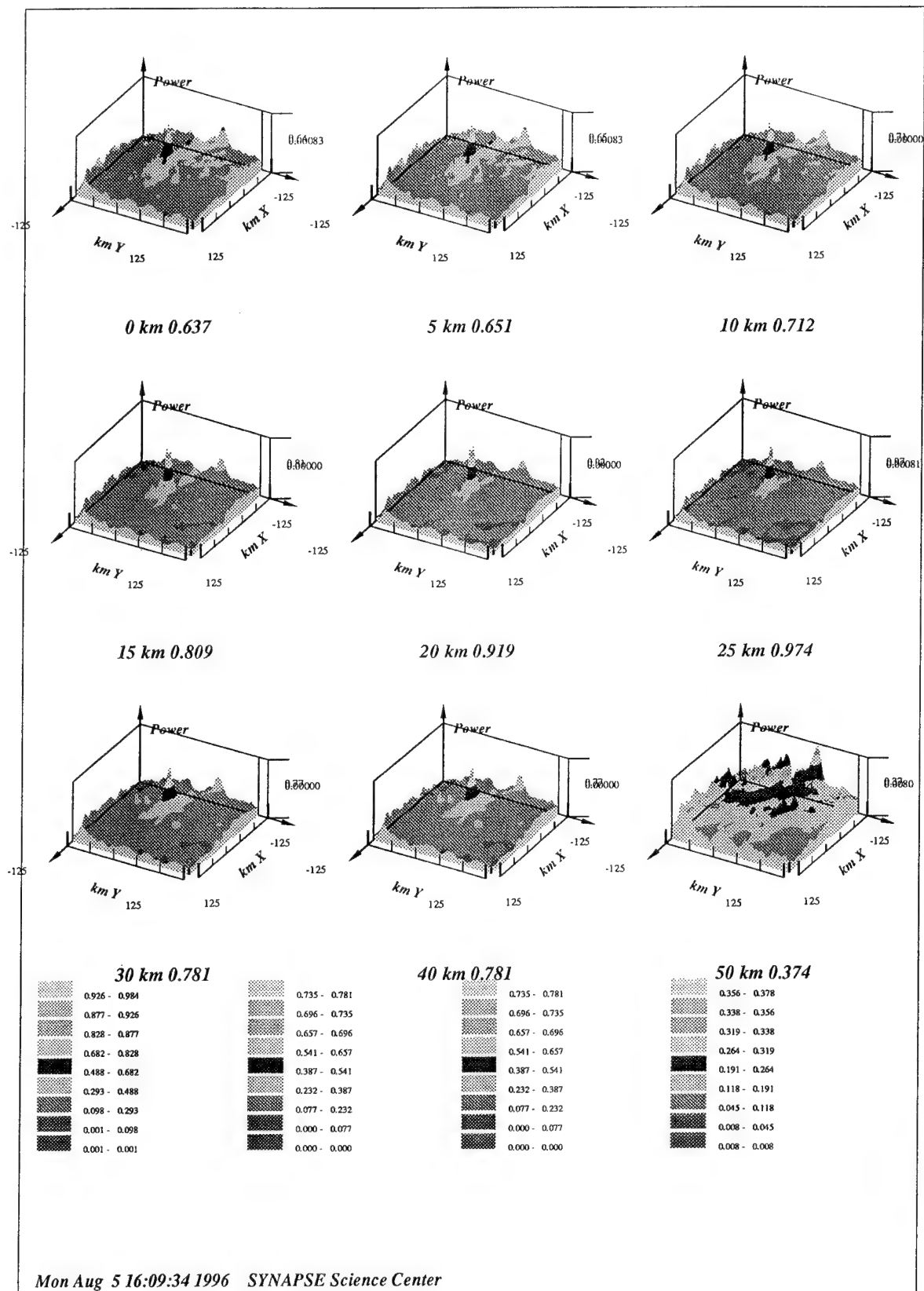


Fig. 2e. The output SNR-map, calculated by SCANLOC program
 The scanning grid area is 255 km x 255 km, grid intervals are 5 km,
 the depths are: 0km, 5km, 10km, 15km, 20km, 25km, 30km, 40km, 50km.

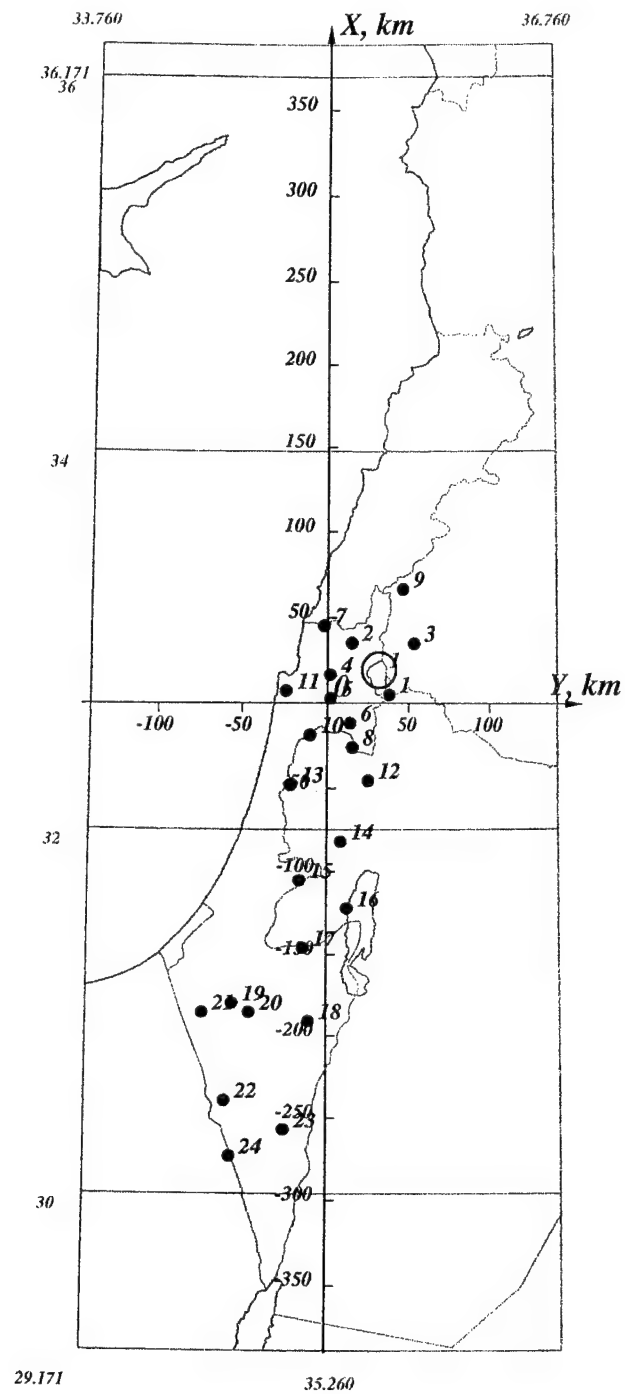


Fig. 3a. The deployment of Israel Seismic Network station which recorded the event 9104150120.

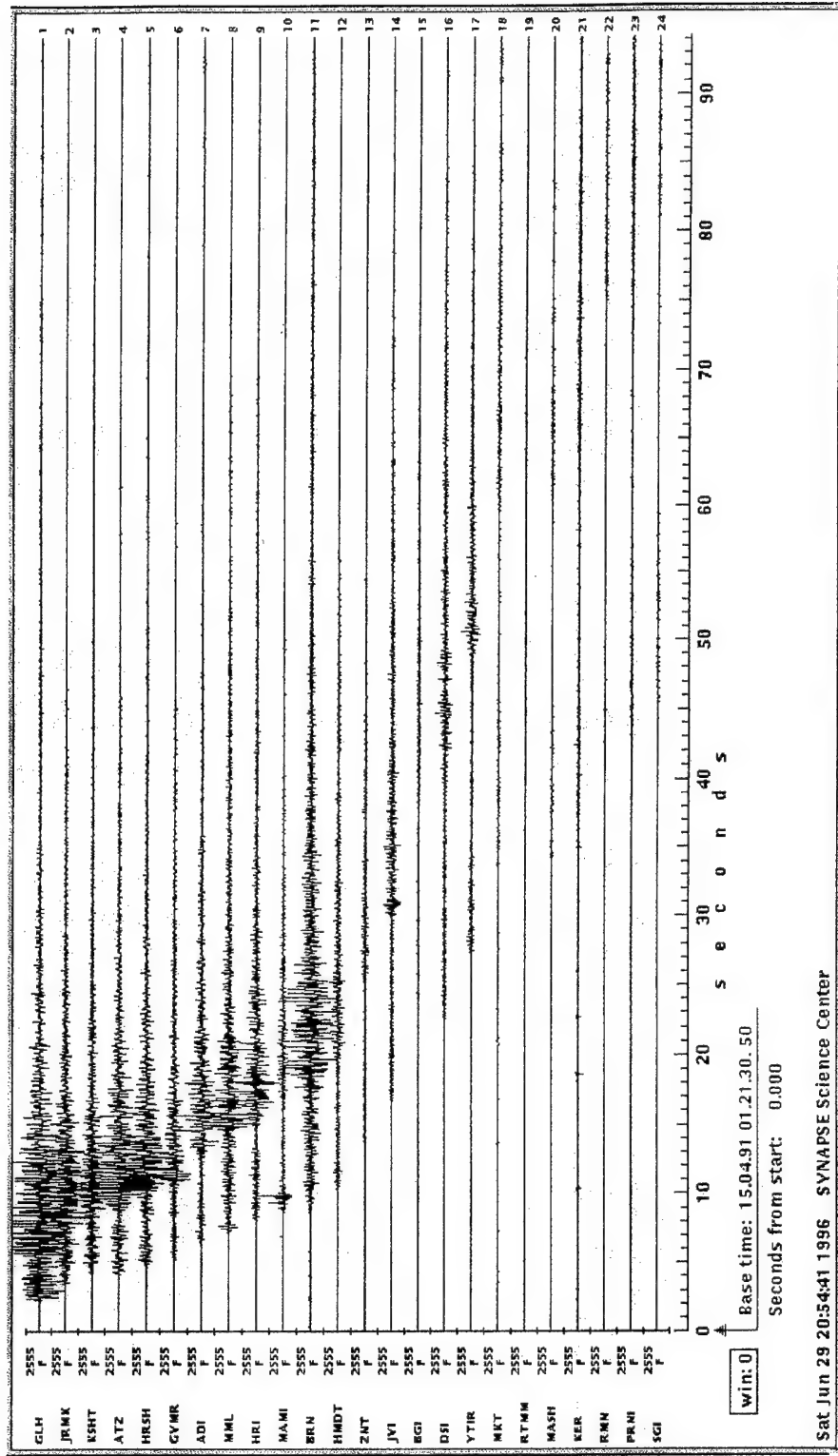


Fig. 3b. The seismogram of event 9104150120 recorded by 24 selected Israel Seismic Network stations.

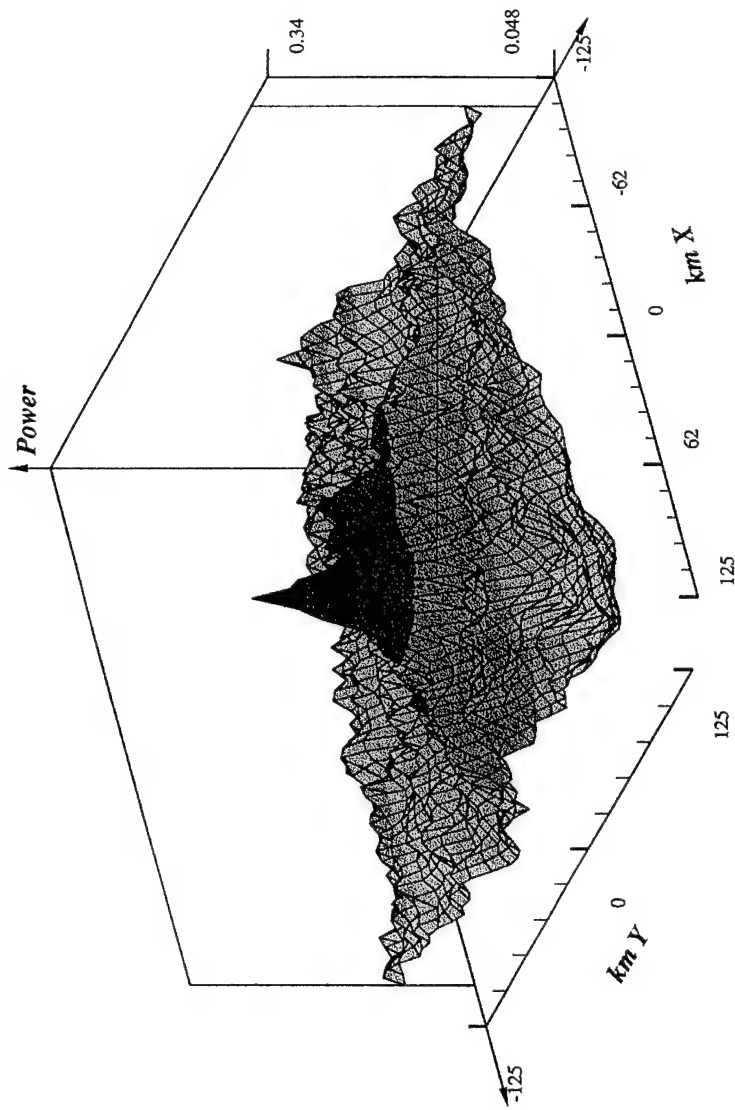
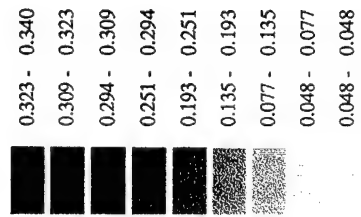


Fig. 3c. The output *SNR*-map, calculated by SCANLOC program.
 The scanning grid area is 255 km x 255 km,
 grid intervals are 5 km, depth is 0 km.

—	0.323
—	0.309
—	0.294
—	0.251
—	0.193
—	0.135
—	0.077
—	0.048

Zmin = 0.048

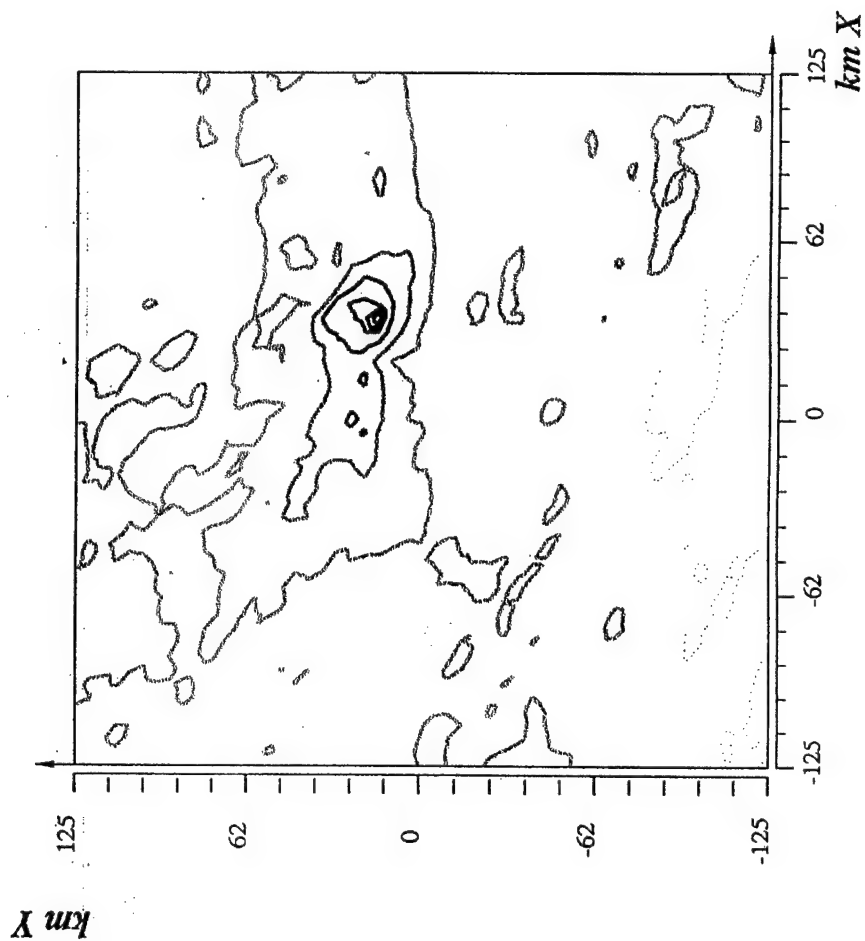


Fig. 3d. The output contour *SNR*-map, calculated by SCANLOC program.
The scanning grid area is 255 km x 255 km,
grid intervals are 5 km, depth is 0 km.

2.6 References

1. Y.Gitterman and T. van Eck (1993). Spectra of quarry blasts and microearthquakes recorded at local distances in Israel, *Bull.Seism.Soc.Am.*, 83, 1799-1812.
2. V.A.Gurevich, V.L.Kiselevich, B.M.Shoubik (1994) ASET - Array based Seismic Emission Tomography, *IRIS Newsletter*, Vol.XIV, No 1, 10-11.
3. S.A.Katz and B.M.Shoubik (1986). Implementation of Multichannel Adaptive Filters in Seismic Researches. Publication of Institute of Physics of the Earth, RAS, Moscow, "Nauka", 221 (in Russian).
4. B.L.N.Kennet (1996). Event location and source characterization, in E.Husebye, A.Dainty (eds.) "Monitoring a comprehensive test ban treaty", Kluwer Academic Publishers, Dortrecht, 501-520.
5. A.F.Kushnir (ed), L.M. Haikin, V.M. Lapshin, B.M. Shoubik, E.V. Troitsky (1995). Seismic monitoring with small aperture arrays under strong noise conditions: algorithms, technique, system design and experimental data processing. Scientific report on AFOSR Special Project SPC-94-4039.
6. N.S.Nadel and M.T.Taner (1971). Semblance and other coherency measures for multichannel data. *Geophysics*, v. 36, 482.
7. A.V.Nicolaev, P.A.Troitsky (1987). Lithospheric studies based on array analysis of P-coda and microseisms. *Tectonophysics*, vol. 140, 103-113.
8. B.M.Shoubik, V.L.Kiselevich, A.V.Nicolaev, L.N.Rykounov and O.G.Flovens (1996). Seismic Emission Tomography, XXV General Assembly European Seismological Commission, Reykjavik, 9-14 September. Abstracts, 37.
9. B.M.Shoubik, V.L.Kiselevich (1993). Microseismic activity in hydrothermal areas and problems of the seismic monitoring., in: "Concepts of the natural and engineering media monitoring". RAS, Moscow, "Nauka" (in Russian).
10. B.M.Shoubik, V.L.Kiselevich, A.V.Nicolaev, L.N.Rykounov (1991). Microseismic activity in hydrothermal areas, in: "Physics basis of the seismic methods", Publication of Institute of Physics of the Earth, RAS, Moscow, "Nauka", 143-158 (in Russian).
11. B.M.Shoubik (1980). Mask-Filters, *Geophysical Prospecting*, No.88, Moscow, "Nedra" (in Russian).
12. F. Ringdal and T. Kvarna (1989). A multichannel processing approach to real time network detection, phase association and threshold monitoring, *Bulletin of the Seismological Society of America*, Vol.79, 1927-1940.
13. G.A.Ryzhikov, M.S.Birulina and E.S.Husebye (1995). Automatic event location using local network data, *Proceedings of the 17th Annual Seismic Research Symposium on Monitoring of Comprehensive Test Ban Treaty 12-15 September of 1995*, 393-400.
14. C.J.Young, J.I.Beiriger, J.R.Trujillo, M.M.Withers, R.C.Aster, L.Astiz and P.M.Shearer (1995). WCEDS: A Waveform Correlation Event Detection System, *Proceedings of the 17th Annual Seismic Research Symposium on Monitoring of Comprehensive Test Ban Treaty 12-15 September of 1995*, 931-940.

2.7. Appendix

Descriptions of SNDA JCL scripts and SCANLOC input file

Appendix 1

Script "recsel.scr" for screening and selecting
the Israel Local Seismic Network seismograms
to further processing by the SCANLOC package:

```
#script boris/recsel.scr
#This script is designed to screening and selecting the ISN
#recordings to further processing by SCANLOC package

. char dt[29][10]
. && dt[1] = "8710071514";    dt[2] = "8802241537"
. && dt[3] = "8803031315";    dt[4] = "8904140553"
. && dt[5] = "9008112214";    dt[6] = "9008210621"
. && dt[7] = "9009041643";    dt[8] = "9009160941"
. && dt[9] = "9011170729";    dt[10] = "9012200001"
. && dt[11] = "9012211524";   dt[12] = "9101090230"
. && dt[13] = "9101261746";   dt[14] = "9101261902"
. && dt[15] = "9101270305";   dt[16] = "9102120832"
. && dt[17] = "9102250633";   dt[18] = "9104051807"
. && dt[19] = "9104071717";   dt[20] = "9104150120"
. && dt[21] = "9104150503";   dt[22] = "9104160637"
. && dt[23] = "9104270713";   dt[24] = "9105011435"
. && dt[25] = "9105012046";   dt[26] = "9105032206"
. && dt[27] = "9105160249";   dt[28] = "8808061449"
. char path[] = "/detseis/seis/alex/data/israel/earthq/"
. int I

. for (i=1;i<29;i= i+1)
    map plot/israelregcom.par
    && clearstack; readpack &path.&dt[i]..pk
    && episort1; plot all -y
. echo PLEASE ASSIGN THE TIME WINDOW and NUMBERS OF CHANNELS CHOOSSED:
    pause
    winon &sndf1 &sndf2
    && keep (&sndc1); cut all; plot all -y
    flist all data/boris/&dt[i].locb.flist
    pause
. echo YOU MAY PUSH "READ" BUTTON to display MAP
    savepack &path.&dt[i].locb.pk
. endfor
end of script
```

Appendix 2

Script "locproc.scr" for processing the preliminary selected seismograms
of Israel Local Seismic Network by the SCANLOC package in order
to obtain the spatial distribution of seismic sources
located in the scanning area.

```
# script boris/locproc.scr
# This script is designed to processing the preliminary selected
# 19 ISN recordings by SCANLOC package in order to obtain spatial
# distribution of seismic sources located in the scanning area.
```

```
. char dt[29][10],          dn[29][10]
. && dt[1]  = "8710071514";  dn[1]  = "1"
. && dt[2]  = "8802241537";  dn[2]  = "2"
. && dt[3]  = "9008210621";  dn[3]  = "3"
. && dt[4]  = "9009160941";  dn[4]  = "4"
. && dt[5]  = "9011170729";  dn[5]  = "5"
. && dt[6]  = "9012211524";  dn[6]  = "6"
. && dt[7]  = "9101090230";  dn[7]  = "7"
. && dt[8]  = "9101261746";  dn[8]  = "8"
. && dt[9]  = "9101270305";  dn[9]  = "9"
. && dt[10] = "9102120832";  dn[10] = "10"
. && dt[11] = "9102250633";  dn[11] = "11"
. && dt[12] = "9104071717";  dn[12] = "12"
. && dt[13] = "9104150120";  dn[13] = "13"
. && dt[14] = "9104150503";  dn[14] = "14"
. && dt[15] = "9104160637";  dn[15] = "15"
. && dt[16] = "9104270713";  dn[16] = "16"
. && dt[17] = "9105012046";  dn[17] = "17"
. && dt[18] = "9105032206";  dn[18] = "18"
. && dt[19] = "9105160249";  dn[19] = "19"
. char path1[80] = "/detseis/seis/alex/data/israel/earthq/"
. char path2[80] = "/detseis/seis/aset/boris/scngr/"
. int I

. for (I=1; i<20;i= i+1)
.   clearstack
.   readpack &path1.&dt[i].locb.pk
.   savessa &path2.indat
.   unix cp &path2.ifisrloc&dn[i] &path2.infloc.inp
.   unix &path2.scanloc
.   unix cp &path2.outdat &path2.outSMAPloc&dn[i]
. endfor
end of script
```

Appendix 3

Script "locview.scr" for screening the original seismograms,
mapping of selected station deployments and imaging of *SNR*-maps
calculated by the SCANLOC package for 19 selected events
registered by the Israel Local Seismic Network

```
# script boris/locview.scr
# This script is designed to screening the original recording,
# map of recorded seismic stations deployment and SNR-maps calculated by
# the SCANLOC package on the 19 ISN recordings
. char dt[29][10],          dn[29][10]
. && dt[1] = "8710071514";   dn[1] = "1"
. && dt[2] = "8802241537";   dn[2] = "2"
. && dt[3] = "9008210621";   dn[3] = "3"
. && dt[4] = "9009160941";   dn[4] = "4"
. && dt[5] = "9011170729";   dn[5] = "5"
. && dt[6] = "9012211524";   dn[6] = "6"
. && dt[7] = "9101090230";   dn[7] = "7"
. && dt[8] = "9101261746";   dn[8] = "8"
. && dt[9] = "9101270305";   dn[9] = "9"
. && dt[10] = "9102120832";   dn[10] = "10"
. && dt[11] = "9102250633";   dn[11] = "11"
. && dt[12] = "9104071717";   dn[12] = "12"
. && dt[13] = "9104150120";   dn[13] = "13"
. && dt[14] = "9104150503";   dn[14] = "14"
. && dt[15] = "9104160637";   dn[15] = "15"
. && dt[16] = "9104270713";   dn[16] = "16"
. && dt[17] = "9105012046";   dn[17] = "17"
. && dt[18] = "9105032206";   dn[18] = "18"
. && dt[19] = "9105160249";   dn[19] = "19"
. char path1[] = "/detseis/seis/alex/data/israel/earthq/"
. char path2[] = "/detseis/seis/aset/boris/scngr/"
. char path3[] = "data/israel/earthq/"
. char path4[] = "/home/lap/snda/sun4/scr/boris/"
. int i
. for (i=1; i< 20; i= i+1)
    unix rm &path2.OUT
    clearstack
    readpack &path1.&dt[i].locb.pk
    plot all -y
    flist all data/boris/mask11
    unix cp &path2.outSMAPloc&dn[i] &path4.OUT
    when (i=1)
        map plot/israelregcom1.par
        surfer &path4.surmapOUT.par
    endwhen
    pause
. endfor
end of script
```

Appendix 4

Example of input file "infloc.inp" for SCANLOC program
intended for processing of event 9104150120 seismograms

4700					NUMBER OF SAMPLES
0.02					SAMPLING INTERVAL
24					NUMBER OF STATIONS
2	6196.	3367.			NUMBER OF PHASES AND PHASE VELOCITIES
-125000.	5000.	51			Y-AXIS GRID PARAMETERS
-125000.	5000.	51			X-AXIS GRID PARAMETERS
0.	1000.	1			Z-AXIS GRID PARAMETERS
37783	4952	0.0	1.0	GLH	
14487	35500	0.0	1.0	JRMK	
52904	35188	0.0	1.0	KSHT	
1686	16858	0.0	1.0	ATZ	
1969	2884	0.0	1.0	HRSH	
13617	-11635	0.0	1.0	GVMR	
-2054	45360	0.0	1.0	ADI	
15047	-25828	0.0	1.0	MML	
45747	66319	0.0	1.0	HRI	
-10149	-18515	0.0	1.0	MAMI	
-24464	7239	0.0	1.0	BRN	
24876	-45548	0.0	1.0	HMDT	STATIONS INFORMATION
-21583	-47995	0.0	1.0	ZNT	
8322	-81726	0.0	1.0	JVI	
-16112	-105224	0.0	1.0	BGI	
12247	-122194	0.0	1.0	DSI	
-13797	-146143	0.0	1.0	YTIR	
-10416	-191051	0.0	1.0	MKT	
-55653	-179933	0.0	1.0	RTMM	
-45367	-185637	0.0	1.0	MASH	
-73832	-185699	0.0	1.0	KER	
-60283	-239448	0.0	1.0	RMN	
-25094	-257213	0.0	1.0	PRNI	
-57100	-273390	0.0	1.0	SGI	
9104150120					LABEL OF EVENT

Explanation of program input parameters:

NUMBER OF SAMPLES

This string defines the number of samples containing in the each seismic trace of processed seismogram. In the our experiments with ISN data processing this parameter took a value from range 800 - 5000. This value is limited by available computer memory capacity only.

SAMPLING INTERVAL

This string defines the each seismic trace sampling rate expressed in second. In the our experiments with ISN data processing this parameter took a value 0.02 sec.

NUMBER OF STATIONS

This string defines the number of seismic traces containing in the processed seismogram. In the our experiments with ISN data processing this parameter took a

value from range 8 - 24. This value is limited by available computer memory capacity only.

NUMBER OF PHASES AND PHASE VELOCITIES

This string defines the number of seismic phases (first parameter) and their velocities expressed in m/sec (following parameters). If the incoherent stacking is used the first parameter determined by the number of seismic phases which could be detected by one channel mask-filter. Phase velocities determined by the a priori velocity model of the medium. In the our experiments with ISN data processing we have used 2 phases (P and S) and the homogeneous *a priori* seismic velocity model with velocities of P and S waves equal to: $V_p = 6196$ m/sec and $V_s = 3367$ m/sec.

Y-AXIS GRID PARAMETERS

This string defines the part of scanning grid parameters. The first parameter is the beginning value of scanning grid coordinates by Y axis expressed in meter. The second parameter is the grid step expressed in meter. Coordinates are given in the local orthogonal system. The third parameter is the number of grid units by the Y axis. In the our experiments with ISN data processing we have specified this value from 1 to 100 grid units by Y axis.

X-AXIS GRID PARAMETERS

This string defines the part of scanning grid parameters. The first parameter is the beginning value of scanning grid coordinates by X axis expressed in meter. The second parameter is the grid step expressed in meter. Coordinates are given in the local orthogonal system. The third parameter is the number of grid units by the X axis. In the our experiments with ISN data processing we have specified this value from 1 to 100 grid units by X axis.

Z-AXIS GRID PARAMETERS

This string defines the part of scanning grid parameters. The first parameter is the beginning value of scanning grid coordinates by Z axis expressed in meter. The second parameter is the grid step expressed in meter. Coordinates are given in the local orthogonal system. The third parameter is the number of grid units by the Z axis. In the our experiments with ISN data processing we have specified this value from 1 to 100 grid units by Z axis.

STATION INFORMATION

This section of infloc.inp file contains the strings which number are equal to number of station. Each string includes 5 parameters. The first parameter is the X coordinate of station expressed in meter. The second parameter is the Y coordinate of station expressed in meter. The third parameter is the Z coordinate of station (the station elevation with respect to sea level) expressed in meter. The coordinates of seismic stations are defined in the local orthogonal system which is the same as coordinate system to scanning grid units. The forth parameter may take two values: 0 or 1. If it is equal to 0 the data of corresponding station does not take part in event location procedure. Sometimes it could be necessary to exclude part of data from further processing by arbitrary reasons. The fifth parameter is the short name of station.

LABEL OF EVENT

This string contents the identification information about processed event.

2.8. Study of Israel regional velocity model on the basis of Israel Seismic Network catalogue of local events.

The travel time tables of seismic wave phases typical for a given region are necessary for the seismic event location based on seismic array and local network data. The accuracy of event hypocenter determination depends on correspondence of phase travel times estimated from the tables used in the location procedure to the real phase time delays for the event under study. The regional travel time tables are usually created in the result of seismic sounding the regional medium by artificial (mainly explosion) sources. Such tables turns to be as a rule rather "smoothed" and not always adequate to the real medium structure in different areas of the region. Detailing of the medium structure and revealing of the local medium heterogeneity demands rather expensive field experimental studies. At the same time the estimates of onset times of wave phases from regional and local events can be utilized for this purpose. If collected statistic become representative enough then for every source-station pair the corrections of the preliminary time travel table can be calculated.

$$t_{ij} = t_{ij}^0 + \delta_{ij}$$

where t_{ij}^0 is the interpolated value of travel time table, δ_{ij} is the correction obtained from experiments. Such work for travel time table correction are conducting at many seismological organizations running local seismic networks for a long time. If the structure of earth medium in the area of seismic network deployment is homogeneous enough then analytic equations can be constructed for regional phase travel time curves against an epicenter distance. This can be done if sufficient amount of arrival time estimates is accumulated in the results of long period of observations.

We made the attempt to determine such equations for the Israel region using the method of regression analysis applied to data acquired by Seismological Division of the Institute for Petroleum Researches and Geophysics (IPRG) in Holon, Israel, during the period 1987 - 1991. The deployment of Israel Local Network stations is shown at the map in Fig.4. The source locations of weak earthquake and explosion events contained in the available IPRG data base are depicted at the map in Fig.5.

The purposes of our study were:

- 1) to check the correspondence between the theoretical regional travel time table available from NORSAR publications and real travel times observed from seismic phases detected in Israel events.
- 2) to correct the regional travel time table in accordance with results of observations.
- 3) to derive analytic equations for travel time curves in depending on epicenter distance; these equations could be used in fast algorithms for event location by scanning of the medium with the beam formed using P and S phase traces in seismograms registered by the local network stations.
- 4) to investigate the character of variations of P-and S-phases apparent velocities in depending on the epicenter distance.

We have analyzed the catalog of weak earthquakes containing arrival times for 4 regional seismic phases: Pg, Sg, Pn and Sn, originated from the sources located in the region Galilee-Kinneret-Coast Tzor. The earthquakes were recorded by the stations of the Israel Local Network; their source parameters are presented in Table 1. The maximum distance between a source and a station was about 350 km. The catalogue contains for given sources the information about onset times of 313 Pg phases, 121 Sg phases, 262 Pn phases and 225 Sn phases. The sufficient amount of experimental data allowed us to obtain analytical equations for the travel time curves of these phases and to study the behavior of the phase apparent velocities against the distance from the source.

Table 1.

N	Year	Month	Date	Origin time	Latitude	Longitude	Name of region
1	1987	OCT	7	15:15: 4.7	32.671 N	35.260 E	Galilee Reg
2	1988	FEB	24	15:37:26.6	32.717 N	35.251 E	Galilee Reg
3	1988	MAR	3	13:15:25.4	32.743 N	35.258 E	Galilee Reg
4	1988	JUL	29	23:33:28.6	32.664 N	35.218 E	Galilee Reg
5	1988	AUG	6	14:49:27.5	32.712 N	35.142 E	Galilee Reg
7	1989	AUG	19	9:17: 5.4	32.790 N	35.283 E	Galilee Reg
8	1990	AUG	11	22:14:59.6	32.987 N	35.413 E	Galilee Reg
9	1990	AUG	17	9:30:32.1	33.140 N	35.262 E	Tzor (Tyre) Reg
10	1990	AUG	21	6:22:23.0	32.663 N	35.152 E	Galilee Reg
11	1990	SEP	4	16:44:21.1	32.908 N	35.035 E	Galilee Reg
12	1990	SEP	16	9:41:44.4	32.961 N	34.981 E	Off Coast Haifa Reg
13	1990	NOV	17	7:30:16.1	32.792 N	35.270 E	Galilee Reg
14	1990	DEC	20	0: 2:18.5	32.547 N	35.226 E	Galilee Reg
15	1990	DEC	21	15:24:50.4	32.853 N	35.571 E	Kinneret Reg
16	1991	JAN	9	2:30:42.2	32.781 N	35.272 E	Galilee Reg
17	1991	JAN	26	17:46:55.7	32.782 N	35.273 E	Galilee Reg
18	1991	JAN	26	19 3:24.0	32.792 N	35.296 E	Galilee Reg

19	1991	JAN	27	3:5:37.2	32.808 N	35.324 E	Galilee Reg
20	1991	FEB	12	8:32:56.9	32.857 N	35.468 E	Galilee Reg
21	1991	FEB	25	6:33:55.4	32.581 N	35.306 E	Galilee Reg
22	1991	APR	5	18:8:24.2	33.084 N	35.039 E	Tzor (Tyre) Reg
23	1991	APR	7	17:18:19.7	32.845 N	35.584 E	Kinneret Reg
24	1991	APR	15	1:21:28.3	32.848 N	35.594 E	Kinneret Reg
25	1991	APR	15	5:3:49.8	32.826 N	35.574 E	Kinneret Reg
26	1991	APR	16	6:38:1.3	32.844 N	35.587 E	Kinneret Reg
27	1991	APR	27	7:13:22.3	32.852 N	35.580 E	Kinneret Reg
28	1991	MAY	1	14:36:22.4	32.847 N	35.580 E	Kinneret Reg
29	1991	MAY	1	20:47:12.1	32.835 N	35.578 E	Kinneret Reg
30	1991	MAY	3	22: 7:19.2	32.830 N	35.583 E	Kinneret Reg
31	1991	MAY	16	2:50:17.2	33.080 N	34.981 E	Off Coast Tzor Reg

We have used the RMS method of regression analysis for creating of a statistical model of phase travel time curves. We assumed that regression is not linear and time travel curves may be approximated by second-order polynomial:

$$T(s) = b_0 + b_1 s + b_2 s^2,$$

where T is the travel time, s is the distance from source to station, $\mathbf{b} = (b_0, b_1, b_2)^T$ is a vector of regressions coefficients. To obtain the regression equation $T = f(s)$ let us introduce the matrices

$$\mathbf{t} = \begin{pmatrix} t_1 \\ t_2 \\ \vdots \\ t_N \end{pmatrix}, \quad \mathbf{S} = \begin{pmatrix} 1 & s_1 & s_1^2 \\ 1 & s_2 & s_2^2 \\ \vdots & \vdots & \vdots \\ 1 & s_N & s_N^2 \end{pmatrix}, \quad \mathbf{b} = \begin{pmatrix} b_0 \\ b_1 \\ b_2 \end{pmatrix}.$$

The results of observations form the column vector \mathbf{t} and values of regression curve - vector \mathbf{T} . Our task is to estimate the coefficients b_0, b_1, b_2 of column vector \mathbf{b} . If to denote by $\mathbf{X} = \mathbf{S}'\mathbf{S}$, then RMS estimations of \mathbf{b} are got as the solution of matrix equation $\mathbf{X}\mathbf{b} = \mathbf{S}'\mathbf{t}$:

$$\mathbf{b} = \mathbf{X}^{-1}\mathbf{S}'\mathbf{t}.$$

The results of estimation of regression coefficient are presented in Table 2.

Table 2.

Coefficients	Values of coefficients for different phases			
	Pg	Sg	Pn	Sn
b0	0.00047	0.00219	1.1745	1.9951
b1	0.16137	0.29682	0.1671	0.2900
b2	18*10 ⁻⁷	16*10 ⁻⁷	-0.0001	-0.0001

For developing of our 2-order regression time travel curves we assumed the following statistical model of estimated phase onset times

$$t_i = b_0 + b_1 s_i + b_2 s_i^2 + e_i,$$

where epicentral distances s are free of mistakes as and e_i are random independent Gaussian variables with mean zeros and equal variances. Also we assumed that the random error of travel time estimation e_i depends on accuracy of event origin time determination and accuracy of P- and S-phase arrival time estimation by a stations operator. This error is regarded as the same for all observations over networks stations:

$$\sigma_{e_i} = \sqrt{\sigma_{t_0}^2 + \sigma_{t_i}^2},$$

where σ_{t_0} is the standard deviation of origin time, σ_{t_i} is the standard deviation of arrival time.

Note, that the most correct approach consists in accounting for the fact that any source location method is based on minimizing the sum of residual times. So, ellipse of source coordinate errors is defined by the sum of squares of phase travel time residuals. In other words, both the origin time and arrival time errors are not independent. But this approach is rather complex one and we confine the analysis by the above assumption about independence of origin and arrival time errors.

We have carried out the variance analysis of the regression to evaluate its significance and have applied the F-criteria for estimating the significance of every coefficient in the regression equation. The statistic of F-criteria is defined by the equation:

$$F_{2,N-3} = \frac{\mathbf{b}'\mathbf{S}'\mathbf{t} - N\bar{t}^2}{\mathbf{t}'\mathbf{t} - \mathbf{b}'\mathbf{S}'\mathbf{t}},$$

where \bar{t} is mean value of the components of vector \mathbf{t}

The results of variance analysis for 2-order regression are shown in Table 3.

Table 3.

Phase type	$(\mathbf{b}'\mathbf{S}'\mathbf{t})10^4$	$(\mathbf{t}'\mathbf{t})10^4$	$\sqrt{\sum (T_i - t_i)^2} 10^3$	$(F_{2,N-3})10^3$
Pg	2.706851	2.706859	0.0028	3690
Sg	2.5100179	2.5100181	0.0044	3613
Pn	16.80232	16.8037	0.2337	3.931
Sn	48.91412	48.9176	0.3942	4.685

One may infer that the regression has the high significance in regard of the table values of F-distribution even on the 2.5% level and thus regression model developed is adequate to real crust velocity features.

The straightforward equations obtained for phase travel times against distances can be employed in a fast real-time algorithms for source location without loss of accuracy in comparison with more time consuming procedure of interpolating experimental travel time tables.

For the initial fitting in these procedures the more precise first order regression also could be helpful. The regressions coefficients for 1-order regression are shown in Table 4.

Table 4.

Values of coefficients for different phases				
Coefficient	Pg	Sg	Pn	Sn
b0	-0.0001	-0.0016	2.2169	3.9868
b1	0.1614	0.2971	0.1442	0.2488

The results of dispersion analysis of 1-order regression coefficients are shown in Table 5.

Table 5.

Phase type	$(b'S't)10^4$	$(t't)10^4$	$10^3 \sqrt{\sum (T_i - t_i)^2}$	$10^3 F_{3,N-3}$
Pg	2.7068595	2.7068597	0.0028	3660
Sg	2.5100179	2.5100181	0.0047	3137
Pn	16.793	16.8037	0.6321	0.54
Sn	48.889	48.9176	1.1312	0.56

The application of the F-criterion to the regression coefficients shows that on the 5% confidence level the coefficients b_0 and b_1 are statistically significant for the all phase regression equations being analyzed. However on the 2.5%-level only the coefficients for Pg and Sg phases are significant. So for the Pn and Sn phases the 2-order regressions have to be adopted. Hence, the linear equations for the travel time against the distance with the coefficients given in Table 4 can be recommended for the Pg and Sg phases.

The linear and quadratic regression functions for the Pn and Sn phase travel time in depending on epicenter distance with the experimental phase onsets are depicted in Fig.6. We see that even visually the quadratic functions provide the much better fitting than linear ones with the sets of Pn and Sn arrival time observations. The linear regression functions for the Pg and Sg phase travel time in depending on epicenter distance with the experimental phase onsets are depicted in Fig.7. We see that for "g"-phases the arrival time observations are in a good accordance with the linear regression curves.

The estimates for variances of regression coefficients can be determined from the covariance matrix using the known equation: $cov\{b\} = \sigma_e^2 X^{-1}$. For the linear regression model it implied the following equations:

$$var\{b_0\} = \sigma_e^2 (X_{00})^{-1} \quad var\{b_1\} = \sigma_e^2 (X_{11})^{-1}$$

The determined by this method values of standard deviation for linear regression coefficients are presented in Table 6.

Table 6.

Values of coefficient standard deviations for different phases				
Coefficient	Pg	Sg	Pn	Sn
b0	0.19145	0.2926	0.1708	0.195
b1	0.00695	0.0121	0.0028	0.003

Employment of the linear travel time equations at local distances provides the opportunity to simplify the minimum mean square source location algorithm while its application to local network data. This algorithm uses the linearization method for solving the inverse location problem so the assumption on the linearity of distance-velocity curves leads to decreasing of computing.

The results discussed above concerned the developing of the relations between phase travel time and epicenter distance: $T=f(s)$. The inverse relations (the distance against the travel time) gives one a impression about the variations of phase apparent velocities along the horizontal distance of phase propagation. For this reason we developed also the similar quadratic and linear regression equations for the relation $s=f(T)$. The coefficients of the linear regressions for the all regional phases are shown in Table 7. The plots of horizontal distance of the Pn and Sn propagation paths in depend of travel time with the quadratic regression fitting curves are presented in Fig. 8. The

analogous plots for Pg and Sg phases with the linear regression curves are shown in Fig. 9.

Table 7.

Coefficient	Values of coefficients for different phases			
	Pg	Sg	Pn	Sn
b0	0.0008	0.0056	-15.0643	-15.6602
b1	6.1959	3.3668	6.9221	4.0102

Israel seismic local network

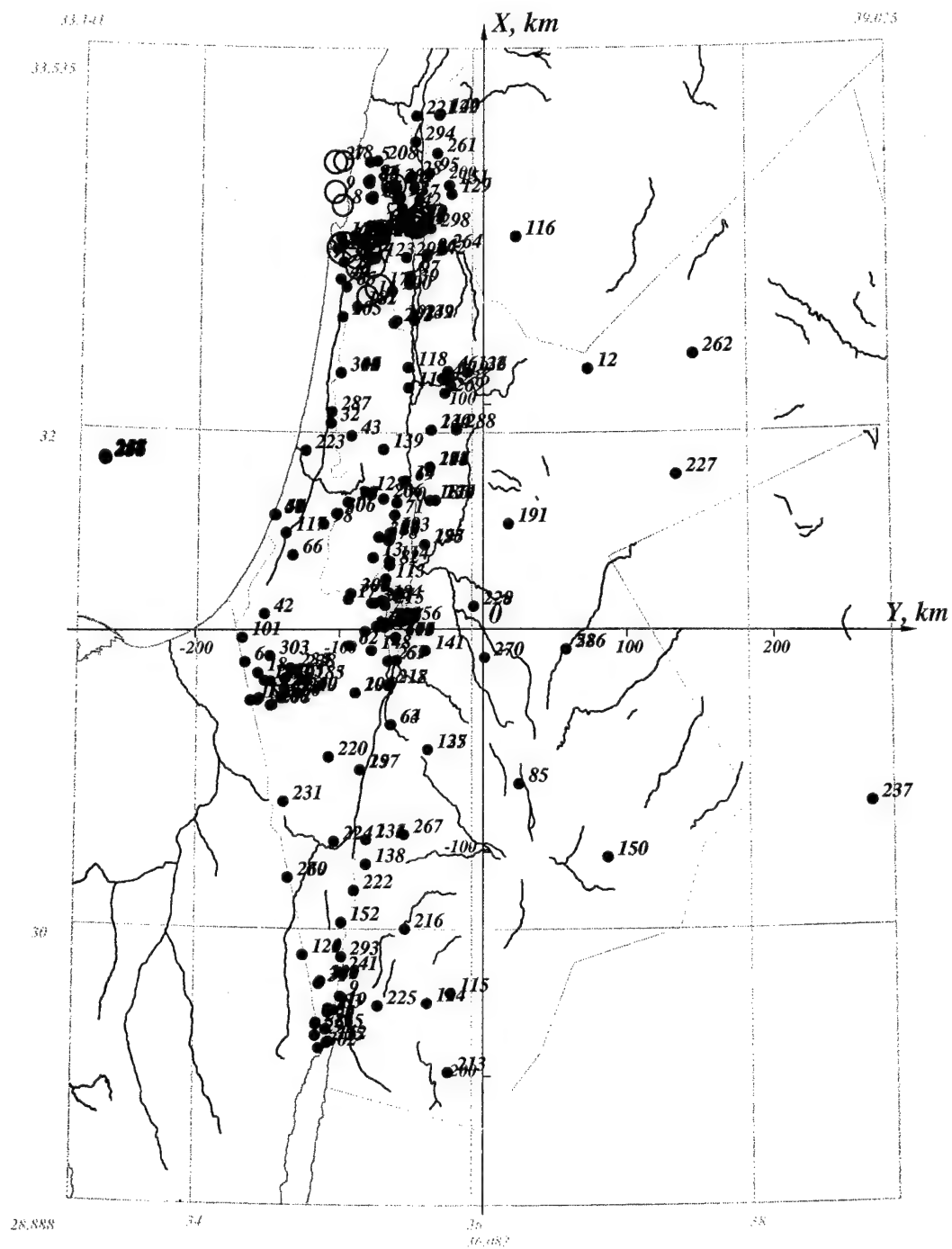


Fig. 4. Deployment of stations of the Israel Local network.

Israel seismic local network

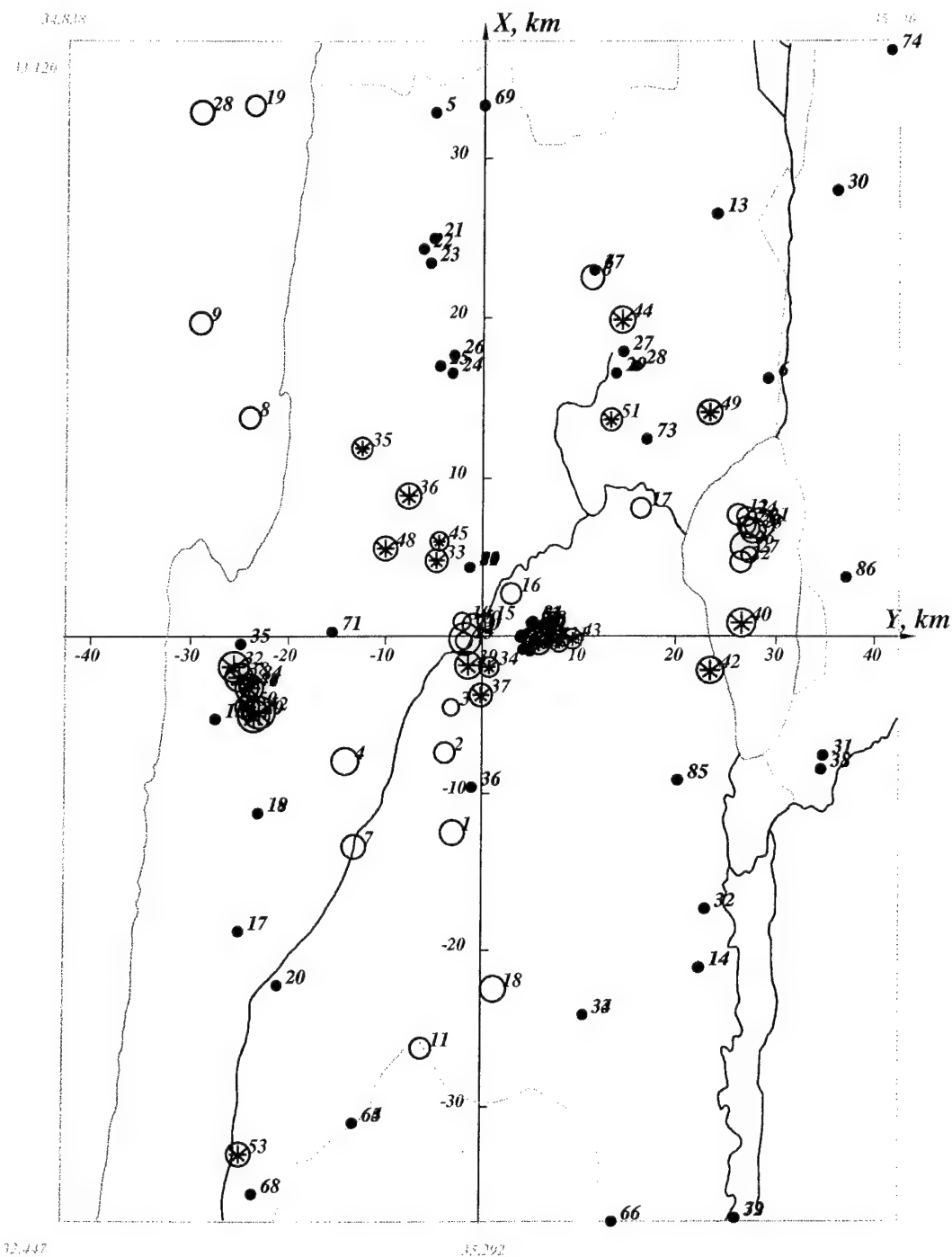


Fig. 5. Locations of Israel weak earthquakes and explosions.
Circles are the earthquake sources;
stars are the explosion sources.

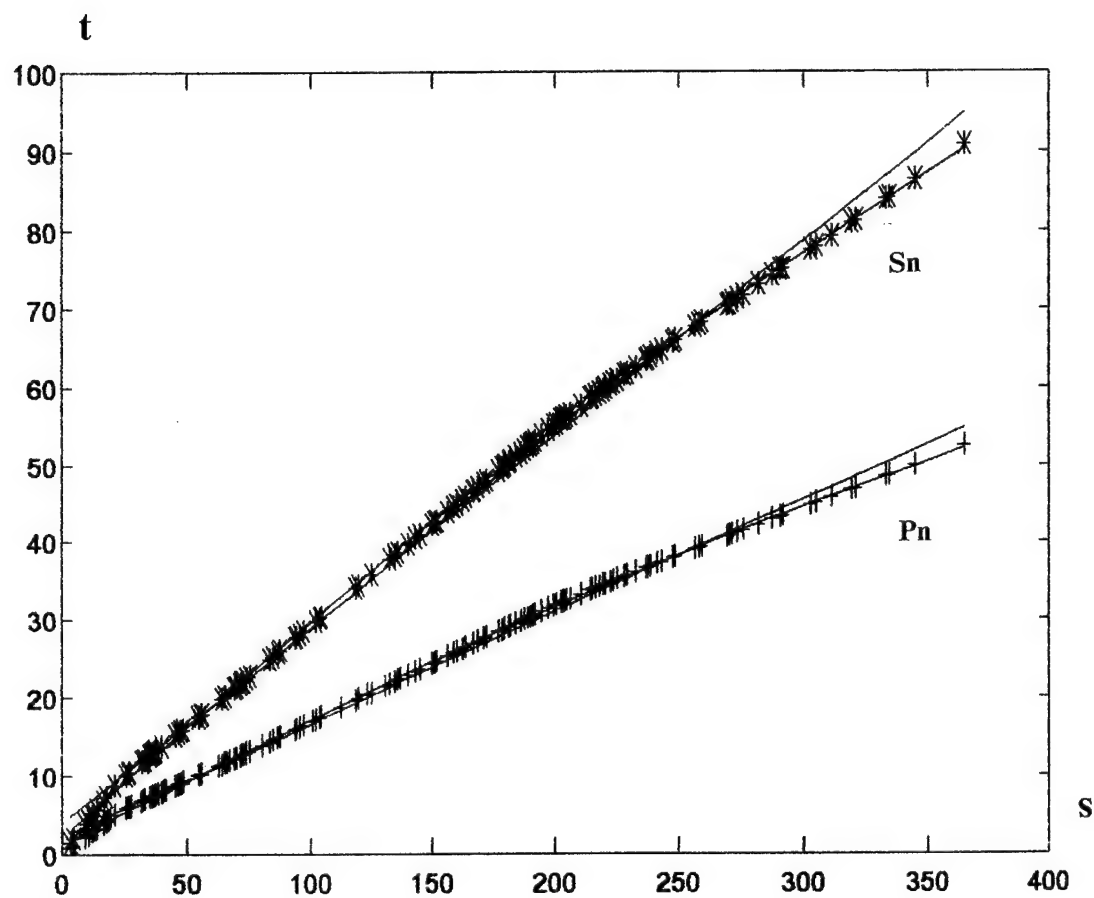


Fig. 6. Linear and quadratic regressions
for Pn and Sn phase travel time
in dependent on epicenter distance.

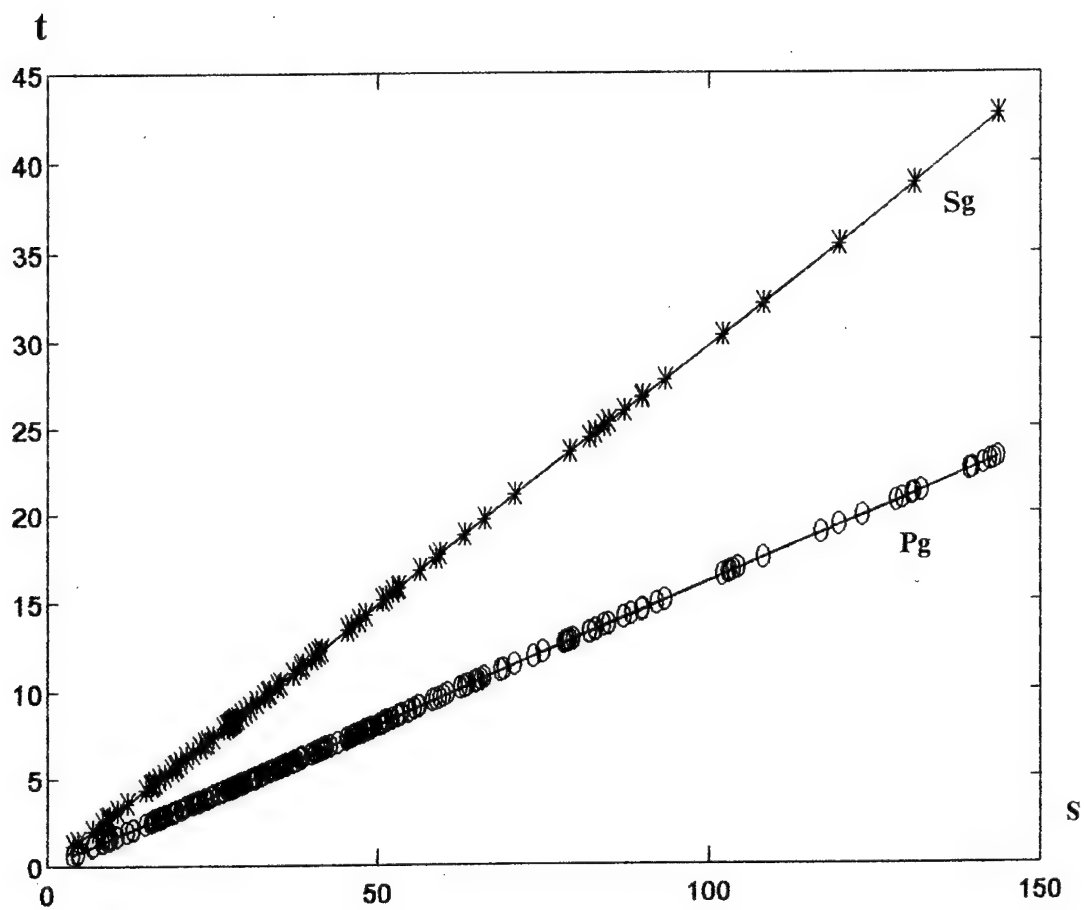


Fig. 7. Linear regressions
for Pg and Sg phase travel time
in dependent on epicenter distance.

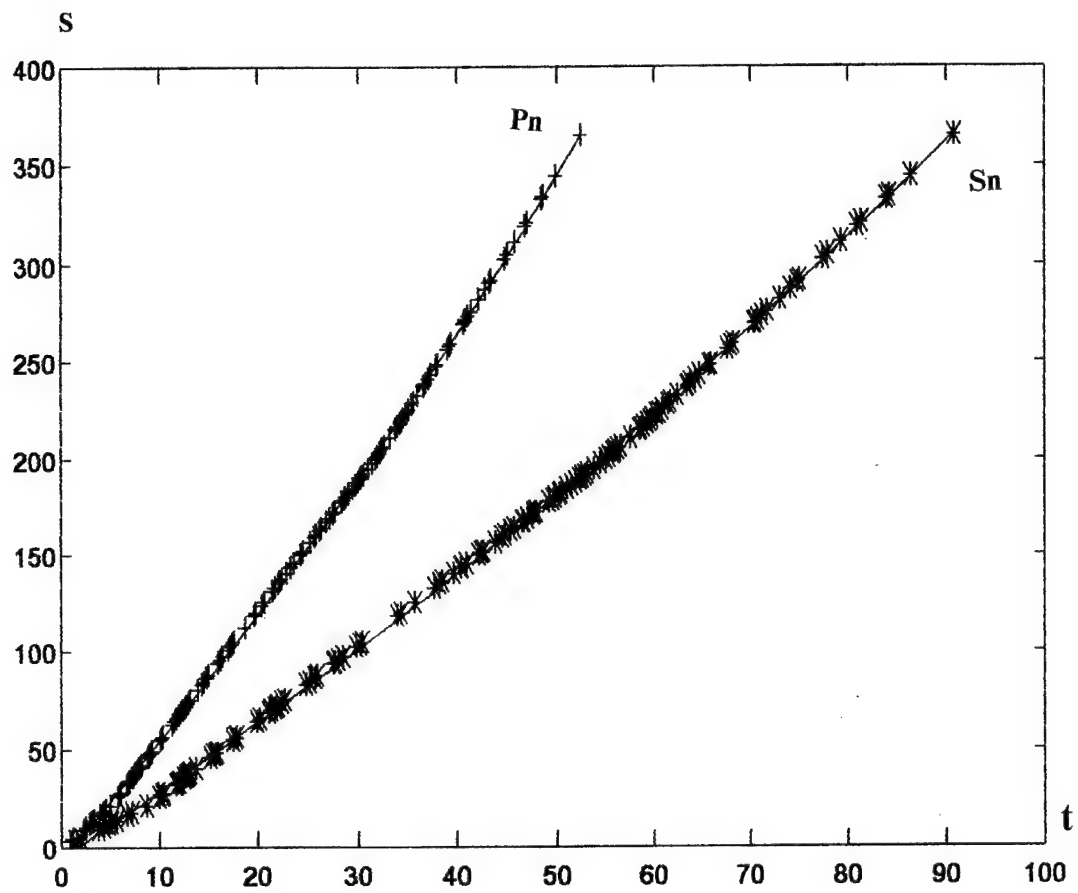


Fig. 8. Horizontal distance of P_n and S_n propagation paths in dependent on travel time.

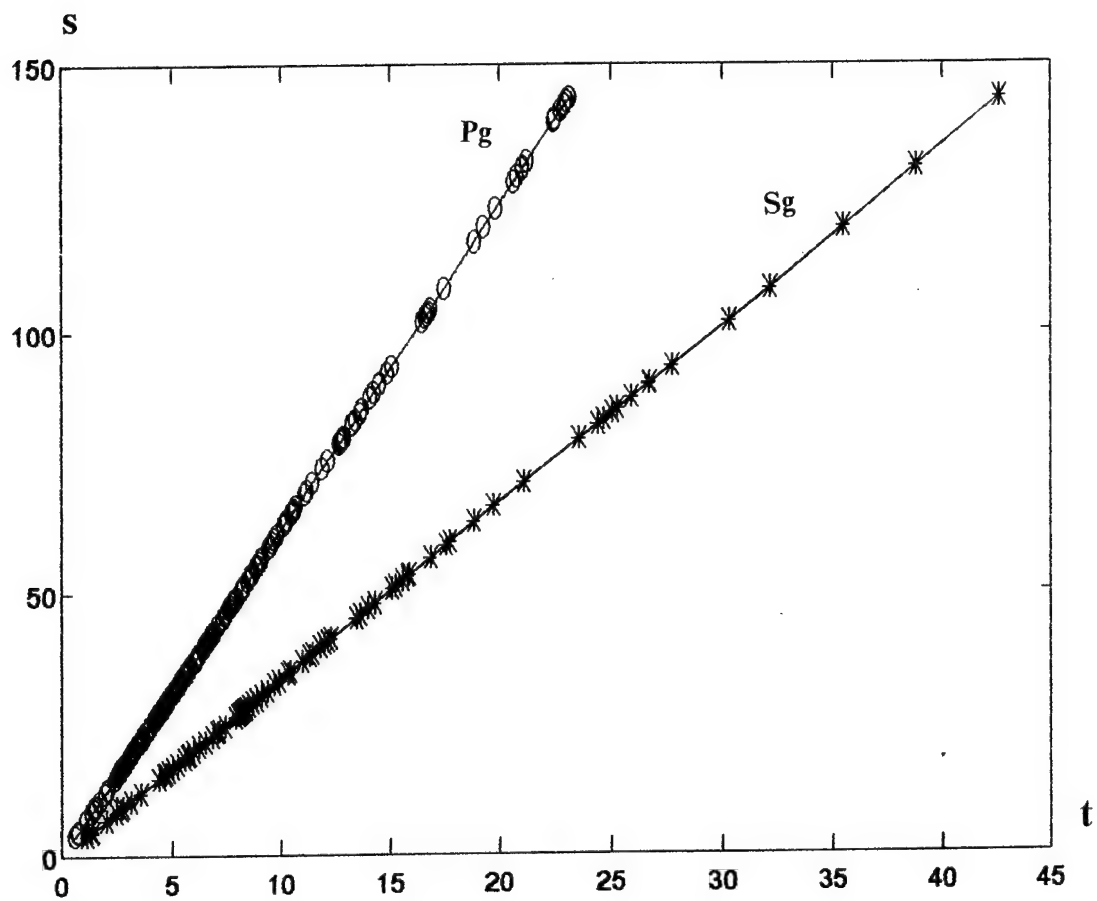


Fig. 9. Horizontal distance of Pg and Sg propagation paths in dependent on travel time.

3. ADAPTIVE PROCESSING OF 3-COMPONENT SMALL APERTURE AND MICRO-ARRAY DATA (THEORY AND ALGORITHMS)

CONTENT

]

3.1. Mathematical models of 3-component small aperture seismic array records	1
3.2. Coherent noise suppression and seismic waveform extraction using data from 3-component arrays	7
3.2.1. Introduction	7
3.2.2. Statistically optimal group filter (Wiener filter)	8
3.2.3. Adaptation of optimal group filter to variations of noise spectrum	10
3.2.4. Spatial Rejecting Group Filter	12
3.2.5. Optimal group filter with additional constraints	14
3.3. Adaptive statistical algorithms for estimation of azimuth and apparent velocity of seismic phases using data from 3-component arrays	16
3.3.1. Introduction	16
3.3.2. Mathematical models of observations as a random time series with informative and nuisance parameters	17
3.3.3. Asymptotically efficient estimates of apparent slowness vector for random signal waveforms	19
3.3.4. Asymptotically efficient estimates of apparent slowness vector for small signal-to-noise ratio	22
3.3.5. Apparent slowness estimates for completely unknown signal waveforms	24
3.4. References	27

3. ADAPTIVE PROCESSING OF 3-COMPONENT SMALL APERTURE AND MICRO-ARRAY DATA (THEORY AND ALGORITHMS)

3.1. Mathematical models of 3-component small aperture seismic array records

Let us suppose hereinafter that seismic waves are generated by remote seismic source and each of the seismic phases (P , S , L , R , etc.) is a plain wave. It is supposed as well that the body wave phases arrive from the homogeneous lower half space on a surface batch of laterally homogeneous layers in accordance with unit steering vectors $\mathbf{a}_w = (a_{wx}, a_{wy}, a_{wz})^T$, where w represents the wave-type index. We designate as v_w a velocity of a w -type wave in the half space directly beneath the batch of layers. Let us assume the origin of coordinates to be settled on the surface of the half space, with the Z -axis directed down, Y -axis to the North and X -axis to the East; the wave azimuth α be counted clockwise from the positive direction of the Y axis, and the wave incidence angle β_w - from the positive direction of the Z axis. Then the vector \mathbf{a}_w can be written as $\mathbf{a}_w = (\sin\alpha \sin\beta_w, \cos\alpha \sin\beta_w, \cos\beta_w)^T$ (T is the sign of transposition). For surface waves $\beta_w = \pi/2$ and $\cos\beta_w = 0$.

A medium displacement $\mathbf{w}(t, \mathbf{r}) = (w_x(t, \mathbf{r}), w_y(t, \mathbf{r}), w_z(t, \mathbf{r}))^T$ for a particular seismic phase at an arbitrary point $\mathbf{r} = (r_x, r_y, r_z)^T$ of the homogeneous half space can be expressed as follows:

$$\mathbf{w}(t, \mathbf{r}) = s_w(t - (\mathbf{r}^T \mathbf{a}_w)/V_w) \mathbf{b}_w \quad (1)$$

where $s_w(t)$ is a waveform of a seismic phase at the origin of coordinates, $\mathbf{b} = (b_{wx}, b_{wy}, b_{wz})^T$ - is a unit vector of seismic phase oscillations which is determined by a wave the incidence angle β , azimuth α and the model of transformations of the plain wave at the day surface boundary. For the simplest medium model without consideration of affecting of the day surface on the wave field the vector \mathbf{b} is expressed by the following simple geometric equations [6]:

$$\text{for P-waves} \quad \mathbf{b}_P = \begin{bmatrix} \sin\alpha \sin\beta \\ \cos\alpha \sin\beta \\ \cos\beta \end{bmatrix}; \quad (2a)$$

$$\text{for SH-waves and for Love waves} \quad \mathbf{b}_L = \begin{bmatrix} \cos\alpha \\ \sin\alpha \\ 0 \end{bmatrix}; \quad (2b)$$

for SV-waves

$$\mathbf{b}_V = \begin{bmatrix} \sin \alpha \cos \beta \\ \cos \alpha \cos \beta \\ \sin \beta \end{bmatrix}; \quad (2c)$$

for Rayleigh waves

$$\mathbf{b}_R = \begin{bmatrix} i \sin \alpha \sin \beta \\ i \cos \alpha \sin \beta \\ \cos \beta \end{bmatrix}; \quad (2d)$$

where $\psi = \arctg(e)$, e represents the ellipticity of a Rayleigh wave, e.g. the ratio of the small axis of a polarization ellipse to the large one; $i = \sqrt{-1}$ characterises the phase shift of $\pi/2$ between the vertical and horizontal components of Rayleigh wave displacements.

In the frequency domain eq.(1) has the form

$$\mathbf{w}(f, \mathbf{r}) = s_w(f) \exp[-i2\pi f(\mathbf{r}^T \mathbf{a}_w)/V_w] \mathbf{b}_w \quad (3)$$

where $s_w(f)$ is the complex spectrum of phase waveform. Let us introduce the 3-dimensional phase slowness vector: $\mathbf{q}_w = (p_x, p_y, p_z)^T = \mathbf{a}/V_w$. Then the wave field eq.(2) can be expressed as a function of the vector \mathbf{q}_w as follows:

$$\mathbf{w}(f, \mathbf{r}) = s_w(f) \exp[-i2\pi f(\mathbf{r}^T \mathbf{q}_w)] \mathbf{b}(\mathbf{q}_w, V_w) \quad (4)$$

Dependence of the vector \mathbf{b} from the vector \mathbf{q}_w in eq.(4) is based on the following simple geometric relations:

$$\sin \alpha = p_x/p_h; \quad \cos \alpha = p_y/p_h; \quad \sin \beta_w = p_h/V_w; \quad p_h = (p_x^2 + p_y^2)^{-1/2}. \quad (5)$$

Equations (2) and (5) imply that for simplest media model the vector \mathbf{b} depends only on the values of apparent velocities p_x, p_y, p_h and phase velocities V_p, V_s via the following equations:

for P-waves

$$\mathbf{b}_P = \begin{bmatrix} p_x \\ p_y \\ \sqrt{V_p^{-2} - p_h^2} \end{bmatrix} V_P \quad (6a)$$

for SH-waves and Love waves

$$\mathbf{b}_L = \begin{bmatrix} p_y \\ p_x \\ 0 \end{bmatrix} \cdot p_h^{-1} \quad (6b)$$

for SV - waves

$$\mathbf{b}_V = \begin{bmatrix} p_x \\ p_y \\ p_h^2 / \sqrt{V_v^{-2} - p_h^2} \end{bmatrix} \sqrt{p_h^{-2} - V_v^2} \quad (6c)$$

for Rayleigh waves

$$\mathbf{b}_R = \begin{bmatrix} p_x \\ p_y \\ -i \quad \text{ctg} \psi \quad p_h \end{bmatrix} \cdot i p_h^{-1} \sin \psi \quad (6d)$$

Note that for Rayleigh and Love waves values of p_x and p_y depend on frequency f .

The model above is the simplest in the sense that it does not take into account the reflections and transformations of the different wave phases while arriving to the day surface. The more complex but more realistic model of seismic wave propagation in a vicinity of the day surface is proposed by B.Kennett [9]. From this model one obtains the following equations for vector \mathbf{b} :

for P-wave:
$$\mathbf{b}_P = \begin{bmatrix} -\sin \alpha \cdot V_P p_h C_2 \\ -\cos \alpha \cdot V_P p_h C_2 \\ V_P q_P C_1 \end{bmatrix} \quad (6a^*)$$

for SH and Love waves:
$$\mathbf{b}_L = \begin{bmatrix} 2 \cos \alpha \\ -2 \sin \alpha \\ 0 \end{bmatrix} \quad (6b^*)$$

for SV-wave:
$$\mathbf{b}_V = \begin{bmatrix} \sin \alpha \cdot V_S q_S C_1 \\ \cos \alpha \cdot V_S q_S C_1 \\ V_S p_h C_2 \end{bmatrix} \quad (6c^*)$$

for Rayleigh wave:
$$\mathbf{b}_R = \begin{bmatrix} -i \sin \alpha \cdot \sin \psi \\ -i \cos \alpha \cdot \sin \psi \\ \cos \psi \end{bmatrix} \quad (6d^*)$$

where V_P , V_S are phase velocities of the P and S waves correspondingly; $\sin \alpha = p_x / p_h$,

$\cos \alpha = p_y / p_h$, p_h is the horizontal apparent slowness of the wave phase: $p_h = (p_x^2 + p_y^2)^{-1/2}$

$$q_P = (V_P^{-2} - p_h^2)^{1/2}; \quad q_S = (V_S^{-2} - p_h^2)^{1/2};$$

$$C_1 = \frac{2 \cdot V_S^{-2} \cdot (V_S^{-2} - 2 \cdot p_h^2)}{(V_S^{-2} - 2 \cdot p_h^2)^2 + 4 \cdot p_h^2 \cdot q_P \cdot q_S}; \quad C_2 = \frac{4 \cdot V_S^{-2} \cdot q_P \cdot q_S}{(V_S^{-2} - 2 \cdot p_h^2)^2 + 4 \cdot p_h^2 \cdot q_P \cdot q_S}.$$

If one neglects the effects of wave reflection from inner medium layer borders and conversion of wave types on these borders while plane wave propagates through layered medium, and restrict himself to taking into account only the effects of wave refraction (the ray propagation approximation), then according to the Snellius law [1] a value of $p_h = \sin \beta_w / V_w$ at any point within a batch of layers (and beneath the day surface) is constant and equal to its value in the half space. As $p_x = \sin \alpha \cdot p_h$ and $p_y = \cos \alpha \cdot p_h$, a value of 2-dimensional vector

$\mathbf{p}=(p_x, p_y)^T$ of horizontal apparent slowness is also constant in all medium points. This vector value is a ray parameter and determines a propagation path of a seismic ray in such layered medium [1]. Based upon eq.(5) and eq.(6) one can come to conclusion that a wave seismic field in any point \mathbf{r} of a laterally homogeneous medium is determined only by the vector \mathbf{p} and a wave velocity V_w in that layer where the point \mathbf{r} is located and is independent from other parameters of layers. Thus, eq.(4) initially written for the homogeneous space is valid for any point of a laterally homogeneous (layered) medium and in particular for points just beneath the day surface, if to neglect a reflection from the day surface.

Considering eq.(4) enables us to interpret the field $w(f, \mathbf{r})$ on the day surface, e.g. for $\mathbf{r}=\mathbf{u}=(x, y, 0)$ as a result of a signal $s_w(f)$ propagation through a linear system:

$$w(f, \mathbf{u}) = g_w(f, \mathbf{u}, \mathbf{p}) s_w(f). \quad (7)$$

The frequency response of this system (in a case of laterally homogeneous medium) is

$$g_w(f, \mathbf{u}, \mathbf{p}) = \exp[-i2\pi f(\mathbf{u}^T \mathbf{p})] b(\mathbf{p}, V_w) \quad (8)$$

If a batch of layers is a fine-stratified and contrasting enough so it is impossible to neglect the effects of wave reflection and wave type transformation, then a field $w(f, \mathbf{u})$ on the day surface admits yet the representation by eq.(7). However, in this case the frequency response of the corresponding linear system can not be expressed by such simple formula as eq.(8). Nevertheless for an arbitrary laterally homogeneous batch it can be determined with the help of rather effective computational methods like the ones of Thompson-Haskel or Kennett [10].

Let us consider a system of seismic observations consisting of m 3-component seismometers registering displacements of medium particles and located at the day surface at points \mathbf{u}_i . If distances between points \mathbf{u}_i are rather small so the medium can be considered permanent within the aperture of the system then such system of seismic observations can be referred as a 3-component array. For this case the set of complex spectra of seismometer outputs - a $3m$ -dimensional column vector $\mathbf{y}_w(f)=(y_{wi}(f), i=\overline{1, 3m})$ - may be expressed as

$$\mathbf{y}_w(f) = \mathbf{h}_w(f, \mathbf{p}) s_w(f) \quad (9)$$

where $\mathbf{h}_w(f, \mathbf{p})=(g_w(f, \mathbf{u}_i, \mathbf{p}), i=\overline{1, 3m})$ is a $3m$ -dimensional column vector of frequency responses of linear systems that are determined by propagation paths of a plain wave from the lower half space to seismometers outputs. In particular, for ray approximation one can write

$$\mathbf{h}_w(f, \mathbf{p}, V) = (\exp[-i2\pi f(\mathbf{u}_i^T \mathbf{p})] b_w(\mathbf{p}, V), i=\overline{1, m}) \quad (10)$$

The considerations made before allow to conclude that in the framework of ray propagation approximation without any loss of generality the origin of coordinates may be placed at \mathbf{u}_I - a point of location of the central array sensor. Then $s_w(f)$ can be interpreted as the waveform of a seismic phase at the central sensor.

Eq.(9), (10) demonstrate that in the framework of ray propagation approach signals from an array of 3-component seismometers contain information on seismic phase apparent slowness vector \mathbf{p} , wave velocity V_w in the layer beneath the surface and phase waveform $s_w(f)$. In seismic monitoring estimation of the apparent slowness vector \mathbf{p} appears to be crucial for effective location of seismic event epicentres using data from single observational site. Determination of seismic phase waveforms $s_w(f)$ is necessary for identification of a seismic source type and estimation of a source seismic moment tensor. Estimation of wave velocity v_w is important for investigation of regional medium structure on the basis of seismic data. Usually these problems are solved sequentially: after a vector \mathbf{p} value is determined a phase velocity V_w can be estimated from polarisation characteristics of three component observations based on eq.(6). And at last, if \mathbf{p} and v_w are known there appear the best conditions for retrieving a seismic phase waveform $s_w(f)$ (or $s_w(t)$) from 3-component multidimensional observations (using eq.(9), (10)), e.g. extracting a function $s_w(f)$ from a noise background. The latter is quite substantial for seismic source identification of small events.

Information on apparent slowness vector \mathbf{p} is contained in relative time delays $\tau_k = (\mathbf{u}_k - \mathbf{u}_I)^T \mathbf{p}$ of sensor signals and in polarisation characteristics of each 3-component seismometer output (mathematically expressed by the vectors $\mathbf{b}_w(\mathbf{p}, V)$). It is important that relative delays τ_k do not depend on velocity V_w of a seismic wave phase in the layer where seismometers are placed. In the contrast, the polarisation characteristics are strongly dependent on V_w . The upper subsurface layer in many regions has small phase velocities, often known with a high uncertainty. In this cases angles of incidence β_w of body seismic waves to the day surface are small even for regional events. As the result the accuracy of β_w measurements based on polarisation characteristics is rather poor [23]. In this conditions more accurate methods to measure apparent slowness \mathbf{p} are those based on time delays τ_k , for example, methods of the spatial spectral analysis (F-K analysis).

Nevertheless, 3-component array observations submit some information about wave azimuth which is additional to the relative time delays τ_k and also do not depend on wave velocity V_w in the surface layer. Really, as it follows from eq.(3) and eq.(6) an amplitude ratio

between signals of seismometer horizontal components is determined only by a seismic wave azimuth.

Hence, with the purpose to extract all information about apparent slowness vector \mathbf{p} , contained in 3-component array observations, one should combine the both: polarisation analysis and F-K analysis approaches, in a single 3C-data processing algorithm. Some of such algorithms are described in Section 3.

Signals of seismometers are usually being observed against a noise background $\xi(t) = (\xi_{kj}(t), k=\overline{1,m}; j=\overline{1,3})$. Therefore output signals of a multichannel system of seismic observations compose a multidimensional random time series

$$\mathbf{x}_w(t) = \mathbf{y}_w(t) + \xi(t) = \mathbf{h}_w(t, \mathbf{p}, V) * s_w(t) + \xi(t) \quad (11)$$

where $\mathbf{h}_w(t, \mathbf{p}, V)$ is a vector impulse response of a medium for given wave phase equal to Fourier transform of a vector-function (10), $*$ is the sign of convolution. In the frequency domain eq.(14) can be written as

$$\mathbf{x}_w(f) = \mathbf{h}_w(f, \mathbf{p}, V) s_w(f) + \xi(f) \quad (12)$$

where $\xi(f)$ is a column $3m$ dimensional vector of a noise complex spectrum.

The noise presence in observations results in the necessity to take into account distorting effects of noise while resolving the discussed above problems of seismic phase parameter determination. E.g. these problems should be formulated as problems of statistical time series analysis. Theory of optimal statistical inferences [3,7] should be implemented for their solution. It meets some difficulties because this theory has been mostly developed for case of known statistical characteristics of noise. For seismic noise it is usually not so.

Numerous investigations have brought enough proves for seismic noise $\xi(t)$ to be considered as a Gaussian process, which may be assumed as a stationary one (at time intervals typical for seismic signal duration) with zero mean and the smooth matrix power spectrum density (MPSD) $\mathbf{F}(f) = E\{\xi(f)\xi^T(f)\}$. Here E represents the sign of mathematical expectation. A MPSD $\mathbf{F}(f)$ reflects seismic noise space and time correlations, which are as a rule non-zero and mostly developed in a low-frequency band. It is especially typical for seismic noise in regions close to sea and ocean shores where seismic noise are generated mostly by a surf. In such regions the space correlation of noise (coherence of noise) is so high that for frequencies lower than 1-3 Hz the MPSD $\mathbf{F}(f)$ of a noise vector time series $\xi(t)$ registered by a small aperture seismic array is nearby to singular [5,18]. The proximity of a determinant of $\mathbf{F}(f)$ to zero forms the criteria for noise coherency in regard to a given observational system.

As it follows from the general points of mathematical statistics if a determinant of $F(f)$ is close to zero the probabilities of errors for statistically optimal decision rules are close to zero as well. Note that for non-optimal procedures, it is by no means necessary. Hence it seems to be rather desirable to take into account an information on noise MPSD $F(f)$ for synthesis of statistically optimal algorithms for processing of multicomponent seismic observations. It often provides a significant increase in accuracy of seismic signals parameter estimation due to the effect of "compensation" (suppression) of noise by statistically optimal data processing procedures.

In order to achieve the theoretical efficiency of noise suppression the strict information about its MPSD $F(f)$ is demanded. But for long time intervals a noise time series $\xi(t)$ can not be regarded as a multidimensional stationary process: its MPSD $F(f)$, being defined by current characteristics of a seismic noise field, is changing in time. Therefore the statistically optimal procedures of multicomponent seismic data analysis can be efficient only in the framework of adaptive approach where the noise MPSD is continuously or periodically estimated using current noise observations.

3.2. Coherent noise suppression and seismic waveform extraction using data from 3-component arrays

3.2.1. Introduction

The adaptive group filtering technique developed and tested in the previous research stages can be gained for processing data from 3-component small aperture and micro arrays. The latter is the subject of the primary interest as Alpha-stations of the International Monitoring Network being developed for verification of Test Ban Treaties. The usage of 3-component array data allows to significantly enhance the quality of extraction of seismic phase waveforms from background noise especially if to employ the adaptive optimal group filtering (AOGF) method. The possibilities are opened to extract waveforms of different event phases which are characterised by different polarisation features, including some of them which are impossible to be handled using only 1-component array data: regional SH, teleseismic Love and so on.

The seismic noise (especially in the sea-shore regions) often is the transient one and is constituted by the surface waves generated by a surf or industrial sources. In these cases it exhibits explicit coherent and polarisation features. As shown, the coherency of noise can be successfully utilised by the AOGF method for the case of 1-component array data processing. This method can be expanded for 3-component (3C) array data processing. The $(3m \times 3m)$ matrix power spectral density (MPSD) of 3C noise records have to be estimated in this case and

the polarisation characteristics of noise are automatically captured in this MPSD. To adjust correctly the AOGF for an extraction of waveform of given seismic phase one have to account the polarisation feature of this phase at the site of 3C observations. So different phases should be treated by the different AOG filters. Parallel processing of the same 3-component array recording by these filters produces three output traces reflecting wavetrain oscillations in longitudinal, transverse and vertical direction generated by the P, SH and SV body waves, Lg, Rayleigh and Love surface waves. Such analysis can be very helpful for investigation of complex wave-field in the regions with strong laterally heterogeneous media structure. It can be implemented for enhancing of event source location and identification quality in regional monitoring with the help of a 3-component array.

Some complication of computing while the processing is justified by the advantages of the described combined procedure accounting for differences in both: relative delays and the polarisation characteristics of the array signal and noise. The application of this procedure can provide for our assessment, the same quality of signal extraction using data of 3C micro array, as using data of 1C small aperture array with 2 - 3 times larger amount of sensors.

The testing of this technique was accomplished using seismograms of the Geyocha 3C array temporary deployed within the framework of PASSCAL Project in Turkmenistan near Ashgabad town and was operated during 1993-1994. The major interest of this PASSCAL experiment in regard of our study purposes is that the Geyocha array contained the 3C small aperture subarray composed by 12 3C very broad band STS-2 seismometers which have registered the wave-fields from a set of local, regional and teleseismic events in extremely wide frequency range 0,002-10 Hz. This open a possibility to extract the waveforms of body-wave and surface-wave event phases from the single multichannel array seismogram and thus eliminate interference usually introduced by frequency responses of different seismometers registering event signals in the distinct bands of seismic range. This array is interesting also as an example of seismic installation deployed in a thick sedimentary basin with strong laterally heterogeneous media characteristics.

3.2.2. Statistically optimal group filter (Wiener filter)

According to eq.(1.11), to restore a waveform $s(t)$ from a seismic data $x(t)$ recorded by a 3-component (3C) seismic array, one should make up for a distorting effect of the medium and clear the signal off the noise. As it follows from statistical theory of time series analysis, if distribution of noises $\xi(f)$ is Gaussian the best procedure for restoring the function $s(f)$ is a group filtering, according to which the scalar complex estimation $\hat{s}(f)$ of a waveform $s(f)$ is found as follows:

$$\hat{s}(f) = \phi^*(f) x(f) \quad (1)$$

where $\phi(f) = (\phi_{jk}(f), j=\overline{1,m}, k=\overline{1,3})$ is a 3m-component vector frequency response of the group filter, symbol * designate the Hermitian conjugation.

The problem of statistically optimal estimation of a waveform $s(f)$ (the optimal group filtering) consists in seeking for a frequency response $\phi_o^*(f)$ which minimises the square mean deviation

$$E_S \{ [\hat{s}(f) - s(f)]^2 \} = \min \quad (2)$$

under the condition of unbiased signal estimation:

$$E_S \{ \hat{s}(f) \} = s(f) \quad (3)$$

In the above equations E_S is the sign of conditional mathematical expectation under the condition that signal is given; the eq.(2),(3) have to be valid for each frequency f for any signal realisation. The requirements by eq.(2),(3) are equivalent to the requirement on the signal estimate dispersion to be minimal:

$$D_S \{ \hat{s}(f) \} = \min \quad (4)$$

The minimisation of dispersion of signal estimate eq.(4) under condition eq.(3) results in the following expression for the frequency response of the OGF [4,5,16,27]:

$$\phi_o^*(f) = [h_w^*(f,p,V) F^{-1}(f)] / [h_w^*(f,p,V) F^{-1}(f) h_w(f,p,V)] \quad (6)$$

where $F^{-1}(f)$ is a inverse $[3m \times 3m]$ - matrix spectral density of 3C array noise $\xi(t)$; $F(f) = E[\xi(f)\xi^*(f)]$, a 3m-vector function $h_w(f,p,V)$ is the frequency response of a medium for the given seismic phase w propagation paths from the first 3C array sensor to another ones. For the ray approximation of seismic wave propagation $h_w(f,p,V)$ is expressed by eq.(1.10).

The OGF output signal in the no noise condition coincides with a phase waveform $s_w(f)$. Indeed, in agree with eq.(1) and (1.9), if a noise is absent ($\xi(t) = 0$)

$$\hat{s}(f) = \{ [h_w^*(f,p,V) F^{-1}(f)] / [h_w^*(f,p,V) F^{-1}(f) h_w(f,p,V)] \} h_w(f,p,V) s_w(f) = s_w(f). \quad (7)$$

If a noise consists of only a diffusion seismic noise i.e. noise records $\xi_{it}(t)$ at all 3C array sensor components are non-correlated, then $F^{-1}(f) = \sigma^{-2} D(f)$ e.g. is a diagonal matrix. In this case, it is often (and groundlessly) assumed that a diffusion noise is white: $D(t) = I$. Then the optimal group filtering procedure coincides with the classical 1C array beamforming (BF)

procedure applied to 1C seismograms, recorded after rotating 1C sensor to a direction of particle motion for a seismic phase being processed. To perform the last procedure one should previously determine a type of the phase.

The optimal group filter eq.(6) does not distort a signal waveform and provides a maximum signal-to noise ratio only if a vector-function $\mathbf{h}_w(f, \mathbf{p}, V)$ used well corresponds to the true frequency response of the medium for the signal propagation paths. For a plain wave and the ray propagation approach it is to have a form given by eq.(1.10), where the 3C vector function $\mathbf{b}_w(\mathbf{p}, V)$ corresponds to a phase type (eq.(1.6)), vector \mathbf{p} coincides with the true apparent slowness vector of the signal wave and V - with the true wave velocity of the seismic phase in the medium subsurface layer. The last values should be preliminary estimated (with the help of procedures described in Section 3 below). An other possible approach consists in scanning the expected signal arrival directions (and/or wave velocities) with the help of a "fan" of filters eq.(6) with different functions $\mathbf{h}_w(f, \mathbf{p}, V)$. The values of \mathbf{p} and v on which the maximum power of some filter output is attained can serve as the seismic wave parameter estimates. The OGF output signal for this direction is an estimate of a signal waveform.

It is easy to show, that a group filter with the following frequency response

$$\phi_w^*(f) = [\mathbf{h}_w^*(f, \mathbf{p}, V) \mathbf{F}^{-1}(f)] / [\mathbf{h}_w^*(f, \mathbf{p}, V) \mathbf{F}^{-1}(f) \mathbf{h}_w(f, \mathbf{p}, V)]^{1/2} \quad (8)$$

also suppresses a coherent component of the noise with the MPSD $\mathbf{F}(f)$ but provides a whitened residual noise output $\eta(t) = \phi_w^*(f) \xi(t)$, for which $E\eta(t)\eta^*(t) = \mathbf{I}$, where \mathbf{I} is identical matrix. However, this group filter distorts the signal waveform. We call it as whitening group filter (WGF). As it is shown in Section 3, WGF procedure is a general intermediate procedure for a statistical estimation of seismic wave apparent velocity.

3.2.3 Adaptation of optimal group filter to variations of noise spectrum.

If the $[3m \times 3m]$ matrix function $\mathbf{F}(f)$, used for calculation of the OGF frequency response via equation (6) well approximates the real MPSD of current array noise then the OGF provides an output with significantly greater SNR then conventional beamforming does. Theoretically the OGF SNR gain tends to infinity if a determinant of $\mathbf{F}(f)$ tends to zero. This occurs in the case of purely coherent noise. The determinant of $\mathbf{F}(f)$ thus can serves as a measure of noise coherency and indicates situations where implementation of the OGF would be successful

As seismic noise is usually not stationary and its MPSD varies in time, the OGF method can be effective only in an adaptive processing system, where a MPSD $\mathbf{F}(f)$ is periodically estimated (updated) using current noise observations. We call such array data processing procedure as the adaptive optimal group filtering (AOGF).

We have found that the AOGF procedure with group filter frequency response by eq.(6) in most cases has a better performance than the conventional beamforming (BF) procedure if a noise MPSD is estimated with the multidimensional autoregressive moving average (ARMA) modelling of noise records [16]. It means that an inverse MPSD is evaluated in the form of the matrix rational function [7]:

$$\hat{F}(f) = \left(\sum_{k=0}^p A_k e^{-i2\pi f k \Delta} \right) \left(\sum_{l=-q}^q L_l e^{-i2\pi f l \Delta} \right)^{-1} \left(\sum_{k=0}^p A_k^T e^{i2\pi f k \Delta} \right), \quad (9)$$

where Δ is the data sampling interval, $[3m \times 3m]$ -matrices A_k , $k \in 0, p$, are determined using first $p+1$ sample matrix autocorrelations of noise observations with the help of a computationally effective multichannel version of the Levinson-Durbin procedure [16,19,28]. MA-coefficients: $[3m, 3m]$ -matrices L_l are calculated as weighted autocovariance matrices with lags $l \in -q, q$ for the time series which is produced from noise data by the multichannel whitening filtering using matrix AR-coefficients A_k

In any case where a MPSD of noise $F(f)$ have to be determined from observations, the following two situations can be faced:

- a) 3C array records comprises an interval where only "pure" noise is present;
- b) all observations are a mixture of signal and noise.

In the first case a rather precise estimate of a noise MPSD $F(f)$ can be obtained from the observations of a "pure" noise. In the second case it seems at a first glance impossible to get a good estimate of $F(f)$ since the MPSD of observations is equal

$$F_{XW}(f) = F(f) + h_w(f) h_w^*(f) \mu(f), \quad (10)$$

where $\mu(f)$ is a power spectral density of a seismic phase waveform. Just the function eq.(10) will be really estimated from a signal and noise mixture. The estimate of $F_{XW}(f)$ being obtained in this case can be quite different from the noise MPSD $F(f)$, especially if a signal-to-noise ratio is large enough.

The following property of the OGF by eq.(6) (which can be called as the "adaptation stability") presents a some theoretical advantage of the OGF: it is easy to show [12,15] that substitution of $F_{XW}(f)$ (eq.(10)) in eq.(6) instead of $F(f)$ does not change the value of the OGF frequency response $\phi_o(f)$. This theoretical advantage is however practically meaningful if an estimate of $F_{XW}(f)$ is accurate enough.

3.2.4. Spatial Rejecting Group Filter

The best noise suppression using group filtering procedures can be achieved if noise is close to coherent. This property possesses transient noise generated by one or several sources localised in a medium. Real seismic noise consists normally of such noise superposing with diffusion microseismic noise caused by a huge number of independent sources. I.e. a real noise process at 3C array sensor outputs can be written down as follows:

$$\xi(t) = \sum_{k=1}^s \mathbf{q}_k(t) * \zeta_k(t) + \delta(t), \quad (11)$$

where $\zeta_k(t)$ is a scalar noise process in k -th source of coherent noise; $\mathbf{q}_k(t)$ is a $3m$ -dimensional vector of impulse transfer functions for the noise along propagation paths through the medium from k -th noise source to 3C array sensors; s is a number of coherent noise sources; $\delta(t)$ - is a vector of diffusion noise processes, $*$ is the sign of convolution.

If processes $\zeta_k(t)$, $k=\overline{1,s}$ and $\delta(t)$ are mutually non-correlated, a matrix power spectral density of the process $\xi(t)$ has the following form [16,17]:

$$\mathbf{F}(f) = \sum_{k=1}^s \mathbf{q}_k(f) J_k(f) \mathbf{q}_k^*(f) + \sigma^2 \mathbf{D}(f) = \mathbf{R}_s(f) + \sigma^2 \mathbf{D}(f); \quad (12)$$

where

$$\mathbf{R}_s = \mathbf{Q}_s(f) \Lambda_s(f); \quad \mathbf{Q}_s(f) = [\mathbf{q}_1(f), \dots, \mathbf{q}_s(f)];$$

$$\Lambda_s(f) = \begin{bmatrix} J_1(f) & \cdot & 0 \\ \cdot & \cdot & \cdot \\ 0 & \cdot & J_s(f) \end{bmatrix}$$

where $J_k(f)$ - is a power spectral density of process $\zeta_k(t)$; $\mathbf{D}(f)$ - is a matrix power spectral density of diffusion noise $\delta(t)$; σ^2 - is a diffusion noise power (for simplicity's sake we consider it to be equal for each array sensor); $\mathbf{q}_k(f)$ - is a $3m$ -dimensional vector frequency response of the medium at propagation paths from k -th source of coherent noise to 3C array sensors..

If the diffusion noise is absent, i.e. $\sigma^2 = 0$ and a number of coherent noise sources is fewer than that of array sensors (in our case, $s < 3m$) the matrix $\mathbf{F}(f)$ become singular. It is shown [12,17] that if diffusion noise power tends to zero ($\sigma^2 \rightarrow 0$)

$$\phi_r^*(f) = \lim_{\sigma \rightarrow 0} \phi_o(f) = [\mathbf{h}_w^*(f, \mathbf{p}, V) \mathbf{B}_s(f) / \mathbf{h}_w^*(f, \mathbf{p}, V) \mathbf{B}_s(f) \mathbf{h}_w(f, \mathbf{p}, V)], \quad (13)$$

where $\mathbf{B}_s = [\mathbf{I} - \mathbf{R}_s(\mathbf{R}_s^* \mathbf{R}_s)^{-1} \mathbf{R}_s^*]$, \mathbf{I} - is a $[s \times s]$ -unit matrix.

In the most significant particular cases, where only one source of coherent noise exists ($s=1$)

$$B_f(f) = [I - q(f)q^*(f) / |q(f)|^2]. \quad (14)$$

In the absence of diffusion noise, the noise at the output of group filter with frequency response by eq.(13) is equal to zero:

$$\eta(f) = \phi_r(f) Q_s(f) \zeta(f) = 0, \quad (15)$$

where $\zeta(f) = (\zeta_k(f), k=\overline{1, s})$ is a vector of processes in the noise sources. Eq.(13) results from the equation: $B_s(f) Q_s(f) = 0$, which is very easy to prove for $s = 1$:

$$B_f(f) Q_f(f) = [q(f) - q(f)q^*(f)q(f) / |q(f)|^2] = 0 \quad (16)$$

Thus, in the absence of diffusion noise, i.e. when seismic noise is fully coherent, it will be completely suppressed by the group filter with frequency response by eq.(13). We call this group filter as the 'spatial rejection group filter'(SRGF).

Note that coherent noise suppression with the help of the SRGF by eq.(13) calls for information on the frequency response vectors $q_k(f)$ of noise propagation paths in the medium. This causes serious problems for its practical implementation.

In some cases a coherent noise can be considered as caused by some surface wave ($k=1$). In such case the vector $q_1(f)$ can be found from eq.(1.10) where p is an apparent slowness vector of coherent noise wave, $b_w(p, V)$ are determined by the type of a noise wave with the help of eq.(1.6b) or eq.(1.6d). The apparent slowness vector p of such interfering noise wave can be estimated with the help of F-K analysis of array records made at a time interval where only coherent noise is present. The another variant of the adaptive SRGF can be obtained if one uses as the of vectors $q_k(f)$ estimates the principal eigen vectors of a MPSD of coherent noise records. The evaluation of the MPSD is preferably to be done by multidimensional ARMA modelling of the noise time series.

Nevertheless the design of spatial rejection filter using eq.(13), (14) always suffers from some uncertainty with respect to a number of coherent noise waves, their types and parameters p , V_w . The experimental investigations of such filters in case of NORESS type small aperture seismic arrays showed that the zones of noise suppression over the apparent slowness plane (p_x, p_y) are rather narrow for any SRJF (although are deep enough). Therefore, a SRGF provides a strong suppression of coherent noise only if medium frequency response vectors $q_k(f)$ used for the noise wave characterisation precisely correspond to reality: one should know accurately the types of noise wave phases, apparent velocities of these waves and be sure that the waves are really close to plain. Naturally, all these conditions are seldom met in practice.

At the same time, if one uses for coherent noise suppression the adaptive optimal group filter in its canonical version eq.(6), this calls for the estimation of matrix power spectral density (MPSD) $F(f)$ of array sensor noise, irrespectively of a physical essence of the noise origin. It is obvious that in practice there is no ideally coherent noise and $F(f)$ is always non singular (although it may be poorly conditioned). Therefore, in practice the suppression of coherent noise with the help of the AOGF is computationally correct procedure (provided the calculations are accurate enough, that is quite feasible task for present-day computers).

3.2.5. Optimal group filter with additional constraints

As it was discusses in Section 3.2.2, in the case of known MPSD of array noise the statistically optimal (Wiener) group filter (OGF), not distorting a phase waveform frequency content have to has the vector frequency response given by eq.(6). The filter minimises the output residual noise if the matrix function $F^{-1}(f)$ used in eq.(6) corresponds to the inverse MPSD of real noise at the array sensors. To ensure this correspondence the adaptation of OGF should be currently or periodically provided, i.e. the adaptive optimal group filter (AOGF) should be implemented in seismological practice.

Our studies of AOGF spatial sensitivity diagrams (SSD) for different array configurations and different noise conditions revealed that maps of these diagrams (depending on apparent slowness vectors (ASV) of seismic wave arrival directions) has deep minima to suppress coherent noise waves and always has the value equal to 1 at the ASV_0 -point corresponding to expected signal arrival direction (on which the AOGF have been steered). These AOGF SSD features are implied by the assumptions eq.(2)-(4) made in the procedure of AOGF design. However the AOGF SSD as a rule has a rather high maximum exceeding 1 and positioned aside of the ASV_0 point. This can lead to deterioration of AOGF noise suppression capability if the coherent noise features (e.g. its arrival direction) abruptly change during AOGF performance before the consequent cycle of adaptation.

The some methods were proposed to improve this AOGF potential disadvantage. One of them was discussed in [5] and consists in applying additional constrains in the procedure of synthesis of AOGF frequency response. The constraint (3) to pass the signal undistorted can be formulated as

$$\phi^*(f) h_w(f, p, V) = I. \quad (17)$$

It is possible to apply the general form linear constraint:

$$\phi^*(f) H_w(f, p, V) = a, \quad (18)$$

where $H_w(f, p, V)$ is some matrix, depending on f, p, V and the phase type w ; a is come constant vector. Under constraint (18) the optimal group filter design is performed by deriving

analytically such filter vector frequency response which provides the minimum of the filter output power

$$\phi^*(f) = \arg \min_{\phi(f)} \{\phi^*(f) F_x(f) \phi(f)\}, \quad (19)$$

where $F_x(f)$ is the matrix spectral density of the signal + noise array observations.

The vector group filter frequency response satisfying conditions by eq.(18), (19) can be found by the method of Lagrange factors which implies the minimisation of the Lagrange functional

$$A = \phi^*(f) F_x(f) \phi(f) - \lambda^* (\phi^*(f) H_w(f, p, V) - a) - (\phi^*(f) H_w(f, p, V) - a) \lambda, \quad (20)$$

with subsequent determination of the Lagrange factor vector λ from constraints by eq.(18).

This method provides the following equation for vector frequency response of the constrained optimal group filter:

$$\phi_{oc}^*(f) = F^{-1}_x(f) H_w(f, p, V) [H_w^*(f, p, V) F^{-1}_x(f) H_w(f, p, V)]^{-1} a \quad (21)$$

For the purpose to design the robust AOGF which would be less sensitive to changes of the supposed (or previously estimated) noise MPSD, the following constraints are relevant [5]:

$$H_w(f, p, V) = [h_w(f, p_0, V) | \frac{\partial}{\partial p_x} h_w(f, p_0, V) | \frac{\partial}{\partial p_y} h_w(f, p_0, V)]; \quad a = (1, 0, 0)^T \quad (22)$$

The constraints defined by eq.(22) guarantee that the AOGF with the frequency response (21) will not possess a high "side lobes" in a vicinity of the arrival direction with ASV p_0 (at which the AOGF is steered). This AOGF peculiarity can be valuable in the case of strongly nonstationary noise conditions.

Note that the constrained AOGF by eq.(21), (22) has the very valuable feature similar to one for the conventional Wiener AOGF: the vector function $\phi_{oc}^*(f)$ does not change if to substitute in to (21) instead the inverse MPSD $F^{-1}_x(f)$ of signal + noise observations the inverse MPSD $F^{-1}_\xi(f)$ corresponding to the "pure" noise. This allows to perform the AOGF adaptation using the noise recordings at time intervals, preceding or succeeding the signal phase intervals. The practice showed that in real AOGF implementations this leads to higher noise suppression capability.

3.3. Adaptive statistical algorithms for estimation of azimuth and apparent velocity of seismic phases using data from 3-component arrays

3.3.1. Introduction.

For estimation of arrival direction (AD) parameters: azimuth and apparent velocity, of seismic phases the two conventional techniques are currently used: polarisation analysis of 3-component (3C) records from a single seismic station and F-K analysis of data from 1-component seismic arrays. The different modifications of these techniques have been developed. Some of them, as the high resolution F-K analysis on the basis of ARMA modelling of 1-component array signals, were investigated in [12,16].

The wide use of 3C small aperture and micro arrays compels seismologists to develop the new methods of azimuth (AZ) and apparent velocity (APV) estimation, that extracts all information about this parameters contained in 3C array records in both: the relative time delays of array signals and their polarisation characteristics. The theoretical background for statistically optimal estimation of AD parameters using 3C array observations obscured by coherent noise was investigated in [11,13]. Three algorithms are proposed which are optimal under different assumptions about a phase waveform. The peculiarity of these algorithms is that the parameters AZ and APV have to be estimated simultaneously with the wave velocity (WV) of given seismic phase in the medium beneath the array (if this velocity is unknown).

The theoretical assessments and computer simulations reveal that significant enhancement of estimation accuracy can be achieved in the case where this algorithms are applied to micro array data obscured by intensive coherent noise. Nevertheless the extensive experiments have to be made with real 3C array records to prove an expediency of practical application of these algorithms.

In this section the evaluation of azimuth and apparent velocity of a plane wave using data from *3-component* small aperture seismic array is treated as a statistical problem of estimation of multidimensional stochastic time series parameters in condition where these parameters comprize the informative and nuisance ones. This approach is new and distinct from the conventional one, according to which the evaluation of arrival directions is interpreted in the framework of spatial spectral (F-K) analysis [24,26].

3.3.2. Mathematical models of observations as a random time series with informative and nuisance parameters.

The mathematical model of seismic signals and noise in array sensors was discussed in Section I. Let us remember that in the time domain this model is

$$x(t) = y(t) + \xi(t) = h_w(f, p, V) s_w(f) + \xi(t) \quad (1)$$

where the notations are the same as in Section 1.

In this section we use to make two alternative assumptions about $s(t)$ - time function (waveform) of seismic phase:

a) A signal $s(t)$ is a realisation of a Gaussian stationary random time series with zero mean and a power spectral density $\mu_s(f)$.

Though this assumption seems to be artificial from the point of view of seismological practice, actually it means that during a synthesis and analysis of estimation algorithms we confine ourselves by taking into account only an averaged signal power spectrum without any consideration of signal phase spectrum. From this point of view the assumption a) is a mere a proper way to enable us to use the technique of statistical time series analysis [12,17]

b) $s(t)$ is an unknown deterministic time series.

In seismological practice the problem of seismic wave AD estimation has often to be resolved without any knowledge of a waveform $s(t)$. The reason is that the seismic event waveforms (and their power spectra) strongly vary for one case or another.

With the purpose to estimate the informative parameters $p = (p_x, p_y)$ of observations fitting eq.(1.1) in the conditions of a priori uncertainty of a signal waveform we have to introduce unknown nuisance parameters of the signal. A seismic wave velocity in the surface layer of the Earth crust is often also unknown and for 3C array data analysis one has to regard it as an additional nuisance parameter.

When modelling $s(t)$ as a random Gaussian time series let us suppose that its power spectral density is a known function $\varphi(f, c)$ depending on q nuisance parameters $c = (c_1, \dots, c_q)^T$. The linear model seems to be the simplest in this case:

$$\varphi(f, c) = \sum_{k=0}^p c_k \varphi_k(f) \quad (2)$$

where $\varphi_k(f)$ may be typical power spectra of seismic signals for different frequency bands: $\varphi_k(f) = \varphi(f - f_k)$, where f_k are central frequencies of such bands. Herewith the fact that $s(t)$ is a

broadband signal provides for q in eq.(2) to be small, i.e. the parametric representation in eq.(2) is efficient with a rather small number q of nuisance parameters.

For the signal model b) where a seismic phase waveform is assumed to be deterministic time series, let us suppose that the all elements of this time series are unknown a'priori. That is in this approach in addition to informative parameters $\mathbf{p}=(p_x, p_y)$ we have N unknown nuisance parameters $s(t)$, $t \in 1, N$. Thus, for this case the number of nuisance scalar parameters is equal to the number of vector observations $\mathbf{x}(t)$, $t \in 1, N$.

The rigorous statistical approach implies that apparent slowness vector determination using records from a 3C array to be regarded as the statistical estimation problem involving nuisance parameters. To make the problem formulation fitting practical conditions we assume observations $\mathbf{x}(t)$, $t \in 1, N$ to be correlated for both: different $t \in 1, N$ and different coordinates $x_j(t)$, $j \in 1, m$ of vectors $\mathbf{x}(t)$. We will suppose below that the matrix power spectral density (MSPD) $\mathbf{F}(f)$ of a noise is known. Such constraint can be justified in many cases by an ability to observe noise $\xi(t)$ records just before a wave phase arrival. Hence the spectral density of noise may be estimated by means of a special adaptation procedure, discussed in Section 2. The estimate $\hat{\mathbf{F}}(f)$ can be used hereafter in algorithms of apparent slowness vector estimation.

A synthesis of statistically optimal algorithms is based on a criterion of accuracy of estimation which must be properly chosen for a problem under consideration. Hereafter we use as the accuracy criterion for any apparent slowness vector estimate $\mathbf{p}_N^*=(p_{xN}^*, p_{yN}^*)^T$ the asymptotic covariance matrix of the estimate

$$\lim_{N \rightarrow \infty} \text{NE}\{(\mathbf{p}_N^* - \mathbf{p})(\mathbf{p}_N^* - \mathbf{p})^T\} = \Psi_{\mathbf{p}} \quad (3)$$

The estimate \mathbf{p}_N^* of apparent slowness vector \mathbf{p} which provides the minimal value of $\text{tr}(\Psi_{\mathbf{p}})$ we will call as the asymptotically efficient (AE) estimate [17]. Note that $\text{tr}(\Psi_{\mathbf{p}})$ is the sum of asymptotic mean square deviations of estimates (p_{xN}^*, p_{yN}^*) from true parameter values (p_x, p_y) . The criterion of asymptotic accuracy by eq.(3) allows one to use analytical techniques of the asymptotic estimation theory [2]. This enables one to derive up to the end both synthesis and analysis of the asymptotically optimal estimates and to gain an explicit estimation algorithms and formulas for their asymptotic covariance matrices. Note, that it is an unresolvable task (both from theoretical and practical points of view) to develop an explicit estimation algorithm, which would be the best in terms of any non-asymptotic accuracy criterion, for example, an algorithm having the smallest mean square deviations for any finite sample size N .

3.3.3. Asymptotically efficient estimates of apparent slowness vector for random signal waveforms.

Under assumption that the signal $s(t)$ is a stationary zero mean Gaussian random process a vector time series $\mathbf{x}(t)$ being observed is a multidimensional zero mean stationary Gaussian time series, which distribution is entirely determined by its matrix power spectral density (MPSD) $F_x(f)$, $f \in [0, f_s/2]$, where f_s is a sampling frequency. With the natural additional assumption that a signal waveform $s(t)$ and a noise $\xi(t)$ are statistically independent it is easy to derive that

$$F_x(f) = F(f) + H_w(f, \mathbf{p}, V) \varphi_s(f, \mathbf{c}) \quad (4)$$

where: $H(f, \mathbf{p}, V) = \mathbf{h}(f, \mathbf{p}, V) \mathbf{h}^*(f, \mathbf{p}, V)$; is the $[3m \times 3m]$ matrix;

$\mathbf{h}(f, \mathbf{p}, V) = (\exp[-i2\pi f(\mathbf{u}_i^T \mathbf{p})] \mathbf{b}(\mathbf{p}, V), i = \overline{1, m})$ is the $3m$ -dimensional column vector of medium frequency responses along paths of seismic wave propagation from the first array sensor to the other ones; $\varphi_s(f, \mathbf{c})$ is a signal power spectral density which has a linear parametric representation in accordance with eq.(1.2). Note, that the MPSD $F_x(f)$ explicitly depends on informative and nuisance parameters of the problem under consideration.

It has been demonstrated in [16,17] that if a probability distribution of observations satisfies rather weak constraints the asymptotically efficient (AE) estimate \mathbf{p}^*_N of informative parameter \mathbf{p} can be obtained (simultaneously with the estimate $\boldsymbol{\theta}^*_N = (\mathbf{c}^*_N, V^*_N)$ of the nuisance parameter $\boldsymbol{\theta} = (\mathbf{c}, V)$) by means of the maximum likelihood approach. According to this approach

$$(\mathbf{p}^*_N, \boldsymbol{\theta}^*_N) = \arg \max_{\mathbf{p}, \boldsymbol{\theta}} (L(X_N, \mathbf{p}, \boldsymbol{\theta})); \quad (5)$$

where $L(X_N, \mathbf{p}, \boldsymbol{\theta}) = \ln(W(X_N, \mathbf{p}, \boldsymbol{\theta}))$ is the logarithm of multivariate probability density of observations, $X_N = (\mathbf{x}_1^T, \dots, \mathbf{x}_N^T)^T$ is the combined column vector of all observations.

Let us construct a computational algorithm for the AE estimate of the parameter $\mathbf{v} = (\mathbf{p}, \mathbf{c}, V)$ based on observations that fit the model eq. (1). A likelihood function for the observations X_N is the logarithm of Gaussian multivariate probability density of X_N , regarded as the function of parameter \mathbf{v} . It can be represented a

$$L(X_N, \mathbf{v}) = -(MN/2) \ln(2\pi) - (1/2) \ln(\det\{C_N(\mathbf{v})\}) - (1/2) X_N^T C_N^{-1}(\mathbf{v}) X_N \quad (6)$$

where C_N is a block Teplitz $[mN \times mN]$ matrix, composed with the blocks

$$\mathbf{C}_\tau = E\{\mathbf{x}(t)\mathbf{x}^T(t+\tau)\} = E\{\mathbf{y}(t)\mathbf{y}^T(t+\tau)\} + E\{\xi(t)\xi^T(t+\tau)\}$$

The likelihood function (2.3) depends on the problems parameters via elements of the inverse matrix $\mathbf{C}^{-1}_N(\mathbf{v})$ and its determinant. It's clear that should the value of mN be of any significance the construction of a computational procedure for maximisation of $L(X_N, \mathbf{v})$ seems to be a difficult task. However, a simple approximation of this functional in the frequency domain is possible if a number of observations N is sufficiently large.

Let us treat the observations which fit the model eq.(1) in the discrete frequency domain provided by Discrete Finite Fourier Transform (DFFT) [3]. In this domain the observations are:

$$\mathbf{x}_j = \mathbf{h}_j(\mathbf{p}, V)s_j + \xi_j + \mathbf{O}_j(1/\sqrt{N}) \quad j=1, N \quad (7)$$

where N is a number of discrete observations; $\mathbf{x}_j \leftrightarrow \mathbf{x}(t)$, and $\xi_j \leftrightarrow \xi(t)$ are DFFT of $\mathbf{x}(t)$, and $\xi(t)$, $t \in 1, N$, consequently, $\mathbf{h}_j(\mathbf{p}, V) = (\exp(i\lambda_j f_s \mathbf{u}_k^T \mathbf{p}) \mathbf{b}_w(\mathbf{p}, V))$, $k \in 1, m$; f_s is the sampling frequency, $\lambda_j = (2\pi j/N)$; $s_j \leftrightarrow s_w(t)$ is a discrete complex spectrum of a seismic phase waveform. It is known, that DFFT frequency observations \mathbf{x}_j have weak mutual correlations for large N even if noise observations themselves are significantly correlated in time. I.e. DFFT appears to be an asymptotically decorrelating transform. If to ignore a weak statistic dependence of \mathbf{x}_j for different j (i.e. to drop the terms $\mathbf{O}_j(1/\sqrt{N})$ in eq. (2.4) one can get the following approximate expression for the likelihood function eq.(2.3) in the discrete frequency domain:

$$L(X_N, \mathbf{v}) = -C + \sum_{j=1}^N \sum_{j=1}^N \ln \det Q_j(\mathbf{p}, \theta) + \sum_{j=1}^N |z_j(\mathbf{p}, \theta)|^2 \quad (8)$$

where $C = \sum_{j=1}^N \ln \det \mathbf{F}_j^{-1} + \sum_{j=1}^N \mathbf{x}_j^* \mathbf{F}_j^{-1} \mathbf{x}_j$ is the term independent on the parameter \mathbf{v} ;

$$\mathbf{F}_j^{-1} = \mathbf{F}^{-1}(\lambda_j f_s),$$

$$Q_j(\mathbf{p}, \theta) = \left[\mathbf{I} - \frac{\mathbf{F}_j^{-1} \mathbf{H}_j(\mathbf{p}, V)}{\varphi_j^{-1}(c) + \text{tr} \mathbf{F}_j^{-1} \mathbf{H}_j(\mathbf{p}, V)} \right];$$

$$z_j(\mathbf{p}, \theta) = \frac{\mathbf{h}_j^*(\mathbf{p}, V) \mathbf{F}_j^{-1} \mathbf{x}_j}{\sqrt{\varphi_j^{-1}(c) + \mathbf{h}_j^*(\mathbf{p}, V) \mathbf{F}_j^{-1} \mathbf{h}_j(\mathbf{p}, V)}},$$

$$H_j(\mathbf{p}, V) = H(\lambda_j f_s, \mathbf{p}, V), \quad h_j(\mathbf{p}, V) = h(\lambda_j f_s, \mathbf{p}, V).$$

Note, that z_1, \dots, z_N are discrete frequency domain output of the conditional optimal Wiener group filter applied to the array data $\mathbf{x}(t)$. The latter transforms a multichannel input signal to a scalar trace and maximises the signal/noise ratio along this trace under the condition of whitening output noise.

It is rather easy to derive an analytical expression for the limit of normalised Fisher matrix for parameters \mathbf{v} [12]. It enable us to calculate the asymptotic covariance matrix for AE estimate of apparent slowness vector.

An analysis of eq.(8) reveals that if signal/noise ratio is sufficiently large values the $\phi_j^{-1}(\mathbf{c})$ become negligible for all j in comparison with $\mathbf{h}_j^*(\mathbf{p}, V) \mathbf{F}_j^{-1} \mathbf{h}_j(\mathbf{p}, V)$. Hence, the dependence of functional $\Lambda(X_N, \mathbf{p}, \mathbf{c}, V)$ upon an unknown signal spectrum $\phi_j(\mathbf{c})$ is weakening up to completely vanishing when $\phi^{-1} \rightarrow 0$. So if a signal/noise ratio is large enough the AE estimate of apparent velocity become close to the estimate maximising the following functional

$$\tilde{\Lambda}(X_N, \mathbf{p}, V) = \sum_{j=1}^N |z_j(\mathbf{p}, V)|^2 \quad (9)$$

where

$$z_j(\mathbf{p}, V) = \frac{\mathbf{h}_j^*(\mathbf{p}, V) \mathbf{F}_j^{-1} \mathbf{x}_j}{\sqrt{\mathbf{h}_j^*(\mathbf{p}, V) \mathbf{F}_j^{-1} \mathbf{h}_j(\mathbf{p}, V)}} \quad (10)$$

is an output of the noise whitening optimal group filter [16], $\mathbf{F}_j = \mathbf{F}(\lambda_j f_s)$ are values of noise MPSD for DFFT frequencies. In other words, if a signal/noise ratio is large enough one must take into account only the noise matrix spectral density meanwhile an information on a signal spectrum become insignificant.

3.3.4. Asymptotically efficient estimates of apparent slowness vector for small signal-to-noise ratio

The AE estimate of apparent slowness vector, considered in Section 3.3 is the best in the terms of asymptotic quality criterion by eq.(3). However it demands a numerical technique for finding a maximum of the functional eq.(8) that makes the computational algorithm rather labour consuming. The iterative estimation procedure is aggravated and slowed down by the necessity to maximise the functional eq.(8) in $(q+3)$ parameters, $q+1$ of which are nuisance, e.g. actually unnecessary for the main estimation problem.

An additional assumption that signal/noise ratio is small allows for a significant simplification of asymptotically efficient estimation algorithm. A mathematically correct formulation of the apparent slowness estimation problem under this assumption is to estimate parameters of a weak signal $y_s(t)$ in the following model of observations

$$\mathbf{x}(t) = (\delta/\sqrt[4]{N}) \mathbf{y}(t) + \xi(t), \quad t \in 1, N \quad (11)$$

In accordance with this model a matrix power spectral density (MPSD) of the time series $\mathbf{x}(t)$, $t \in 1, N$ is equal to

$$\mathbf{F}_x(f) = \mathbf{F}(f) + (1/\sqrt{N}) \mathbf{H}(f, \mathbf{p}, V) \sum_{k=1}^q c_k \varphi_k(f) \quad (12)$$

It can be shown [12,17] that under weak restrictions on noise MPSD $\mathbf{F}(f)$ the likelihood function (LF) eq.(6) of observations by eq.(1), (2) has the following asymptotic representation:

$$L(X_N | \mathbf{c}/\sqrt{N}, \mathbf{p}, V) = -L(X_N, 0) + \mathbf{c}^T \delta(X_N, \mathbf{p}, V) - (1/2) \mathbf{c}^T \Gamma(\mathbf{p}, V) \mathbf{c} + \alpha_N(X_N, \mathbf{p}, V, \mathbf{c}), \quad (13)$$

where

$$\delta(X_N, \mathbf{p}, V) = (1/\sqrt{N}) \sum_{j=1}^N [|\mathbf{h}_j^*(\mathbf{p}, V) \mathbf{F}_j^{-1} \mathbf{x}_j|^2 - \mathbf{h}_j^*(\mathbf{p}, V) \mathbf{F}_j^{-1} \mathbf{h}_j(\mathbf{p}, V)] \varphi_j$$

is the vector asymptotically sufficient statistic for the small nuisance parameters \mathbf{c}/\sqrt{N}

$$\Gamma(\mathbf{p}, V) = (1/N) \sum_{j=1}^N [\mathbf{h}_j^*(\mathbf{p}, V) \mathbf{F}_j^{-1} \mathbf{h}_j(\mathbf{p}, V)]^2 \varphi_j \varphi_j^*$$

is the limit of normalised Fisher matrix for the small nuisance parameters \mathbf{c}/\sqrt{N} [12,16,17]; $\alpha(X_N, \mathbf{p}, \mathbf{c}, V)$ is a residual term of the LF asymptotic decomposition, converging to zero in probability as a random process in the space $\mathbf{C}[\wp \times \Theta]$ of continues functions from (\mathbf{p}, θ) with a uniform metric, where Θ is a bounded set of nuisance parameters $\theta = (\mathbf{c}, V)$, \wp is a

bounded set of informative parameters \mathbf{p} ; $L(X_N, \theta)$ is the likelihood function of "pure" noise. Due to independence of this term on the parameters $(\mathbf{p}, \mathbf{c}, V)$ it may be dropped hereinafter.

As follows from eq.(13) the AE parameter estimate for observations fitting the model eq. (1), (2) has the form

$$\tilde{\boldsymbol{\theta}}_N = (\tilde{\mathbf{p}}_N, \tilde{\boldsymbol{\theta}}_N) = \arg \max_{\mathbf{c}, \mathbf{p}, V} [\mathbf{c}^T \boldsymbol{\delta}(X_N, \mathbf{p}, V) - (1/2) \mathbf{c}^T \Gamma(\mathbf{p}, V) \mathbf{c}]. \quad (14)$$

The estimate $\tilde{\boldsymbol{\theta}}_N$ appears to be significantly simpler than the common case AE estimate obtained by maximising eq.(8). Indeed, by maximising eq.(14) in \mathbf{c} with fixed \mathbf{p} and V it is easy to derive

$$\tilde{\mathbf{c}}_N(\mathbf{p}, V) = \arg \max_{\mathbf{c}} [\mathbf{c}^T \boldsymbol{\delta}(X_N, \mathbf{p}, V) - (1/2) \mathbf{c}^T \Gamma(\mathbf{p}, V) \mathbf{c}] = \Gamma^{-1}(\mathbf{p}, V) \boldsymbol{\delta}(X_N, \mathbf{p}, V) \quad (15)$$

The substitution of eq.(3.5) into eq.(3.4) gives

$$(\tilde{\mathbf{p}}_N, \tilde{V}_N) = \arg \max_{\mathbf{p}, V} R(X_N, \mathbf{p}, V) \quad (16)$$

where

$$R(X_N, \mathbf{p}, V) = \boldsymbol{\delta}^T(X_N, \mathbf{p}, V) \Gamma^{-1}(\mathbf{p}, V) \boldsymbol{\delta}(X_N, \mathbf{p}, V) \quad (17)$$

Thus when a signal/noise ratio is small the problem of apparent slowness vector and seismic wave phase velocity estimation can be reduced to maximisation of the functional eq.(17) in \mathbf{p} and V . This is essentially simpler task than the maximisation of functional eq.(8). It is attributed both to the less number of calculations for evaluating the values of $R(X_N, \mathbf{p}, V)$ as well as its derivatives by p_x, p_y and V , and to the fact that the procedure of optimisation involves only three parameters: p_x, p_y and V , instead of $(q+3)$ parameters $(\mathbf{c}, \mathbf{p}, V)$. As a rule this yields to a significant increase in the speed of iterative procedures of numerical optimisation. A maximisation of the functional eq.(17) becomes easier also due to the existence of simple explicit expressions for its partial derivatives of the first and the second order for parameters \mathbf{p}, V .

With the purpose to investigate an asymptotic quality of estimates by eq.(16) one needs first to proof the \sqrt{N} -consistency of the estimates $(\tilde{\mathbf{p}}_N, \tilde{V}_N)$, e.g. the convergence $(\tilde{\mathbf{p}}_N, \tilde{V}_N)$ in probability with speed $1/\sqrt{N}$ to the true parameters values (\mathbf{p}_0, V_0) . Then one needs to find an asymptotic covariance of apparent slowness vector estimate $\tilde{\mathbf{p}}_N$ i.e. the limit

$$\lim_{n \rightarrow \infty} E_{\mathbf{p}_0, V_0} N(\tilde{\mathbf{p}}_N - \mathbf{p}_0)(\tilde{\mathbf{p}}_N - \mathbf{p}_0)^T = K_p(\mathbf{p}_0, \mathbf{c}_0, V_0). \quad (18)$$

Comparison of $\text{tr} K_p(\mathbf{p}_0, \mathbf{c}_0, V_0)$ with the lower bound for estimation errors guaranteed by asymptotically efficient algorithm eq.(8) enables one to determine a possible loss in asymptotic

quality of apparent slowness by estimate eq.(16) comparing with the AE estimate. Such investigations may be performed based upon techniques developed in [12].

Note, that formula for asymptotically sufficient statistic (see eq.(13)) may be transformed to the following form

$$\delta(X_N, \mathbf{p}, V) = ((1/\sqrt{N}) \sum_{j=1}^N (|z_j|^2 - 1)^2 r_j(\mathbf{p}, V) \varphi_j) \quad (19)$$

where $r_j(\mathbf{p}, V) = \mathbf{h}_j^*(\mathbf{p}, V) \mathbf{F}_j^{-1} \mathbf{h}_j(\mathbf{p}, V)$; and z_j are determined by eq.(10). One can see from eq.(10) that for the case of small signal/noise ratio the AE estimation procedure includes as a main part the calculation of output z_1, \dots, z_N of the whitening group filter.

3.3.5. Apparent slowness estimates for completely unknown signal waveforms.

If the waveform $s(t)$ of seismic phase is completely unknown (Section 3.3.1, model b) the spectral samples $s_j, j \in 1, N$ in eq.(7) are completely unknown too and have to be considered as a set of nuisance parameters for the problem. If to drop small terms $O_f(1/\sqrt{N})$ in eq.(7) then observations in the discrete frequency domain fit a non-linear regression model with unknown "repressors" s_j . As a number of nuisance parameters s_j tends to infinity with an increase of the number of data samples N , a reasonable question arises: do such formulation of the problem provides existence of some \sqrt{N} -consistent estimate, for which estimation errors tend to zero if N tends to infinity and the asymptotic covariance matrix eq.(3) exists. Hereafter we are to construct an example of such estimate by means of the maximum likelihood techniques. The proof of the \sqrt{N} -consistency of this estimate and analytical expression for its asymptotic covariance matrix may be obtained using the results of [12].

Let us derive a maximum likelihood estimate of apparent slowness vector \mathbf{p} and wave velocity v for the case of completely unknown waveform $s_j, j \in 1, N$. We will use an approximate expression for the likelihood function in the frequency domain, similar to eq.(8). As s_j are deterministic (though unknown) complex values, and ξ_j are Gaussian vectors then the same considerations which have led to eq.(6) allow us to derive the following asymptotic expression for the likelihood function in the case under discussion

$$\begin{aligned} L(X_N | \mathbf{p}, V, \{s_j\}) &= C - (1/2) \sum_{j=1}^N \ln \det \mathbf{F}_j - (1/2) \sum_{j=1}^N (\mathbf{x}_j - \mathbf{h}_j(\mathbf{p}, V) s_j)^* \mathbf{F}_j^{-1} (\mathbf{x}_j - \mathbf{h}_j(\mathbf{p}, V) s_j) = \\ &= l_f(X_N | \mathbf{p}, V, \{s_j\}) + O_f(1/\sqrt{N}) \end{aligned} \quad (20)$$

The joint maximum likelihood (ML) estimates of informative parameters \mathbf{p}, V and unknown nuisance parameters $s_j, j \in 1, N$ are the solution of the following set of equations

$$\frac{\partial}{\partial \operatorname{Re} s_j} l_f(X_N | \mathbf{p}, V, \{s\}) = 0; \quad \frac{\partial}{\partial \operatorname{Im} s_j} l_f(X_N | \mathbf{p}, V, \{s\}) = 0; \quad j \in 1, N; \quad (21)$$

$$\frac{\partial}{\partial p_\alpha} l_f(X_N | \mathbf{p}, V, \{s\}) = 0; \quad \alpha \in x, y; \quad \frac{\partial}{\partial v} l_f(X_N | \mathbf{p}, V, \{s\}) = 0;$$

where $\operatorname{Re} s_j$ and $\operatorname{Im} s_j$ are the real and imaginary parts of complex signal spectral samples.

Having positively defined Hermitian matrix \mathbf{F}_j^{-1} expressed in the form: $\mathbf{F}_j^{-1} = \mathbf{F}_j^{-1/2} \mathbf{F}_j^{-1/2}$ one can write the main term of eq.(4.1) like

$$L(X_N | \mathbf{p}, V, \{s\}) = C - (1/2) \sum_{j=1}^N \ln \det \mathbf{F}_j - (1/2) \sum_{j=1}^N |\mathbf{n}_j - \mathbf{d}_j(\mathbf{p}, V) s_j|^2; \quad (22)$$

$$\text{where} \quad \mathbf{n}_j = \mathbf{F}_j^{-1/2} \mathbf{x}_j, \quad \mathbf{d}_j = \mathbf{F}_j^{-1/2} \mathbf{h}_j(\mathbf{p}, V). \quad (23)$$

The first subsystem of equations (21) is linear and as it is easy to verify has the following solution

$$s_j^+ (\mathbf{p}, V) = [\mathbf{d}_j^* (\mathbf{p}, V) \mathbf{x}_j] / |\mathbf{d}_j (\mathbf{p}, V)|^2; \quad j \in 1, N. \quad (24)$$

Substituting $s_j^+ (\mathbf{p}, V)$ into the second subsystem of eq.(21) one obtains (after some simple algebraic transformations) that in the problem being considered the ML estimates of apparent slowness vector and wave velocity are solutions of the following set of non-linear equations

$$\rho_\alpha(X_N, \mathbf{p}, V) = \sum_{j=1}^N \mathbf{x}_j^* \left(\frac{\partial}{\partial p_\alpha} A_j(\mathbf{p}, V) \right) \mathbf{x}_j = 0; \quad \alpha \in x, y; \quad (25)$$

$$\rho(X_N, \mathbf{p}, V) = \sum_{j=1}^N \mathbf{x}_j^* \left(\frac{\partial}{\partial v} A_j(\mathbf{p}, V) \right) \mathbf{x}_j = 0;$$

$$\text{where} \quad A_j(\mathbf{p}, V) = \left(\mathbf{I} - \frac{\mathbf{F}_j^{-1} \mathbf{H}_j(\mathbf{p}, V)}{\operatorname{tr} \mathbf{F}_j^{-1} \mathbf{H}_j(\mathbf{p}, V)} \right) \mathbf{F}_j^{-1}. \quad (26)$$

The all discussed above provides the important conclusion that ML-estimates of seismic wave apparent slowness vector \mathbf{p} and velocity V in the case of completely unknown waveform have to minimise the functional

$$\Gamma(X_N, \mathbf{p}, V) = \sum_{j=1}^N \mathbf{x}_j^* A_j(\mathbf{p}, V) \mathbf{x}_j \quad (27)$$

The functional eq.(27) has a clear geometrical interpretation. According to eq.(7) the signal frequency samples \mathbf{x}_j belong (with an accuracy up to $O_f(1/N)$) to some 1-dimensional subspaces $\mathfrak{R}_j(\mathbf{p}, V)$ of the complex m -dimensional \mathbf{x}_j -vector spaces \mathbf{C}_j^m . It is easy to demonstrate that the functional eq.(27) is the sum of squares of distances from the observations \mathbf{x}_j to the

corresponding subspaces $\mathfrak{R}_j(\mathbf{p}, V)$, the distances are calculated in the metrics determined by the inner products

$$(\mathbf{a}, \mathbf{b}) = \mathbf{a}^* \mathbf{F}_j^{-1} \mathbf{b}, \quad \mathbf{a}, \mathbf{b} \in C_j^m \quad (28)$$

Thus in the problem being considered the maximum likelihood techniques brings to the vector (\mathbf{p}, V) estimate which is a generalisation of the known estimate by the orthogonal statistical regression method.

By a simple transformation of the functional eq.(27) one can verify that the method described really provides exactly the same estimates of apparent slowness vector \mathbf{p} and velocity V as the functional eq.(9),(10), which provides the AE estimates for random Gaussian signal with a large signal/noise ratio. It is evident, that eq.(26) and eq.(27) result in

$$\Gamma(X_N, \mathbf{p}, V) = \sum_{j=1}^N \mathbf{x}_j^* \mathbf{F}_j^{-1} \mathbf{x}_j - \sum_{j=1}^N \left(\frac{|\mathbf{h}_j^*(\mathbf{p}, V) \mathbf{F}_j^{-1} \mathbf{x}_j|^2}{\mathbf{h}_j^*(\mathbf{p}, V) \mathbf{F}_j^{-1} \mathbf{h}_j(\mathbf{p}, V)} \right) \quad (29)$$

The first term in eq.(29) does not depend on parameters (\mathbf{p}, V) , so the estimation of (\mathbf{p}, V) is reduced to maximisation of the second term, which coincides exactly with the functional $\tilde{\Lambda}(X_N, \mathbf{p}, V)$ by eq.(9),(10). This is the very important coincidence which exhibits the close connection between so different at first glance mathematical models of observations: the model of random Gaussian signal with an unknown power spectrum density and the model of deterministic signal with completely unknown waveform. This interesting (but natural) correlation of these models has been discussed in [12].

3.4. References

1. Aki, K., Richards, P., 1980, Quantitative seismology. Theory and Methods, Freeman and Comp., San Francisco.
2. Backus, M., Burg, J., Boldwin, D., Bryan, E., 1964, Wide-band extraction of mantle P-waves from ambient noise, *Geophysics*, vol.29, pp.672-692.
3. Brillinjer, D., 1976, Time series. Theory and data processing. J.Willey and sons, N-Y.
4. Capon, J., 1970, Application of space-time domain decision and estimation theory to antenna processing system design, *Proc. IEEE*, vol.58, pp.170-180.
5. Claassen, J.P., 1992, The application of multiply constrained minimum variance adaptive beamforming to regional monitoring, *Bull.Seism.Soc.Am.*, vol.82, pp.2191-2212.
6. Esmer soy, C., Cormier, V.F., Toksoz, M.N., 1985, Three-component array processing, in *The VELA Program: A twenty-five year review of basic research*, ed.: A.V. Kerr, DARPA, Washington, D.C., pp.565-578.
7. Hannan, E.J., 1970, Multiple time series, J.Willey and sons, N-Y.
8. Harris, D.B., 1990, Comparison of the direction estimation performance of high-frequency seismic arrays and three-component stations, *Bull.Seism.Soc.Am.*, vol.80, pp.1951-1968.
9. Jepsen, D.C., Kennett, B.L.N., 1990, Three-component analysis of regional seismograms, *Bull.Seism.Soc.Am.*, vol.80, pp.2032-2052.
10. Kennett, B.L.N., 1980, Seismic wave propagation in stratified media, Cambridge, University Press.
11. Kushnir, A.F., 1995, Algorithms for adaptive statistical processing of seismic array data, *Proceedings of NATO Advanced Study Institute on Monitoring of a Comprehensive Test Ban Treaty*, Portugal, Kluwer Pub.Comp., Amsterdam, Netherland, 1996.
12. Kushnir, A.F., 1989, Asymptotically optimal statistical analysis of geophysical fields, Dr.Sc. Dissertation, Moscow, IPE, Acad.Sc. USSR (in Russian).
13. Kushnir, A.F. (ed), 1995, Seismic monitoring with small aperture arrays under strong noise conditions: algorithms, technique, system design and experimental data processing, Technical Report on EOARD Special Project SPC-94-4039.
14. Kushnir, A.F., Fyen, F., Kvarna, T., 1991, Studying of multichannel statistical data processing algorithms in the framework of the NORSAR event processing program package, Semiannual Technical Summary, NORSAR Sci.Rep. 2-90/91, Kjeller, Norway, pp.82-103.

15. Kushnir, A.F., Kvarna, T., 1991, Initial testing of mixed event separation using statistically optimal adaptive algorithms, Semiannual Technical Summary, NORSAR Sci.Rep. 1-91/92, Kjeller, Norway, pp.112-126.
16. Kushnir, A.F., Lapshin, V.M., 1986, Parametric methods of analysis of multiple time series, Moscow, Nauka, Publ.Inst.Phys.Earth, Acad.Sci. USSR (in Russian).
17. Kushnir, A.F., Mostovoy, C.V., 1990, Statistical processing of geophysical fields, Naukova Dumka, Kiev (in Russian).
18. Kushnir, A.F., Pinsky, V.I., Tsvang, S.L., Fyen, J., Makkeltveit, S., Ringdal, F., 1990, Optimal group filtering and noise attenuation for NORESS and ARCESS arrays, Semiannual Technical Summary, NORSAR Sci.Rep. 1-90/91, Kjeller, Norway, pp.115-134.
19. Kushnir, A.F., Pisarenko, V.F., Rukavishnikova, T.A., 1980, Noise compensation in multidimensional geophysical observations. I. Theory and methods of data processing, Computational Seismology, vol.13, Allerton Press Inc., pp.146-151.
20. Kvarna, T., 1993, Intelligent post-processing of seismic events. Part 2: Accurate determination of phase arrival times using autoregressive likelihood estimation, Semiannual Technical Summary, NORSAR Sci.Rep. 2-92/93, Kjeller, Norway, pp.68-92.
21. Kvarna, T., 1993, A generic algorithm for accurate determination of P-phase arrival times, Semiannual Technical Summary, NORSAR Sci.Rep. 2-93/94, Kjeller, Norway, pp.98-108.
22. Kvarna, T., Ringdal, F., 1992, Integrated array and three-component processing using a seismic microarray, Bull.Seism.Soc.Am., vol.82, pp.870-882.
23. Lokshtanov, D.E., Ruud, B.O., Husebye E.S., 1991, The crustal transfer function in seismic three-component slowness estimation, Geophys.Res.Lett., vol.18, pp.1393-1396.
24. Mykkeltveit, S., Ringdal, F., Kvarna, T., Alewin, R., 1990, Application of regional arrays in seismic verification research, Bull.Seism.Soc.Am., vol.80, pp.1777-1800.
25. Pisarenko, V.F., Kushnir, A.F., Savin, I.V., 1987, Statistical adaptive algorithms for estimations of onset moments of seismic phases, Phys.Earth Planet.Inter., vol.47, pp.888-900.
26. Ringdal, F., Husebye, E.S., 1982, Application of arrays in the detection, location and identification of seismic events, Bull.Seism.Soc.Am., vol.72, pp.2201-2224.
27. Shen, W.W., 1979, A constrained minimum power adaptive beamforming with time varying adaptation rate, Geophysics, vol.44, pp.1088-1096.
28. Wiggins, R.A., Robinson, E.A., 1968, Recursive solution of the multichannel filtering problem, J.Geophys.Res., vol.70, pp.1885-1890.

4. EXPERIMENTAL STUDY OF ADAPTIVE ALGORITHM APPLICATIONS TO 3-COMPONENT VERY BROAD BAND SMALL APERTURE ARRAY DATA PROCESSING

CONTENT

4.1 Introduction.....	1
4.2. Geyocha array noise feature study.....	2
4.3. Simulating experiments with real Geyocha 3C noise recordings.....	5
4.4. Analysis of Geyocha 3C seismograms from Lop Nor explosion on 07.10.1994.....	6
4.4.1. P-phase arrival direction estimation.....	6
4.4.2. Extracting of phase waveforms from background noise.....	7
4.5. Analysis of Geyocha 3C seismograms from Lop Nor explosion on 10.06.1994.....	9
4.5.1. P-phase arrival direction estimation.....	9
4.5.2. Extracting of phase waveforms from background of noise and coda of previous phases.....	11
4.6. Analysis of Geyocha 3C seismograms from Oman gulf earthquake on 18.10.1993.....	14
4.6.1. Onset time estimation of the event wave phases.....	14
4.6.2. Extraction of body wave phase waveforms using adaptive array seismogram processing	17
4.6.3. Study of event surface wave characteristics.....	19
Figures.....	
4.7. Detection and parameter estimation of explosion signal obscured by coda of strong interfering earthquake using data from small aperture array.....	21
Figures	
4.8. References.....	24

4. EXPERIMENTAL STUDY OF ADAPTIVE ALGORITHM APPLICATIONS TO 3-COMPONENT VERY BROAD BAND SMALL APERTURE ARRAY DATA PROCESSING

4.1 Introduction

The well tested NORESS-type small aperture arrays are essentially oriented to the regional seismic monitoring [5] and are equipped by short period instruments which record a seismic energy above 0.5 Hz. For this reason there were not so much studies of low frequency noise field coherency in the limits of these array aperture. The α -stations of the International Monitoring Network currently being deployed are expected to be designed as 3-component wide band small aperture arrays containing about ten very broad band (VBB) 3C sensors within an aperture about 1.5 km [9]. Prototypes of the α -stations were tested in the framework of the IRIS PASSCAL project. For example, the VBB subarrays of Pinjon Flat (USA) and Geyocha (Turkmenistan) experimental arrays can be treated as such prototypes. Fig.1 shows the configuration of VBB subarray of the Geyocha array deployed not so far from Turkmenistan capital Ashgabad. The array having been exploited during 93-94 years. It was situated on thick sedimentary rocks and hence was affected by intensive seismic noise (especially in the low frequency range). This sedimentary basin has been subjected to intensive geological crumpling, so multiple folds have been formed. These folds and other medium inhomogenities cause intensive scattering of seismic waves. For this reason the extraction of seismic phase waveforms and estimation of phase parameters relaying only on the wave polarization characteristics is very difficult task in this region. Employment of 3C VBB seismic arrays significantly gains the information about characteristics of complex wave-fields generated in the medium by seismic events and greatly facilitates event analysis. Registering of the three spatial components of seismic wave field by different array receivers allows to distinct the seismic phases based on their polarization characteristics and to extract the SH and Love phases which are not registered by 1C vertical sensors. Observation of an event wave-field at spaced sites allows to eliminate influence of media lateral ingomogeneties by "smoothing" of their impacts on local wave-field behavior. This leads to the much higher accuracy of event parameter measurements. Besides, by analyzing seismic noise 3C array recordings one can study spatial and polarization characteristics of the noise wave-field. This provides the better noise suppression by the 3C adaptive processing procedures as compared with 1C ones. However, the data from 3C arrays should be handled with some care, because involving horizontal seismograms into processing one may in some cases diminish the quality of event analysis. This can occur, for example, while extracting waveforms of teleseismic longitudinal body waves. The seismic power of such waves is mainly concentrated in the vertical component of an event wave-field while seismic

noise fields often has the most power in the horizontal components. So signal-to-noise ratio in horizontal seismograms of 3C array can be rather low in such cases, and processing of the horizontal seismograms altogether with the vertical seismograms can lead only to deterioration of waveform extraction quality.

Below we discuss results of analysis of the noise field in the Geyocha array region and adaptive processing of seismograms from several regional events recorded by this array. We are grateful to Dr. A.Dainty from the Earth Division of US AF Phillips Laboratory who collected these array multichannel recordings and transferred them to computer network of Moscow IRIS Data Analysis Center. Owing to the Dr. A.Dainty help our research group has got the relevant real data for thorough testing and refinement of the adaptive 3-component array data processing technique being developed.

Some characteristics of the events are enclosed in the Table 1

Table 1

Ev. n	Origin time	Source coordinates degr.	Source depth km.	Magnitude mb	Epicenter distance degr.	Back azimuth degr.	P-wave appar. veloc.	Source type
1	07.10.94 03:25:58.1	41.66° N 88.75° E	0	6.0	23.74°	71.29°	11.46	China nuclear test
2	10.06.94 06:25:58.0	41.69° N 88.79° E	0	5.7	23.77°	71.22°	11.46	China nuclear test (6 3C st)
3	18.10.93 13:57:14.6	22.13° N 62.85° E	10	5.2	16.29°	164.13°	8.67	Earthquake (11 3C st.)
4	02.10.93 01:17:30.4	39.07° N 69.97° E	14	5.0	9.35°	79.37°	8.04	Earthquake

The apparent velocities of the P-phase arrival were calculated based on the known source coordinates using travel time tables originated from the Jeffreys-Bullen Earth model.

4.2. Geyocha array noise feature study

As we noted above the main reason for employing of the adaptive statistical array data processing is the coherence feature of the noise field observing in the many practical situations. So the first stage of our experimental studies of the Geyocha array recordings was investigating of noise field characteristics. The typical Geyocha sensor noise recordings are shown at Fig.2a. The noise seismograms were registered at the N, E and Z components of the central Geyocha seismometer ORGH. Power spectral densities (PSD) of the noise field components estimated using the noise realizations in Fig.2a are shown in Fig.2b for frequency range 0-10 Hz and in Fig.2c (with more resolving power) - for frequency range 0-1 Hz. We see that the PSD has four peaks at frequencies 0.07, 0.2, 1.5 and 3.5 Hz. The peaks in the low frequency range are

produced by the storm microseisms. Their genesis is discussed below. The peaks in the high frequency range are split because as we guess, the resolving power of the spectral analysis was excessive in this range, that lead to statistical fluctuations of the PSD estimate. But may be these peaks are connected with some man made periodical sources.

In Fig.2d the noise PSD for the central vertical sensor is compared with the PSD of a beam composed from noise records of all 12 vertical VBB instruments; beam was steered to Lop Nor China Test Site (azimuth 71.7° , app. velocity 3.55 km/sec). We see that the noise with frequencies below 1 Hz is not suppressed by the beamforming procedure. This indicates that the noise field has high spatially correlations for this frequencies. Fig.3a shows noise coherence functions for the vertical components of the most close located (B32, C22) and the most distant apart (NHB, SEH) array sensors. We see that the first function preserves magnitudes very close to 1 over all frequency band 0-1 Hz and the second function has values larger then 0.8 up to 0.5 Hz. Fig.2d and Fig.3a convinced us that for extraction of seismic phase waveforms in the frequency band below 1 Hz one has to apply the adaptive optimal group filtering algorithm instead of the conventional beamforming procedure. At Fig.3b the noise coherence functions calculated for the different pairs of components of central Geyocha 3C seismometer are displayed. All three functions have the very low magnitude that give rise to doubts that the 3-component AOGF procedure provides much signal-to-noise ratio gain in comparison with 1-component one. In fact, our experiments showed that gain about 4.5 dB can be achieved (as it is theoretically predicted for the case of uncorrelated spatial noise components). Nevertheless, there was demonstrated that 3-component modification of the AOGF method is very helpful for separation of the seismic phases having main oscillation energy in different spatial components: longitudinal, transverse and vertical, if these phases are obscured by coherent seismic noise or the coda waves of the previous phases.

The following analysis will be mainly accomplished for the frequency range 0.01-2.5 Hz, so let us study the noise characteristic for this range in more details. At first, note that for the frequencies exceeding 0.3 Hz noise PSD is almost the same for the all spatial components. This is valid also for the band 0.05-0.1 Hz. In contrast, in the vicinity of the peak frequency 0.2 Hz the vertical noise component has the power exceeding the power of the horizontal noise components more then 4 times. The first can be explained by the noise polarization elongated in Z-direction that allows us to suspect that this noise component is propagated as the longitudinal body waves arriving to the array from below. This conclusion is confirmed by the results of F-K analysis, discussed below.

In the very low frequency band (below 0.03 Hz) the situation is opposite: noise power for the Z-component is about 10 times less then for horizontal components. This can be explained

by the physical nature of these noise oscillations caused by the fluctuations of the atmospheric pressure. The impact of these fluctuations on the horizontal seismometer components is much stronger than on its vertical component [10].

The same power of the noise field components in the frequency band 0.05-0.1 Hz leads to hypothesis that this noise component could be the transient one propagating as the Rayleigh waves with the small elliptic factor. This conclusion also is confirmed by the F-K analysis.

The spatial spectrum map (F-K map) for Geyocha array noise in the frequency band 0.15-0.25 Hz (corresponding to the most strong spectral peak of the Fig.2c spectra) is depicted in Fig.4a. According to the map this noise component could be treated as a composition of body waves arriving with very low incidence angles. In regard of the thick sedimentary layers beneath the array it is not contradicted with the description of this component as a scattered field generated by the ocean storms. Judging the back azimuth of this noise component (230°) the "source" of this microseisms is situated in Indian Ocean. The F-K map for the other low frequency noise peak in the band 0.05-0.07 Hz (Fig.4b) testifies that this noise component could be composed with surface waves arriving from Caspian Sea (note that apparent velocity of this surface waves is slightly greater than typical Rayleigh wave velocity).

Because of the small aperture and the high correlation of noise for different sensors one may erroneously declare that the Geyocha type VBB array is a bad instrument for analyzing teleseismic and far regional surface waves. Really, the beamforming method does not provide any improvement in SNR for these waves, their F-K analysis is hampered by the coherence low frequency noise. To demonstrate applicability of the AOGF method for the case we simulated seismograms of a Rayleigh wave generated by a teleseismic explosion and recorded by the 1-component Geyocha array. The waveforms of seismograms from different array sensors were modeled as the Berlage pulses with frequency 0.06 Hz and duration 150 sec. The pulses were shifted in time as for the Rayleigh wave originated from the Chinese Lop Nor test site. Note that the central frequency of the simulated wave was chosen equal to the frequency of Geyocha coherent noise peak. The simulated seismograms were then mixed with real Z-component records of Geyocha VBB array noise. The mixture (with the power SNR=0.1) was processed by the AOGF in the frequency band 0-1 Hz. The results shown in Fig.5 allow to assert that the AOGF has in this case the great potentials: the Rayleigh phase SNR was improved in 40 times due to effective suppression not only the transient (0.06 Hz) but also scattered (0.2 Hz) noise components.

4.3. Simulating experiments with real Geyocha 3C noise recordings

To assess advantages which the adaptive statistical approach has for 3C broad band array data processing in comparison with the 1C case we simulated Geyocha array 3C seismograms as produced by the Lg regional seismic phase with central frequency 0.2 Hz, arrival azimuth 71.7° and velocity 4 km/sec. Note that the signal frequency was chosen coinciding with the most strong noise spectral peak (originated from the scattered storm microseisms). The simulated seismograms were mixed with real 3C recordings of Geyocha VBB noise to provide the power SNR=0.1. The mixture was processed by the 1C (for vertical components only) and 3C beamforming and adaptive group filtering algorithms. The results are shown in Fig.6. Fig.6a demonstrates the output traces of the one-component beamforming (trace 2), AOGF (trace 3) and WOGF (trace 4) algorithms applied to the all 12 VBB vertical array channels (in the frequency band 0-1 Hz). Trace 1 is a record of simulated Lg waveform. We see that as for the previous case (extracting a teleseismic long period surface wave) the conventional beamforming fails to recover the signal waveform but the AOGF provides a high suppression of coherent array noise and the good extraction of weak seismic Lg phase only due to a difference in the signal and noise spatial characteristics

In Fig.6b the results are shown for the same procedures applied to the vertical components of only four most distantly spaced VBB instruments: ORGH, NH, SWH and SEH (see Fig.1). We see that the micro array consisting only 4 1C stations also provides rather good noise suppression and signal extraction. But the quality of signal recovering while using only 4 1C stations are significantly poorer than for the total Geyocha vertical subarray.

Fig.6c shows the processing results for the simulated data from 12 3C stations. The quality of signal recovering here is approximately the same as for 12 vertical channels (Fig.6a) if do not take into account very long period (about 100 sec.) noise oscillations. The latter are very strong in the horizontal E-component noise recordings and are leaking in the output AOGF traces. So addition of horizontal instruments in this experiment apparently does not enhance the array processing capability because the 1C AOGF procedure already compensates all coherent noise and leave at the output only incoherent noise residuals.

Fig.6d exhibits the processing results for data from the described above micro-array consisting of four 3C stations. The quality of signal waveform recovering in this case is close to one for the case of array consisting of 12 vertical instruments (Fig.6a). Though the number of seismic channels in the both cases are the same, a deployment of array consisting of 12 vertical stations is much expensive than deployment of four 3C stations due to the cost of additional station volts and wiring from volts to the central hub.

The simulation experiments made with the Geyocha array modeled LF signals and real noise recordings allows to assert that VBB small aperture micro-arrays have the potentials to be a good tool for measurement of parameters of surface waves generated by teleseismic and far regional events. Expanding of adaptive processing technique to the 3C case provides the procedure for recovering of waveforms of low frequency seismic phases obscured by long period coherent noise; the good results can be achieved with the help of 3C micro-arrays consisting of 4-6 3C VBB instruments.

4.4. Analysis of Geyocha 3C seismograms from Lop Nor explosion on 07.10.1994

4.4.1. *P-phase arrival direction estimation.*

The simulations discussed above were made for the assumption that the medium in the vicinity of the array is laterally homogeneous one and the event waves are the plane ones. However the real medium beneath the array has very complex geological characteristics and this seriously hamper the analysis of event phase characteristics. The multiple scatterers generate the scattered waves arriving to the array sensors with small delays relatively the main phase wave. This leads to distortions of polarization characteristics of this wave. As result, even at the first seconds after phase onsets the particle motion has the form much more complicated then theoretically predicted one.

The particle motion of the P-wave of event *n2* from Table 1 is shown in the Fig.7. It has the elliptic feature that is peculiar to inhomogeneous and anizotropic media [1]. Table 2 encloses the results of polarization analysis of the P-wave of event *n1* made for recordings of the 12 VBB 3C Geyocha seismometers

Table 2

Seismometer	Back azimuth α	Incidence angle β
ORGH	63.8	18.4
NH	43.6	11.2
SWH	44.6	19.3
SEH	67.4	13.9
A22	68.7	19.2
B32	70.3	16.0
C22	76.6	12.2
D33	55.7	12.4
E22	61.1	16.0
F32	53.9	18.1
G22	46.2	17.9
H32	61.8	19.6
Mean values	59.5	16.2
RMS error	10.3	3.0

We see that deviation of the azimuth and incidence angle estimates relative to their mean value are very high. This testifies that serious medium inhomogeneity exists even inside the small array aperture (less than 2 Km). The mean value of the azimuth is about 22° less than the real azimuth value (Table 1). This can be connected with anomalous polarization of the longitudinal waves in the area which is already mentioned in [6].

At the same time the F-K analysis of the event P-wave-field made using recordings from 12 vertical Geyocha seismometers (Fig.8) gave the P-phase arrival azimuth estimate equal 67.6° that is much closer to the real value equal to 71.3° . The 4° deviation of the azimuth estimate to the North can be explained by the impact of the great Tibet and Tjan-Shan mountain provinces at the path of the wave propagation. The F-K estimate of the P-wave apparent velocity equal to 11.9 km/sec is also well corresponds to the value determined from the Jeffreys-Bullen travel time tables (11.46 km/sec). Some estimate excess of the theoretical value may be connected with the impact of low speed upper sedimentary layer in the Geyocha area.

The estimation of P-wave velocity in the medium beneath the array can be done by comparison of the results of polarization and F-K analysis. Employment of the simplest relation $\sin\beta_p = p_h V_p$ gives the value $V_p = 3.6$ km/sec, that is significantly less than value $V_p = 5.5$ km/sec assumed in the Jeffreys-Bullen Earth model. So low velocity value obtained compels us to suspect that for the V_p estimation in the given case one should employ the Kennett's model of the P-wave interaction with the day surface which takes into account the wave transformations while reflecting this border.

4.4.2. Extracting of phase waveforms from background noise.

The experimental study of 3C AOGF method effectiveness in comparison with 1C case while extracting the weak event P-phase waveforms from background coherent seismic noise was performed with the help of the following simulation. The Geyocha 3C recordings of the event *n1* P-wave (shown in Fig.9a for the central sensor components) were scaled and mixed with the Geyocha noise recordings (shown in Fig.2a for the same components) to get the signal-to-noise ratio $SNR=1$ (in the frequency band 0.01-2.5 Hz). The 3C seismogram of the mixture for the central Geyocha sensor is shown at Fig.9b. The vertical lines at this figure marks the time interval at which the explosion P-wave signal was inserted to the noise. For signal waveform extraction from noise we uses as total set of seismograms from 12 3C Geyocha sensors, as the seismograms from the subarray consisting of 3 outer Geyocha 3C sensors (NH,SWH,SEH) and the central 3C sensor ORGH. For data processing we used the following procedures:

- -conventional beamforming procedure;
- -traditional undistorting adaptive optimal group filtering procedure (AOGF1, Section 3.2.2);

- -AOGF-procedure with additional constrains to have the zero partial derivatives of the sensitivity function by x and y apparent slowness (AOGF2, Section 3.2.5);
- -adaptive whitening group filtering procedure (AWGF, Section 3.2.2);

The 1- and 3-component versions of these procedures was employed, being applied to 1C vertical array data set and to 3C array data set correspondingly. For noise adaptation the multichannel ARMA model was used with AR part order equal to 2 and MA part order equal to 8. The noise matrix covariance function was estimated using multichannel data at the time intervals which does not contain the signal (the outer intervals in Fig.9b).

The signal-to-noise ratios obtained in result of application of the all procedures described are contained in Table 3.

Table 3

Output signal-to-noise ratio		
Procedure used	Total array	4-sensor array
Z-component beam	0.7	0.64
Z-component AOGF1	27.6	2.4
Z-component AOGF2	25.8	1.2
Z-component AWGF	491.6	154.7
3-component AOGF1	30.3	5.5
3-component AOGF2	32.7	4.7
3-component AWGF	731.1	200.4

The output traces of the procedures for 12 Z-sensor array are depicted in Fig.10a, for 12 3C-sensor array - in Fig.10b, for 4 Z-sensor subarray - in Fig.10c and for 4 3C-sensor array - in Fig.10d. Comparison of the results presented in Table 3 and in Fig.10 allows us to make the following conclusions:

- a) The conventional one-component beamforming does not provide the extraction of the signal waveform in the wide frequency band of the study: 0.01-2.5 Hz.
- b) The optimal group filtering procedure extracts the P-phase waveform with undistorting reproduction of all frequency components of the signal in the wide frequency band. The procedure provides the gain in power SNR in comparison with beamforming equal to ≈ 30 for 12 3C-sensor array and ≈ 9 - for 4 3C-sensor array;
- c) The results of the experiment do not reveal an advantage of the adaptive optimal group filtering with the additional constrains on the spatial sensitivity diagram (AOGF2) in comparison with the traditional AOGF (AOGF1). At the same time the AOGF2 procedure involves additional computational resources and more time consuming then AOGF1.
- d) The adaptive whitening group filtering procedure (AWGF) provides extremely high noise suppression and signal extraction by combining the optimal filtering in the spatial and

frequency domains. Even for 4 3C-sensor microarray it produced in the experiment the power SNR gain equal to 200. As it is seen from Fig.10 the procedure preserves the most structural features of the phase waveform: the phase onset time is determined from the AWGF trace with the most precision; the appearance of the distinct wavelets inside the waveform is also not smoothed that allows to detect weak secondary phases on the background of the main phase oscillations, and so on. The only thing which can not to be guaranteed is the preserving of the phase power spectral density shape. This can hamper the estimation of the m_b magnitude based on the AWGF trace. Nevertheless the hope exists to develop some method for correction of such magnitude estimates for the characteristics of the whitening procedure.

e) The employment of 3C AOGF procedure instead of 1C procedure for phase waveform extraction from total Geyocha array recording set does not lead to significant improvement in SNR: 30-33 - for the 3C case instead 26-28 - for the 1C case. This can be explained by very low noise coherence between the 3C sensor spatial components and by many times larger amount of parameters which have to be estimated while 3C array noise modeling, in comparison with 1C modeling. Nevertheless, for the case of microarray consisting of 4 3C-sensors the 3C AOGF filtering provides the SNR gain in comparison with 1C variant close to the theoretically predicted 4.5 dB.

4.5. Analysis of Geyocha 3C seismograms from Lop Nor explosion on 10.06.94

The second event analyzed in our experimental study was Chinese nuclear test made on 10.06.94 at the Lop Nor test site. For some technical reasons we have the event recordings only from six 3C sensors of the Geyocha array. These sensors are marked by the crosses at the Fig.1. We see that the disposition of the sensors is close to be symmetric in respect to the straight line connecting the outer sensors NH and SEH. This allows to predict that the spatial sensitivity diagrams of the microarray being composed with these sensors have the central symmetry (in respect to the point $p_x=p_y=0$) for any steering direction and that for steering directions close to perpendicular to the line of symmetry the array spatial sensitivity diagram is very wide. The effective subarray aperture in the latter direction is less then 0.5 km, so it is really a equivalent to a microarray.

4.5.1. *P-phase arrival direction estimation.*

The disposition of the Geyocha seismometers which recordings were available is very unlucky for the F-K analyses of signals arriving from the Lop Nor test site direction. For this reason the P-wave F-K map calculated by conventional algorithm applied to the Z-component subarray seismograms has the very smoothed maximum (Fig.11). The estimates of wave arrival direction

(azimuth $\alpha=77.5^\circ$ and apparent velocity $v_p=10.9$ km/sec) are farther from theoretically predicted values than for the discussed above Lop Nor event *n1* (see Fig.8). The F-K estimates made using different time intervals of P-phase waveform demonstrated rather strong variability. We explain this by the poor sensor disposition combined with the complex structure of P-wave polarization. The latter preserves plausible linearity only during the first 4 seconds after the P-phase onset. The F-K map in Fig.11 was calculated just for this interval.

Such instability of the conventional Z-component F-K analysis stimulated us to employ generalized F-K analysis based on 2-components (horizontal) and 3-component seismograms recorded by the subarray. As it is seen from Fig.12 the event P-phase has the rather powerful horizontal components that is related with the complex medium structure beneath the array. The generalized 2-component F-K analysis taking into account only transverse phase oscillations produced in the case the F-K map shown in Fig.13. The azimuth and apparent velocity estimates ($\alpha=69.5^\circ$, $v_{ap}=11.7$ km/sec) provided by this map significantly less differ from the theoretical values ($\alpha=71.3^\circ$, $v_{ap}=11.5$ km/sec) than in the case of conventional Z-component F-K analysis.

The procedure of generalized 3-component F-K analysis of P-phase wave-field requires the information about longitudinal wave velocity V_p beneath the array. If this information is absent the generalized 3C F-K analysis can be made repeatedly with different suspected V_p values. The V_p value which provides the highest maximum of the F-K map can be regarded as the estimate of the real V_p value. (Note, that this method is statistically well grounded). This procedure applied to the 3C P-wave seismograms of the Lop Nor event *n2* gave the V_p estimate equal to 4.3 km/sec. The generalized 3C F-K map corresponding to this velocity value is shown in Fig.14. It provides the azimuth estimate equal 67.7° which is closer to real value and almost the same as for the F-K azimuth estimate got for the Lop Nor event *n1* (67.5°). However, the apparent velocity estimate obtained by this method turned to be excessively high: 16.1 km/sec, that is almost in 1.5 times larger then the theoretical value. This ensure us that the simplest model of the P-wave interacting with the day surface border (employed in the tested version of the generalized 3C F-K algorithm) does not correspond the real Geyocha conditions. Possibly the best accuracy can be achieved if to employ the Kennett interacting model, with a properly assigned factor μ in the relation $V_p=\mu V_s$. This conclusion is confirmed by the result of velocity V_p estimation based on polarization and F-K analysis of the set of 3C seismograms for Lop Nor event *n2*. The azimuth and incidence angle estimates calculated from the available P-phase recordings of 6 3C seismometers are listed in Table 4.

Table 4

Seismometer name	Back azimuth α	Incidence angle β
ORGH	60.3	22.6
NH	36.3	9.5
SEH	39.8	22.6
A22	66.8	20.0
B32	74.0	19.7
C22	71.6	17.5
Mean values	61.5	18.3
RMS error	15.2	4.5

The P-wave medium velocity estimate based on the simplest equation $\sin\beta = V_p/v_{ap}$ is equal in this case: $V_p=3.7$, that is corresponds well to the value obtained for Lop Nor event *n1*. This value is too low and can not be explained by the properties of the upper sedimentary layer.

Since the P-phase polarization even at the first seconds after onset moment is the strongly elliptic one (Fig.7) it is natural to employ for the generalized 3C F-K analysis the mathematical model for elliptic particle motion (really, the theoretical Rayleigh wave polarization model). This attempt provided the F-K map shown in Fig.15. The P-phase azimuth and apparent velocity estimates got with the help of this algorithm ($\alpha=71.7^\circ$, $v_{ap}=12.1$ km/sec) are greatly close to the theoretical values ($\alpha=71.3^\circ$, $v_{ap}=11.5$ km/sec).

Discussion above allows to assert that employment of horizontal component seismograms in the framework of the generalized F-K analysis provides significant improvement of accuracy of seismic phase azimuth and apparent velocity measurements based on data from 3C microarrays. The accuracy of such analysis in the case of 6 station microarray with effective aperture about 0.5 km is comparable with the accuracy of conventional Z-component F-K analysis in the case of NORESS type array with aperture 25 km. In any case the F-K analysis of microarray data provides much higher accuracy of arrival direction estimation then the polarization analysis of single 3C seismometer.

4.5.2. Extracting of phase waveforms from background of noise and coda of previous phases.

The wavetrain components of the Lop Nor event on 10.06.1994 registered by the central Geyocha 3C seismometer are shown in Fig.16 for frequency band 0.01-2 Hz. The signal-to-noise ratio of event P-phase is rather high, so the employment of AOGF seems to be expedient and one should use the conventional beamforming. However, Fig.17 shows that there exists a significant difference in the waveforms produced by the 1-component beamforming and 1-component AOGF procedures on the basis of subarray P-phase Z-seismograms in the frequency band 0.01-2 Hz. The decisive distinction is that the AOGF output trace reveal the thin

structure of the P-phase wavetrain: the sequence of distinct wavelets is seen in this trace. The secondary wavelets have almost the same form as the first one and can be interpreted as the reflections from the medium layer borders. These wavelets are almost not seen in the 1-component beam trace being hampered by the leaking of low frequency (coherent) noise. Note that the power of beam trace is about 2 times greater than for the AOGF trace. This is connected with the large width of subarray beam steered to the Lop Nor direction (the effective aperture of subarray for this direction is less than 0.5 km). For this reason the beamforming procedure collects the energy of waves arriving from a large range of directions, and accumulates besides the straight P-wave the multiple reflected and scattered waves generated by inhomogeneities of the medium beneath the array. The significant difference (in 2,7 times) exists for the maximal amplitudes of beam and AOGF traces, that leads to excess of 0.4 magnitude units while the event magnitude is estimated based on the beam trace instead of the AOGF trace.

Involving into the AOGF processing the recordings of horizontal subarray components does not provide a significant signal-to-noise ratio improvement in the extracted P-phase waveform as compared with Z-component AOGF trace. However this allows to separate the different constitutions of the complex P-phase particle motion. Fig.18 shows the results of 3-component AOGF filtering which extracts the waveforms of P-phase particle motions along the P-ray, in transversal (SH) and orthogonal (SV) directions relatively to this ray. The 3-component filtering algorithm used was based on the simplest model of the wave interaction with the day surface border neglecting the wave type transformations. One can see from the figure that already at the first seconds after the "pure" P-wave have arrived along the ray there exists the powerful motions in the orthogonal direction to the ray (SV-component). The oscillations of these two components are shifted in phase that leads to the elliptic P-wave polarization mentioned above. The power of the particle motions in the transverse direction to the ray is significantly less than in the other two directions and these oscillations can be related with the scattered wave fields.

Modified version of the 3-component AOGF algorithm which considers the wave transformations on the day surface border produced the output traces depicted in Fig.19. It is noticeable that the waveforms extracted for the longitudinal, transverse and orthogonal ray directions are exactly the same as for the simplest 3C AOGF version. The difference is only in power of the extracted waves which is in two times less than in the previous case, that is quite correct from the theoretical consideration.

As it is seen from Fig.16 the broad band event wavetrain does not contain any evidence of the shear wave arrivals. The application of 3-component AOGF processing also has not

provided the extracting of the regional or teleseismic S-phases. We regard this as peculiarity of this explosion may be connected with its source physical characteristics.

The 3-component seismogram of the central Geyocha sensor filtered in the frequency band 0.01-0.1 Hz is shown in Fig.20. The intensive Rayleigh and Love phase oscillations are explicitly seen in this figure. It is interesting that the 3-component AOGF algorithm gives the chance to extract the oscillations of these waves even in the broad frequency band 0.01-2 Hz. Before to demonstrate this we discuss the estimation of Rayleigh and Love surface wave arrival parameters.

The 3-component subarray seismograms filtered in the band 0.01-0.1 Hz gave the possibility to estimate these parameters with the help of generalized 3-component F-K analysis. The output maps of the analysis for the Rayleigh and Love waves are shown in Fig.21 and Fig.22. These maps provides the following estimates: for the Rayleigh wave - $\alpha=66.1^\circ$ and $v_{ap}=2.2$ km/sec; for the Love wave - $\alpha=64.1^\circ$ and $v_{ap}=3.3$ km/sec. The azimuth estimates for the both waves differ from theoretical value equal to 71.5° . This undoubtedly connected with the impact of Pamir and Tjan-Shan mountains which lie at the theoretical path of the wave propagation. The same reason can explain the low apparent velocities of the surface waves which differ from velocities predicted by Jeffreys-Bullen Earth model (3.0 km/sec- for Rayleigh and 3.5 km/sec for Love waves).

Fig.23 presents the output traces of 1-component and 3-component AOGF procedures applied to the subarray seismograms in frequency band 0.01-2 Hz. One can see that the 1-component AOGF steered to the azimuth 66.1° and apparent velocity 2.2 km/sec did not revealed any surface wave. At the same time the 3-component AOGF with the same steering detected the strong Rayleigh wave oscillations at the longitudinal output component and (with steering $\alpha=64.1$, $v_{ap}=3.1$ km/sec) - the intensive Love wave oscillations at the transverse output component. Note that the orthogonal output component of 3C AOGF did not show any surface wave oscillations (exactly as the 1C AOGF trace did). This attests to the explosion Rayleigh wave has the very low ellipticity and its vertical component have the less power than noise and body wave coda.

The AOGF filter adaptation in the previous case was made using noise recordings before event P-wave arrival. If to include in the adaptation interval the P-phase and its coda (up to 500 sec) then the 3-component AOG filtering of the surface waves gives the much better results (Fig.24). The 1C AOGF in this case also failed to detect the Rayleigh wave oscillations, but the longitudinal component of 3C AOGF revealed these oscillations very clearly due to suppression of the coherent P-wave + P-coda oscillations. The 3C AOGF extraction of the Love wave at transverse component turned to be the most effective: the high frequency P-wave + P-coda

oscillations were strongly suppressed and the multi-mode structure of the Love wave oscillations became clearly seen. Note that the orthogonal component of 3C AOGF also did not provide the detection of vertical Rayleigh wave component, though the P-wave power is suppressed there in great extent then for 1C AOGF.

The last experiment with the surface waveform extraction was made in the frequency band 0.01-0.1 Hz with adaptation including the interval of event P-wave (up to 500 sec). The results of this experiment are presented in Fig.25. We see that in this frequency band the Z-component AOGF provided the refinement of Rayleigh vertical component waveform that allows to detect the wave multi-mode structure. The Z-AOGF trace and the orthogonal 3C AOGF trace demonstrates a very good coincidence of the Rayleigh wave oscillations that convince us that the noise impact is practically eliminated. Nevertheless, the 3C AOGF orthogonal trace looks slightly more noisy that is explained by the low frequency noise leakage into this trace from the original array horizontal seismograms (where this noise is always more powerful than in the vertical seismograms). Association of the Z-AOGF trace with the longitudinal 3C AOGF trace provides the possibilities for comprehensive analysis of event Rayleigh wave characteristics. It is noticeable that the amplitude of vertical Rayleigh component is almost in 5 times less than the amplitude of longitudinal component. This Rayleigh wave feature is obviously connected with some peculiarities of regional medium structure which should be the object of further study.

Comparison of 3C AOGF transverse components in Fig.24 and Fig.25 confirmed the conclusion about the multi-mode structure of event Love wave. Some distinctions in local amplitudes at the traces we prone to explain by the distortions due to preliminary low band filtering of array seismograms. We would prefer to recommend for the further comprehensive analysis the Love waveform after 3C AOGF broad band processing shown at the last trace in Fig.24: this trace has almost the same signal-to-noise ratio, preserves the high frequency signal components and are free from distortions connected with low band filtering.

4.6. Analysis of Geyocha 3C seismograms from Oman gulf earthquake on 18.10.93

4.6.1. Onset time estimation of the event wave phases.

The seismograms of the earthquake recorded by the central Geyocha sensor are depicted in Fig.26. The several explicit wave phases are seen in the event wavetrain: P-phase manifesting at the all components, a share wave phase manifesting at the horizontal components in the form of SH oscillations and practically not visible at the vertical component and also very strong oscillations of the surface waves: the Love wave - at the horizontal components (starting from 300 sec), and Rayleigh wave - at the vertical component (starting from 450-500 sec).

Due to known coordinates of the earthquake source and Geyocha array location it is possible to calculate the onset times for various regional and teleseismic phases by employing regional and global travel time tables. For the first one we employed the NORSAR regional travel time table: this was the single regional table being available in the course of our study. The teleseismic travel time table used was originated from Jeffreys-Bullen Earth model. We realize that the NORSAR regional travel time table does not correspond to the medium structure in the Geyocha array region and this inevitably leads to deviations of calculated and observed onset times for regional phases of the event. The calculated onset times are presented in Table 5.

The estimation of phase onset times was accomplished with the help of Maximum Likelihood (ML) algorithm which design and performance quality are described in [8,3,4]. This procedure is installed as the interactive tool in the SNDA System that provides great facilities for interactive seismogram phase picking. Fig.27 illustrates the procedure of interactive onset time estimation for teleseismic and regional phases of the event using E-component recording of body waves in frequency band (0.01-10)Hz. The upper trace is the original E-seismogram, second trace is the result of this seismogram adaptive whitening, third trace is the onset time ML function calculated for the total wavetrain interval: this is the first, exploratory onset determination which can give information about a number of strongest phases and approximate moments of their onsets. The next four traces are the ML functions calculated in the local intervals around the phase onsets.

The same procedures were accomplished with the another two component seismograms. The results of the onset time measuring are collected in Table 6.

Table 5

Theoretical onset times

Teleseismic phases		Regional phases	
Phase type	Onset time: h:min:sec	Phase type	Onset time: h:min:sec
P	14:01:06.39	Pn	14:01:02.92
S	14:04:07.60	Pg	14:02:06.78
L	14:05:51.93	Sn	14:03:50.14
R	14:07:29.09	Sg	14:06:12.87
		Lg	14:05:52.18
		Rg	14:07:28.32

Table 6

Measured onset times

Seismometer component	Phase type:			
	Pn	Pg	Sn	S
E-component	14:01:07.05	14:01:55.32	14:03:28.77	14:04:07.16
N-component	14:01:03.75	14:02:00.47	14:03:25.78	14:04:28.09
Z-component	14:01:03.30	14:02:00.07	14:03:27.67	

The analysis of tables above allows to make the following conclusions:

The Pn phase onsets estimated using Z and N components have the delays 0.4-0.8 sec relatively to theoretically predicted value. The additional 3.5 sec relative delay of the Pn-onset at the E-component may be explained by impact of the teleseismic P-phase: this phase theoretical onset is close to the estimate got for the E-component (see Tables 5,6).

The Pg phase is almost not visible at the seismograms, nevertheless it is reliably detected by ML onset algorithm at all components with excellent coincidence of the onsets at N and Z components. Pg arrival precedes the theoretical time for 6.5 sec, that we explain by disagreement of the NORSAR medium model with the real medium characteristics.

The Sn phase is also poorly seen in the seismograms but undoubtedly revealed by ML algorithm at all components with good coincidence of the onsets at E and Z components. This testifies that the Sn phase is composed by as SH as SV oscillations. It also arrives earlier then the NORSAR travel time prediction, and time shift here is already equal about 23 sec.

The teleseismic S-wave onset time estimated using the E-seismogram demonstrates a very good accordance with the value provided by the Jeffreys-Bullen Earth model: the divergence here is only in 0.4 sec. The great error of onset estimate made using the N-component is explained by the impact of low-frequency noise pulse in the vicinity of S-phase onset: this pulse is clearly seen at the N-component seismogram depicted in Fig.28.

In connection with the described results of application of the ML algorithm for onset time estimation of weak regional phases the following recommendations can be stated:

1) This would be helpful to install in the SNDA system the 3-component version of ML onset estimation algorithm which designed and tested by the authors of the paper [8]. The algorithm accounts the changes as in power spectrums of the seismogram components as in the polarization of these component oscillations at the moment of phase arrival. So it could be preferable for applications in case of 3-component array data processing.

2) While using the ML onset estimation algorithm it would be more expedient to perform the preliminary adaptive whitening procedure just at the same local time interval which is chosen for calculating the onset ML function. This promises some gain in accuracy of the ML onset estimation procedure, though leads to some time consumption when estimating the multiply phase onsets.

Fig.28 shows the event body wave 3C seismograms of the central Geyocha sensor with the margins of Pn, Pg and Sn time intervals chosen for calculating phase power spectra and for estimating their arrival direction parameters with the help of wide-band F-K analysis. The power spectra of these phases are shown in Fig.29a - 29c. As it is theoretically predicted, the Pn phase has the most high frequency content: its spectrum maximum is situated at 0.7 Hz but there

exists the second powerful spectral peak with frequency 0.4; the Pg phase has the single spectral peak at 0.55 Hz, and the Sn phase - at 0.33 Hz. The F-K analysis maps for these phases are presented in Fig.30a - 30c. The most impressive in this maps is that estimates of Pn and Sn waves azimuths are equal 184.7° and 183.8° , i.e. coincides with the accuracy less than 1° (the apparent velocities of this phases are $V_{ap}(Pn)=8.7$ and $V_{ap}(Sn)=8.0$). Note however, that these azimuth values differ from theoretical one (equal to $\alpha=164.1^\circ$) of about 20° . Such divergence can not be explained by the estimation error and obviously connected with the peculiarities of these wave propagation in the region. Note the both phases propagates along the boundary between the Earth crust and upper mantle and evidently this boundary has a laterally heterogeneous structure in the region. At the same time, the Pg-phase F-K azimuth estimate is equal to 169.1° and differ from the theoretical azimuth only in 5° (the Pg apparent velocity is $V_{ap}(Pn)=6.8$). Because the Pg phase propagates within the Earth crust the mentioned lateral heterogeneity of the crust-mantle boundary apparently does not affect strongly on this wave propagation. This matter is already discussed in the papers [6,7], where was stated, that various wave phases demonstrate the different arrival azimuths in Central Asia region. However, the authors of these papers observed this effect only for the surface waves.

4.6.2. Extraction of body wave phase waveforms using adaptive array seismogram processing.

Fig.31 shows the example of Geyocha sensor 3C seismogram in the time interval comprising the regional and teleseismic body waves. The oscillations of different regional phases are not seen explicitly enough. Below we make the attempt to make more detailed conclusions about these phase waveforms. In Fig.32 the results are presented connected with Pn waveform extraction in frequency band (0.01-2) Hz by the beamforming and AOGF procedures using only Z-component Geyocha seismograms. Trace 1 is the result of conventional beamforming procedure steered to the Pn wave direction. We see in the trace the presence of strong low frequency noise oscillations. The trace 2 is the result of AOGF procedure with the adaptation interval preceding the Pn onset. Only very low frequency noise components remain in the trace and the Pg phase with onset time 120 sec is explicitly revealed. Trace 3 is the output of AOGF with adaptation made using the total interval of event wavetrain recording (0-1000) sec and trace 4 is the same for adaptation made using the "tail" of the event wavetrain recordings succeeding the body wave interval (200-1000) sec. We see from these traces that the low frequency noise oscillations are completely suppressed and the thin structure of the Pn coda is revealed: one can notice the distinct high frequency wavelets starting after Pn phase at the moments 80 and 92 sec.

Fig.32 shows the results of analysis of Pn wave oscillations produced by the 3-component AOGF using set of 3C Geyocha seismograms. We see that longitudinal Pn oscillations have

relatively low frequency: less than 0.4 Hz, but there exists strong high frequency SV coda in time interval (70-80) sec and high frequency elliptic shear wave (SH-SV) coda oscillations in interval (80-92). Apparently these coda waves are some transformations of the Pn wave at the heterogeneity in a vicinity of Geyocha array. Thus we can assert that 1C and 3C AOGF analysis of the event Pn phase allows to reveal the thin structure of this wave and its coda waves in the broad frequency band which is not evident from original seismograms and conventional beamforming traces.

Fig.34 and Fig.35 demonstrate the extracting of Pg phase waveform using Z-component and 3-component Geyocha array seismograms correspondingly. Traces 1-4 in Fig.34 are produced with the same procedures as the analogous traces in Fig.32, the difference is only that the group filters were steered to the Pg apparent velocity instead Pn one. Trace 5 in Fig.35 is the output of the AOGF with adaptation made using Z-seismograms at the interval preceding the Pg onset (0-100 sec.). Traces 1-4 in Fig.34 are very similar to traces 1-4 in Fig.32 that is explained by the small difference in the arrival directions of Pn and Pg phases which is not discerned by the small aperture Geyocha array. Trace 5 in Fig.5 provides the most clear impression about the Pg phase waveform in comparison with the another traces. From Fig.35 one can get the impression about sophisticated polarization of the Pg wave oscillations which include the intensive motions not only in the longitudinal, but in the orthogonal and even transverse directions. This is consequence of the intensive Pg wave scattering along the path in heterogeneous Earth crust in the region.

Fig.36 and Fig.37 presents the results of extraction of Sn and teleseismic S phase waveforms using ZC and 3C Geyocha array seismograms, correspondingly. Traces 1-5 in Fig.36 are produced by the same procedures as the analogous traces in Fig.34. The difference is only that the group filters were steered to the S-wave arrival direction and AOGF adaptation in trace 5 was made using time interval (0-180) sec, which precedes the Sn-phase onset. At all traces there are no evidence of the S-phase oscillations. It is explained by the low power of Sn-phase and the close to transverse polarization of teleseismic S-phase. Some hint on the appearance of Sn-phase can be get from trace 5 where the time series oscillations become evidently low frequent after the Sn-phase onset moment. This can be explained by the scattering of the relatively low frequent SH-polarized Sn-phase on the medium heterogeneity. The very different image presents the 3C AOGF output traces depicted in Fig.37. Though the regional Sn phase became apparent in transverse and orthogonal components only due to slight decreasing the dominant frequency of oscillations, the teleseismic S-phase oscillations are explicitly manifested in transverse and orthogonal components. In comparison for example, with the initial

seismograms of the central Geyocha sensor these oscillations are evidently cleared from low frequency noise components.

4.6.3. Study of event surface wave characteristics.

Fig.38 shows the 3-component seismogram of central Geyocha sensor rotated in direction of theoretical surface wave arrival. The very powerful Love and Rayleigh surface wave oscillations allow to investigate their polarization and spectral-velocity features. The results of nonlinear Flinn polarization filtering applied to the 3C seismograms of the central Geyocha sensor are presented in Fig.39. At least three distinct oscillation modes are seen for the Rayleigh waves (at the longitudinal and orthogonal components) and two modes - for the Love wave. The evidence of these mode existence can be observed in the "raw" traces of Fig.38, but the nonlinear Flinn polarization filtering exhibits in this example its undoubted helpfulness.

Fig.40 demonstrates the results of the Love wave spectral analysis in the time and spatial domains. In Fig.40.a the power spectral density is depicted for the Love wave oscillations being observed at Fig.38 trace 2 during (300-600) sec time interval. As it follows from Fig.39, this is the spectrum of main Love wave mode. The spectrum peak is focused in frequency band (0.025-0.09) with maximum at 0.05 Hz. The detailed spectral analysis revealed that the signal frequency content smoothly changes from 0.025Hz for the beginning of Love wave at 300 sec to 0.09Hz for the end of its main mode at 600 sec. Thus this Love wave mode has the strong dispersion: its frequency changes almost in 4 time.

The Fig.40.b shows the wide-band F-K analysis map for frequency band (0.03-0.08) Hz. It revealed the arrival azimuth and apparent velocity of the Love wave equal to $\alpha=157.6^\circ$ and $V_{ap} = 3$ km/sec. The azimuth of the Love wave arrival is less than theoretical one (164.1°) for 6.5° , and demonstrates the very high consistency in different frequency bands. This follows from the results of multiple narrow band F-K analysis presented in Fig.40.c and Fig.40.d. The F-K analysis was performed for 6 equidistant frequency bands with width equal 0.1 Hz in the range (0.03-0.08). From Fig.40.c one can see that the Love wave arrival azimuth does not practically change depending on the wave period. This contradicts with the results of paper [7] where such dependence were mentioned, however, for the other arrival direction of surface waves.

Fig.40.d presents the Love main mode dispersion curve i.e. dependence of apparent velocity upon the wave period. This curve was gained in the result of multiple narrow band F-K analysis mentioned above. The dispersion curve good corresponds to the theoretical one following from the Gutenberg Earth model. In Fig.41 the results are presented obtained after 3C AOGF filtering of Love wave phase using 3C Geyocha array seismograms. Adaptation of the 3C AOGF was made using array data at time interval (0-300) sec., preceding the Love wave

onset. The traces in Fig.41 allow to calculate the trajectory of Love wave particle motions in the ray transverse-longitudinal directions corresponding to time interval (350-600) sec. and frequency band (0.01-2)Hz. This trajectory is depicted in Fig.42.a and one can see that in the time interval of main Love mode waveform the Rayleigh wave interfering longitudinal component has the amplitudes in three times less than Love wave transverse oscillations.

The power spectral density of Rayleigh wave longitudinal oscillations is shown in Fig.42.b. the spectrum was calculated using trace 1 of Fig.38 in time interval (400-650) sec. We see from this figure that the Rayleigh wave spectrum has the rather narrow peak concentrated in frequency band (0.05-0.1)Hz. with maximum at 0.08 Hz. The results of wide-band F-K analysis for time interval (400-550) sec in frequency band (0.05-0.1)Hz are shown in Fig.42.c. The Rayleigh wave arrival azimuth estimate is equal 168.8° , that exceeds the theoretical value (164.1°) at 4.7° and the arrival azimuth estimate for the Love wave at 11.2° . (Note that the theoretical azimuth is almost in the middle between the above surface waves azimuths). Such great difference between the Love and Rayleigh azimuth estimates can not be explained by the errors of the F-K analysis accounting for the very high signal-to noise ratio in the both phases. Here we again have to refer to complexity of the Earth crust and upper mantle in the region under study and propose to implement thorough investigation of the wave propagation peculiarities in this region, which attract the assiduous attention in regard of CTBT monitoring.

For the Rayleigh phase we can not produce the stable estimation of dispersion curve (the apparent velocity in depending on the period) with the help of multiple narrow band F-K analysis. It possibly is connected with the interference of the Rayleigh wave main and upper modes which is strong due to rather low epicenter distance of the event. We plan to implement for this purpose the sonogram (time-frequency) analysis.

The 3C AOGF filtering of the 3-component Geyocha array seismograms with the purpose to extract the Rayleigh wave oscillations at longitudinal and transverse directions produced the traces similar to ones depicted in Fig.41. For this reason we do not provide the additional figure with this traces. We used the extracted Rayleigh wave traces to calculate the trajectory of Rayleigh wave particle motions in the longitudinal and orthogonal (vertical) directions to the ray. This trajectory is drawn in Fig.42.d. One can see that the trajectory has the elongated elliptic form with the ratio of ellipse axes equal to 4.3 and with the main axis having the angle about 30° with the longitudinal direction. This information can be used for characterization of the medium structure in the region.

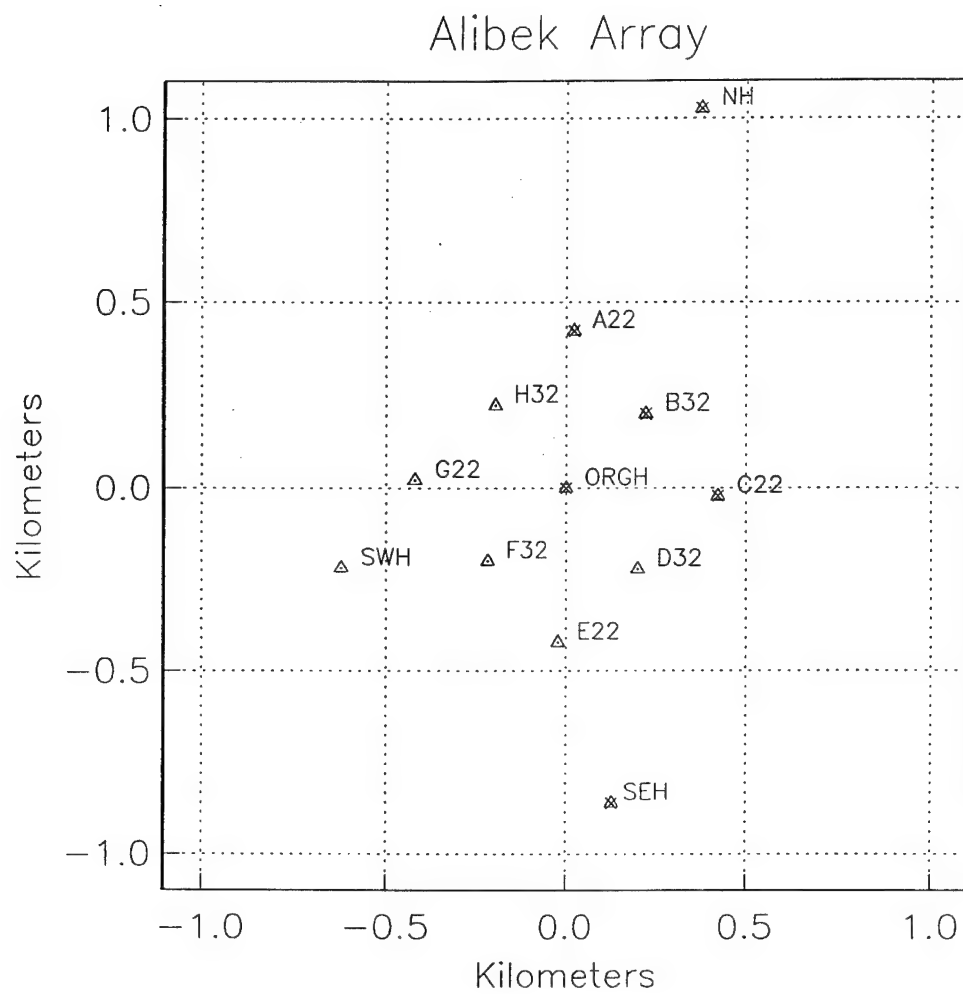
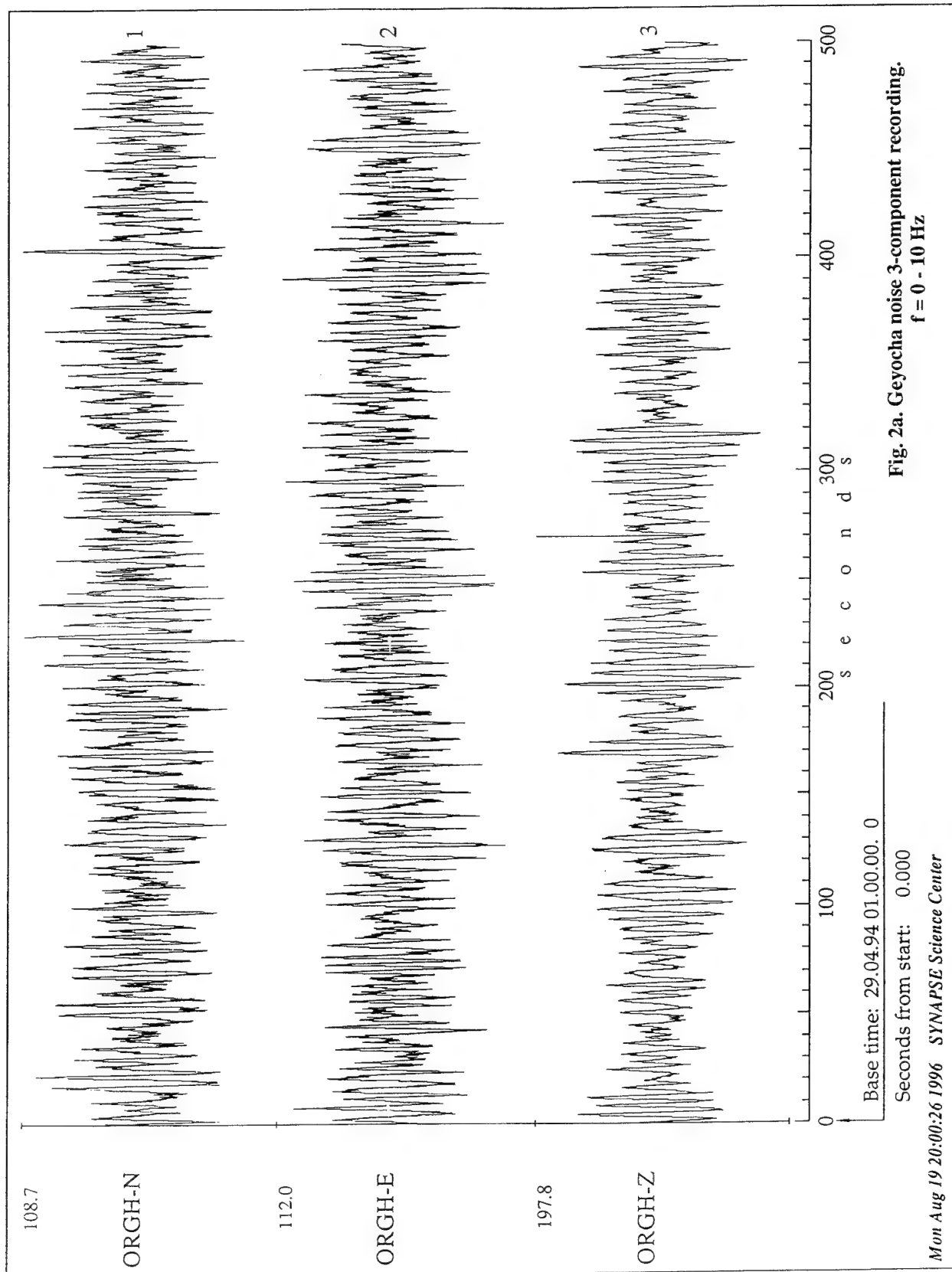


Fig. 1. Geyocha seismic array configuration.
Stations used in analysis of the explosion on 10.06.91
are marked by crosses.



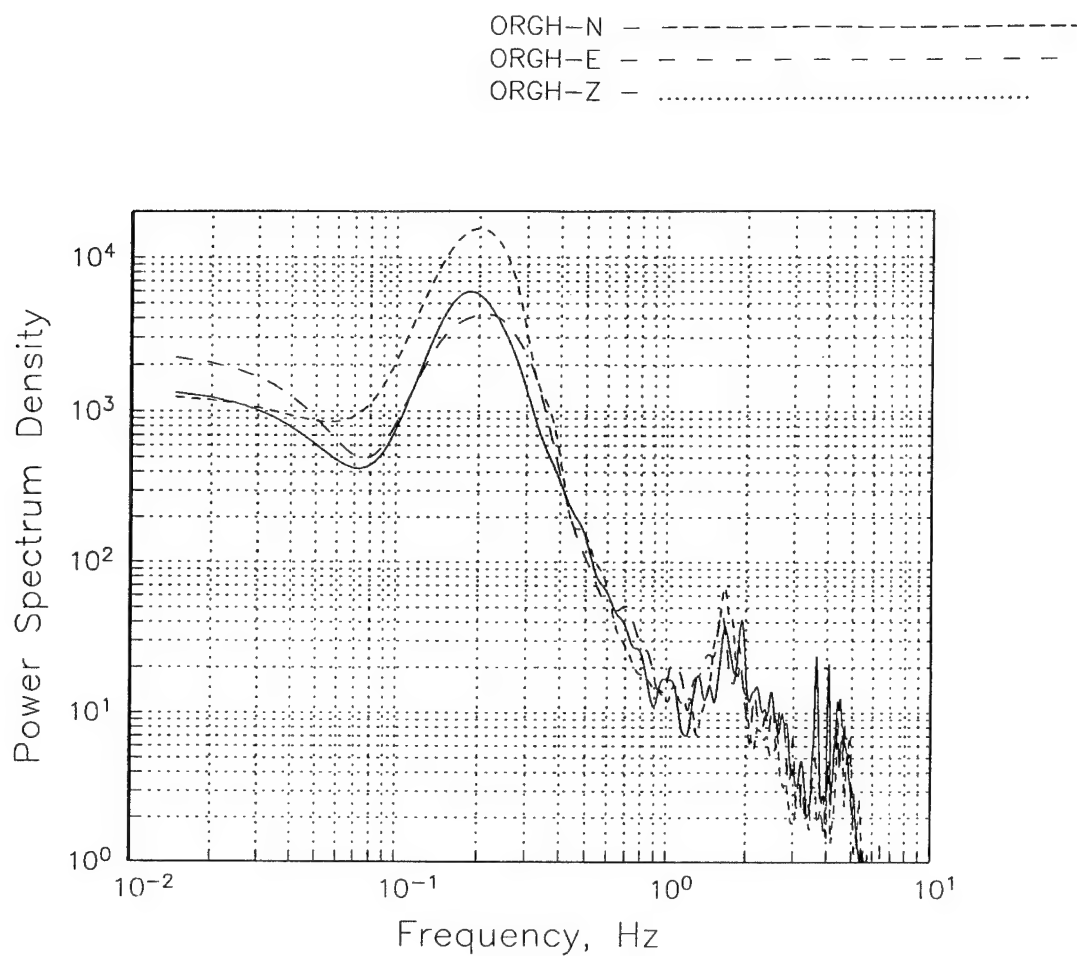


Fig. 2b. Power spectra of noise records on 29.04.94 01:00:00
T = 0 - 200 sec
f = 0.01 - 10 Hz

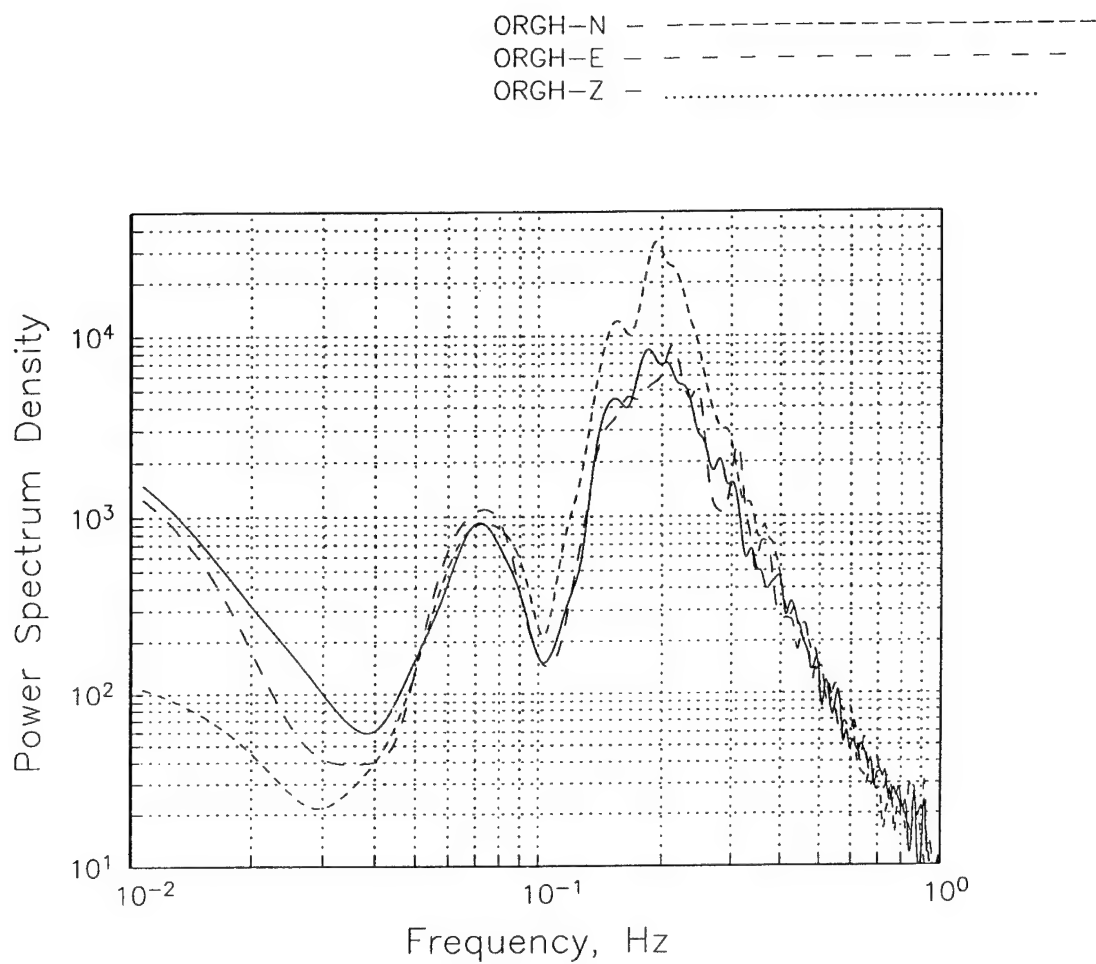


Fig. 2c. Power spectra of noise records on 29.04.94 01:00:00
T = 0 - 1000 sec
f = 0.01 - 1 Hz

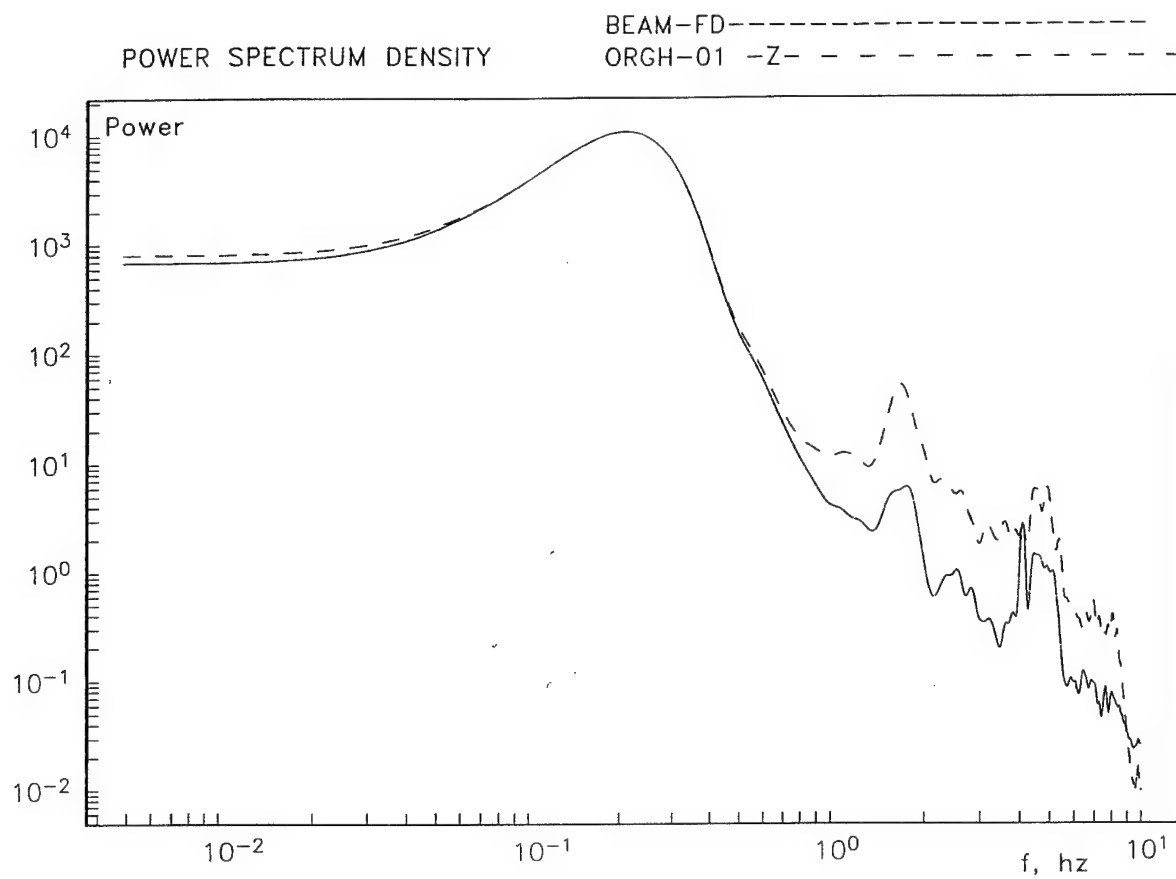


Fig. 2d. Power spectra of noise recorded by Z-component of ORGH (solid curve) and of a beam composed from noise records (dashed curve).

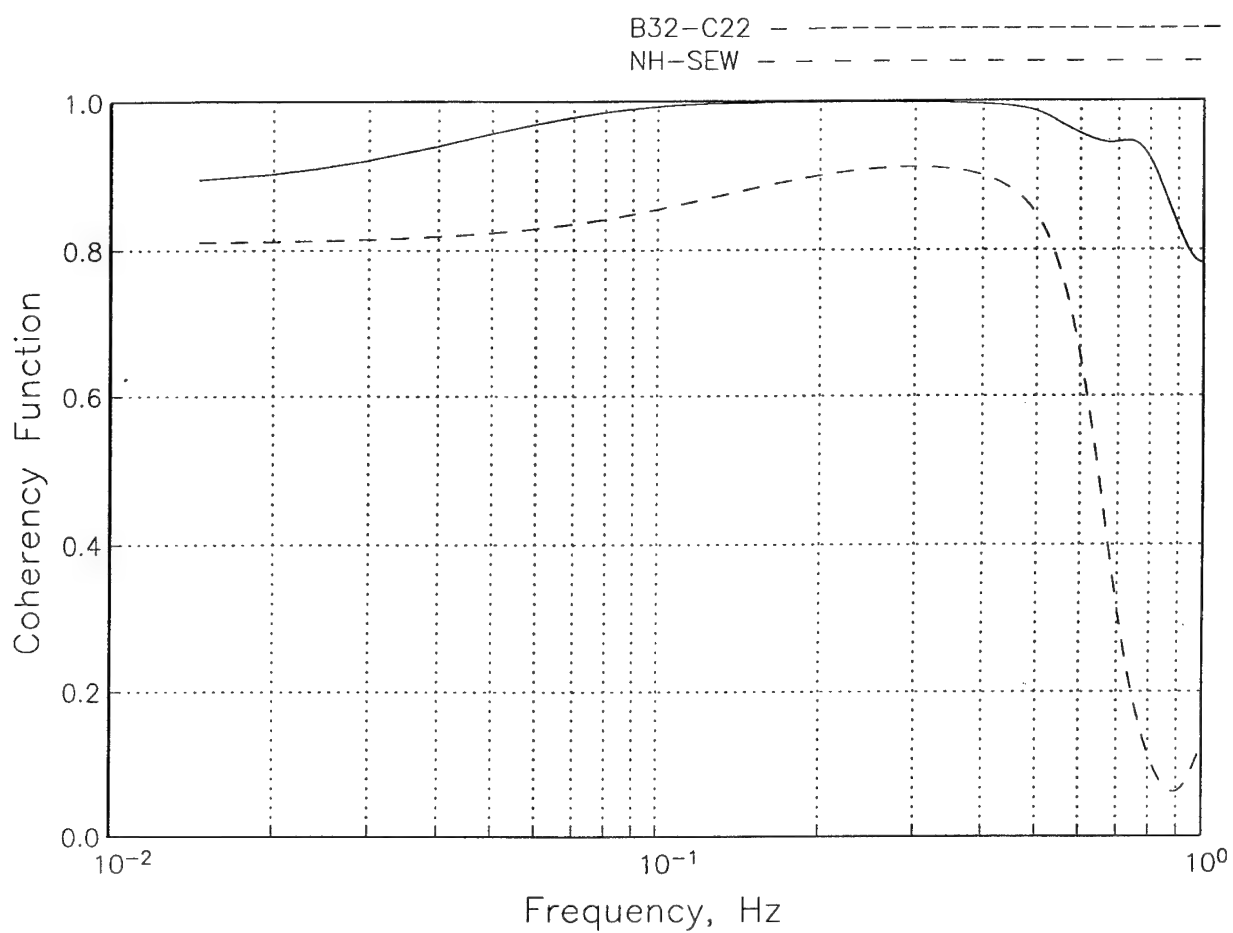
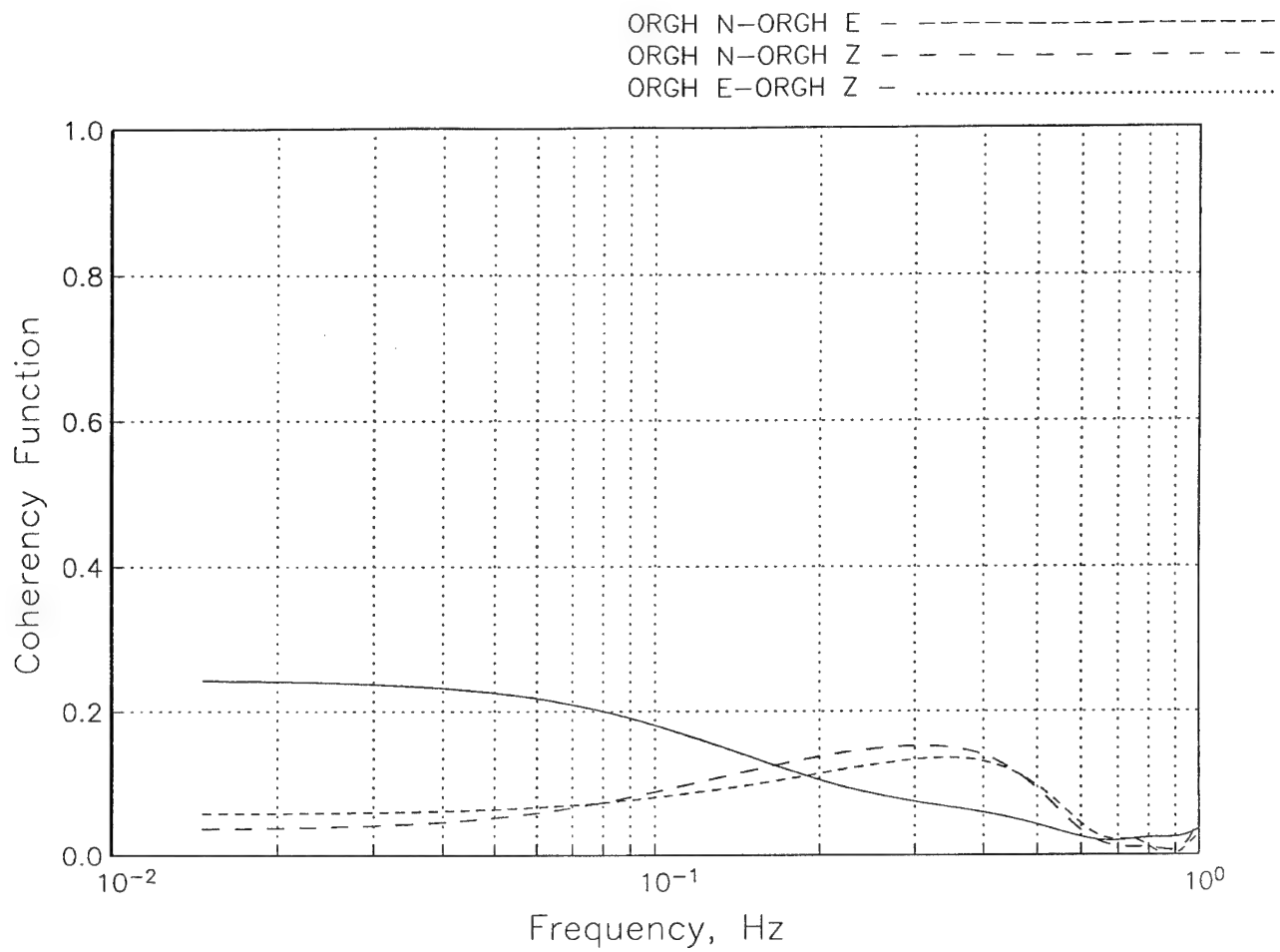
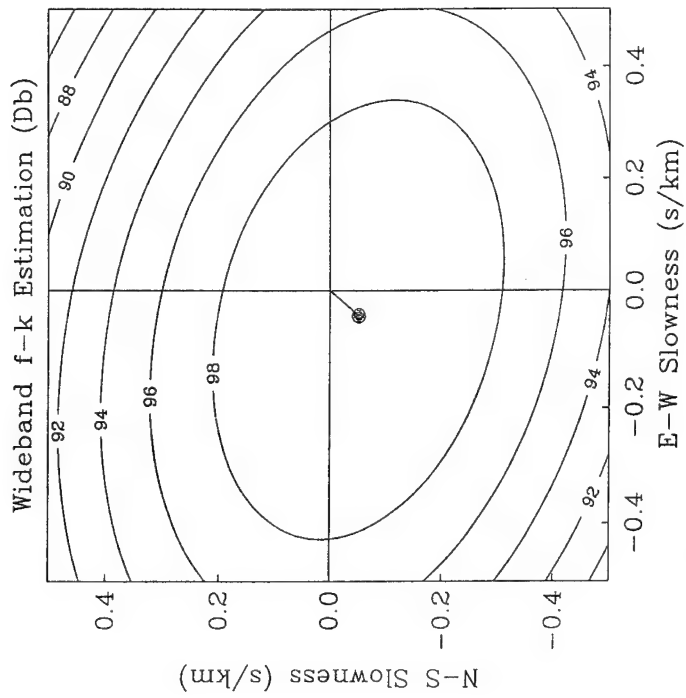


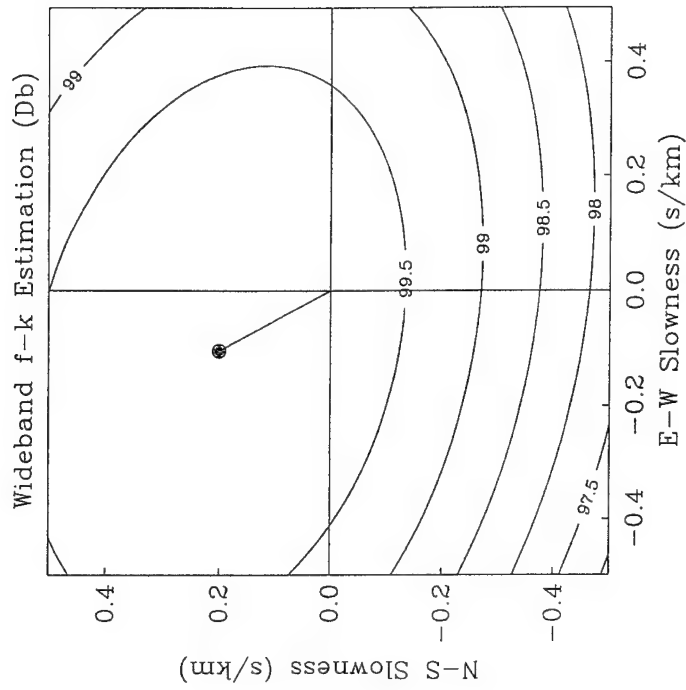
Fig. 3a. Coherence between Z-components of the nearest (B32 and C22) (solid curve) and the most remote (NH and SEH) (dashed curve) Geyocha stations. Noise records on 29.04.94 01:00:00



**Fig. 3b. Coherency between different components
of 3C-seismometer ORGH.
Noise records on 29.04.94 01:00:00**



a



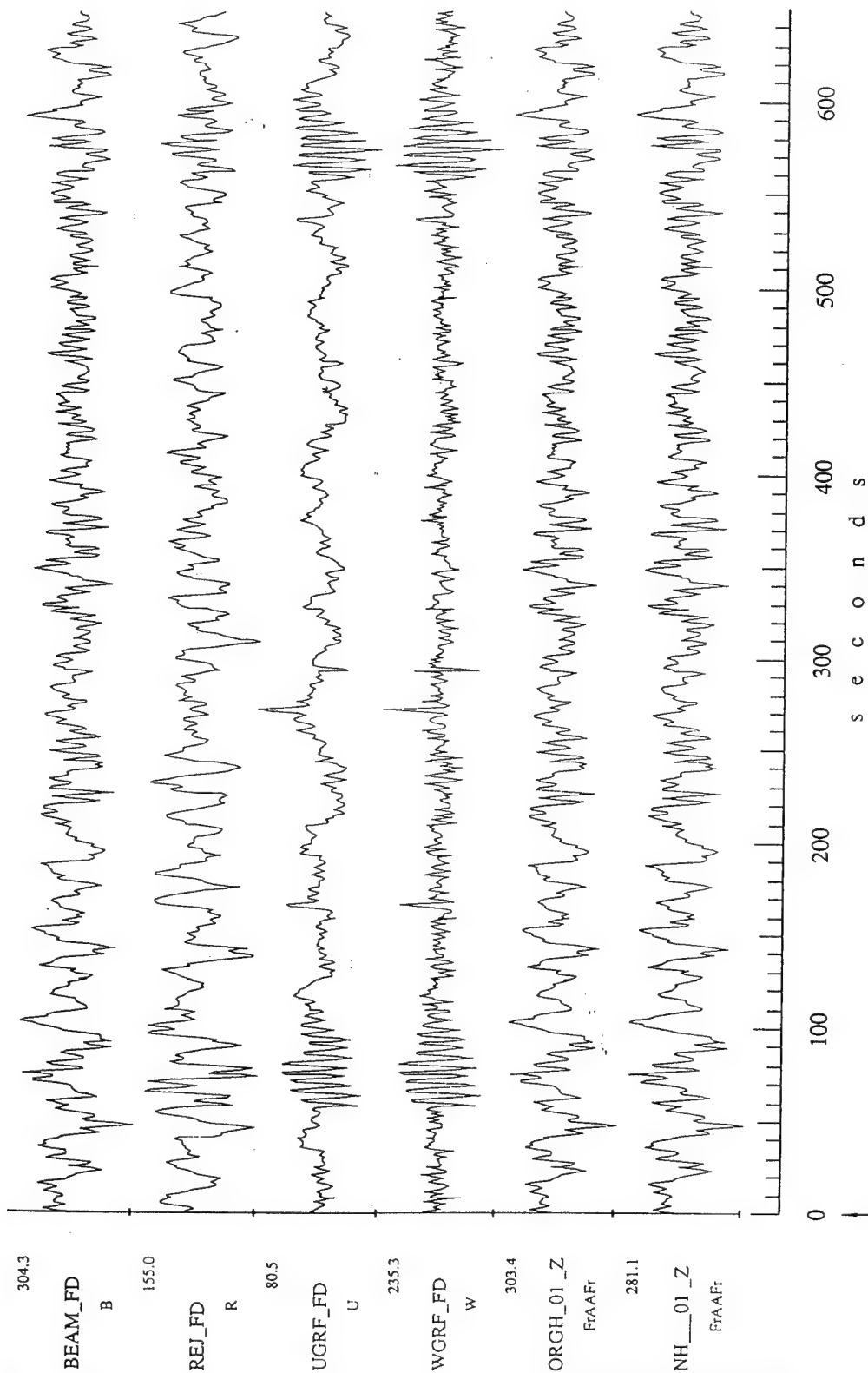
b

Fig. 4. Estimation of microseism wave arrival parameters.

Noise records on 29.04.94 01:00:00

a. $f = 0.2$ Hz

b. $f = 0.07$ Hz



Base time: 29.04.94 13:28:19.589

Fig. 5. Extraction of simulated Rayleigh waveforms from real Geyocha noise using Z-component array recordings. SNR=0.1

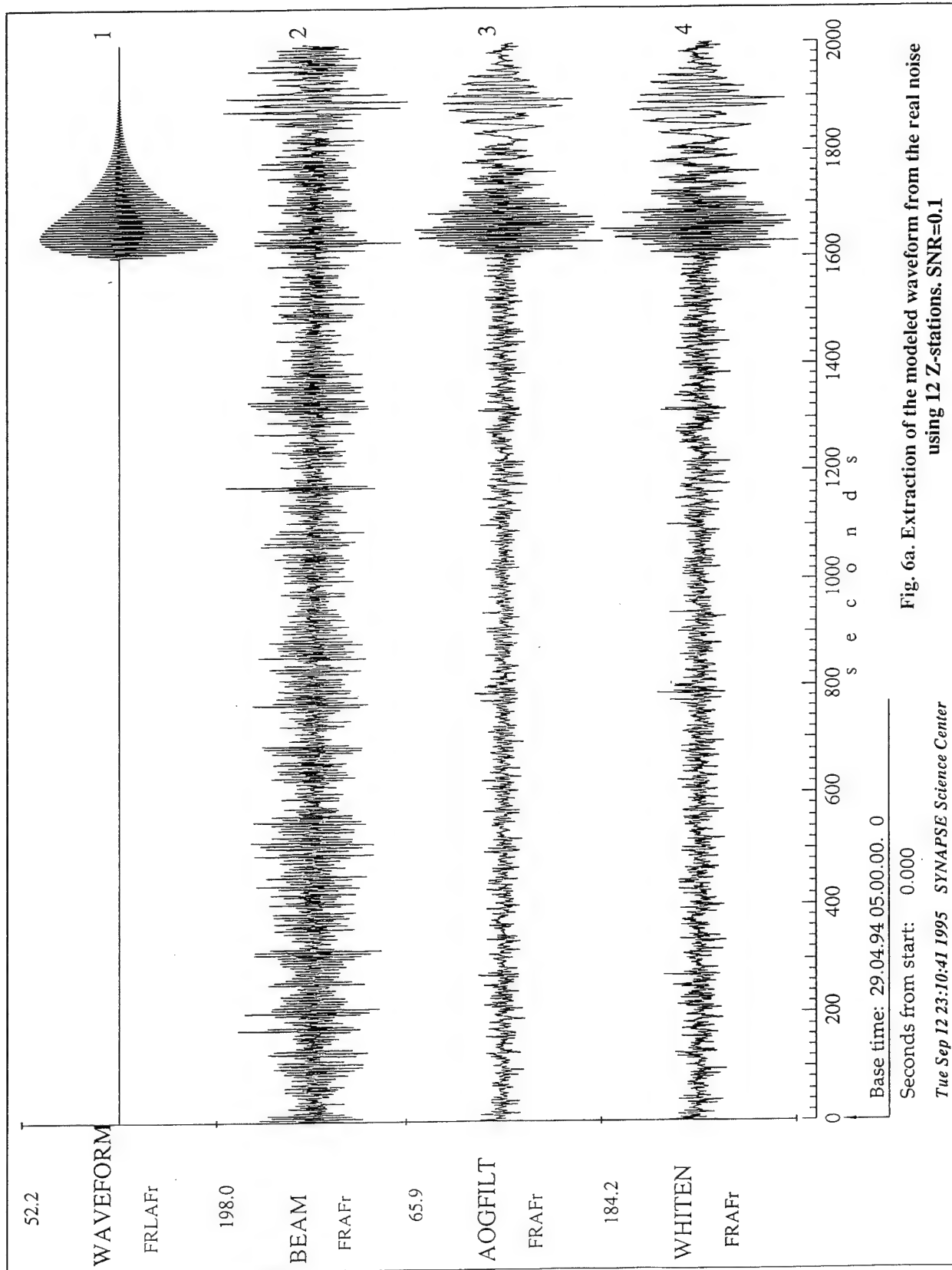


Fig. 6a. Extraction of the modeled waveform from the real noise using 12 Z-stations. SNR=0.1

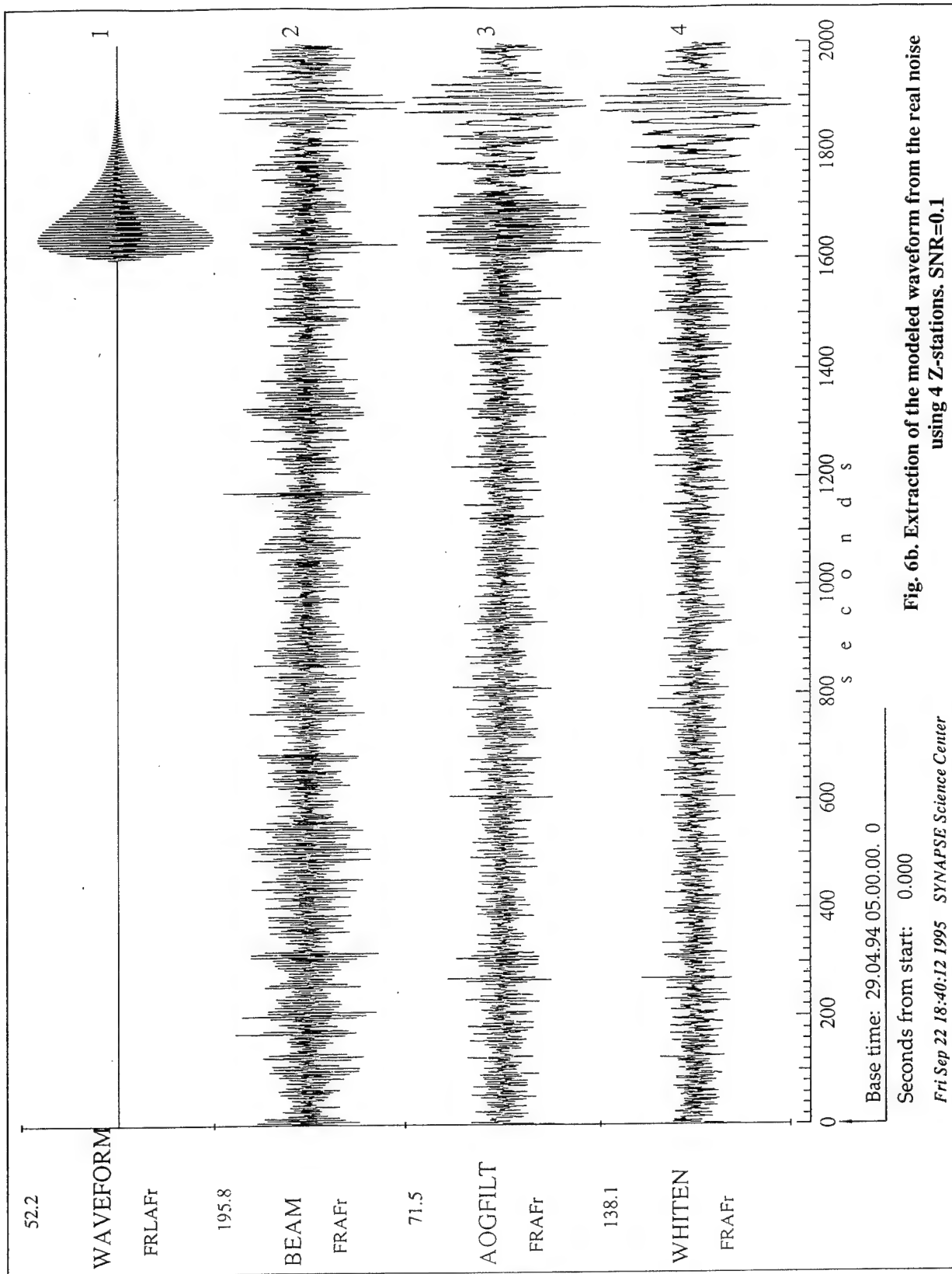


Fig. 6b. Extraction of the modeled waveform from the real noise using 4 Z-stations. SNR=0.1

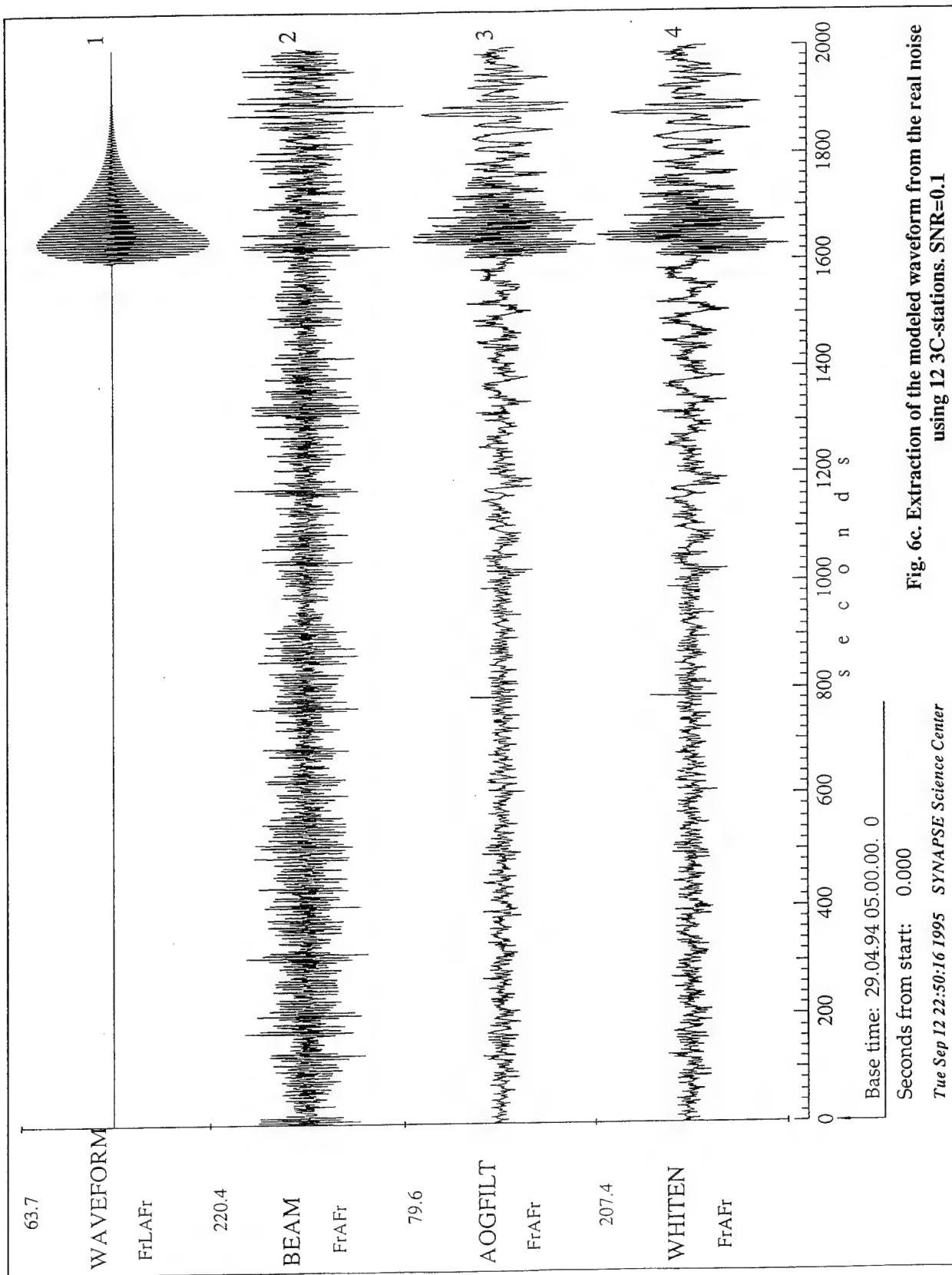


Fig. 6c. Extraction of the modeled waveform from the real noise
using 12 3C-stations. SNR=0.1

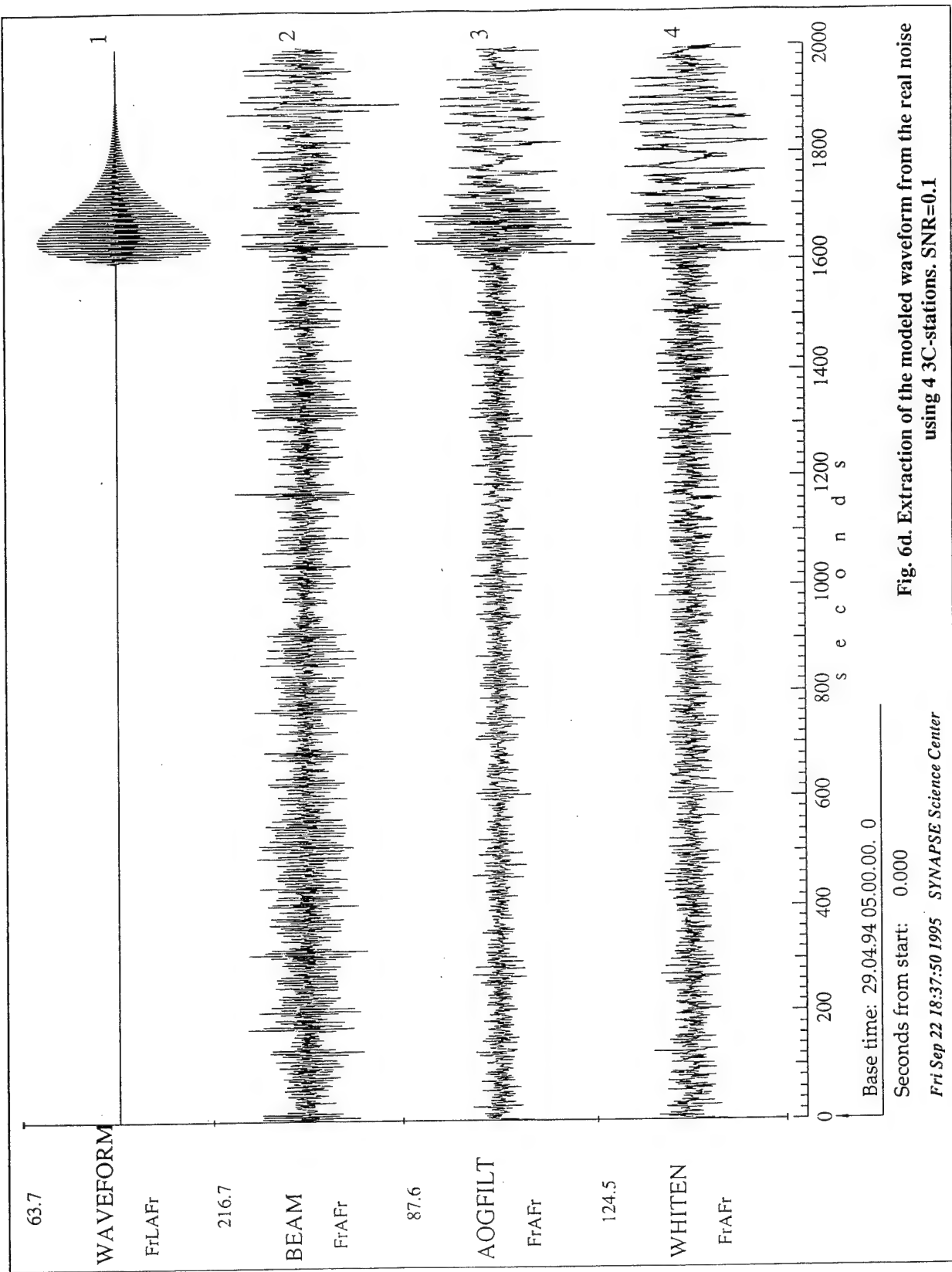
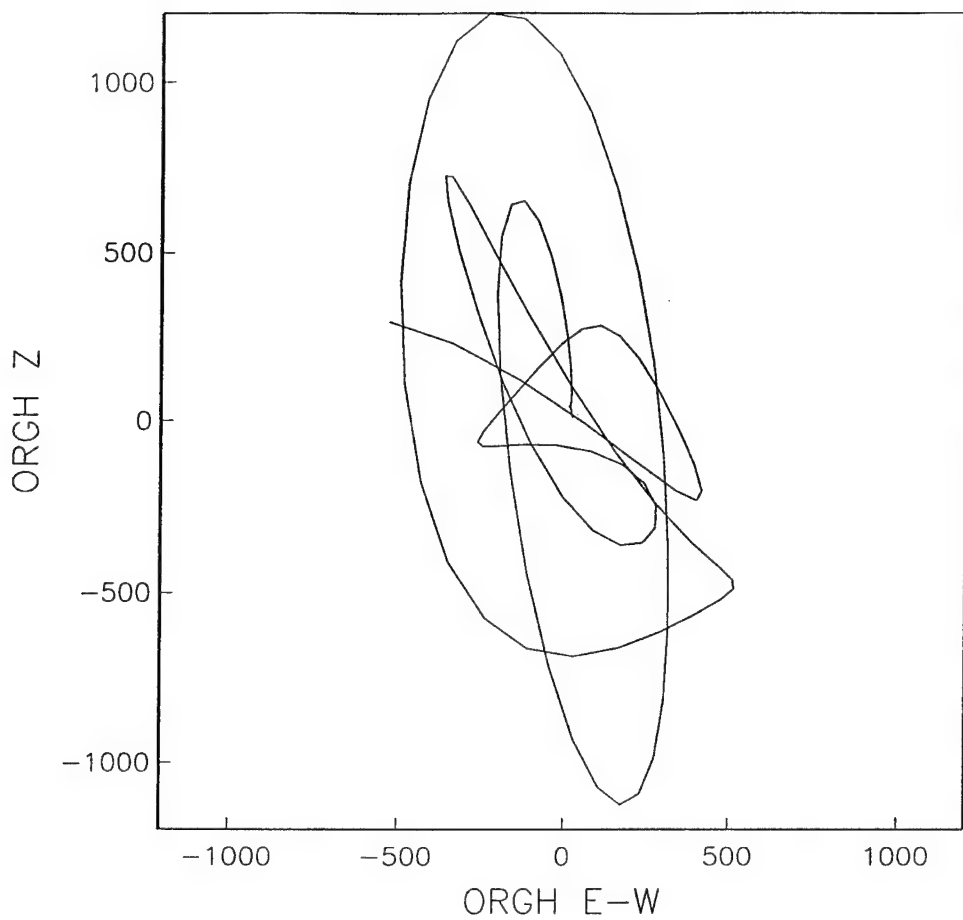
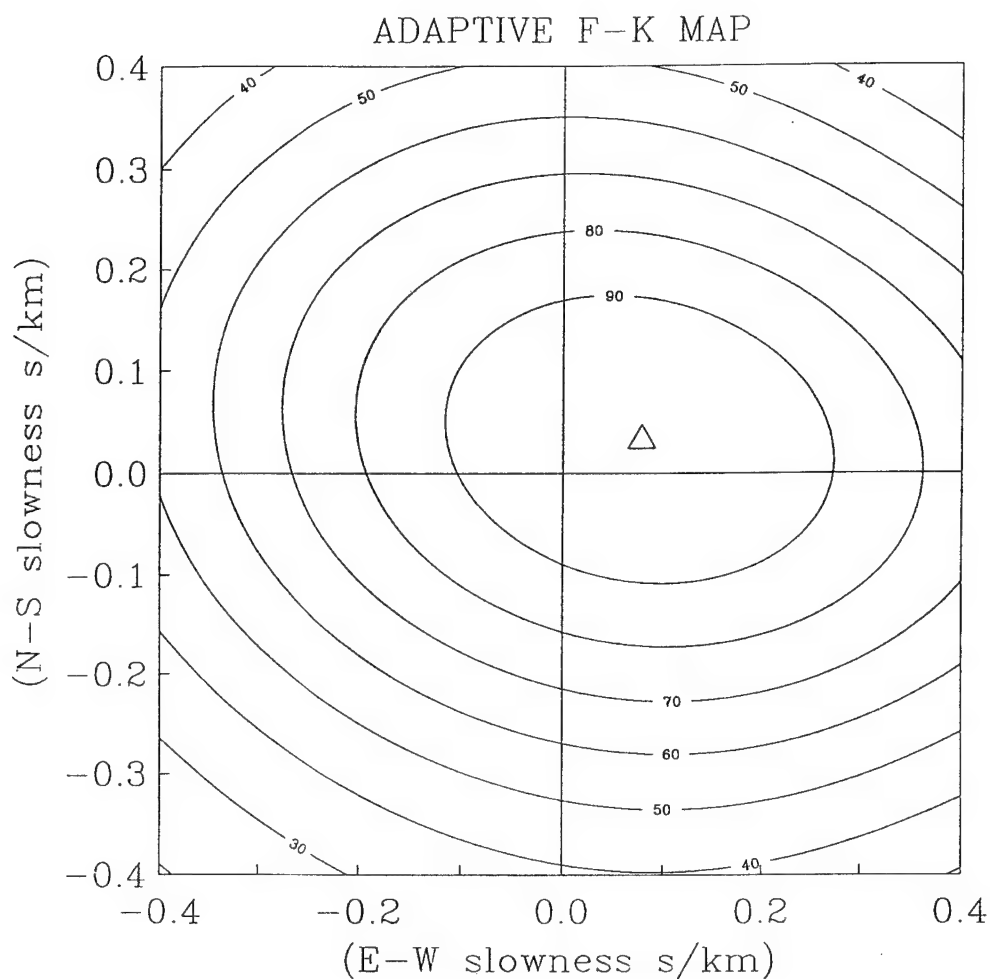


Fig. 6d. Extraction of the modeled waveform from the real noise using 4 3C-stations. SNR=0.1



**Fig. 7. Particles motion for first 5 seconds
of explosion P-wave on 3C ORGH station on 10.06.94.
 $f = 0.01 - 2$ Hz**



Frequency = 0.800 Hz, Azim. of max =
 67.59 Ap. vel. of max = 11.90 Power
 max = 100.00 Adapt. AR order IP = 0
 Adapt. MA order IQ = 0
 Regulariz. = .0000000 Adapt. mode = 0

**Fig. 8. Estimation of P-wave arrival parameters
 for explosion on 07.10.94.
 $f = 0.8 - 1.2$ Hz**

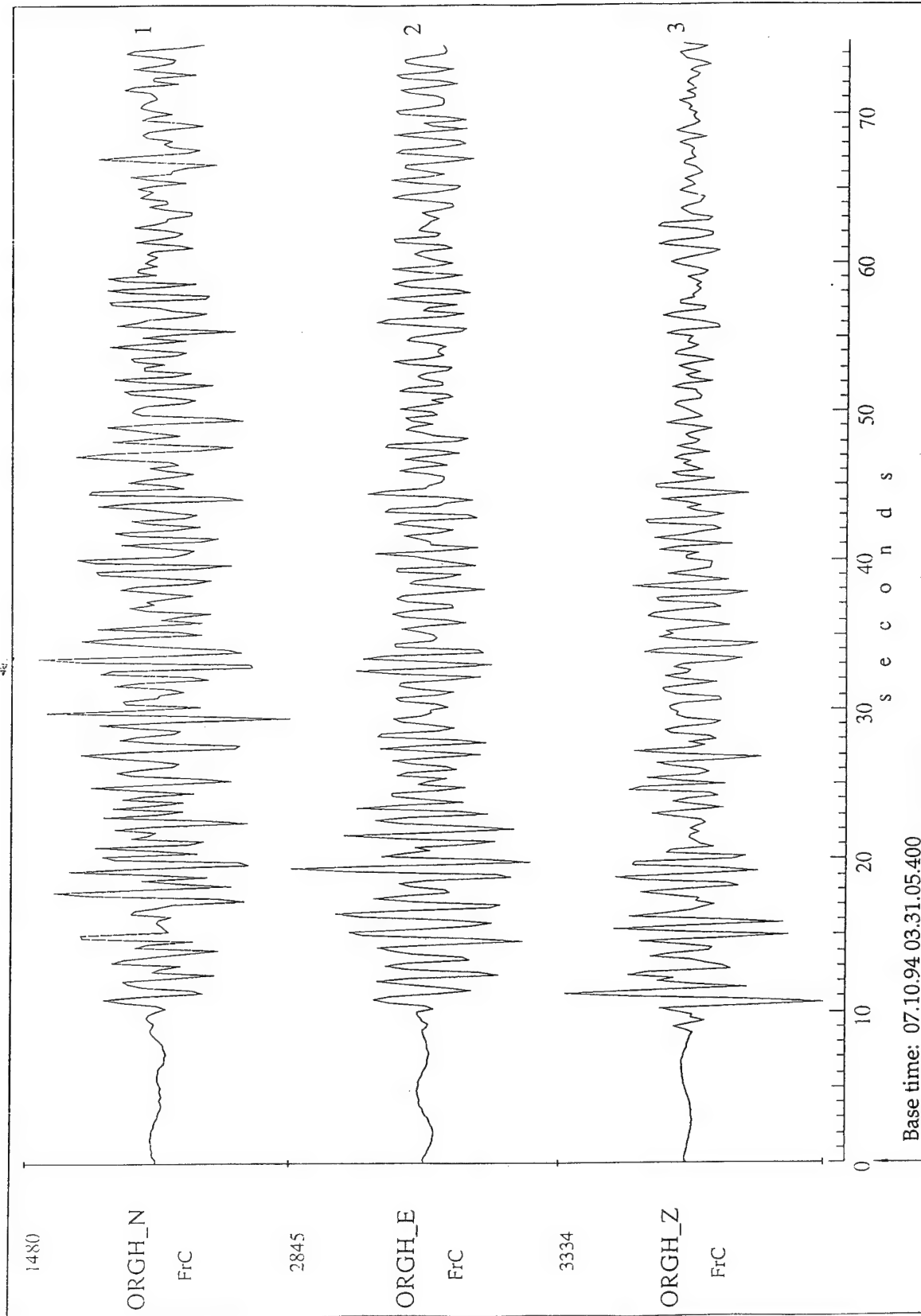
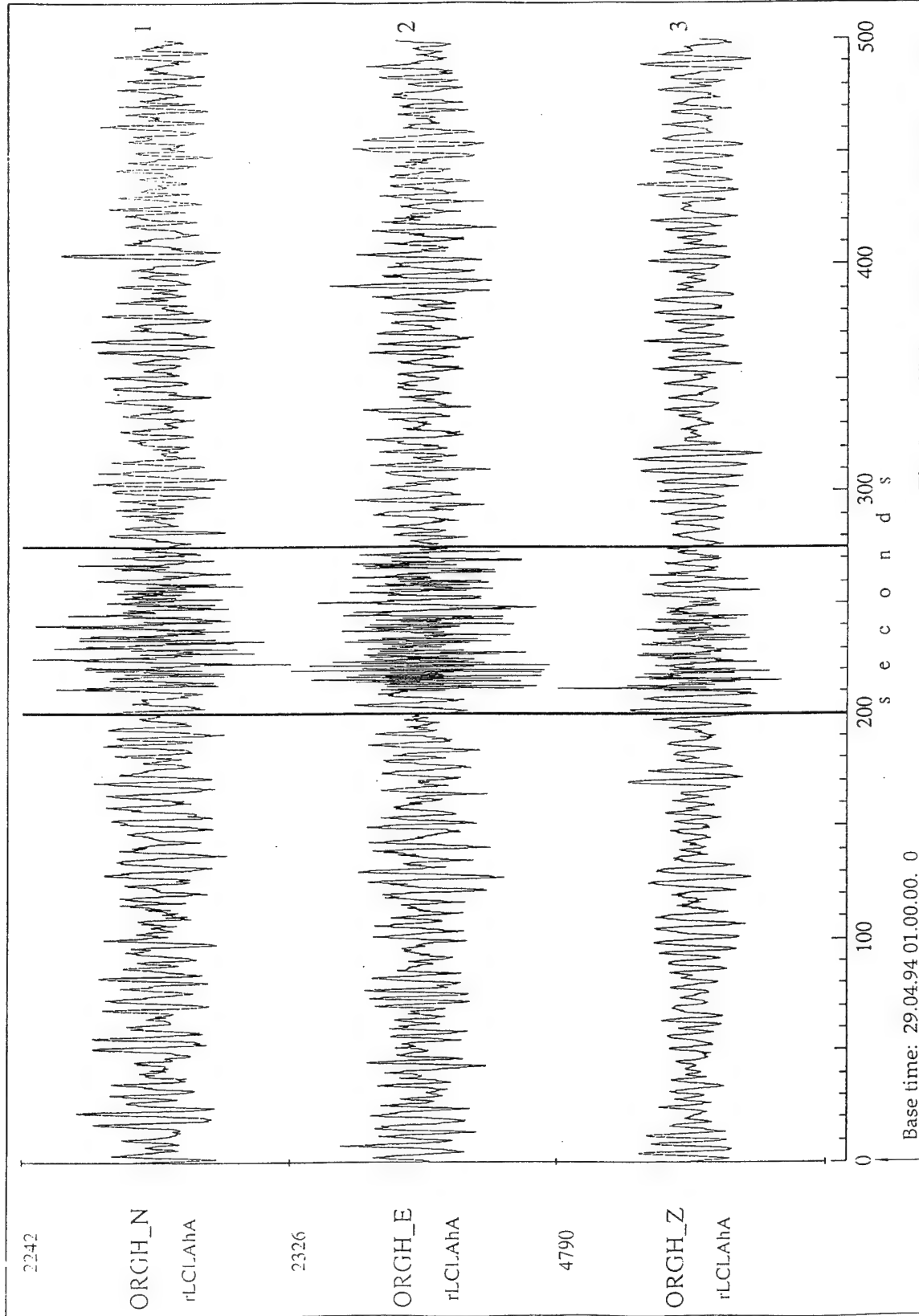


Fig. 9a. P-waveform for the Lop Nor explosion on 07.10.94.
 $f = 0.01 - 2.5 \text{ Hz}$



Base time: 29.04.94 01.00.00. 0

Seconds from start: 0.000

Tue Jul 9 00:47:44 1996 SYNAPSE Science Center

Fig. 9b. Artificial mixture of the explosion P-wave and real noise 3-component records.
 $f = 0.01 - 2.5 \text{ Hz}$, $\text{SNR} = 1$

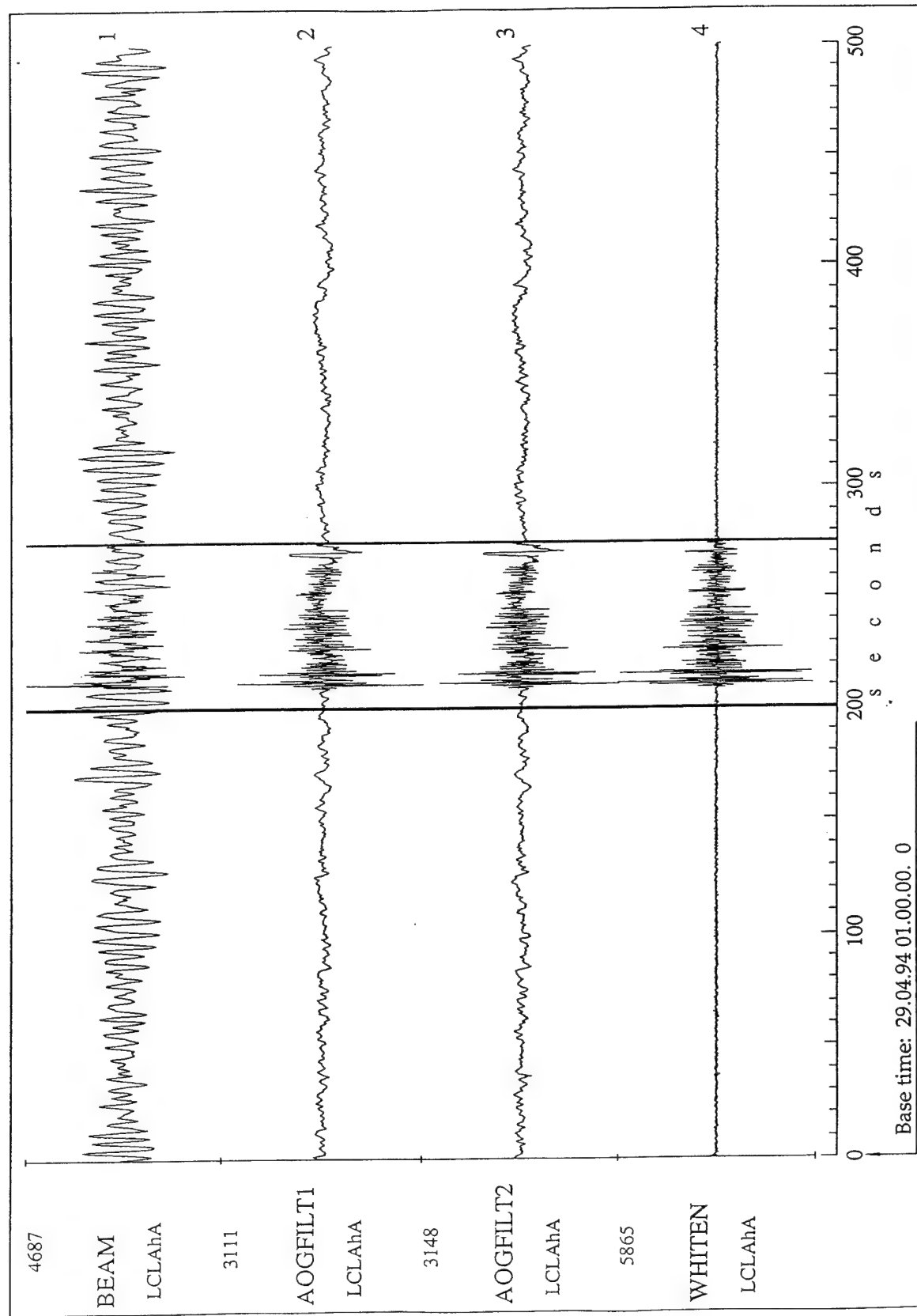


Fig. 10a. Extraction of P-phase waveform using 12 Z-stations.
 $f = 0.01 - 2.5 \text{ Hz}$

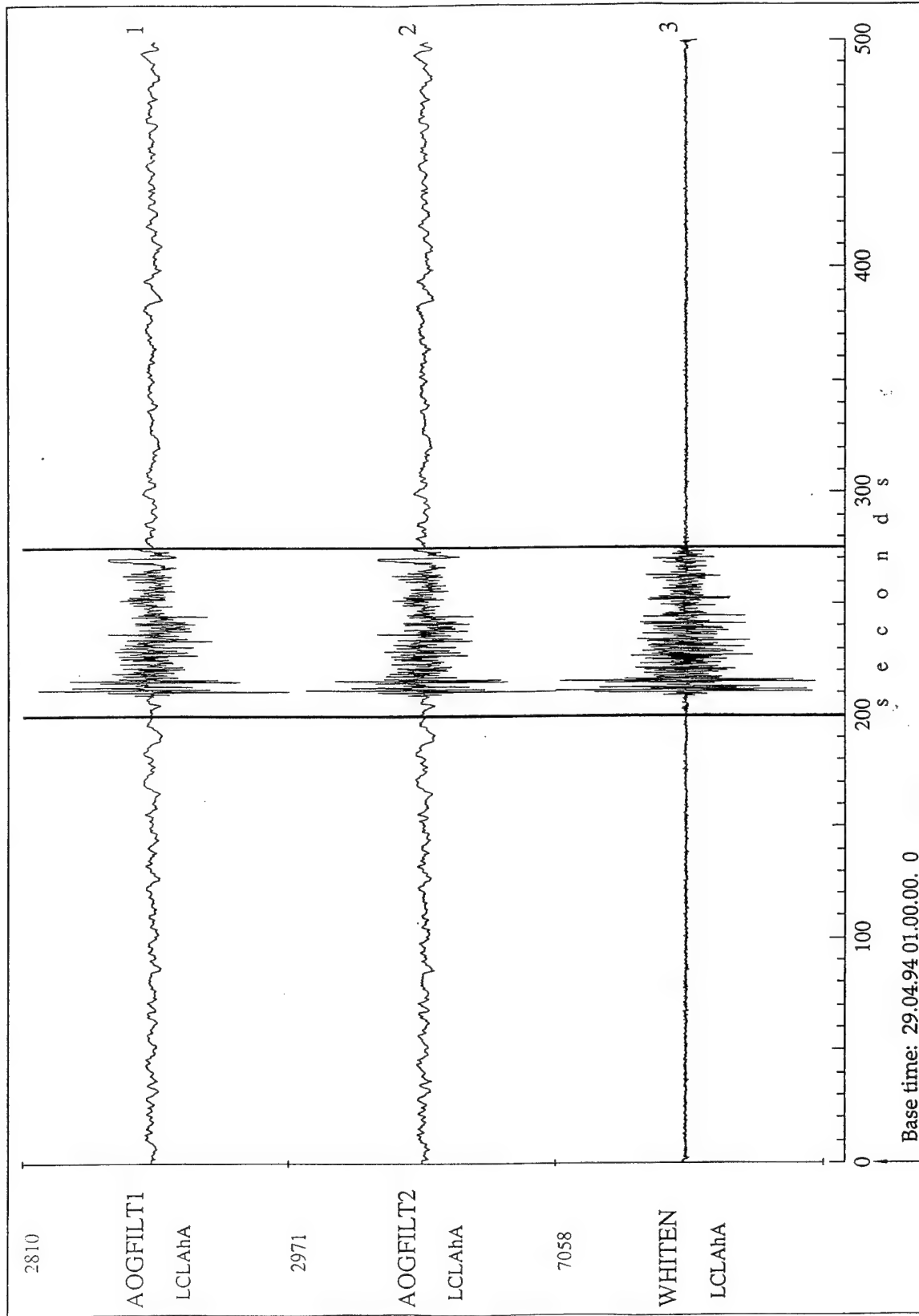


Fig. 10b. Extraction of P-phase waveform using 12 3C-stations.
 $f = 0.01 - 2.5 \text{ Hz}$

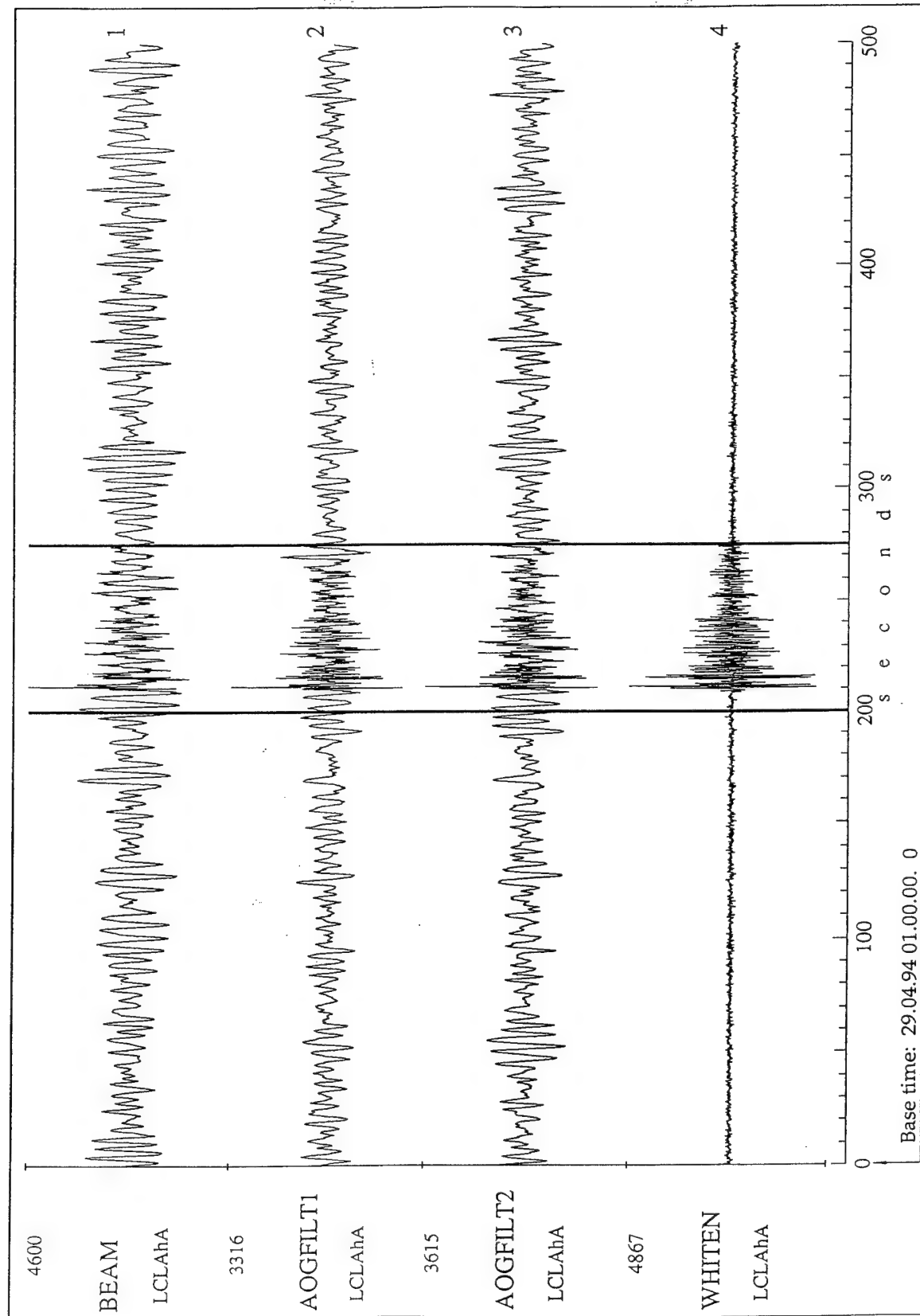


Fig. 10c. Extraction of P-phase waveform using 4 Z-stations.
 $f = 0.01 - 2.5 \text{ Hz}$

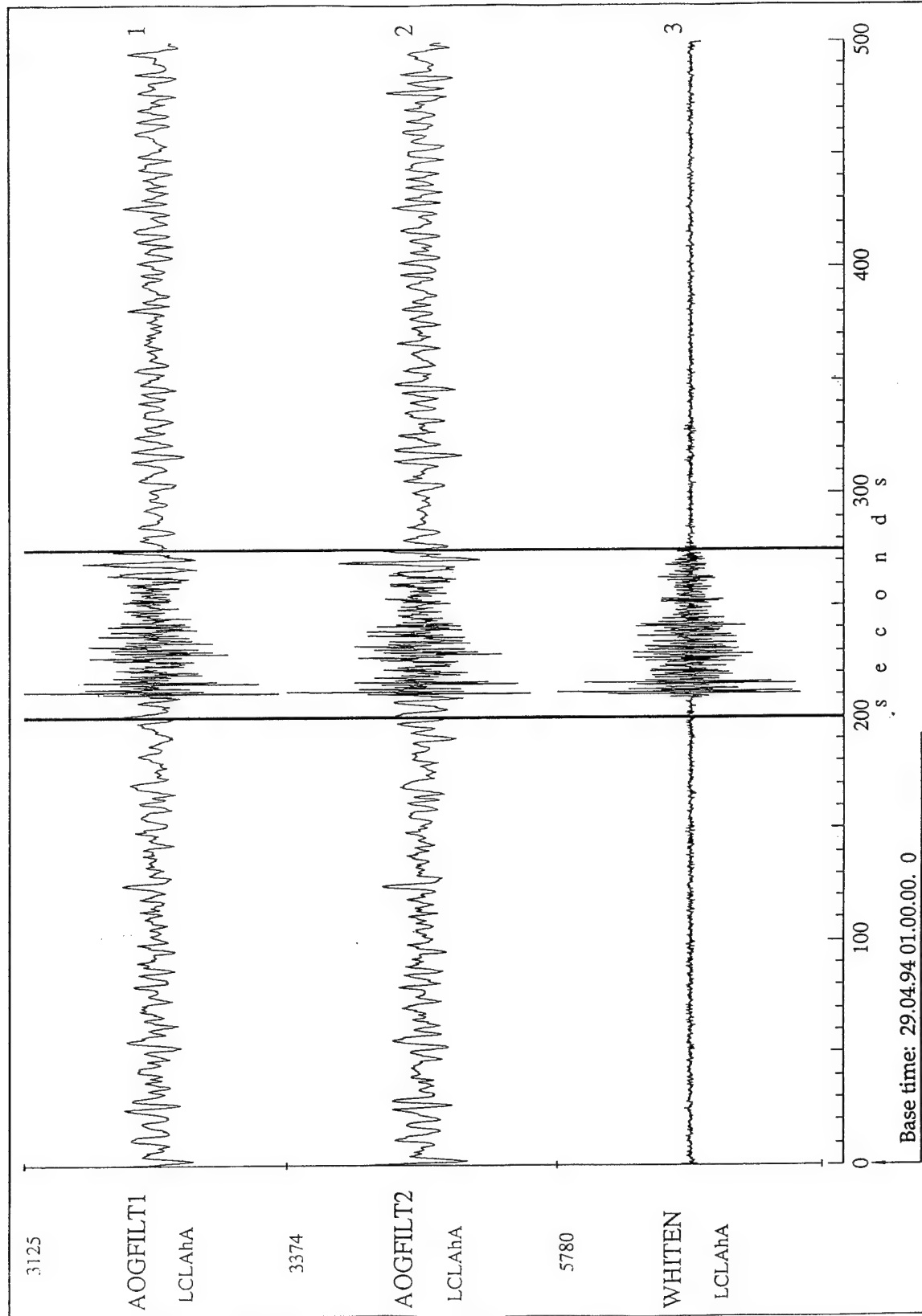
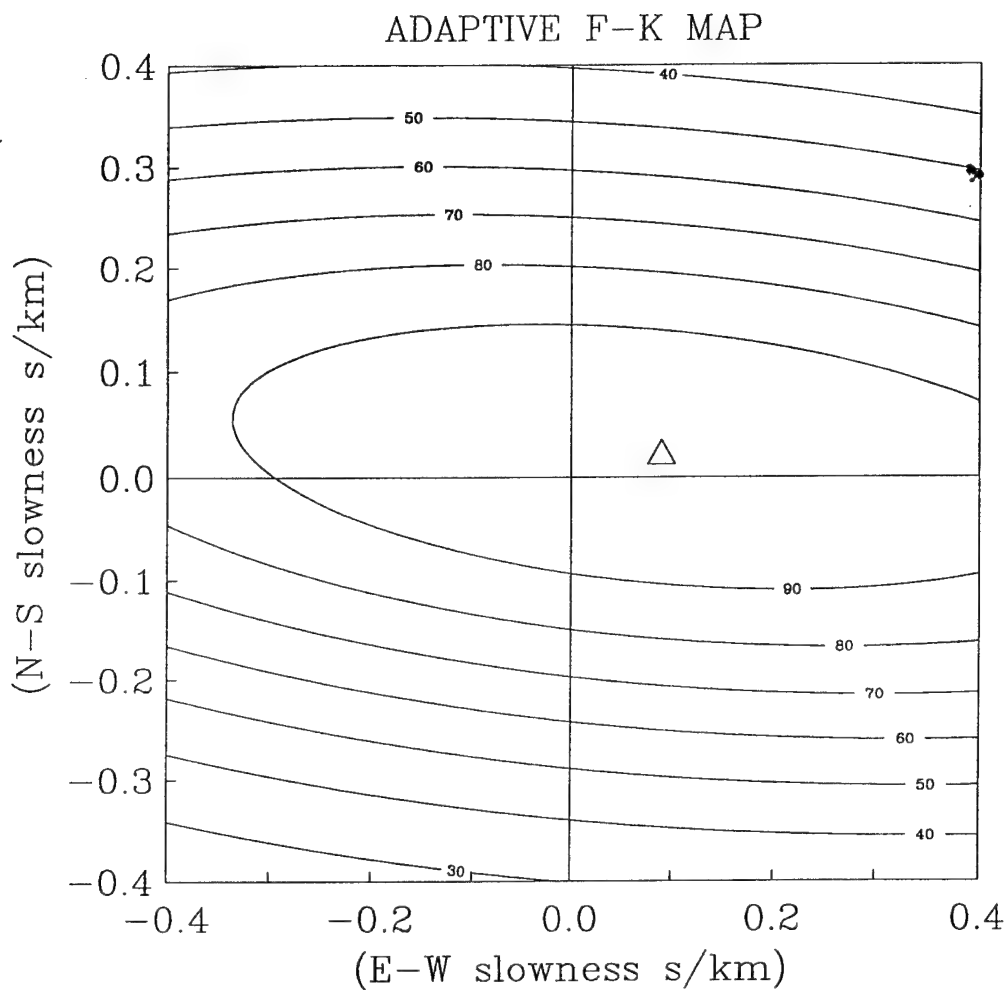


Fig. 10d. Extraction of P-phase waveform using 4 3C-stations.
 $f = 0.01 - 2.5 \text{ Hz}$



Frequency = 0.700-1.0 Hz, HIGH
 RESOLUTION Azim. of max= 77.47 Ap.
 vel. of max= 10.85 Power max= 100.00
 Adapt. AR order IP= 0 Adapt. MA order
 IQ= 0 Regulariz.=.0000000 Adapt. mode
 = 0

Fig. 11. F-K analysis map for P-phase of Lop-Nor event
 on 10.06.94.

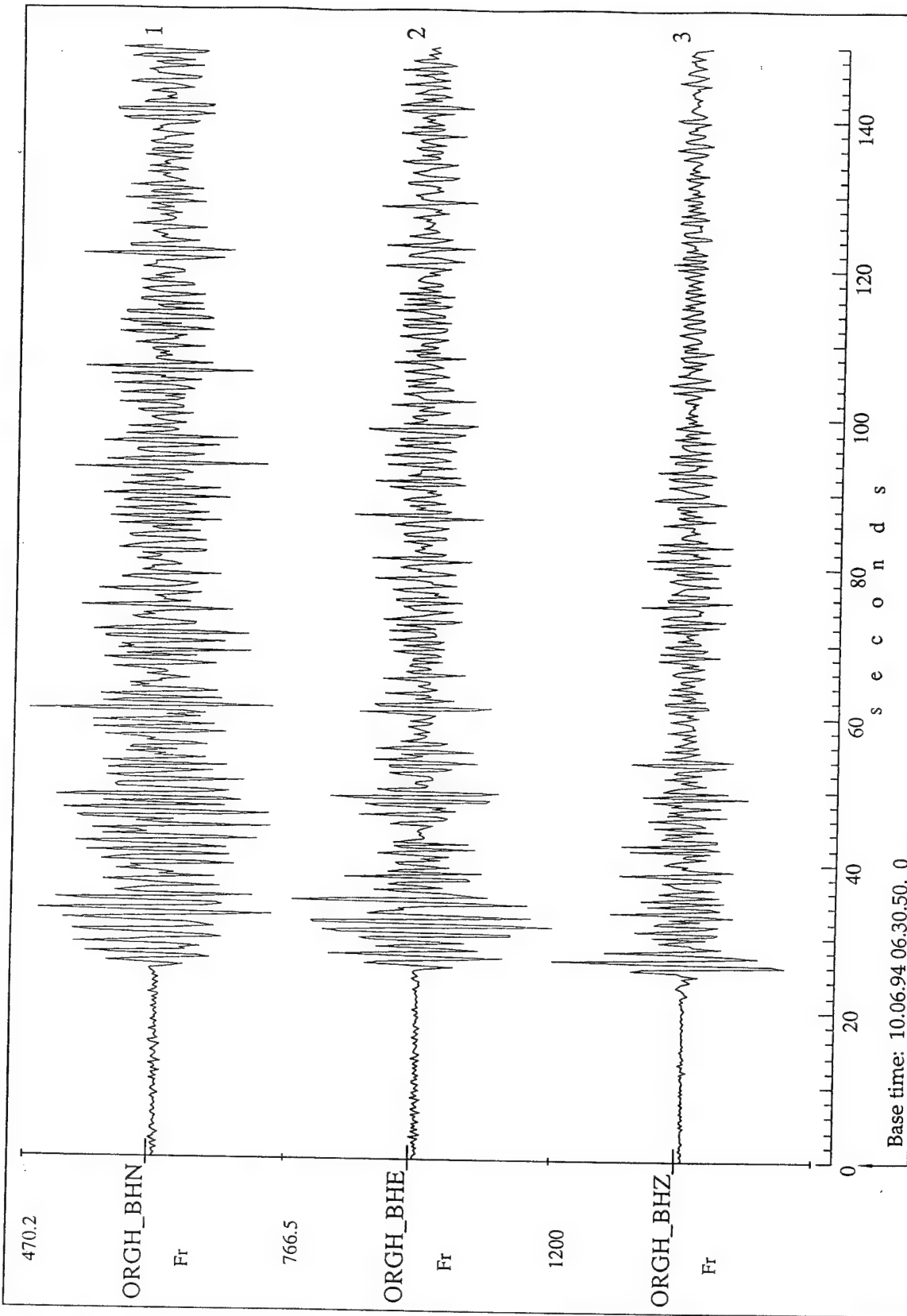
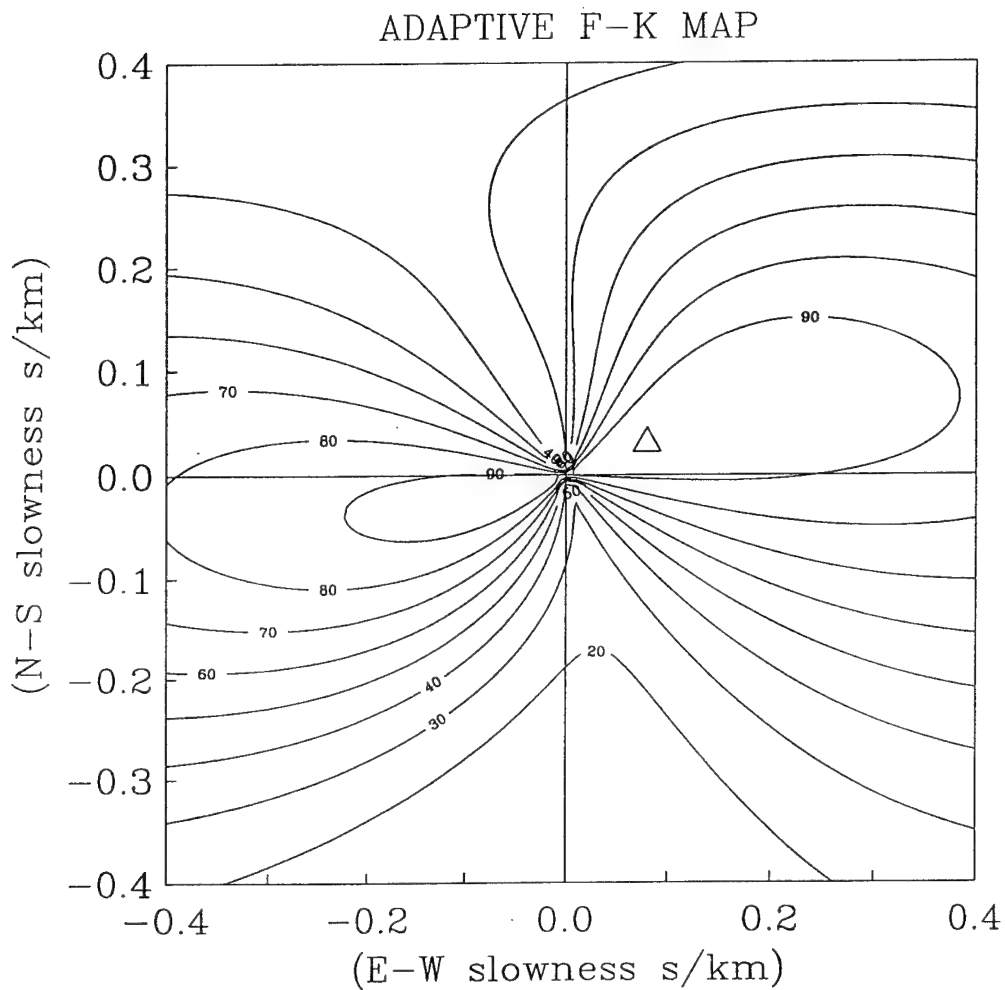
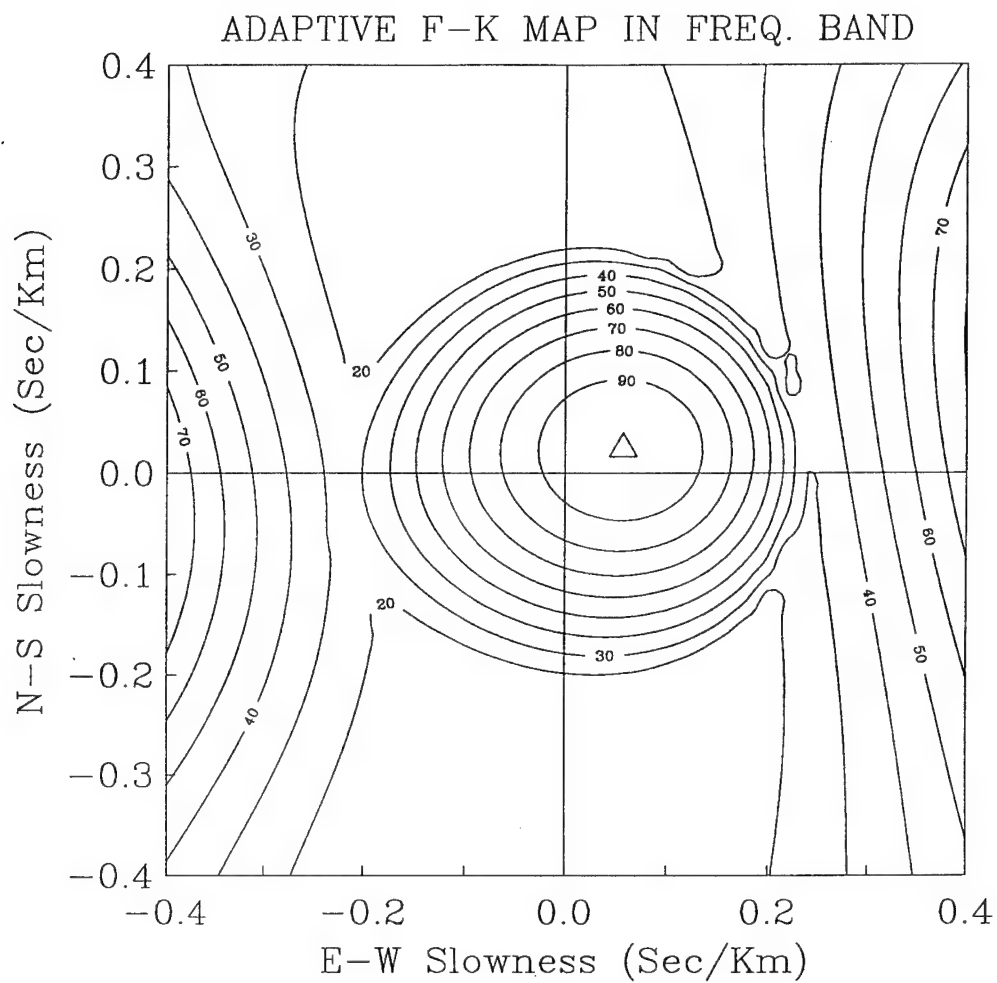


Fig. 12. P-phase 3C waveform for Lop-Nor event on 10.06.94.
 $f = 0.5 - 2 \text{ Hz}$



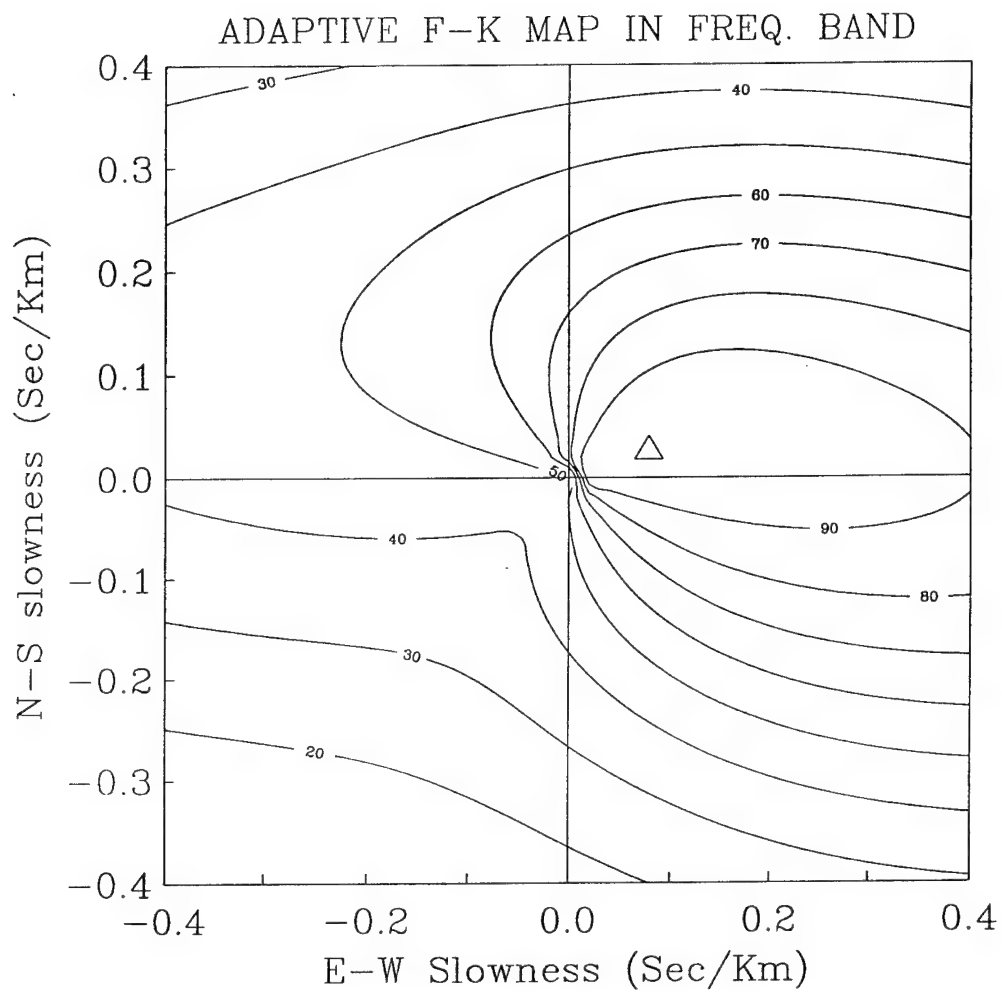
Frequency = 0.700-1.0 Hz, HIGH
 RESOLUTION Azim. of max= 69.44 Ap.
 vel. of max= 11.70 Power max= 100.00
 Adapt. AR order IP= 0 Adapt. MA order
 IQ= 0 Regulariz.=.0000000 Adapt. mode
 = 0

Fig. 13. Map for P-phase generalized F-K analysis
 based on horizontal components.



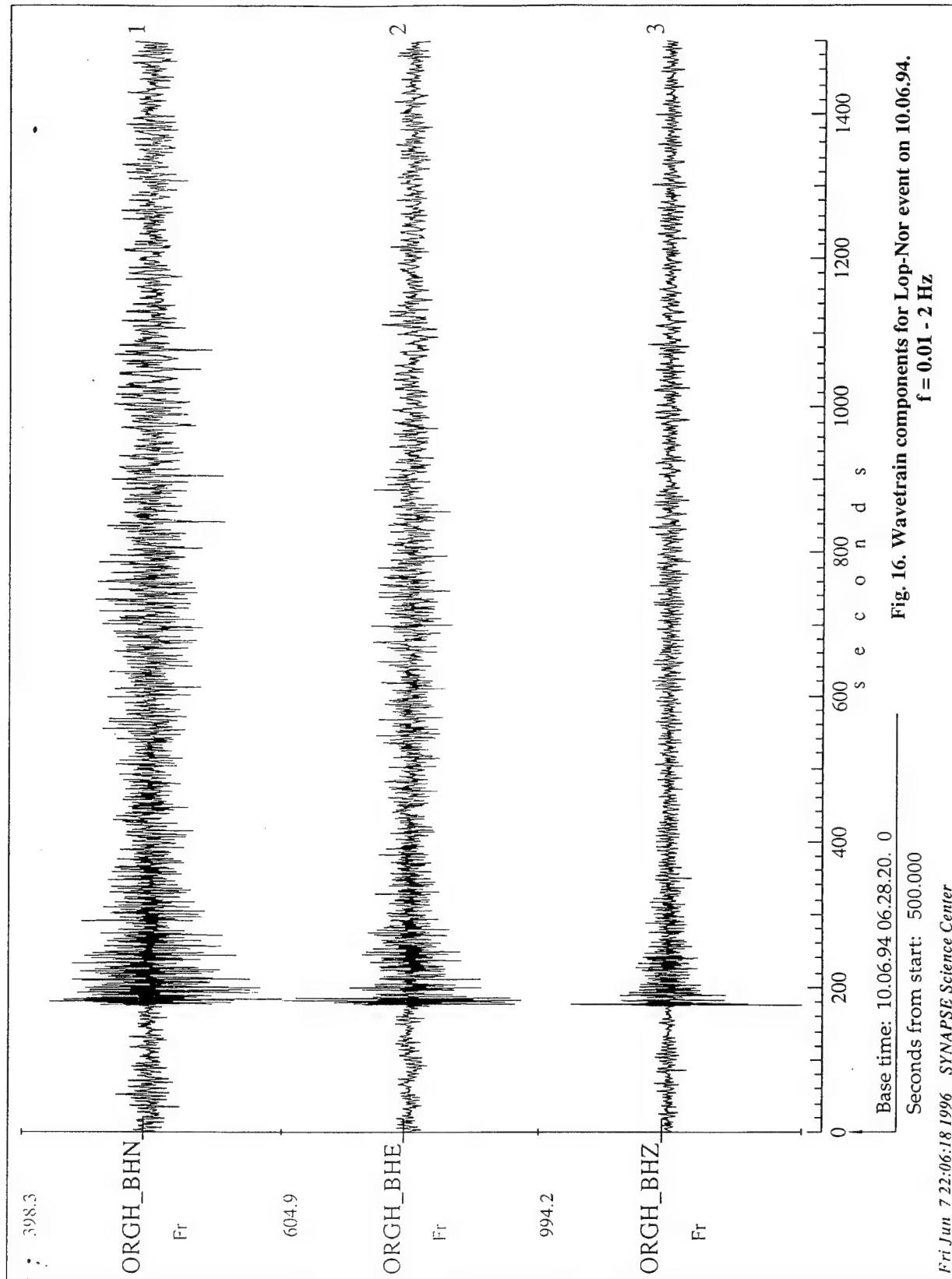
Frequency band: 0.70 - 1.00 Hz;
Azimuth: 67.73 Degrees; Apparent
Velocity: 16.10 Km/Sec.

Fig. 14. Map for P-phase generalized 3C F-K analysis
with linear polarization model.



Frequency band: 0.70 - 1.00 Hz;
 Azimuth: 71.74 Degrees; Apparent
 Velocity: 12.08 Km/Sec.

**Fig. 15. Map for P-phase generalized 3C F-K analysis
 with elliptic polarization model.**



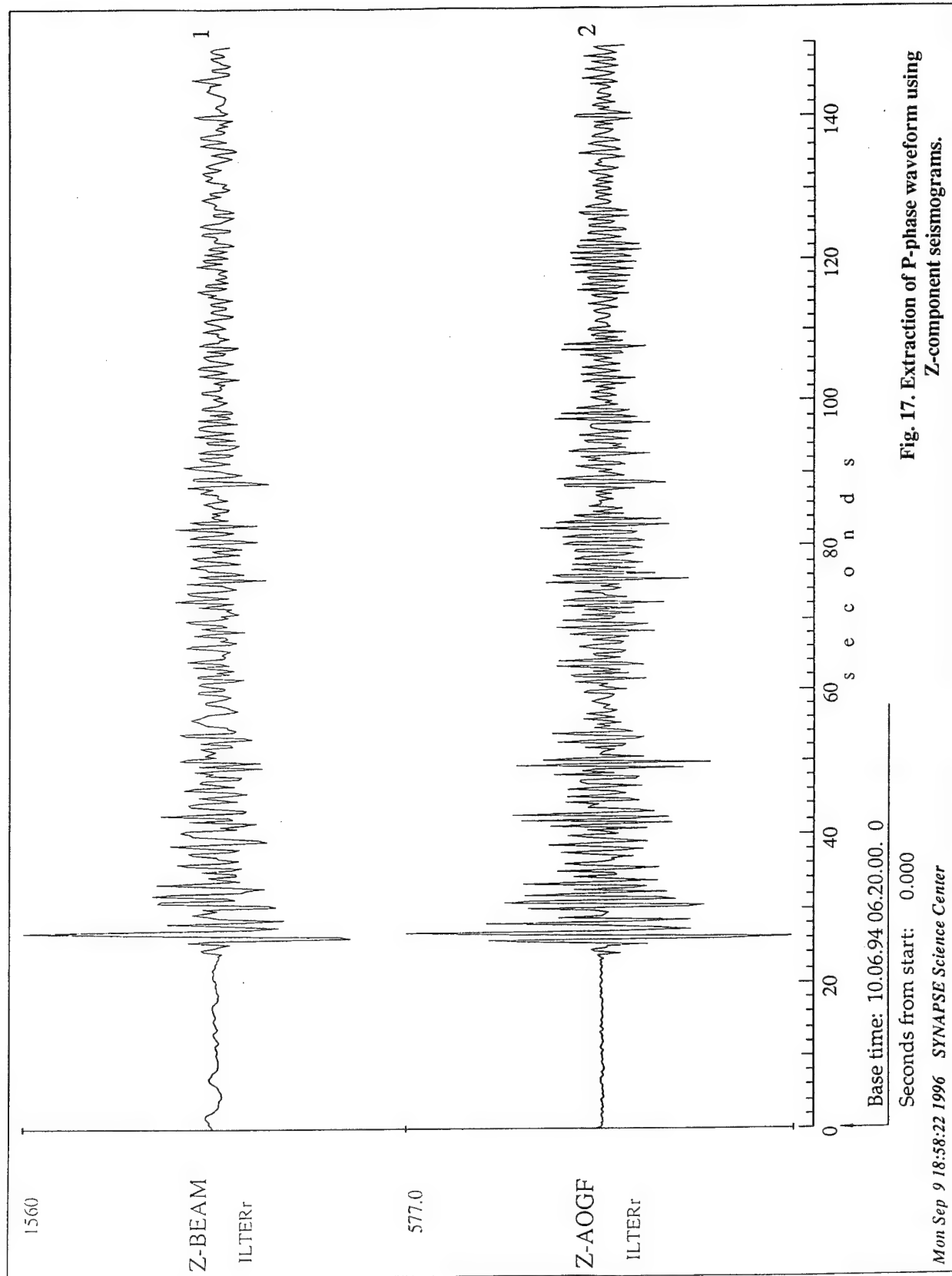


Fig. 17. Extraction of P-phase waveform using Z-component seismograms.

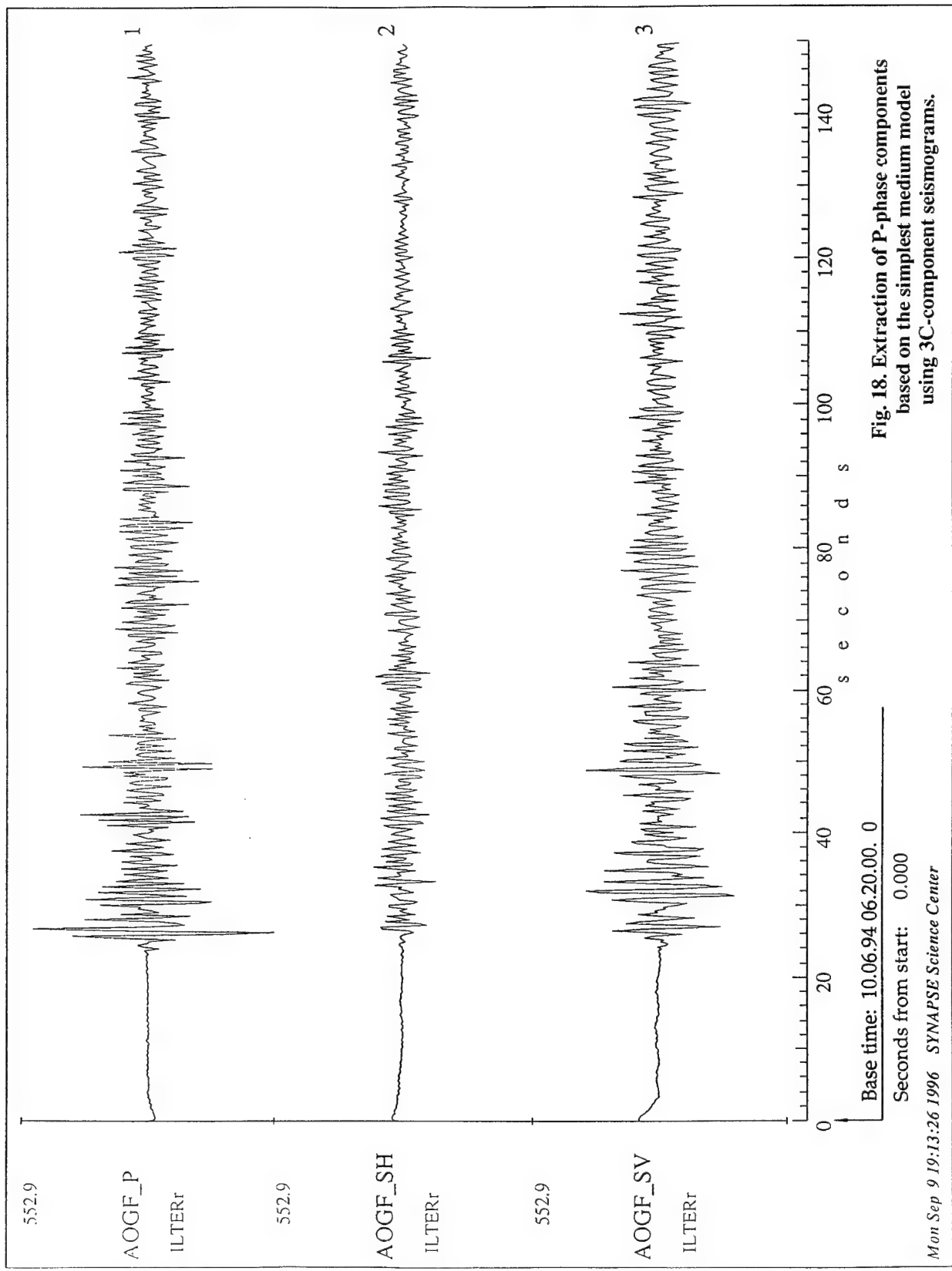
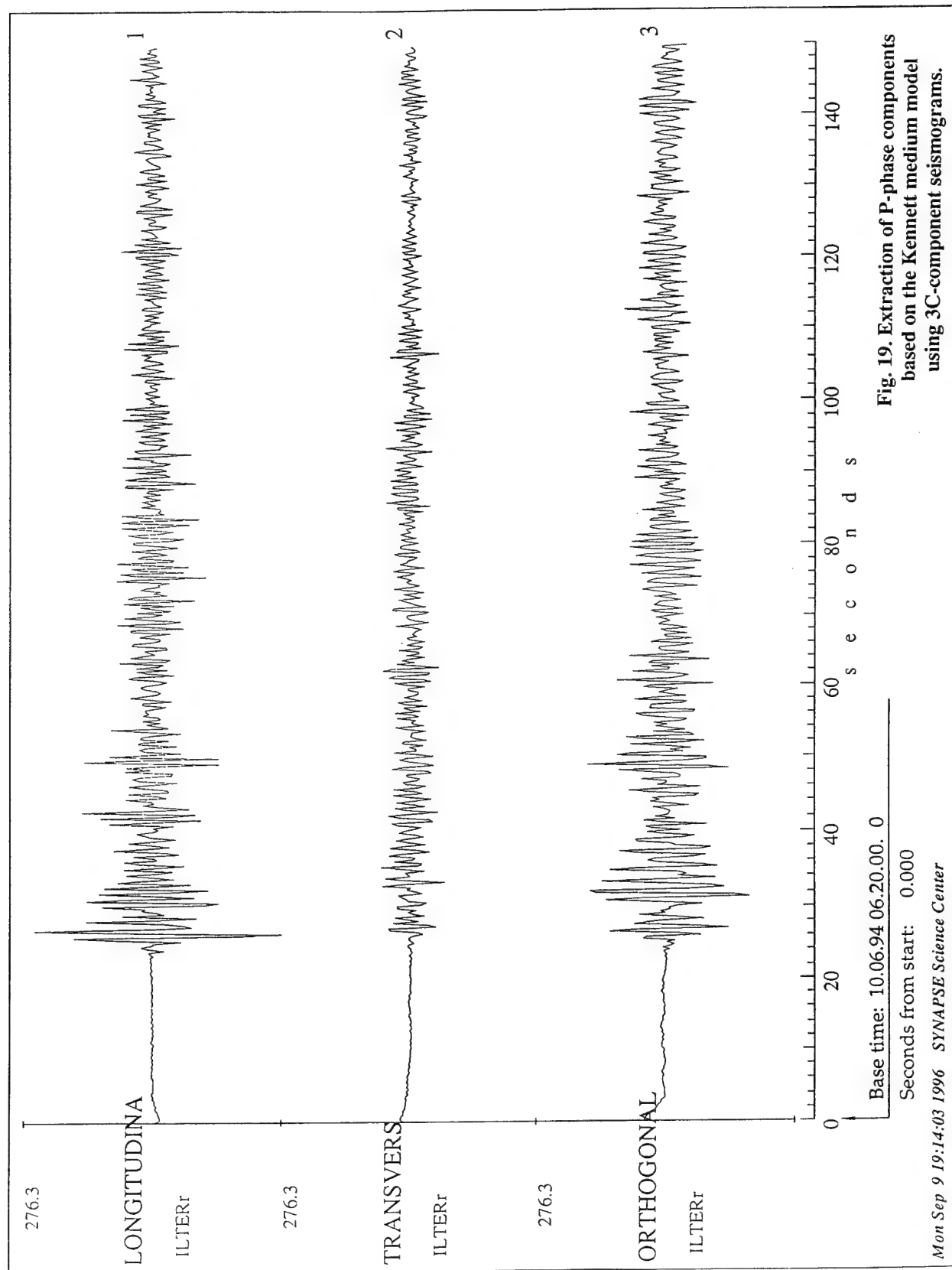
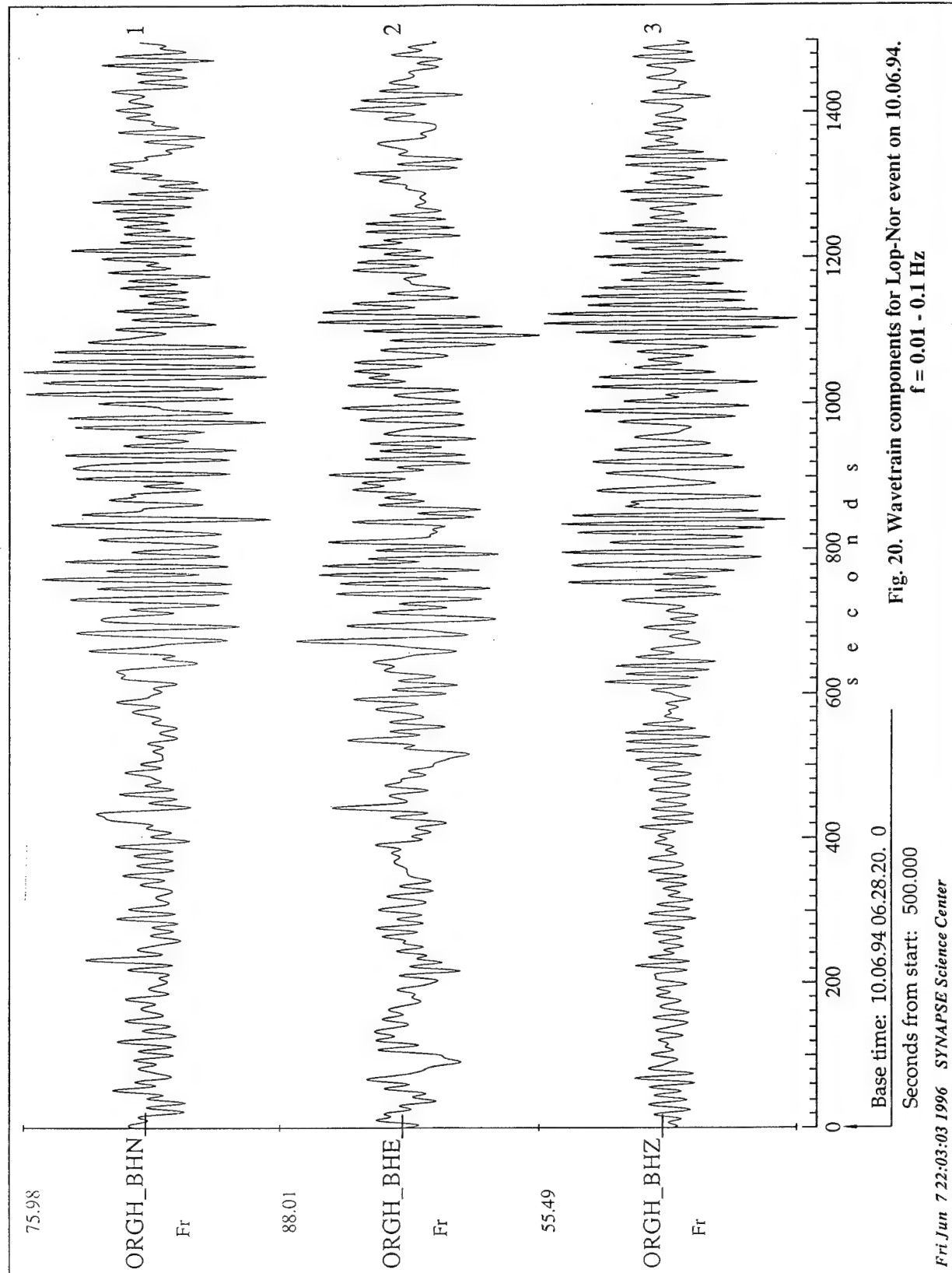
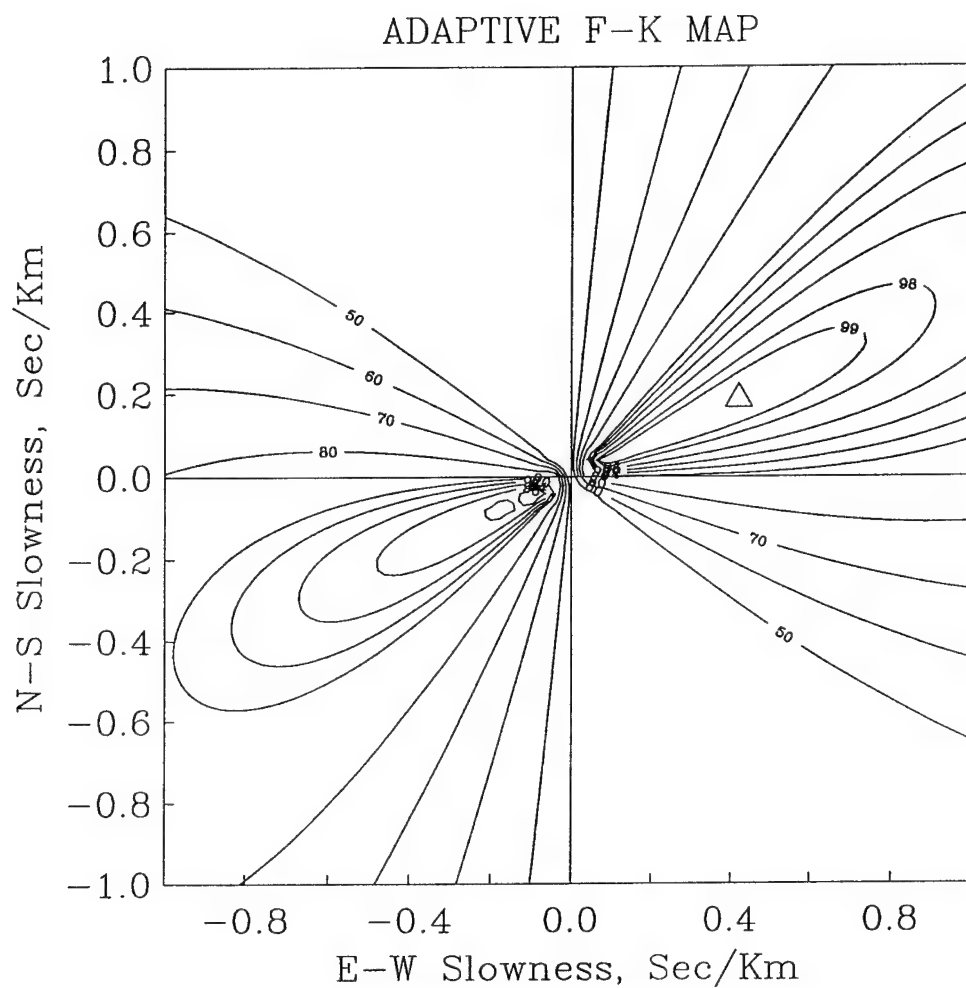


Fig. 18. Extraction of P-phase components based on the simplest medium model using 3C-component seismograms.

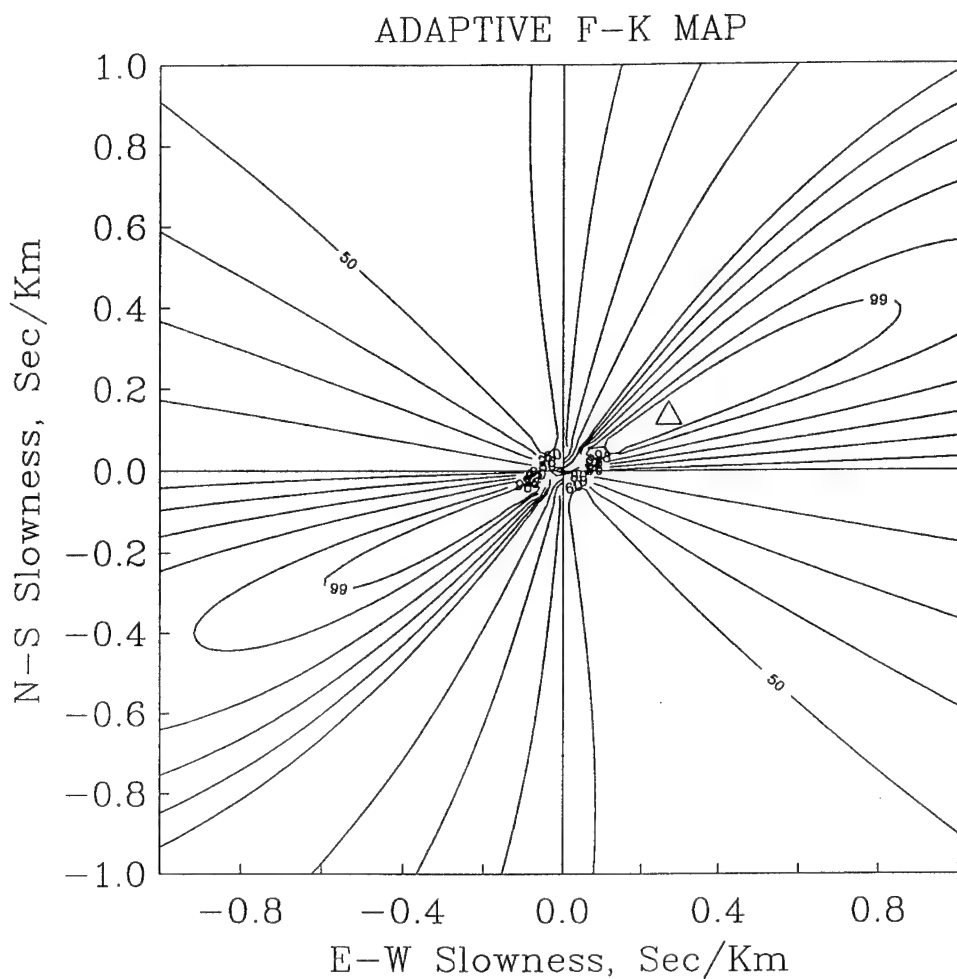






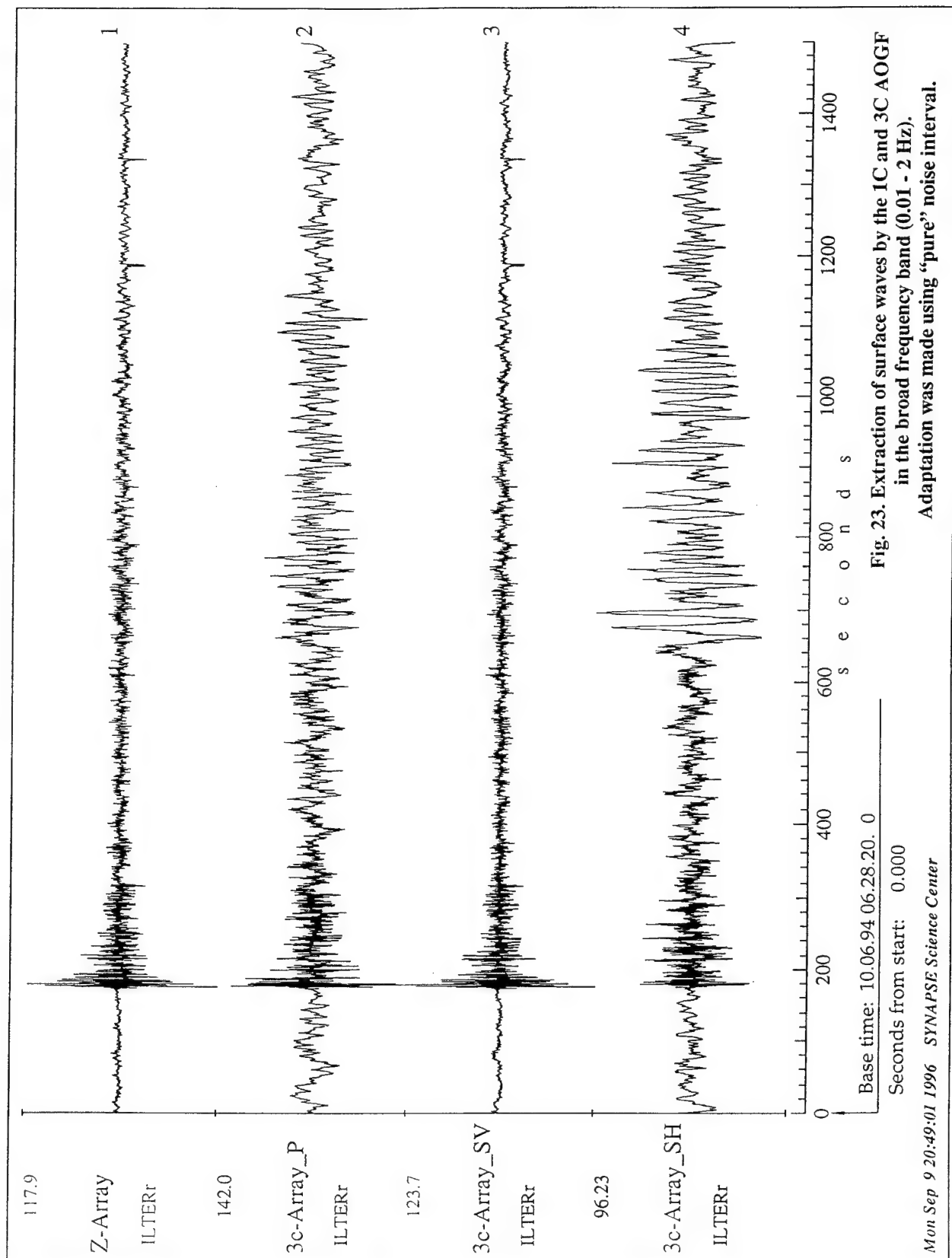
Frequency Band 0.060 - 0.09 Hz;
 Azimuth - 66.15 Degrees; Apparent
 Velocity - 2.17 Km/Sec; Model for
 Adaptation - ARMA; AR-Order - 2;
 MA-Order - 8.

Fig. 21. Map for Rayleigh wave generalized 3C F-K analysis of
 10.06.94. Lop Nor event.



Frequency Band 0.04 - 0.09 Hz;
Azimuth - 64.09 Degrees; Apparent
Velocity - 3.31 Km/Sec; Model for
Adaptation - ARMA; AR-Order - 2;
MA-Order - 8.

Fig. 22. Map for Love wave generalized 3C F-K analysis of
10.06.94. Lop Nor event.



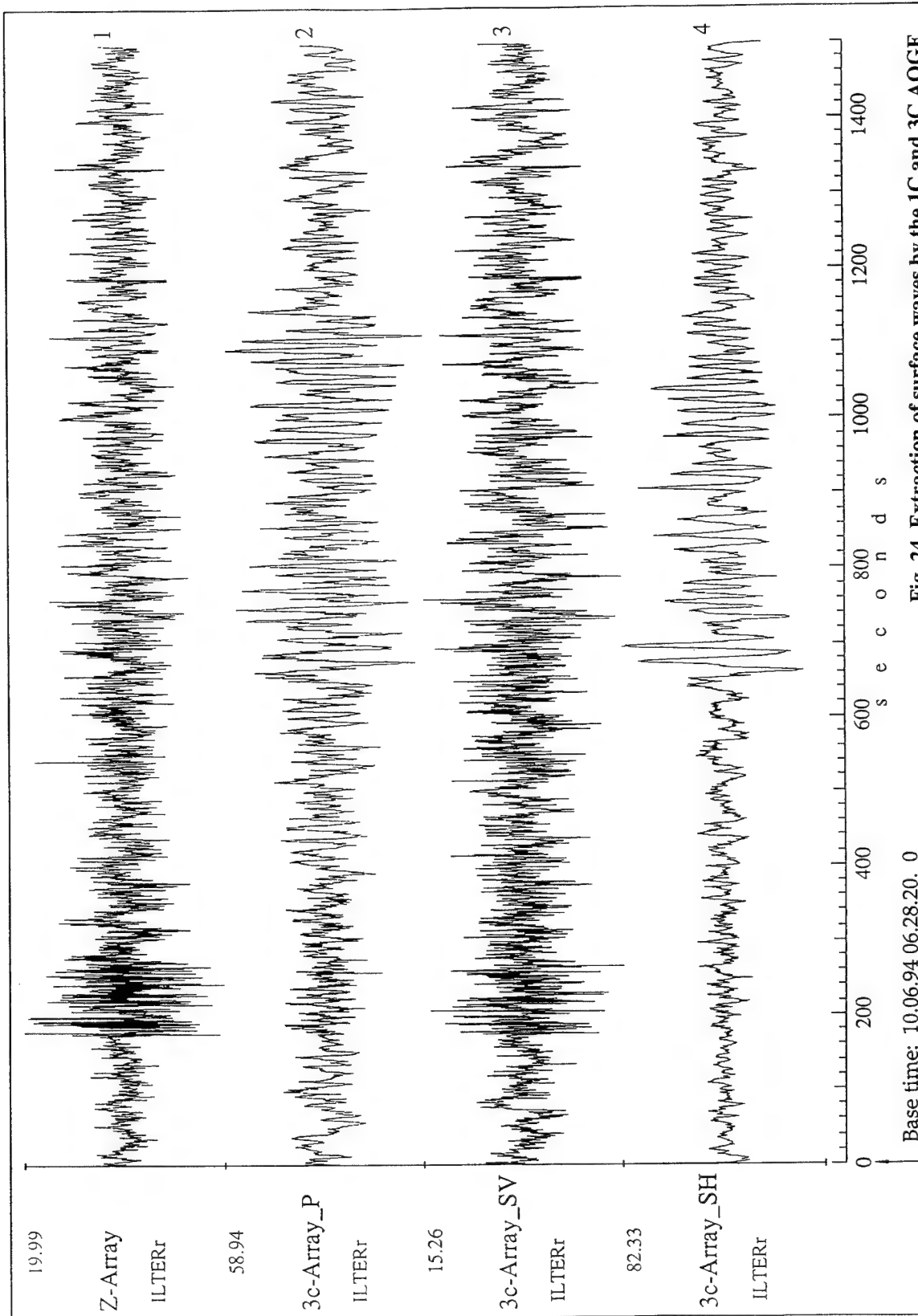
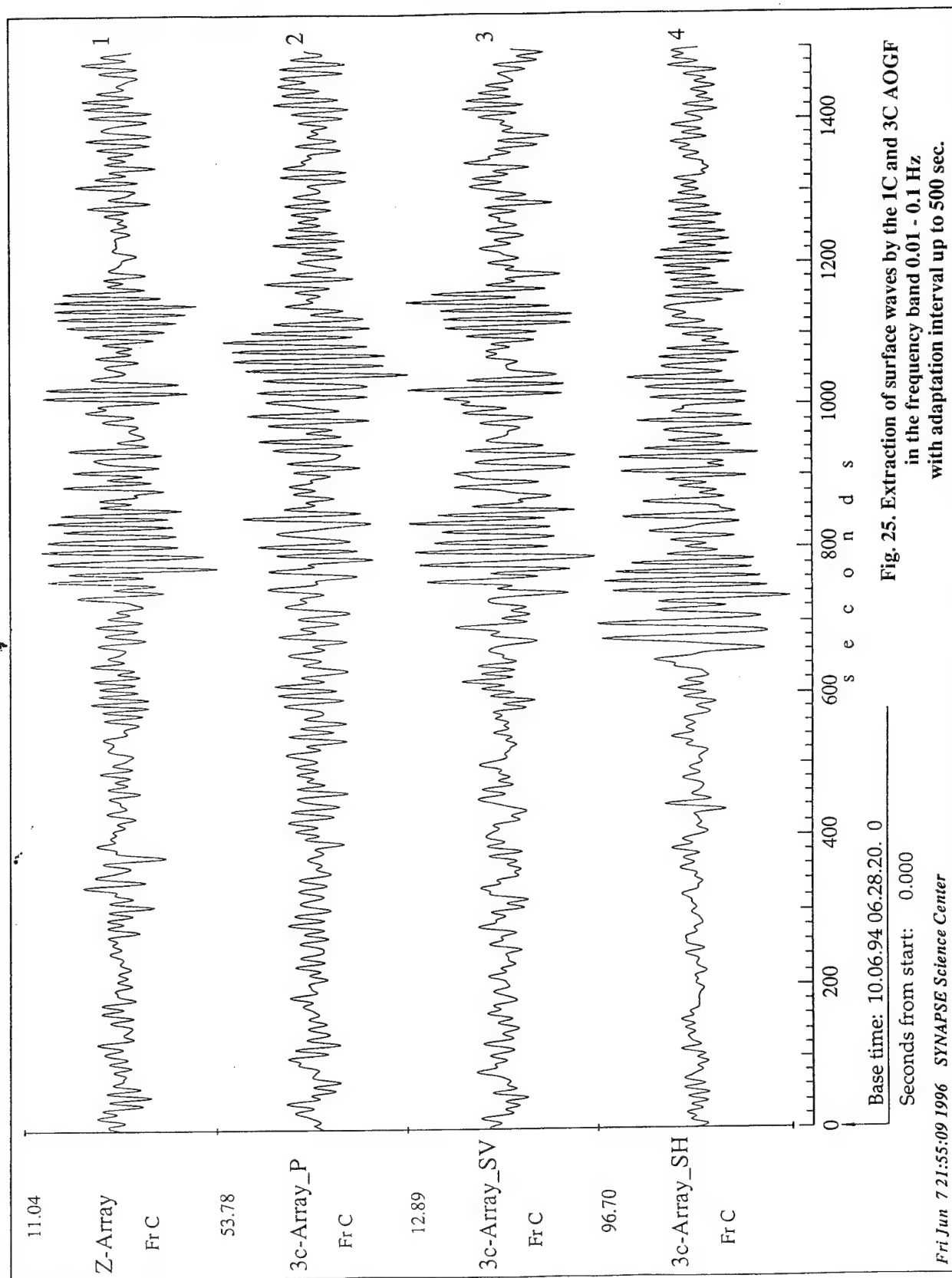


Fig. 24. Extraction of surface waves by the 1C and 3C AOGF
in the broad frequency band (0.01 - 2 Hz)
with adaptation interval up to 500 sec.



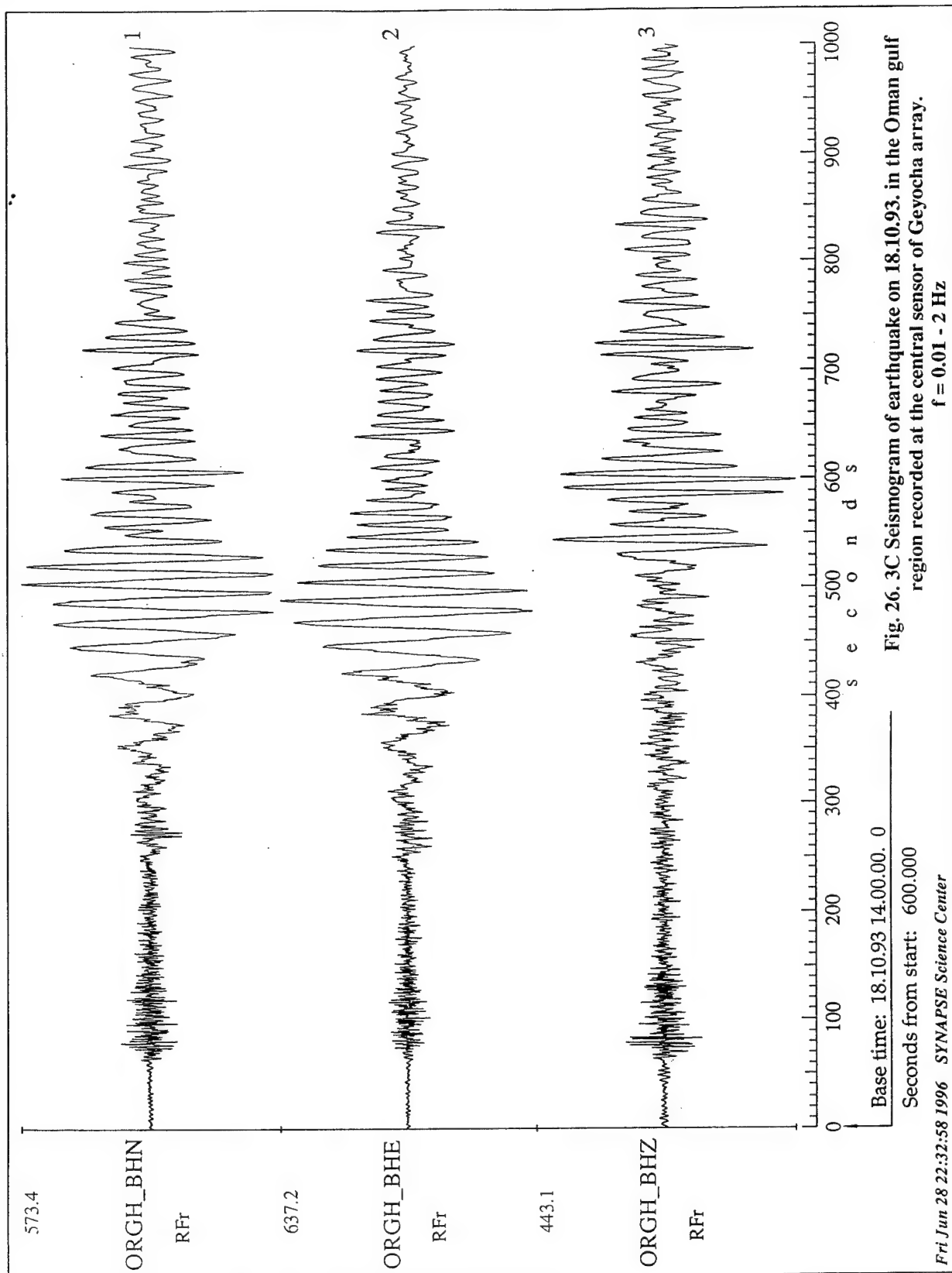
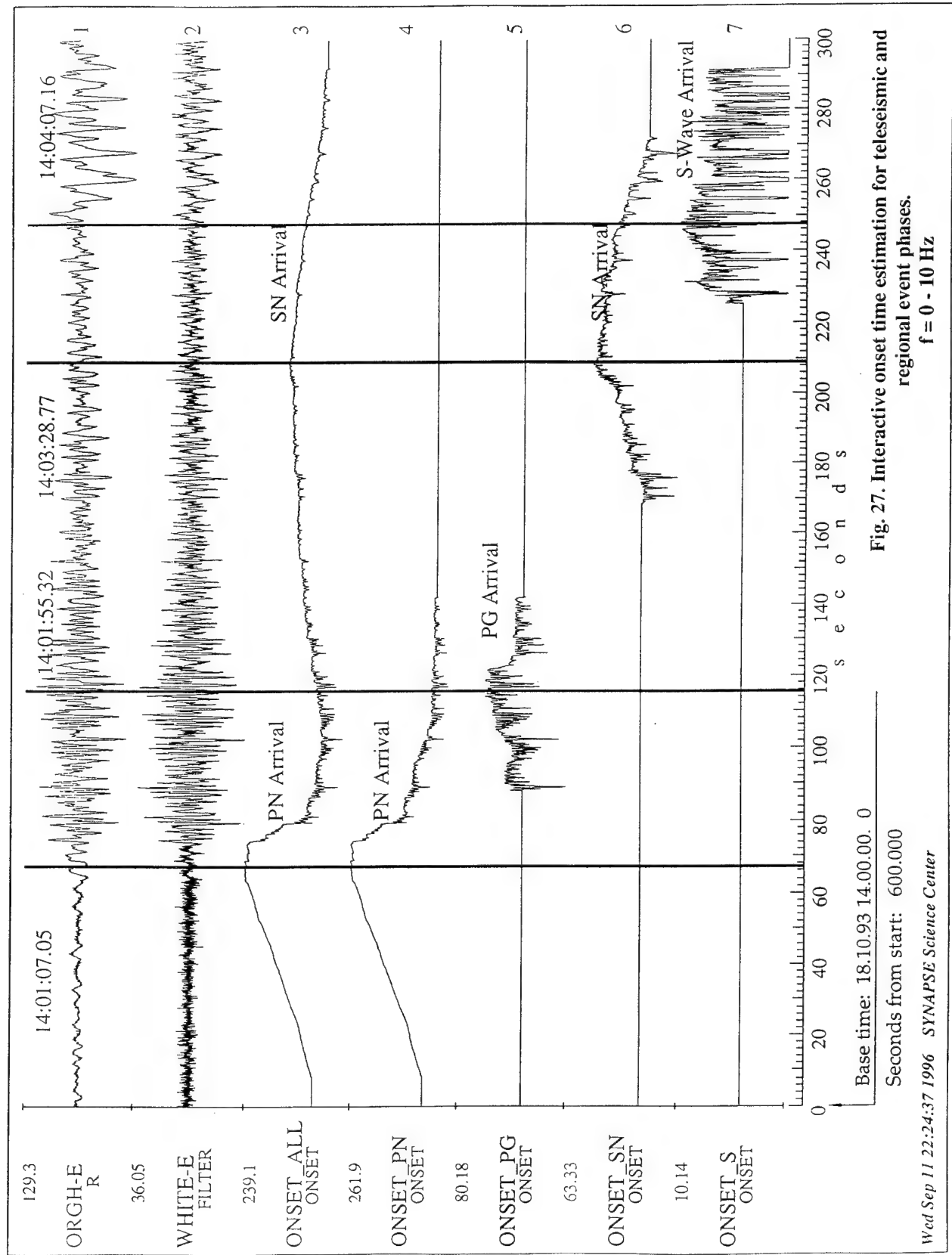


Fig. 26. 3C Seismogram of earthquake on 18.10.93. in the Oman gulf region recorded at the central sensor of Geyocha array.



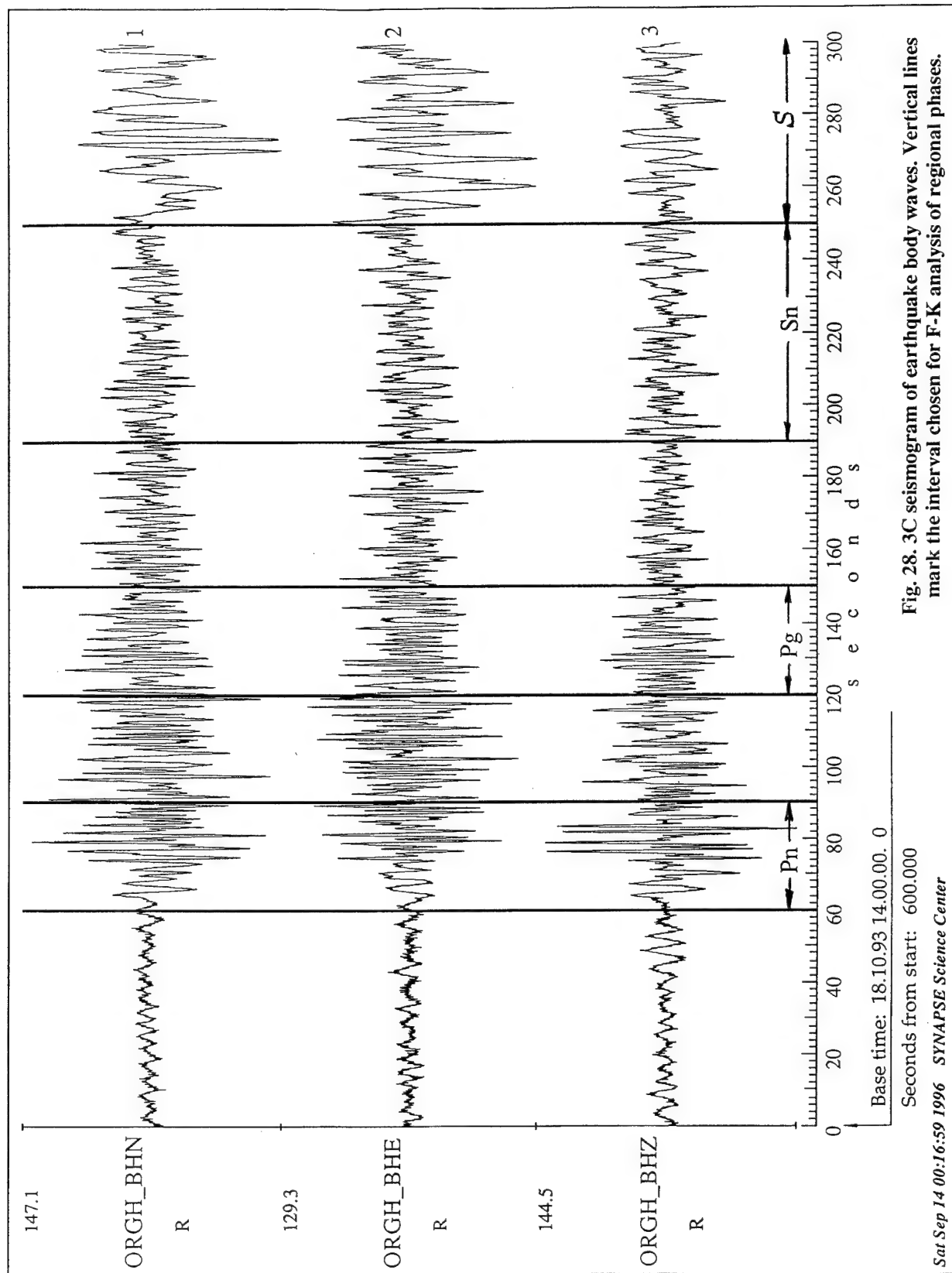


Fig. 28. 3C seismogram of earthquake body waves. Vertical lines mark the interval chosen for F-K analysis of regional phases.

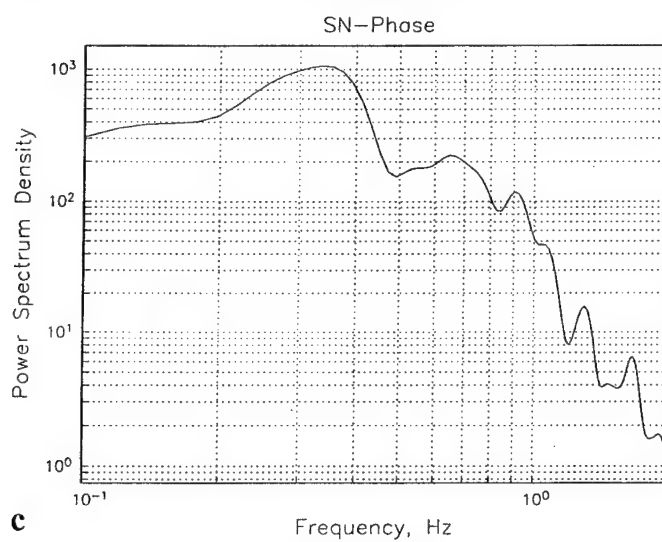
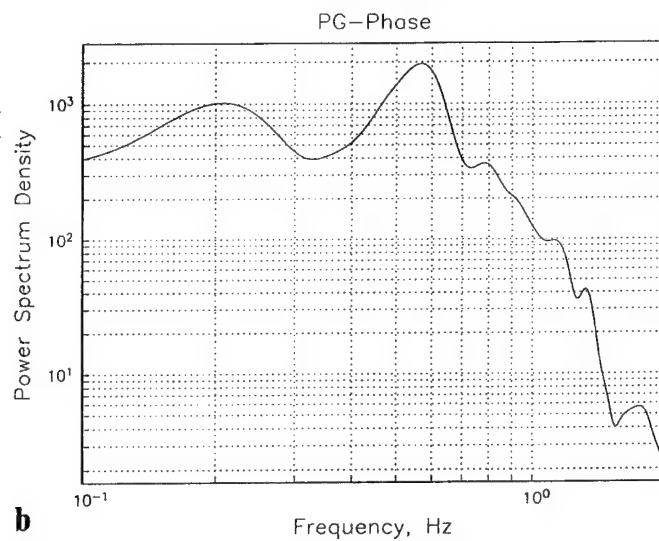
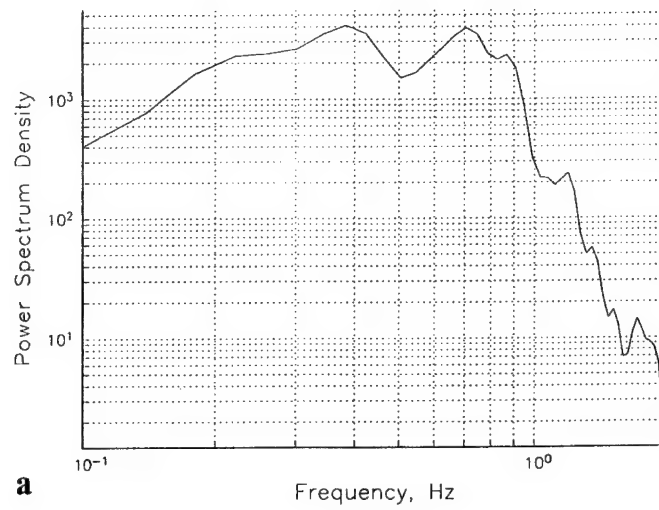


Fig. 29. Power spectral densities of earthquake regional phases.
a. Pn-phase.
b. Pg-phase.
c. Sn-phase.

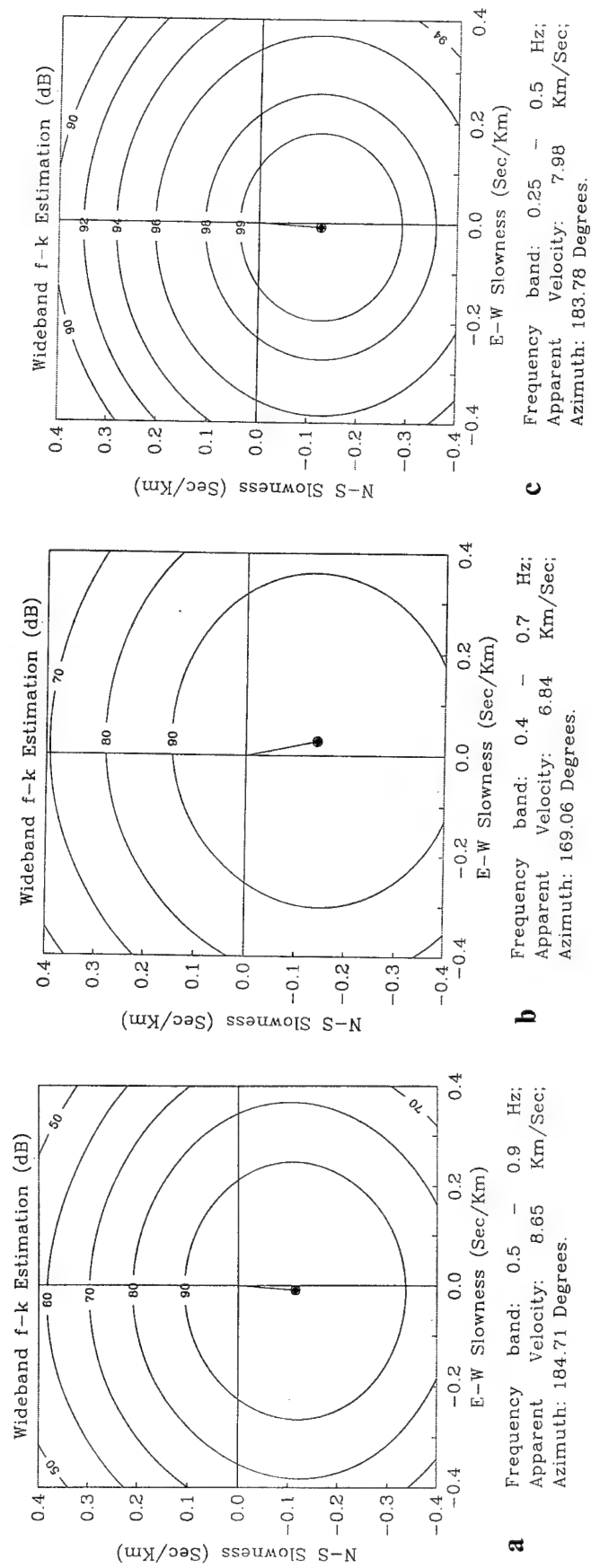


Fig. 30. F-K analysis maps for earthquake regional phases.
a. Pn-phase.
b. Pg-phase.
c. Sn-phase.

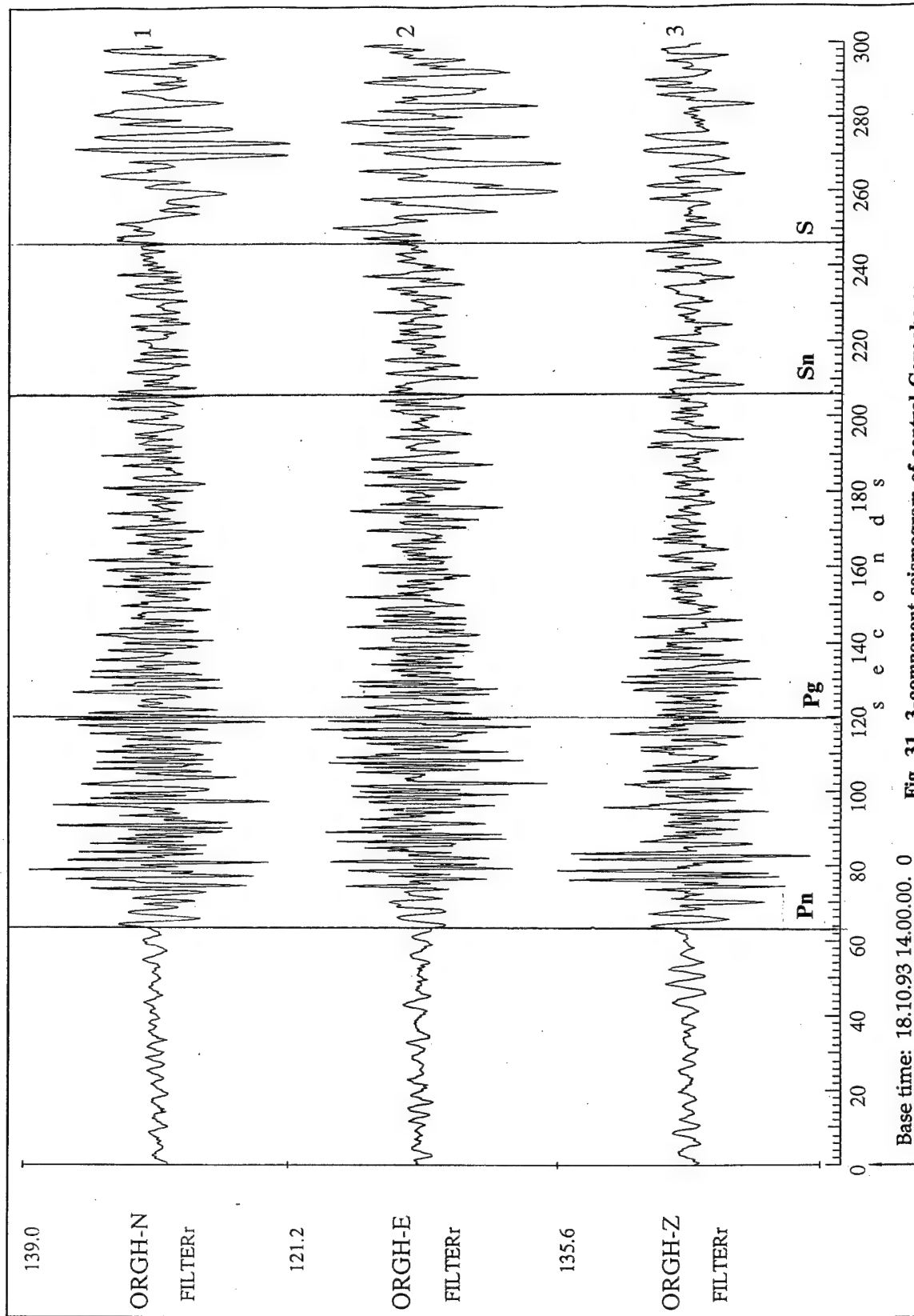


Fig. 31. 3-component seismogram of central Geyocha sensor
at time interval of body waves (0.1 - 2) Hz.

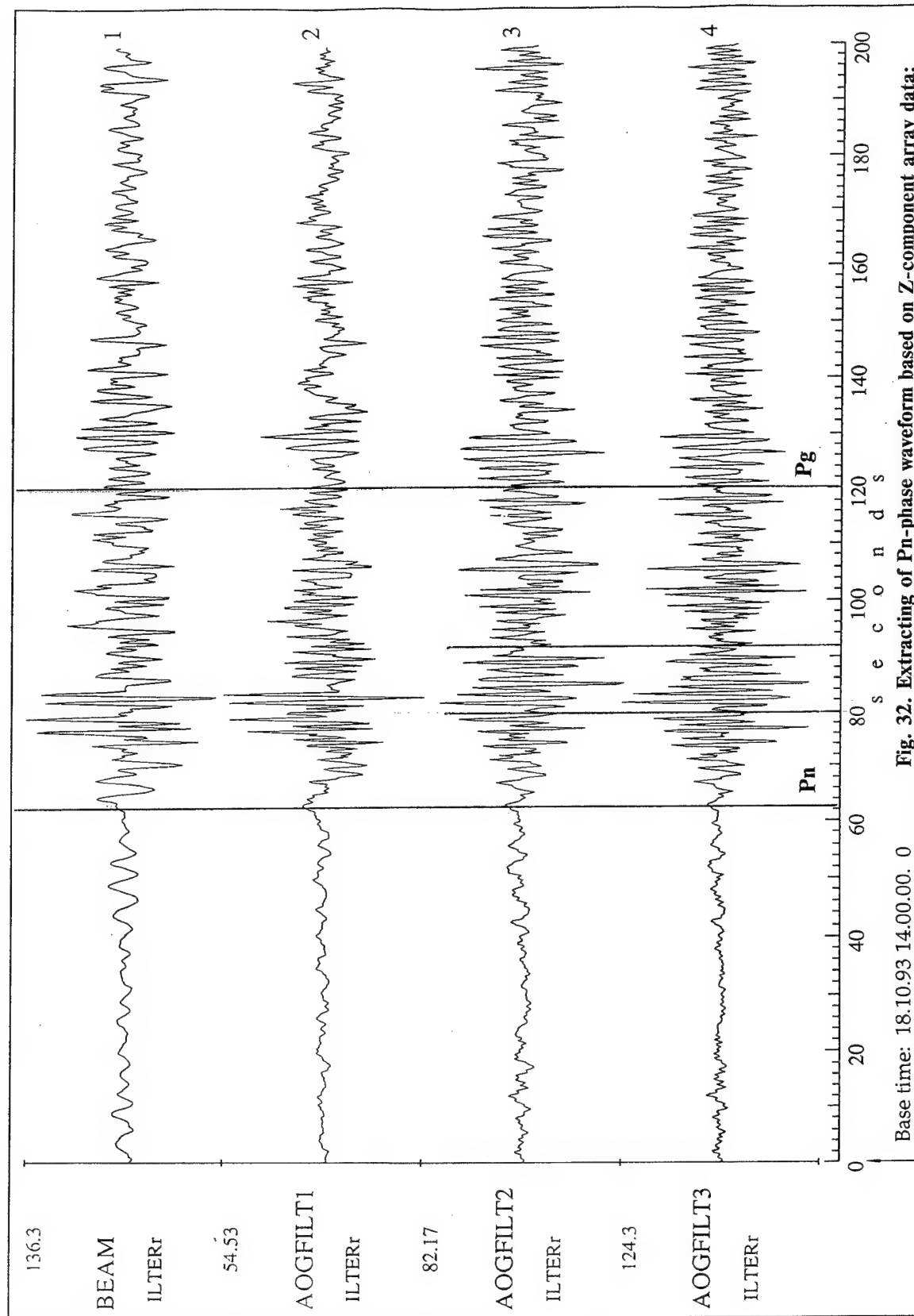


Fig. 32. Extracting of Pn-phase waveform based on Z-component array data:
1) beam trace; 2) AOGF trace with adaptation on preceding noise; 3) AOGF trace
with adaptation using total event wavetrane (0-1000) sec.; 4) AOGF trace with
adaptation using only wavetrane succeeding the Pn + Pg phases (200-1000 sec).

Base time: 18.10.93 14.00.00. 0

Seconds from start: 0.000

Thu Sep 12 22:48:43 1996 SYNAPSE Science Center

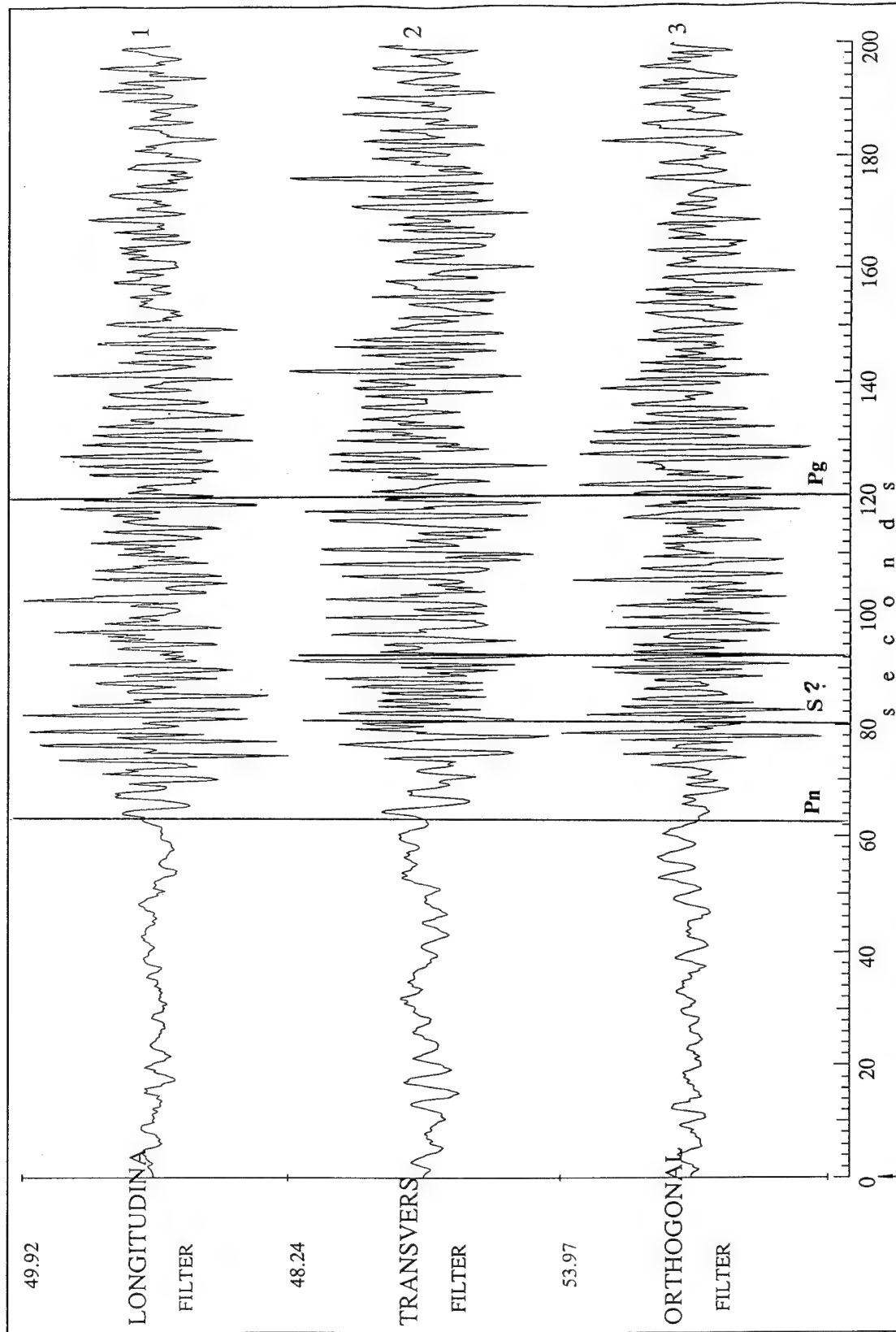


Fig. 33. Extracting of Pn-phase 3-component oscillations based on 3-component Geyocha array seismograms. (Note the onset of SH high frequency phase at 80 sec. and onset of SV transformed wave at 70 sec.)

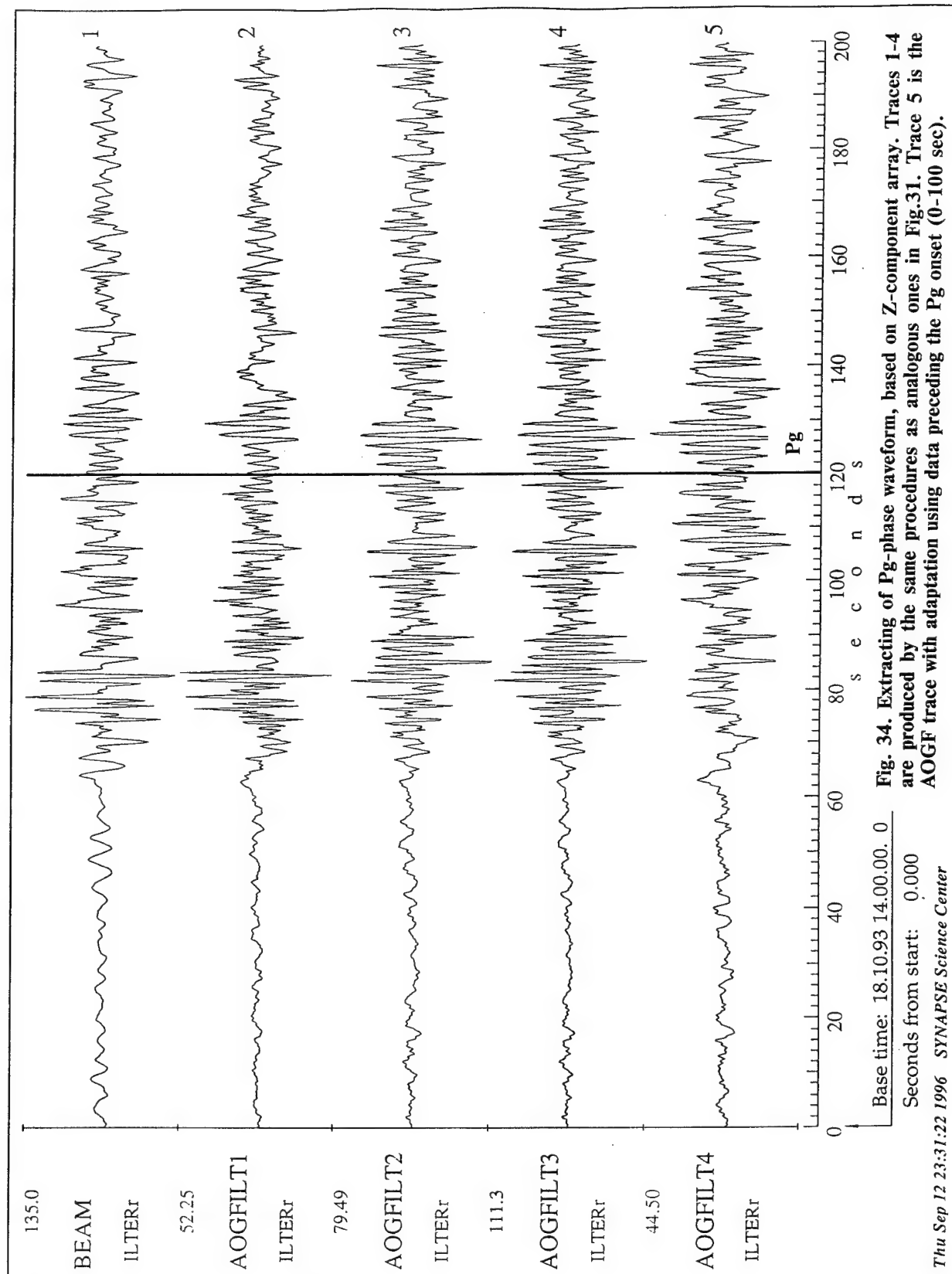


Fig. 34. Extracting of Pg-phase waveform, based on Z-component array. Traces 1-4 are produced by the same procedures as analogous ones in Fig.31. Trace 5 is the AOGF trace with adaptation using data preceding the Pg onset (0-100 sec).

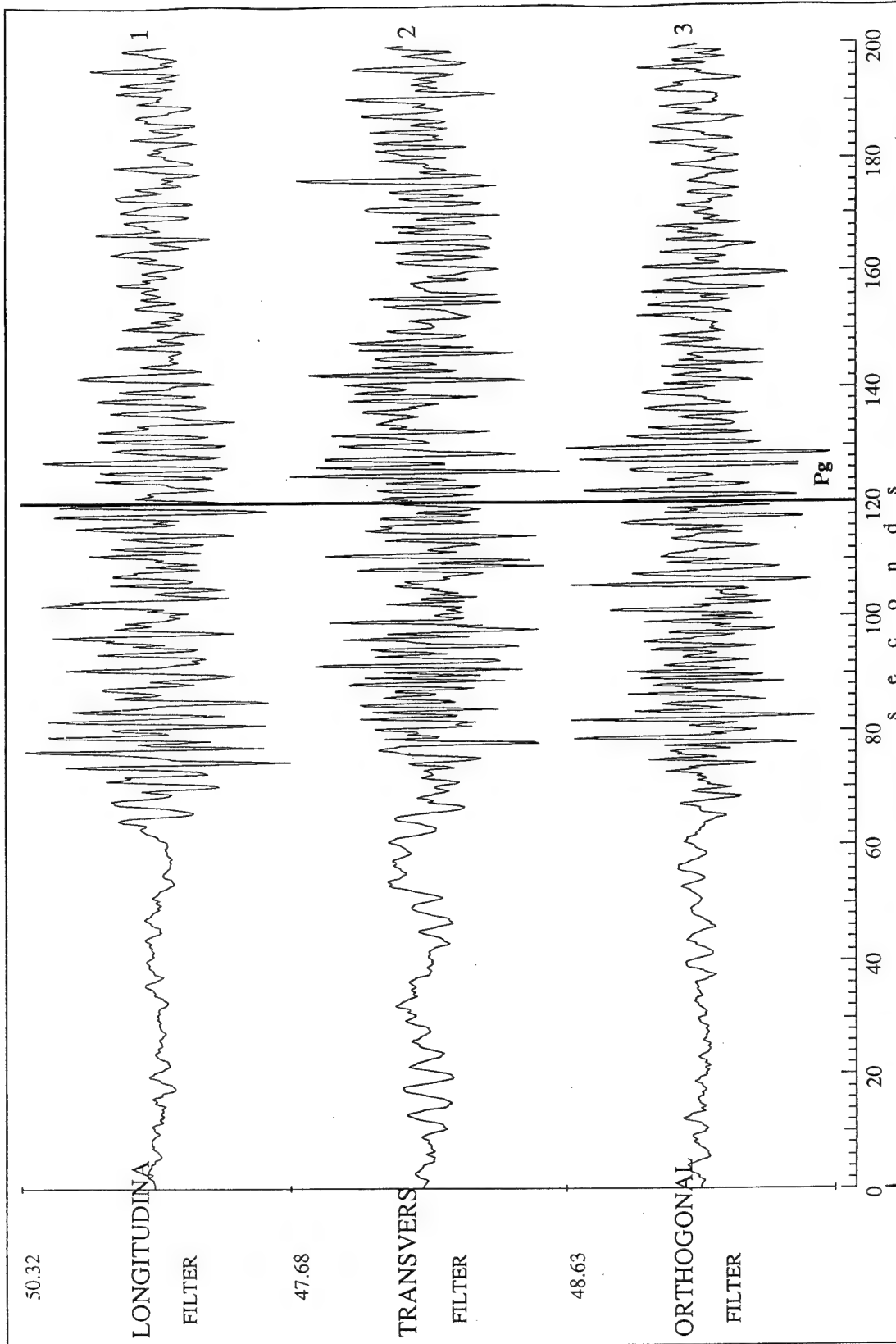


Fig. 35. Extracting of Pg-phase 3-component oscillations based on 3-component array seismograms. Note the complex character of wave polarization.

Base time: 18.10.93 14.00.00. 0

Seconds from start: 0.000

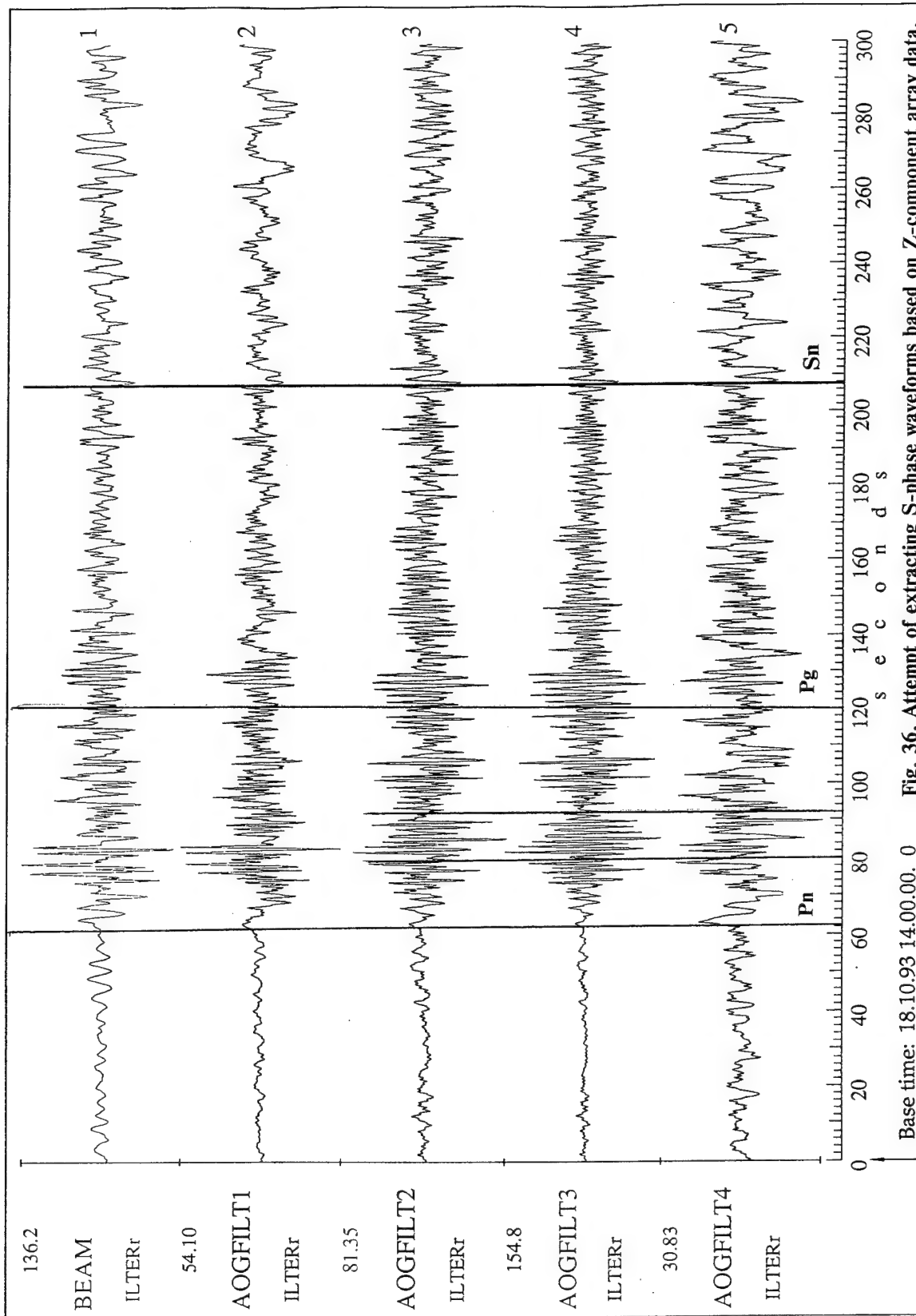


Fig. 36. Attempt of extracting S-phase waveforms based on Z-component array data. The AOGF adaptation for traces 2-4 was the same as for analogous traces in Fig 32. The adaptation for trace 5 was made using time interval (0-180) sec.

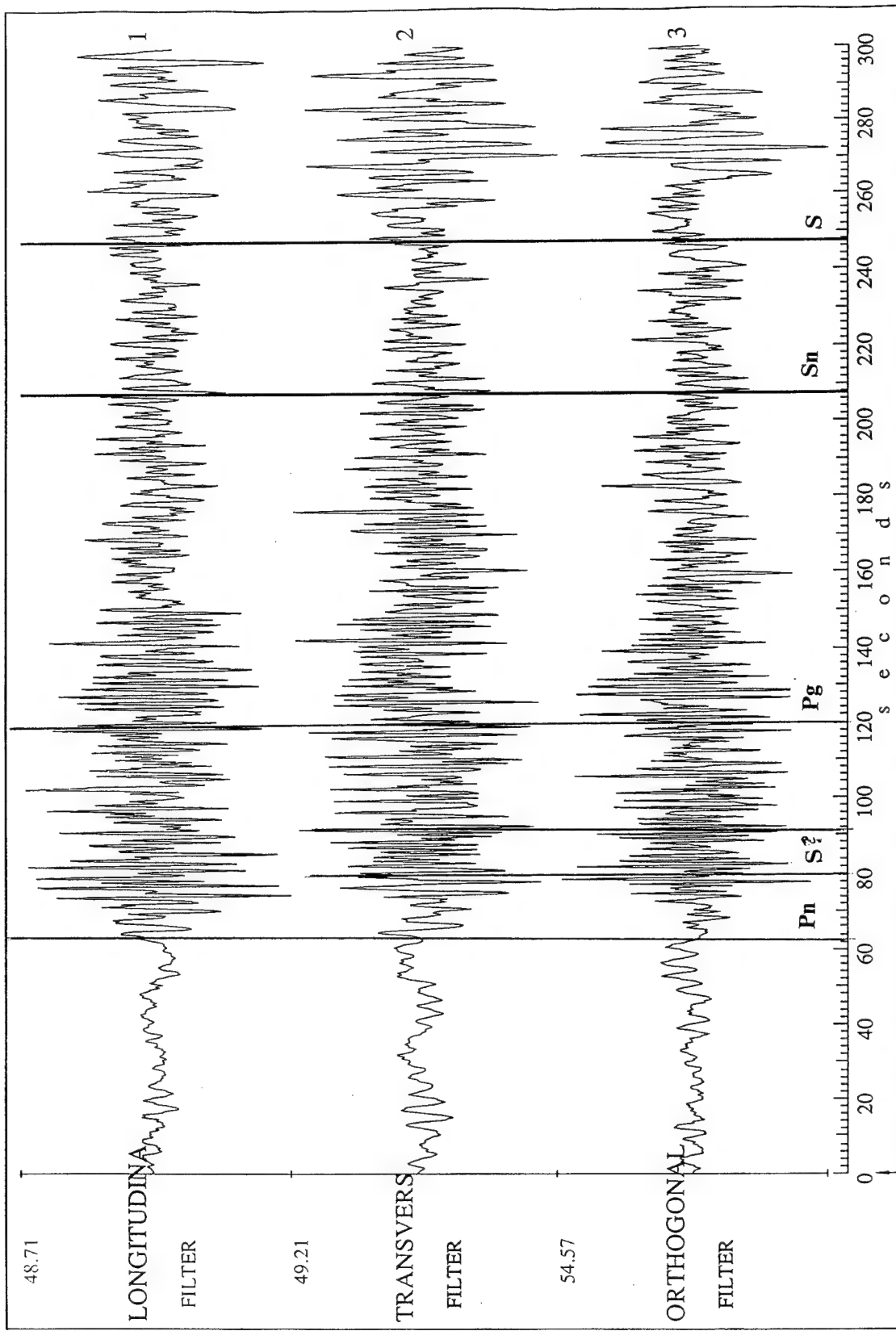


Fig. 37. Extracting of teleseismic S-phase waveform based on 3-component array seismograms. Note, that Sn phase is practically not seen.

Base time: 18.10.93 14.00.00. 0
Seconds from start: 0.000

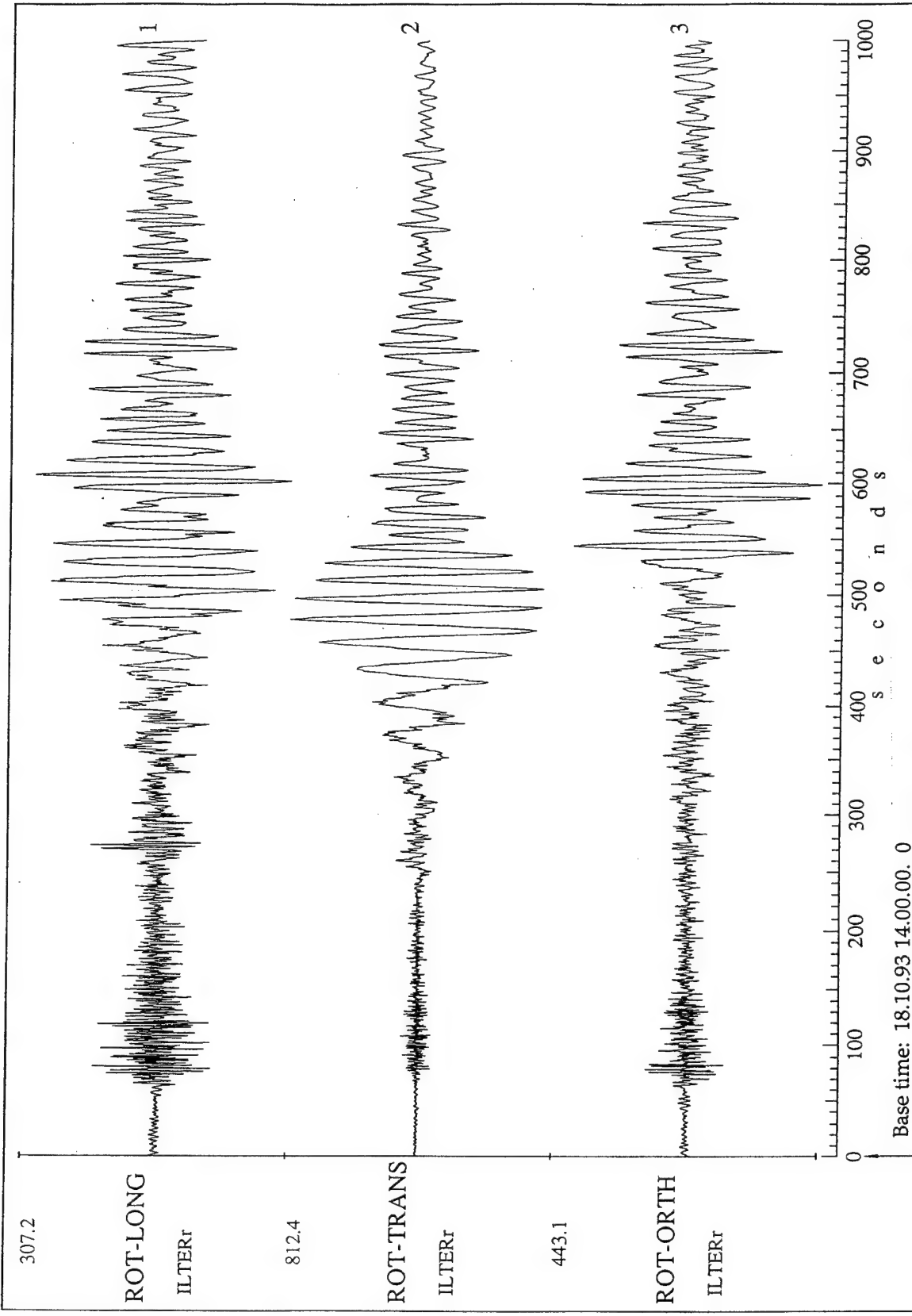


Fig. 38. 3-component seismogram of central Geyocha sensor, rotated in longitudinal, transverse and orthogonal directions.

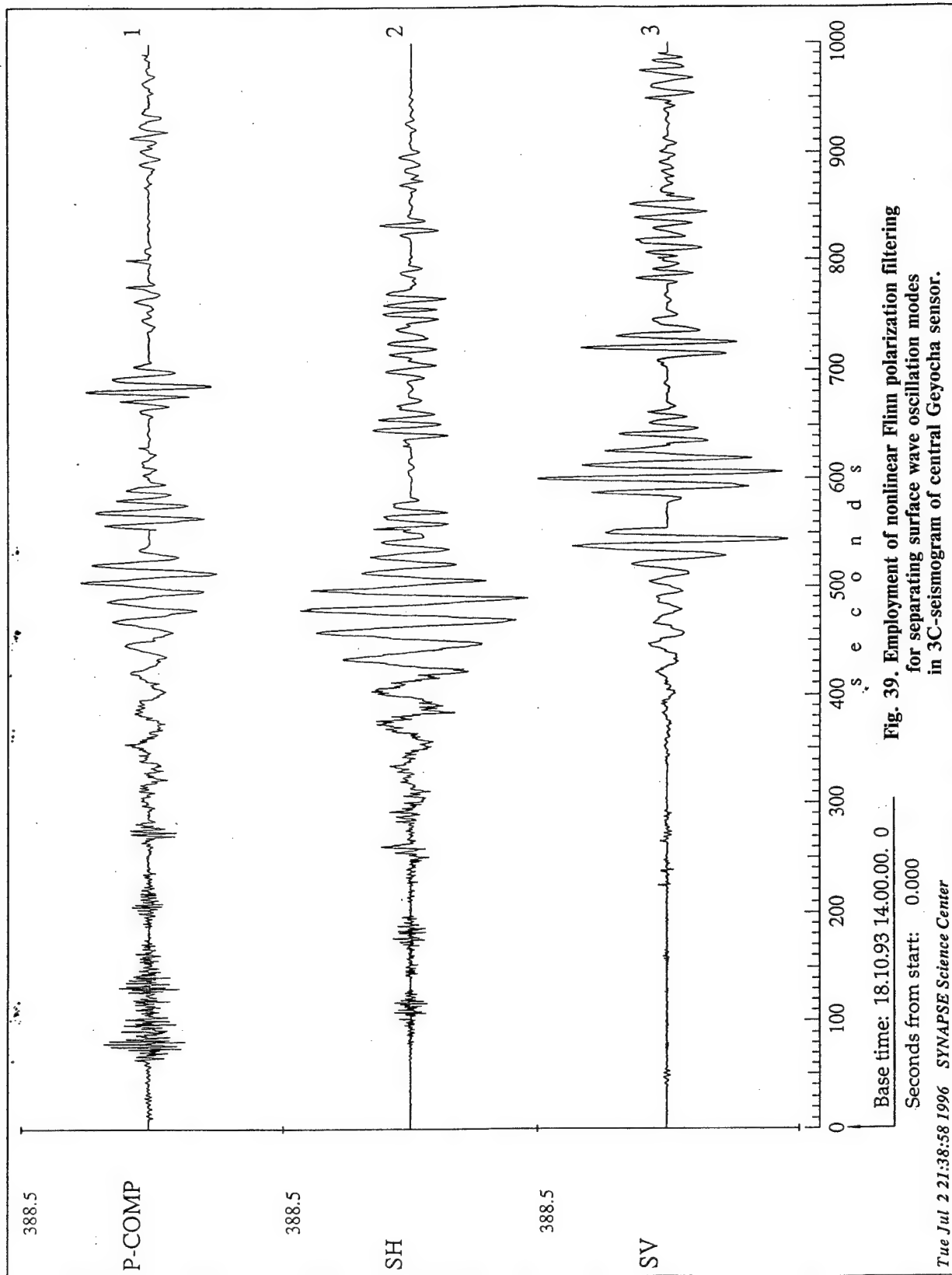


Fig. 39. Employment of nonlinear Flinn polarization filtering for separating surface wave oscillation modes in 3C-seismogram of central Geyocha sensor.

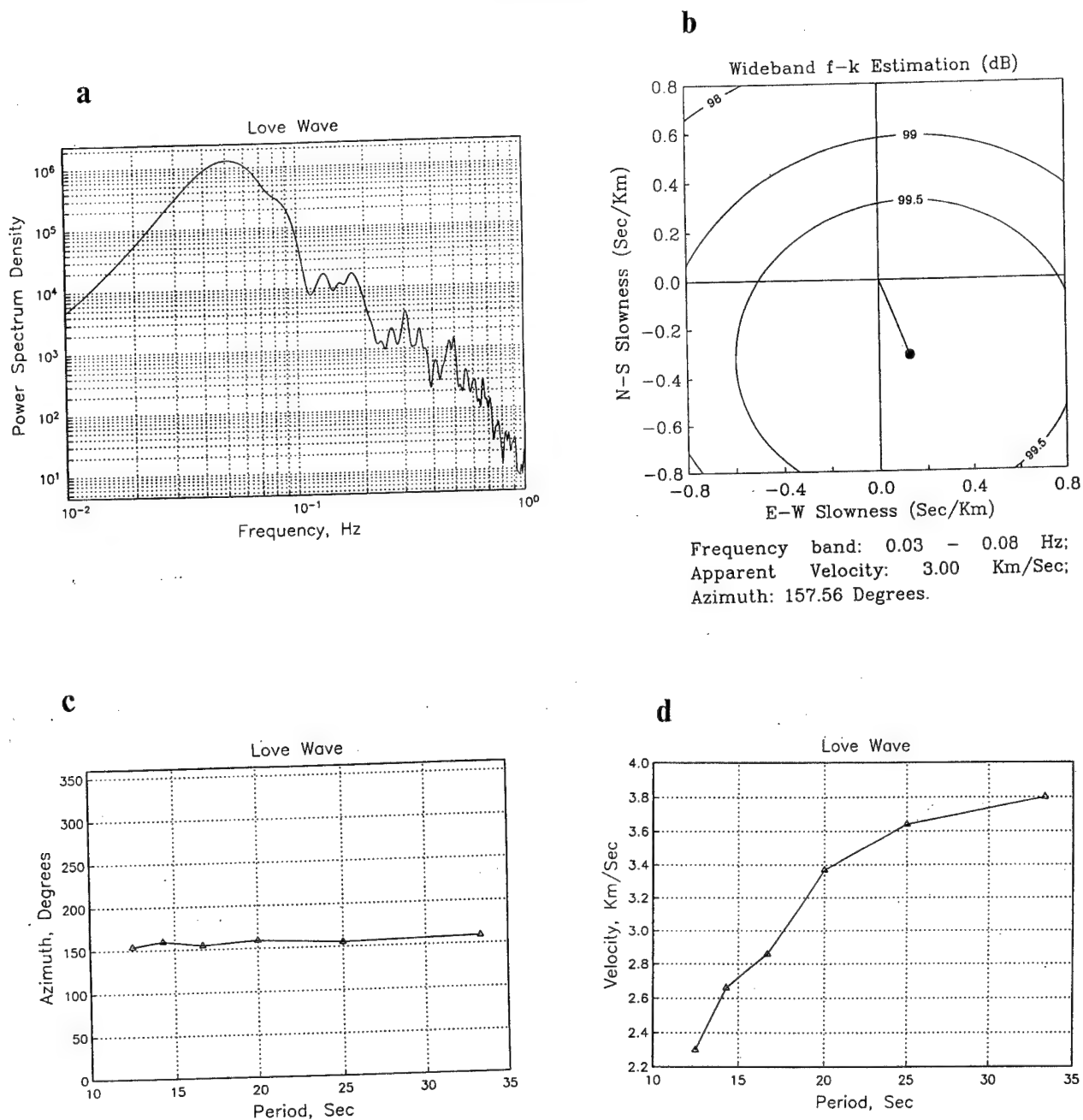
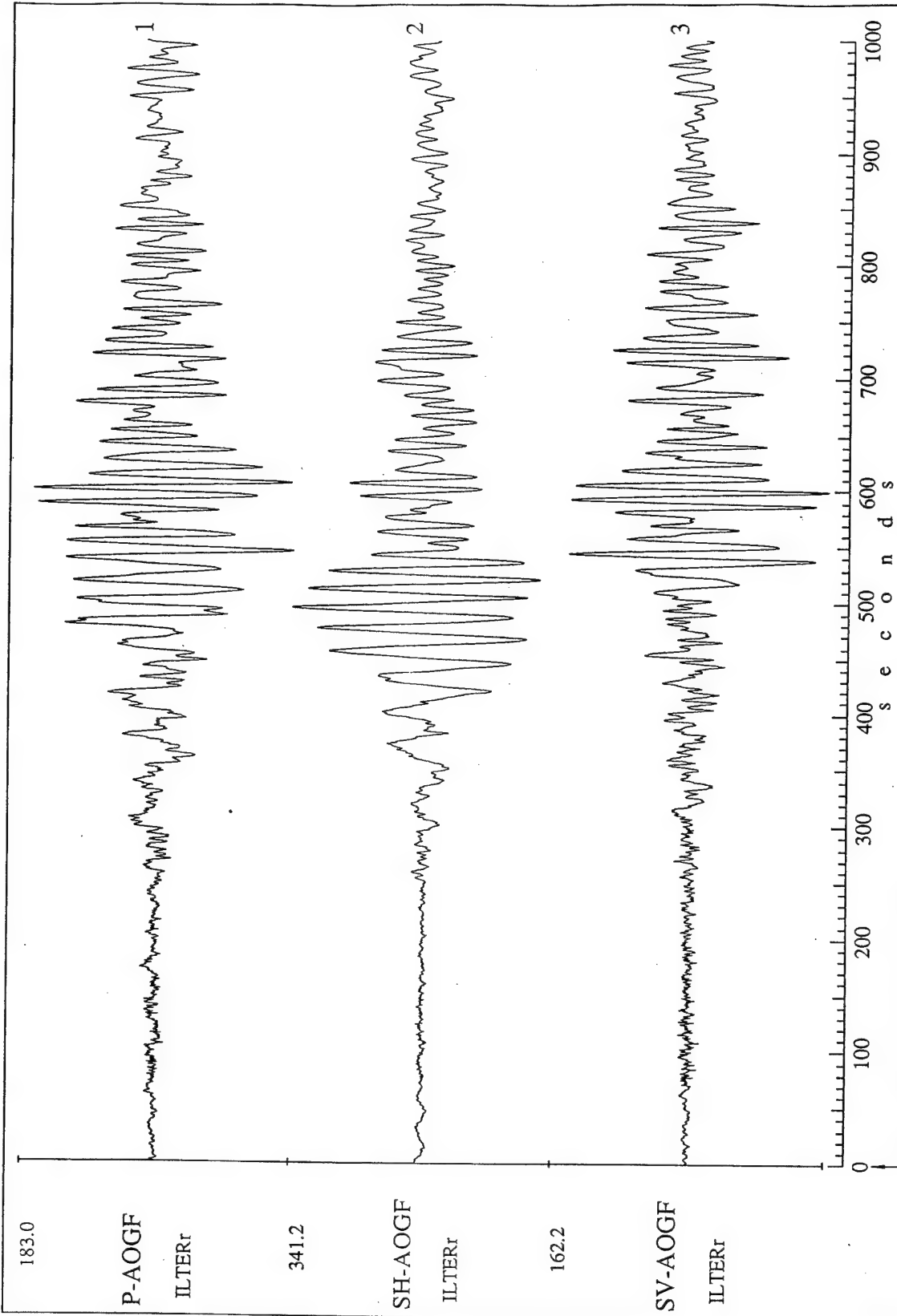


Fig. 40. Study of Love wave spectral-velocity features.

- a) Spectrum of Love wave at time interval 350-600 sec.
- b) Wide band estimation of Love wave arrival direction for frequency range (0.03-0.08)Hz, corresponding to its power peak at time interval 350-600 sec.
- c) Variations of Love wave arrival azimuth in depending on period.
- d) Variations of Love wave apparent velocity (dispersion curve) in depending on period.



Base time: 18.10.93 14.00.00. 0
Seconds from start: 0.000

Fig. 41. Broad band extracting of Love wave oscillations
in frequency band (0.01-2) Hz using
3-component array seismograms.

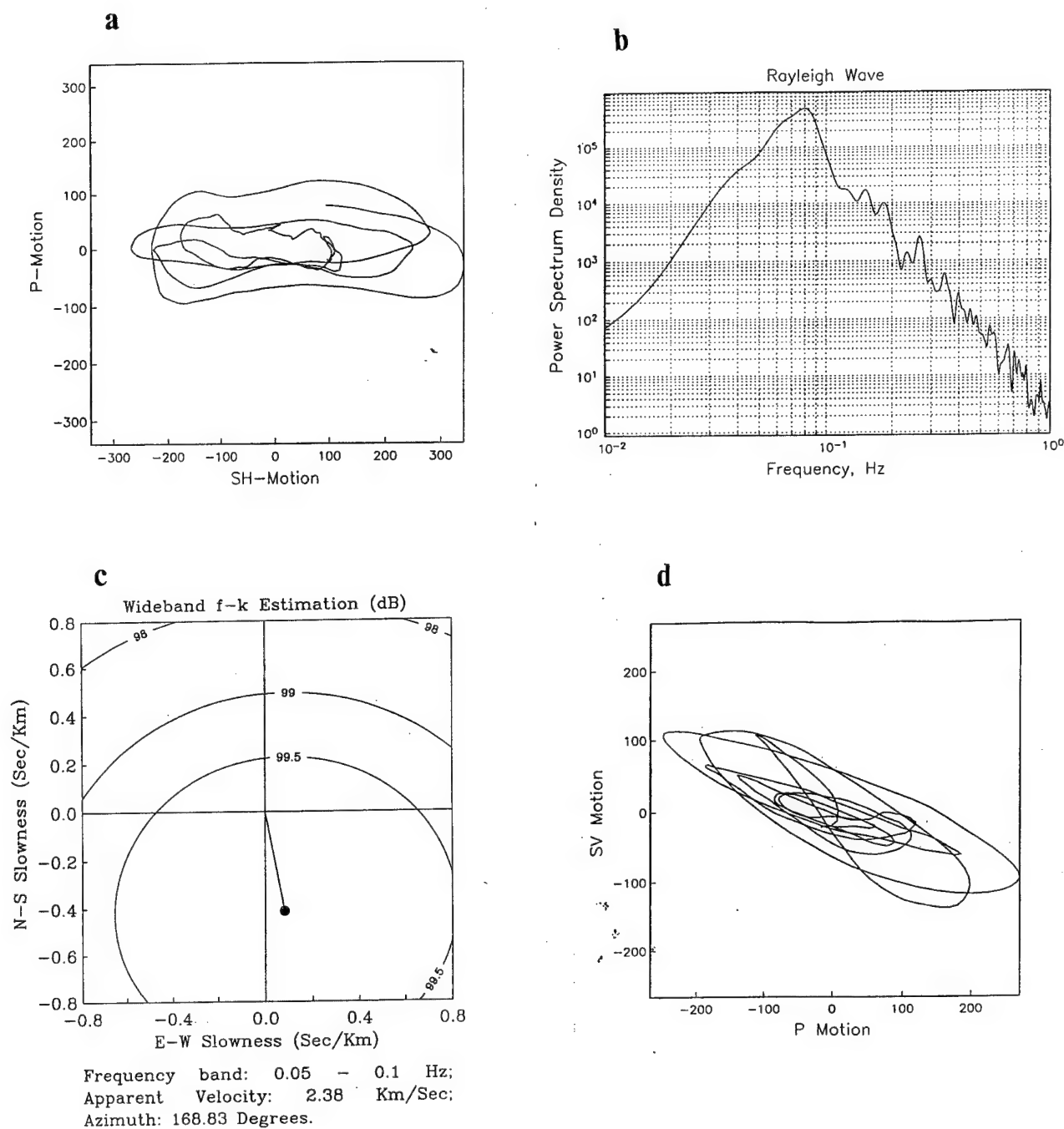


Fig. 42. Study of Love and Rayleigh wave features.

- a) Trajectory of Love wave particle motions in the ray transverse and longitudinal directions for time interval 350-500 sec. and frequency band (0.01-2) Hz.
- b) Spectrum of Rayleigh wave at time interval 400-650 sec.
- c) Wide band estimation of Rayleigh wave arrival direction for frequency band (0.05-0.1) Hz corresponding to it power peak at time interval 400-550 sec.
- d) Trajectory of Rayleigh wave particle motions in the vertical plane along the ray for time interval 500-650 sec. and frequency band (0.01-2) Hz.

4.7. Detection and parameter estimation of explosion signal obscured by coda of strong interfering earthquake using data from small aperture array

Capabilities of the adaptive statistical algorithms for analyzing data from small aperture seismic arrays (SASA) are illustrated below by algorithms application to the problem of detection and parameter estimation of a so called "hidden explosion" seismic signal. The SNDA system with its functional and operational facilities provided the convenient framework for the automated analysis of SASA data in this illustration.

The possible scenario of avoiding a Comprehensive Test Ban Treaty is to perform secret nuclear test by triggering a nuclear device with the help of seismic signal from a rather strong earthquake. In this case the explosion wave phases are obscured by coda waves of the earthquake. Latter typically are much stronger than seismic noise at the observational sites of monitoring network and often do not allow to detect the explosion signal using data from single seismic station. Nevertheless, current estimating the noise field statistical feature by a SASA and processing SASA recordings by the statistically optimal algorithms provides a chance of reliable CTBT monitoring even in conditions of implementing the described avoiding scenario .

Fig.7.1-7.3 illustrates results of application of the adaptive statistical processing methods to the "hidden explosion" problem. In this study we used multichannel seismograms from underground nuclear test at Novaya Zemlya site (24 Oct. 1990) and earthquake in Hindu Kush (25 Oct. 1990) registered by NORESS. The simulation a mixture of the NORESS seismograms from the above events to provide a "hidden explosion" signal obscured by an earthquake coda and further seismogram processing for the explosion signal detection and parameter estimation were made with the help of special SNDA script, comprising a variety of the SNDA stack commands and adaptive statistical procedures.

Fig.7.1.a shows P-wave seismogram from Novaya Zemlya explosion (NZE) (trace (1)) and P-wave with coda wave seismogram from Hindu Kush earthquake (HKE) recorded by the central NORESS sensor. The seismograms were filtered in the frequency band (0.5-5)Hz, resampled, shifted in time and scaled by the SNDA stack commands. The simulated "hidden explosion's" 25-channel NORESS data are displayed in Fig.7.1.b. This mixture of real NZE and HKE NORESS seismograms contains the NZE P-wave obscured by the HKE coda with the RMS SNR=0.5 and the onset time at 23 sec later the HKE P-wave arrival. This data is the raw material for the succeeded analysis. Note that the explosion signal is not recognizable in this seismogram mixture du to similarity of amplitude and frequency contents of the NZE P-waves and HKE coda waves.

Fig. 7.1.c demonstrates the detecting of NZE P-wave on the background of HKE coda by the adaptive statistically optimal detector (ASOD) [8,11,12]. The detection procedure is

applied to the output of the beam steered to NZ site (trace (3)). The output of the same beamforming procedure applied to the "pure" HKE seismograms is shown at the trace (4) to compare it with the trace (3). One can see that conventional beamforming does not suppress the HKE coda waves sufficiently enough to provide the reliable signal detecting by the standard STA/LTA detector. At the same time trace (2), containing the ASOD time series demonstrates the presence of strong peak from NZE P-wave. This peak significantly exceeds the ASOD fluctuations caused by HKE coda wave oscillations. Triggering of the trace (2) with the help of the automatically chosen threshold (equal to the doubled root mean square value of the total trace) allows to detect reliably the NZE P-wave and to chose the appropriate time interval (containing suspected "hidden explosion" signal) as the object for succeeded thorough analysis (trace (1)).

Fig.7.1.d illustrates capability of the adaptive group filtering (AOGF) algorithm for extracting of waveform of a weak seismic phase obscured by coda waves. The HKE coda is a strongly coherent one that yields in insufficient suppression capability of the conventional beamforming in this case (trace (3)). At the same time, just the strong HKE coda coherence allows the AOGF procedure to gain the effective coda wave suppression that is seen in the AOGF output trace (3). Trace (1) shows the output of AOGF applied to the "pure" NZE seismograms (to compare it with the trace (3)). One can see that the waveform of NZE P-wave is reproduced by the AOGF rather accurately. Note, that adaptation of AOGF algorithm was made using the NZE+HKE seismogram mixture at the time intervals (0-22) sec and (35-60) sec., i.e. before and after the interval containing the NZE P-wave. These adaptation intervals were automatically chosen in result of detection procedure described.

In Fig.7.2.a one can see the output traces of the AOGF procedure applied to the "pure" NZE and to the mixture of NZE+HKE seismograms. Superposition of these traces by the SNDA graphic means (Fig.7.2b) allows to assess the distortions of NZE P-waveform which are produced by this waveform extracting from the HKE coda waves (note that it was rather difficult case where initial SNR did not exceed 0.5).

Fig.7.2.c illustrates the estimation of NZE P-wave onset time with the help of maximum likelihood algorithm [8,11,12] applied to the AOGF output (to trace (3) in Fig. 7.1.d). Note, that this algorithm is realized in the SNDA in two forms: as the stack command (used mainly for scripts) and as the interactive graphic command.

In Fig.7.2.d the power spectra of beamforming and AOGF outputs are shown. They are calculated for the time interval containing the NZE P-wave. The figure demonstrates the small distinction the spectrum of extracted NZE P-waveform (after AOGF) from the spectrum of initial NZE P-waveform. At the same time, due to small SNR=0.5 the beam output does not

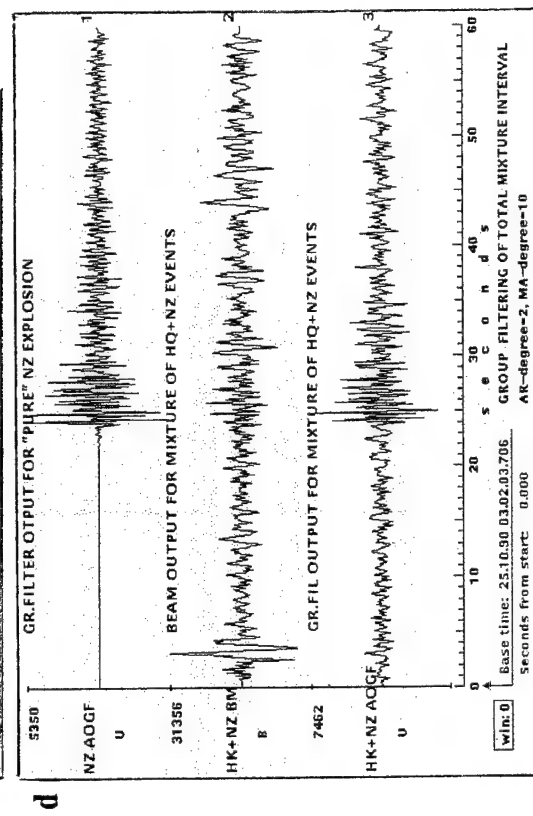
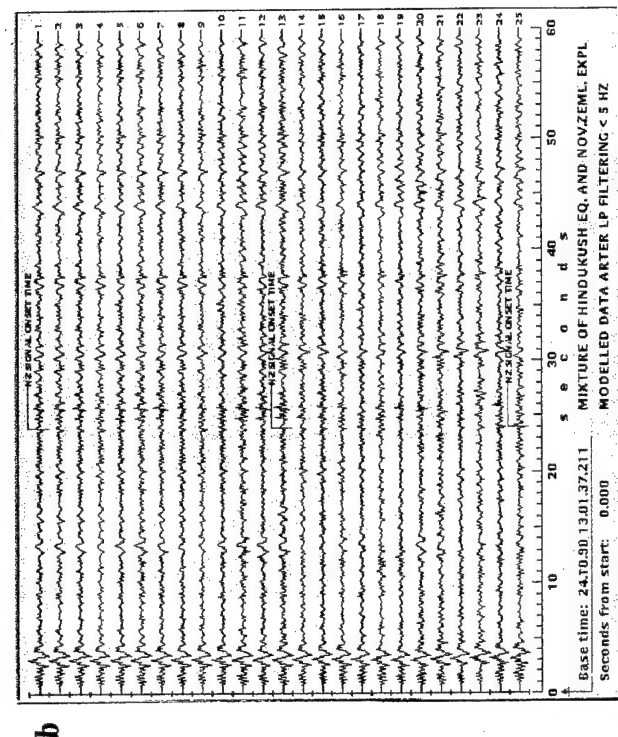
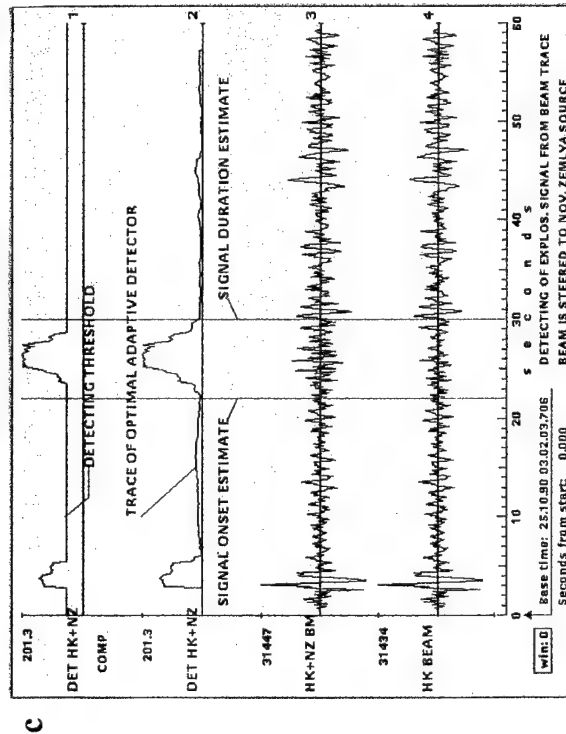
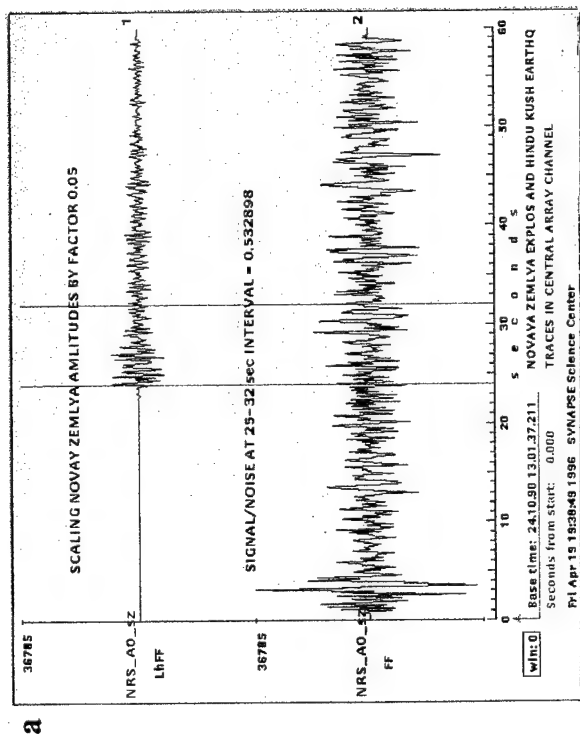


Fig. 7.1. a, b) Simulating of signal + noise mixture with SNR=0.5 using real NORESS seismograms. c) Detecting of weak explosion signal by statistically optimal detector. d) Extracting of explosion waveform by beam and AOGF

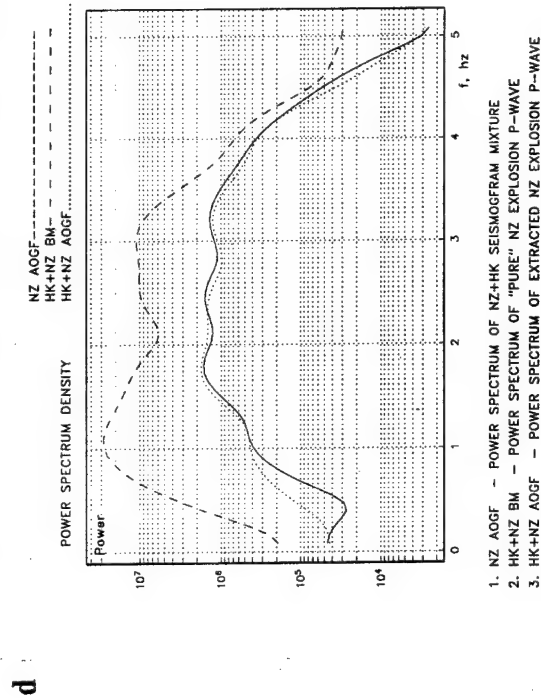
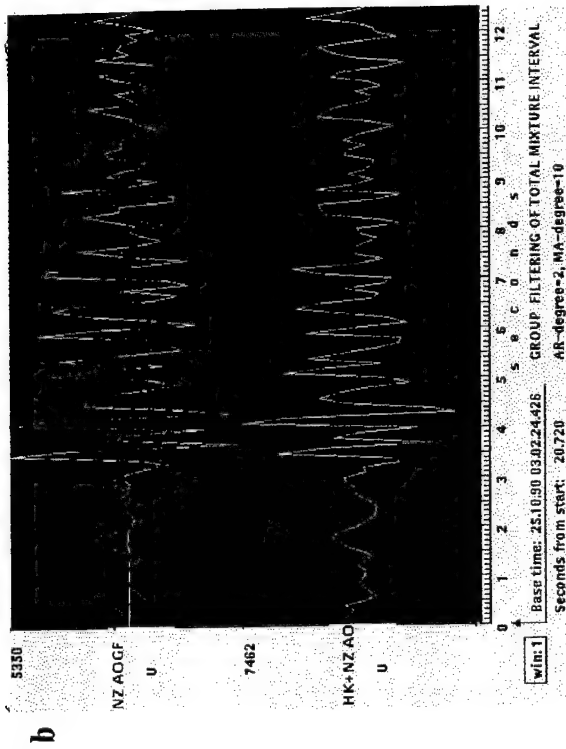
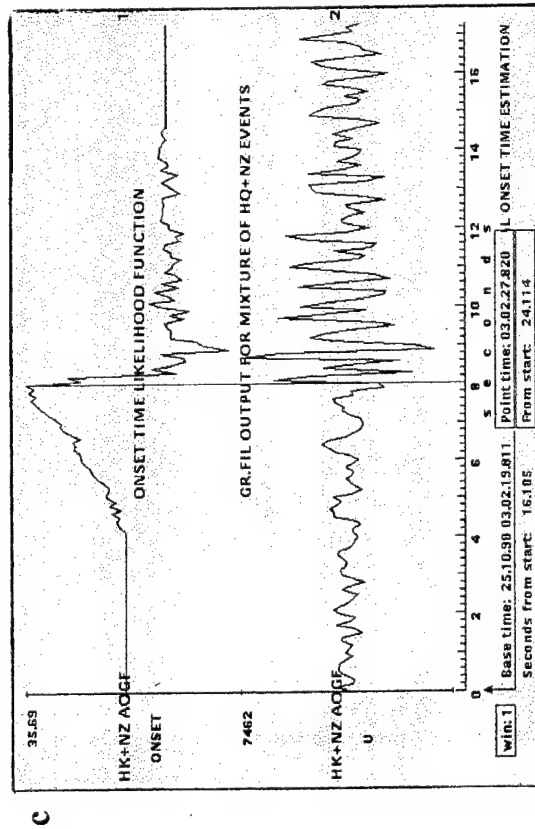
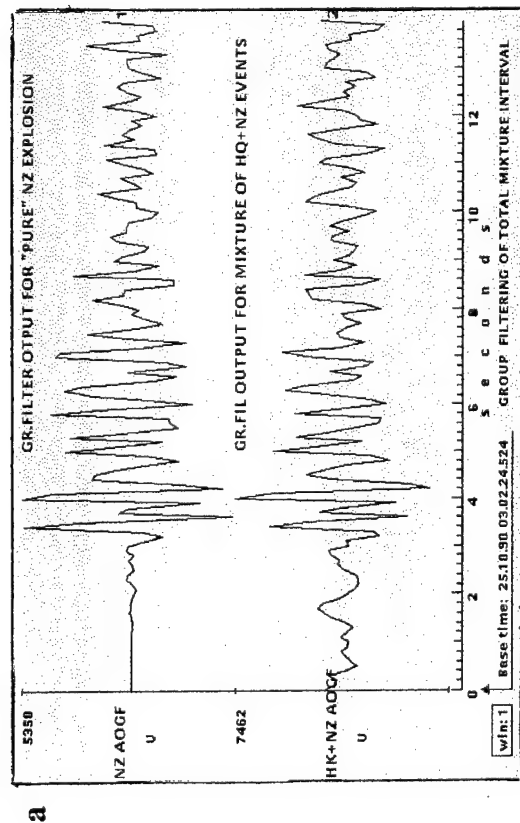


Fig.7.2. a, b) Comparison of waveforms for "pure" and extracted from noise explosion signals. c) Explosion onset time estimation by Maximum Likelihood algorithm. d) Comparison of spectra of "pure" explosion signal with beam and AOGF outputs.

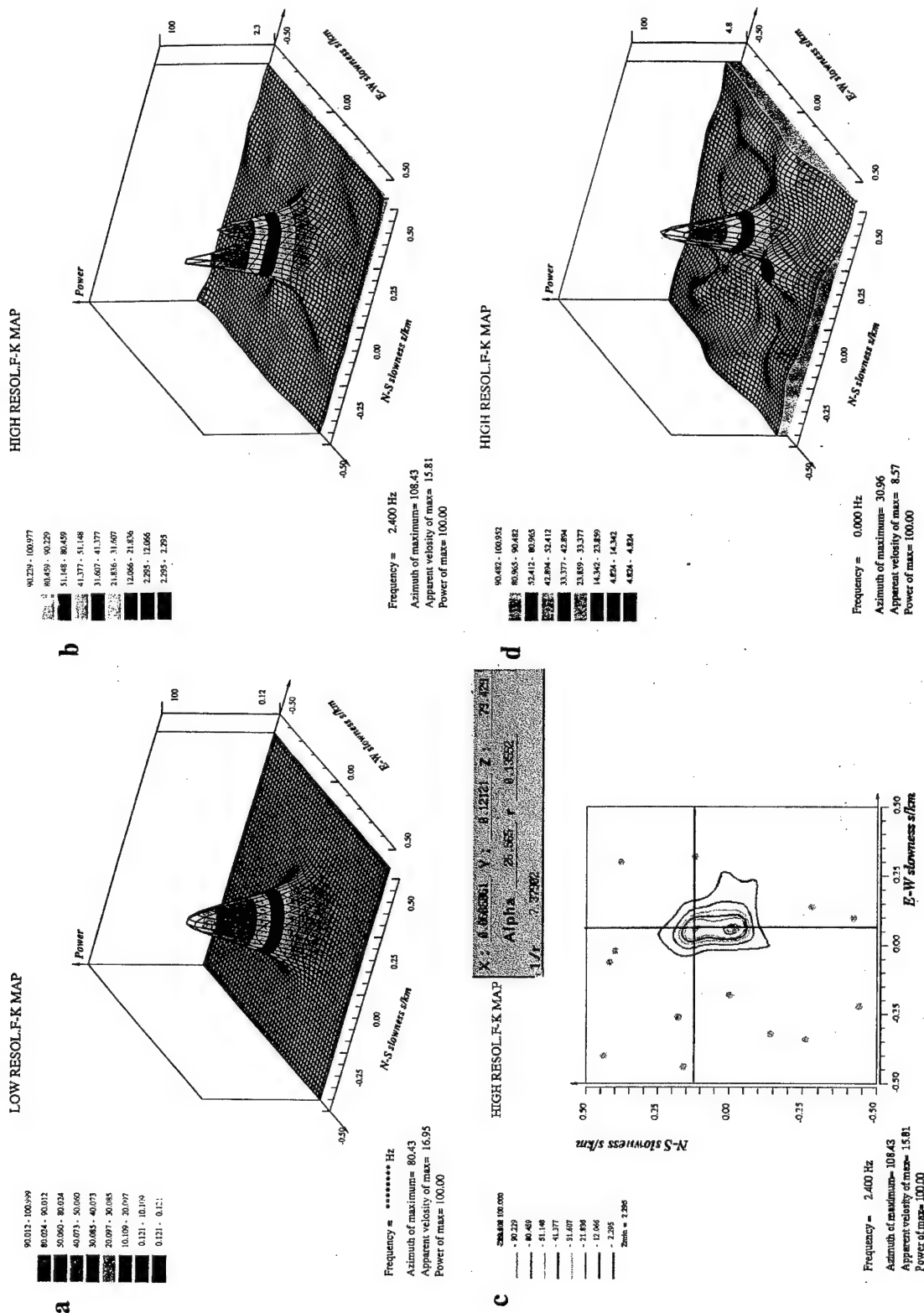


Fig. 7.3. Estimation of explosion wave arrival parameters on background of earthquake coda (SNR=0.5; real parameters are: AZ=32.9°, V_{ap}=10.4 km/sec. a) Wide band F-K map for the wave mixture. b, c) High resolution F-K map for the wave mixture. Explosion parameter estimates are: AZ=26.6°, V_{ap}=7.4. d) Adaptive F-K map for the wave mixture. Explosion

allow to catch any impression about the NZE P-wave spectrum, that makes it impossible to implement the standard source identification procedures.

Fig. 7.3 presents the results of arrival direction estimation for the suspicious wave detected in the HKE coda. This estimation is the very difficult task and was performed in our study by means of various F-K analysis algorithms. (Let us emphasize that evaluation of seismic wave arrival direction altogether with estimation of P and S phase onset times provides the information needed for the location of event epicenter based on data from a single SASA). Fig. 7.3.a displays the spatial spectrum calculated by the conventional broad band F-K analysis algorithm [12,13] using the NZE+HKE seismogram mixture at time interval containing NZE P-wave. One can see that the spectrum maximum, which is the estimate of wave arrival direction, only slightly differs from the real arrival direction parameters of HKE P-wave (azimuth= 102.4° and apparent velocity= 14.8 km/sec.). Application to the HKE+NZE seismogram mixture of the high resolution F-K analysis (the modified Capon algorithm with the estimation of array data matrix power spectrum by the multidimensional autoregressive-moving average modeling [12,13]) allows to detect at the time interval being analyzed the two waves (Fig.7.b). The global maximum of the F-K map testifies to the presence of HKE P-wave. Measuring the second maximum location (made with graphic interactive SNDA tool, Fig.7.c) gives the estimates for the second wave arrival parameters equal to: azimuth= 26.5° , apparent velocity= 7.4 km/sec. These values are rather far from the real NZE P-wave arrival parameters equal to: azimuth= 32.9° , apparent velocity= 10.4 km/sec.

At last, the advanced algorithm was implemented for the accurate estimation of NZE P-wave arrival direction from the NZE+HKE seismogram mixture. This is the adaptive Maximum Likelihood F-K algorithm for direction estimation of a signal plane wave arriving to a SASA site together with coherent interfering waves. The algorithm is described in Section 3.3. In our case the HK coda wave spatial characteristics can be analyzed independently at the time intervals which does not contain the signal wave, and the adaptation of ML F-K algorithm was made using this observations. The employment of algorithm resulted in the spatial spectrum estimate shown in Fig.7.3.d. The F-K map contains the single strong peak with the maximum located at the point with azimuth= 31.0° and apparent velocity= 8.6 km/sec. These values are more close to the real arrival parameters of the NZE P-wave than those obtained by the high resolution F-K analysis. Note also that the high resolution F-K analysis demanded in our case the rather thin fitting of the program parameters to obtain the impressive map depicted in Fig.7.b. At the same time the adaptive ML F-K algorithm is much more robust in applications to broad band array seismograms.

4.8. References

1. Der, Z.A., Baumgardt, D.R., Shumway, R.H., 1993, The nature of particle motion in regional seismograms and its utilization for phase identification, *Geophys.J.Int.*, vol.115, pp.1012-1024.
2. Kushnir, A.F., Fyen, F., Kvarna, T., 1991, Studying of multichannel statistical data processing algorithms in the framework of the NORSAR event processing program package, *Semiannual Technical Summary, NORSAR Sci.Rep. 2-90/91, Kjeller, Norway*, pp.82-103.
3. Kvarna, T., 1993, Intelligent post-processing of seismic events. Part 2: Accurate determination of phase arrival times using autoregressive likelihood estimation, *Semiannual Technical Summary, NORSAR Sci.Rep. 2-92/93, Kjeller, Norway*, pp.68-92.
4. Kvarna, T., 1993, A generic algorithm for accurate determination of P-phase arrival times, *Semiannual Technical Summary, NORSAR Sci.Rep. 2-93/94, Kjeller, Norway*, pp.98-108.
5. Mykkeltveit, S., Ringdal, F., Kvarna, T., Alewin, R., 1990, Application of regional arrays in seismic verification research, *Bull. Seism. Soc. Am.*, vol.80, pp.1777-1800.
6. Pavlis, G., Al-Shukri, H., Mahdi, H., Repin, D., 1994, JPS arrays and networks in Central Asia, *IRIS Newsletters*, vol.XIII, pp.9-13.
7. Pavlis, G., Mahdi, H., Vernon, F.L., 1994, Surface wave propagation in Central Asia: Observations of scattering and multipathing with the Kyrgyz broadband array, *Proc. of the 16th Annual Seismic Research Symposium*, pp.291-297.
8. Pisarenko, V.F., Kushnir, A.F., Savin, I.V., 1987, Statistical adaptive algorithms for estimations of onset moments of seismic phases, *Phys. Earth Planet. Inter.*, vol.47, pp.888-900.
9. Prototype arrays incorporate new technology and reduce costs, 1994, *The Monitor*, vol.4, pp.8-11.
10. Sorrels, G.G., 1971, A preliminary investigation into the relationship between long-period seismic noise and local fluctuations in the atmospheric pressure field, *Geophys. J.*, vol.26, pp.71-82.
11. Kushnir, A.F., V.M. Lapshin, V.I. Pinsky, and J. Fyen (1990) Statistically optimal event detection using small array data, *Bull. Seism. Soc. Am.*, 80, 1934-1947.
12. Kushnir A.F. (1995) Algorithms for adaptive statistical processing of seismic array data, *E.S. Husebye and A. Dainty (eds), Monitoring a Comprehensive Test Ban Treaty, Kluwer Academic Publishers, Dordrecht / Boston / London*, 565-586.
13. Kushnir A.F. (ed), L.M. Haikin, V.M. Lapshin, B.M. Shoubik, E.V. Troitsky (1995) Seismic monitoring with small aperture arrays under strong noise conditions: algorithms, technique, system design and experimental data processing. *Scientific report on AFOSR Special Project SPC-94-4039*.

CONTENT

5.	FURTHER DEVELOPMENT OF THE SNDA SYSTEM	2
5.1.	New high level language	2
5.2.	Surfer	6
5.3.	Map	7
5.4.	Cluster	8
5.5.	Other developments	10

5. FURTHER DEVELOPMENT OF THE SNDA SYSTEM

Within the framework of this study the problem oriented computer shell SNDA was significantly advanced to provide the high level facilities for the scientific investigations involving processing a large amount of experimental data. A high level object oriented **language** was developed to support the full and complete processing the data. The three new original color graphic packages were created and incorporated into SNDA: "**Surfer**" - for plotting and graphic analysis the different spatial diagrams and other surfaces, "**Map**" - for depicting and analysis of mutual dispositions of local seismic network stations and seismic events sources on a geographic background and "**Cluster**" - for graphic support of the cluster analysis in procedures of seismic events discriminating. Besides the set of Stack commands was significantly expanded and some of them were improved with account of SNDA operation experience accumulated at SYNAPSE Science Center and other institutes for the last years.

5.1. New high level language

The SNDA job control language (JCL) is developed to facilitate an implementation of SNDA Stack commands and problem oriented data processing procedures (SA-procedures). JCL is a high level problem oriented object language (such as well known MATLAB language). The difference is in the entity of objects. Here we deal with seismograms and other time series, spectra, matrices, studying their structures and properties in the course of processing procedures. Being intended for mass data processing in seismology the language meets demands of the conventional structure programming. He possesses the well known syntax constructions, which allows to compose the clear and plain (without goto) programs. As the result the program robustness, flexibility, and modification simplicity is guaranteed. JCL provides a user with possibilities to perform various graphic interactive actions during the program execution after commands **plot** and **pause**. This extremely facilitates comprehensive analysis of the great volume of experimental data.

The main JCL constructions are:

```
block ... endblock
perform
when ... elseif ... elseif ... else endwhen
for ... endfor
```

Statements **block ... endblock** together with operator **perform** allows to separate some completed logical unit into the isolated part of program.

Construction **when ... elseif ... elseif ... else ... endwhen** provides the choice of some variant from several ones in dependent of condition.

Construction **for ... endfor** provides organizing the cycles.

Below is an example of the program written in SNDA JCL.

```
. int i,j
. char tx[10], time [12]
. perform initial
. for (tx = "NRJ",i=0; i<28 ; i=i+1 )
.   for (time ="12.01", j<3 ; j=j+1 )
.     perform processing
.     perform savereslt
.   endfor
. endfor
. perform estimate
. return # main program

. block initial
... # operators
. endblock

. block processing
.   float aaa,bb,cc
.   int ee,ff,gg
.   readcss30 /detseis/seis/israel/data/exposions/9410031539
.   filterC (3-7) 0.1 30 0.12 4
.   powspec (3-7) 100 5
.   plotspec 5 -AOGF -expl.cmnt
... # other operators
. endblock

. block savereslt
.   savevar plot/kush/parms.bb a c k l
.   savesnd plot/kush/values.bb sndi1 sndi2 sndf10 sndf1 sndc7
. endblock
. block estimate
... # operators
. endblock
```

The programs written in the SNDA language, (in contrast to problem oriented C or FORTRAN procedures) we refer as **script**. The structure operators are the backbone of any script while the specific processing functions are performed by the language commands classified onto three groups: SA-procedures, stack commands, and control statements. Note that even a sophisticated SA-procedure in terms of the SNDA language stand out as a simple JCL command. This is a main peculiarity of the object languages.

The control statements mainly operate with the Black Board Variables (BB-variables). The latter allow to control a data analysis by modifying parameters of procedures (or even algorithms at whole) in depend on intermediate processing results. This possibility is realized by the implementation of the BB-variables in the Stack commands (with predecessor "&") instead of numerical or character operands. The current values of BB-variables substitute the operands (or arbitrary parts of text) in command. Thus they allow to manage a communication between SA-procedures during a script execution. By making computational cycles and choice operators dependent on current values of BB-variables a user can change a sequence of program processing steps (e.g. to execute or skip any SA procedure or Stack command in accordance with results of previous steps).

The JCL control statements serves for declaration of BB-variables, their initialization and modification as well as for change an order of execution of SNDA commands in dependent on BB-variables values. The following JCL control statements exist now in the SNDA: **BBV declaration**, **BBV assignment**, **BBV print** and **save**, statement **label**, conditional and unconditional **goto**. Besides there exists a possibility of interactive graphic assignment of BB-variables during measuring of time and amplitude trace characteristics in main graphic window (see 6.6, 6.7 of the appendix). Unlike the Stack commands and SA-procedures, JCL Control Statements must have the "."(dot) character at the beginning of the Statement string.

The one-dimensional arrays of the float, integer and character BB-variables are supported in the JCL. They are also accessible within SA-procedure by the special system call. The following conventional algebraic functions may be used in expressions for assignment of BB-variables:

```
trigonometric: sin, cos, tan, asin, acos, atan;
hyperbolic:    sinh, cosh, tanh, asinh, acosh, atanh;
other:         log (natural), exp, sqrt.
```

Below an example of such expression is shown.

```
. r = 1- sin ((m [m [a* sqrt((c-b)**2)] - 6.77] -5.77)/2 *pi/6 )
```

A length of any script Statement must not exceed 125 characters. Statement operands are to be separated by the blanks. Several sequential blanks are considered as the one blank. Empty lines can be set among script statements for the better script fashioning. Any statement, starting with the "#" (hash mark) character, is considered as a comment and is skipped during a script execution.

After a script is started the SNDA performs its preprocessing to examine the script structure and convert it into the sequence of primitive statement (with **goto** operators). As a result a new intermediate script version is composed and saved in current directory *snda/sun4*, which composed of primitive operators. The new name of this file is ended with **.mid**. Then SNDA performs the syntax checking of the commands, verification of variable specifications and the validation of correctness of their applications. All needed diagnostic messages are displayed on command window. If the script text is correct the direct access file is mapped into computer memory and executed. This concept provides multiple jumps to labels inside the script without time losses.

Before being executed, every script statement with its number is displayed on the console. The statement **echo** enables to protocol the desirable BB-variables in the process of script execution.

If the **pause** (or **plot**) command is met the script execution is halted (for the **plot** case - after displaying the Stack traces in the SNDA graphic window). To resume execution a user has to click the **GO** button in the Stack command window. While script is halted a user may perform some interactive actions: measuring of trace characteristics in the main graphic window and after that to modify BB-variables. This allows to manage the changes in the further script execution.

Detail description of the language is presented in the Section 5 of the appendix.

5.2. Surfer

Surfer is a graphic program package for plotting the images of functions of two-dimensional variable in forms of different surfaces and maps. The program creates a special color graphic window for plotting the function images. The latter may be a three or two dimensional. The two-dimensional image may have two types: in the form of isolines of levels, drawn by the different colors (contour image) and in the form of topographic map with a gradual transformation of wide spectrum colors (map image).

Any plot is created by the executable module "surfer", that reads a control file (as the well known UNIX packages "contour", "plotxy", and "gnuplot" do). A name of the control file is a single (and obligatory) argument of the "surfer" command. A structure of the control file is described below.

After the **surfer** starts a graphic window with a color 3-dimensional figure emerges. A user may push the **Opt** button to prescribe some additional parameters of the image (see below) and then push the **3d** button (or right mouse button) to replot the image. A user may also rotate figure around vertical and horizontal axes in the range $(-90^\circ, +90^\circ)$ - by mowing the middle mouse button or turn the image back by setting an appropriate option. In order to get a contour image a user has to push **Contour** button, while to get a map image - push the **Topo** button. After plotting the color image a user may create a PostScript file and view its image on the screen. For this purpose he has to push the **Create PS** button (the name of PostScript file may be also prescribed in the corresponding panel string), after that a new window is created with a PostScript (color or monochrome) image. The PostScript file can be printer using the standard UNIX command.

A user may currently correct the surfer control and data files without exit the program **surfer**. He may also change the names of both files and then push the **Read** button. A new control file and corresponding data-file will be read. After renewing the data a user may continue the graphic analysis of the different function images.

A user may fit a color palette of the objects on the screen (3D-figure, contour or topo maps) in accordance with his own taste. For this purpose he has to click the

Palette button The changes of palette, made by the user, are retained to be valid for the PostScript image too.

A user may exchange the X,Y axes or invert the image along the axis.

A user may cut the desirable horizontal layer of the 3D image. The clipped layer is automatically expanded up to whole range of Z-axis. This mean enables one to make the thorough graphic investigation of some rather thin layer in details, if the ordinary image of the whole figure does not display a detailed configuration of the layer of interest. The mode providing this option is set by the **Cut** button.

A user may graphically measure the values of arguments as well as the function in any point of surface. Measuring of point coordinates is provided in the **Contour** and **Topo** modes This allows for example to provide the graphic analysis of the surface near its different local extremums. The mode for coordinate measuring is set by the **Measure** button.

In the **Contour** or **Topo** mode there exists a possibility to make a zooming. So the little piece of surface may be expanded up to the whole image box and total color palette will be used in the limits of chosen figure part. This enables to achieve the more high precision of coordinates measurement. The standard X-window resize function is realized, so a user may significantly enlarge the image to provide the detailed graphic investigation of some local region of interest. At last a user has an opportunity to compose a collection of the images on one page (in the single PostScript file) in order to prepare the illustrations for reports or scientific papers. Detailed description of the Surfer is presented in the Section 7 of the appendix.

5.3. Map

The package is intended for the graphic interactive analysis of the disposition of the local network stations and possible regional seismic event on the geographic background. The two coordinate system are used simultaneously for the image: Geographic and plane Gauss-Kruger one. The center of latter is supposed to be moved from equator to the geometrical center of the region. To convert the Geographic coordinates to the Gauss-Kruger system and back the approximate polynomials are used. The distortions of graphic distance measurements of points on the plane depend on the point separation from the central meridian of selected zone.

They are close to zero when measuring is made along the meridian and rise hundreds meters close to borders of a 6-grades zone. The further expansion of the zone causes the rather large distortions.

Nevertheless the package provides rather exact measurements of a distance between two arbitrary points over the ellipsoid arc on the earth surface (deviation is less then 0.1 m.) regardless of positions and separation of these two points.

The package provides the following facilities:

- selection of the needed stations from the total station list using special characters masks, applied to the station labels;
- plotting the selected station network and selected set of event epicenters on the geographic background forming the file with the station selected list;
- reducing the scale of the image in order to plot the rather large geographical area around the station network to include the event sources under interest.;
- zooming the selected local zone to display the more detailed configuration of the station and event groups;
- graphic interactive measurement of the selected point coordinates as well the distances between two arbitrary points using one of the two measuring modes: over the plane and over the ellipsoid arc;
- creating the file with the network station epicentral distances relative to chosen event (for further sorting the multichannel seismogram);
- drawing the different geographic objects on the map: coast lines, states boundaries, rivers and so on.
- creating the PostScript file to be printed out onto the laser printer.

Detailed description of the Map package is presented in the Section 8 of the Appendix.

5.4. Cluster

Cluster is a package for graphical support of the source identification procedures. It provides imaging of the numerical event feature vectors in the 3-dimensional coordinate space. This enables user to study interactively the discrimination capabilities of the used discrimination features.

The learning events of every class have to be contained in the separate files in which every event is to be represented by the one feature vector, composing the row of values in integer, float or exponential format. Thus the file may be regarded as matrix of N row and M columns, where N - is amount of events in this class and M - is a total number of features (the same for all events). The unknown events to be attributed to one of the classes must be also in the separate file of the same structure. The total number of features must be more or equal to 3.

The System creates a special color graphic window with an image. The plot is created by the executable module **cluster**, which read a control file. A name of the control file is a single (and obligatory) argument of the **cluster** command.

After the **cluster** starts a color graphic window arises with 3-dimensional box with color point clusters. Each event is depicted as a point, which symbol and color correspond to the appropriate class. A user may push the **List** button to view the list of events. Then he may rotate a box by the moving middle mouse button to achieve a maximum separation of the event clusters for known classes. The position of tested event point in this plot enables user to classify event, i.e. to attribute it to the one of learning clusters.

There exist two alternative ways to initiate the cluster program.

1) A user defines in control file three desirable components of feature vectors as first operands of the corresponding operators: **xlabel**, **ylabel**, **zlabel**. Here he defines also the linear or logarithm scale mode for each axis and the name of feature applied. The cluster image appears just after starting.

2) A user does not define in control file the specific numbers of desirable features. The program starts with empty graphic window without any image. The selection of desirable features is performed interactively in the special "Select features" window. To do this a user must push the **Select** button of the "cluster" main menu, after that a new window arises with the total list of features numbers

positioned in the small boxes. The user should select the desirable three numbers by the left mouse button (the boxes selected are highlighted by the red color), set an appropriate scale mode, click the corresponding choice buttons, and push the **plot** button or right mouse button. The cluster image will appear. By this interactive way a user may easily study many combinations of features to achieve a maximum separation of the event point clusters for different classes.

The cluster program recognizes both ways with the help of **labfile** operator. If **labfile** operator is present in the control file, then it is supposed to be the second way of starting. If **labfile** operator is omitted (but xlabel, ylabel, zlabel is applied), then the program chooses the first way. The standard X-window resize function is realized in the program, that allows to adjust the convenient size of the "cluster" window.

After plotting the image at the screen a user has a possibility to compose and preview a PostScript file of the image. It is made by pushing the **Form PS-file** button (the name of file may be also prescribed in corresponding panel string), a new window is created with postscript image. The Postscript file with the assigned name can be printed then using the standard UNIX tool. As in the "Surfer" package a user can compose the collection of the images on one page.

Detailed description of the Cluster package is presented in the Section 9 of the Appendix.

5.5. Other developments

5.5.1. The most important Stack trace processing commands are included to the interactive graphic toolkit to the main graphic menu of the multichannel graphic frame. The new button **GP** (Graphic processing) opens the next processing procedures: onset time estimation, direct fast Fourier transform, power and cross Spectra estimation, filtering by the different methods (see Section 6.13 of the Appendix). All Stack commands with this names are also retained.

5.5.2. The more convenient way to select channels and time window is developed in addition to the old way: a user may select channels and simultaneously set a new window in "TW-mode" by drawing a rectangle in the graphic window with the help of middle mouse button (see Section 6.5 of the Appendix). Besides Magnify mode is significantly advanced (see Section 6.9 of the Appendix).

5.5.3. Some new stack commands are added (see section 4. of the Appendix):

read/save commands: **savestack**, **readstack**, **readtab**, **read_im_pk**, **readdem**;

window handle commands: **win1** , **winmax**;

trace handle commands: **stcopy**;

trace arithmetic commands: **mult**, **addc**;

trace processing commands: **abs**, **receipr**, **sqr**, **msqr**, **sqr**, **msqrt**, **power**, **ln**, **log**, **mean**, **meansqr**, **meanabs**, **tmax**, **tmin**; **gc** (composing a new trace with cosine signal);

network trace sorting commands: **sort**, **synchro**, **episort**, **episort1**, **episort2**

displaying and plot commands: **flist**, **surfer** **map** **cluster**;

5.5.4. Some stack commands are improved, namely:

plotspec - frequency interval may be set and comments are provided;

savetab, **savepack**, **savefloat** are performed in regard to current winon.

5.5.5. The **channels**-operand for stack commands has now a more free form: it can be channel numbers or intervals of numbers, separated by the blanks or commas, the total string to be inserted into the parenthesis (see Section 4.1. of the Appendix), for example:

(1,3 5 10-13 20-23 25)

5.5.6. The installation of the whole SNDA tree at a user computer is simplified and provided by the just one command "tar -xvf".

6. DESCRIPTION OF PROGRAMS FOR 3-COMPONENT ARRAY DATA PROCESSING

CONTENTS

6.1. Program "MODELS" Modeling of 3-component array seismograms...	1
6.2. Program "POL" Polarization filtering of data from single 3-component station by Flinn method	7
6.3. Program "POLCFLTS" Vector polarization filtering of multichannel data	11
6.4. Program "ARMAFS" Estimating of inverse matrix power spectral density of multichannel data by ARMA modeling	14
6.5. Program "GRFILTFES" Optimal Wiener group filtering of 3-component array data for different types of wave polarization	18
6.6. Program "GRFLTFCS" Extraction of waveforms of differently polarized seismic phases using 3-component array data with the help of optimal Wiener group filtering	25
6.7. Program "GRFLTFK" Adaptive 3-component F-K analysis	32
6.8. Program SP3C Adaptive multimode F-K analysis of 3-component array data	37

6. DESCRIPTION OF PROGRAMS FOR 3-COMPONENT ARRAY DATA PROCESSING

6.1. Program "MODELS"

Modeling of 3-component array seismograms

The program simulates multichannel seismograms at the output of 3 component (3C) array. First, let us emphasize that the program does not calculate the synthetic seismogram for some given medium model and location of a seismic source. It provides much more simple imitation of a multichannel seismogram needed for testing of algorithms and programs intended for advanced 3C array data processing. At the first step a seismic phase signal is generated with an assigned deterministic waveform or a random waveform with given power spectral density. The signal corresponds to a recording of a seismic wave phase by a 1C sensor located at the point with coordinates $(x,y,z)=(0,0,0)$ and oriented in the direction of the seismic phase oscillations. Then using this basic waveform the program calculates the phase waveforms for every sensor of a 3C array taking into account the array geometry, direction of plane seismic wave arrival and phase type: P, SH, SV, L & R.

Let X-axis be directed to the West, Y-axis - to the North and Z - along to upper perpendicular to the day surface. Assume that wave field registered is generated by a distant seismic source and thus every seismic wave phase has the plane wave front. Suppose that a body wave phase arrives to the day surface from a laterally homogeneous lower half-space and denote $\mathbf{a}=(a_x, a_y, a_z)^T$ wave-front unit directional vector, α and β - the back azimuth and incidence angle of the arrival direction and V - the wave velocity just beneath the day surface. Using this notations we have:

$$\mathbf{a}=(-\sin(\alpha)\sin(\beta), -\cos(\alpha)\sin(\beta), \cos(\beta))^T.$$

Displacements of media particles $\mathbf{u}(t, \mathbf{r})=(u_x(t, \mathbf{r}), u_y(t, \mathbf{r}), u_z(t, \mathbf{r}))^T$ in a point $\mathbf{r}=(r_x, r_y, r_z)^T$ for a given wave phase oscillations can be written as

$$\mathbf{u}(t, \mathbf{r})=s(t-(\mathbf{r}^T \mathbf{a})/V) \mathbf{b},$$

where $s(t)$ is a scalar phase waveform registered in the coordinate origin; $\mathbf{b}=(b_x, b_y, b_z)^T$ - unit vector reflecting the oscillation direction (polarization) of given wave phase.

In the frequency domain this equation has the form:

$$\mathbf{u}(f, \mathbf{r})=s(f)\exp(-i2\pi f(\mathbf{r}^T \mathbf{a})/V)\mathbf{b}$$

For the simplest medium model without consideration of affecting of the day surface on the wave field the vector \mathbf{b} is expressed by the following simple geometric equations:

for P-wave:
$$\mathbf{b}_P = \begin{bmatrix} -\sin \alpha \cdot \sin \beta \\ -\cos \alpha \cdot \sin \beta \\ \cos \varphi_P \end{bmatrix};$$

for SH and Love-waves:
$$\mathbf{b}_L = \begin{bmatrix} \cos \alpha \\ -\sin \alpha \\ 0 \end{bmatrix};$$

for SV-wave:
$$\mathbf{b}_V = \begin{bmatrix} \sin \alpha \cdot \cos \beta \\ \cos \alpha \cdot \cos \beta \\ \sin \beta \end{bmatrix};$$

for Rayleigh wave:
$$\mathbf{b}_R = \begin{bmatrix} -i \sin \alpha \cdot \sin \psi \\ -i \cos \alpha \cdot \sin \psi \\ \cos \psi \end{bmatrix};$$

where $\psi = \arctg(e)$, e is Rayleigh wave elliptic coefficient (ratio of the small and large axes of the wave polarization ellipse); $i = \sqrt{-1}$ characterizes the $\pi/2$ phase shift between horizontal and vertical components of Rayleigh phase displacements.

The model above is the simplest in the sense that it does not take into account the reflections and transformations of the different wave phases while arriving to the day surface. The more complex but more realistic model of seismic wave propagation in a vicinity of the day surface is proposed by D.Kennet. From this model one obtains the following equations for vector \mathbf{b} :

for P-wave:
$$\mathbf{b}_P = \begin{bmatrix} -\sin \alpha \cdot V_P p_h C_2 \\ -\cos \alpha \cdot V_P p_h C_2 \\ V_P q_P C_1 \end{bmatrix}$$

for SH and Love waves:
$$\mathbf{b}_L = \begin{bmatrix} 2 \cos \alpha \\ -2 \sin \alpha \\ 0 \end{bmatrix}$$

for SV-wave:
$$\mathbf{b}_V = \begin{bmatrix} \sin \alpha \cdot V_S q_S C_1 \\ \cos \alpha \cdot V_S q_S C_1 \\ V_S p_h C_2 \end{bmatrix}$$

for Rayleigh wave:
$$\mathbf{b}_R = \begin{bmatrix} -i \sin \alpha \cdot \sin \psi \\ -i \cos \alpha \cdot \sin \psi \\ \cos \psi \end{bmatrix}$$

where V_p , V_s are phase velocities of the P and S waves correspondingly; p_h is the horizontal apparent slowness of the wave phase;

$$q_P = (V_P^{-2} - p_h^2)^{1/2}; \quad q_S = (V_S^{-2} - p_h^2)^{1/2};$$

$$C_1 = \frac{2 \cdot V_S^{-2} \cdot (V_S^{-2} - 2 \cdot p_h^2)}{(V_S^{-2} - 2 \cdot p_h^2)^2 + 4 \cdot p_h^2 \cdot q_P \cdot q_S}; \quad C_2 = \frac{4 \cdot V_S^{-2} \cdot q_P \cdot q_S}{(V_S^{-2} - 2 \cdot p_h^2)^2 + 4 \cdot p_h^2 \cdot q_P \cdot q_S}.$$

Besides modeling of a multichannel seismogram at the output of 3C array the program can simulate the output of the so-called Strain-Inertial Micro Array (SIMA) - seismic field recording installation consisting of a single 3C seismometer and two horizontal (E-W and N-S directed strainmeters) deployed in the same site. The known relation between recordings $d_i(t)$ and $u_i(t)$, $i=x,y$ of the similarly directed horizontal sensors of seismometer and strainmeter: $d_i(t) = -p_i u_i(t)$, where p_i is horizontal apparent velocity in the i -th direction, is used for this simulation.

Input parameters of the program

All the program parameters are to be contained in a disk file with the name "models.inp". An example of the file is given below.

```
*** FILE OF INPUT PARAMETERS FOR PROGRAM "MODELS": standard ***
INSTALLATION TYPE: 3C ARRAY=1; 1C ARRAY=2; 2C HORIZ. ARRAY=3; SIMA=4
1
NUMBER OF SEISMOMETERS
12
NAME OF FILE WITH SEISMOMETER COORDINATES
alibek.crd
TYPE OF WAVE PHASE: P = 1; SH or LOVE = 2; SV = 3; RAYLEIGH = 4
1
RAYLEIGH WAVE ELLIPTIC COEFFICIENT
0.7
P- AND S-WAVE MEDIUM PHASE VELOCITIES
6. 3.5
NAME OF FILE WITH DISPERSION CURVE (IF NAME=' ' - WITHOUT DISPERSION)
disp.dat
MEDIUM MODEL: SIMPLEST = -1; KENNET MODEL = 1
-1
WAVEFORM TYPE: WHITE UNCORRELATED CHANNEL SIGNALS = -2; WHITE NOISE
WAVEFORM = -1; BERLAGUE PULSE = 0; AR-PROCESS = 1; PATTERN WAVEFORM = 2;
1
10. CENTRAL FREQUENCY FOR BERLAGUE PULSE (HZ)
0.2
AR-MODEL ORDER
4
INPUT FILE FOR WAVEFORM DESIGN (FOR MODEL TYPE 1 OR 2): '*.dat'-TIME
SERIES; '*.arc'-AR-COEFFICIENTS
pwform.dat
```



```

PARAMETERS C & B OF WAVEFORM ENVELOPE: ENV(T)=C*T*EXP(-B*T) (IF C=0 -
ENV=1)
10. 0.002
ARRIVAL AZIMUTH (DEGREES)
10.
ANGLE OF INCIDENCE (DEGREES)
20.
ONSET TIME OF WAVE PHASE (SEC)
20.
LENGTH OF WAVE PHASE (SEC)
80.
OUTPUT DATA SAMPLING INTERVAL (SEC)
0.05
POWER OF OUTPUT WAVEFORM
500.
WRITE MODE: TO DISK FILE = -1; TO SYSTEM STACK = 1
1
NAME OF FILE FOR OUTPUT DATA PARAMETERS (FOR WRITE MODE = -1)
models.par
NAME OF FILE FOR OUTPUT DATA SAMPLES (FOR WRITE MODE = -1)
models.dat
INITIAL VALUE FOR RANDOM NUMBER GENERATOR
11

```

Explanation of the input parameters

1. ARRAY TYPE: 3C ARRAY = 1; 1C ARRAY = 2; 2C HORIZ. ARRAY = 3; SIMA = 4

The parameter defines the type of recording installation and can have the values:

1 - for a 3-component array or single 3-component station (if parameter NUMBER OF SEISMOMETERS equal 1);

2 - for 1-component array consisting of similarly oriented sensors;

3 - for 2-component horizontal array;

4- for strain-seismometer microarray (SIMA), consisting of a single 3C seismometer and two horizontal strainmeters located at the same site.

2. NUMBER OF SEISMOMETERS

The number of 1, 2 or 3-component seismic receivers composing the array;

3. NAME OF FILE WITH SEISMOMETER COORDINATES

The name of file with coordinates (in km) of seismic receivers composing the array (1C, 2C, 3C seismometers or SIMA) If the number of seismometers is equal 1 then it is assumed to be located at the point with coordinates (0,0). The file has to consist of two ASCII columns: first one with X-coordinates (East-West orientation) and second one with Y-coordinates (South-North orientation). In this version of the program the Z seismometer coordinates are assumed to be equal 0.

4. TYPE OF WAVE PHASE: P = 1; SH or LOVE = 2; SV = 3; RAYLEIGH = 4

The parameter determines the type of seismic phase to be simulated: (1)- for P-wave, (2) - for SH or Love wave, (3) - for SV wave and (4) - for Railegh wave. The given version of program generates array recordings for a single wave phase;

5. RAYLEIGH WAVE ELLIPTIC COEFFICIENT

This is the elliptic coefficient of the Railegh wave: the ratio of small axis of oscillation polarization to the large one;

6. P- AND S-WAVE MEDIUM PHASE VELOCITIES

This is the phase velocities of P and S waves in the medium just beneath the array. When modeling the Railegh (Love) waves if the parameter "Name of file with

dispersion curve" consists of 5 blanks then the P-wave velocity (i.e. the first from two assigned here parameters) is used as the surface phase velocity.

7. NAME OF FILE WITH DISPERSION CURVE (IF NAME=' ' - WITHOUT DISPERSION)

The name of file containing the surface wave dispersion curve. If this parameter value the name contains blanks at 5 first positions it means that the dispersion is absent and the surface wave has to be modeled using the frequency independent phase velocity. The file has to consist of two ASCII format columns: the frequency in Hz and velocity in Km/Sec;

8. MEDIUM MODEL: SIMPLE = -1; KENNETH MODEL = 1

The "medium model" = -1 is used for the simple laterally homogeneous model without accounting for the day surface affect on the wave arrival parameters; the "medium model" = 1 is used for the Kennet model accounting for the frequency independent wave reflections and transformation at the day surface.

9. WAVEFORM TYPE: WHITE UNCORRELATED CHANNEL SIGNALS = -2; WHITE NOISE WAVEFORM = -1; BERLAGE PULSE = 0; AR-PROCESS = 1; PATTERN WAVEFORM = 2;

The parameter determines a type of phase waveform:

(-2) - in this case all channel waveforms are modeled as realizations of independent white Gaussian random processes with zero mean and equal dispersions (defined by the value of parameter "Power of output waveform");

(-1) - in this case the waveform of wave phase oscillations is assumed to be a white Gaussian time series, the channel waveforms are generated on this basis using array configuration, wave type, wave arrival direction and wave velocity in the medium.

0 - in this case the phase waveform has the shape of the Berlage pulse: $u(t) = t^a \exp(-2\pi f_0 b t) \sin(2\pi f_0 t)$, where f_0 is the central frequency of the waveform spectrum; a, b are the parameters of pulse shape;

(1) - in this case the phase waveform is modeled as an autoregressive random process

(with assigned power spectrum) using the equation: $u(t) = \sum_{k=1}^p a(k)u(t-k) + \sigma^2 \varepsilon(t)$,

where $a(k)$, $k=1, \dots, p$ are the autoregression coefficients, p is the autoregression order, $\varepsilon(t)$ is the innovation whiter random time series with zero mean and unit dispersion, σ^2 is the dispersion of autoregression residuals;

(2) - in this case a pattern time series stored in the special disk file is used for simulation of phase waveform to be modeled.

10. CENTRAL FREQUENCY FOR BERLAGE PULSE (HZ)

If the phase waveform is modeled as the Berlage pulse the parameter defines the pulse central frequency.

11. AR-MODEL ORDER

If the phase waveform is modeled as autoregression (AR) process this parameter defines the order of autoregression.

12. INPUT FILE FOR WAVEFORM DESIGN (FOR MODEL TYPE 1 OR 2):
.dat'-TIME SERIES; '.arc'-AR-COEFFICIENTS

The parameter defines the name of file used when MODEL TYPE value is equal 1 or 2. In the first case the file has to have the extensions ".dat" or ".arc" The file with extension ".dat" have to contain some pattern waveform (time series) which is approximated by an AR-process with given order p . The autoregressive coefficients calculated in result of this approximation are then used for phase waveform simulating. This provides the opportunity to generate a great number of statistically

independent seismograms with a given power spectrum that is necessary for Monte Carlo investigation of array data processing algorithm characteristics.

The file with the extension ".arc" have to contain AR coefficients for generating of phase waveform to be modeled.

In case when WAVEFORM TYPE = 2 the file can have an arbitrary name and has to contain the pattern phase waveform (usually originated from real seismic recording) which must be used for generating of a multichannel array seismogram.

In any case file has to contain one ASCII format column: N waveform samples or p AR coefficients

13. PARAMETERS C & B OF WAVEFORM ENVELOPE: $ENV(T)=C*T*EXP(-B*T)$ (IF $C=0 \Rightarrow ENV=1$)

These are the parameters of the phase waveform envelope. For all values of parameter MODEL TYPE excluding 0 (Berlage pulse) and 2 (pattern time series) the waveform being generated is multiplied with the function $x(t)=Ct \cdot \exp(-Bt)$ determining the waveform envelope. If $C=0$ then $x(t)=1$.

For MODEL TYPE=0 these parameters define the coefficients of Berlage pulse, for MODEL TYPE=2 the parameters are not used.

14. ARRIVAL AZIMUTH (DEGREES)

This parameter defines the arrival back azimuth of modeled wave to the receiving installation (for direction from the receiver to a seismic source). The azimuth is counted clockwise from the Y (South-North) axis.

15. ANGLE OF INCIDENCE (DEGREES)

This is the incidence angle of modeled wave arrival to the receiving installation. The angle is counted from the vertical to the day surface.

16. ONSET TIME OF WAVE PHASE (SEC)

This is the onset time of the wave phase in the point with the coordinates (0,0). It is assumed that the first sample of the seismogram to be modeled corresponds to the time moment equal to zero. From this moment to the phase onset time the modeled seismogram has the zero values.

17. LENGTH OF WAVE PHASE (SEC)

This is the length (in sec.) of the wave phase to be modeled. This parameter jointly with the phase onset time defines the total length of the simulated seismogram.

18. OUTPUT DATA SAMPLING INTERVAL (SEC)

The parameter determines the sampling interval of the seismogram being simulated.

19. POWER OF OUTPUT WAVEFORM

The parameter determines the averaged power of the seismogram being simulated.

20. WRITE MODE: TO DISK FILE = -1; TO SYSTEM STACK = 1

The parameter determines a device for saving simulated multichannel seismogram: (-1) if it is a disk file, (1) - if it is the SNDA System stack

21. NAME OF FILE FOR OUTPUT DATA PARAMETERS (FOR WRITE MODE = -1)

If the simulated multichannel seismogram has to be written to the disk file this parameter determines the name of file for saving the seismogram parameters: number of channels, number of samples in each channel, sampling interval (in sec) These values are saved in the ASCII format row.

22. NAME OF OUTPUT DATA FILE (FOR WRITE MODE = -1)

If the simulated multichannel seismogram has to be written to the disk file this parameter determines the name of file for saving of the seismogram sample data. The data is written in the ASCII format multiplex form without any header.

23. INITIAL VALUE FOR RANDOM NUMBER GENERATOR (MODEL TYPE=(-2), (-1), (1)).

The parameter determines the initial value (integer) for starting the random number generator used for a modeling stochastic white time series.

Output data format

The program output consists of N-channel array seismogram. The number of channels depends on chosen array configuration. The general ordering of the output traces for every recording installation (1C, 2C, 3C seismometers or SIMA) composing the array is the following: 1) Strainmeter S-N, 2) Strainmeter W-E, 3) Seismometer S-N, 4) Seismometer W-E, 5) Seismometer Z. Some of the above traces can be absent in the simulated multichannel seismogram that depends on the program input parameters for the array configuration. The ordering of the seismometer 1, 2 or 3-component outputs is determined by the file of array seismometer coordinates. If simulated seismogram is written to the SNDA Stack (parameter WRITE MODE=1) all traces are placed to the beginning of the stack.

6.2. Program "POL"

Polarization filtering of data from single 3-component station by Flinn method

The program realizes the classic Flinn algorithm of polarization filtering 3 component (3C) data. Its basic idea is utilization of the linear polarization feature of P, SH and SV waves while propagating through layered laterally homogeneous medium and possibility to transform elliptic polarized Rayley type wave recordings to the quasi-linear polarized 3c time series.

A moving time window consisting of N data samples is chosen inside the time interval under investigation. A length of the window is to meet the following two restrictions: 1) Number of samples N should be sufficiently large to provide the statistically reliable suppression of seismic noise interfering with the signal waveform. 2) The window length should not exceed duration of the seismic wave phases with different polarization and the intervals between these phases: if two such phases are contained in the same time window it would not be possible to distinct this waves by any polarization filter. Thus for successful polarization filtering the compromise has to be achieved between resolving power and reliability of extraction of the waves with different polarization.

The 3×3 covariance matrix C of the 3-component data within chosen time window is estimated and its eigen values λ_i and eigen vectors e_i , $i=1, \dots, 3$ are calculated. Using these values weight functions F and D characterizing a linearity quality and direction of wave phase polarization are evaluated. The function F is the same for the longitudinal and transverse waves and equal $F = (1 - (\lambda_1/\lambda_2)^m)^n$, where

λ_1 and λ_2 are the largest and a second in the magnitude eigen values of the power spectrum matrix C . The function D is calculated for each type of wave phases P, SH and SV using different formulas:

$$D_P = (e_1^T U_P)^l, \quad D_{SH} = (e_1^T U_{SH})^l, \quad D_{SV} = (e_1^T U_{SV})^l.$$

Here e_1 is the eigen vector corresponding the largest eigen value λ_1 ; U_P is a unit column vector normal to the assumed phase wave front positioning; U_{SH} , U_{SV} are the unit column vectors orthogonal to the U_P and belonging to the horizontal and vertical planes correspondingly; exponent powers n , m and l determine the order of nonlinearity of the polarization filter and are chosen empirically.

Magnitude of weight function F is equal 1 for purely linearly polarized wave phase and diminishes up to zero while increasing of ellipticity of wave polarization up to pure spherical one. The function D_P emphasis phase oscillations in the current time window if direction of eigen vector e_1 is close to assumed phase arrival direction, functions D_{SH} and D_{SV} do so if e_1 is orthogonal to this direction.

The following three values are calculated for every current position t of the time window middle point:

$$P_t = F_t D_P(X_t^T U_P); \quad SH_t = F_t D_{SH}(X_t^T U_{SH}); \quad SV_t = F_t D_{SV}(X_t^T U_{SV});$$

A user can perform polarization filtering in two assumptions: a location of the seismic source is known or unknown. For the first case it is possible to calculate the vectors U_P , U_{SH} , U_{SV} and then to accomplish the filtering using given vector values. For the second case vector U_P should be estimated from observations. As a rule the value of eigen vector e_1 corresponding to a maximum magnitude of the weight function F is used as such estimate. It is justified by the fact that maximum polarization linearity of the 3C observations coincide with an arrival of the P-phase. However for small signal to noise ratio the maximal F value can be connected with a S-phase arrival. This leads to mistake in identification of P and SV phases. So for a weak events one should use information about P-phase onset time and seek a maximum of the weight function F just after this moment. Estimated value of U_P allows to calculate U_{SH} , U_{SV} and then perform the polarization filtering.

Input parameters of the program

All input parameters of the program have to be contained in the file "pol.inp". Example of the file is given below:

```
***** FILE OF INPUT PARAMETERS FOR PROGRAM "POL": standard*****
READ/WRITE MODE: -1 - FROM/TO DISC FILE; 1 - FROM/TO SYSTEM STACK
```

```

1      1
CHANNELS FOR PROCESSING (FOR READ MODE = 1)
3
PROCESSING MODE: 0-GIVEN AZIMUTH AND INCIDENCE; 1-MAXIMUM LINEARITY;
2-MAXIMUM LINEARITY IN CURRENT WINDOW; 3-SCANNING THROUGH AZIMUTH;
4-SCANNING THROUGH INCIDENCE
2
BACK-AZIMUTH FROM STATION TO THE SOURCE, DEGREES
71.22
INCIDENCE ANGLE (FROM VERTICAL) OF WAVE ARRIVAL, DEGREES
20
LENGTH OF TIME WINDOW FOR FILTER ADAPTATION, SEC
4.
DELAY OF TIME WINDOW FROM START POINT OF TRACES, SEC
176.
LINEARITY ORDER 1
1
LINEARITY ORDER 2
2
DIRECTION ORDER
2
NUMBER OF RAYS (NR<=100)
20
NAME OF DATA PARAMETER FILE (FOR READ MODE = -1)
data.par
NAME OF DATA FILE (FOR READ MODE = -1)
data.dat
NAME OF OUTPUT FILE (FOR WRITE MODE = -1)
out.dat

```

Explanation of the input parameters

1. READ/WRITE MODE: FROM/TO DISC FILE = -1; FROM/TO SYSTEM STACK = 1;

The parameter determines the location of input data and the device on which the processing results are stored: -1 is a disk file, 1 is the stack of the SNDA System;

2. CHANNELS FOR PROCESSING (FOR READ MODE = 1)

If data are read from the SNDA stack this parameter assigns the numbers of channels chosen for the processing

3. PROCESSING MODE: 0 - GIVEN AZIMUTH AND INCIDENCE; 1 - MAXIMUM LINEARITY; 2-MAXIMUM LINEARITY WITH GIVEN TIME; 3 - SCANNING THROUGH AZIMUTHS; 4 - SCANNING THROUGH INCIDENCE ANGLES

The parameter determines a mode of the filtering:

0 means that the normal vector to the P-wave front is known;

1 means that the normal vector to the P-wave front is determined in the program based on maximum of polarization linearity inside of a total data interval being processed

2 means that the normal vector to the P-wave front is determined in the program based of polarization inside of a assigned time window position;

3 means that the scanning through arrival azimuths is performed (for assigned incidence angle) to estimate the arrival direction

3 means that the scanning through arrival incidence angles is performed (for assigned azimuth) to estimate the arrival direction

4. BACK-AZIMUTH FROM STATION TO THE SOURCE (DEGREES)

The parameter assigns a value of arrival back-azimuth for using in 0 and 3 filtering mode.

5. INCIDENCE ANGLE OF WAVE ARRIVAL (FROM VERTICAL, DEGREES)

The parameter assigns a value of arrival incidence angle for using in 0 and 4 filtering mode

6. LENGTH OF TIME WINDOW FOR FILTER TEACHING, SEC

A length of moving time widow for calculation of a filter output value (sec)

7. DELAY OF TIME WINDOW FROM START POINT OF TRACES, SEC

Time from data start to the start of time window for determination of P-wave arrival direction

8. LINEARITY ORDER 1

The power m of exponent for calculation of weight function F

9. LINEARITY ORDER 2

The power n of exponent for calculation of weight function F

10. DIRECTION ORDER

The power l of exponent for calculation of weight function D

11. NUMBER OF RAYS FOR SCANNING (≤ 100)

The number of rays used for scanning arrival directions in 3 and 4 filtering modes

12. NAME OF DATA PARAMETER FILE (FOR READ MODE = -1)

The name of disk file containing the parameters of data for processing: a number of channels, a number of channel data points, data sampling interval (

13. NAME OF DATA FILE (FOR READ MODE = -1)

The name of disk file containing data to be processed. Data have to be written in ASCII format in multiplex form without any header.

14. NAME OF OUTPUT FILE (FOR WRITE MODE = -1)

The name of output disk file for saving of filtering results. The output data are written in ASCII format in the multiplex form without any header

Input data format

The program performs polarization filtering of data recorded single 3-component station. The 3 channel data to be processed have to correspond the SN, EW and Z sensor components. Mixing up the channel order does not cause the failure of the program but leads to wrong results. The channel number exceeding 3 is not permissible. The number of data samples has to be the same in every channel and less then 10000.

Output data format

The number and types of the program output traces depends on PROCESSING MODE parameter value. When this parameter is equal 0, 1 or 2 there are 8 traces:

- 1) Resulting trace for filtering in the current polarization direction (main eigen vector direction) of 3C data being processed;
- 2) Resulting trace for filtering in P-wave oscillation direction;
- 3) Resulting trace for filtering in SH-wave oscillation direction;
- 4) Resulting trace for filtering in SV-wave oscillation direction;
- 5) Polarization linearity weights F_i ;
- 6) Directional weights D_i ;
- 7) Azimuths of the main axis (eigen vector) of a current data polarization;
- 8) Angle of incidence of the main axes (eigen vector) of a current data polarization.

When PROCESSING MODE parameter is equal to 3 there are N output filtered traces (where N equal to value of parameter NUMBER OF RAYS FOR SCANNING) corresponding to different azimuths (in the range of 0,360 degrees) and

incidence angle assigned by parameter INCIDENCE ANGLE OF WAVE ARRIVAL. When PROCESSING MODE parameter is equal 4 there are N output filtered traces corresponding different incidence angles in the range of (0,90) degrees and azimuth assigned by parameter BACK-AZIMUTH FROM STATION TO THE SOURCE.

6.3. Program "POLCFLTS" Vector polarization filtering of multichannel data

The program realizes the method of multichannel data polarization filtering, put forward by Dj.Samson and Dj.Olson. The most known from literature polarization filtering algorithms have a vector frequency response: they use as an input a multidimensional time series and produce at the output a single trace which is a result of polarization filtering in the direction of the main axis of data covariance matrix. Dj.Samson and Dj.Olson proposed the alternative approach when polarization filter has a scalar frequency response and produces the same number output traces as it has at the input:

$$Y(t) = \sum_{i=0}^{N-1} X(t-i) \cdot H(i)$$

where $X(t)=[X_1(t), X_2(t), \dots, X_M(t)]^T$ - vector input time series of the filter; $Y(t)=[Y_1(t), Y_2(t), \dots, Y_M(t)]^T$ - filter output vector time series having the same dimension as the input one; $h(t)$ - scalar frequency response of the filter; N - length of time window used for calculation of the filter output for a current time moment t ; M - number of data channels.

The major information needed for constructing of filter frequency response $H(t)$ is frequency dependent characteristic of polarization of the input signal $X(t)$. Let us consider the smoothed estimation of matrix power spectral density (MPSD) of the input signal $X(t)$:

$$C(f, \delta) = \sum_{k=K_1}^{K_2} a(k) \cdot Z(k) Z^*(k)$$

where $Z(k) = \sum_{t=0}^{N-1} X(t) \cdot \exp(-i2\pi kt)$ - is the Fourier transform of the input signal;

$k=0, 1, \dots, N-1$; (K_1, K_2) is the interval for smoothing through frequencies; $f=(K_1+K_2)/(2N\Delta t)$; $\delta=(K_2-K_1)/(N\Delta t)$; Δt is the data sampling interval; $*$ is the

symbol of Hermitic conjugation; $a(k)$ is a smoothing window, satisfying the

condition: $\sum_{k=K_1}^{K_2} a(k) = 1.$

Number of freedom degrees ν of smoothed estimation $C(f)$ of data MPSD is equal:

$$\nu = \left[\sum_{k=K_1}^{K_2} a^2(k) \right]^{-1}$$

The measure $P(f)$ of polarization of the input multichannel data $X(t)$ is determined by the spectrum of matrix $C(f)$ eigen values (for purely polarized $X(t)$ there exist only one nonzero eigen value). A computationally efficient measure $P(f)$ can be derived from the characteristic polynomial of the matrix $C(f)$ and has the form:

$$P = \frac{M \cdot (tr(C^2) - (tr(C))^2)}{(M-1) \cdot (tr(C))^2}$$

where $tr(C)$ is the track of matrix C (dependence on P and C from f is omitted for simplicity).

As the polarization filter frequency response one may choose some proper function from polarization measure $P(f)$. It is convenient to use for a such function $h(f) = P^g(f)$ where g is some positive quantity, determining the degree of nonlinearity of the filter. An increasing of g leads to a more severe suppression of the input data at intervals where data contains strong unpolarized components (e.g. have small signal to noise ratio)

The algorithm of vector polarization filtering of multichannel data can now be written as following:

$$Y(t) = N^{-1} \sum_{k=0}^{N-1} Z(k) \cdot P^g \cdot \exp(i2\pi kt), \quad t=0, 1, \dots, N-1.$$

Mean value and dispersion of the estimated polarization characteristic $P(f)$ strongly depend on ν - freedom degrees number of MPSD estimation $C(f)$. With increasing ν the mean value of $P(f)$ trends to its truth value and the dispersion decreases. However, using a large values of ν is not expediently because this implicate a bad frequency resolution of the polarization filtering. The number of channels M

strongly affects to dispersion of $P(f)$ and for large M it can be recommended to increase the filter nonlinearity order g .

The program being described implements the above algorithm for the case of a moving time window. This variant of filter realization is most expedient for processing of nonstationary time series such as multichannel seismic recordings. In this case the data polarization characteristics can significantly change along the time interval being processed. Note that the given program version uses the rectangular time windows (with number of freedom degrees equal N) which are not overlapping for the sake of saving computational resources.

Input parameters of the program

All input parameters of the program have to be contained in the file "polcflt.inp". Example of the file is given below:

```
***FILE OF INPUT PARAMETERS FOR PROGRAM "POLCFLTS": standard ***
READ/WRITE MODE: FROM/TO DISK FILE =-1; - FROM/TO SYSTEM STACK = 1
  1  1
ORDER OF POLARIZATION FILTER
  3
LENGTH OF MOVING WINDOW FOR PROCESSING (IN SEC)
  50
NUMBER OF FREEDOM DEGREES
  6
DATA CHANNELS FOR PROCESSING (FOR READ MODE = 1)
all
DATA PARAMETER FILE NAME (FOR READ MODE = -1)
data.par
DATA FILE NAME (FOR READ MODE = -1)
data.dat
NUMBER OF FIRST POINT FOR PROCESSING (FOR READ MODE = -1)
  1
NUMBER OF DATA POINTS FOR PROCESSING (FOR READ MODE = -1)
1000
NAME OF OUTPUT FILE (FOR WRITE MODE = -1)
out.dat
```

Explanation of the input parameters

1. READ/WRITE MODE: FROM/TO DISK FILE =-1 ; FROM/TO SYSTEM STACK =1

The parameter determines the location of input data and the device on which the processing results are stored: -1 is a disk file, 1 is the stack of the SNDA System;

2. ORDER OF POLARIZATION FILTER

The parameter determines the nonlinearity feature of the filter: power g of the exponent P_g ;

3. LENGTH OF MOVING WINDOW FOR FILTERING (IN SEC)

The length of moving time window for data processing (sec);

4. NUMBER OF FREEDOM DEGREES

The number of freedom degrees for the estimate of matrix power spectral density $C(f)$.

The parameter determines the length of triangular smoothing frequency window

5. DATA CHANNELS FOR PROCESSING (FOR READ MODE = 1)

If data are read from the SNDA stack this parameter assigns the numbers of channels chosen for the processing;

5. NAME OF DATA FILE (FOR READ MODE = -1)

The name of disk file containing data to be processed. Data have to be written in ASCII format in multiplex form without any header.

6. NAME OF FILE WITH DATA PARAMETERS (FOR READ MODE = -1)

The name of disk file containing the parameters of data for processing: a number of channels, a number of channel data points, data sampling interval;

7. NUMBER OF FIRST POINT FOR PROCESSING (FOR READ MODE = -1)

If data are read from disk file this parameter defines the number of a first sample of data interval chosen for the processing. The preceding samples are omitted

8. NUMBER OF DATA POINTS FOR PROCESSING (FOR READ MODE = -1)

If data are read from disk file this parameter defines the length of data interval for processing (in samples). This interval is then divided to some number of unoverlapping time windows which length is assigned by the parameter LENGTH OF MOVING WINDOW FOR FILTERING.

9. NAME OF OUTPUT FILE (FOR WRITE MODE = -1)

The name of output disk file for saving of filtering results. The output data are written in ASCII format in the multiplex form without any header

Input data format

As the input data of the program one may use no more then 50 time series with the same number of samples in every series not exceeding 4096 ones. An ordering of the input channels is not meaningful for the program.

Output data format

In result of program performing one gets $M+1$ traces. The first M traces are the filtered time series (there are the same number of traces and the same channel ordering as for the input data). In the last output trace the averaged through frequencies filter response P^g is presented for each moving time window inside the total interval of processed data. If program output is put into the SNDA stack the all traces is placed at the end of stack.

6.4. Program "ARMAFS"

**Estimating of inverse matrix power spectral density of multichannel data
by ARMA modeling**

The program is designed for estimating of inverse matrix spectral density of multichannel data. The estimating is performed by multidimensional autoregressive-moving averaged (ARMA) modeling of the multichannel time series $\mathbf{x}(t) = (x_1(t), x_2(t), \dots, x_M(t))^T$ that means the approximation of $\mathbf{x}(t)$ by the random process $\mathbf{y}(t)$ satisfying to the following equation

$$\mathbf{y}(t) = \sum_{l=1}^P \mathbf{A}(l) \mathbf{y}(t-l) + \sum_{l=0}^Q \mathbf{B}(l) \mathbf{e}(t-l), \quad t=1, \dots, N$$

where N is the length of time series being modeled; P is the order of autoregression (AR) part of the model; Q is the order of moving averaged (MA) part of the model; $A(l)$, $l \in 1, P$ are the $M \times M$ matrices of AR parameters; $B(l)$, $l \in 1, Q$ are the $M \times M$ matrices of MA parameters; M is the dimension of time series; $e(t)$ is the M -dimensional Gaussian white time series with the zero mean and unit covariance matrix. The procedure for calculation of parameters $A(l)$ and $B(l)$ is chosen to provide the good adjusting of the model $y(t)$ to the observations $x(t)$ under the condition of saving the computational time.

The estimate $F^{-1}(f)$ of inverse matrix power spectrum density of the multichannel observations is evaluated from $A(l)$ and $B(l)$ estimates using the equation:

$$F^{-1} = \left(\sum_{k=1}^P A(k) \cdot \exp(i2\pi kf) \right) \cdot \left(\sum_{k=1}^Q B(k) \cdot \exp(i2\pi kf) \right)^{-1} \cdot \left(\sum_{k=1}^P A^T(k) \cdot \exp(-i2\pi kf) \right)$$

Input parameters of the program

All input parameters of the program have to be contained in the file "armafs.inp". Example of the file is given below:

```
*** FILE OF INPUT PARAMETERS FOR PROGRAM ARMAFS: standard***
ADAPTATION MODE: ARWF = -1; ARLD = -2; MA = -3; ARMA = -4
-4
ORDER OF MULTIDIMENSIONAL AUTOREGRESSIVE MODEL
10
ORDER OF MULTIDIMENSIONAL MOVING-AVERAGE MODEL
10
VALUE OF A REGULARIZATOR FOR MATRIX AUTOCOVARANCE FUNCTION
0.0001
LOW & HIGH FREQUENCIES OF FREQUENCY RANGE
0. 5.
FILTERING MODE: WITH INTERPOLATION = 1, WITHOUT = -1
1
NUMBER OF FREQUENCIES (IF FILTERING MODE IS = 1)
128
NAME OF OUTPUT FILE FOR INVERSE MATRICES
insp.mtrs
NAME OF OUTPUT FILE FOR INVERSE MATRIX PARAMETERS
insp.par
READ MODE: FROM DISK FILE = -1; FROM SYSTEM STACK = 1
1
DATA CHANNELS TO BE PROCESSED (IF READ FROM DISK FILE THEN AT THE END OF
LIST MUST BE 0)
25
NAME OF DATA FILE (FOR READ MODE = -1)
fchn.dat
```

NAME OF DATA PARAMETER FILE (FOR READ MODE = -1)
fchn.par

Explanation of input parameters

1. ADAPTATION MODE: ARWF = -1; ARLD = -2; MA = -3; ARMA = -4

The parameter determines the type of multichannel data model:

(-1) means the data modeling by the autoregressive (AR) process with the order P ($Q=0$); the AR matrix coefficients $A(l)$, $l=1, \dots, P$ are calculated with the help of computational efficient Levinson-Durbin procedure, the covariance matrix of residuals $B(0)$ are estimated as covariance matrix of an output signal of the multichannel whitening filter:

$$B(0) = \frac{1}{N} \sum_{t=1}^N y(t)y^*(t), \text{ where } y(t) = \sum_{k=1}^P A(k)x(t-k).$$

(-2) - the data are also modeled by AR process with the order P ($Q=0$), but in distinction with the (-1) mode the all AR model matrix parameters: $A(l)$ and $B(0)$, are estimated by the Levinson-Darbin procedure. This is less time consuming in comparison with (-1) mode, but for strongly coherent data can lead to computational instability.

(-3) means the data modeling by the moving average (MA) process with the order Q ($P=0$); MA matrix coefficients $B(l)$, $l=0, \dots, Q$ are calculated by the equation:

$$B(l) = \frac{1}{N} \sum_{t=1}^N x(t)x^*(t-l).$$

(-4) means the data modeling by the autoregressive-moving average (ARMA) process with the orders P and Q ; The AR matrix coefficients $A(l)$, $l=1, \dots, P$ are calculated with the help of multichannel Levinson-Darbin procedure, MA matrix coefficients $B(k)$, $k=0, \dots, Q$ are estimated as the matrix covariances with lags $0, \dots, Q$ of output process of the multichannel whitening filter:

$$B(k) = \frac{1}{N} \sum_{t=1}^N y(t)y^*(t-k), \quad k=0, \dots, Q, \text{ where } y(t) = \sum_{k=1}^P A(k)x(t-k).$$

2. ORDER OF MULTIDIMENSIONAL AUTOREGRESSIVE MODEL PART

The order of model AR part has not to exceed 50.

3. ORDER OF MULTIDIMENSIONAL MOVING-AVERAGE MODEL PART

The order of model MA part has not to exceed 50.

4. VALUE OF A REGULARIZATOR FOR MATRIX AUTOCOVARANCE FUNCTION

If multidimensional time series being modeled has high correlations between component processes then it is expedient to add to the diagonal elements $B_{ii}(0)$ of the estimated data covariance matrix some regularization quantities by the formula: $B'_{ii}(0) = B_{ii}(0)(1+REG)$, where REG is the regularization parameter with recommended values: 0.01 - 0.0001

5. LOW & HIGH FREQUENCIES OF FREQUENCY RANGE

These two parameters assign the frequency interval ($f_l f_h$) in which margins the data inverse matrix power spectral density (MPSD) is calculated.

6. FILTERING MODE: WITH INTERPOLATION = 1, WITHOUT = -1

If this parameter is equal 1 (with interpolation) then data inverse MPSD is calculated for equidistant grid in the interval ($f_l f_h$); number N_f of the grid points is determined by the parameter NUMBER OF FREQUENCIES.

If this parameter is equal -1 (without interpolation) then the number of the grid points is determined by the $N_f = 2^x < N_d/2$ - the greatest power-of-two value which is less then half of the every channel data samples. In both cases it has to be: $N_f < 257$

7. NUMBER OF FREQUENCIES (IF FILTERING MODE IS 1)

This parameter determines the number of frequencies for inverse MPSD calculation in the case where parameter FILTERING MODE=1. The parameter value has to be less then 257.

8. NAME OF OUTPUT FILE FOR INVERSE MATRIX

This is the name of disk file in which the values of calculated inverse MPSD is to be stored.

9. NAME OF OUTPUT FILE FOR INVERSE MATRIX PARAMETERS

This is the name of disk file in which the parameters of calculated inverse MPSD are to be stored.

10. READ MODE: FROM DISK FILE = -1; FROM SYSTEM STACK = 1

This switch allows to choose the device to read the input data for processing: (-1) means that data are read from a disk file, (1) -

11. DATA CHANNELS TO BE PROCESSED (IF READ FROM DISK FILE - 0 - END OF LIST)

The parameter determines the channel numbers of multidimensional time series to be processed. If the data are read from the SNDA Stack the parameter value must be a string having one of the following shapes: 15; (1,3-10,14); all (in accordance with CHANNELS format in the SNDA System stack command parameters). If the data are read from a disk file the parameter value is a column of channel numbers ended by 0. In both cases the total number of channels choosed has to be less then 50.

12. NAME OF DATA FILE (FOR READ MODE -1)

If parameter READ MODE = -1, then the name of file containing the samples of data to be processed is assigned here. The data must be in the ASCII multiplex format without any header.

13. NAME OF DATA PARAMETER FILE (FOR READ MODE -1)

If parameter READ MODE = -1, then the name of file containing the parameters of input data is assigned here. The parameters are: number of data channels, number of samples in every channel and the data sampling interval; the file must have the form of ASCII string.

Input data format

The multichannel time series which can be processed by the program have to consist of no more then 50 channels with no more then 4096 samples in every channel.

Output data format

In result of program performing the two files are created: first contains the inverse MPSD matrices of the input data calculated for the given set of frequencies, second contains the parameters of the data and MPSD estimate calculated: the number of channels processed, type and orders of the ARMA model, and so on. The both files are written in the ASCII format.

6.5. Program "GRFILTF5"

Optimal Wiener group filtering of 3-component array data for different types of wave polarization

The program is designed for performing of optimal Wiener group filtering of the multichannel seismic recordings with the purpose of extraction from coherent seismic noise of "useful" seismic wave phase waveforms. The wave phase is assumed to arrive from definite direction and be polarized in accordance with one of the following polarization types: P, SH (or L), SV and R.

Let the coordinate system has the X-axis directed to the East, Y-axis - to the North and Z-axis to the Zenith. Assume that the plane seismic wave phase arrives to recording site from direction being determined by the azimuth α , incidence angle β and has the phase velocity V . Designate as $s(t)$ the waveform of the seismic phase in the coordinate origin $\mathbf{r}_0=(0,0,0)$. Then the vector signal at the output of the 3-component array can be written in the frequency domain as

$$\mathbf{u}(f)=\mathbf{h}(f) \cdot s(f); \quad \mathbf{h}(f)=(h_1(f), \dots, h_{3M}(f))^T = \boldsymbol{\varphi}(f) \otimes \mathbf{b};$$

where $\boldsymbol{\varphi}(f)=\{\exp(-i2\pi f(\mathbf{r}_i^T \mathbf{a})/V), i=1, \dots, M\}$ is the M -dimensional column vector of the signal phase delays in the array seismometers; \otimes is the Kronecker product of $\boldsymbol{\varphi}$ and 3-dimensional vector \mathbf{b} ; $s(f)$ is the Fourier transform of the signal $s(t)$; $\mathbf{h}(f)$ is the vector frequency response of the seismic wave propagation paths from the coordinate origin \mathbf{r}_0 to the array sensors; \mathbf{b} is the vector reflecting the polarization features of the seismic wave phase; $\mathbf{a}=(\sin\alpha \cdot \sin\beta, \cos\alpha \cdot \sin\beta, \cos\beta)^T$ is the unit vector orthogonal to the phase wave front.

The vector \mathbf{b} depends on the wave phase type (P, SH, SV Love or Rayleigh) and for the simplest laterally homogeneous medium model without accounting for the day surface affecting to the wave propagation has the form

For P-wave:
$$\mathbf{b}_P = \begin{bmatrix} -\sin\alpha \cdot \sin\beta \\ -\cos\alpha \cdot \sin\beta \\ \cos\beta \end{bmatrix}$$

For SH and Love waves:
$$\mathbf{b}_L = \begin{bmatrix} \cos\alpha \\ -\sin\alpha \\ 0 \end{bmatrix}$$

For SV-waves
$$\mathbf{b}_V = \begin{bmatrix} \sin\alpha \cdot \cos\beta \\ \cos\alpha \cdot \cos\beta \\ \sin\beta \end{bmatrix}$$

For Rayleigh waves:
$$\mathbf{b}_R = \begin{bmatrix} -i \sin \alpha \cdot \sin \psi \\ -i \cos \alpha \cdot \sin \psi \\ \cos \psi \end{bmatrix}$$

In the practical applications the seismic signal is as a rule recorded on the background of the additive seismic noise. So the multichannel recordings of the 3-component array can be expressed by the following equation: $\mathbf{u}(f) = \mathbf{h}(f) \cdot s(f) + \zeta(f)$ where $\zeta(f)$ is the Fourier transform of array seismic noise recordings.

The optimal undistorting group filter (OUGF) is known as the filter providing maximum suppression of a seismic noise containing a coherent components and extraction without distortions a waveform of the seismic phase arriving from the known direction. Its frequency response is equal: $\Phi_I(f) = F^{-1}(f) \mathbf{h}(f) (\mathbf{h}^*(f) F^{-1}(f) \mathbf{h}(f))^{-1}$ where $F(f) = E\{\zeta(f) \zeta^*(f)\}$ is matrix power spectral density (MPSD) of the array noise recordings. The restriction on the OUGF frequency response to not distort the waveform of phase arriving from the given direction with given polarization leads to the following equation: $\Phi_I^*(f) \mathbf{h}(f) = 1$

In more common case it is possible to impose arbitrary restrictions on the group filter frequency response: $\Phi^* \mathbf{H} = \mathbf{c}$, where the matrix \mathbf{H} specifies restriction types and vector \mathbf{c} defines the desired filter response under these restrictions. In this version of the program the variant proposed by J. Classen is realized where the following three restrictions are imposed: one for the response amplitude to be unit for the assigned arrival direction and other two - for the x, y -spatial derivations of the response function which have to be equal zero for the same direction:

$$\mathbf{H} = [\mathbf{h}, \partial \mathbf{h} / \partial p_x, \partial \mathbf{h} / \partial p_y]$$

$$\mathbf{c} = (1, 0, 0)^T$$

where $p_x = \sin \alpha \cdot \sin \beta / V$ is apparent slowness of the wave phase in the X -axis direction; $p_y = \cos \alpha \cdot \sin \beta / V$ is the same for the Y -axis.

The group filter frequency response in this case has the form

$$\Phi_2(f) = F^{-1}(f) \mathbf{H}(f) (\mathbf{H}^*(f) F^{-1}(f) \mathbf{H}(f))^{-1} \mathbf{c}$$

We call such filter as optimal undistorting constrained group filter (OUCGF)

One can easily verify that the noise power spectral density at the output of OUGF $\Phi_I(f)$ equal to $\sigma^2(f) = (\mathbf{h}^*(f) F^{-1}(f) \mathbf{h}(f))^{-1}$. Thus the group filter with the frequency response $\Phi_2(f) = F^{-1}(f) \mathbf{h}(f) (\mathbf{h}^*(f) F^{-1}(f) \mathbf{h}(f))^{-1/2}$ produces at the output the

noise with unit power spectral density. We call such filter as the optimal whitening group filter (OWGF)

If the seismic signal is recorded at a background of transient interference waves generated by the spatially localized source with known parameters, then the inverse noise MPSD can be found analytically: $F^{-1}(f)=[I-q(q^*q)^{-1}q^*]$, where I is the identity matrix, $q(f)$ is the vector frequency response of propagation paths of the interfering wave while it propagates from the noise source to the array sensors. For the plane interfering wave the vector $q(f)$ has the same structure as the vector $h(f)$. The undistorting optimal group filter designed for this form of MPSD is called the spatially rejecting filter.

Input parameters of the program

All input parameters of the program have to be contained in the file "grflfts.inp". Example of the file is given below:

```
*** FILE OF INPUT PARAMETERS FOR PROGRAM GRFLTFS: standard ***
ARRAY TYPE: 3C ARRAY=1; 1C ARRAY=2; 2C HORIZONTAL ARRAY=3; SIMA=4
2
FILTER TYPE: UNDISTORTING(1)=1; UNDISTORTING(2)=2; WHITENING=3
1
PHASE TYPE: P = 1; SH & LOVE = 2; SV = 3; RAYLEIGH. =4
1
INITIAL AND FINAL POINTS FOR SCANNING AT AZIMUTH (DEGREES FROM NORTH)
0. 350.
INITIAL AND FINAL POINTS FOR SCANNING AT INCIDENCE ANGLE (DEGREES FROM
VERT.)
0. 90.
INCREMENTS FOR SCANNING (DEGREES)
10. 10.
RAYLEIGH WAVE ELLIPTIC COEFFICIENT (HORIZ/VERT)
0.8
MEDIUM PHASE VELOCITY (KM/SEC)
5.
NAME OF FILE WITH PHASE VELOCITY DISPERSION CURVE FOR SURFACE WAVE (IF
NAME="" - WITHOUT DISPERSION)

LOW AND HIGH FREQUENCIES OF FILTERING RANGE (HZ)
0. 5.
NUMBER OF FREQUENCY BANDS
1
MARGINS OF BANDS (HZ)
1. 2. 3. 4.
NOISE MATRIX TYPE: IDENTICAL = -1; FOR REJECTION FILTER=0; ADAPTIVE=1
1
NOISE WAVE DIRECTION (AZ. & INC. ANGLE), VELOCITY & WAVE TYPE FOR
REJECTION FILTERING
340. 75. 3. 1
NAME OF FILE WITH ARRAY SEISMOMETER COORDINATES (IN KM)
```

```

arcess.crd
NAME OF FILE FOR INVERSE MATR. SP. PARAMETERS
insp.par
NAME OF FILE FOR INVERSE MATR. SP. VALUES
insp.mtrs
READ/WRITE MODE: FROM/TO STACK = 1; FROM/TO DISK FILE = -1
1 1
DATA CHANNELS TO BE PROCESSED (IF READ FROM STACK)
25
OUTPUT PRESENTATION: AS TIME SERIES = 0; TRACE POWERS = 1
0
NAME OF FILE WITH DATA PARAMETERS (IF READ FROM DISK FILE)
grfltfs.par
NAME OF FILE WITH DATA SAMPLES (IF READ FROM DISK FILE)
grfltfs.dat
NAME OF FILE FOR SAVING OUTPUT (IF WRITE TO DISC FILE)
grfltfs.out

```

Explanation of program parameters

1. ARRAY TYPE: 3C ARRAY = 1; 1C ARRAY = 2; 2C HORIZONTAL ARRAY = 3; SIMA = 4

The parameter defines the type of recording installation and can have the values:

- (1) - for a 3-component array or single 3-component station (if parameter NUMBER OF SEISMOMETERS equal 1);
- (2) - for 1-component array consisting of similarly oriented sensors;
- (3) - for 2-component horizontal array;
- (4) - for strain-seismometer microarray (SIMA), consisting of a single 3C seismometer and two horizontal strainmeters located at the same site.

2. FILTER TYPE: UNDISTORTING(1) = 1; UNDISTORTING(2) = 2; WHITENING = 3

The parameter defines the type of group filter to be used:

- (1) - for undistorting filter with single restriction (frequency response (FR) Φ_1);
- (2) - for undistorting with restrictions on the FR spatial derivatives (FR Φ_2);
- (3) - for whitening group filter (FR Φ_3).

3. PHASE TYPE: P = 1; SH & LOVE = 2; SV = 3; RAYLEIGH = 4

The parameter defines the type of seismic wave phase to be extracted. This program version intended for extracting only single phase with specific polarization:

- (1) - for the P-phase;
- (2) - for the SH or Love phases;
- (3) - for the SV phase;
- (4) - for the Rayleigh phase.

4. INITIAL AND FINAL POINTS FOR SCANNING AT AZIMUTH (DEGREES FROM NORTH)

The given program version allows to perform the optimal group filtering of 3-component array data not only for the single arrival direction but for the "fan" of directions inside given ranges of azimuth and incidence angles of wave front (i.e. it provides scanning the medium with the assigned angle increments). The parameter assigns the initial and final values of wave arrival back azimuths (from recording site to the seismic source) to be used while scanning the medium. If the initial value is equal to the final one then the group filtering is performed for this single azimuth.

5. INITIAL AND FINAL POINTS FOR SCANNING AT INCIDENCE ANGLE (DEGREES FROM VERT.)

The parameter assigns the initial and final values of wave arrival incidence angle (counted from lower perpendicular to the day surface) to be used while scanning the medium. If the initial value is equal the final one then the group filtering is performed for the single incidence angle.

6. INCREMENTS FOR SCANNING (DEGREES)

These two parameters define the increments for scanning at azimuth and incidence angle.

7. RAYLEIGH WAVE ELLIPTIC COEFFICIENT (HORIZ/VERT)

This is the elliptic coefficient of the Rayleigh wave: the ratio of small axis of oscillation polarization to the large one;

8. MEDIUM PHASE VELOCITY (KM/SEC)

This is the phase velocity of the P or S wave in the medium just beneath the array. If value of parameter "Name of file with dispersion curve" while filtering of the Rayleigh or Love waves consist of 5 blanks this velocity is used as the average surface phase velocity

9. NAME OF FILE WITH PHASE VELOCITY DISPERSION CURVE FOR SURFACE WAVE (IF NAME=' ' - WITHOUT DISPERSION)

This is the name of file containing the surface wave dispersion curve (the phase velocity as function of frequency). If the name contains the blanks at 5 first positions it means that the dispersion is absent and the surface wave is regarded as possessing the frequency independent (mean) phase velocity. The file has to consist of two ASCII format columns: the frequency in Hz and velocity in Km/Sec;

10. LOW AND HIGH FREQUENCIES OF FILTER RANGE (HZ)

These two parameters assign the low and high frequencies of the range of group filtering to be performed.

11. NUMBER OF FREQUENCY BANDS

The given program version allows to calculate simultaneously the group filtering of input traces for several (maximum 5) frequency bands inside the assigned frequency range. This parameter defines the number of bands

12. MARGINS OF BANDS (HZ)

The parameter is valid only if the NUMBER OF FREQUENCY BANDS is more then 1; it defines the inner margins of frequency bands for filtering. It is assumed in the program that the frequency bands do not overlap, low frequency of the first band and high frequency of the last one are equal correspondingly to the low and high frequencies of the filter range (the values of the above parameter). Thus the "margins of the bands" are the points of partition of the previously assigned filter frequency range.

13. NOISE MATRIX TYPE: IDENTICAL = -1; FOR REJECTION FILTER = 0; ADAPTIVE = 1

For design of any type optimal group filter it is needed to evaluate the inverse matrix power spectral density (IMPSD) $F^{-1}(f)$ of array noise. The following options of the IMPSD can be used in the program, being specified by the parameter values:

(-1) means the identity IMPSD corresponding the assumption that the noise field at the recording site is the spatially uncorrelated white one. The optimal group filtering coincides in this case with the conventional 3-component beamforming procedure.

(0) means the IMPSD corresponding the coherent noise field generated by the random plane wave arriving to the recording site with an assigned direction. The

IMPSD is calculated in the program. In this case the group filtering procedure realizes the algorithm of spatial rejecting filtering.

(1) means adaptive IMPSD. If noise field contains a strong coherent components of unknown genesis the both above assumptions about the noise IMPSD are not satisfactory. In this most common case the optimal group filtering has to involve an estimate of the array noise IMPSD. The latter should be preferably made using the array noise recordings at a time interval just before the seismic event signal onset. The IMPSD estimate can be supplied by the program "*armafs*". While using the parameter value = 1 this program have to be executed before running the program "*grfltf*". The same array channel ordering must be guaranteed in the both program input data.

14. NOISE WAVE DIRECTION: AZ. & INC. ANGLE; VELOCITY & WAVE TYPE (FOR REJECTION FILTERING)

If the rejection filtering (NOISE MATRIX TYPE = 0) is chosen as optimal group filtering option, this parameter specifies the features of interfering plane wave: its arrival azimuth, incidence angle, phase velocity in the medium and the polarization type.

15. NAME OF FILE WITH ARRAY SEISMOMETER COORDINATES (IN KM)

The name of file with coordinates of array receivers (1C, 2C, 3C seismometers or SIMA). If the number of seismometers is equal to 1 then it's site is assumed to have coordinates (0,0). The file must consist of two ASCII columns: first one with X-coordinates (West-East orientation) and second one with Y-coordinates (South-North orientation). In this version of the program the Z seismometer coordinates are assumed to be equal 0.

16. NAME OF FILE FOR INVERSE MATR. SP. PARAMETERS

This is the name of file containing parameters of the IMPSD estimate (if NOISE MATRIX TYPE = 1).

17. NAME OF FILE FOR INVERSE MATR. SP. VALUES

This is the name of file containing values of the IMPSD estimate (if NOISE MATRIX TYPE = 1).

18. READ/WRITE MODE: FROM/TO STACK = 1; FROM/TO DISK FILE = -1

The first of these two parameters defines the device for reading the program input data of and the second one - the device for saving results of the program performing: (1) is for the SNDA stack, (-1) is for the disk file.

19. DATA CHANNELS TO BE PROCESSED (IF READ FROM STACK)

This parameter is valid if the input data are read from the SNDA Stack. It must have a form of strings corresponding to CHANNELS parameter format used in the SNDA stack commands. For example, it can be as following: 15; (1,3-10,14); all. The total number of specified data channels has not to exceed 50.

20. OUTPUT PRESENTATION: AS TIME SERIES = 0; TRACE POWERS = 1

The presentation of filtering results is possible in two forms:

(0) - in the form of output time series. In this case after the program execution a user gets the set of time series (traces).

(1) - in the form of tables of filtered trace powers. For every frequency band the table is produced. It is composed by the powers of group filter output traces corresponding to the all scanning directions.

21. NAME OF FILE WITH DATA PARAMETERS (IF READ FROM DISK FILE)

If parameter READ MODE=-1, then the name of file containing the parameters of input data has to be assigned here. The parameters are: number of data channels,

number of samples in every channel and the data sampling interval; the file must have the form of ASCII string.

22. NAME OF FILE WITH DATA SAMPLES (IF READ FROM DISK FILE)

If parameter READ MODE=-1, then the name of file containing the samples of data to be processed must be assigned here. The data must be in the ASCII multiplex format without any header.

23. NAME OF FILE FOR SAVING OUTPUT (IF WRITE MODE=-1)

If WRITE MODE=-1 the parameter assigns the name of file for saving the filtering results to the disk. The output traces are saved in the ASCII demultiplex form. The every output trace has a header containing the filtering direction (azimuth and incidence angle) frequency band and the number of trace points.

Input data format

The input data for the program are to be the multidimensional time series with total number of channels no more then 50 and number of samples in the every channel no more then 4096. If the data are stored in the disk file the latter must have the ASCII multiplex format. The channel ordering for every array recording instrument has to be in generally the following: S-N strainmeter, W-E strainmeter, N-S seismometer, W-E seismometer, Z-seismometer. For a particular array configuration some of the channels above can be omitted.

Output data format

In depend on a value of parameter OUTPUT PRESENTATION the program output can have the following forms:

(a) A set of time series which are the results of input data group filtering for the frequency bands specified by the parameter MARGINS OF BANDS and for the signal arrival directions specified by the scanning parameters. For every direction there is the sequence of traces corresponding to the different bands. If output data are saved to the disk file they are written in the ASCII multiplex format with the header containing the filtering direction (azimuth and incidence angle), frequency band and the number of trace points. If output data are saved to the SNDA stack they are placed to the end of the stack and are followed by all needed information

(b) A set of tables containing only the averaged powers of output traces. For every frequency band the table is composed by the powers of group filter outputs corresponding to the all scanning directions. The minimum and maximum values of the tables are calculated and the arrival directions are indicated at which these extremum values are attained. In this version of the program these tables are only displayed to the screen and do not saved into a file.

6.6. Program "GRFLTFCS"

Extraction of waveforms of differently polarized seismic phases using 3-component array data with the help of optimal Wiener group filtering

The program is designed for waveform extraction of the spatial oscillation components of a seismic wave field, registered by a 3-component array. The oscillations in three conventionally examined directions ('longitudinal' - along the wave propagation ray, 'transversal' - in the horizontal direction orthogonal to the ray, and 'orthogonal' - in vertical direction orthogonal to the ray) are extracted from the background of seismic noise with adaptive suppression of the noise coherent component with the help of multichannel Wiener filtering. The array data processing is performed in the frequency domain.

Let the coordinate system has the X -axis directed to the East, Y -axis - directed to the North and Z -axis to the zenith and denoted as $\mathbf{p}=(p_x, p_y)^T$, $p_x=\sin\alpha\cdot\sin\beta/V$, $p_y=\cos\alpha\cdot\sin\beta/V$, the vector of apparent velocities of the wave in the X and Y directions; here α is the back azimuth of wave arrival, β is its incidence angle and V is the wave phase velocity in the medium just beneath the array. Let the registered wave field is a wavetrain composed by superposition of seismic phases with different polarization. If the all phases are generated by the same seismic source and every phase arrival direction can be characterized by the single apparent velocity vector \mathbf{p} (the ray propagation approximation) then the multichannel signal registered by the array of 3-component seismometers can be expressed in the frequency domain by the equation:

$$\mathbf{u}(f)=\boldsymbol{\varphi}(f)\otimes\mathbf{B}(f)\cdot\mathbf{s}(f), \quad \boldsymbol{\varphi}(f)=(\varphi_1(f),\dots,\varphi_M(f))^T, \quad \varphi_j(f)=\exp(-i2\pi f\tau_j),$$

where $\mathbf{s}(f)=(s_P(f), s_T(f), s_O(f))^T$; $s_P(f)$, $s_T(f)$, $s_O(f)$ are the Fourier transforms of longitudinal, transversal and orthogonal components of wave oscillations; $\tau_j(\mathbf{p})$ is the wave time delay at the site of j -th seismometer (depending from the phase apparent velocity vector), \otimes is the Kronecker product of the vector $\boldsymbol{\varphi}$ and (3×3) matrix \mathbf{B} ; M is the number of array seismometers; matrix $\mathbf{B}(f)$ has the form: $\mathbf{B}(f)=\mathbf{A}_1\mathbf{A}_2$. The matrix \mathbf{A}_1 is equal

$$\mathbf{A}_1 = \begin{bmatrix} -\sin\alpha & \cos\alpha & 0 \\ -\cos\alpha & -\sin\alpha & 0 \\ 0 & 0 & 1 \end{bmatrix}$$

It realizes the rotation of the coordinate system, associated with the seismic source (for which the X -axis is directed along the day surface to the source epicenter, the Z -axis is directed to the zenith and Y -axis is orthogonal to X and Z axes) to the geographical coordinate system introduced above.

The matrix A_2 reflects our model of wave propagation in the medium in the vicinity of the array. For the simplest model without accounting for wave reflection and transformation at the day surface this matrix has the form

$$A_2 = \begin{bmatrix} \sin \beta_P & 0 & -\cos \beta_V \\ 0 & 1 & 0 \\ \cos \beta_P & 0 & \sin \beta_V \end{bmatrix}$$

where β_P и β_V -incidence angles for P and S waves correspondingly.

The model above is too simple to reflect all features of wave field registered by a 3-component array, so it is mainly relevant for investigation of surface waves (for which $\beta_P = \beta_V = \pi/2$) and for preliminary (exploration) array data analysis because it does not consume much computational time. For comprehensive body wave investigations it is expedient to implement more complex but more realistic frequency independent propagation model proposed by D.Kennet, which reflects the impact of the day surface to body wave propagation. For this model the matrix A_2 has the form:

$$A_2 = \begin{bmatrix} V_P \cdot p_h \cdot C_2 & 0 & -V_S \cdot q_S \cdot C_1 \\ 0 & 2 & 0 \\ V_P \cdot q_P \cdot C_1 & 0 & V_S \cdot p_h \cdot C_2 \end{bmatrix};$$

where V_P , V_S are the phase velocities of the P and S waves accordingly;

$$q_P = (V_P^{-2} - p_h^2)^{1/2}; \quad q_S = (V_S^{-2} - p_h^2)^{1/2}; \quad C_1 = \frac{2 \cdot V_S^{-2} \cdot (V_S^{-2} - 2 \cdot p_h^2)}{(V_S^{-2} - 2 \cdot p_h^2)^2 + 4 \cdot p_h^2 \cdot q_P \cdot q_S}$$

$$C_2 = \frac{4 \cdot V_S^{-2} \cdot q_P \cdot q_S}{(V_S^{-2} - 2 \cdot p_h^2)^2 + 4 \cdot p_h^2 \cdot q_P \cdot q_S}; \quad p_h^2 = p_x^2 + p_y^2$$

In practical applications the seismic event signals are registered by an array at the background of additive seismic noise. So 3-component array recordings can be expressed by the following equation: $u(f) = \varphi(f) \otimes B(f)s(f) + \zeta(f)$, where $\zeta(f)$ is Fourier transform of the multichannel array noise component.

The group filter frequency response providing the optimal suppression of the noise component and the undistorting extraction of wave oscillations in the described

above longitudinal, transverse and the orthogonal directions is given by the following equation:

$$\Phi_I(f) = F^{-1}(f)H(f)(H^*(f) F^{-1}(f) H(f))^{-1},$$

where $\Phi(f)$ is $(3M \times 3)$ matrix function; $F(f) = \zeta(f)\zeta^*(f)$ is $(3M \times 3M)$ inverse noise matrix spectral density (IMPSD) of array noise recordings; $H(f) = \varphi(f) \otimes B(f)$ is $3M \times 3$ matrix. The filter transforms the $3M$ channel array seismogram to 3 output traces, each trace is composed by extracted wavetrain oscillations in the one of the three conventional directions. The single restriction used for filter design is the condition to undistortingly reproduce the oscillation components of signal arriving from the given direction. It is reflected in the following equation $\Phi_I^*(f)H(f) = (1, 1, 1)^T$

One can easily check that the noise power spectral densities of the filter output traces are given by the equation

$$\sigma^2(f) = (\sigma_P \sigma_T \sigma_O)^T = ((H(f)F^{-1}(f)H(f))^{-1})^T$$

Thus the group filter with frequency response $\Phi_S(f) = F(f)H(f)(H^*(f)F^{-1}(f)H(f))^{-1/2}$, produces at the every direction output the white noise. Such a filter we call the whitening optimal group filter.

If the seismic signal is recorded at a background of transient interference waves generated by the spatially localized source with known parameters, then the inverse noise MPSD can be found analytically: $F^{-1}(f) = [I - Q(Q^*Q)^{-1}Q^*]$, where I is the $(3M \times 3M)$ identity matrix, $Q(f)$ is the $(3M \times 3)$ matrix frequency response of propagation paths of the interfering wave while it propagates from the noise source to the array sensors. For the plane interfering wave the matrix $Q(f)$ has the same structure as the matrix $H(f)$. The undistorting optimal group filter designed for this form of MPSD is known as spatially rejecting filter.

Input parameters of the program

All input parameters of the program have to be contained in the file "grfltfcs.inp". Example of the file is given below:

```
***FILE OF INPUT PARAMETERS FOR PROGRAM "GRFLTFCS": standard***
ARRAY TYPE: 3C = 1; 2C HORIZONTAL = 2; SIMA = 3
1
FILTER TYPE: UNDISTORTING(1) = 1; WHITENING = 3
1
INITIAL AND FINAL POINTS FOR SCANNING AT W-E SLOWNESS (SEC/KM)
-0.4      0.4
```



```

INITIAL AND FINAL POINTS FOR SCANNING AT S-N SLOWNESS (SEC/KM)
-0.4    0.4
INCREMENTS FOR SCANNING AT DIRECTIONS (SEC/KM)
0.02    0.02
MEDIUM MODEL: SIMPLEST (WITHOUT INTERACTIONS)= -1; FREQUENCY INDEPENDENT
(D.KENNET) = 1
-1
P & S-WAVES MEDIUM PHASE VELOCITIES (KM/SEC)
6.    4.
NAME OF FILE WITH MEDIUM PHASE VELOCITY DISPERSION CURVE (FOR LOVE &
RAYLEIGH WAVES)

LOW AND HIGH FREQUENCIES FOR FILTERING RANGE (HZ)
0.    5.
NUMBER OF FREQUENCY BANDS
3
MARGINS OF BANDS (HZ)
1.    1.5    3.    4.
NOISE MATRIX TYPE: IDENTICAL= -1; FOR REJECTION FILTER=0; ADAPTIVE=1
1
NOISE DIRECTION (E-W & N-S SLOWNESS) AND MEDIUM MODEL FOR REJECTION
FILTERING
0.4    0.4    -1
NAME OF FILE WITH ARRAY SEISMOMETER COORDINATES (IN KM)
alibek.crd
NAME OF FILE FOR INVERSE MATR. SP. PARAMETERS
insp.par
NAME OF FILE FOR INVERSE MATR. SP. VALUES
insp.mtrs
OUTPUT PRESENTATION: AS FILTERED TIME SERIES = -1; AS POWER MAPS = 1
-1
READ/WRITE MODE: FROM/TO STACK = 1; FROM/TO DISK FILE = -1
1    1
DATA CHANNELS TO BE PROCESSED (IF READ FROM SYSTEM STACK)
36
NAME OF FILE WITH DATA PARAMETERS (IF READ FROM DISK FILE)
grfltfs.par
NAME OF FILE WITH DATA SAMPLES (IF READ FROM DISK FILE)
grfltfs.dat
NAME OF FILE FOR SAVING OUTPUT (IF WRITE TO DISC FILE)
grfltfs.out

```

Explanation of parameters

1. ARRAY TYPE: 3C = 1; 2C HORIZONTAL = 2; SIMA = 3
 The parameter defines the type of recording installation and can have the values:
 - (1) - for a 3-component array or single 3-component station (if parameter NUMBER OF SEISMOMETERS equal 1);
 - (2) - for 2-component horizontal array;
 - (3)- for strain-seismometer microarray (SIMA), consisting of a single 3C seismometer and two horizontal strainmeters located at the same site.
2. FILTER TYPE: UNDISTORTING(1) = 1; WHITENING = 3
 The parameter defines the type of group filter to be used:
 - (1) - for undistorting filter with single restriction (frequency response (FR) Φ_1);

(3) - for whitening group filter (FR Φ_3).

3. INITIAL AND FINAL POINTS FOR SCANNING AT W-E SLOWNESS (SEC/KM)

The given program version allows to perform the optimal group filtering of 3-component array data not only for the single arrival direction but for the "fan" of directions inside of given ranges of W-E and S-N slowness of wave arrival (i.e. it provides scanning of the medium with the assigned slowness increments). The parameter assigns the initial and final values of wave arrival W-E horizontal slowness to be used while scanning the medium. If the initial value is equal the final one then the group filtering is performed for the single W-E slowness value.

4. INITIAL AND FINAL POINTS FOR SCANNING AT N-S SLOWNESS (SEC/KM)

The parameter assigns the initial and final values of wave arrival S-N horizontal slowness to be used while scanning the medium. If the initial value is equal to the final one then the group filtering is performed for the single S-N slowness value.

5. INCREMENTS FOR SCANNING AT DIRECTIONS (SEC/KM)

These two parameters define the increments for scanning at W-E and S-N slowness of wave arrival.

6. MEDIUM MODEL: SIMPLEST (WITHOUT WAVE TRANSFORM) = -1; FREQUENCY INDEPENDENT (D.KENNET) = 1

The parameter defines the medium model used:

(-1) corresponds to the simplest model not accounting for the day surface impact to the wave propagation;

(1) corresponds to the frequency independent model proposed by D.Kennet accounting the wave reflections and transformations at the day surface.

7. P & S-WAVES MEDIUM PHASE VELOCITIES (KM/SEC)

These two parameters determine phase velocities of the P and S waves in the medium beneath the array. If the Rayleigh wave is studied the both value must have the same values equal to the Rayleigh wave phase velocity: $V_P = V_S = V_R$

8. NAME OF FILE WITH PHASE VELOCITY DISPERSION CURVE FOR SURFACE WAVE (IF NAME=' ' - WITHOUT DISPERSION)

This is the name of file containing the surface wave dispersion curve (the phase velocity as function of frequency). If the parameter value contains the blanks at 5 first positions, it means that the dispersion is absent and the surface wave is regarded as possessing the frequency independent (mean) phase velocity. The file has to consist of two ASCII format columns: the frequency in Hz and velocity in Km/Sec;

9. LOW AND HIGH FREQUENCIES OF FILTER RANGE (HZ)

These two parameters assign the low and high frequencies of the range of group filtering to be performed.

10. NUMBER OF FREQUENCY BANDS

The given program version allows to calculate simultaneously the group filtering output traces for several (maximum 5) frequency bands inside the assigned frequency range. The parameter defines the number of bands

11. MARGINS OF BANDS (HZ)

The parameter is valid only if the NUMBER OF FREQUENCY BANDS is more than 1; it defines the inner margins of frequency bands for filtering. It is assumed in the program that the frequency bands do not overlap, low frequency of the first band and high frequency of the last one are equal correspondingly to the low and high frequencies of the filter range (the values of the above parameter). Thus the "margins

of the bands" are the points of partition of the previously assigned filter frequency range.

12. NOISE MATRIX TYPE: IDENTICAL = -1; FOR REJECTION FILTER = 0; ADAPTIVE = 1

For design of any type optimal group filter it is needed to evaluate the inverse matrix power spectral density (IMPSD) $F^{-1}(f)$ of array noise. The following options of the IMPSD can be used in the program, being specified by the parameter values:

(-1) means the identity IMPSD corresponding the assumption that the noise field at the recording site is the spatially uncorrelated white one. The optimal group filtering coincides in this case with the conventional 3-component beamforming procedure.

(0) means the IMPSD corresponding the coherent noise field generated by the random plane wave arriving to the recording site with an assigned direction. The IMPSD is calculated in the program. In this case the optional group filtering procedure realizes the algorithm of spatial rejecting filtering.

(1) means adaptive IMPSD. If noise field contains a strong coherent components of unknown genesis the both above assumptions about the noise IMPSD are not satisfactory. In this most common case the optimal group filtering has to involve an estimate of the array noise IMPSD. The latter should be preferably made using the array noise recordings at a time interval just before the seismic event signal onset. The IMPSD estimate can be supplied by the program "*armafs*". While using the parameter value = 1 this program has to be executed before running the program "*grflts*". The same array channel ordering must be guaranteed in the both program input data.

13. NOISE WAVE DIRECTION: AZ. & INC. ANGLE; VELOCITY & WAVE TYPE (FOR REJECTION FILTERING)

If the rejection filtering (NOISE MATRIX TYPE = 0) is chosen as optimal group filtering option, this parameter specifies the features of interfering plane wave: its arrival azimuth, incidence angle, phase velocity in the medium and the polarization type.

14. NAME OF FILE WITH ARRAY SEISMOMETER COORDINATES (IN KM)

The name of file with coordinates of array recording installations composing the array (1C, 2C, 3C seismometers or SIMA). If the number of seismometers is equal 1 then it's site is assumed to has coordinates (0,0). The file must consist of two ASCII columns: first one with X-coordinates (West-East orientation) and second one with Y-coordinates (South-North orientation). In this version of the program the Z seismometer coordinates are assumed to be equal 0.

15. NAME OF FILE FOR INVERSE MATR. SP. PARAMETERS

This is the name of file containing parameters of the IMPSD estimate (if NOISE MATRIX TYPE = 1).

16. NAME OF FILE FOR INVERSE MATR. SP. VALUES

This is the name of file containing values of the IMPSD estimate (if NOISE MATRIX TYPE = 1).

17. OUTPUT PRESENTATION: AS TIME SERIES = 0; TRACE POWER MAPS = 1

The presentation of filtering results is possible in two forms:

(0) - in the form of output time series. In this case after the program execution a user gets the set of time series (traces).

(1) - in the form of filtered trace power maps. For every frequency band and every wave oscillation component the map with coordinates X-slowness - Y-slowness is

produced. The map are composed by the powers of group filter output traces corresponding to the all scanning wave arrival directions.

18. READ/WRITE MODE: FROM/TO STACK = 1; FROM/TO DISK FILE = -1

The first of these two parameters defines the device for reading the program input data and the second one - the device for saving results of the program performing: (1) is for the SNDA stack, (-1) is for the disk file.

19. DATA CHANNELS TO BE PROCESSED (IF READ FROM SNDA STACK)

This parameter is valid if the input data are read from the SNDA Stack. It must have a form of strings corresponding to CHANNELS parameter format used in the SNDA stack commands. For example, it can be as following: 15; (1,3-10,14); all. The total number of specified data channels has not to exceed 50.

20. NAME OF FILE WITH DATA PARAMETERS (IF READ FROM DISK FILE)

If parameter READ MODE = -1, then the name of file containing the parameters of input data has to be assigned here. The parameters are: number of data channels, number of samples in every channel and the data sampling interval; the file must have the form of ASCII string.

21. NAME OF FILE WITH DATA SAMPLES (IF READ FROM DISK FILE)

If parameter READ MODE = -1, then the name of file containing the samples of data to be processed must be assigned here. The data has to be in the ASCII multiplex form without any header.

22. NAME OF FILE FOR SAVING OUTPUT (IF WRITE MODE = -1)

If WRITE MODE = -1 the parameter assigns the name of file for saving the filtering results to the disk. The output traces are saved in the ASCII demultiplex form. The every output trace has a header containing the filtering direction (X and Y slowness), frequency band and the number of trace points.

Input data format

The input data for the program are to be the multidimensional time series with total number of channels no more then 50 and number of samples in the every channel no more then 4096. If the data are stored in the disk file the latter must have the ASCII multiplex format. The channel ordering for every array recording instrument has to be in generally the following: S-N strainmeter, W-E strainmeter, N-S seismometer, W-E seismometer, Z-seismometer. For a particular array configuration some of the channels above can be omitted.

Output data format

In depend on a value of parameter OUTPUT PRESENTATION the program output can have the following forms:

(a) A set of time series which are the results of input data group filtering for the frequency bands specified by the parameter MARGINS OF BANDS and for the signal arrival directions specified by the scanning parameters. For every direction there is the sequence of traces corresponding to the different bands. If output data are saved to the disk file they are written in the ASCII multiplex format with the header containing the filtering direction (X, Y slowness), frequency band and the number of trace points. If output data are saved to the SNDA stack they are placed to the end of the stack and are followed by all needed information

(b) A set of maps in coordinates X-slowness - Y-slowness containing the averaged powers of output traces (F-K maps). Such maps (composed by the powers of group filter outputs corresponding to the all scanning directions) are produced for every component of wave oscillation and every frequency band. The minimum and maximum values of the maps are calculated and the arrival directions are indicated at

which these extremum values are attained. The maps are saved into a disc file and displayed to the screen with the help of SNDA "*Surfer*" routine.

6.7. Program "GRFLTFK" Adaptive 3-component F-K analysis

Program is intended for adaptive estimation of the horizontal slowness vector of seismic wave phase using the observations from a 3-component (3C) 2-component or 1-component (1C) seismic array. The following model of the multidimensional time series at the output of 3C array sensors is used (being written in the frequency domain)

$$\mathbf{x}(f) = \mathbf{y}(f) + \xi(f) = \mathbf{h}_w(f, \mathbf{p}, V) s_w(f) + \xi(f) \quad (1)$$

where $\mathbf{x}(f) = (x_1(f), \dots, x_{3M}(f))^T$ is $3M$ dimensional vector of array observations in the frequency domain; $\xi(f)$ is the $3M$ dimensional vector of additive array noise component, $\mathbf{h}_w(f, \mathbf{p}, V)$ is the $3M$ dimensional vector frequency response VFR of the medium beneath the array which converts the complex spectrum $s_w(f)$ of wave phase oscillations to oscillations at the outputs of of $3M$ array sensors. The equation for the VFR calculations based on two different models of the laterally homogeneous medium are given in Section 3.1 (see also in the description of program "*grfiltfs*"). Note that the type of analyzed wave polarization directly defines the form of the function $\mathbf{h}_w(f, \mathbf{p}, V)$, along with the value of the wave velocity in the medium and array sensor coordinates.

In general case the array is assumed as consisting of M 3-component seismometers with N-S, E-W, Z, sensors. In case of a Z-component array or an array consisting of horizontal N-S, E-W seismometers some of the sensors are regarded as being off and the corresponding elements in the all vectors of eq.(1) are substituted by zeros. For the adaptive mode of program execution the additional assumption is used that additional observation of the "pure" noise realization $\xi_o(f)$ is available. Usually this is some noise array recordings at time intervals preceding or succeeding the interval containing the signal wave phase being analyzed. It is supposed, that the current seismic noise field is rather stationary one and the noise $[3M \times 3M]$ matrix power spectrum density

(MPSD) $F_o(f)$ calculated using “pure” noise realization $\xi_o(f)$ with the help of program “*armafs*” well corresponds to the MPSD of noise realization $\xi(f)$ obscuring the signal waveforms at the array sensors.

As it is shown in Section 3.3 under assumptions above the statistically optimal (Maximum Likelihood) estimate of wave phase apparent slowness vector $\mathbf{p}=(p_n, p_e)$ can be calculated in accordance with the following formula

$$\hat{\mathbf{p}} = \arg \max_{\mathbf{p}} \sum_{j=j_{min}}^{j_{max}} \frac{\mathbf{h}_w^*(f_j, \mathbf{p}, V) F_0^{-1}(f_j) \mathbf{x}(f_j) \mathbf{x}^*(f_j) F_0^{-1}(f_j) \mathbf{x}_w(f_j, \mathbf{p}, V)}{\mathbf{h}_w^*(f_j, \mathbf{p}, V) F_0^{-1}(f_j) \mathbf{h}_w(f_j, \mathbf{p}, V)} \quad (2)$$

where $\mathbf{x}(f_j)$ are the complex spectral components of array observations by eq.(1) in the frequency points of the Discrete Fourier Transform (DFT), j_{min} and j_{max} are the DFT points defined the frequency band of the F-K analysis

The program realizing the ML algorithm of apparent slowness vector estimation creates the map consisting of values of functional corresponding to p_n , p_e slowness, in the assigned range of the wave arrival directions i.e. Maximum value of the map corresponds to the ML estimate of apparent slowness vector of wave arrival.

The program “*grfiltfk*” can also work in the nonadaptive mode. In this case the two variants exist. For the first variant the noise MPSD is supposed to be identity matrix: $F_o(f) \equiv \mathbf{I}$. This corresponds to the assumption that the array noise is originated from the spatially uncorrelated white noise field. In this case the ML apparent slowness estimate coincides with the conventional 3-component wide band F-K analysis. For the second variant the assumption is made that the array noise is pure coherent one and generated by transient nuisance wave with the known apparent slowness vector, polarization type and phase velocity in the medium. The MPSD $F_o(f)$ corresponding to this nuisance wave is calculated in the program using above parameters by equations for kernel matrix of rejection group filter (see eq.(12)-(14) in Section 3.2.4).

The program “*grfiltfk*” allows to calculate a series of maps corresponding to different frequency bands. This provides the possibility to analyze the wave arrival direction parameters in depending on frequency, for example to calculate the dispersion curves of the teleseismic surface waves.

Input parameters of the program

All parameters of the program are to be contained in a disk file with the name "grfiltfk.inp". An example of the file is given below.

```

*** FILE OF INPUT PARAMETERS FOR PROGRAM "GRFILTFK": standard ***
ARRAY TYPE: 3C ARRAY=1; 1C ARRAY=2; 2C HORIZONTAL ARRAY=3; SSI=4;
2
FILTER TYPE: UNDISTORTING(1)=1; UNDISTORTING(2)=2; WHITENING=3
3
WAVE TYPE: P=1; SH & LOVE=2; SV=3; RAYLEIGH=4;
1
IMAGE: CONTOUR MAP=0; 3D IMAGE=1; BOTH=2
2
PLOTING: FROM PROGRAM=0; FROM SCRIPT=1
0
INITIAL AND FINAL POINTS FOR SCANNING AT E-W-SLOWNESS (SEC/KM)
-0.2 0.2
INITIAL AND FINAL POINTS FOR SCANNING AT N-S SLOWNESS (SEC/KM)
-0.2 0.2
INCREMENTS FOR SCANNING AT SLOWNESS (SEC/KM)
0.02 0.02
RAYLEIGH WAVE ELLIPTIC COEFFICIENT (HORIZ/VERT)
0.8
MEDIUM PHASE VELOCITY (KM/SEC)
5.
NAME OF FILE WITH PHASE VELOCITY DISPERSION CURVE FOR SURFACE WAVE (IF
NAME=' ' - WITHOUT DISPERSION)

LOW AND HIGH FREQUENCIES FOR GROUP FILTERING (HZ)
1. 3.
NUMBER OF FREQUENCY BANDS
1
MARGINS OF BANDS (HZ)
3. 4.
CALCULATION OF AVERAGED MAP FOR DIFFERENT FREQUENCES: YES=1; NO=0
1
NOISE MATRIX TYPE: IDENTICAL=-1; CALC. FOR REJECTION FILTER=0;
ADAPTIVE=1;
1
NOISE DIRECTION (EW & NS SLOWN.), VELOCITY AND WAVE TYPE (FOR REJECTION
FILTER)
0.2 0.2 3. 1
NAME OF WITH ARRAY COORDINATE (COORDINATES IN KM)
data/lapshin/noress.crd
NAME OF FILE FOR INOISE INVERSE SPECTRUM PARAMETERS
ssa/lapshin/insp.par
NAME OF FILE FOR NOISE INVERSE MATRIX SPECTRUM
ssa/lapshin/insp.mtrs
READ/WRITE MODE: FROM/TO SYSTEM STACK=1; FROM/TO DISC FILE=-1
1 1
DATA CHANNELS TO BE PROCESSED (IF READ FROM SYSTEM STACK)
25
NAME OF FILE WITH DATA PARAMETERS (IF READ FROM DATA FILE)

```

ssa/lapshin/data/grfltfs.par
 NAME OF FILE WITH DATA SAMPLES (IF READ FROM DATA FILE)
 ssa/lapshin/data/grfltfs.dat

Explanation of the input parameters

1. ARRAY TYPE: 3C ARRAY = 1; 1C ARRAY = 2; 2C HORIZ. ARRAY = 3; SIMA = 4

The parameter defines the type of recording installation and can have the values:

- 1 - for a 3-component array or single 3-component station
- 2 - for 1-component array consisting of similarly oriented sensors;
- 3 - for 2-component horizontal array;
- 4- for strain-seismometer microarray (SIMA), consisting of a single 3C seismometer and two horizontal strainmeters located at the same site.

2. FILTER TYPE: UNDISTORTING(1) = 1; UNDISTORTING(2) = 2; WHITENING = 3

The parameter defines the type of group filter to be used:

- (1) - for undistorting filter with single restriction (frequency response (FR) Φ_1);
- (2) - for undistorting with restrictions on the FR spatial derivatives (FR Φ_2);
- (3) - for whitening group filter (FR Φ_3).

3. WAVE TYPE: P = 1; SH & LOVE = 2; SV = 3; RAYLEIGH = 4

The parameter defines the type of seismic wave phase to be extracted. This program version intended for extracting only single phase with specific polarization:

- (1) - for the P-phase;
- (2) - for the SH or Love phases;
- (3) - for the SV phase;
- (4) - for the Rayleigh phase.

4. IMAGE: CONTOUR MAP=0; 3D IMAGE=1; BOTH=2

The parameter defines the type of program output control file which is used by the utility providing the plotting of F-K map. A user can choose one (or both) from the two specified programs: the standard UNIX graphic routine "contour" or the SNDA graphic program "surfer"

5. PLOTTING: FROM PROGRAM=0; FROM SCRIPT=1

The parameter allows to start the execution of the graphic utility for the F-K map imaging inside the program "grfiltfk" or to transfer this function to the special SNDA command.

6. INICIAL AND FINAL POINTS FOR SCANNING AT E-W-SLOWNESS (SEC/KM)

The parameter assigns the initial and final values of wave W-E horizontal slowness to be used while scanning the medium for creating the F-K map.

7. INITIAL AND FINAL POINTS FOR SCANNING AT N-S SLOWNESS (SEC/KM)

The parameter assigns the initial and final values of wave S-N horizontal slowness to be used while scanning the medium for creating the F-K map.

8. INCREMENTS FOR SCANNING AT DIRECTIONS (SEC/KM)

These two parameters define the increments for scanning at W-E and S-N slowness of wave arrival while creating the F-K map.

9. RAYLEIGH WAVE ELLIPTIC COEFFICIENT (HORIZ/VERT)

This is the elliptic coefficient of the Rayleigh wave: the ratio of small axis of oscillation polarization to the large one;

10. MEDIUM PHASE VELOCITY (KM/SEC)

This is the phase velocity of the P or S wave in the medium just beneath the array. If value of parameter "Name of file with dispersion curve" while filtering of the Rayleigh or Love waves consist of 5 blanks this velocity is used as the average surface wave velocity

11. NAME OF FILE WITH PHASE VELOCITY DISPERSION CURVE FOR SURFACE WAVE (IF NAME=' ' - WITHOUT DISPERSION)

This is the name of file containing the surface wave dispersion curve (the phase velocity as function of frequency). If the name contains the blanks at 5 first positions it means that the dispersion is absent and the surface wave is regarded as possessing the frequency independent (mean) phase velocity. The file has to consist of two ASCII format columns: the frequency in Hz and velocity in Km/Sec;

12. LOW AND HIGH FREQUENCIES OF F-K ANALYSIS RANGE (HZ)

These two parameters assign the low and high frequencies of the range within which the F-K analysis is to be performed.

13. NUMBER OF FREQUENCY BANDS

The given program version allows to calculate simultaneously the F-K analysis of input traces for several (maximum 5) frequency bands inside the assigned frequency range. This parameter defines the number of bands

14. MARGINS OF BANDS (HZ)

The parameter is valid only if the NUMBER OF FREQUENCY BANDS is more than 1; it defines the inner margins of frequency bands for filtering. It is assumed in the program that the frequency bands do not overlap, low frequency of the first band and high frequency of the last one are equal correspondingly to the low and high frequencies of the filter range (the values of the above parameter). Thus the "margins of the bands" are the points of partition of the previously assigned filter frequency range.

15. CALCULATION OF AVERAGED MAP FOR DIFFERENT FREQUENCIES:

YES=1; NO=0

This is the switch to the option for computing the averaged F-K map composed from the set of maps previously calculated for different frequency bands.

16. NOISE MATRIX TYPE: IDENTICAL = -1; FOR REJECTION FILTER = 0; ADAPTIVE = 1

For creating of the adaptive F-K map it is needed to evaluate the inverse matrix power spectral density (IMPSD) $F^{-1}(f)$ of array noise. The following options for the IMPSD can be used in the program, being specified by the parameter values:

(-1) means the identity IMPSD corresponding the assumption that the noise field at the recording site is the spatially uncorrelated white one. The adaptive F-K analysis coincides in this case with the conventional (3-component) wide band F-K analysis.

(0) means the IMPSD corresponding to the coherent noise field generated by the nuisance plane wave arriving to the recording site with an assigned direction. The IMPSD is calculated in the program.

(1) means adaptive IMPSD. If the noise field contains a strong coherent components with unknown genesis the both above assumptions about the noise IMPSD are not satisfactory. In this most common case the optimal group filtering has to involve an estimate of the array noise IMPSD. The latter should be preferably made using the array noise recordings at a time interval just before the seismic signal onset. The IMPSD estimate can be supplied by the program "armafs". While using the parameter value = 1 this program have to be executed before running the program "grfiltfk". The same array channel ordering must be guaranteed for both program input data.

17. NOISE DIRECTION (EW & NS SLOWN.), VELOCITY AND WAVE TYPE
(FOR REJECTION NOISE SUPPRESSION)

If the NOISE MATRIX TYPE = 0 is chosen as the option for adaptive F-K analysis, this parameter specifies the features of interfering plane wave: its apparent slowness vector, wave velocity in the medium and the polarization type.

18. NAME OF FILE WITH ARRAY SEISMOMETER COORDINATES (IN KM)

This is the name of file with coordinates of array receivers (1C, 2C, 3C seismometers or SIMA). If the number of seismometers is equal to 1 then it's site is assumed to have coordinates (0,0). The file must consist of two ASCII columns: first one with X-coordinates (West-East orientation) and second one with Y-coordinates (South-North orientation). In this version of the program the Z seismometer coordinates are assumed to be equal 0.

19. NAME OF FILE FOR INVERSE MATRIX SPECTRUM PARAMETERS

This is the name of file containing the parameters of IMPSD estimate (if NOISE MATRIX TYPE = 1).

20. NAME OF FILE FOR INVERSE MATRIX SPECTRUM VALUES

This is the name of file containing the values of IMPSD estimate (if NOISE MATRIX TYPE = 1).

21. READ/WRITE MODE: FROM/TO STACK = 1; FROM/TO DISK FILE = -1

The first of these two parameters defines the device for reading of the program input data; the second one - the device for saving results of the program performing: (1) is for the SNDA stack, (-1) is for the disk file.

22. DATA CHANNELS TO BE PROCESSED (IF READING FROM STACK)

This parameter is valid if the input data are read from the SNDA Stack. It must have the form of string corresponding to CHANNELS parameter format used in the SNDA stack commands. For example, it can be as following: 15; (1,3-10,14); all. The total number of specified data channels has not to exceed 50.

23. NAME OF FILE WITH DATA PARAMETERS (IF READING FROM DISK FILE)

If parameter READ MODE = -1, then the name of file containing the parameters of input data has to be assigned here. The parameters are: number of data channels, number of samples in every channel and the data sampling interval; the file must have the form of ASCII string.

24. NAME OF FILE WITH DATA SAMPLES (IF READING FROM DISK FILE)

If parameter READ MODE = -1, then the name of file containing the samples of data to be processed must be assigned here. The data must be in the ASCII multiplex format without any header.

6.8. Program SP3C

Adaptive multimode F-K analysis of 3-component array data

The program is intended for adaptive estimating of slowness vectors of the seismic waves using observations of 3-component (3C) seismic arrays. In the nonadaptive mode the program allows to calculate estimates of spatial spectra of array recordings using the conventional low resolution and different high resolution methods. In the adaptive mode it provides the low resolution estimation of spatial spectrum of "signal" wave with suppression of noise spatial spectral components. The

last program functions coincides with the purposes of the program “*grfltfk*”, which is really the theoretical prototype of the program “*sp3c*”.

The necessity of program “*sp3c*” development is due to the fact that performance of the prototype program “*grfltfk*” is rather time consuming. As it is seen from eq.(1) of the program “*grfltfk*” description there is needed to calculate and invert the $M \times M$ matrices (where M is a number of the array sensors) for the all Discrete Fourier Transform (DFT) frequencies of the seismic range being analyzed e.g. to perform the thousands computational cycles. The program “*sp3C*” is based on an approximate formula for the calculations of multimode adaptive spatial spectrum. It runs in tens times faster than the prototype program “*grfltfk*”.

The modifying of calculating algorithm is connected with the next assumptions. Let frequency band being analyzed is quite narrow, and we can neglect variations of the functions $h(f_j, p, V)$ and $F_0^{-1}(f_j)$ in this frequency band. Then equation (1) in the description of program “*grfltfk*” can be transformed in the following form:

$$\hat{p} = \arg \max_p \frac{h^*(f_0, p, V) F_0^{-1}(f_0) \left[\sum_{j=jmin}^{j=jmax} x(f_j) x^*(f_j) \right] F_0^{-1}(f_0) h(f_0, p, V)}{h^*(f_0, p, V) F_0^{-1}(f_0) h(f_0, p, V)} \quad (1)$$

where f_0 - is a frequency in the middle of the band being analyzed; $jmin$, $jmax$ are the lower and upper DFT frequencies in the band. The expression in the square brackets is the averaging of matrix periodogram of $3M$ vector array observations in the frequency domain. This averaged matrix is really the estimate of MPSD of the being analyzed array seismograms containing the signal wave obscured by array noise components. We can substitute instead the expression in the square brackets other more statistically grounded estimate $F_x(f_0)$ of the averaged MPSD of the signal observations in the given frequency band. Remind, that the matrix $F_0(f_0)$ in eq.(1) is the MPSD of the “pure” array noise calculated during adaptation using “pure” array noise recordings. This is performed in the program “*sp3c*” based on matrix coefficients of the noise ARMA model produced by the program “*marmamo*” at the stage of adaptation to noise.

So the computational formula for narrow band adaptive F-K estimate of apparent slowness vector has the form:

$$\hat{p} = \arg \max_p \frac{h^*(f_0, p, V) F_0^{-1}(f_0) F_x(f_0) F_0^{-1}(f_0) h(f_0, p, V)}{h^*(f_0, p, V) F_0^{-1}(f_0) h(f_0, p, V)} \quad (2)$$

As for the program "*grfiltfk*" in the case of 1-component or two-component (with horizontal sensors) array the matrices $F_x(f)$ and $F_0(f)$ will have the dimensions $[M \times M]$ or $[2M \times 2M]$ correspondingly. Note that the general formula eq.(2) has numerous partial cases that allow to design the program providing multimode F-K analysis: 1) adaptive low resolution, 2) conventional low resolution and high resolution with ARMA modeling for the estimation of signal data MPSD $F_x(f)$. In the case 1) calculations is performed using general eq.(2). In the case 2) matrix $F_0^{-1}(f)$ is substituted in eq.(2) by the identity matrix I ; this implies that the denominator of eq.(1) become equal to 1 and eq.(2) itself coincides with the conventional formula for narrow band low resolution F-K analysis. In the case 3) the matrix $F_0^{-1}(f)$ in eq.(2) is substituted by the matrix $F_x(f)$; this implies that the nominator of eq.(2) become equal to 1 and eq.(2) itself coincides with the conventional formula of Capon high resolution F-K analysis. All this options are realized in the program "*sp3c*".

Note that in any described modes the matrix functions $F_x(f)$ and $F_0^{-1}(f)$ are calculated in the program based on the matrix coefficients of ARMA models of the signal and noise time series. The latter are produced by the program "*marmamo*" which have to be executed before running the program "*sp3c*", moreover, for the adaptive mode this program have to process the signal and the noise data separately. The matrix coefficients of the data ARMA models transferred to the program "*sp3c*" via disc files with the standard names. So this mutual execution of these two programs is not so borrowing for a user, especially if F-K analysis processing is performed with the help of special SNDA script.

Input parameters of the program

All parameters of the program are to be contained in a disk file with the name "*sp3c.inp*". An example of the file is given below.

```
*** FILE OF INPUT PARAMETERS FOR PROGRAM "sp3c": standard ***
TYPE OF ANALYSIS: LOW RESOLUTION = 0; HIGH RESOLUTION = 1
1
ARRAY TYPE: 3C ARRAY = 1; 1C ARRAY = 2; 2C HORIZONTAL ARRAY = 3; SSI = 4
1
WAVE TYPE: P = 1; SH & LOVE = 2; SV = 3; RAYLEIGH = 4
IMAGE: CONTOUR MAP = 0; 3D IMAGE = 1; BOTH = 2
2
PLOTING: FROM PROGRAM = 0; FROM SCRIPT = 1
```

```

0
ADAPTIVE MODE = 1; WITHOUT ADAPTATION = 0;
1
INITIAL AND FINAL POINTS FOR SCANNING AT E-W-SLOWNESS (SEC/KM)
-0.2    0.2
INITIAL AND FINAL POINTS FOR SCANNING AT N-S SLOWNESS (SEC/KM)
-0.2    0.2
INCREMENTS FOR SCANNING AT SLOWNESS (SEC/KM)
0.02    0.02
RAYLEIGH WAVE ELLIPTIC FACTOR (HORIZ/VERT)
0.7
MEDIUM PHASE VELOCITY (KM/SEC)
6.
NAME OF FILE WITH PHASE VELOCITY DISPERSION CURVE FOR SURFACE
WAVE (IF NAME=' ' - WITHOUT DISPERSION)
disp.crv
LIST OF FREQUENCY VALUES (<=10 in the limits of data freq band), HZ
1.5  0  0  2.4  0  0  0  0  0  0
PLOTING SUM OF MAPS FOR DIFFERENT FREQUENCIES: YES - 1; NO - 0 (ISUM)
0
NOISE REGULATIZATION VALUE: QUANTATY IN [0,1], REAL NOISE: 0, WHITE
NOISE: 1
0

```

Explanation of the input parameters

1. TYPE OF ANALYSIS: LOW RESOLUTION = 0; HIGH RESOLUTION = 1
The parameter specifies the method of high or low resolution FK-analysis. Note that this parameter is valid only for nonadaptive mode. If the method "Low resolution" is selected, then the spectrum matrix $F_0^{-1}(f)$ in eq.(2) is replaced by the identity matrix. If the method "High resolution" is selected, then the spectrum matrix $F_0^{-1}(f)$ in eq.(2) is replaced by the $F_x(f)$, thus the only denominator of eq.(2) with this matrix substituted is computed.
2. ARRAY TYPE: 3C ARRAY = 1; 1C ARRAY = 2; 2C HORIZONTAL ARRAY = 3; SSI = 4
The parameter determines the structure of seismic recording system. The possible variants are: array consisting of 3C-seismometers, array of 1C-vertical seismometers, array of 2C-(vertical and horizontal) seismometers, the recording system SSI consisting of single 3C-seismometer and 2C horizontal strainmeter.
3. WAVE TYPE: P = 1; SH & LOVE = 2; SV = 3; RAYLEIGH = 4
The parameter allows to select the wave phase type which specific polarization will be used in the F-K analysis.
4. IMAGE: CONTOUR MAP = 0; 3D IMAGE = 1; BOTH = 2
The parameter defines the type of program output control file which is used by the utility providing the plotting of F-K map. A user can choose one (or both) from the two specified programs: the standard UNIX graphic routine "contour" or the SNDA graphic program "surfer".
5. PLOTING: FROM PROGRAM=0; FROM SCRIPT=1
The parameter allows to start the execution of the graphic utility for the F-K map imaging inside the program "grfiltfk" or to transfer this function to the special SNDA command.

6. ADAPTIVE MODE = 1; WITHOUT ADAPTATION = 0;

The parameter swithes the program to the modes of conventional low resolution or high resolution F-K analysis (without adation) or to the adaptive F-K analysis mode. In the latter case the parameter "TYPE OF ANALYSIS" must be set to the "Low resolution" mode.

7. INICIAL AND FINAL POINTS FOR SCANNING AT E-W-SLOWNESS (SEC/KM)

The parameter assigns the initial and final values of wave W-E horizontal slowness to be used while scanning the medium for creating the F-K map.

8. INITIAL AND FINAL POINTS FOR SCANNING AT N-S SLOWNESS (SEC/KM)

The parameter assigns the initial and final values of wave S-N horizontal slowness to be used while scanning the medium for creating the F-K map.

9. INCREMENTS FOR SCANNING AT DIRECTIONS (SEC/KM)

These two parameters define the increments for scanning at W-E and S-N slowness of wave arrival while creatinf the F-K map.

10. RAYLEIGH WAVE ELLIPTIC COEFFICIENT (HORIZ/VERT)

This is the elliptic coefficient of the Rayleigh wave: the ratio of small axis of oscillation polarization to the large one;

11. MEDIUM PHASE VELOCITY (KM/SEC)

This is the phase velocity of the P or S wave in the medium just beneath the array. If value of parameter "Name of file with dispersion curve" while filtering of the Rayleigh or Love waves consist of 5 blanks this velocity is used as the average surface wave velocity

12. NAME OF FILE WITH PHASE VELOCITY DISPERSION CURVE FOR SURFACE WAVE (IF NAME=' ' - WITHOUT DISPERSION)

This is the name of file containing the surface wave dispersion curve (the phase velocity as function of frequency). If the name contains the blanks at 5 first positions it means that the dispersion is absent and the surface wave is regarded as possessing the frequency independent (mean) phase velocity. The file has to consist of two ASCII format columns: the frequency in Hz and velocity in Km/Sec;

13. LIST OF FREQUENSY VALUES (<=10 in the limits of data freq band), HZ

The parameter deterimines the set of central frequencies of narrow band F-K analysis. The F-K maps are calculated for frequency bands around these central frequencies. The width of bands depends on parameters of array data ARMA model assigned in the program "marmamo" and transferred to the program "sp3c" via the file with standard name.

14. CALCULATION OF AVERAGED MAP FOR DIFFERENT FREQUENCES:

YES=1; NO=0

This is the switch to the option for computing the averaged F-K map composed from the set of maps previously calculated for different frequency bands.

15. NOISE REGULATIZATION VALUE: QUANTATY IN THE LIMITS [0,1]:

FOR REAL NOISE = 0, FOR WHITE NOISE = 1

The parameter allows to relax the noise suppression in the adaptive F-K mode. If it hase the value equal to 0, the calculations are made in accordance with eq.(2). For other values noise matrix $F_0^{-1}(f)$ is substitutes in eq.(2) by the matrix $\Phi = (1-\rho)F_0^{-1}(f) + \rho I$, where I is the identity matrix, ρ is the parameter value.